Novel covalent FAP inhibitors: preparation and validation of target binding by ^{18}F release

Inaugural-Dissertation
zur
Erlangung des Doktorgrades
der Mathematisch Naturwissenschaftlichen Fakultät
der Universität zu Köln

vorgelegt von
Anna-Lena Elsner
aus Nettetal

angenommen im Jahr 2026

Meiner Familie

“One never notices what has been done; one can only see what remains to be done.”

Marie Curie

Abstract

Endoradiotherapy is a systemic treatment approach to selectively deliver a cytotoxic dose of radiation to tumors or other abnormal tissue. For this purpose, compounds labeled with therapeutic radionuclides (usually α- or β^--emitters with a suitable half-life) are used, which are capable of selectively interfere with macromolecules, structures, or biological processes in the target tissue. Fibroblast activation protein (FAP) is a membrane-anchored protein that is overexpressed in the microenvironment of most malignant solid tumors but absent in benign tumors or healthy tissue, making it a promising target for endoradiotherapy. Numerous radiolabeled FAP inhibitors (FAPIs) are widely applied for diagnostic imaging. However, the application of existing FAPIs labeled with therapeutic radionuclides is limited by their insufficient tumor retention.

A primary objective of this study was therefore to improve tumor retention through the development of FAPIs capable of forming an irreversible covalent bond with the enzyme's active site. The novel compounds were designed based on the core structure of the most popular FAPI, UAMC-1110, with the nitrile moiety replaced by a covalently binding ^{18}F-substituted warhead. Release of [^{18}F]fluoride upon covalent interaction of the inhibitors with the active site of FAP was intended to provide indirect evidence of covalent bond formation.

Three FAPIs with an ^{18}F-labeled warhead were synthesized and their stability was assessed in aqueous media across various pH values and under physiological conditions in phosphate-buffered saline (PBS) and human blood plasma. An inhibitor bearing a sulfonyl [^{18}F]fluoride warhead could be labeled with radiochemical conversions (RCCs) of 58 ± 12% using SuFEx-based ultra-fast ^{18}F/^{19}F isotopic exchange and isolated in radiochemical yields (RCYs) of 24 ± 3%. However, due to its insufficient stability, this inhibitor was not further pursued.

Following the synthesis and successful radiofluorination of model phosphonate compounds, a FAPI with an ^{18}F-labeled phosphonofluoridate warhead was prepared in RCYs of 56 ± 9%. This compound proved to be stable for at least 2 h in aqueous media (pH 2−10) and in human blood plasma, with no evidence of defluorination. In enzyme assays with FAP, [^{18}F]fluoride release was observed, whereas no release occurred in the presence of the FAP-related peptidases DPP 2, DPP 4 and DPP 9, indicating selectivity for FAP. However, even greater [^{18}F]fluoride release was observed in the presence of PREP, suggesting higher affinity for this enzyme.

A third FAPI was developed by replacement of the nitrile group with an ^{18}F-labeled phosphonofluoridodithoate warhead. A model radiofluorinated phosphonofluoridodithoate was first prepared and its *in vitro* stability was subsequently investigated. These experiments confirmed the high stability of the labeled compounds. Afterwards, the ^{18}F-labeled FAPI was

produced from the respective oxydithiaphospholan-2-sulfide precursor in RCYs of 46 ± 11%. The candidate demonstrated sufficient stability over a period of 2 h under physiological conditions. However, no coupling to FAP was detected, as demonstrated by the absence of [^{18}F]fluoride release in all enzymatic assays.

In summary, three potential FAPIs with novel ^{18}F-labeled warheads instead of the conventional cyano group were prepared, whereby the candidate with a phosphonofluoridate moiety demonstrated sufficient stability and covalent binding to FAP in *in vitro* experiments. This compound could serve as a lead candidate for the development of FAP-specific radiotherapeutics exhibiting prolonged retention in tumor tissue.

Kurzzusammenfassung

Die Endoradiotherapie ist ein systemischer Therapieansatz, bei dem eine zytotoxische Strahlendosis selektiv an Tumorgewebe abgegeben wird. Dazu werden Verbindungen eingesetzt, die mit therapeutischen Radionukliden (in der Regel α- or β^--Strahler mit einer geeigneten Halbwertszeit) markiert sind und selektiv mit Molekülen, Strukturen oder Stoffwechselprozessen des Targetgewebes wechselwirken. Das Fibroblasten-Aktivierungsprotein (FAP) ist ein membrangebundenes Protein, das im Tumormikromilieu der meisten bösartigen soliden Tumoren überexprimiert wird, jedoch in gutartigen Tumoren oder gesundem Gewebe nicht nachweisbar ist. Damit stellt es ein vielversprechendes Ziel für die Endoradiotherapie dar. Zahlreiche radioaktiv markierte FAP-Inhibitoren (FAPIs) werden bereits für die diagnostische Bildgebung eingesetzt. Die Anwendung bestehender, mit therapeutischen Radionukliden markierter FAPIs ist jedoch aufgrund ihrer unzureichenden Tumorretention begrenzt.

Ein zentrales Ziel dieser Arbeit war daher die Verbesserung der Tumorretention durch die Entwicklung von FAPIs, die eine irreversible kovalente Bindung mit dem aktiven Zentrum des Enzyms eingehen können. Die neuartigen Verbindungen wurden auf der Basis der Struktur des meistgenutzten FAPIs, UAMC-1110, entwickelt, wobei die Nitril-Gruppe durch eine kovalent bindende ^{18}Fluor-substituierte Wirkkomponente ersetzt wurde. Die Freisetzung von [^{18}F]Fluorid bei kovalenter Wechselwirkung der Inhibitoren mit dem aktiven Zentrum des FAP-Enzyms sollte einen indirekten Nachweis für die Bildung einer kovalenten Bindung liefern.

Drei FAPIs mit einer ^{18}F-markierten Wirkkomponente wurden synthetisiert und ihre Stabilität in wässrigen Medien bei verschiedenen pH-Werten sowie unter physiologischen Bedingungen in phosphatgepufferter Kochsalzlösung (PBS) und humanem Blutplasma untersucht. Ein Inhibitor mit einem Sulfonyl[^{18}F]fluorid-Warhead konnte mittels SuFEx-basiertem ultraschnellem ^{18}F/^{19}F Isotopenaustausch mit radiochemischen Umsätzen (RCUs) von 58 ± 12% markiert und in radiochemischen Ausbeuten (RCAs) von 24 ± 3% isoliert werden. Aufgrund seiner unzureichenden Stabilität wurde dieser Inhibitor jedoch nicht weiterverfolgt.

Nach der Synthese und erfolgreichen Radiofluorierung von Modell-Phosphonatverbindungen wurde ein FAPI mit einem ^{18}F-markierten Phosphonofluoridate-Warhead in RCAs von 56 ± 9% hergestellt. Diese Verbindung war in wässrigen Medien (pH 2–10) und in humanem Blutplasma für mindestens zwei Stunden stabil, ohne dass Anzeichen für eine Defluorierung beobachtet wurden. In Enzymassays mit FAP wurde eine Freisetzung von [^{18}F]Fluorid beobachtet, während in Gegenwart der FAP-verwandten Peptidasen DPP 2, DPP 4 und DPP 9 keine Freisetzung auftrat, was auf eine Selektivität für FAP hinweist. In Gegenwart von PREP wurde jedoch eine höhere Freisetzung von [^{18}F]Fluorid beobachtet, was auf eine größere Affinität für dieses Enzym hinweist.

Ein dritter FAPI wurde durch Substitution der Nitrilgruppe mit einem ^{18}F-markierten Phosphonofluoridodithoat-Warhead entwickelt. Zunächst wurde eine radiofluorierte Phosphonofluoridodithoat-Modellverbindung hergestellt und deren *In-vitro*-Stabilität untersucht. Die markierten Verbindungen zeigten in diesen Experimenten eine hohe Stabilität. Anschließend wurde das ^{18}F-markierte FAPI aus dem entsprechenden Oxydithiaphospholan-2-sulfid-Vorläufer in RCAs von 46 ± 11% hergestellt. Der Kandidat zeigte über einen Zeitraum von zwei Stunden unter physiologischen Bedingungen eine ausreichende Stabilität. Es wurde jedoch keine Bindung an FAP festgestellt, was durch die fehlende [^{18}F]Fluorid-Freisetzung in Enzymassays belegt wurde.

Insgesamt wurden drei potenzielle FAPI mit den neuen ^{18}F-markierten Wirkkomponenten anstelle der konventionellen Cyano-Gruppe hergestellt, wobei die Phosphonofluoridate-Verbindung eine ausreichende Stabilität und in *In-vitro*-Experimeten eine kovalente Bindung zu FAP zeigte. Diese Verbindung kann als Leitmotiv für die Entwicklung von FAP-spezifischen Radiotherapeutika mit einer längeren Tumorretention dienen.

Acknowledgements

First and foremost, I would like to express my sincere gratitude to my doctoral supervisor, Prof. Dr. Bernd Neumaier. I would like to thank him for giving me the opportunity to carry out this work at INM-5 and for providing me with an interesting research question and constant support throughout the project.

I would like to express my sincere thanks to Prof. Dr. Axel Klein for agreeing to take on the second review. I would also like to thank Prof. Dr. Ines Neundorf for her mentorship in the Thesis Advisory Committee and for agreeing to chair the examination committee.

I would also like to thank Prof. Dr. Boris Zlatopolskiy for his outstanding supervision throughout the project. Without his support, this work would not have been possible.

My thanks also go to Dr. Marcus Holschbach and Dr. Birte Drewes for their invaluable support and the countless NMR measurements that made my everyday lab work easier.

I would also like to thank Dr. Dirk Bier and Dr. Daniela Schneider for the biological evaluations and numerous enzyme experiments. Their ideas have enhanced the quality and advanced the progress of my work.

Many thanks also go to Dr. Swen Humpert, who always answered my questions patiently and was always willing to listen.

Thanks also to my co-doctoral students for the good working atmosphere, their advice and the occasional beer. Special thanks go to my lab colleague, Dr. Yannick Keuthen, who bore witness to the occasional nervous breakdown and becoming a good friend, and to Dr. Chris Hoffmann, who fostered a pleasant office atmosphere and usually organized the afternoon beer.

I would also like to thank Melanie Brugger, Tobias Wachten and Jana Honert, who always listened sympathetically and made my daily lab routine a little better. I would like to thank Dr. Roberta Cologni for her friendship – I could talk to her about anything at any time. I would also like to thank Dr. Jonas Strecker for his friendship and the occasional gaming night. Thanks to all the other INM-5 colleagues for the pleasant working atmosphere and their active support.

Finally, I would like to express my heartfelt thanks to my friends and family, especially my boyfriend Christian, who had to endure a lot from me during this time yet always supported me. Without you, I would never have been able to complete this work. Thank you!

Table of Contents

Abstract ..... **i**

Kurzzusammenfassung ..... **iii**

Acknowledgements ..... **v**

1 Introduction **1**

1.1 Radiotracers in life science 1
1.1.1 Principles of positron emission tomography 2
1.1.2 Endoradiotherapy 7

1.2 Radiolabeling strategies with ^{18}F 13
1.2.1 Electrophilic Radiofluorination 13
1.2.2 Nucleophilic Radiofluorination 14
1.2.3 Transition metal-mediated radiofluorination 20
1.2.4 Indirect radiofluorination 24
1.2.5 Radiofluorinations at heteroatoms 26

1.3 Fibroblast activation protein (FAP) as target for tumor imaging and radiotherapy 39
1.3.1 FAP inhibitors based on UAMC-1110 40

2 Aim **44**

3 Results and Discussion **45**

3.1 Synthesis and stability investigation of a potential covalent FAP inhibitor containing a sulfonyl [^{18}F]fluoride functionality 45
3.1.1 Introduction 45
3.1.2 Results and Discussion 46
3.1.3 Conclusion 53

3.2 Synthesis and radiolabeling of phosphonate model compounds 54
3.2.1 Synthesis of tritylphosphono[^{18}F]fluoridate (**[^{18}F]13**) 54
3.2.2 Preparation of (4-(*tert*-butoxy)-2-methyl-4-oxobutan-2-yl)phosphono[^{18}F]fluoridate (**[^{18}F]16**) 57

3.3 Synthesis and preliminary *in vitro* evaluation of a potential covalent FAP inhibitor containing a phosphor[^{18}F]fluoridate functionality as warhead 60
3.3.1 Abstract 60
3.3.2 Results and Discussion 61
3.3.3 Conclusion 74

3.4 Synthesis and preliminary *in vitro* evaluation of an ^{18}F-labeled covalent FAP inhibitor containing a phosphono[^{18}F]fluoridodithioate functionality as warhead 75
3.4.1 Abstract 75

3.4.2 Results and Discussion 75
3.4.3 Conclusion 83
4 Summary and Outlook 84
5 Experimental part 86
5.1 General 86
5.1.1 Organic synthesis 86
5.1.2 Solvents and chemicals 86
5.1.3 Spectroscopy 86
5.1.4 Chromatography 87
5.2 Radiochemistry 87
5.2.1 [^{18}F]F$^-$ production 87
5.2.2 Materials 87
5.2.3 Chromatography 88
5.2.4 Characteristic parameters for describing radiolabeled substances 88
5.2.5 Radiosyntheses 89
5.3 Supporting Information to chapter 3.1 90
5.3.1 Organic preparative syntheses 90
5.3.2 NMR spectra 104
5.3.3 Radiosynthesis 113
5.3.4 Stability studies in aqueous media 114
5.3.5 Stability study in human blood plasma 115
5.3.6 Radio-TLC 115
5.4 Experimental part to chapter 3.2 116
5.4.1 Organic preparative syntheses 116
5.4.2 NMR spectra 122
5.4.3 Radiosyntheses 130
5.5 Supporting Information to chapter 3.3 132
5.5.1 Organic preparative syntheses 132
5.5.2 NMR-spectra 145
5.5.3 Determination of enantiomeric excess 165
5.5.4 Radiosyntheses 166
5.5.5 Stability studies in aqueous media 170

5.5.6 Stability studies in human blood plasma for [^{18}F]**23** 171

5.5.7 Radio-TLC 176

5.6 Supporting Information to chapter 3.4 180
5.6.1 Organic preparative syntheses 180

5.6.2 NMR-spectra 187

5.6.3 Radiosyntheses 195

5.6.4 Stability studies in aqueous solutions 198

5.6.5 Stability studies in human blood plasma 199

5.6.6 Enzyme experiments 199

5.6.7 Chromatograms 200

6 References 211

7 Annex 227

7.1 Prostate-specific membrane antigen (PSMA) as biological target 227
7.1.1 PSMA inhibitors 227

7.2 Aim 230
7.3 Results and discussion 231
7.3.1 Preliminary work on the synthesis of the novel ^{18}F-labeled 2-PMPA analog 231

7.4 Summary 240
7.5 Experimental part 241
7.5.1 Organic preparative syntheses 241

7.5.2 NMR-spectra 252

7.5.3 Radiosyntheses 262

7.6 References 264
8 List of abbreviations 266

9 List of figures 272

10 List of schemes 279

11 List of tables 283

1 Introduction

1.1 Radiotracers in life science

Radiolabeled compounds have become indispensable tools in routine clinical practice. They are primarily utilized as probes for different molecular imaging modalities, which enable the visualization of physiological and pathological processes at the cellular or molecular level. A prerequisite for the latter is that the tracer should be applied in amounts, which does not perturb the biological process under investigation and that the radiation generated during or shortly after the decay of the radioactive label (radionuclide) is penetrative enough to be externally detected using suitable methods. This so-called tracer principle was first introduced by George Charles de Hevesy, who is widely regarded as the "father of nuclear medicine" due to his pioneering contributions to the application of radioisotopes in life science. His groundbreaking research in this area was recognized with the Nobel Prize in Chemistry in 1943.[1] Even though Marie Curie had already developed concepts for diagnosing and treating cancer with external radiation during World War I, it was de Hevesy who first used radioactivity to quantify biological processes in 1923.[2,3] Specifically, he investigated the uptake of ^{212}Pb in plants, predominantly *Vicia faba*, by analyzing the ashes of plant parts via electroscopy.[4] His findings not only demonstrated the incorporation of radioactive lead into plant tissues, but also showed that radioactive lead and stable lead can be substituted for each other.[3,5] These results emerged from unsuccessful attempts by de Hevesy, on behalf of Rutheford[6], to separate the two. He concluded that different lead isotopes are biologically and chemically indistinguishable, and that the radioactive species could be utilized to study biological processes, thus establishing the conceptual basis of the tracer principle.[3]

Morphological imaging modalities such as magnetic resonance imaging (MRI), X-ray, and computed tomography (CT) primarily provide structural information. In contrast, nuclear medicine techniques like positron emission tomography (PET) or single-photon emission computed tomography (SPECT) utilize the tracer principle to visualize biochemical processes (e.g., metabolism, receptor expression, surface antigen properties) at the molecular level. As such, these imaging modalities often allow for the detection of pathological alterations even before anatomical changes become apparent, facilitating early diagnosis and potentially improving the outcome for affected patients.

The tracers used for PET and SPECT are typically administered in (sub)nanomolar quantities, which do not interfere the processes under investigation. Structurally, they consist of at least two components: a radionuclide, which emits detectable tissue-penetrating radiation, and a pharmacophore, which confers selectivity for the biological target or process of interest (Figure 1). When a radiometal is used for labeling, the tracer also contains a chelator (to complex the

radiometal) usually coupled to the pharmacophore via a linker. The linker can significantly influence the pharmacokinetics of the tracer, for example by altering its lipophilicity and net charge.

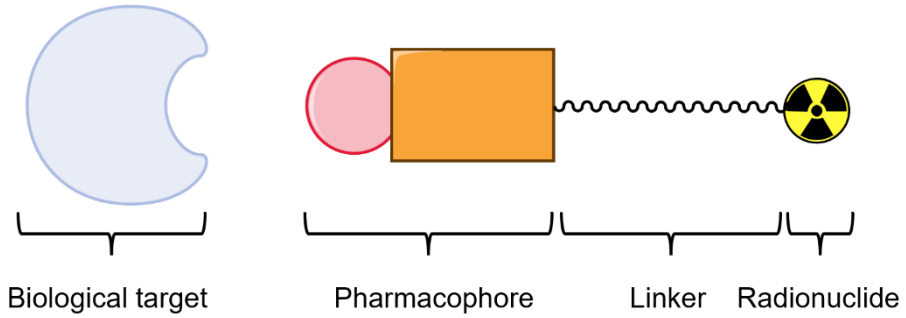

Figure 1: Schematic presentation of a radiotracer consisting of a pharmacophore, a linker, and a radionuclide.

Following administration, the emitted radiation enables localization of the radionuclide by the PET or SPECT scanner, so that the distribution of the tracer in the organism under investigation can be observed non-invasively. The pharmacophore is designed to selectively interact with the target molecule or process of interest. Molecular imaging thus allows for the visualization of even minuscule alterations, supporting not only the diagnosis of various diseases but also therapy monitoring, drug development, and studies on the pharmacokinetics of novel pharmaceuticals.[7]

1.1.1 Principles of positron emission tomography

As mentioned above, the two primary molecular imaging techniques in nuclear medicine are SPECT and PET. As neither method provides morphological information, they are typically combined with anatomical imaging modalities such as CT (SPECT/CT and PET/CT) or MRI (PET/MRI) to enable precise localization of the investigated processes.

SPECT was first described by Kuhl and Edward in 1963 as a refinement of planar scintigraphy that provides three-dimensional data.[8,9] It is based on the use of tracers containing gamma-emitting radionuclides with relatively low photon energies (preferably about 150 keV), such as ^{99m}Tc, ^{123}I, ^{131}I ^{67}Ga, or ^{111}In[10,11], to match the sensitivity range of the detectors used. The gamma cameras used as detectors contain a collimator that only registers radiation entering perpendicular to the detector surface and a photomultiplier to amplify the signal. Acquisition of multiple planar images by one to three camera heads that rotate around the patient enables reconstruction of tomographic images of the three-dimensional radiotracer distribution.

The concept of PET was first introduced by Rankowitz and Robertson in 1962[12], with the first commercially viable PET scanner developed in the mid-1970s by Ter-Pogossian, Phelps and Hoffman.[9,13] It is based on the use of tracers labeled with positron-emitting radionuclides (β^+-

emitters), which typically possess an excess of protons relative to their stable isotope. Such radionuclides decay by either β^+ emission or electron capture, depending on the mass difference between parent and daughter nuclides.[14] If the mass of the daughter nuclide is at least two electron masses higher than that of the parent nuclide, the parent nuclide can undergo β^+ decay. If this condition is not met, the parent nuclide can compensate for the excess of protons by electron capture (ε). Many radionuclides that decay by β^+ decay can undergo both decay types, with the ratio being nuclide dependent.[14]

In β^+ decay, a proton (p) is converted into a neutron (n), emitting an electron neutrino (ν_e) and a positron (e^+, the antiparticle of an electron) (*1*):[14]

$$ {}^{1}_{1}\mathrm{p} \rightarrow {}^{1}_{0}\mathrm{n} + \mathrm{e}^{+} + \nu_{\mathrm{e}} \qquad (1) $$

The positron released by the emission loses kinetic energy and can either annihilate directly by emitting two gamma photons with an energy of 511 keV each in an angle of approximately 180°, or convert to a positronium by combining with an electron (Figure 2, A). Direct annihilation occurs in 60% in biological tissue, whereas positronium is produced in 40%.[15] This can exist as *ortho*-positronium with a parallel spin and an average lifetime of 142 ns (in a vacuum) or as *para*-positronium with an opposite spin and an average lifetime of 125 ps (in a vacuum).[16] In biological tissue, the ratio of *ortho*- to *para*-positronium formation is 3:1.[17] In most cases, *ortho*-positronium reacts with an electron and undergoes pick-off annihilation or forms *para*-positronium through reaction with oxygen, while only 0.5% of *ortho*-positronium decays into three gamma photons.[15–17] The decay of *para*-positronium and pick-off annihilation in turn lead to the emission of two gamma photons.[15–17]

These annihilation photons can then be detected as coincidence events by a ring-shaped array of scintillation detectors in the PET scanner. A coincidence event is recorded when two 511 keV photons are detected nearly simultaneously (within the coincidence time window) by an opposing detector pair (Figure 2, B). Each such event is assumed to originate from a single annihilation located along a straight line between the two detectors (line of response), allowing spatial assignment of the decay. Reconstructing a large number of such events enables three-dimensional visualization of the tracer distribution.

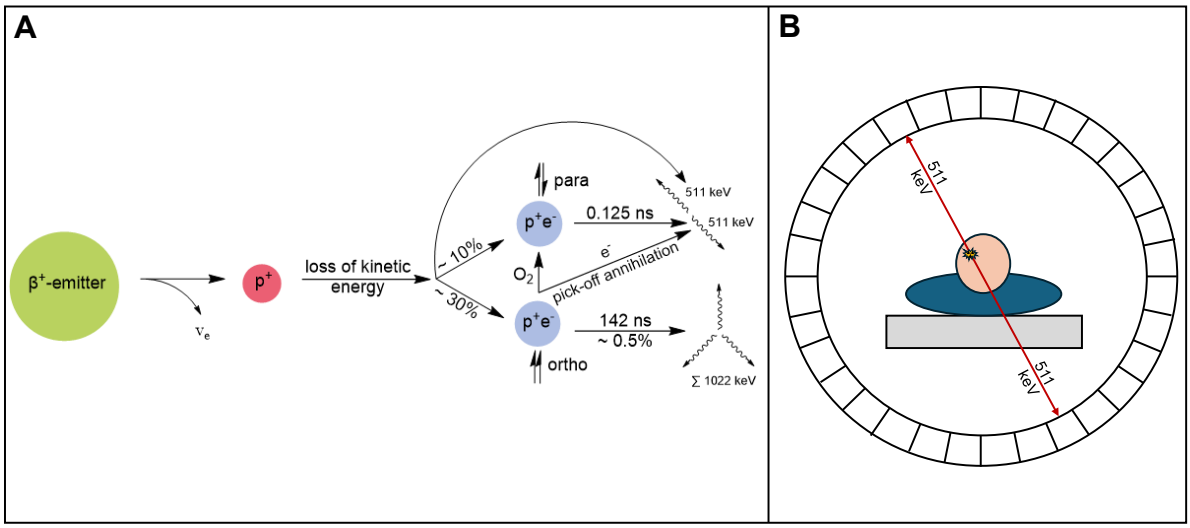

Figure 2: Schematic illustration of ß⁺ decay (**A**[18]) and a PET scan (**B**).

Unlike SPECT, PET does not require physical collimation, resulting in significantly higher sensitivity. However, the spatial resolution of PET images is limited by the distance between the site of positron emission and the site of annihilation, with lower distances corresponding to a higher theoretically achievable resolution. This distance is influenced by the density of surrounding tissues (i.e. the path length of positrons is shorter in high-density tissues than in low-density tissues) and by the initial kinetic energy of the positron, which varies by radionuclide. Therefore, the choice of radionuclide is important for the resolution of the PET images.

1.1.1.1 Radionuclides for PET

In addition to the design of the pharmacophore and linker, the choice of radionuclide is critical for successful PET imaging. Some radionuclides suitable for PET applications are shown in Table 1.[11] Key factors influencing radionuclide selection include the probability of positron emission, the maximum positron energy, and the physical half-life. As mentioned above, the positron energy directly affects the spatial resolution, while a high positron emission probability minimizes signal disturbances. The half-life is an important factor for radiotracer synthesis and should be compatible with the timescale of the biological process under investigation.

Table 1: Data of the most common PET nuclides.[11,19]

Entry	Radionuclide	Half-life	$E_{\beta+}$ max [keV]	Mode of decay (%)
1	^{18}F	110 min	635	β^+ 97 ε 3
2	^{68}Ga	67.6 min	1900	β^+ 90 ε 10
3	^{11}C	20.4 min	960	β^+ 99.8 ε 0.2
4	^{13}N	10.0 min	1190	β^+ 100
5	^{15}O	2.0 min	1723	β^+ 99.9 ε 0.1
6	^{89}Zr	78.4 h	909	β^+ 22.7 ε 77.3
7	^{124}I	4.18 d	2138	β^+ 22.7 ε 77.3

In addition to its decay properties, the chemical properties of the radionuclide also need to be considered. Ideally, introduction of the radionuclide should not alter the biological and pharmacokinetic properties of the radiotracer compared to its non-radioactive analogs. ^{11}C, ^{13}N, and ^{15}O are isotopes of three most frequent elements in organic chemistry: carbon, nitrogen, and oxygen. Since all isotopes of a given element share very similar chemical behavior (apart from isotope effects, which are most prominent for isotopes of hydrogen and are much lower or even negligible for isotopes of heavier elements), radiotracers containing these nuclides can be synthesized without structural modification and should exhibit the same chemical and pharmacological properties as their non-radioactive analogs. However, the short half-lives of ^{15}O ($t_{1/2}$ = 2.0 min)[11] and ^{13}N ($t_{1/2}$ = 10.0 min)[11] render them unsuitable for complex radiosyntheses or the investigation of slower biological processes. Consequently, both nuclides are primarily employed in simple radiotracers such as [^{13}N]NH_3[20,21] or [^{15}O]H_2O[22–24], and are best suited for imaging rapid physiological processes like myocardial perfusion or cerebral blood flow.[20–25] In contrast, ^{11}C with a half-life of 20.4 min[11] can be used for the synthesis of more complex radiotracers that are accessible through fast labeling reactions. For instance, ^{11}C-labeling via methylation with [^{11}C]CH_3I provides access to a broad array of clinically relevant radiotracers, including [^{11}C]PIB for imaging of amyloid plaques in Alzheimer's disease or frontotemporal lobar degeneration[26], [^{11}C]MET for brain tumor imaging [27], and [^{11}C]DASB for imaging of the serotonin transporter (Figure 3).[28,29] Nevertheless, a major disadvantage of all three short-lived radionuclides mentioned (^{13}N, ^{15}O, and ^{11}C) is the

necessity for local production, which restricts their use to specialized facilities with an on-site cyclotron.

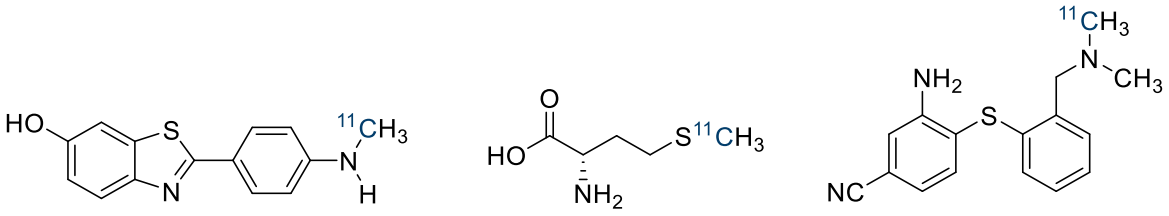

[^{11}C]PIB [^{11}C]MET [^{11}C]DASB

Figure 3: ^{11}C-labeled radiotracers.[26–29]

For this reason and owing to its good accessibility in the form of [^{18}F]fluoride and favorable physical and chemical properties, ^{18}F has become the most widely used PET radionuclide. It can be produced with a cyclotron by bombardment of ^{18}O-enriched water ([^{18}O]H_2O) with protons (^{18}O(p,n)^{18}F) or by bombardment of ^{20}Ne with deuterons (^{20}Ne(d,α)^{18}F). With a half-life of nearly 2 hours (109.7 minutes), ^{18}F enables time-intensive, multi-step syntheses and supports centralized production and subsequent delivery of tracers to surrounding clinics according to the so-called “satellite” concept. This obviates the need for a local cyclotron, facilitating broader clinical adoption and commercialization of radiotracers. In addition, the half-life of ^{18}F is sufficiently long to investigate even slow biological processes, yet short enough to keep radiation exposure for the patients low.

^{18}F also has a unique and versatile chemistry, enabling its integration into a diverse array of small organic molecules, proteins, or peptides. Moreover, since its physical properties make fluorine an important building block in medical chemistry, many pharmaceutical drugs contain fluorine substituent(s) and can thus be radiofluorinated without structural modification.[30] Fluorine's compact van der Waals radius (1.47 Å) makes it nearly isosteric with hydrogen (1.20 Å), and the C–F bond length (1.35 Å) is very similar to that of C–H bonds (1.09 Å).[30,31] Consequently, substitution of hydrogen atoms by fluorine atoms does typically not result in substantial alterations in overall molecule size or shape. However, fluorine's high electronegativity (EN: 4.0) relative to hydrogen (EN: 2.1)[32] can significantly affect the dipole moment, pK_a, and/or general reactivity of the labeled molecule.[30,32] These electronic effects must be considered when designing ^{18}F-labeled radiotracers.

In addition, the C–F bond confers enhanced thermal and metabolic stability as well as increased oxidative resistance due to its higher bond strength (C–F: 112 kcal/mol vs. C–H: 98 kcal/mol).[30,32,33] Unlike hydrogen, fluorine also acts as a hydrogen bond acceptor and increases the lipophilicity of a compound.[32] These attributes contribute to the widespread use of fluorine in medicinal chemistry, as reflected in the growing proportion of fluorinated FDA-approved drugs over the last five decades.[34]

Despite its less favorable decay properties compared to ^{18}F, ^{68}Ga is another widely utilized radionuclide for PET imaging. Its high maximum positron energy (1900 keV)[11] results in reduced spatial resolution, and its shorter half-life (68 minutes)[11] makes application of the "satellite" concept challenging. Labeling with ^{68}Ga necessitates the presence of the suitable chelator in the tracer molecule. This has implications for the properties of ^{68}Ga-labeled tracers. Nevertheless, ^{68}Ga-labeled probes are frequently employed in the clinical practice since it can be obtained in commercially available ^{68}Ge/^{68}Ga radionuclide generators. These generators are compact and easily transportable facilitating their clinical use in resource-limited settings.

1.1.2 Endoradiotherapy

Endoradiotherapy, also known as targeted radionuclide therapy[35,36], is a systemic treatment strategy in which a radiolabeled compound is used to selectively deliver a cytotoxic dose of ionizing radiation to disease sites, such as neoplastic lesions in cancer or inflamed joints in rheumatoid arthritis.[36] In contrast to external beam radiotherapy, this approach treats diseases from within the body by exploiting the targeting specificity of molecular carriers.[37] Structurally, these compounds are radiotracers (see section 1.1), which contain therapeutic instead of diagnostic radionuclides. Since most therapeutic radionuclides are radiometals, they are typically complexed using suitable chelators, such as DOTA, NOTA or DTPA.[36] Importantly, the therapeutic effect is not due to the pharmacological action of the pharmacophore itself, but rather due to the ionizing radiation emitted by the radionuclide. As already described in section 1.1, the pharmacophore serves to guide the radiopharmaceutical to its biological target. Peptides, antibodies or small molecule ligands are mainly used for this purpose.[35]

Ionizing radiation induces molecular damage primarily by destruction of covalent bonds in critical biomolecules, ultimately leading to subcellular dysfunction and cell death. DNA fragmentation, one of the most lethal effects, is largely driven by ionization and radical formation through radiolysis, mediated by the linear energy transfer (LET) of the emitted particles.[36] LET is defined as the energy per unit distance released by an ionizing particle and is directly proportional to the density of ionization events along the particle's path.[14]

Radionuclides used for endoradiotherapy are most commonly β^- emitters (such as ^{90}Y, ^{131}I, ^{177}Lu, or ^{186}Re), although alpha emitters (such as ^{211}At, ^{213}Bi, or ^{225}Ac) are increasingly used as well. In some cases, Auger electron emitters, which decay by electron capture (ε) or internal conversion (e.g., ^{111}In or ^{125}I), are also suitable for endoradiotherapy.[36]

β^- decay occurs in nuclides with an excess of neutrons and involves conversion of a neutron (n) from the nucleus into a proton (p), an electron (e), and an electron antineutrino (2):[14]

$$^{1}_{0}\mathrm{n} \rightarrow {}^{1}_{1}\mathrm{p} + \mathrm{e}^{-} + \bar{\nu}_{\mathrm{e}} \qquad (2)$$

β^- particles have a relatively low LET (~0.2 keV/µm) and a path length of up to several centimeters, depending on their energy (50−2300 keV).[38] Heavy nuclides (atomic number Z greater than 83) and some nuclide groups that are distant from the line of β stability on the nuclide map undergo α decay, which involves emission of helium nuclei ($^4He^{2+}$) (*3*):[14]

$$^{A}Z \rightarrow {}^{A-4}(Z-2) + {}^{4}_{2}He^{2+} \quad (3)$$

Due to their large mass and high energy (5–9 MeV), these α particles have a high LET (80–100 keV/µm) and travel less than one cell diameter in tissue[36,38], making them extremely potent in inducing localized cytotoxicity.[36]

Auger electrons are generated following electron capture or internal conversion,[38] which creates a vacancy in the inner atomic shell. Relaxation of electrons from a higher shell then initiates a cascade of atomic electron transitions, which culminates in the emission of Auger or Coster-Kroning electrons and characteristic X-rays. These electrons have low kinetic energies (a few eV to approx. 1 keV) and extremely short tissue ranges (<0.5 µm), necessitating intracellular or even intranuclear delivery for effective DNA damage.[38] However, their short range and high LET (4−26 keV/µm) render them highly cytotoxic and limit damage to surrounding tissues.[39,40]

Notably, therapeutic particles can also affect non-target cells, a phenomenon known as the "crossfire effect".[36] For example, high-energy emitters like ^{90}Y produce radiation tracks long enough to irradiate adjacent tumor cells even without direct uptake. While this improves therapeutic efficiency against tumors with heterogeneous receptor expression or poor vascularization,[36,41] it can also increase off-target toxicity in healthy tissues. Conversely, low-energy β^--emitters such as ^{177}Lu as well as α- or Auger electron emitters cause less damage to healthy tissue but also reach fewer tumor cells, making them useful in cases involving small tumors, tumor clusters or metastases.[40] Another effect observed is the so-called "radiation-induced bystander effect", where cells that are not directly crossed by charged particles exhibit cytotoxic responses. This phenomenon is presumably caused by intercellular communication or paracrine signaling via free radicals and inflammatory mediators like cytokines.[36,42]

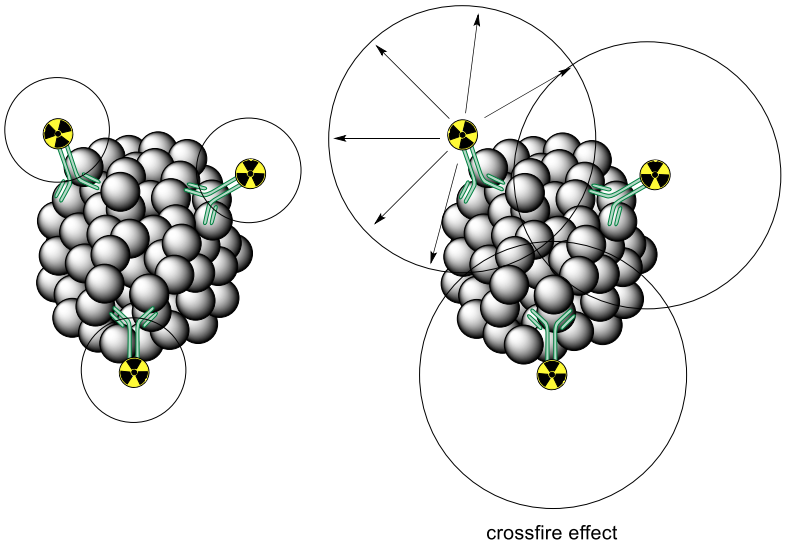

Figure 4: Schematic representation of the ranges of various β^--emitters, including the crossfire effect (left).

Chemotherapy remains one of the most prevalent systemic cancer treatments, particularly for tumors that are not operable or that have been deemed unsuitable for radiation therapy.[36] This is partly due to the availability of a variety of chemotherapeutic agents for different types of cancer, especially metastatic tumors, and partly because it does not necessitate the complex infrastructure required for radiotherapy. Nevertheless, the side effects of chemotherapy, such as organ toxicity, immunosuppression, or cardiac arrhythmia, are substantial and associated with a considerable burden for the patients. In contrast, endoradiotherapy requires only minimal quantities of the radiopharmaceutical, which are typically below the threshold for (pharmacological) side effects.[36] Another significant advantage of endoradiotherapy over other treatment modalities is the capacity to assess treatment responses and perform patient-specific dosimetry with SPECT or PET.[36] This can be achieved through the use of radiotracers with the same general structure as the therapeutic radiopharmaceutical, which contain a suitable radionuclide for imaging instead of the therapeutic radionuclide (theranostic pairs). This approach enables the utilization of suitable radioisotopes of the same element or chemically related nuclides with disparate decay properties for both diagnostic and therapeutic purposes. Theranostic pairs generally consist of a PET or SPECT radiotracer and a therapeutic radiopharmaceutical, which exhibit equivalent biodistribution within the body. The theranostic approach not only enable monitoring of the therapy status but also the measurement of patient-specific uptake kinetics, thereby facilitating a more precise and individualized dosimetry prior to therapy.[43]

Endoradiotherapy also has some key disadvantages that must be considered. For example, the maximum tolerated dose is limited by the radiosensitivity of off-target organs like liver, kidneys, thyroid or bone marrow, where significant uptake of the radiopharmaceutical may occur.[36,44] Thyroid uptake of radioiodine-labelled radiopharmaceuticals can be minimized by

prior administration of potassium iodide, which saturates the thyroid gland and competitively reduces absorption of radioactive iodine.[36,45] Likewise, uptake of radiolabeled DOTATOC derivatives by the kidneys can be reduced e.g. by the cationic amino acids lysine and arginine.[36,46] Due to these aspects, it is essential that radiopharmaceuticals exhibit a high target affinity and specificity, rapid and sustained target accumulation, fast washout from healthy tissues and a high metabolic stability.[36] The goal of endoradiotherapy is to selectively irradiate the diseases tissues, usually tumors, while minimizing damage to healthy tissues.[40] In addition to selecting the appropriate pharmacophore for the disease, the choice of a suitable radionuclide is also imperative.

1.1.2.1 Radionuclides for endoradiotherapy

The selection of an appropriate radionuclide for endoradiotherapy depends on multiple factors, most importantly the decay properties, such as the type of decay and the energy of the emitted particle. Additionally, the half-life and the decay products of the radionuclide must be taken into consideration.[37] The nuclide purity and product route should also be considered.[47–49] A selection of possible therapeutic nuclides is listed in Table 2.

Table 2: Overview of selected radionuclides used for endoradiotherapy.[36]

Entry	Radionuclide	Half-life	Mode of decay [%]	E_{ave} [keV]	Mean range
1	^{90}Y	64.1 h	β^- (100)	935	4.0 mm
2	^{131}I	8.0 d	β^- (100)	182	0.39 mm
3	^{177}Lu	6.7 d	β^- (100)	133	0.23 mm
4	^{186}Re	3.8 d	β^- (100)	764	3.1 mm
5	^{211}At	7.2 h	α (42)	6790	60 µm
6	^{213}Bi	46 min	α (36)	8320	84 µm
7	^{225}Ac	10.0 d	α (100)	5750	61 µm
8	^{111}In	2.8 d	ε (100)/Auger	0.02	> 100 nm
9	^{125}I	60.1 d	ε (100)/Auger	0.015	> 100 nm

As already mentioned above, the mode of decay should align with the characteristics of the disease to be treated. While β^--particles with the millimeter or centimeter range are suitable for the treatment of large or heterogenous tumors, α-particles with a short range and high LET are ideal for treating small tumors or micrometastases. Auger electrons are effective when the radiopharmaceutical is able to cross the cell membrane and localizes in close proximity to the DNA in the nucleus.[35] The radionuclide's half-life should match the biological half-life of the

radiopharmaceutical, and most of the decay should take place when the radiopharmaceutical has reached the target site (i.e., when a sufficient ratio of target-to-non-target accumulation has been achieved). A longer half-life can be advantageous if the ratio between target and non-target organs is high or increases over time. However, longer half-lives reduce the dose rate and may thus decrease the biological effect. Conversely, short-lived radionuclides can also be used when rapid radiosynthesis and fast accumulation of the radiopharmaceutical in the lesions are feasible.[37] Ideally, the half-life of therapeutic radionuclides should fall within the range of six hours to seven days.[50]

Currently, there are 13 therapeutic radiopharmaceuticals on the market, all of which are used in cancer therapy.[51] Early agents, such as [^{223}Ra]$RaCl_2$ or sodium [^{32}P]orthophosphate, exhibited non-specific accumulation and were therefore associated with significant off-target toxicity.[51] One of the first and most enduring radionuclides for cancer therapy was ^{131}I, initially used to treat thyroid cancer and hyperthyroidism.[47,49,52] Hertz and Roberts first used ^{130}I in 1941, before it was replaced by the more cost-effective ^{131}I in 1946.[47,53,54] ^{131}I is a β^- and γ emitter with a half-life of 8.05 days[47] that can either be obtained as a fission by-product of ^{99}Mo production, or produced via the $^{130}Te(n,\gamma)^{131m,g}Te \xrightarrow{\beta^-} {}^{131}I$ reaction in a nuclear reactor.[43] In addition to the therapeutic radiation of β^- particles with a maximal energy of 0.606 MeV,[36] and a range of approximately 3 mm in tissue, its γ emission enables concurrent imaging.[47,53] Sodium [^{131}I]iodinate accumulates in the thyroid gland and delivers cytotoxic radiation to thyroid cancer cells.[51,55] Beyond thyroid cancer, ^{131}I is also employed for the treatment of adult pheochromocytoma and childhood neuroblastoma ([^{131}I]MIBG)[51,56], as well as for monoclonal antibody-based therapies against hepatocellular carcinoma ([^{131}I]Metuximab) and non-Hodgkin's follicular lymphoma ([^{131}I]Tositumomab).[51] Together with ^{124}I, ^{131}I forms a theranostic pair.[43]

Another clinically relevant therapeutic radionuclide is the β^- emitter ^{90}Y ($t_{1/2}$ = 2.7 d[43]), which has been used for the treatment of (metastatic) liver cancer[47,57], neuroendocrine tumors (NETs), ovarian cancer, and hematologic malignancies.[47,58,59] ^{90}Y forms a theranostic pair with ^{86}Y and can be produced via the $^{89}Y(n,\gamma)^{90}Y$ reaction, albeit in very low specific activity. Alternatively, no-carrier-added ^{90}Y can be obtained from commercially available ^{90}Sr/^{90}Y generators with typical yields of 3–5 GBq.[43]

^{177}Lu ($t_{1/2}$ = 6.7 d) is a low-energy β^--emitter that has gained clinical relevance through recent FDA approval of the peptides [^{177}Lu]Lu-DOTA-TATE (2018) and [^{177}Lu]Lu-PSMA-617 (2022)[51] for treating NETs and metastatic castration-resistant prostate cancer, respectively (Figure 5).[51,60] In addition to peptides, ^{177}Lu has been demonstrated to be suitable for the labeling of antibodies[47] and forms a theranostic pair with ^{68}Ga.

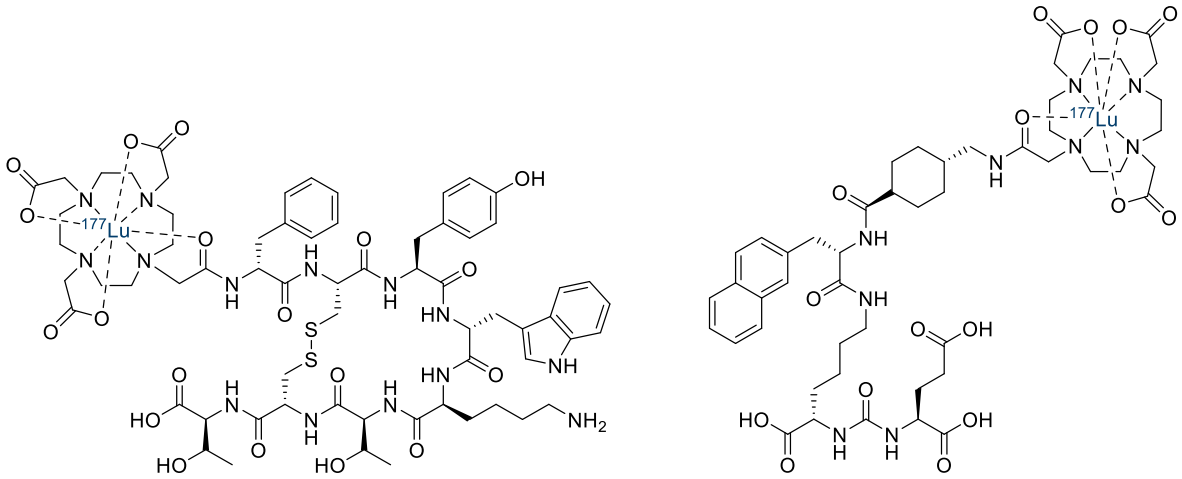

Figure 5: Chemical structures of [^{177}Lu]Lu-DOTA-TATE (left)[61] and [^{177}Lu]Lu-PSMA-617 (right)[62].

An α emitter of interest for targeted a-therapy (TAT) is ^{225}Ac, the parent nuclide of ^{312}Bi, which is also used for TAT. ^{225}Ac has a half-life of 9.9 days[47,63] and is obtained by neutron transmutation of ^{225}Ra or as a decay product of ^{233}U.[47,58,63,64] It has been utilized for the treatment of NETs and has also demonstrated efficacy in prostate cancer therapy with ^{225}Ac-labeled ligands of prostate-specific membrane antigen (PSMA).[47,58,63,65,66] PSMA ligands labeled with ^{225}Ac have recently garnered attention as an alternative to ^{177}Lu-PSMA.[47,58,63,65] Daughter nuclides of ^{225}Ac , such as ^{213}Bi, ^{217}At and ^{221}Fr could damage healthy cells.[47,67] Their pharmacokinetic behavior should be taken into consideration, as they have the potential to accumulate in healthy tissue, for example ^{213}Bi, which has been known to accumulate in the renal cortex.[47,67] Research on the labeling and application of ^{211}At is highly topical. ^{211}At has been identified as a promising alpha emitter for TAT, with a half-life of 7.2 hours.[68,69] Like other halogens, ^{211}At accumulates in the thyroid gland and is therefore a candidate for the treatment of thyroid cancer. However, release of free ^{211}At can also result in unwanted radioactivity accumulation in the thyroid gland when ^{211}At-labeled radiopharmaceuticals with insufficient stability are used to treat other cancers, necessitating blocking strategies to prevent unintended thyroid exposure.[68] ^{211}At can be produced via the ^{209}Bi(α,2n)^{211}At nuclear reaction using cyclotrons operating at 20−28.4 MeV[68,70], a capability possessed by only a few facilities worldwide, including one at our research institution. Two ^{211}At-labeled radiopharmaceuticals are already in phase I clinical trials: [^{211}At]At-ch81C6, a radiolabeled monoclonal antibody that binds specifically to tenogenin and is being tested for the treatment of brain tumors[68,71]; and [^{211}At]At-MX35 F(ab')$_2$, a radiolabeled antibody fragment that targets the sodium-dependent phosphate transporter protein 2b (NaPi 2b) present in 90% of human epithelial ovarian cancers and is therefore being tested for the treatment of ovarian cancer.[68,72] Furthermore, several ^{211}At-labeled pharmaceuticals are currently evaluated in preclinical studies. These include

radiopharmaceuticals that target PSMA, cluster of differentiation (CD) and human epidermal growth factor receptor-2 (HER2).[68]

1.2 Radiolabeling strategies with ^{18}F

Radiofluorination is typically performed using one of two distinct strategies, selected based on the desired product. The first approach, direct radiofluorination, involves incorporating ^{18}F directly into the precursor molecule. This involves the radiofluorination step itself, followed (if necessary) by the removal of protecting groups. Owing to the relatively short synthesis times and higher overall radiochemical yields (RCYs), direct radiofluorination is often preferred if feasible. However, this strategy necessitates that the radiolabeling precursor is soluble in the reaction medium, stable under the radiolabeling conditions, and does not possess functional groups that could interfere with the radiolabeling reaction. Biomolecules such as proteins, peptides, or antibodies often do not meet these requirements and thus cannot be labeled using this strategy. In such cases, the second labeling strategy, indirect radiolabeling, can be employed. In this approach, a prosthetic group is first labeled and then coupled with the pharmacophore under suitably mild conditions.

From a mechanistic perspective, two types of fluorination reactions with ^{18}F can be distinguished: electrophilic radiofluorination typically uses gaseous $[^{18}F]F_2$ or another electrophilic radiofluorinating agent whereas nucleophilic radiofluorination is based on the use of $[^{18}F]$fluoride ($[^{18}F]F^-$).

1.2.1 Electrophilic Radiofluorination

Electrophilic $[^{18}F]F_2$ is produced as an anhydrous gas via the $^{20}Ne(d,\alpha)^{18}F$[73] or $^{18}O(p,n)^{18}F$[74] nuclear reaction in a cyclotron. The highly reactive ^{18}F atoms produced during this process tend to adsorb onto the walls of the target chamber, complicating their recovery. To facilitate efficient recovery, 50–200 µmol of $[^{19}F]F_2$ is typically added as a carrier,[75] resulting in formation of gaseous $[^{18}F]F_2$ via isotopic exchange.[75,76] However, the addition of carrier fluorine limits the theoretical RCYs to a maximum of 50%, as two ^{18}F atoms are statistically unlikely to combine and form $[^{18}F]F_2$.[30] Furthermore, the attainable molar activities (A_M) are significantly reduced,[75] a drawback which can be critical for certain applications requiring high specific activity (e.g., imaging of low-abundance targets).

Electrophilic radiofluorination enables the ^{18}F-labeling of olefins via electrophilic addition and aromatics via electrophilic substitution. Nevertheless, the high reactivity of $[^{18}F]F_2$ often results in low selectivity, giving rise to complex product mixtures that are difficult to separate. A

prominent example is the first synthesis of 2-[^{18}F]fluoro-deoxy-2-glucose ([^{18}F]FDG) from 3,4,6-tri-*O*-acetyl-*D*-glucal via electrophilic radiofluorination.

[^{18}F]FDG is the most widely used PET tracer. Contrary to glucose, it is not fully metabolized due to its ^{18}F label, accumulates in metabolically active cells, and can be used to visualize tissues with high metabolic activity throughout the body. Its utility in tumor diagnostics stems from the increased glucose consumption of rapidly proliferating tumor cells.

Addition of [^{18}F]F_2 to the unsaturated bond proceeds non-regioselective and results in a 3:1 mixture of 1,2-difluorinated glucose and 1,2-difluorinated mannose isomers.[77] Subsequent basic or acidic cleavage of the protection groups yields not only [^{18}F]FDG, but also 2-[^{18}F]fluoro-2-deoxy-mannose ([^{18}F]FDM) and their non-radioactive counterparts ([^{19}F]FDG and [^{19}F]FDM) due to the presence of the carrier (Scheme 1).[77]

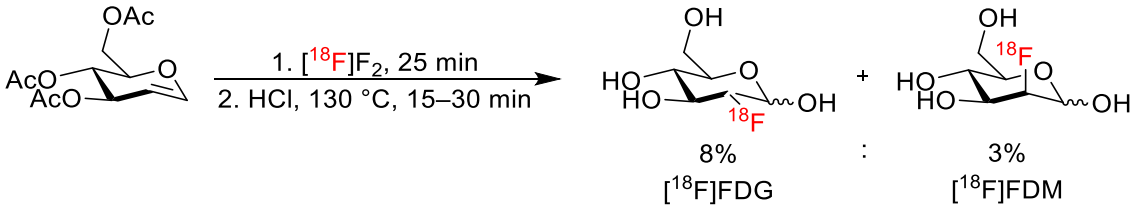

Scheme 1: Synthesis of [^{18}F]FDG via electrophilic radiofluorination of 3,4,6-tri-*O*-acetyl-*D*-glucal as described by Ido *et al*.[77]

The problems associated with the high reactivity of [^{18}F]F_2 can sometimes be circumvented through the use of secondary electrophilic fluorinating agents such as [^{18}F]XeF, [^{18}F]Selectfluor bistriflate or acetyl [^{18}F]hypofluorite.[75,78] In addition, the regioselectivity can often be improved by using metal-organic leaving groups such as $Sn(Me)_3$.[75,79] In contrast, the inherently low achievable A_M of approx. 100 MBq/µmol (for [^{18}F]F_2 produced via the ^{20}Ne(d,α)^{18}F reaction) or approx. 600 MBq/µmol[76] (for [^{18}F]F_2 produced via the ^{18}O(p,n)^{18}F reaction) remains a major limitation.[75] Currently, electrophilic radiofluorination is rarely used in PET-chemistry.

1.2.2 Nucleophilic Radiofluorination

Nucleophilic, no-carrier-added [^{18}F]F^- can be produced in a cyclotron via the ^{18}O(p,n)^{18}F nuclear reaction using ^{18}O-enriched water ([^{18}O]H_2O) as the target material. This reaction route provides high production yields (2.22 GBq/µAh compared to 0.40 and 1.0 GBq/µAh for the ^{20}Ne(d,α)^{18}F and ^{18}O(p,n)^{18}F nuclear reactions, respectively) and molar activities of up to 600 GBq/µmol.[75] Further advantages include simplified handling of dissolved [^{18}F]F^-, a higher production efficiency, and the fact that no carrier needs to be added. However, since [^{18}F]F^- is highly hydrated in aqueous solution due to its high charge density, the nucleophilicity is significantly reduced and thus insufficient for nucleophilic radiofluorinations.[75] This in turn

necessitates preprocessing of the aqueous [^{18}F]F$^-$ prior to nucleophilic radiofluorination. The standard method involves anion exchange chromatography followed by azeotropic drying. To this end, [^{18}F]F$^-$ is loaded fixed onto an anion exchange cartridge (AEC), effectively separating it from a bulk of [^{18}O]H_2O, which can be recovered and reused. This step also removes (radio)metal impurities originating from the target chamber, the tubing, or the [^{18}O]H_2O, thereby ensuring the absence of radionuclide impurities in the final product.[80] The [^{18}F]F$^-$ is then eluted from the AEC using a solution of salt (usually basic) dissolved in protic medium, followed by complete removal of volatiles. The residual [^{18}F]fluoride salt is usually additionally dehydrated by repetitive azeotropic drying with MeCN. Typically, a combination of K_2CO_3 and the cryptand Kryptofix® 2.2.2 is employed for chelation of K^+, resulting in the formation of a highly reactive "naked" [^{18}F]fluoride.[81] In addition to being time-intensive, a disadvantage of this [^{18}F]F$^-$ preprocessing method is that the relatively high basicity of K_2CO_3 can promote side reactions, lead to the formation of chemical impurities and so interfere the sequential radiolabeling step. In the case of S_N2 or S_NAr radiofluorination, the anhydrous [^{18}F]F$^-$ is taken up into a solution of the suitable labeling precursor in the appropriate aprotic solvent and briefly heated to afford after (if necessary) deprotection and isolation by HPLC or SPE the desired ^{18}F-fluorinated compound.

In 2014, Richarz *et al*. introduced a simplified alternative to the conventional S_N radiofluorination known as the "minimalist approach".[82] This method obviates time-consuming azeotropic drying and application of bases, and other additives. Instead, [^{18}F]F$^-$ is eluted directly from the AEC using an alcoholic solution of a suitable onium salt (e.g., iodonium or trialkylammonium salt), which also serves as the radiolabeling precursor. The basicity of the reaction can be controlled by the choice of an appropriate counterion, while the high solubility of onium salts in organic solvents eliminates the need for a phase transfer catalyst. MeOH has been identified as the preferred elution solvent due to its rapid evaporation under reduced pressure and [^{18}F]F$^-$ recovery rates of 90–98%. After evaporation of the alcohol, an appropriate reaction solvent is added and the radiofluorination reaction is performed by heating to the desired temperature.[82] For radiofluorination of non-onium salt precursors, a "minimalist-like approach" can be used. In this method, [^{18}F]F$^-$ is eluted with a solution of an onium salt, such as triethylammonium bicarbonate or triflate, in MeOH. After evaporation of the MeOH, a solution of the labeling precursor in an appropriate reaction solvent is added and the radiolabeling reaction is performed as described above.[83,84]

Nucleophilic ^{18}F-fluorinations are typically performed in polar aprotic solvents like MeCN, DMSO, or DMF. Due to their polarity range, these solvents support the formation of dissociated ion pairs with [^{18}F]F$^-$ and thus enhance the nucleophilicity. However, they are insufficiently polar to fully solvate [^{18}F]F$^-$ by themselves. Depending on the functional groups present in the radiolabeling precursor, it may also be necessary to introduce protecting groups prior to the

radiolabeling step, as some groups can otherwise interfere with radiolabeling due to their nucleophilicity and/or the high basicity of [^{18}F]F$^-$. Functional groups that usually require protection include carboxylic acids, primary and secondary amines, phenols, and thiols.
Depending on the type of precursor and position of the leaving group, a distinction is made between aliphatic and aromatic nucleophilic radiofluorination. Each approach involves different mechanisms and precursor requirements for efficient formation of C-F bonds.

1.2.2.1 Aliphatic radiofluorination

Nucleophilic radiolabeling of aliphatic substrates proceeds according to an S_N mechanism, with the S_N2 pathway being the preferred mechanism for radiofluorination. In this reaction, ^{18}F replaces the leaving group through a Walden inversion, resulting in inversion of the configuration at the stereocenter (Scheme 2). Suitable leaving groups include halogens (e.g., bromine, iodine) and particularly sulfonates like triflates, mesylates, and tosylates, which provide favorable kinetics for the S_N2 reaction.

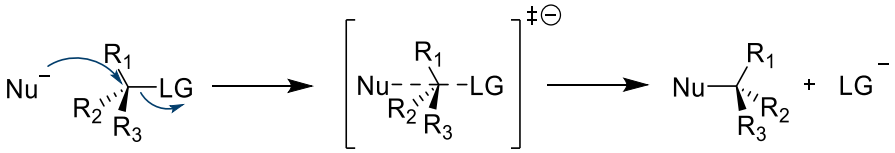

Scheme 2: S_N2 reaction mechanism. Nu = nucleophile, LG = leaving group.[85]

An illustrative example of aliphatic nucleophilic radiofluorination is the nucleophilic synthesis of [^{18}F]FDG. Here, 1,3,4,6-tetra-*O*-acetyl-2-*O*-trifluoromethanesulfonyl-ß-*D*-mannopyranose is used as the precursor, with [^{18}F]F$^-$ attacking at the 2-position. Following acid- or base-mediated cleavage of the acetyl groups, [^{18}F]FDG is obtained with nearly 100% purity and without detectable by-products. (Scheme 3).[86,87]

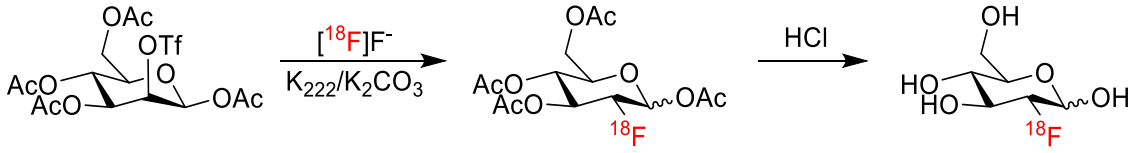

Scheme 3: Synthesis of [^{18}F]FDG via aliphatic nucleophilic radiofluorination.[86,87]

Several parameters critically influence the RCYs of aliphatic S_N2 radiofluorinations, including precursor concentration, solvent, temperature, reaction time, and the type and quantity of base used.[88,89] These reactions require a basic environment to activate the [^{18}F]F$^-$ nucleophile, yet excessive basicity can promote side reactions, such as hydrolysis or E2 eliminations.[89,90] Consequently, minimizing the addition of base is often crucial for optimizing RCYs, especially

for base-sensitive tracers.[89,91] Various elution methods have been investigated to address this issue. Although no base is deliberately added in the "minimalist approach", trace amounts of basic carbonate are still introduced during [^{18}F]F$^-$ elution due to the anion metathesis with the AEC in the carbonate form.[82,89] To further reduce basicity, Lee *et al*. preconditioned AECs with non-basic mesylate anions before trapping of [^{18}F]F$^-$.[89,92] This approach enhanced the radiochemical conversion (RCCs) for base-labile tracers, such as *N*-(3-[^{18}F]fluoropropyl)-2*ß*-carbomethoxy-3*ß*-(4-iodophenyl)nortropane ([^{18}F]FP-CIT).[89,93]

1.2.2.2 Aromatic radiofluorination

Aromatic C-^{18}F bonds can be formed through nucleophilic aromatic substitution (S_NAr). When conventional leaving groups, such as halogens, -NO_2 or -$^+NMe_3$, are employed, the choice of precursors is restricted to highly activated electron poor aromatics.[94] It was long assumed that the S_NAr reaction proceeds via the so called Meisenheimer complex, whereby the nucleophile adds to the aromatic ring under forming of the complex. Subsequent rearomatization via the cleavage of the leaving group afforded the desired product. In 2018, however, Kwan *et al*. corrected this assumption, showing that S_NAr reactions proceed via three different mechanism depending on the leaving group.[95] The mechanism involving the Meisenheimer complex is only feasible for extremely electron-deficient aromatics, like 1,3,5-trinitrobenzene with poor leaving groups like -OMe or -NR_2 whereby the anionic Meisenheimer complex is stabilized by electron-withdrawing groups (Scheme 4, A).[95] The S_NAr reaction of weaker activated (hetero)arenes with good leaving groups, such as -Br, occurs via a concerted mechanism (Scheme 4, B). Conversely, if the arene is stabilized by strongly electron-withdrawing groups and simultaneously destabilised by good leaving groups, such as -Cl, the reaction procees via a borderline mechanism between the formation of the Meisenheimer complex and the concerted mechanism (Scheme 4, C).[95]

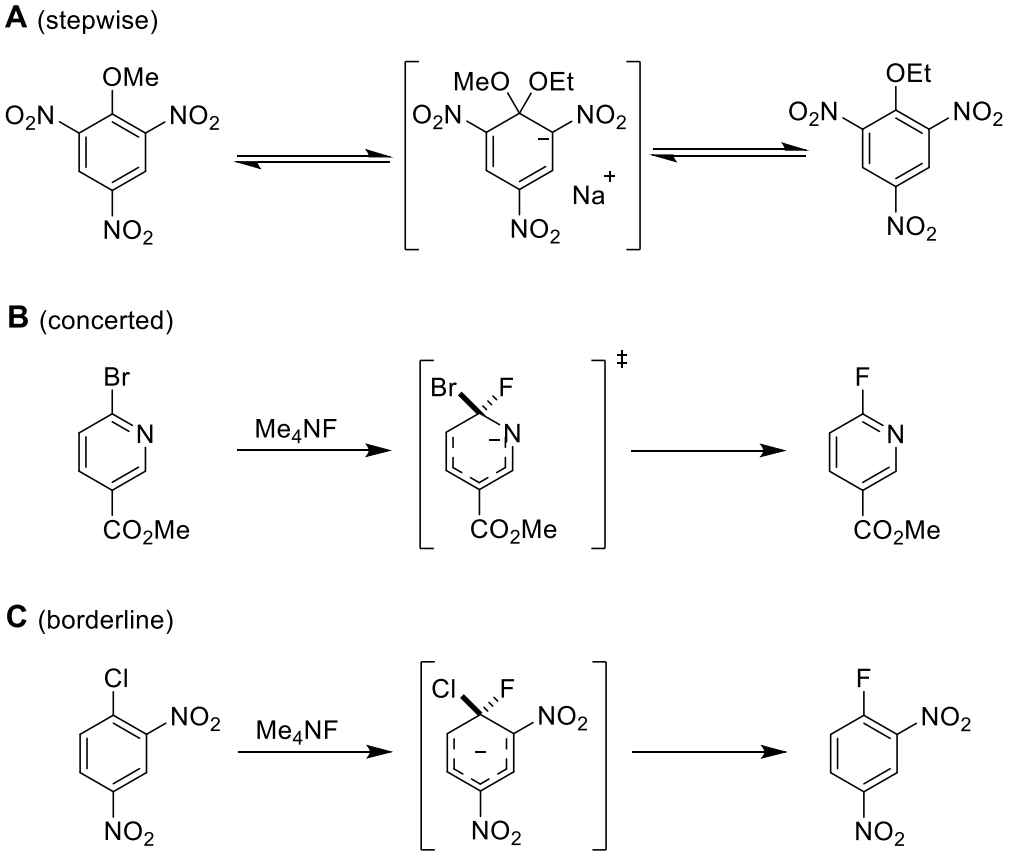

Scheme 4: The various mechanisms of the SNAr reaction described by Meisenheimer (A)[96] and Kwan *et al.*[95]

The requirement for strongly electron-deficient aromatic system restricted the scope of conventional S_NAr radiofluorination. However, some notable examples, including [^{18}F]altanserin[97,98] have been successfully prepared using S_NAr with conventional leaving groups (Scheme 5).[30]

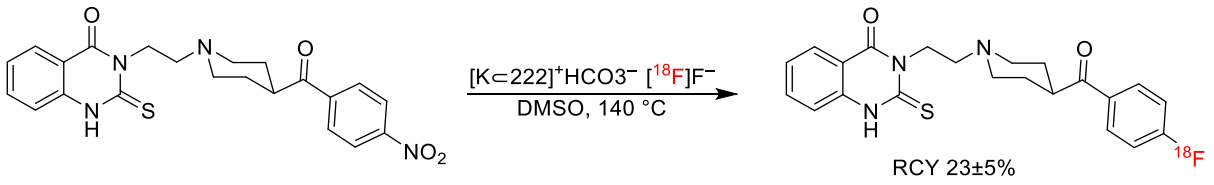

Scheme 5: Synthesis of [^{18}F]altanserin described by Hamacher *et al.*[97]

A more variable method for the production of [^{18}F]fluoroarenes is the nucleophilic aromatic substitution of diaryliodonium salts.[30,99,100] Pike *et al.* in 1995 were the first to use aryl iodonium salts as precursors for radiofluorination, thereby demonstrating that arenes without strongly electron-withdrawing substituents can be radiofluorinated using nucleophilic [^{18}F]F$^-$.[99] Consequently, radiofluorination of electron-neutral or moderate electron-rich aromatics became feasible (Scheme 6, A).[99] The electronic and steric properties of the two aromatic rings determine the regioselectivity of the reaction,[30,101,102] with substitution occurring at the

aromatic ring with the greater electron deficiency in the case of asymmetric diaryliodonium salts.[30] Another underlying effect on regioselectivity is the *ortho* effect, whereby substitution preferentially occurs on the aromatic ring that has a substituent(s) in *ortho* position(s) to the iodonium group.[30,75] The *ortho* effect is likely facilitated by the formation of an iodine-centered trigonal bipyramidal intermediate during the nucleophilic attack and by the introduction of [^{18}F]F$^-$ through the sterically restricted *ortho*-substituted ring in the equatorial position.[102,103] Ross *et al*. introduced aryl(2-theinyl)iodonium salts, whereby the 2-thienyl group serves as dummy ligand, which enables the production of ^{18}F-labled moderately electron-rich arenes in one step with complete regioselectivity (Scheme 6, B).[102]

Aryl iodonium ylides can also be used as labeling precursors, enabling the synthesis of electron-rich fluoroarenes.[104] However, the reactions of iodonium ylided are regiospecific compared to those of diaryliodonium salts. Most ylides exhibit relatively low thermal stability and therefore can only be handled at low temperatures or generated *in situ*, which often results in low RCYs.[104] Thermal stability could be enhanced by introducing sterically hindered sibstituents such as adamantane. (Scheme 6, C).[105]

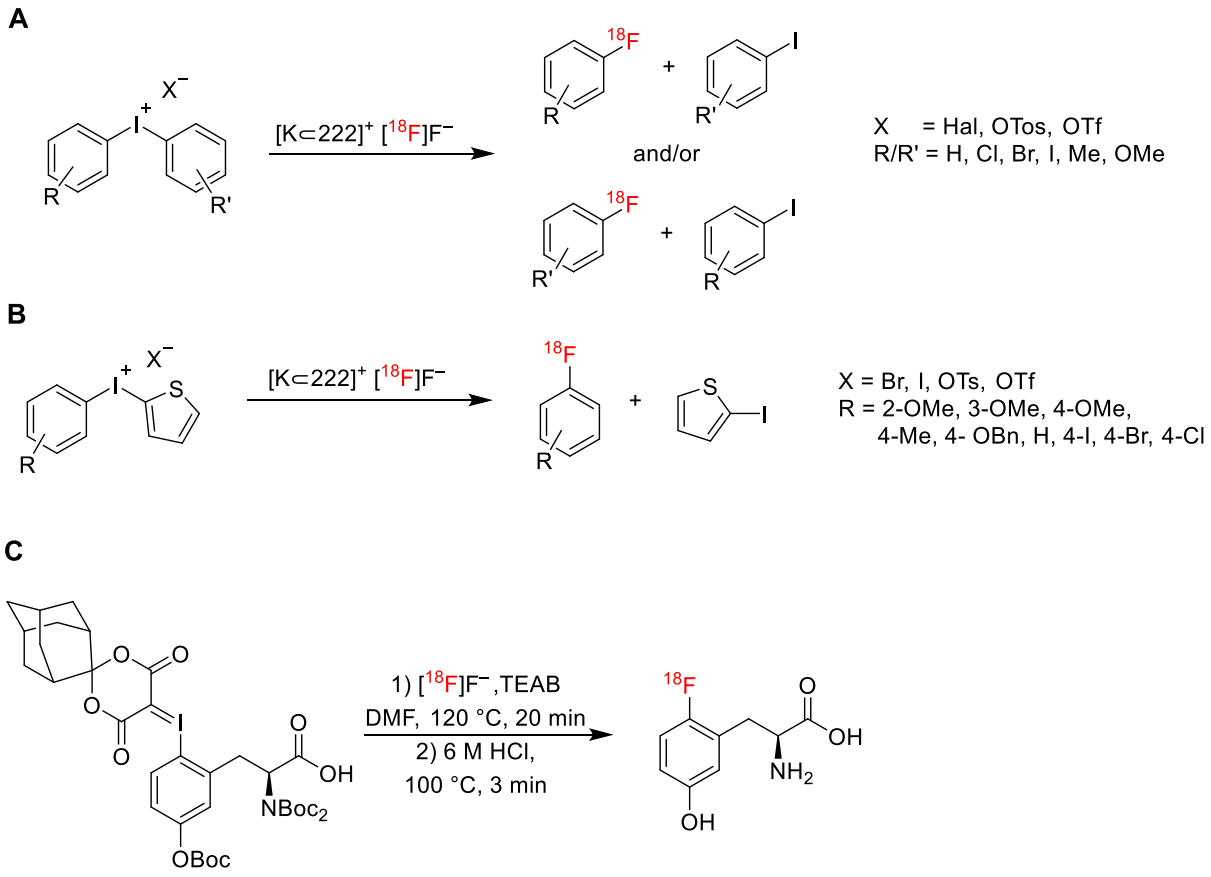

Scheme 6: Radiofluorination by nucleophilic aromatic substitution of various iodonium precursors: A: diaryliodonium salts;[99] B: aryl(2-theinyl)iodonium salts;[102] C: iodonium ylides.[105]

Another class of molecules that can be used as precursors for S_NAr reactions of non-activated aromatic compounds are triarylsulfonium salts, which were first used for radiofluorination by Mu *et al.* (Scheme 7, A).[106] Årstad and co-workers introduced dibenzothiophenesulfonium salts as radiolabeling substrates and applied them to efficiently produce PET tracers such as [^{18}F]FPEB or 3-[^{18}F]fluorodeprenyl (Scheme 7, B).[107] In 2019, Ritter and co-workers published a simplified one-step synthesis of dibenzothiophenylsulfonium salts and described the fine tuning of the electronic properties of dibenzothiophene leaving group as the way for more efficient production of radiofluorinated aromatics (Scheme 7, C).[108,109]

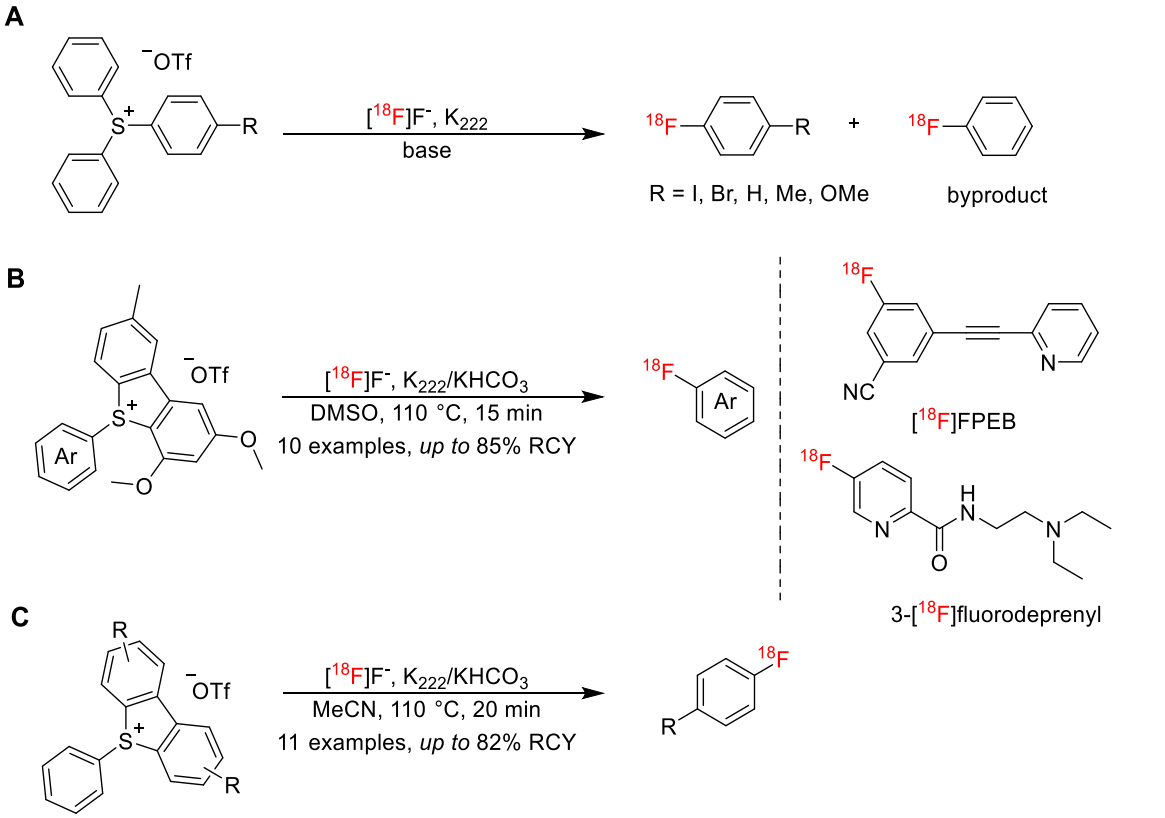

Scheme 7: Radiofluorination of triarylsulfonium salts described by A: Mu *et al.*[106]; B: Årstad and co-workers;[107] C: Ritter and co-workers.[109]

1.2.3 Transition metal-mediated radiofluorination

Over the past decade, transition metal-mediated radiofluorination has emerged as a powerful tool for the preparation of ^{18}F-labeled PET tracers. Especially, copper-mediated radiofluorination is characterized by versatility and robustness, which facilitates efficient introduction of ^{18}F into a broad range of substrates.[110,111] The method has been demonstrated to be particularly useful for the production of electron-rich (hetero)aromatics, which were previously difficult or impossible to prepare. The underlying mechanism involves a “Umpolung” that enables nucleophilic [^{18}F]F$^-$ to react with electron-rich systems by leveraging the electronic

activation provided by transition metals. This approach offers several advantages, including high efficiency and selectivity as well as a broad substrate scope.[89,110,112]

This approach was pioneered by Ritter and co-workers, who described in 2011 radiofluorination using two Pd complexes.[113] The radiofluorinating agent (B) is formed by reaction of a cationic Pd(IV) species (A) and [^{18}F]fluoride. This agent reacts in an oxidative fluorine transfer with a Pd(II) complex (C), which is formed by transmetalation from an aryl boronate ester. The radiofluorinated product is then formed via a reductive elimination step of the previously formed intermediate (D). The disadvantage of working with such palladium complexes is that they are not easily accessible and are extremely sensitive to moisture and oxygen.[113]

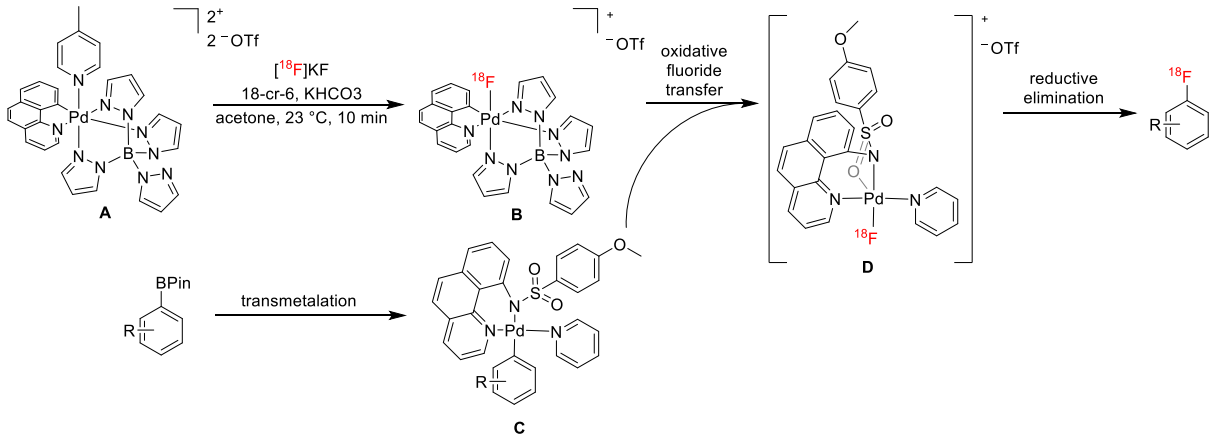

Scheme 8: Pd-mediated electrophilic radiofluorination of aryl boronate described by Ritter and co-workers.[113]

In 2012, the same group presented aryl-nickel complexes as metal mediators for the radiofluorination of aromatics.[114] A radiofluorinated hypervalent iodine compound (B) is used as an oxidant. Unfortunately, the thermal instability and moisture sensitivity of the oxidant severe impaired the practical value of the method.[114]

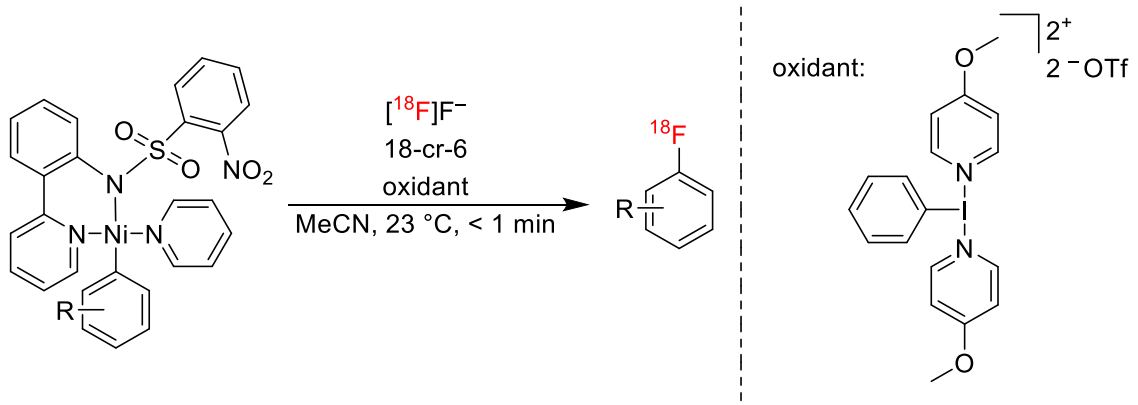

Scheme 9: Ni-mediated oxidative radiofluorination described by Ritter and co-workers.[114]

1.2.3.1 Copper-mediated radiofluorination

In 2014, Scott and co-workers and Gouverneur and co-workers independently reported the first examples for copper-mediated radiofluorination of aromatics.[110,115,116] Scott and co-workers employed aryl(mesityl)iodonium precursors with $(CH_3CN)_4CuOTf$ as the catalyst and a $[^{18}F]KF{\cdot}18\text{-crown-}6{\cdot}K_2CO_3$ complex as $[^{18}F]F^-$ source (Scheme 10, A). This enabled the radiofluorination of aromatics independent on their electronic properties. The applicability of the protocol for the synthesis of clinically relevant radiotracers was demonstrated by preparation of protected 6-[^{18}F]fluoro-DOPA and 4-[^{18}F]fluorophenylalanine.[110,115] Gouverneur and co-workers utilized aryl boronate ester precursors and labeled them using $[Cu(OTf)_2(py)_4]$ as copper catalyst and $[^{18}F]KF{\cdot}K2.2.2$ as $[^{18}F]F^-$ source (Scheme 10, B).[110,116] Scott and co-workers extended the approach to aryl boronic acid (Scheme 10, C)[117] and trialkylstannanes (Scheme 10, D).[110,117,118] Furthermore, Sanford and co-workers developed a Cu-catalyzed C-H radiofluorination of aromatic 8-aminoquinolinyl benzamides and NHC-Copper mediated ligand directed ^{18}F-fluorination of aryl halogenides (Scheme 10, E, F).[119,120]

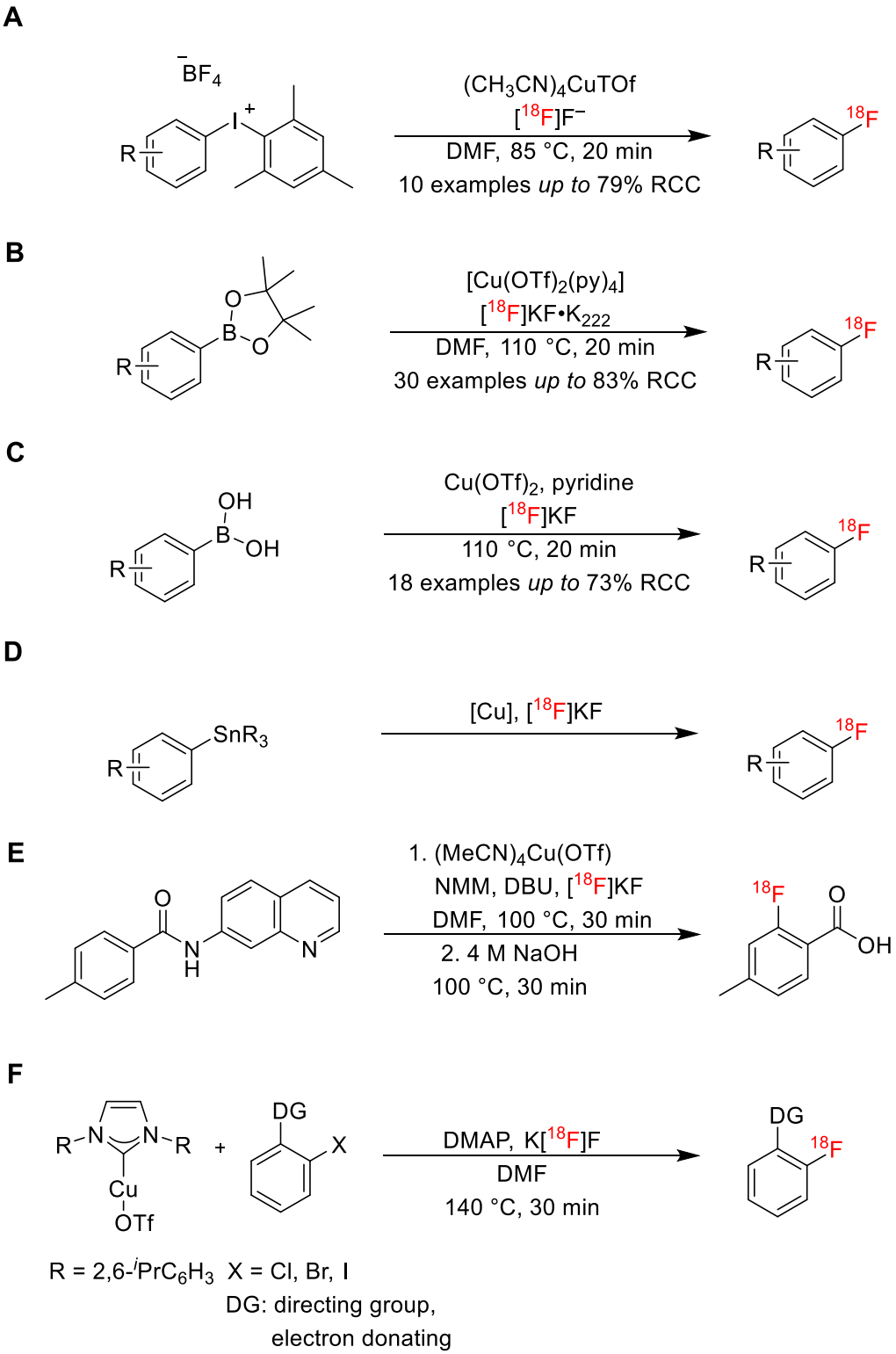

Scheme 10: Various copper-mediated radiofluorinations. A: Radiolabeling of diaryliodonium salts described by Scott and co-workers[115]; B: Radiofluorination of aryl boronate esters described by Gouverneur and co-workers[116]; C: Radiofluorination of aryl boronic acids described by Scott and co-workers[117]; D: Radiofluorination of trialkylstannanes described by Scott and co-workers[118]; E: Cu-catalyzed C-H radiofluorination of aromatic carboxylic acids described by Sanford and co-workers[119]; F: NHC-Copper mediated ligand directed 18F-fluorination of aryl halogenides described by Sanford and co-workers.[120]

In 2015, Neumaier and co-workers developed a “low-base approach”, recognizing that large quantities of base have a negative effect on the Cu-mediated radiofluorination of (aryl)(mesityl)iodonium and arylboronate precursors. They also applied the “minimalist approach” to Cu-mediated radiolabeling of the same substrates eliminating the need for both, base and azeotropic drying.[121] Two years later, Zischler *et al*. demonstrated that the addition of certain alcohols enhances the RCCs for labeling of boronic acids, boronic acid pinacol esters, and stannanes[122], while Zarrad *et al.* proposed a mechanism of the Cu-mediated radiofluorination of stannanes, boronic acids and aryl pinacol boronates (Scheme 11).[83]

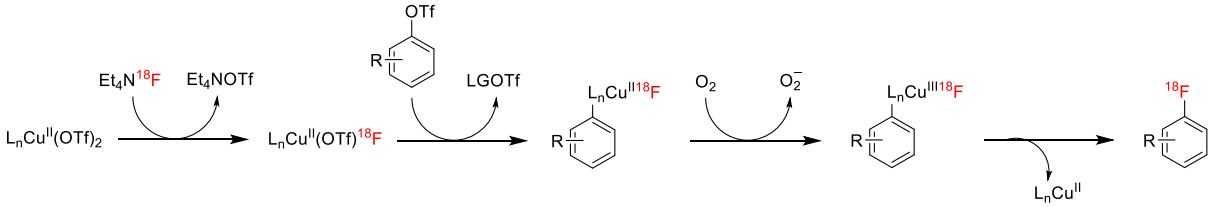

Scheme 11: Proposed mechanism of Cu-mediated radiofluorination described by Zarrad *et al*.[83]

More recently, Hoffmann *et al*. identified new copper complexes for the labeling boronic acids, stannanes, and boronic acid pinacol esters (Scheme 12). These complexes enabled improved RCCs despite a reduction in the precursor amount. $[Cu(4\text{-}PhPy)_4(ClO_4)_2]$ and $[Cu(3,4\text{-}Me_2Py)_4(OTf)_2]$ proved to be the most efficient tested copper mediators, while DMI emerged as the optimal solvent, enabling efficient labeling of a large number of model compounds and the synthesis of several PET tracers.[123]

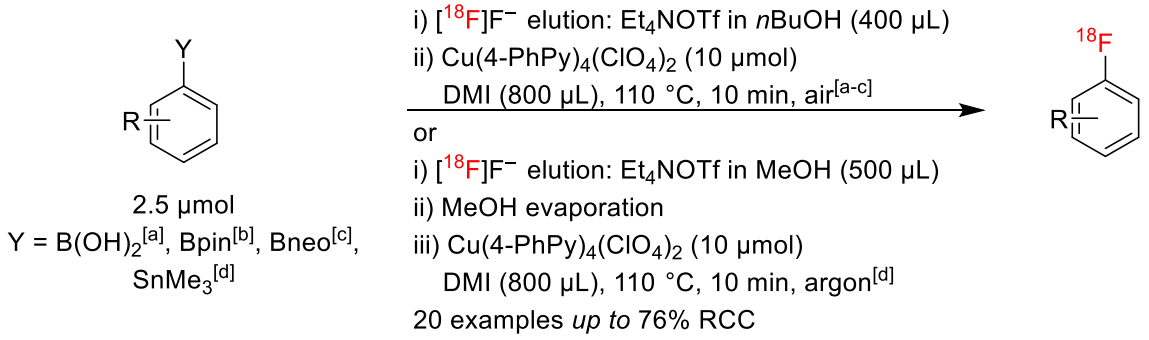

Scheme 12: Optimized radiofluorination of different labeling precursors for the synthesis of ^{18}F-labeled aromatics.[123]

1.2.4 Indirect radiofluorination

Indirect radiofluorination is often necessary when labeling biomolecules such as proteins, antibodies and nucleic acids. This approach is typically employed when the target compound contains a large number of functional groups or does not tolerate the harsh reaction conditions required for direct radiofluorination. In this case, a bifunctional small molecule, designated as

a prosthetic group or labeling synthon, is labeled with ^{18}F and then conjugated to the target molecule under mild conditions. The prosthetic group can be introduced in various ways, depending on the biomolecule. For example, ^{18}F-fluoroalkylation[124] can be used to couple ^{18}F-fluorinated sulfonates or alkyl halides to thiol and amino groups in peptides or proteins. *N*-succinimidyl 4-[^{18}F]fluorobenzoate ([^{18}F]SFB)[125] or 2,3,5,6-tetrafluorophenyl 6-[^{18}F]fluoronicotinate ([^{18}F]FPy-TFP)[126] are amino reactive and can be conjugated, e.g., to the amino groups in the side chain of lysine residues.[127] Cysteine-containing biomolecules can be selectively labeled by Michael addition with ^{18}F-labeled maleimide derivatives, such as *N*-[2-(4-[^{18}F]fluorobenzoamido)ethyl]maleimide ([^{18}F]FBEM).[128,129]

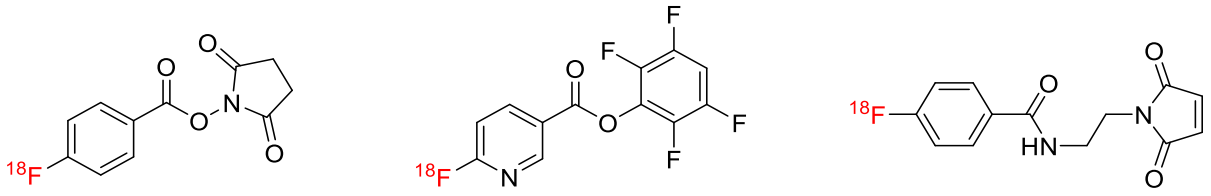

[^{18}F]SFB [^{18}F]FPy-TFP [^{18}F]FBEM

Figure 6: Prosthetic groups for the indirect radiofluorination of biomolecules.[125,126,128,129]

The Cu-mediated or strain-promoted 1,3-cycloadditions of alkynes to azides, which are widely used in the modern organic chemistry, known as the “click reaction”, can also be used for indirect radiofluorination. This reaction exhibits several advantages, including a high regioselectivity, excellent yields and mild reaction conditions.[130] Marik *et al*. were the first to employ the Cu-catalyzed reaction in 2006 to label an azide-functionalized peptide with an ^{18}F-labeled alkyne (Scheme 13, A).[131] Carpenter *et al*. and Bouvert *et al*. later implemented to the PET-chemistry the copper-free strain-promoted variant of the reaction (Scheme 13).[132]

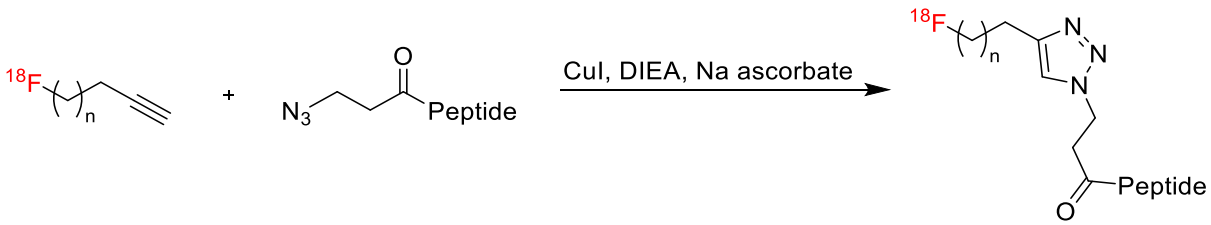

Scheme 13: Cu-catalyzed 1,3-dipolar cycloaddition between an azide-functionalized peptide and an ^{18}F-labeled alkyne.[131]

Transition metal-mediated cross-coupling reactions, including Sonogashira and Suzuki-Miyaura cross-couplings, have also been adapted for indirect ^{18}F-labeling. For example, Gao *et al*. utilized Suzuki-Miyaura cross-coupling to attach [^{18}F]fluorophenylboronic acid to a phenyl iodide-functionalized polypeptide (Scheme 14, A).[133] The labeling of alkyne-functionalized

peptides using the Sonogashira cross-coupling reaction was performed with 1-[^{18}F]fluoro-4-iodobenzene ([^{18}F]FIB, Scheme 14, B).[134]

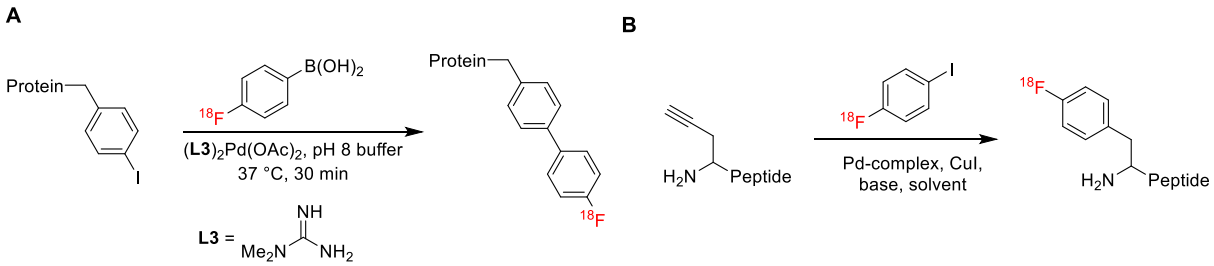

Scheme 14: Indirect radiofluorination via Suzuki-Miyaura cross-coupling (A)[133] and Sonogashira cross-coupling (B).[134]

1.2.5 Radiofluorinations at heteroatoms

Besides the ^{18}F-fluorination at carbon, the radiofluorination at heteroatoms have also been investigated. The respective studies have been conducted on boron, silicon, sulfur and phosphorus-containing compounds as well as aluminum chelates. These forms with F highly stable bonds (dissociation energies: B−F: 766 kJ/mol, Si−F: 540 kJ/mol, Al−F: 664 kJ/mol, P−F: 439 kJ/mol, and S−F: 343 kJ/mol; compare with: C−F: 536 kJ/mol).[135,136]

1.2.5.1 Radiofluorination at boron

First studies on the radiofluorination of boron compounds were carried out in the 1960s by Askenasy *et al*.[137] and Entzian *et al*.[138] It took 50 years before interest on this topic was revived. In the early 2000s, Ting *et al*. proposed that organotrifluoroborates could be suitable for radiolabeling via ^{18}F/^{19}F-isotopic exchange.[139] In addition to their hydrophilicity and bioorthogonality, organotrifluoroborates are also non-toxic.[140] In this study, arylboronic acid pinacol esters were used as precursors and labeled in the presence of KHF_2 as a carrier, which resulted in low molar activity (Scheme 15, A).[139,140] Subsequently, Perrin and co-workers investigated the kinetic stability of organotrifluoroborates in water and synthesized several synthons for radiofluorination. These synthons could be labeled with good yields and exhibited promising *in vitro* stability.[140,141] Li *et al*. applied this strategy to synthesize several radiofluorinated peptides for PET imaging by coupling the ^{18}F-labeled synthons to peptides.[140,142] Nevertheless, the method exhibited some disadvantages, including low molar activity due to the addition of a carrier and poor hydrolytic stability of the labeled aryltrifluoroborates. This resulted in low tumor uptake and, in some cases, significant radioactivity accumulation in bone (indicative of *in vivo* radiodefluorination).[140] To overcome the issue of low molar activity, arylborimides were introduced as alternative labeling precursors that require little or no carrier addition (Scheme 15, B).[143]

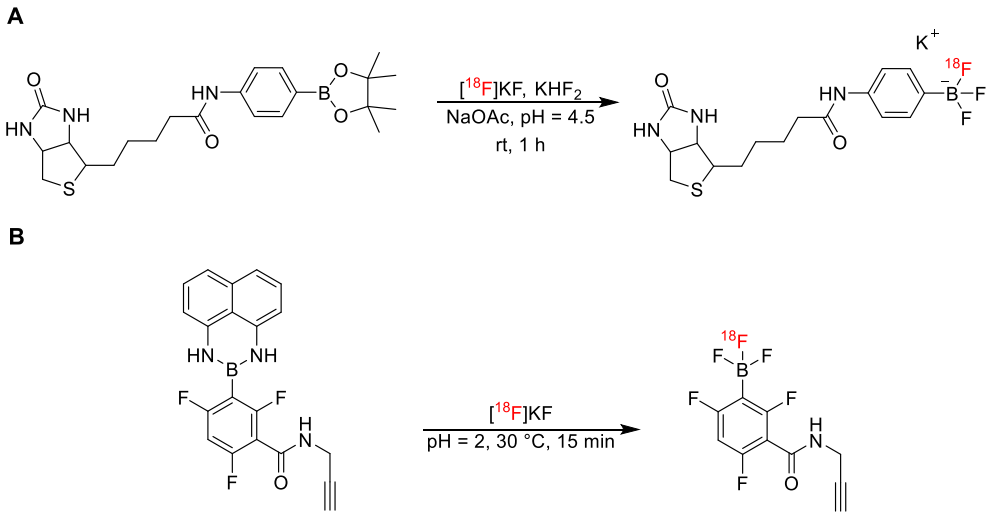

Scheme 15: Synthesis of [^{18}F]aryltrifluoroborate from arylboronic acid pinacol esters as described by Ting *et al*. (A)[139] and from arylborimides as described by Liu *et al*. (B).[143]

Perrin and co-workers further advanced the field by applying ^{19}F/^{18}F isotopic exchange reactions to zwitterionic trifluoroborates, which demonstrated improved hydrolytic and *in vivo* stability (Figure 7).[140,144] This method is straightforward, as the precursor is identical to the product, a property that has proven advantageous in the context of organotrifluoroborates. Zwitterionic trifluoroborates are accessible via well-established preparation procedures and exhibit high storage stability. This method also facilitated the labeling of several complex peptides, including Tyr^3-octreotide and bombesin, through click reactions of the synthons to the peptides.[140,144]

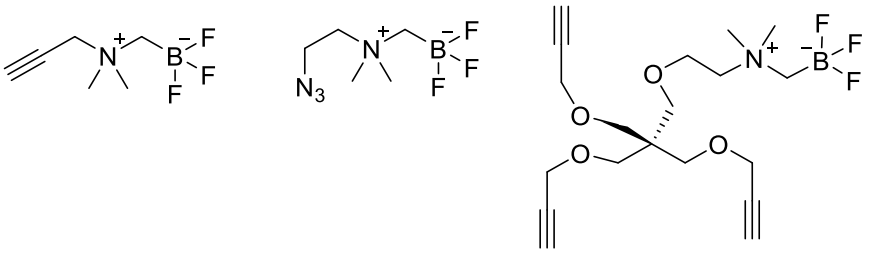

Figure 7: Zwitterionic trifluoroborates suitable as precursors of radiolabeled prosthetic groups for click conjugation.[144]

1.2.5.2 Radiofluorination at silicon

In 1985, Rosenthal *et al*. were the first, who prepared compounds, which contains C–^{18}F bond. [^{18}F]Fluorotrimethylsilane was synthesized using [^{18}F]TBAF as the fluorination reagent in a solution of 65% aqueous MeCN, achieving an RCY of 80% (Scheme 16, A).[136,145] Ting *et al*. resumed research on ^{18}F−Si bonds in 2005 with the labeling of a triethoxysilane biotin derivative. The researchers directly employed irradiated [^{18}O]H_2O for radiolabeling, omitting

any [^{18}F]F$^-$ preprocessing. The labeling of an alkyl tetrafluorosilicate in buffer solutions at pH 4.5 and 7.5 at ambient temperature afforded virtually quantitative radiochemical yields within less than one hour, though required addition of KHF_2 as a carrier (Scheme 16, B).[136,139] The resulting Si−^{18}F bonds exhibited low hydrolytic stability, and the product synthesized by Rosenthal *et al*. proved to be unstable *in vivo*.[136,139,145] As early as 1985, Rosenthal proposed the use of sterically demanding substituents attached to silicon, with the objective of improving the hydrolytic stability.[136,145] This hypothesis was later confirmed by Choudhry *et al*. and Schirrmacher *et al*. in 2006. Choudhry *et al*. demonstrated enhanced hydrolytic and blood serum stability of *tert*-butyldiphenylsilyl [^{18}F]fluoride, while Schirrmacher *et al*. showed significantly higher *in vivo* stability of di-*tert*-butylphenylsilyl [^{18}F]fluoride compared to this compound.[136,146,147]

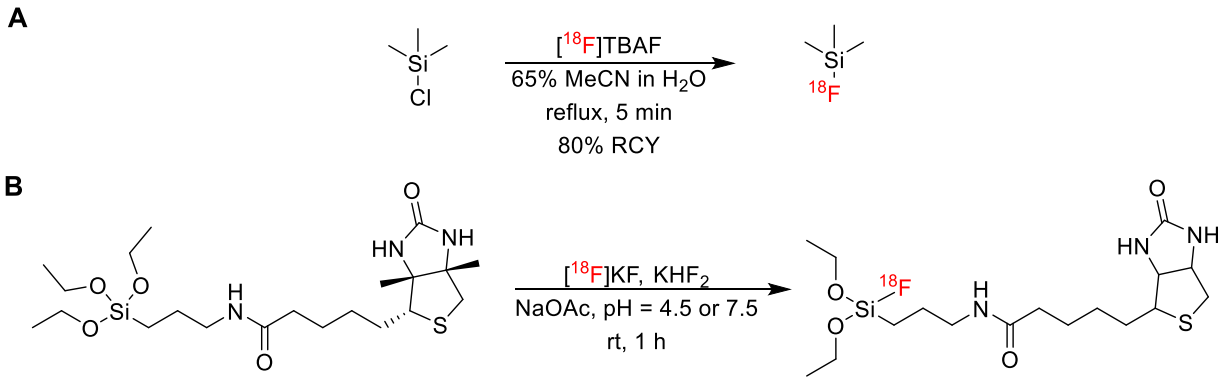

Scheme 16: Preparation of radiolabeled compounds containing Si–^{18}F bonds by Rosenthal *et al*.[145] and Ting *et al*.[139]

Schirrmacher *et al*. also demonstrated that ^{19}F/^{18}F isotopic exchange reactions could be applied for the formation of ^{18}F−Si bonds.[136,147] Specifically, labeling of di-*tert*-butylarylfluorosilanes with [^{18}F]KF/Kryptofix 222 was accomplished within 10−15 minutes at room temperature, with labeling yields of 80−95%. This method was employed to label fluorosilane-functionalized Tyr^3-octreotate, affording yields ranging from 90% to 97%. Furthermore, by doubling the reaction time and increasing the reaction temperature to 95 °C, the same compound could be labeled directly using the irradiated target water (Scheme 17). However, such elevated temperatures pose a significant limitation for the direct labeling of proteins or other sensitive biomolecules.[136,147]

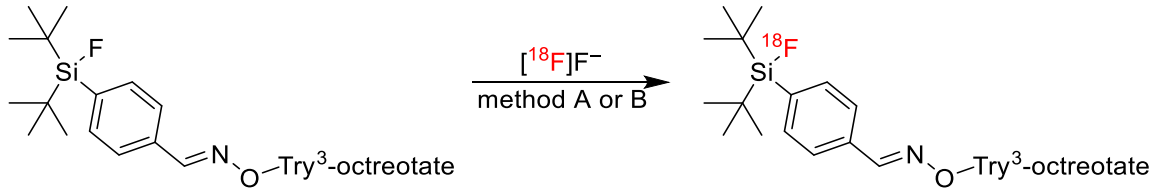

Scheme 17: Radiolabeling of Try^3-octreotate via ^{18}F/^{19}F isotopic exchange. Method A: [^{18}F]KF/Kryptofix 222, MeCN, rt, 10-15 min; Method B: [^{18}F]F$^-$/[^{18}O]H_2O, MeCN (15-20% total volume), 95 °C, 30 min.[147]

1.2.5.3 Radiolabeling at aluminum

In 2009, McBride et al. were the first to radiofluorinate suitable peptides conjugates via chelation of Al[^{18}F]F.[148,149] To this end, DTPA- or NOTA-HSG-hapten conjugates were treated with $AlCl_3$ and [^{18}F]F$^-$. The Al[^{18}F]F-labeled DTPA conjugates exhibited insufficient stability *in vitro*, both in formulation and in serum.[148,149] In contrast, it was demonstrated that Al[^{18}F]F-NOTA complexes are both kinetically inert and thermodynamically stable.[149,150] These complexes are typically synthesized by reacting of conjugates with [^{18}F]F$^-$ and $AlCl_3$ at a pH of 4. The pH range of 4–5 is crucial for the chelation, as pH values below 4 give rise of H[^{18}F]F, while pH values above 5 result in precipitation of insoluble aluminum hydroxide.[149,151] Although Al[^{18}F]F can be produced directly from the [^{18}F]F$^-$-containing target water, the [^{18}F]F$^-$ is often concentrated and purified using QMA cartridges to remove metal ion impurities originating from the cyclotron target.[149,152] The addition of organic co-solvents has been shown to increase the RCYs.[149,153] The chelator NODA was shown to form especially stable Al[^{18}F]F complexes (Figure 8). However, a notable disadvantage of using NOTA or NODA conjugates is the requirement for elevated temperatures for radiolabeling (100−120 °C). While such temperatures are generally tolerated by small peptides, they pose considerable challenges for the labeling of larger proteins or other sensitive biomolecules.[148,149]

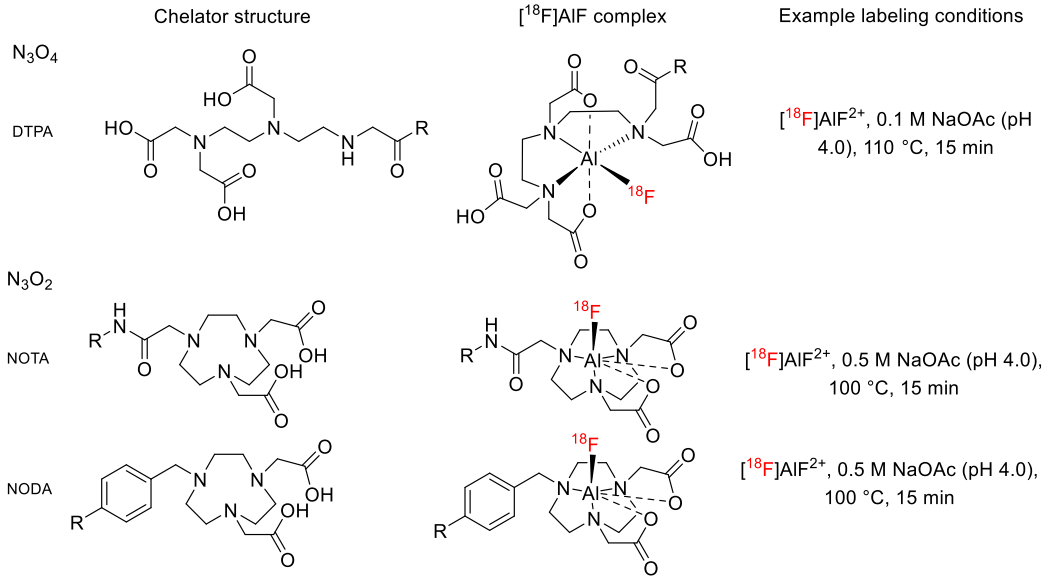

Figure 8: Structures of Al[^{18}F]F chelating chelators, proposed complexes and labeling conditions.[148,149,154]

To address this limitation, Cleeren *et al*. proposed two acyclic chelators that enable efficient radiolabeling at 40 °C. Unfortunately, the resulting labeled conjugates suffered from insufficient stability *in vitro*.[149,155] In 2017, the same group successfully disclosed the novel chelator (±)-H_3RESCA, which could be radiolabeled at ambient temperature. The compound contained a cyclohexyl ring to enhance structural rigidity, which positively influenced on the stability of the corresponding Al[^{18}F]F complexes. The latter demonstrated stability in rat plasma for at least four hours (Figure 9).[149,156] In 2020, Russelli *et al*. developed three new acyclic chelators based on the 2-aminomethylpiperidine (AMP) scaffold, which could be labeled at ambient temperature and pH 5 with good yields. One of them, 2-AMPDA-HB, demonstrated promising *in vivo* stability (Figure 9).[149,157]

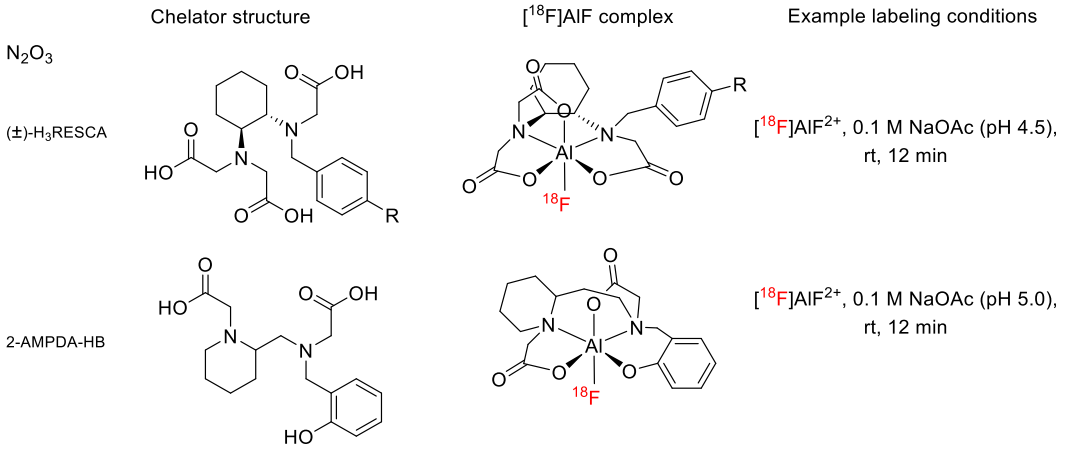

Figure 9: Structure of chelators for Al[^{18}F]F chelation, the resulting complexes and labeling conditions.[149,156,157]

1.2.5.4 Radiolabeling at phosphours

The P−F bond was contained in compounds that have been used in biological studies[158] and as poisons.[159] In 1990, Ghorab *et al*. investigated isotopic exchange reactions between PF_6 and radiofluorinated hexafluorides ([^{18}F]MoF_6, [^{18}F]WF_6, and [^{18}F]UF_6) in MeCN at ambient temperature.[160] However, the synthesis of organic compounds containing ^{18}F−P bonds was not investigated until 2005, when Studenov *et al*. synthesized *N*,*N*,*N*′,*N*′-tetramethylphosphorodiamide [^{18}F]fluoride ([^{18}F]Dimefox, Scheme 18), a radiolabeled pesticide and cholinesterase inhibitor.[161] The model compound was prepared in an RCY of 96% using nucleophilic substitution of the corresponding chloride with [^{18}F]TBAF. It showed moderate stability in aqueous media (75% intact after 30 minutes), but the authors suggested that PET tracers containing phosphorofluoridate monoester groups might exhibit improved stability.[161]

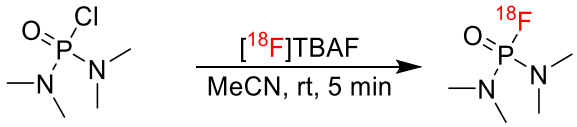

Scheme 18: Radiosynthesis of [^{18}F]Dimefox described by Studenov *et al*.[161]

Phosphorofluoridates can be prepared using either P(V) or P(III) precursors, with a preference for the former due to enhanced stability. Furthermore, the phosphorus in P(III) precursors must first be oxidized[162] or sulfurized[158,163] to the more stable P(V) state, resulting in an additional reaction step.[161]

In 2017, Vabre *et al*. described the preparation of an ^{18}F-labeled organophosphorus-based radiotracer based on an *N*-heterocyclic carbene as a potential adduct for a prosthetic group.[164] They synthesized a 1,3-dimethylimidazol-2-ylidene-PF_5 derivative and labeled the zwitterionic compound using Lewis acid-catalyzed ^{18}F/^{19}F isotopic exchange with [^{18}F]TBAF in MeCN. $SnCl_4$ was selected as the promoter, and the product was obtained in RCYs ranging from 4% to 6%, depending on the temperature employed (Scheme 19). The compound exhibited good *in vitro* and *in vivo* stability, attributable to the Coulomb effects between the imidazolium and the phosphorus moiety.[164]

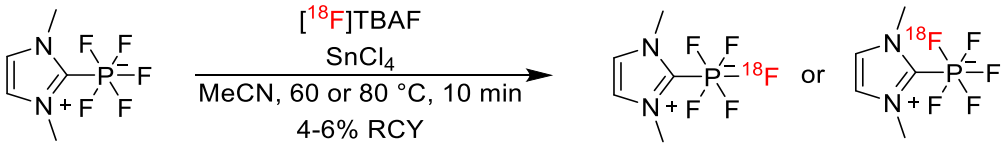

Scheme 19: Radiolabeling of a 1,3-dimethylimidazol-2-ylidene-PF5 derivative via ^{18}F/^{19}F isotopic exchange as described by Vabre *et al*.[164]

In 2018, Jiang *et al*. reported the synthesis of [^{18}F]hexyfluorophosphate ([^{18}F]HFP) as potential radiotracer for PET imaging of the sodium-iodide symporter (NIS).[165] Their tracer was prepared in an automated synthesis module by reacting PF_5 with [^{18}F]KF/Kryptofix 2.2.2, which afforded an RCY of 10% and a molar activity of 604 MBq/µmol. The tracer demonstrated specific uptake in NIS-expressing tissues and, despite low molar activity, promising *in vivo* imaging properties.[165]

Hong *et al*. performed ^{18}F/^{19}F isotopic exchange on phosphorus in aqueous solution, enabling the direct radiofluorination of functionalized biomolecules.[166] Initially, they synthesized small organofluorophosphines, in which the phosphorus was shielded by different groups of varying steric hindrance (Figure 10). Subsequent radiofluorination afforded the corresponding ^{18}F-labeled organofluorophosphines in RCYs of >90% and confirmed that greater steric hindrance is associated with higher RCYs. The compounds demonstrated stability *in vitro* in various solutions for over two hours. Biomolecules functionalized with organofluorophosphines, such

as human serum albumin and c(RGDyk), could also be labeled in aqueous solution, albeit with lower RCYs of >5% and >30%, respectively.[166]

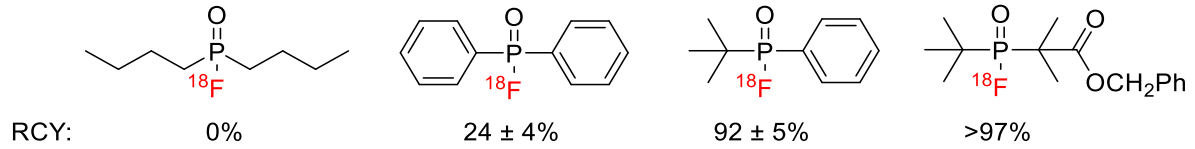

Figure 10: Preparation of ^{18}F-labeled organofluorophosphines via ^{18}F/^{19}F isotopic exchange as described by Hong *et al*.[166]

While ^{18}F-labeled organofluorophosphates have traditionally been synthesized via ^{18}F/^{19}F isotopic exchange with limited molar activities, Mou *et al*. proposed in 2021 a novel strategy for the preparation of ^{18}F-labeled phosphorofluoridates and phosphonofluoridic acids through Zn(II)-catalyzed nucleophilic radiofluorination of imidazole-activated precursors.[167] Radiolabeling was performed with a precursor amount of 0.2 mg and a five-fold excess of Zn(II) for 20 min at 70 °C (Figure 11), which afforded the ^{18}F-labeled compounds in good molar activities and RCYs of >50% for phosphorofluoridates and >80% for benzyl phosphonofluoridic acids. The benzyl phosphorofluoridate and benzyl phosphonofluoridic acid remained stable for 90 minutes in saline and mouse serum at 37 °C.[167]

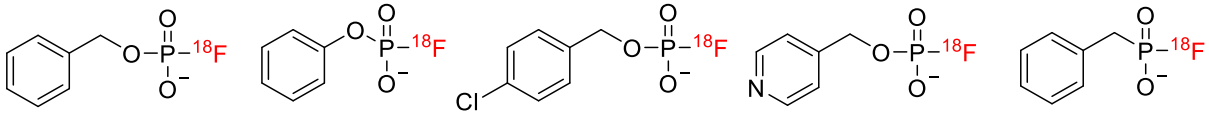

Figure 11: ^{18}F-labeled organofluorophosphates described by Mou *et al*.[167]

Most recently, Tang *et al*. reported the radiolabeling of phosphine oxides via Cu(II)-mediated direct ^{18}F-dehydrofluorination.[168] Using an active ester model compound (Scheme 20, A), the authors investigated the influence of several reaction parameters, including reaction time, temperature, [^{18}F]F$^-$ source, solvent, precursor amount, $Cu(OAc)_2$ equivalents, and water amount, on the RCCs of the reaction. Furthermore, they proposed a mechanism for Cu(II)-mediated dehydrofluorination (Scheme 20, B) and achieved a 15-fold increase in molar activity compared to labeling via ^{18}F/^{19}F isotopic exchange.[168]

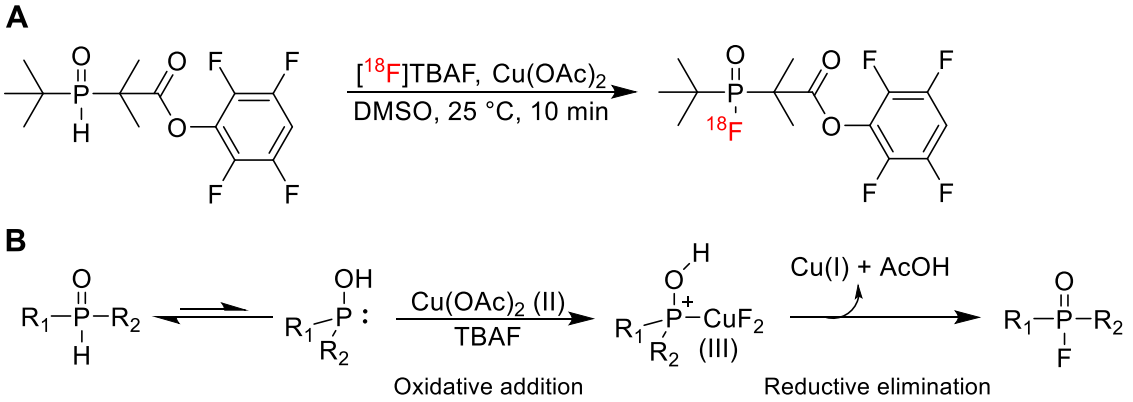

Scheme 20: Cu(II)-mediated direct ^{18}F-dehydrofluorination of a model compound (A); Proposed reaction mechanism for Cu(II)-mediated dehydrofluorination (B).[168]

Shortly thereafter, Wang *et al*. succeeded in synthesizing [^{18}F]phosphonofluoridic acids ([^{18}F]PFAs) at ambient temperature within five minutes.[169] The diphenyl phosphonate precursors were radiofluorinated in two steps, which comprised nucleophilic addition of one phenolate group with [^{18}F]F$^-$, followed by the instant hydrolysis of the second phenolate ion by quenching with H_2O.[169] D'Andrea *et al*. proposed a reaction mechanism involving a difluoride-substituted intermediate in the presence of excess F$^-$ (Scheme 21, A)[169,170], while Wang *et al*. suggested a monofluorinated intermediate for reactions involving small quantities of [^{18}F]F$^-$ (Scheme 21, B).[169]

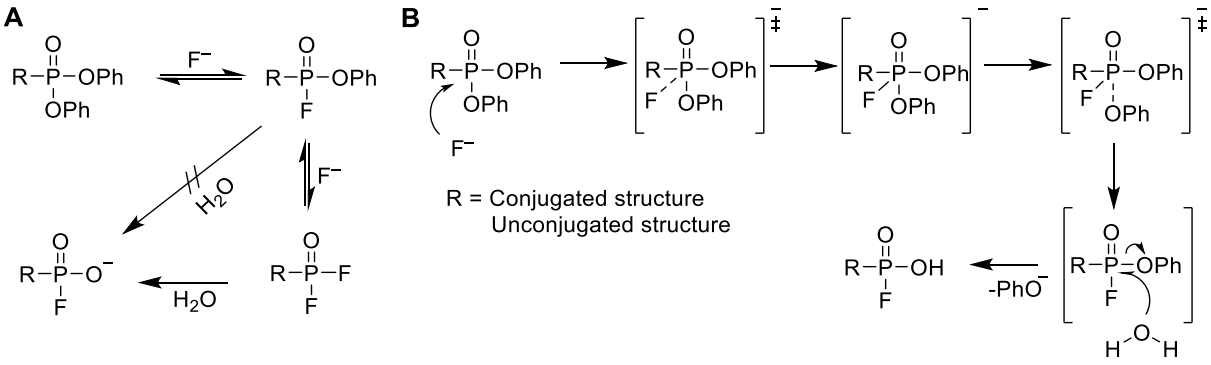

Scheme 21: Proposed fluorination hydrolysis reaction mechanism by d'Andrea *et al*.[170] (A) and Wang *et al*.[169] (B).

The site-selectivity of the phosphonate-specific nucleophilic substitution was investigated in the presence of interfering compounds (up to 10 eq.; 3 µmol), such as amino or hydroxyl groups.[169] Moderate RCYs were observed, indicating reasonable site-selectivity in the presence of interfering groups. The presence of water (up to 8–19%) in the reaction system was also tolerated, although the RCYs decreased with increasing of water content. A variety of substrates with functional groups such as bromine, cyano, methoxy, nitro, or naphthyl, as well as compounds with several heterocyclic structures such as pyridine, benzofuran, and benzothiazole could be labeled in high RCYs. Functional groups like carboxyl, amino, and hydroxyl were also tolerated. ^{18}F-Labeled biomolecules such as [^{18}F]PFA folic acid or [^{18}F]PFA-

pyridoxamine were prepared with RCYs of 46% and 23%, respectively (Figure 12). Two of the synthesized [^{18}F]phosphonofluoridic acids were stable for over 2 hours at 37 °C in both PBS and serum. This method enabled the labeling of a wide range of substrates containing different functional groups with good RCYs under mild conditions, obviating the need for protecting groups.[169]

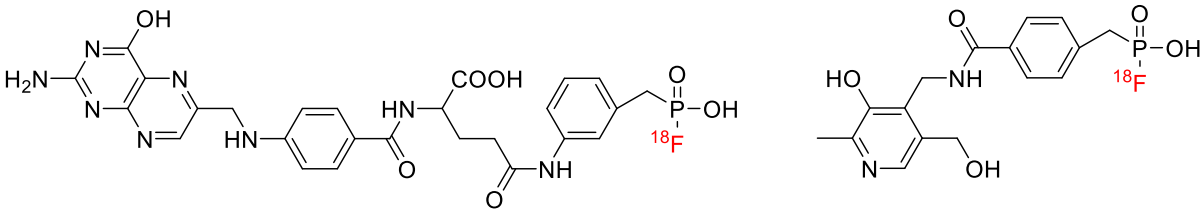

Figure 12: Biologically relevant molecules functionalized with [^{18}F]phosphonofluoridic acids by Wang et al.[169]

In 2022, Yang *et al*. synthesized [^{18}F]fluorothiophosphate ([^{18}F]FTP) synthons via nucleophilic ring opening of oxydithiaphospholane 2-sulfides with concurrent elimination of thiirane, which proceeded at ambient temperature within 30 seconds (Scheme 22).[171] A variety of such substrates, including alkanes, alkenes, halogens, heterocycles, nucleotide and amino acid derivatives were labeled affording the corresponding radiofluorinated products in high RCYs and with high molar activity.[171]

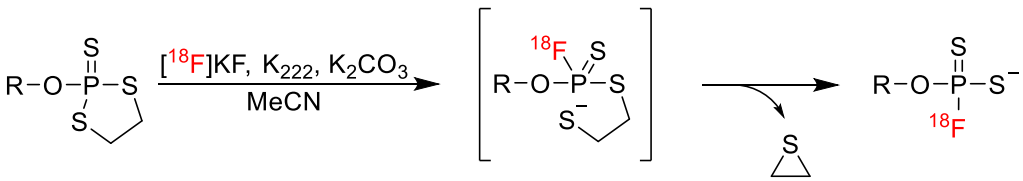

Scheme 22: General reaction equation for the synthesis of [^{18}F]FTPs described by Yang *et al.*[171]

[^{18}F]FTPs demonstrated a good hydrolytic stability under basic and acidic conditions. [^{18}F]FTPs-derived radiolabeled prosthetic groups were also prepared. Their suitability for indirect radiolabeling was demonstrated by the automated synthesis of an ^{18}F-labeled c(RGDyK) conjugate in reasonable isolated RCYs and with a molar activity of 337–517 GBq/µmol.[171]

1.2.5.5 Radiofluorination at sulfur

Organic compounds containing a F−S bond have attracted significant interest in biology and chemistry due to their reactivity and balanced stability under physiological conditions.[172] Such compounds have shown promise as effective protease inhibitors, covalent protein modifiers,

and biological probes.[173] Similarly, different compounds with an $^{18}F-S$ bond were prepared and evaluated for their feasibility as PET tracers.[172,174]

Tosyl [^{18}F]fluoride was the first described compound with $^{18}F-S$ bond. It was synthesized from tosyl chloride by the reaction with aqueous cesium [^{18}F]fluoride in the 1970s by de Kleijn *et al*.[175] Thirty years later, Neal *et al*. observed the formation of tosyl [^{18}F]fluoride as a by-product during the reaction of bis(tosyloxy)methane with [^{18}F]F$^-$ to form [^{18}F]fluoromethyl tosylate. They were able to control the formation of tosyl [^{18}F]fluoride by adjusting the amount of Kryptofix 222, tetrabutylammonium bicarbonate, and water.[176] Sulfonyl [^{18}F]fluorides have since garnered significant attention as prosthetic groups for indirect radiofluorination. Inkster *et al*. synthesized four sulfonyl [^{18}F]fluorides from the corresponding sulfonyl chlorides (Figure 13, A). The 3-formyl analogue showed good stability in PBS at physiological pH and temperature for two hours but underwent partial degradation in mouse serum (55% intact after 15 minutes).[177] Matesic *et al*. later prepared twelve aryl sulfonyl [^{18}F]fluorides from the corresponding chlorides using microfluidic synthesis, achieving RCYs of >75% at 30–180 °C (Figure 13, B). Preliminary stability studies conducted in serum under physiological conditions demonstrated that steric hindrance around the sulfonyl fluoride confers greater resistance against hydrolysis than electronic density.[178] In 2015, Al-Momani *et al*. succeeded in synthesizing a prosthetic group ([^{18}F]FS-PTAD) and conjugating it to tyrosine. The resulting [^{18}F]FS-tyrosine was claimed to be stable (≥95% intact) for at least 2 h in EtOH/PBS (8/92), even without significant steric hindrance around the [^{18}F]SO_2F group (Figure 13, C).[179]

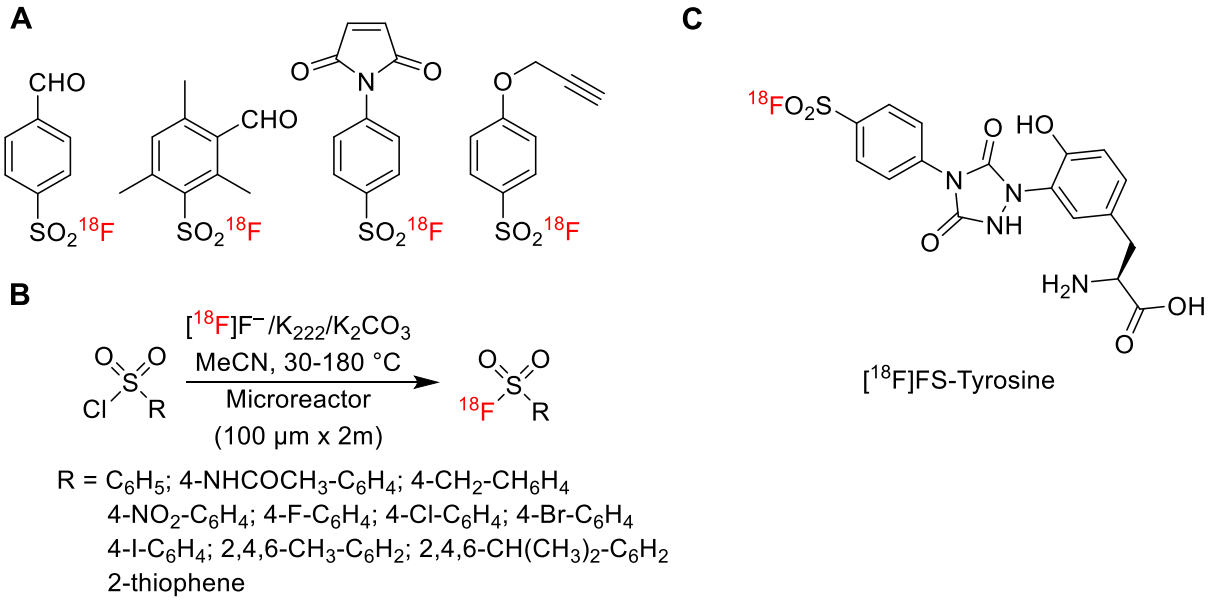

Figure 13: A: [^{18}F]Sulfonyl fluorides synthesized by Inkster *et al*.[177]; B: Radiofluorination of sulfonyl chlorids in a microreactor as described by Matesic *et al*.[178]; C: [^{18}F]FS-Tyrosine synthesized by Al-Momani *et al*.[179]

Ethenesulfonyl fluoride (ESF), identified by Chen *et al*. as a strong Michael acceptor[180], was synthesized in its ^{18}F-labeled form by Pascali *et al*., who proposed it as a prosthetic group for conjugation with "soft" nucleophiles, such as ω-amino group lysine or thiol group of cysteine residues.[174] Due to the small size and hydrophilicity of [^{18}F]ESF, the authors hypothesized that it would be suitable for labeling proteins or polypeptides without drastically altering their polarity or pharmacological properties.[174] The synthesis of [^{18}F]ESF was successfully achieved under both c.a. and n.c.a. conditions, and its conjugation to selected model compounds was accomplished. The conjugates were stable in the reaction mixture, but exhibited degradation in rat serum or when formulated for injection.[181] Additionally, [^{18}F]ESF has been proposed as a versatile [^{18}F]fluoride source for the preparation of radiotracers that could be supplied to hospitals and academic institutions without own cyclotron (Scheme 23).[172,182]

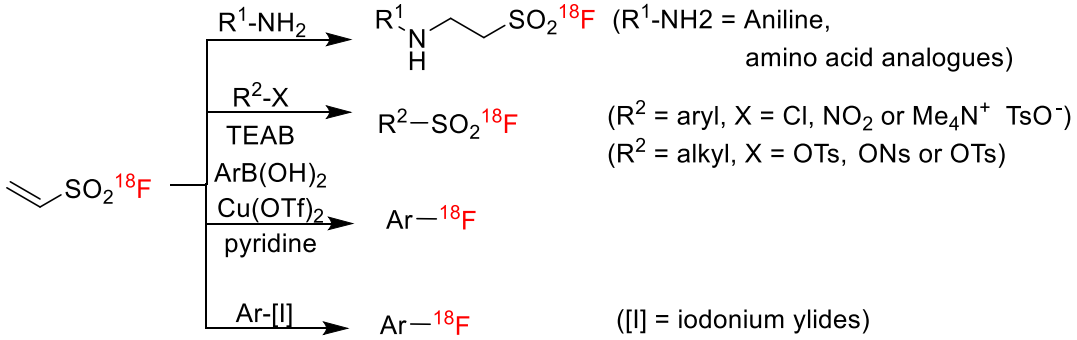

Scheme 23: [^{18}F]ESF as a fluorination reagent.[172,182]

The limited number of publications on aliphatic sulfonyl [^{18}F]fluorides suggests that these compounds have not been extensively investigated, most likely due to insufficient stability.[183,184]

The OSO_2F unit can function as a leaving group or as a robust building block in organic synthesis, depending on the characteristics of the alkyl or aryl moiety it is associated with.[172] $KOSO_2$[^{18}F]F (Scheme 24) was synthesized by Blower and wo-workers in RCYs of 31.6 ± 9.5% and adequate molar activities of 48.5 ± 13.4 GBq/µmol.[185] This compound showed specific uptake via NIS *in vitro* and *in vivo*.[172,185]

Scheme 24: Synthesis of [^{18}F]fluorosulfate.[172,185]

In 2014, Sharpless and colleagues introduced "sulfur(VI) fluoride exchange" (SuFEx) as a new class of click chemistry reaction.[186] In 2021, Zheng *et al*. established a link between click chemistry and radiochemistry by labeling a series of arylfluorosulfates via ultra-fast SuFEx-based $^{18}F/^{19}F$ isotopic exchange within 30 seconds at ambient temperature.[187] The labeled compounds were isolated using solid-phase extraction cartridges and a conventional elution procedure, achieving apparent RCCs of 80–90% but isolated yields of only 20–40% (Scheme 25).[187] This discrepancy was investigated by Walter *et al*. in 2022, who optimized the protocol using a "minimalist-like" $[^{18}F]F^-$ elution approach that eliminated the need for azeotropic drying.[84] Utilizing this robust method, nanomolar precursor quantities (20 µg) could be labeled in high volumes (1 mL), yielding the corresponding aryl $[^{18}F]$fluorosulfates in good to excellent yields (Scheme 25).[84]

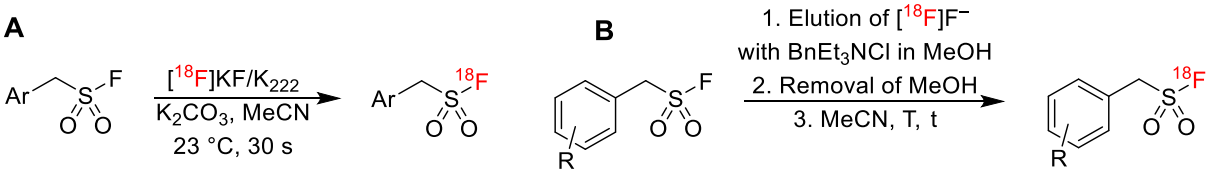

Scheme 25: Synthesis of arylfluorosulfates via SuFEx-based $^{18}F/^{19}F$ isotopic exchange described by Zheng *et al*.[187]; B: Optimized protocol developed by Walter *et al*.[84]

Using $^{18}F/^{19}F$ isotopic exchange, Jeon *et al*. synthesized sulfamoyl $[^{18}F]$fluorides shortly after Zheng et al.[188] They successfully labeled 30 compounds, including both aliphatic and aromatic precursors as well as primary and secondary amines. The RCYs ranged from 50 to 97%, with precursor amounts from 0.5 to 20 µmol and a reaction time of 10 min at 60 °C in an Anton Paar inductive heating reactor.[188]

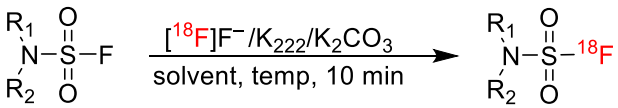

Scheme 26: Radiosynthesis of sulfamoyl $[^{18}F]$fluorides described by Jeon *et al*.[188]

Kim *et al*. developed a method for the direct preparation of sulfamoyl $[^{18}F]$fluorides through radiofluorosulfurylation of amines.[189] In this method, an $[^{18}F]FSO_2^+$ transfer species is generated *in situ* by eluting $[^{18}F]F^-$ from a QMA cartridge with a $MeCN/H_2O$ mixture containing a fluorosulfonylated imidazolium salt, SuFEx-IT. The resulting species reacted efficiently with various amine substrates, including primary and secondary aliphatic and aromatic amines affording the corresponding radiolabeled compounds in fair RCCs. Notably, the reaction did not require strictly anhydrous conditions or the use of a cryptand.[172,189]

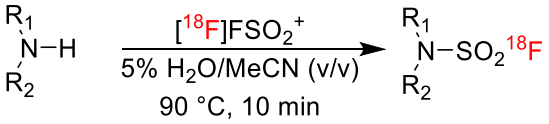

Scheme 27: Synthesis of sulfamoyl [^{18}F]fluorides by direct radiofluorosulfurylation of amines.[172,189]

1.3 Fibroblast activation protein (FAP) as target for tumor imaging and radiotherapy

In 1986, Wolfgang Rettig identified a cell surface antigen expressed on reactive stromal fibroblasts in granulation tissue during wound healing, as well as in most soft tissue sarcomas, epithelial carcinomas, and certain fetal mesenchymal fibroblasts.[190] This antigen was absent in malignant or normal epithelial cells, normal fibroblasts, or the stroma of benign epithelial tumors. Based on these observations, the antigen was designated as “fibroblast activation protein” (FAP). In 1990, Atsuko Aoyama discovered a dimeric 170 kDa membrane-bound gelatinase in the human melanoma cell line LOX, which was termed “seprase” (for surface-expressed protease). Subsequent cloning and sequencing revealed that seprase and FAP were identical.[190,191,192] FAP expression has since also been detected in non-fibroblast cell types, such as epithelial tumors[193], melanomas and melanocytes[192,194], and macrophages[195]. In addition, it has been shown that FAP is not confined to the cell surface and can also be shed from the plasma membrane as soluble FAP.[190,196]

FAP is a type II transmembrane serine protease with a molecular mass of 97 kDa that exhibits both dipeptidyl and endopeptidase activity.[190] It belongs to the prolyl peptidase family, which also includes dipeptidyl peptidases such as DPP 4, DPP 7 (also known as DPP 2), DPP 8, DPP 9, and prolyl oligopeptidase (PREP/POP).[197] These enzymes preferentially cleave peptide substrates after proline residues.[198] Among them, FAP shares the greatest amino acid sequence similarity with DPP 4, reaching up to 70%.[199] FAP is composed of 760 amino acids, with the intracellular domain comprising the first four residues, the transmembrane domain spanning residues 5–25, and the extracellular domain extending from residues 26–760.[196] The β-propeller domain encompasses residues 54–492, while residues 27–53 and 493–760 form the α/β-hydrolase domain. The enzyme's catalytic triad is situated in the hydroxylase domain, at the interface between the α/β-hydroxylase domain and the β-propeller domain.[190] The catalytic triad, which forms the enzyme's active site, consists of serine, aspartic acid, and histidine[200], with serine acting as the nucleophile responsible for cleaving *N*-terminal pro-X peptide bonds (where X indicates an amino acid other than proline or hydroxyproline). While both FAP and DPP 4 exhibit dipeptidyl peptidase activity, endopeptidase activity is unique to FAP and provides a functional distinction for selective detection and inhibition. The optimal amino acid sequence for FAP's endopeptidase activity is Gly-Pro-X, with the highest efficacy observed when X = Met or Phe, and the lowest when X = Glu or His.[190,201]

FAP expression has been linked to several human diseases, including autoimmune diseases, fibrosis, atherosclerosis, metabolic disorders, arthritis and various cancers. In many of these conditions, increased FAP expression correlates with disease progression and severity.[190] FAP is overexpressed in more than 90% of carcinomas, including lung, breast, pancreatic,

colon, bladder, and ovarian cancers, but is typically absent or minimally expressed in normal tissue. In the aforementioned malignancies, FAP is predominantly localized in the tumor stroma, making it a reliable marker for cancer-associated fibroblasts (CAFs).[190] CAFs constitute the primary component of the tumor stroma and function as pivotal modulators of metastasis and cancer progression. In contrast to cancer cells, CAFs exhibit enhanced genetic stability and a reduced propensity to develop resistance to therapy.[202] CAFs can originate from various sources, including local fibroblasts, circulating fibroblasts, or bone marrow-derived stem cells.[203,204] Their emergence is associated with molecular and morphological changes in the tumor stroma, including the upregulation of FAP expression.[204] A meta-analysis published in 2015 found that FAP expression is significantly correlated with a higher risk of lymph node metastasis, increased local tumor invasion and reduced overall survival.[205] Consequently, FAP is considered a key target for tumor diagnosis and therapy.[202]

1.3.1 FAP inhibitors based on UAMC-1110

In 2005, Hu *et al*. described the first small molecules capable of inhibiting FAP. [206,207] Through structure-activity relationship studies, they identified X-*boro*Pro compounds (where X stands for an amino acid at position P2 with unsubstituted or substituted amine) as potential FAP inhibitors (FAPIs). Cyclic and aliphatic alkyl groups, which were initially evaluated as *N*-terminal substituents, did not enhance the inhibitory effect. Despite the known preference of FAP for glycine at the P2 position, inhibition by Val-*boro*Pro was also observed. However, since DPP 4 also accommodates valine in this position, Val-*boro*Pro binds to both enzymes and lacks FAP-selectivity. [206,207] Owing to its high potency (IC_{50} value in the nanomolar range), the inhibitor still progressed to phase II clinical trials under the trade name Talabostat but was subsequently discontinued due to safety concerns, possibly related to the limited selectivity.[206,208,209] Consequently, various research groups have continued the development of selective FAPIs.[210] One major challenge in this field has been to achieve the required selectivity for FAP over PREP, since there is significant overlap in the substrate sequences processed by the two enzymes.[198] In 2013, Jansen *et al*. published a study exploring potential FAPIs based on a 2-cyanopyrrolidine scaffold.[209] Among the 35 compounds examined, two exhibited low nanomolar affinity and high selectivity for FAP over DPPs and PREP. Based on their findings, they identified the *N*-(4-quinolinoyl)-glycyl-(2-cyanopyrrolidine) scaffold as a promising basis for FAPI development.[209] In a follow-up study published one year later, the authors investigated an additional 60 compounds and identified UAMC-1110 (Figure 14) as the most potent candidate.[198] UAMC-1110 exhibited IC_{50} values of 3.2 nM for FAP and 1.8 µM for PREP, along with favorable pharmacokinetic properties.[198]

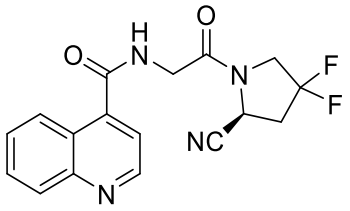

Figure 14: Structure of UAMC-1110.[198]

Building on these findings, Loktev *et al*. synthesized two FAPIs for nuclear medicine applications.[211] The radiotracer [^{125}I]FAPI-01 was prepared by radioiodination of a stannyl precursor derived from an UAMC-1110 analog without fluorine substituents on the pyrrolidine ring (Figure 15). FAPI-02 was obtained by modification of the same pharmacophore with a linker and chelator (Figure 15) connected to the quinolyl fragment at the sixth position, enabling labeling with both diagnostic (^{68}Ga) and therapeutic (^{177}Lu or ^{90}Y) radionuclides. These radioligands exhibited high specificity and affinity, as well as rapid internalization by FAP-expressing cells *in vitro* and *in vivo*. The ^{68}Ga-labeled tracer was also evaluated in cancer patients, demonstrating high tumor uptake and providing high-contrast PET images.[211]

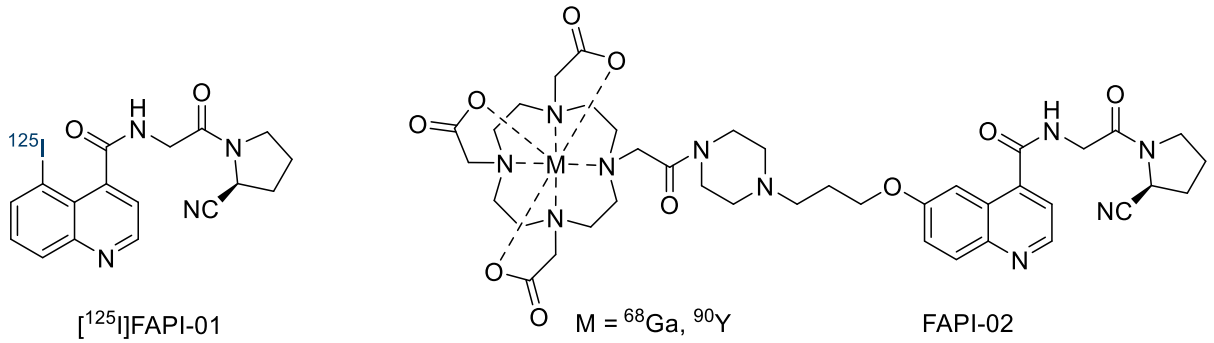

Figure 15: Structures of FAPI-01 and FAPI-02.[211]

The Heidelberg group around Haberkorn *et al*. subsequently synthesized several FAPIs (FAPI-03 – FAPI-15) based on UAMC-1110 or its analogs.[212] Among them, FAPI-04 emerged as a particularly promising candidate for therapeutic applications, offering improved tumor uptake and retention compared to FAPI-02 (Figure 16).[212] Loktev *et al*. later introduced FAPI-46, which exhibited even better tumor retention.[213] Most clinical studies performed to date have utilized radiolabeled analogs of FAPI-04 or FAPI-46.[214] For example, Kratochwil *et al*. published a seminal study with [^{68}Ga]FAPI-04, in which they demonstrated that the tracer exhibits tumor uptake in 28 different types of cancer.[215] Nevertheless, tumor retention of existing FAPIs remains insufficient for therapeutic applications.[216]

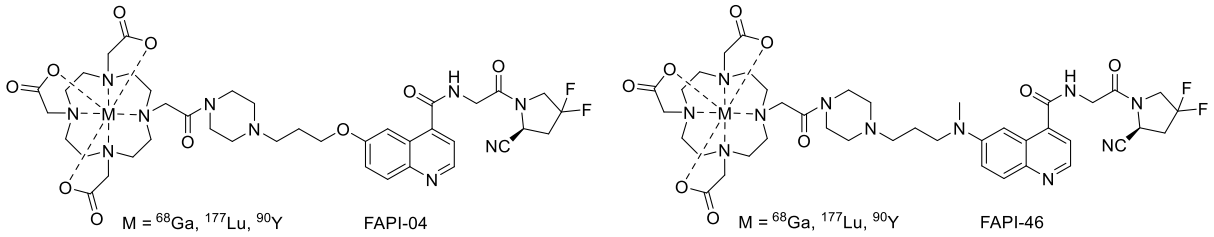

Figure 16: Structures of FAPI-04 and FAPI-46.[212,213]

To simplify the precursor synthesis for FAPIs containing a chelator, Moon *et al*. synthesized FAPIs with a squaric acid (SA)-based linker between the UAMC-1110 motif and the chelator (Figure 17). While [^{68}Ga]DOTA.SA.FAPI showed favorable imaging characteristics, [^{177}Lu]DOTA.SA.FAPI was rapidly cleared from the tumor within 48 hours post-injection.[217] To enhance tumor retention and FAP affinity, dimeric variants like DOTAGA.(SA.FAPI)$_2$ or DOTA.(SA.FAPI)$_2$ were also developed.[218] In an early clinical study, the ^{177}Lu-labeled dimer DOTAGA.(SA.FAPI)$_2$ exhibited promising therapeutic potential.[219] Based on FAPI-47, a chinese research group further extended this concept by producing tetramers to prolong tumor retention.[220]

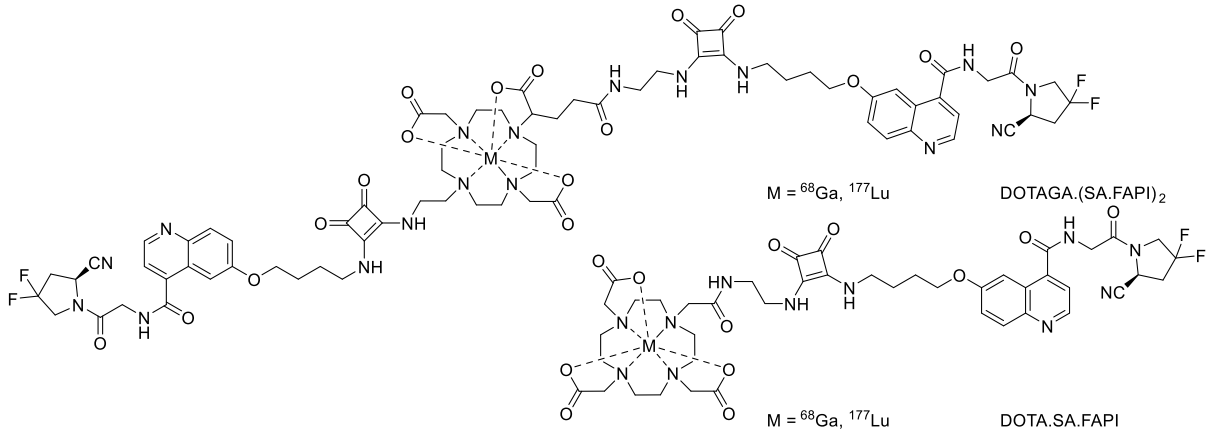

Figure 17: Structures of DOTAGA.(SA.FAPI)$_2$ and DOTA.SA.FAPI.[217,218]

To enable the preparation of radiofluorinated analogs for PET imaging, FAPI derivatives were also modified for ^{18}F labeling. The Heidelberg group substituted the DOTA chelator in FAPI-02 with NOTA, affording an analog (FAPI-74) that could be labeled with either ^{68}Ga or Al[^{18}F]F.[221] In the preceding year, Cui *et al*. introduced CTR-FAPIs, designed to bind irreversibly to FAP.[222] These compounds utilize SuFEx warheads like aryl sulfonyl fluorides or aryl fluorosulfates for covalent modification of tyrosine residues or other amino acids within the protein, rather than directly binding to the enzyme's active site.[186,222] SuFEx warheads were selected due to their proximity-dependent reactivity, which offers increased bioorthogonality and high stability until the target is reached. The study indicated that this approach could

significantly enhance the pharmacokinetics and tumor specificity, resulting in a 13-fold increase in tumor accumulation.[222]

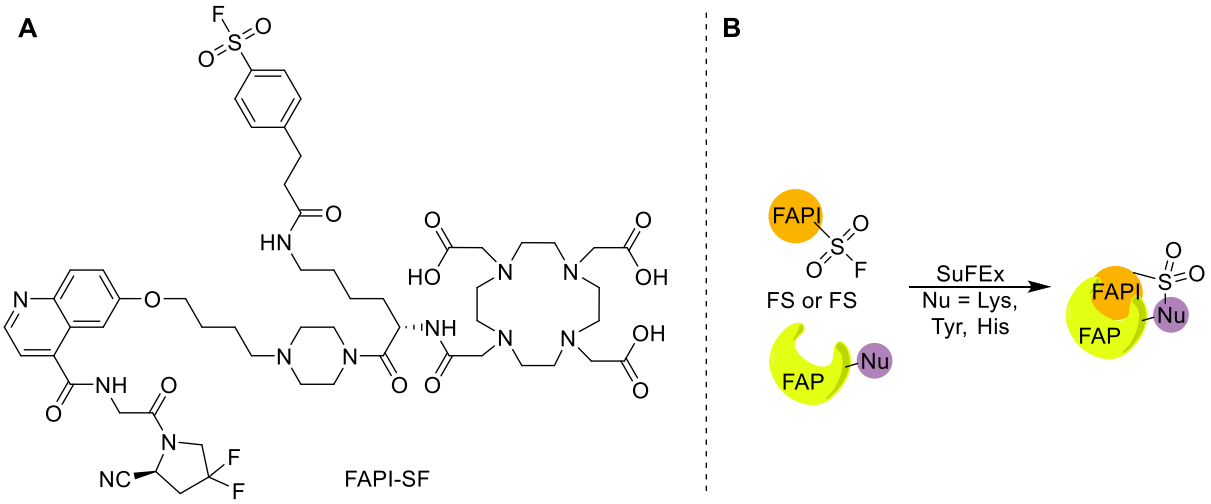

Figure 18: A: Structure of FAPI-SF, a covalent FAPI that binds via the sulfonyl fluoride group; B: Scheme of proximity-based SuFEx ligation on FAP.[222]

2 Aim

The primary aim of this work was to develop novel FAPIs based on UAMC-1110 that can form irreversible covalent bonds with the serine or other nucleophilic residues in the active site of FAP, thereby improving *in vivo* tumor retention. To achieve this, the nitrile group on the pyrrolidine ring should be replaced by more reactive covalent warheads. The warheads, which should be investigated included sulfonyl fluorides, phosphonofluoridates, and fluoridodithioates (Figure 19). These warheads should be labeled with fluorine-18 to enable indirect detection of covalent bond formation through the release of [^{18}F]fluoride. This release results from a nucleophilic attack by serine (or other) residues in the FAP enzyme pocket, which displaces [^{18}F]fluoride as a leaving group during covalent binding.

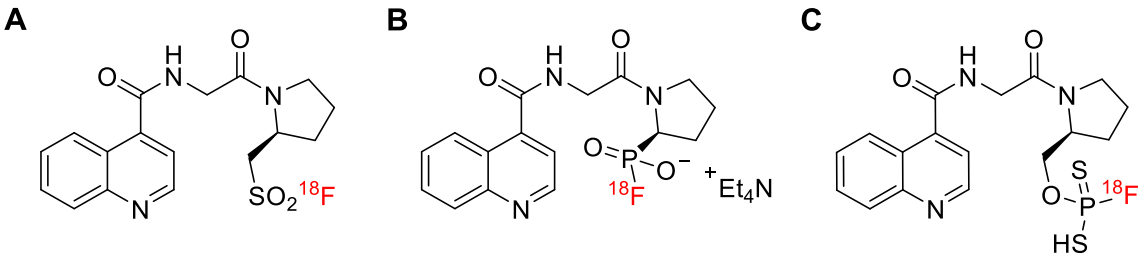

Figure 19: Structures of the target compounds with the corresponding warhead; A: sulfonyl [^{18}F]fluorides; B: phosphono[^{18}F]fluoridates; C: [^{18}F]fluoridodithioates.

The hydrolytic and blood plasma stability of these radiolabeled UAMC-1110 analogs should be first evaluated. The sufficiently stable candidate(s) should further be examined in the [^{18}F]fluoride release test using FAP as well as structurally similar enzymes like DPP 2, DPP 4, DPP 9, and PREP. A sensitive and simple detection method for monitoring [^{18}F]fluoride release in enzyme assays using radio-TLC and/or adsorption on hydroxyapatite should be additionally developed.

The second aim of this work was to prepare an ^{18}F-labeled 2-PMPA derivative with ^{18}F-substitutent attached to phosphor of the phosphate group. 2-PMPA has subnanomolar affinity for prostate specific membrane antigen (PSMA) and represents the current gold standard for assessing the binding affinity of novel PSMA inhibitors *in vitro*. The description of the preparation of the corresponding radiolabeling precursor as well as model radiolabeling substrates, their radiolabeling and attempts to deprotect ^{18}F-fluorinated protected 2-PMPA can be found in **Annex**.

3 Results and Discussion

3.1 Synthesis and stability investigation of a potential covalent FAP inhibitor containing a sulfonyl [^{18}F]fluoride functionality

Radiolabeled fibroblast activation protein (FAP) inhibitors (FAPIs) have emerged as valuable radiotracers for imaging a wide range of tumor types. However, rapid washout from the tumor microenvironment limits their suitability for therapeutic applications. To overcome this limitation through formation of a covalent bond with the serine residue in the active site of FAP, a novel FAPI with a sulfonyl fluoride warhead was synthesized. In addition, an optimized protocol for radiofluorination of the compound via sulfur(VI) fluoride exchange (SuFEx)-based ultrafast ^{18}F/^{19}F isotopic exchange was developed to enable detection of covalent bond formation based on the release of [^{18}F]fluoride. The radiolabeled FAPI was obtained with a radiochemical conversion of 53 ± 12% (n=8) and a radiochemical yield of 24 ± 3% (n=5). Stability tests demonstrated moderate to good stability in phosphate-buffered saline and acidic media, but suffered rapid defluorination in blood plasma.

3.1.1 Introduction

The potential of sulfonyl fluorides as covalent modifiers of serine proteases was demonstrated by Guardiola *et al*. in studies on the serine hydrolase prolyl oligopeptidase (POP), which is closely related to fibroblast activation protein. POP, also referred to as PREP, is a cytosolic protease that hydrolyzes post-proline bonds of small peptides and is prominently expressed in the brain.[223,224] Research has shown that POP interacts with other proteins and contributes to their colocalization in the brains of patients with Parkinson's disease.[223,225] Due to POP's involvement in the pathogenesis of several cognitive disorders, including schizophrenia, several POP inhibitors have been developed.[223] However, clinical trials with these inhibitors were unsuccessful, primarily due to limited selectivity and insufficient blood-brain barrier penetration.[223,226] In the last decade, attention has shifted toward the synthesis of covalent POP inhibitors, though these have often suffered from fast hydrolysis of the covalent bond. In 2018, Guardiola *et al*. used structure-guided design to develop selective and membrane-permeable POP inhibitors capable of covalently binding to serine-554 in the enzyme's active site.[223] These inhibitors are functionalized at position P1 with a sulfonyl fluoride group, which is a slightly reactive electrophile that should form an irreversible covalent bond with the serine residue, thereby inhibiting catalytic activity (Figure 20). In addition to their notable potency in the nanomolar range, these compounds exhibited 1000-fold *in vitro* selectivity for POP over dipeptidyl peptidase 4 (DPP 4) and FAP, two closely related serine proteases. These findings

exemplify the potential of sulfonyl fluoride-functionalized inhibitors as tools for selective POP inhibition and for investigating POP enzyme function in central nervous system diseases.[223]

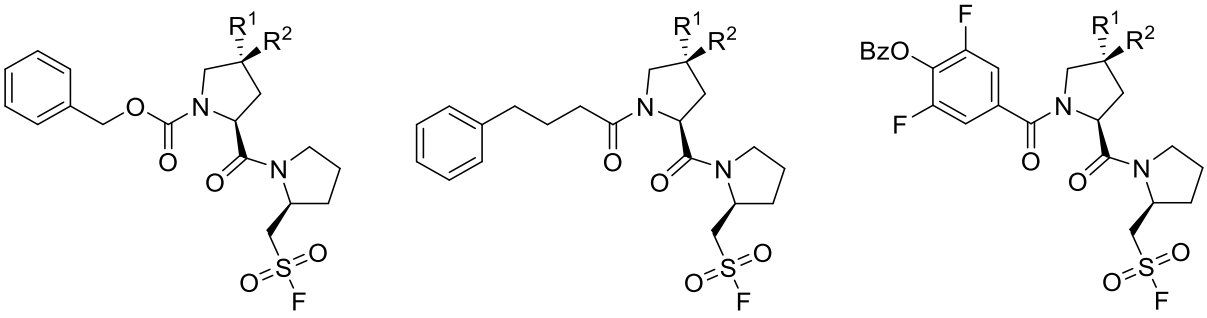

R^1 = H, F
R^2 = H, F, CF_3, CH_3

Figure 20: Structures of POP inhibitors described by Guardiola *et al*.[223]

Inspired by the covalent POP inhibitors developed by Guardiola *et al*., which utilize a sulfonyl fluoride warhead,[223] we replaced the nitrile group on the pyrrolidine moiety of UAMC-1110, the potent FAP inhibitor, developed by Jansen *et al*. [198], with a sulfonyl fluoride functionality, which was further radiofluorinated using the protocol for $^{18}F/^{19}F$-isotpic exchange developed in our group (Figure 21). For the sake of simplicity, the two fluorine substituents on the pyrrolidine ring were additionally substituted by hydrogen ones.

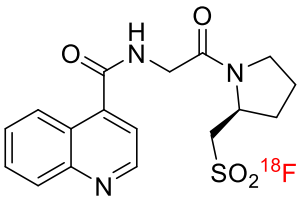

Figure 21: Target compound with a sulfonyl [^{18}F]fluoride warhead.

3.1.2 Results and Discussion

3.1.2.1 Chemistry

The synthesis of the radiolabeling precursor/the reference compound **11** involved two literature-known building blocks: (quinoline-4-carbonyl)glycine (**3**)[198] and (*S*)-pyrrolidin-2-ylmethanesulfonyl fluoride hydrochloride (**8**)[223] (Scheme 28), which could be obtained via three- and four-step synthesis sequences, respectively.

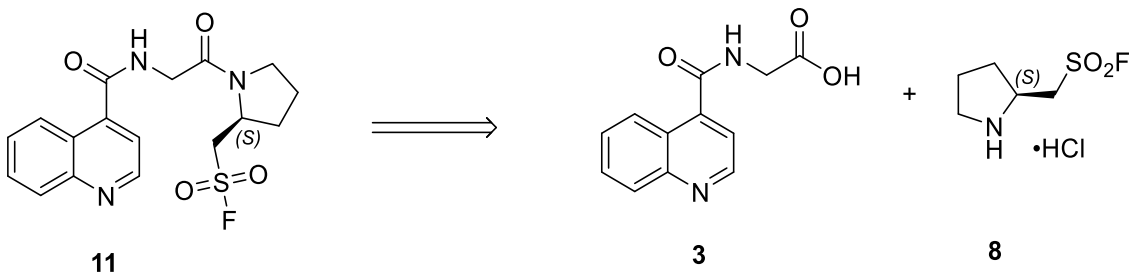

Scheme 28: Synthesis of (*S*)-(1-((quinoline-4-carbonyl)glycyl)pyrrolidin-2-yl)methanesulfonyl fluoride (**11**).

The synthesis of compound **3** was performed according to the protocol by Wilson *et al*.[227] for the first step, and the procedure outlined by Jansen *et al*.[198] for the remaining steps. In the initial step, 4-quinolinecarboxylic acid was quantitatively converted to the corresponding acid chloride **1** using oxalyl chloride under DMF catalysis.[227] This intermediate was then reacted with glycine methyl ester hydrochloride or glycine ethyl ester hydrochloride in the presence of triethylamine, affording the respective amides in excellent yields of 94% for the methyl ester (**2a**) and 97% for the ethyl ester (**2b**). After saponification with NaOH and acidification with HCl, **3** was obtained in yields of 59% and 73%, respectively, from the methyl and ethyl ester (Scheme 29).[198]

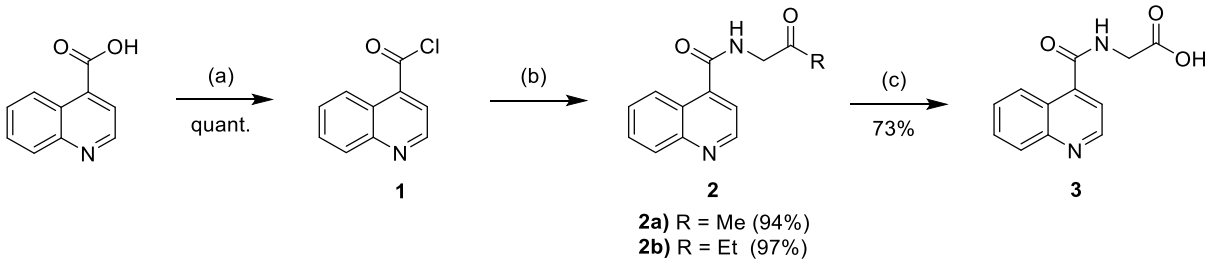

Scheme 29: Synthesis of **3** according to protocols by Wilson *et al*.[227] and Jansen *et al*.[198] Reaction conditions: a) Oxalyl chloride, DMF, CH_2Cl_2, 0 °C – rt, 18 h; b) Glycine methyl ester hydrochloride (**2a**) or Gylcine ethyl ester hydrochloride (**2b**), Et_3N, CH_2Cl_2, 0 °C – rt, 24,5 h; c) NaOH, MeOH/H_2O (1:1), rt, 18 h, then: HCl.

Compound **8** was prepared according to the procedures by Guardiola *et al.*[223] and Brouwer *et al*.[228] In the first step, *Z*-*L*-prolinol was converted to the corresponding mesylate. The resulting sulfonate was subjected to nucleophilic substitution with generated cesium thioacetate, affording the thiol acid ester **4** in 69% yield.[223] Subsequent oxidation of **4** with H_2O_2 and reaction with sodium acetate provided sodium sulfonate **5** in 98% yield,[223] which was fluorinated with XtalFluor-M® to produce the Cbz-protected sulfonyl fluoride **7** in 29% yield (Scheme 30). Finally, deprotection of **7** with HBr in AcOH afforded the desired target compound **8** in 92% yield.[223]

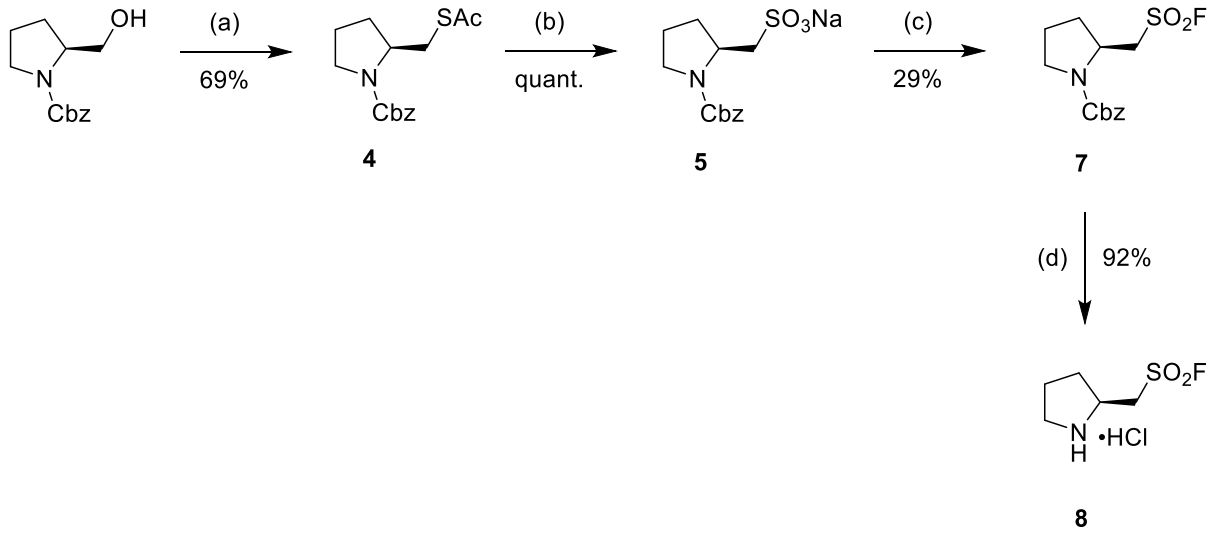

Scheme 30: Synthesis of **8** according to protocols of Guardiola *et al*.[223] Reaction conditions: a) Et_3N, methanesulfonyl chloride, CH_2Cl_2, 0 °C – rt, 17,5 h, then: Cs_2CO_3, thioacetic acid, DMF, rt, 3 d; b) H_2O_2, AcOH, rt, 17 h, then: NaOAc•$3H_2O$, 20 min, rt; c) XtalFluor-M®, Et_3N•HF, reflux, 4d; d) HBr in AcOH, CH_2Cl_2, rt, 1 h.

Due to the low yield of **7** obtained via the XtalFluor-M®-mediated reaction, alternative reaction routes were also evaluated. First, compound **5** was chlorinated using triphosgene and catalytic DMF to obtain sulfonyl chloride **6**[228], which was then fluorinated with KHF_2 at ambient temperature in acetone. Unfortunately, no product could be isolated. As an alternative, **5** was chlorinated with oxalyl chloride[229] in benzene followed by fluorination with potassium bifluoride, which afforded **7** in 65% yield (Scheme 31).[186] To further streamline the synthesis, one reaction step was eliminated by using a modified reaction route: compound **4** was directly chlorinated with *N*-chlorosuccinimide (NCS)[230], giving **6** in 90% yield. Subsequent fluorination of **6** with potassium bifluoride furnished **7** in 73% yield (Scheme 31).

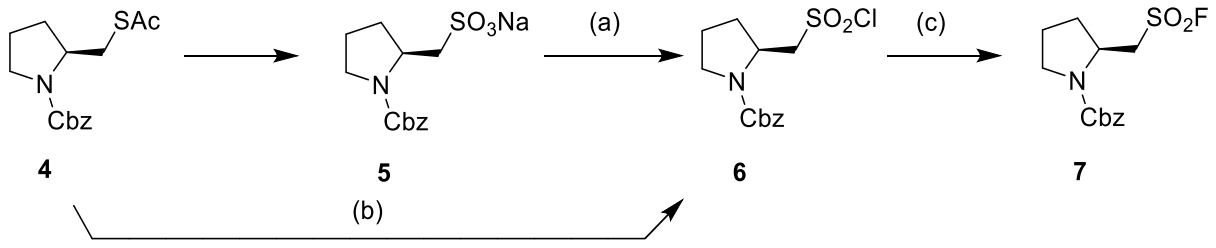

Scheme 31: Synthesis of **7** by alternative reaction routes. Reaction conditions: a) $(COCl)_2$, DMF, C_6H_6, 0 °C – rt, 35 min[229]; b) NCS, HCl, MeCN, 0 °C, 80 min[230], 90%; c) KHF_2, MeCN/H_2O, rt, 92 h[186], 65% via **6** from a), 73% via **6** from b.

Compound **11** should be initially prepared by coupling **8** with the acid chloride obtained from **3**, prepared using $(COCl)_2$/DMF (cat.). As the desired amide was not obtained under these conditions, the coupling reagent *N*-ethoxycarbonyl-2-ethoxy-1,2-dihydroquinoline (EEDQ) was applied instead. EEDQ, originally described by Belleau *et al*.[231,232], is a classic reagent for peptide synthesis. Carboxylic acids can be converted to amides with amines in the presence

of EEDQ[233], whereby the coupling reaction proceeds via reaction of the amine with a mixed carboxylic acid anhydride intermediate (Scheme 32).[232,234] The reaction does not require a tertiary base and, since the mixed anhydride is only formed slowly and immediately consumed by aminolysis in the presence of the amine, the formation of by-products and racemization is minimized.[232,235]

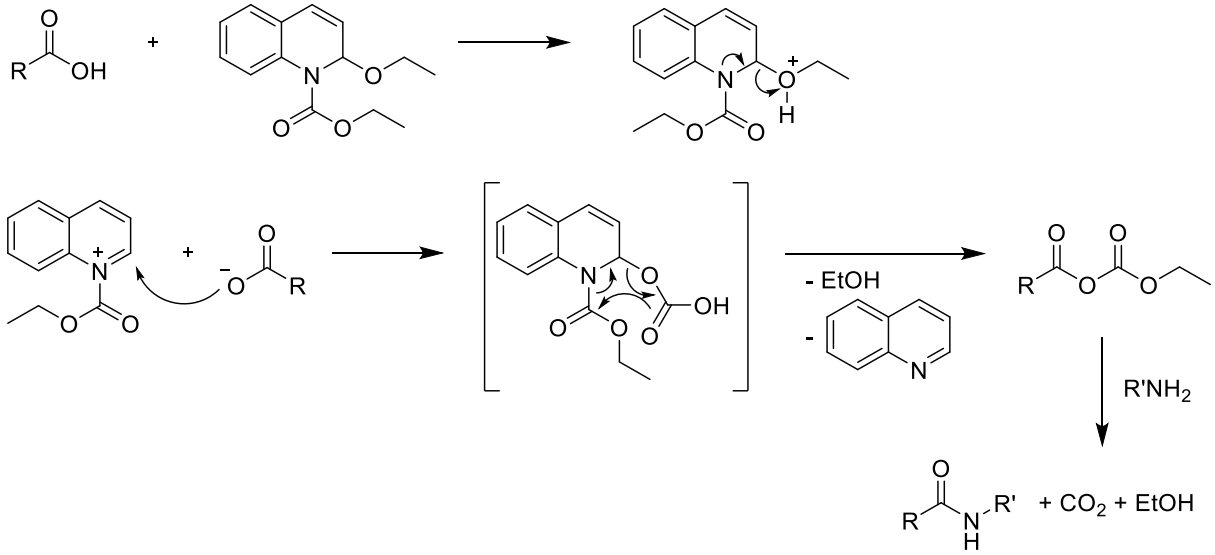

Scheme 32: Formation of mixed anhydrides by EEDQ and subsequent amide formation.[232,234,235]

An analogous model reaction was initially performed with *L*-proline methyl ester hydrochloride (**9**).[236] **9** was then reacted with **3** in the presence of EEDQ to obtain methyl (quinoline-4-carbonyl)glycyl-*L*-prolinate (**10**, Scheme 33) in 27% yield after a reaction time of 45 h.

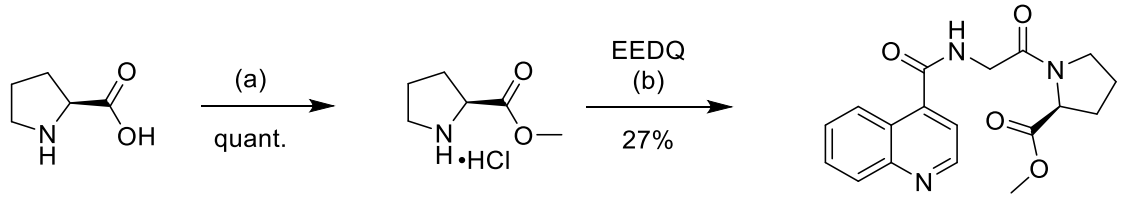

9 **10**

Scheme 33: Synthesis route for the preparation of **10**. Reaction conditions: a) $SOCl_2$, MeOH, 0 °C – rt, 24 h [236]; b) Et_3N, EEDQ, DMF, rt, 45 h.

Finally, compound **11** was prepared by coupling **3** with **8** in the presence of EEDQ, which afforded the desired reference compound and precursor in 19% yield after 119 h.

3.1.2.2 Radiochemistry

Radiolabeling of **11** was performed using the SuFEx-based $^{18}F/^{19}F$ isotopic exchange protocol previously developed in our group.[84] To this end, [^{18}F]fluoride was loaded onto a QMA

cartridge, which thereafter was rinsed with MeOH to remove residual H_2O. The cartridge was dried with air to remove residual MeOH and the [^{18}F]fluoride was eluted with a solution of tetrabutylammonium perchlorate (TBAP, 10 µmol) in dry MeOH (1 mL). The MeOH was removed, a solution of **11** (100 nmol) in MeCN (1 mL) was added, and the reaction mixture was heated for 7 min at 40 °C under argon without stirring. Suprisingly, HPLC analysis after quenching of the reaction mixture with H_2O revealed no detectable formation of the desired product [^{18}F]**11** (Table 3, entry 1). Subsequent attempts to optimize the reaction conditions by reducing the reaction time to 3 min (Table 3, entry 4), or by increasing the reaction temperature to 50−60 °C (Table 3, entry 2–3), likewise yielded no formation of [^{18}F]**11**.

Table 3: Screening (n=1) of reaction conditions for radiofluorination of **11** with TBAP as elution salt.

Entry	TBAP (µmol/mL)	Reaction time (min)	Reaction temperature (°C)	Radiochemical conversion (%)
1	10	7	40	0
2		7	50	0
3		7	60	0
4		3	40	0

Replacing TBAP with benzyltriethylammonium chloride ($BnEt_3NCl$) as the elution salt and reducing the quantity from 10 µmol to 2.5 µmol resulted in no radiochemical conversion (RCC) after 3 min at 60 °C, but afforded [^{18}F]**11** in an RCC of 5% after 3 min at 40 °C (Table 4, entry 2). Further screening using $BnEt_3NCl$ revealed that the RCCs increased with decreasing reaction temperature. Furthermore, the reaction time was systematically varied (Table 4, entries 5–9). The highest RCC was observed after a reaction time of 5 min at 0 °C (Table 4, entry 7). Consequently, the optimized reaction conditions (2.50 µmol $BnEt_3NCl$ as elution salt, a reaction time of 5 min, and a reaction temperature of 0 °C) were adopted for all subsequent radiolabeling experiments with **11**, whereby RCCs of 53 ± 12% (n=8) could be achieved. After isolation by solid-phase extraction and elution with EtOH or DMSO (0.5 mL), the tracer was obtained in radiochemical yields (RCYs) of 24 ± 3% (n=5) and with a radiochemical purity (RCP) of >95%.

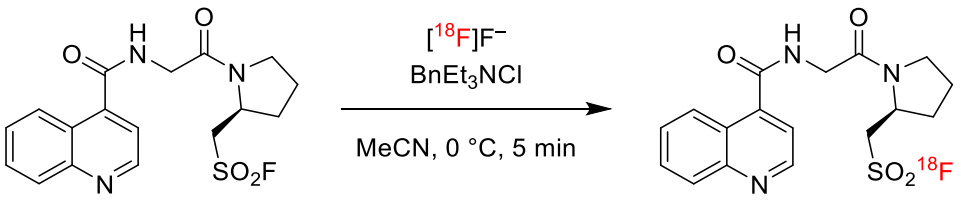

11 [^{18}F]**11**

Scheme 34: Radiofluorination of **11** via ^{18}F/^{19}F isotopic exchange.

Table 4: Screening (n=1) of reaction conditions for the radiofluorination of **11** using 2.50 µmol $BnEt_3NCl$ in MeOH (0.7 mL) as elution salt.

Entry	Reaction time (min)	Reaction temperature (°C)	Radiochemical conversion (%)
1	3	60	0
2	3	40	5
3	3	30	10
4	3	20	38
5	3	0	54
6	4	0	32
7	**5**	**0**	**68**
8	6	0	28
9	7	0	59

*3.1.2.3 Stability study of [^{18}F]**11** in aqueous solutions*

The stability of [^{18}F]**11** was assessed in aqueous solutions across a range of pH values. In addition to H_2O, stability was examined in phosphate-buffered saline (PBS) at a physiological pH of 7.4, as well as in acidic media with pH values between 2 and 5. All stability assessments were conducted at ambient temperature over a period of 2 h, except for a test in sodium acetate buffer at pH 4, in which the solution was heated to 100 °C for 10 min, followed by stability monitoring at ambient temperature.

Significant defluorination of the tracer was observed in both H_2O and PBS (Figure 22). It is well established that alkyl sulfonyl fluorides exhibit lower stability than their aryl counterparts.[183,184] Nevertheless, under certain kinetic and spatial conditions, the conversion of fluoride into a leaving group is desirable, as it is essential for the “click” reactivity characteristic of sulfonyl fluorides.[237] In the experiments conducted here, [^{18}F]**11** exhibited half-lives of 117 min and 124 min in H_2O and PBS, respectively. The released [^{18}F]fluoride could be clearly detected at the baseline of the respective radio-NP-TLC analyses (Figure 22).

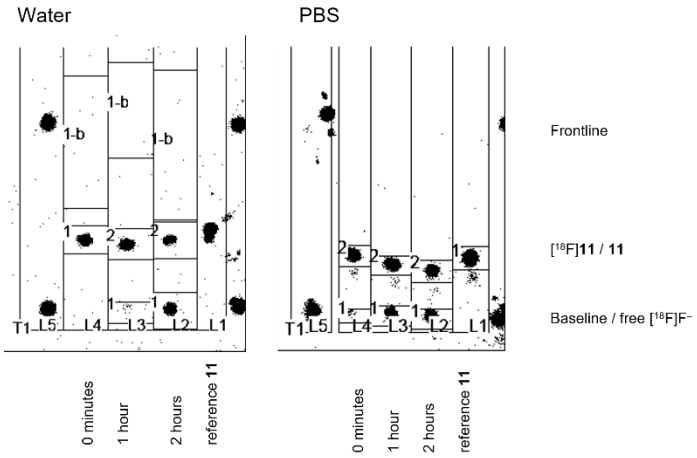

Figure 22: Radio-NP-TLC of stability tests with [^{18}F]**11** in H_2O and PBS, solvent mixture: 4% MeOH in CH_2Cl_2.

In contrast, radio-NP-TLC demonstrated that [^{18}F]**11** was stable in sodium acetate buffer (pH 4) at ambient temperature. Incubation at 100 °C for 10 min in the same buffer resulted in 27% defluorination.

*3.1.2.4 Stability study of [^{18}F]**11** in human blood plasma*

The stability of [^{18}F]**11** was further investigated in human blood plasma. To this end, an aliquot of [^{18}F]**11** in DMSO (1 µL) was added to fresh human blood plasma (1 mL), and the mixture was incubated at 37 °C in a thermoshaker. Aliquots were removed at 5, 15, 30 and 60 min and analyzed by radio-NP-TLC. The results indicated rapid degradation of the tracer: within just 5 min, 40–50% of [^{18}F]**11** had already undergone defluorination. After 15 min, only 10 ± 4.3% of the tracer remained intact, and this was reduced to 3.6 ± 1.6% after 30 min. By the 60-min mark, the complete (>98%) defluorination took place. These data correspond to a calculated half-life of 5.7 min, with recovery of radioactivity in organic solvents ranging from 65% to 86% (Figure 23).

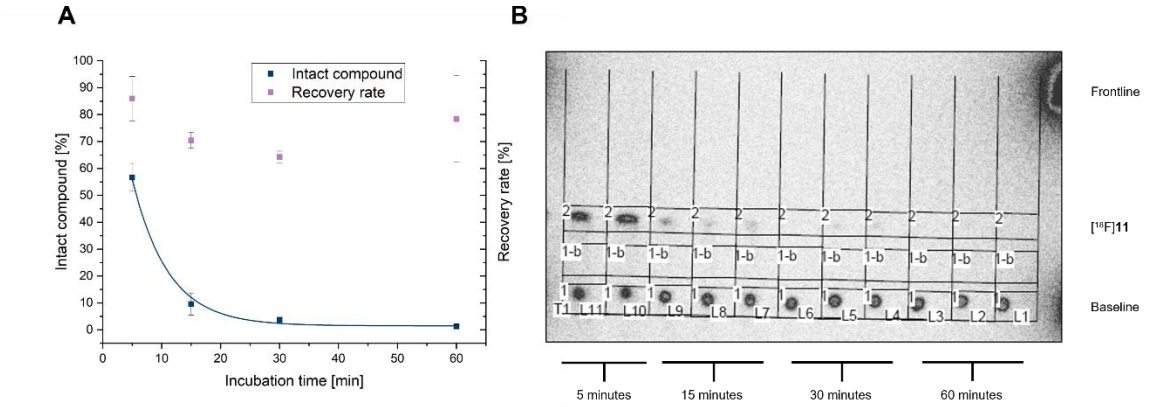

Figure 23: A) Stability of [^{18}F]**11** in human blood plasma and the recovery rate. B) Radio-NP-TLC of the stability test in human blood plasma, solvent mixture: 4% MeOH in CH_2Cl_2.

3.1.3 Conclusion

A novel FAP inhibitor with a sulfonyl fluoride-based warhead was successfully synthesized over eight steps in an overall yield of 11%. Subsequent radiofluorination by SuFEx-based $^{19}F/^{18}F$ isotopic exchange afforded the ^{18}F-labeled isotopolog [^{18}F]**11** in RCCs and RCYs of 58 ± 12% and 24 ± 3%, respectively. [^{18}F]**11** exhibited excellent stability at pH 4 and satisfactory stability in H_2O and PBS. However, the low stability in human blood plasma precluded further evaluation of the tracer. Accordingly, the development of a covalent FAP inhibitor should be focused on the alternative warhead structures.

3.2 Synthesis and radiolabeling of phosphonate model compounds

Fluorophosphonates and diphenylphosphonate are well-established agents for the inactivation of serine hydrolases.[170] Due to their highly electrophilic centers, fluorophosphonates have the capacity to react with or phosphorylate serine residues located in the active site of these enzymes.[170] The aim of this study was to evaluate the potential of phosphonofluoridates as covalent warheads for targeting serine proteases, with a special focus on fibroblast activation protein (FAP). Prior to synthesizing a FAP-specific covalent inhibitor, phosphonate model compounds were synthesized based on the work of Wang *et al.*[169] and radiofluorinated to assess the influence of steric effects on their stability in different media (Figure 24).

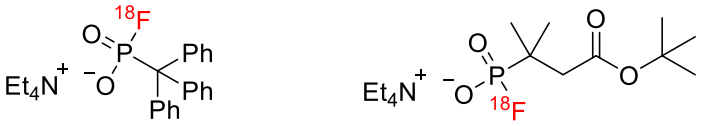

Figure 24: Radiofluorinated phosphonate model compounds.

3.2.1 Synthesis of tritylphosphono[^{18}F]fluoridate (**[^{18}F]13**)

*3.2.1.1 Synthesis of diphenyl tritylphosphonate (**12**) and tritylphosphonofluoridate tetrabutylammonium salt (**13**)*

In order to evaluate the influence of large electron-rich substituents on radiolabeling of substituted diphenyl phosphonates, ^{18}F-fluorination of diphenyl tritylphosphonate (**12**) was studied. The synthesis was achieved by DBU-promoted alkylation of trityl chloride with diphenylphosphite in acetone, which afforded **12** in 57% yield (Scheme 35). The non-radioactive reference compound tritylphosphonofluoridate (**13**) was prepared in 61% yield by nucleophilic substitution of **12** with TBAF according to the protocol of Wang *et al*. (Scheme 35).[169]

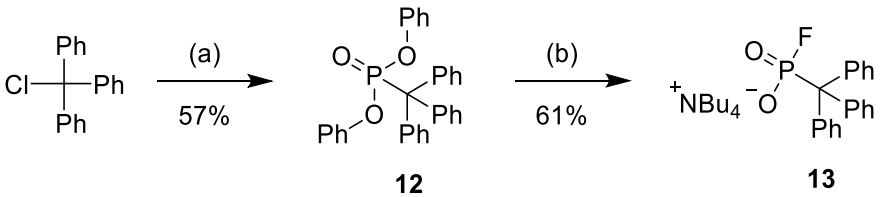

Scheme 35: Reaction scheme for the synthesis of diphenyl tritylphosphonate (**12**) and subsequent synthesis of the non-radioactive reference compound **13**. Reaction conditions: a) diphenyl phosphite, DBU, acetone, 18.5 h, rt; b) TBAF, THF, overnight, rt.

*3.2.1.2 Preparation of tritylphosphono[^{18}F]fluoridate ([^{18}F]**13**)*

12 was labeled using the protocol described by Wang *et al*.[169] Accordingly, [^{18}F]fluoride was fixed on a QMA cartridge, eluted with a solution of Kryptofix® 222 (K_{222}, 8 mg) and K_2CO_3 (1 mg) in MeCN:H_2O (1 mL, 4:1, v/v) and the resulting solution was concentrated under reduced pressure in a flow of argon. After repetitive azeotropic drying of the residue with MeCN (3 × 100 µL) at 100 °C, a solution of precursor **12** (0.5 µmol) in MeCN (100 µL) was added and the reaction mixture was stirred for 15 min at 50 °C. However, no radiochemical conversion (RCC) was observed under these conditions (Table 5, entry 1). Upon increasing the reaction temperature to 80 °C, [^{18}F]**13** was formed in RCCs of 12 ± 6% (n=3) along with three radioactive by-products (Table 5, entry 2; Figure 25). The by-products eluted later than the product from RP HPLC column, suggesting that they were more hydrophobic than [^{18}F]**13**.
In the next set of experiments the K_{222}/K_2CO_3 elution solution was replaced with tetraethylammonium bicarbonate ($TEAHCO_3$) in MeOH (1 mg/mL), which allowed for preprocessing of [^{18}F]fluoride without the need for subsequent azeotropic drying. After the elution of [^{18}F]fluoride, all volatiles were evaporated at 80 °C for a few minutes before **12** in MeCN was added and radiofluorinated as described above. In this case, two radioactive by-products were observed, both eluting prior to the main product (Table 5, entry 3). Switching the solvent from MeCN to DMF and testing additional reaction conditions (Table 5, entry 4–7) did not lead to an increase in RCCs or a reduction in by-product formation (Figure 25).
These results suggest that the choice of elution system, solvent, and temperature probably influences the formation of radioactive by-products, but that none of these variables significantly affects the RCCs. The explanation for the low RCCs could be the steric hindrance imposed by the trityl group. Due to the combination of low RCCs, the presence of multiple radioactive by-products, and the limited solubility of the reaction mixture in H_2O, the product was not isolated, and no stability tests were performed.

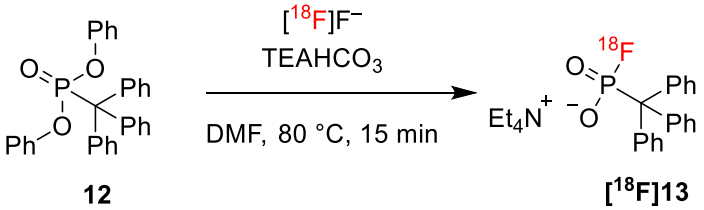

Scheme 36: Radiosynthesis of [^{18}F]**13** from **12**.

Table 5: Optimization of the reaction conditions for radiofluorination of **12** (n=3).

Entry	Elution solution (1.00 mg/mL)	Precursor amount (µmol)	Solvent	Reaction time (min)	Reaction temperature (°C)	Radiochemical conversion (%)		Number of by-products
1	K_{222}/K_2CO_3[a]	0.50	MeCN	15	50	0	*	-

2	K_{222}/K_2CO_3[a]	0.50	MeCN	80	12	±	6	3
3	$TEAHCO_3$	0.50	MeCN	50	5	±	1	2
4	$TEAHCO_3$	0.50	DMF	50	7	±	3	1
5	$TEAHCO_3$	1.00	DMF	50	5		*	1
6	$TEAHCO_3$	0.50	DMF	80	13	±	4	2
7	$TEAHCO_3$	0.50	DMF	rt	1		*	-
8	TEAOTf	0.50	DMF	50	13	±	1**	2

[a] K_{222} (8 mg)/K_2CO_3 (1 mg) in 80% MeCN (1 mL), * n=1; ** n=2.

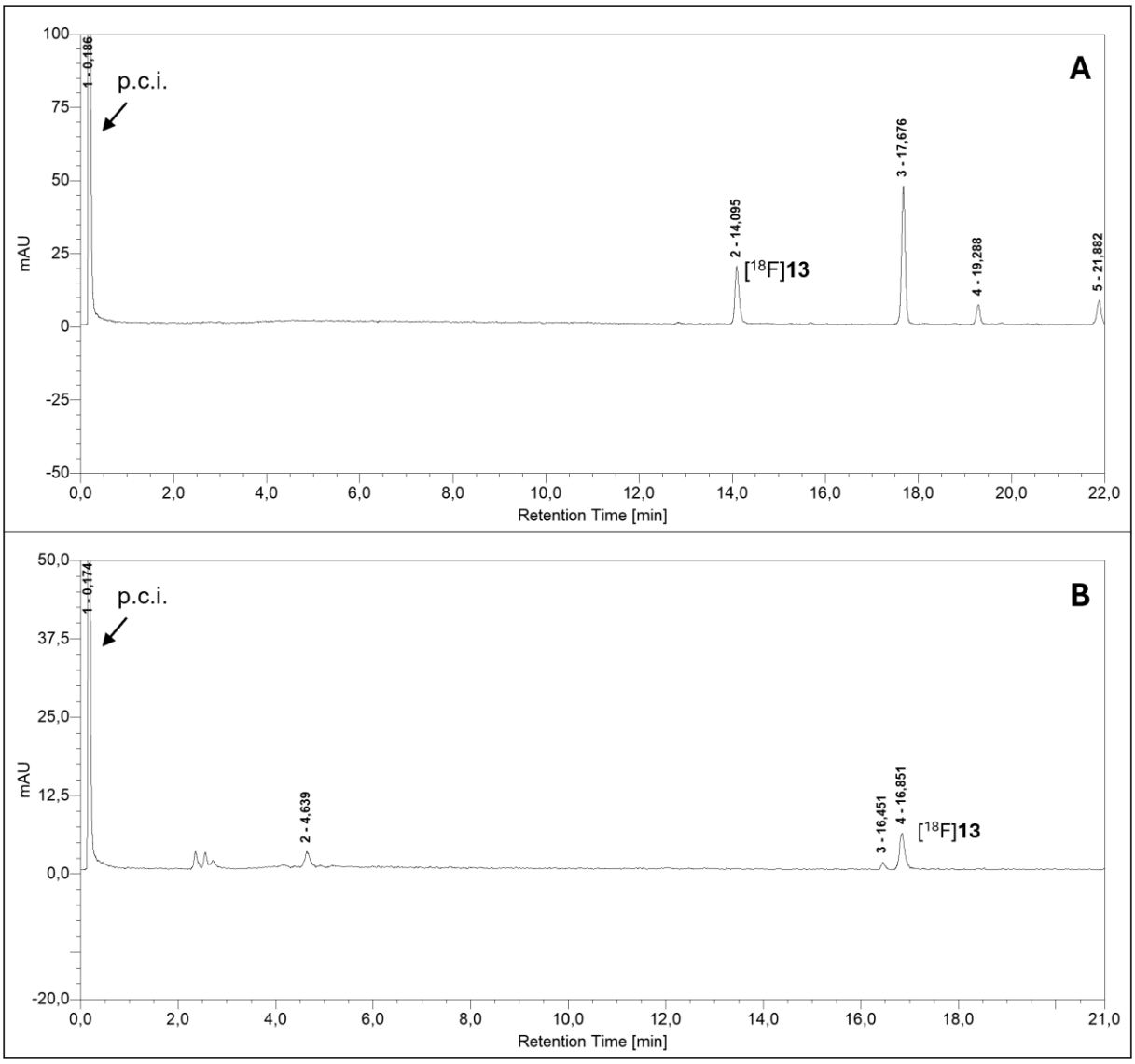

Figure 25: Example HPLC chromatograms of the various radiofluorination reactions of **12**. A) HPLC trace of [^{18}F]**13**. Reaction conditions: Kryptofix® 222 & K_2CO_3 at 80 °C for 15 minutes in MeCN. [^{18}F]**13** elutes at 14.1 min, the radioactive by-products elute later. Column: MultoKrom® 100-5 C18 AQ LC column 250×4.6 mm; eluent: 0–5 min: 20% MeCN (0.1% TFA), 5–17 min: 20→90% MeCN (0.1% TFA), 17–22 min: 90% MeCN (0.1% TFA). Flow rate: 1 mL/min. B) HPLC trace of [^{18}F]**13**. Reaction conditions: $TEAHCO_3$ at 80 °C for 15 min in DMF. [^{18}F]**13** elutes at 16.9 min, the radioactive by-products elute earlier. Column: MultoKrom® 100-5 C18 AQ LC column 2504.6 mm; eluent: 0–5 min: 20% MeCN (0.1% TFA), 5–20 min: 20→80% MeCN (0.1% TFA). The product elutes later under the conditions of B) due to the flatter gradient compared to A). Abbreviation: p.c.i. – post-column injection.

3.2.2 Preparation of (4-(*tert*-butoxy)-2-methyl-4-oxobutan-2-yl)phosphono[^{18}F]fluoridate (**[^{18}F]16**)

The second phosphonate model compound selected for radiofluorination was *tert*-butyl 3-(diphenoxyphosphoryl)-3-methylbutanoate (**15**). This compound contains two methyl groups in alpha position to the phosphorus atom, which should provide steric hindrance. The *tert*-butyl ester was chosen over the free acid, as free acids are often unsuitable for radiofluorination reactions.

*3.2.2.1 Synthesis of tert-butyl-3-(diphenoxyphosphoryl)-3-methylbutanoat (**15**) and (4-(tert-butoxy)-2-methyl-4-oxobutan-2-yl)phosphonofluoridate tetrabutylammonium salt (**16**)*

The synthesis of **15** was accomplished in two steps. Initially, *tert*-butyl 3-methylbut-2-enoate was prepared according to Gillespie.[238] To this end, *tert*-BuOH was deprotonated with *n*-BuLi and the resulting *t*BuOLi was allowed to react with dimethylacryloyl chloride affording the α,β-unsaturated ester **14** in 32% yield (Scheme 37). In the next step, diphenyl phosphite was added to **14** via a trimethylaluminum-mediated conjugate addition (Scheme 37)[239,240], which furnished the labeling precursor **15** in 37% yield.

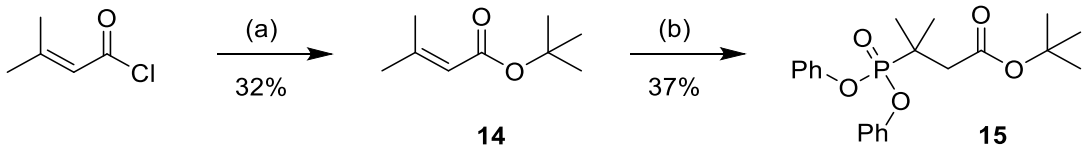

Scheme 37: Synthesis of the labeling precursor **15**. Reaction conditions: a) *t*BuOH, *n*-BuLi, THF, reflux, 1 h; b) diphenyl phosphite, Me_3Al, CH_2Cl_2, rt, overnight.

The non-radioactive reference compound **16** was prepared by nucleophilic substitution of **15** with TBAF in an excellent yield of 96% (Scheme 38).[169]

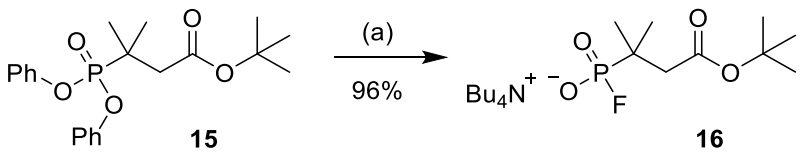

Scheme 38: Fluorination of **15** to obtain the non-radioactive reference compound **16**. Reaction conditions: a) TBAF, THF, rt, overnight.[169]

3.2.2.2 *Radiosynthesis of (4-(tert-butoxy)-2-methyl-4-oxobutan-2-yl)phosphono[^{18}F]fluoridate ([^{18}F]**16**) and stability study in aqueous media*

The radiofluorination of **15** was carried out following the protocol described by Wang *et al.*[169] To this end, [^{18}F]fluoride was eluted from a QMA cartridge with a solution of Kryptofix® 222 (K_{222}, 8 mg) and K_2CO_3 (1 mg) in 80% MeCN (1 mL). After removal of volatiles and repetitive azeotropic drying of the residue with MeCN (3 × 100 µL) at 100 °C, a solution of precursor **15** (0.5 µmol) in MeCN (100 µL) was added, the reaction mixture was stirred for 15 min at 80 °C, and then quenched with H_2O (0.5 mL) before being analyzed by HPLC using the post column injection method.[241] Under these conditions, [^{18}F]**16** was obtained in RCCs of 37 ± 22% (Table 6, entry 1). Application of $TEAHCO_3$ in MeOH (1 mg/mL) for the [^{18}F]fluoride elution resulted in the reduced RCCs to 17 ± 6% (Table 6, entry 2). At 50 °C or ambient temperature, the product formation was observed, even with extended reaction times of up to 20 minutes (Table 6, entries 3–4). Next, the elution with TEAOTf as an elution salt was evaluated affording RCCs of 27 ± 4% at 80 °C (Table 6, entry 8). Given the higher RCCs compared to $TEAHCO_3$ at the same temperatures, further optimization of the reaction parameters was carried out using TEAOTf. Although K_{222}/K_2CO_3 gave even higher RCCs, TEAOTf was favored to avoid the longer overall production times associated with azeotropic drying. Several reaction parameters were varied (Table 6, entries 7–11), including conduction of the reaction under air (Table 6, entry 10–11). The best RCCs of 45 ± 9% were obtained with a reaction temperature of 100 °C and a reaction time of 20 min (Table 6, entry 9).

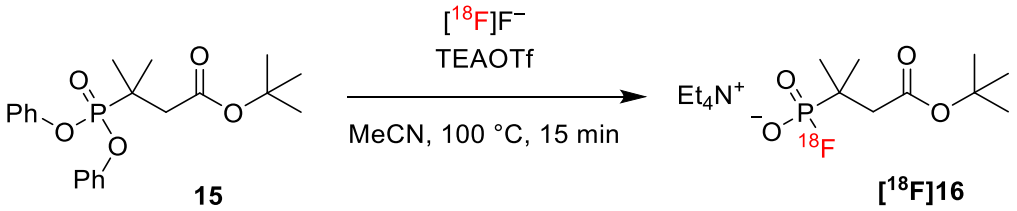

15 **[^{18}F]16**

Scheme 39: Radiosynthesis of [^{18}F]**16** from **15**.

Table 6: Optimization of the reaction conditions for radiofluorination of [^{18}F]**16**.

Entry	Elution solution (1.00 mg/mL)	Reaction time (min)	Reaction temperature (°C)	Radiochemical conversion (%)
1	K_{222}/K_2CO_3[a]	15	80	37 ± 22
2	$TEAHCO_3$	15	80	17 ± 17
3	$TEAHCO_3$	15	rt	0 ± *
4	$TEAHCO_3$	15	50	0 ± *
5	$TEAHCO_3$	20	50	0 ± *
6	TEAOTf	15	80	27 ± 4**

7	TEAOTf	15	60	0	±	*
8	TEAOTf	20	80	40	±	5
9	TEAOTf	20	100	45	±	9***
10	TEAOTf	20	100	37	±	17****/+
11	TEAOTf	15	100	20	±	*/+
12	TEAOTf	15	100	37	±	14***

[a] K_{222} (8 mg)/K_2CO_3 (1 mg) in 1 mL MeCN:H_2O (4:1), * n=1, ** n=4; *** n=7; **** n=3; +: reaction under air.

Attempts to develop a suitable TLC method for [^{18}F]**16** were unsuccessful. However, HPLC analysis of the radiolabeled product spiked with the non-radioactive reference compound confirmed the identity of [^{18}F]**16**.

The product was then isolated by semi-preparative HPLC, followed by solid-phase extraction on a QMA cartridge and formulated in isotonic saline (0.9%). [^{18}F]**16** was obtained in RCYs of 26 ± 12% (n=7) and RCPs in the range of 77–97%. Using a different semi-preparative HPLC column or solvent mixture did not significantly improve the purity.

Stability tests with [^{18}F]**16** over a period of 2 h at ambient temperature were conducted in duplicate in H_2O and PBS (pH 7.4), and in a single trial with 0.1% TFA (pH 2). Immediately after addition of the tracer, and after 1 and 2 h, aliquots were taken and analyzed by HPLC. The results indicated that [^{18}F]**16** is sufficiently stable over a period of 2 h in all three media (Figure 26). Deviations with a tendency toward higher percantages are attributable to the measurement method. These findings suggest that a FAPI based on UAMC-1110 featuring a phosphonate group is likely to exhibit comparable stability, and that steric hindrance does not adversely influence the stability of the phosphonofluoridate moiety.

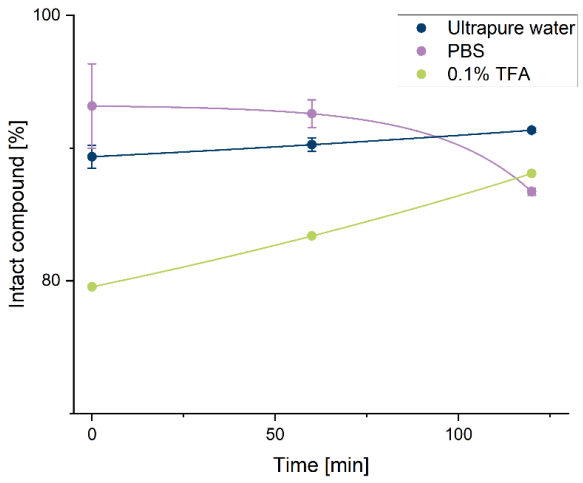

Figure 26: Stability of [^{18}F]**16** in H_2O (blue), PBS (pH 7.4, pink) and 0.1% TFA in H_2O (pH 2, green).

3.3 Synthesis and preliminary *in vitro* evaluation of a potential covalent FAP inhibitor containing a phosphor[^{18}F]fluoridate functionality as warhead

3.3.1 Abstract

Analog of the fibroblast activation protein inhibitor (FAPI) UAMC-1110[198], a derivative, which contains a phosphono[^{18}F]fluoridate instead of nitrile warhead, was prepared (Figure 27).

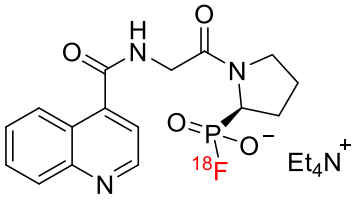

Figure 27: FAPI derivative with a phosphono[^{18}F]fluoridate warhead.

The aim was to determine whether this warhead could form a covalent bond with the active site of FAP,[170] thereby prolonging tumor retention. For simplicity and to facilitate concept verification, the two fluorine atoms on the pyrrolidine ring of UAMC-1110 were omitted. In addition, a second derivative with the same warhead on the pyrrolidine scaffold but lacking the quinolone backbone was synthesized to serve as a negative control (Figure 28).

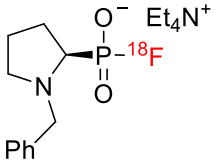

Figure 28: Structure of the second derivative without the quinolone backbone.

Since the inhibitory activity of UAMC-1110 is largely attributable to its quinolone backbone, it was hypothesized that an inhibitor devoid of this fundamental structure would lack affinity for FAP. This experimental design was intended to confirm that the covalent FAPI selectively interacts with FAP, while the structurally distinct control compound does not bind or react with the enzyme's active site despite containing the same warhead.

3.3.2 Results and Discussion

3.3.2.1 Chemistry

Synthesis of the reference compound (**23**) and radiolabeling precursor (**22**) for [^{18}F]**23**

The diphenylphosphonate precursor **22** was prepared by the acylation of diphenyl (*R*)-pyrrolidin-2-ylphosphonate [(*R*)-**21**] with 2,3,5,6-tetrafluorophenyl (quinoline-4-carbonyl)glycinate (**17**) (Scheme 40). Both building blocks were obtained via four-step synthetic routes.

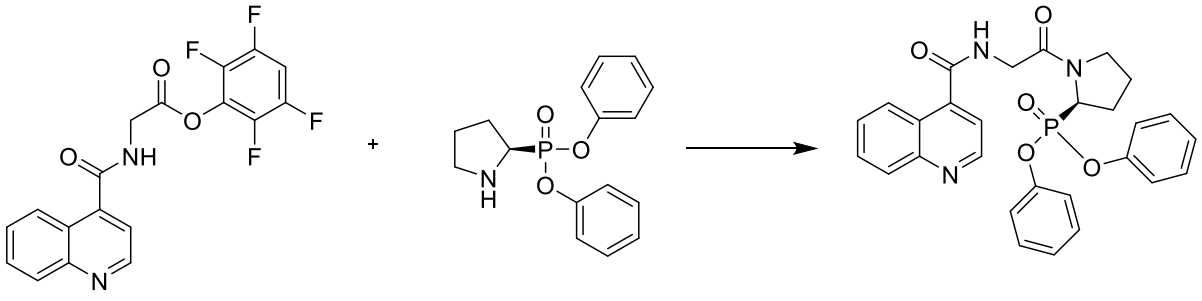

17 (*R*)-**21** **22**

Scheme 40: Synthesis of precursor **22**.

The TFP ester **17** was prepared in 26% yield by reacting **3** (synthesized according to established procedures[198,227], for details see section 3.1.2.1) with 2,3,5,6-tetrafluorophenol in the presence of DCC as coupling agent (Scheme 41).

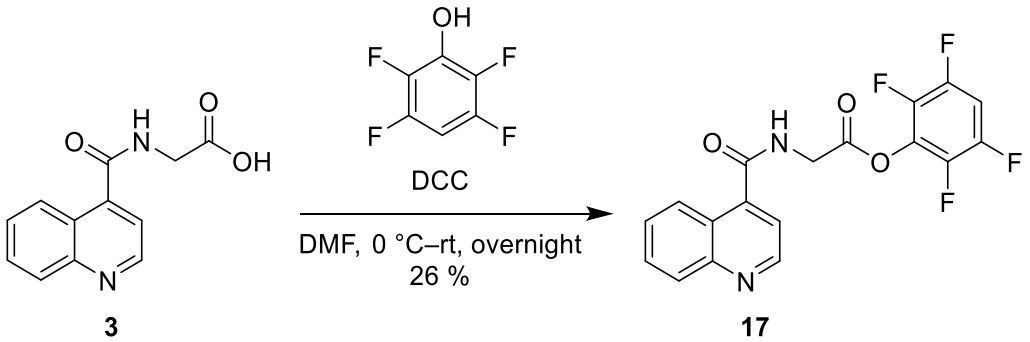

3 **17**

Scheme 41: Synthesis of **17** from **3** and TFP.

The synthesis of (*R*)-**21** was initially attempted via the route described by Katrizky *et al*.[242], which involves a double Robinson-Schöpf condensation to form a chiral oxazolopyrrolodine, followed by an Arbuzov reaction with triethylphosphite and hydrogenation (Scheme 42).[242]

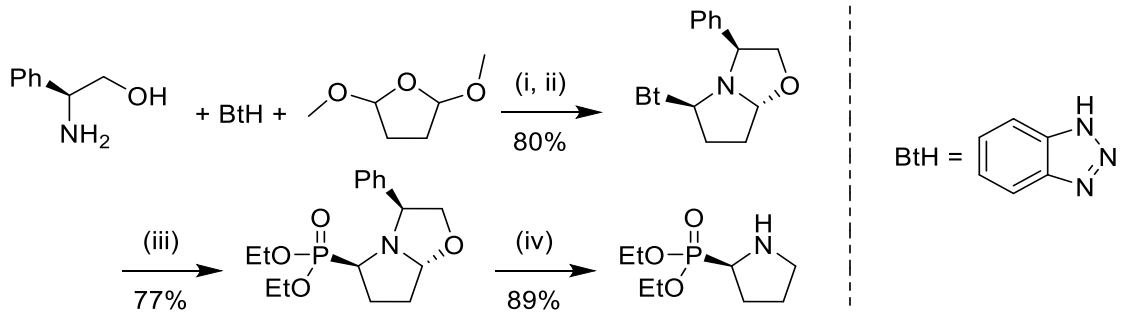

Scheme 42: Reaction route for the synthesis of diethyl (*R*)-pyrrolidin-2-ylphosphonate [(*R*)-**21**] according to Katritzky *et al*.[242] Reaction conditions: i) 0.1 N HCl, 50 °C, 0.5 h; ii) CH_2Cl_2, rt, 12 h; iii) $P(OEt)_3$, $ZnBr_2$, CH_2Cl_2, rt; iii) Pd/C, H_2.

However, this approach was abandoned due to difficulties in purifying the chiral oxazolopyrrolidine intermediate and the incompatibility of the classical Arbuzov reaction with triarylphosphites.[243] Instead, (*R*)-**21** was prepared via asymmetric synthesis starting from masked oxosulfinimines (*N*-sulfinylimines).[244,245] In the first step, 4,4-dimethoxybutanenitrile was reduced with DIBAL-H[246,247] to yield 4,4-dimethoxybutanal (**18**) in an excellent yield of 92% (Scheme 43). Although Davis used (*S*)-(+)-*p*-toluenesulfinamide for sulfinimine formation, *tert*-butyl sulfinamide was selected here as a more sterically hindered chiral auxiliary to direct the diastereoselective follow-up reaction with an organolithium compound.

Ellmann *et al*. were the first to report on the asymmetric synthesis of *tert*-butanesulfinamide and its subsequent reaction with ketone and aldehydes.[248–252] They first used $MgSO_4$ or $CuSO_4$ for the condensation,[248–250,252] then developed conditions with $Ti(OEt)_4$ for the reaction of ketones and aldehydes with Ellmann's sulfinamide, which does not react in the presence of $MgSO_4$ or $CuSO_4$.[249–252]

Several condensation agents were screened, whereby $Ti(OEt)_4$ obtained the highest yield (48%) for (*S*)-**19** (Table 7, Scheme 43).[244,253] In contrast to the reaction conditions described by Elmann, which utilize the aldehyde in excess[250], an excess of the sulfinamide was used here.

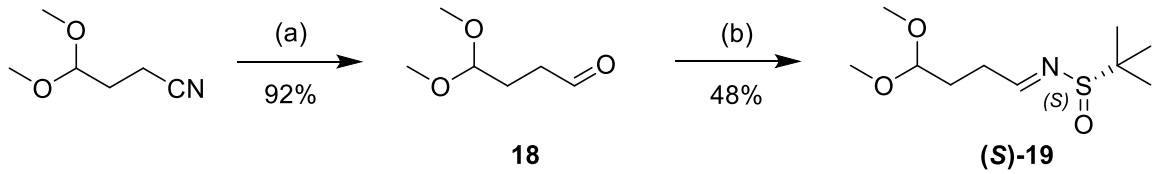

Scheme 43: Synthesis of **18** from 4,4-dimethoxybutanenitrile and subsequent condensation to (*S*)-**19**. Reaction conditions: a) DIBAL-H, CH_2Cl_2, –78 °C to rt, 18 h[246,247]; b) (*S*)-(–)-*t*butylsulfinamide, $Ti(OEt)_4$, CH_2Cl_2, rt, 65.5 h[244].

Table 7: Optimization of the reaction conditions for synthesis of (*S*)-**19** from 4,4-dimethoxybutanal and (*S*)-(–)-^{t}butylsulfinamide.

Entry	Condensation agent (eq)	Equivalent aldehyde	Equivalent sulfinamide	Reaction time (h)	Yield (%)
1	$MgSO_4$ + PPTS (5.00, 0.05)	2.00	1.00	24	26
2	$MgSO_4$ + PPTS (5.00, 0.05)	1.00	1.20	25	24
3	$MgSO_4$ + PPTS (10.0, 0.10)	1.00	1.00	21	21
4	$CuSO_4$ (2.20)	1.10	1.40	42	14
5	$CuSO_4$ (2.25)	1.00	1.65	90	18
6	Cs_2CO_3 (2.00)	1.00	1.00	18	17
7	TTIP (6.00)	1.00	1.00	2	29
8	$Ti(OEt)_4$ (6.00)	1.00	1.00	2	32
9	$Ti(OEt)_4$ (6.00)	1.00	1.00	19	41
10	$Ti(OEt)_4$ (2.00)	1.00	1.00	23	32*
11	$Ti(OEt)_4$ (6.00)	1.00	1.20	65.5	48

* reaction in THF

Subsequently, diphenyl [(*R*)-1-([(*S*)-*tert*-butylsulfinyl]amino)-4,4-dimethoxybutyl]phosphonate [(*S,R*)-**20**] was synthesized by reaction of (*S*)-**19** with lithium diphenylphosphite, prepared *in situ* from triphenylphosphite and LiHMDS, according to the protocol by Davis *et al*.[244] This reaction afforded (*S,R*)-**20** in 74% yield (Scheme 44). The newly formed stereocenter was inferred to have an (*R*)-configuration, as reported by Davis *et al.*, due to addition to the *Si*-face of the imine[244,254] via a "seven-membered twisted chairlike transition state" (Davis *et al.*, *J. Org. Chem.* **2004**, *69.* 3774–3781[244]).[244,254,255] The enantiomeric purity of (*S*)-**21** was later confirmed by two indirect methods (see below). Cleavage of the sulfinamide and simultaneous ring closure in a mixture of TFA and H_2O (95:5), followed by delayed addition of Et_3SiH, yielded diphenyl (*R*)-pyrrolidin-2-ylphosphonate [(*R*)-**21**] in 62% yield (Scheme 44).[256] Ellmann *et al*. found that delayed addition of Et_3SiH prevents formation of the by-product diphenyl (3,4-dihydro-2H-pyrrol-5-yl)phosphonate.[256]

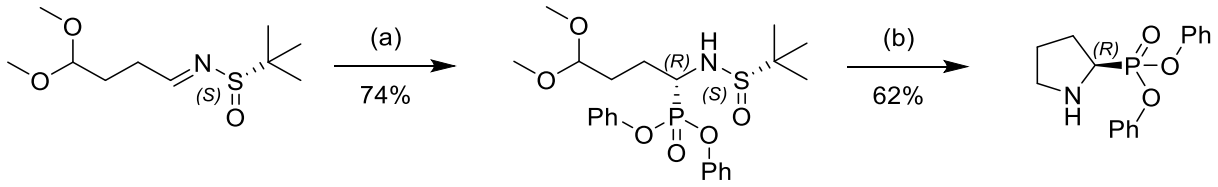

Scheme 44: Synthesis of (*R*)-**21** via (*S,R*)-**20**. Reaction conditions: a) Diphenyl phosphite, LiHMDS, THF, –78 °C, 2.5 h[244]; b) Et_3SiH, TFA, H_2O, rt, 25 h.[256]

Since the stereocenter does not change during the following reaction, it can be assumed that the configuration is the (*R*)-configuration. The enantiomeric purity was confirmed by two indirect methods. First, diphenyl pyrrolidin-2-ylphosphoante [(*S*)-**21**] was synthesized in the (*S*)-configuration (Scheme 45), and the optical rotation angles of (*R*)-**21** and (*S*)-**21** were determined using a polarimeter. The two compounds showed opposite specific rotation angles (α_D = – 5.2 for (*R*)-**21** and α_D = 7.2 for (*S*)-**21**), as expected for two different enantiomers. In addition, a 1:1 racemic mixture of (*R*)-**21** and (*S*)-**21** was dissolved in *n*-hexane:isopropyl alcohol (9:1), and the retention times of both enantiomers were determined by chiral HPLC. Separate injections of the enantiomers onto the chiral HPLC column resulted in distinct retention times of 24.8 min for (*R*)-**21** and 30.5 min for (*S*)-**21**. The enantiomeric purity was determined to be >99% for both enantiomers (Figure 29).

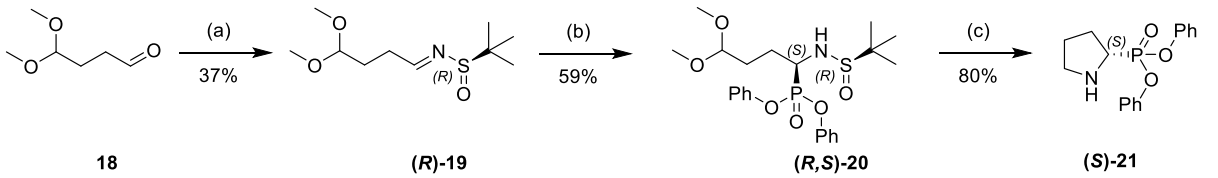

Scheme 45: Synthesis route for preparation of (*S*)-**21**. Reaction conditions: a) (*R*)-(–)-^{t}butylsulfinamide, $Ti(OEt)_4$, CH_2Cl_2, rt, 113 h[244]; b) diphenyl phosphite, LiHMDS, THF, –78 °C, 3.5 h[244]; c) Et_3SiH, TFA, H_2O, rt, 18 h[256].

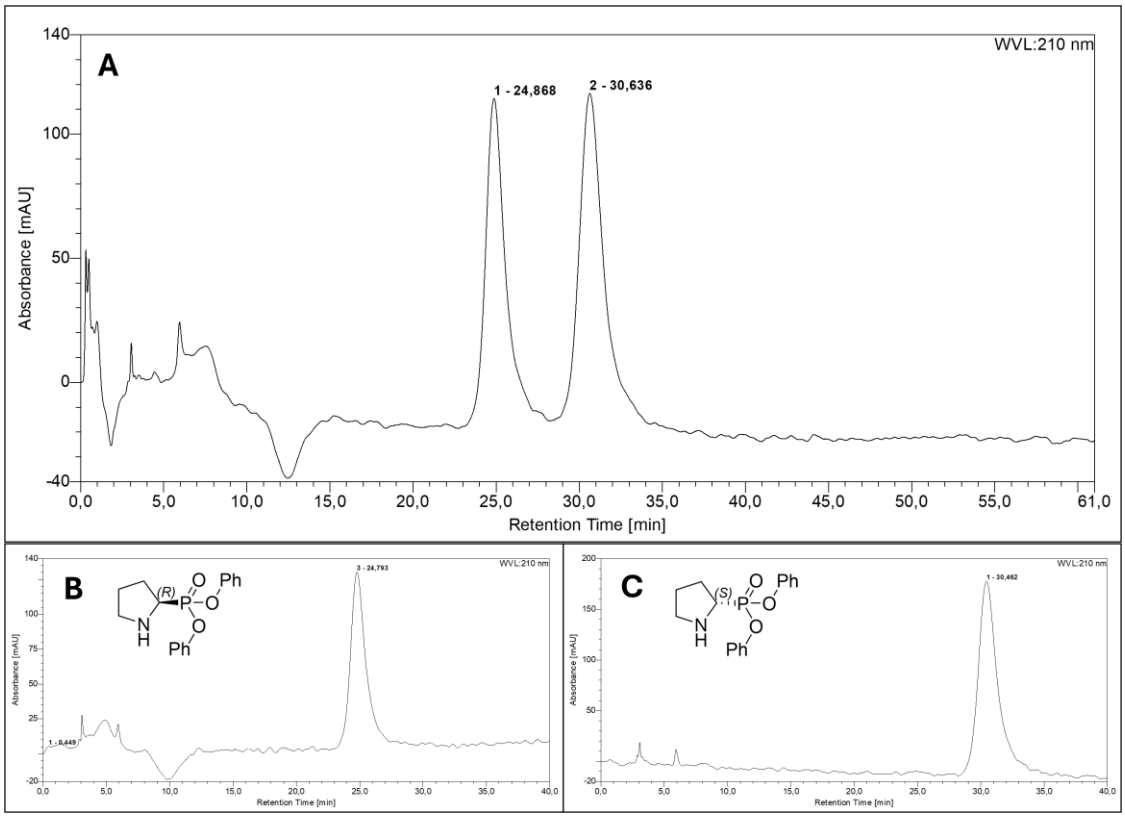

Figure 29: Chiral HPLC of (*R*)-**21** and (*S*)-**21**. HPLC conditions: Column: Daicel CHIRALPAK AD 10 µm (80 Å) 250×4.6 mm; eluent: 10% isopropyl alcohol in *n*-hexane. Flow rate: 1 mL/min. A) Racemic mixture (1:1); B) Chiral HPLC of (*R*)-**21**, t_R = 24.8 min; C) Chiral HPLC of (*S*)-**21**, t_R = 30.5 min.

Taken together, (*R*)-**21** was obtained in an overall yield of 20% over four steps. The final step of the synthesis was the coupling between (*R*)-**21** and **17** (Scheme 46), which afforded precursor **22** in 41% yield, corresponding to a total yield of 14% over the nine reactions steps. The reference compound **23** was synthesized by fluorination of **22** with NH_4F according to the method of d'Andrea *et al*.[170], which yielded the desired product in 50% yield (Scheme 46).

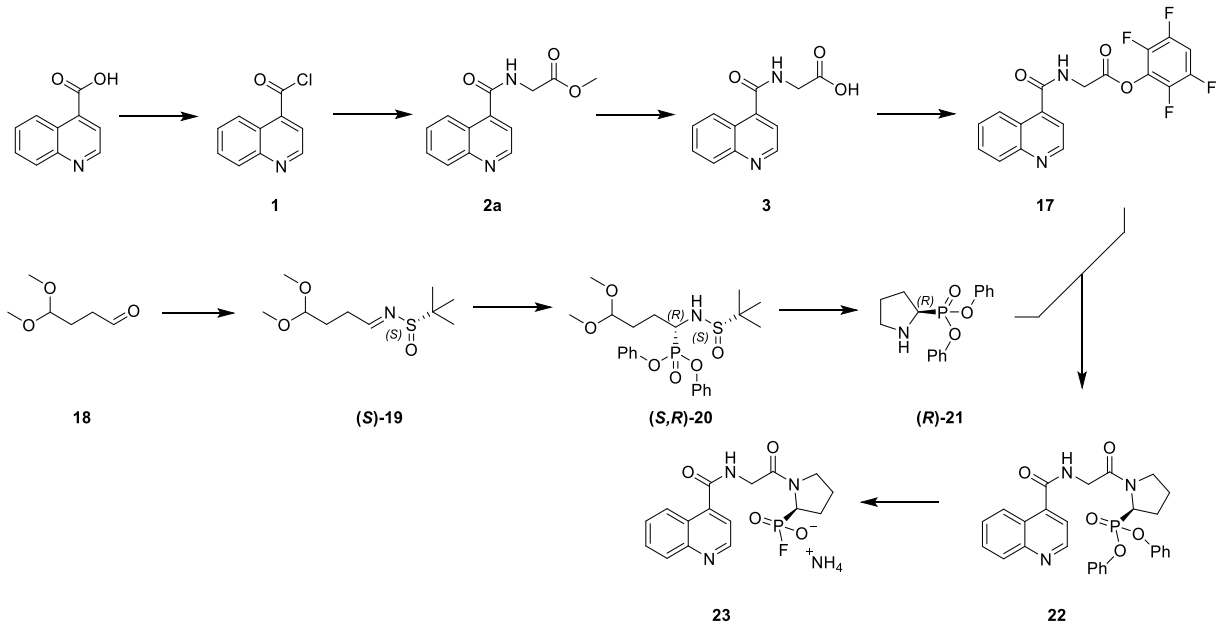

Scheme 46: Overview of the synthesis sequence for precursor **22** and reference compound **23**.

Synthesis of the reference compound (**25**) and radiolabeling precursor (**24**) for [^{18}F]**25**

Diphenyl (*R*)-(1-benzylpyrrolidin-2-yl)phosphonate (**24**) was synthesized in 47% yield by the alkylation of (*R*)-**21** with benzyl bromide in the presence of triethylamine.[257] To obtain the reference compound (*R*)-(1-benzylpyrrolidin-2-yl)phosphonofluoridate (**25**), **24** was stirred with NH_4F at 60 °C for 17 h[170], which afforded **25** in 58% yield (Scheme 47).

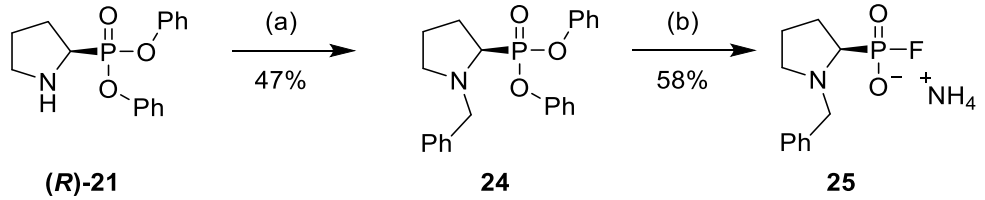

Scheme 47: Synthesis of **24** and **25**. Reaction conditions: a) Benzyl bromide, Et_3N, CH_2Cl_2, 0 °C – rt, 16 h[257]; b) NH_4F, MeCN, 60 °C, 17 h[170].

3.3.2.2 Radiochemistry

Production of (*R*)-(1-((quinoline-4-carbonyl)glycyl)pyrrolidin-2-yl)phosphono[^{18}F]fluoridate ([^{18}F]**23**)

Initially, radiolabeling of **22** was carried out following the protocol by Wang *et al*.[169], using K_{222}/K_2CO_3 for [^{18}F]fluoride elution (Table 8, entry 1). Subsequently, various reaction conditions were explored using only $TEAHCO_3$ or TEAOTf as elution salts (Table 8, entries 2−13) applying

a “minimalist-like” approach. No significant differences in radiochemical conversions (RCCs) were observed among the different elution salts in DMF at ambient temperature with 0.25 µmol precursor (Table 8, entries 2–3). Similarly, quadrupling the precursor amount did not result in a meaningful difference in RCCs when comparing $TEAHCO_3$ and TEAOTf (Table 8, entries 4–5). However, switching the solvent to MeCN and increasing the reaction temperature from rt to 40 °C approximately doubled the RCCs at a precursor amount of 0.25 µmol (Table 8, entries 6–7). A further improvement in RCCs was achieved by doubling the precursor amount (Table 8, entries 7 and 9) and increasing the temperature from 40 to 50 °C (Table 8, entries 9–10). Notably, reducing the reaction time or replacing $TEAHCO_3$ with TEAOTf led to decreased RCCs under otherwise identical conditions (Table 8, entry 11–13).

The optimized protocol for radiolabeling of **22** is with elution of [^{18}F]fluoride with $TEAHCO_3$ in MeOH (Table 8, entry 10). After evaporation of the solvent, **22** (0.5 µmol) in MeCN was added and the reaction mixture was stirred at 50 °C for 20 minutes (Scheme 48). Finally, [^{18}F]**23** was isolated by semi-preparative HPLC and formulated in isotonic saline, which afforded the desired tracer in radiochemical yields (RCYs) of 56 ± 9% (n=19), a radiochemical purity (RCP) of >95%, activity yields (AYs) of 38 ± 8% (n=24) and molar activities of 30−237 GBq/µmol (product activities of 145−526 MBq, n=12).

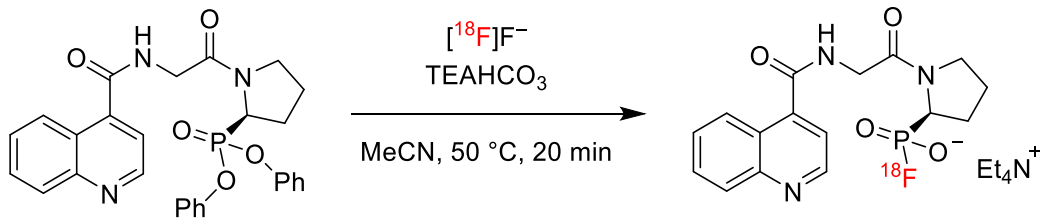

22 **[^{18}F]23**

Scheme 48: Radiosynthesis of [^{18}F]**23** from **22**.

Table 8: Optimization of the reaction conditions for radiolabeling of **22** (n=3).

Entry	Precursor amount [µmol]	Solvent [100 µL]	Elution solution (1.00 mg/mL)	Reaction temperature [°C]	Reaction time [min]	RCC [%]
1	0.25	DMF	K_{222}/K_2CO_3	rt	20	35 ± 14*
2	0.25	DMF	$TEAHCO_3$	rt	20	34 ± 6**
3	0.25	DMF	TEAOTf	rt	20	34 ± 1*
4	1.00	DMF	$TEAHCO_3$	rt	20	37 ± 14
5	1.00	DMF	TEAOTf	rt	20	38 ± 3*

6	0.25	MeCN	$TEAHCO_3$	rt	20	24	±	1*
7	0.25	MeCN	$TEAHCO_3$	40	20	42	±	2*
8	0.25	MeCN	$TEAHCO_3$	60	20	37	±	2*
9	0.50	MeCN	$TEAHCO_3$	40	20	50	±	3
10	**0.50**	**MeCN**	**$TEAHCO_3$**	**50**	**20**	**57**	±	**4****
11	0.50	MeCN	$TEAHCO_3$	50	10	49	±	8**
12	0.50	MeCN	$TEAHCO_3$	50	5	39	±	8
13	0.50	MeCN	TEAOTf	50	20	48	±	4**

* n=2, ** n=4

Production of (*R*)-(1-benzylpyrrolidin-2-yl)phosphono[^{18}F]fluoridate ([^{18}F]**25**)

For radiolabeling of precursor **24**, [^{18}F]fluoride was loaded on a QMA cartridge and eluted with TEAOTf in MeOH. Following evaporation of the solvent, **24** (0.5 µmol) in MeCN was added and the reaction mixture was stirred for 15 min at 60 °C affording the RCCs of 49 ± 7% (n=3). Several alternative radiolabeling conditions were tested (Table 9), which however did not improve RCCs. After isolation by semi-preparative HPLC, [^{18}F]**25** was obtained in RCYs of 44 ± 8% (n=6), an RCP of >98%, AYs of 30 ± 5% (n=6) and molar activities of 13–28 GBq/µmol (192–337 MBq product activity, n=5).

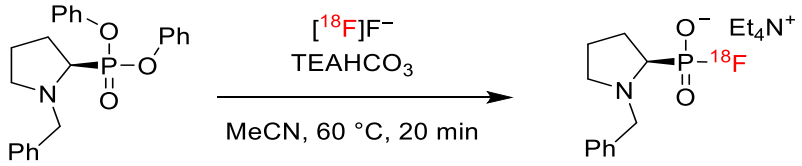

24 **[^{18}F]25**

Scheme 49: Radiosynthesis of [^{18}F]**25** from **24**.

Table 9: Optimization of the reaction conditions for radiolabeling of **24**. Unchanged parameters: 0.5 µmol precursor in 100 µL MeCN. n=3.

Entry	**Elution salt (1.00 mg/mL)**	**Reaction temperature [%]**	**Reaction time [min]**	**RCC [%]**		
1	TEAOTf	60	15	49	±	7
2	TEAOTf	70	15	42	±	5
3	$TEAHCO_3$	60	15	39	±	2
4	$TEAHCO_3$	60	20	48	±	13

* n=6

3.3.2.3 Stability studies in aqueous solutions

Stability studies of [^{18}F]**23** in aqueous solutions

The stability of [^{18}F]**23** was investigated in H_2O, phosphate-buffered saline (PBS) at physiological pH (7.4), FAP assay buffer consisting of 50 mM TRIS buffer (pH 7.5, 1.0 M NaCl, 0.1% BSA), acidic aqueous solutions (pH 1–5), and slightly basic aqueous solutions (pH 8–10). Stability was evaluated over a period of 2 h, with aliquots taken immediately after addition of [^{18}F]**23** or after 10 min of incubation (FAP-buffer), as well as after 1 and 2 h. Furthermore, stability was assessed in aqueous solutions (pH 4) after heating to 100 °C for 5 or 10 min, with aliquots analyzed immediately after addition of [^{18}F]**23** as well as after 1 and 2 h at room temperature. Throughout the 2 h incubation, [^{18}F]**23** remained completely intact in H_2O, PBS, 0.1% TFA (pH 2), NaOAc buffer (pH 4 & 5) and basic media ($NaHCO_3$ solution, pH 8 and NH_4OH/NH_4Cl buffer, pH 10, Figure 47–Figure 50). In FAP-buffer (Figure 51) and NaOAc buffer (pH 4), 2% defluorination was observed over the period of 2 h. In 0.55% TFA (pH 1), defluorination amounted to 6% after 1 h and 11% after 2 h (Figure 48). Heating [^{18}F]**23** for five minutes at 100 °C in NaOAc buffer (pH 4) resulted in 25% defluorination, while heating for 10 minutes at the same temperature led to 50% defluorination. In both cases, the compound remained stable during the subsequent 2 h incubation at ambient temperature (Figure 52).

Stability studies of [^{18}F]**25** in aqueous solutions

The stability of [^{18}F]**25** was examined in H_2O, PBS (pH 7.4) and FAP-buffer (50 mM TRIS buffer [pH 7.5, 1.0 M NaCl, 0.1% BSA]) over a 2 h period and analyzed by radio-RP-TLC. [^{18}F]**25** demonstrated complete stability in all three media tested throughout the entire observation period.

*3.3.2.4 Stability studies of [^{18}F]**23** in human blood plasma*

An aliquot of [^{18}F]**23** in isotonic saline (2 µL) was added to 1 mL of human blood plasma, which had been preheated to 37 °C. After 5, 15, 30, 60, 90 and 120 min, aliquots were taken and proteins were precipitated by addition to MeCN. Each time point was analyzed in triplicate using radio-NP-TLC. During the 2 h measurement period, no defluorination or formation of radiolabeled metabolites was detected.

3.3.2.5 Enzyme experiments

[The enzyme experiments were performed with the support of the radiopharmacology team at INM-5.]

In vitro enzyme experiments were used to evaluate the covalent interaction between [^{18}F]**23** and FAP. The objective was to test the hypothesis that [^{18}F]fluoride is released upon reaction of [^{18}F]**23** with the enzyme. It was assumed that the amount of released [^{18}F]fluoride would be too small for detection by HPLC. Therefore, preliminary tests were conducted using hydroxyapatite (HA), which is known to adsorb [^{18}F]fluoride and commonly applied for water defluorination.[258] These tests demonstrated that 25 mg/mL HA could adsorb 99% of [^{18}F]fluoride, while retaining only 2% of [^{18}F]**23**.

Subsequent enzyme experiments were performed using isolated FAP instead of cell-based systems, enabling precise control of enzyme concentration and thus quantification of [^{18}F]fluoride release. The enzymatic activity of FAP was confirmed using the fluorogenic substrate *Z*-Gly-Pro-AMC (benzyloxycarbonyl-glycine-proline-7-amino-4-methylcoumarin), which is hydrolyzed by prolyl endopeptidases to release fluorescent 7-amino-4-methylcoumarin (Scheme 50).[259]

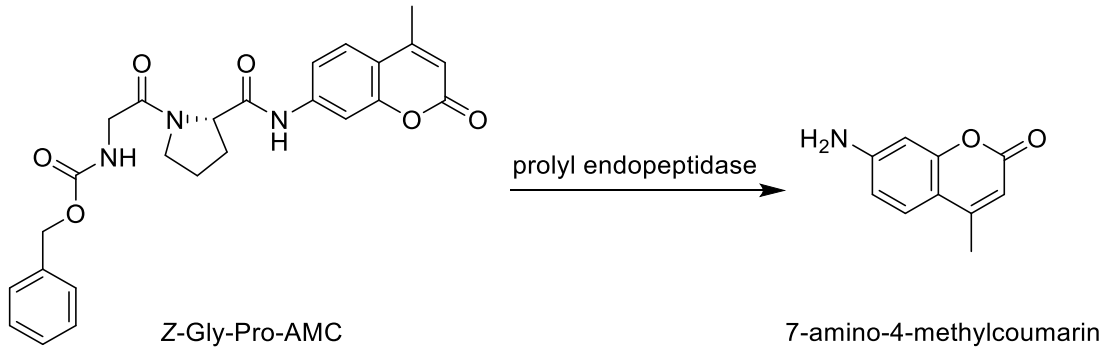

Scheme 50: Hydrolysis of *Z*-Gly-Pro-AMC to 7-amino-4-methylcoumarin by prolyl endopeptidases.[259]

The molar mass of FAP and an estimated molar activity of 40 GBq/µmol for [^{18}F]**23** were used to determine that 0.2 µg of FAP would provide a 10-fold enzyme excess when using 10 kBq of [^{18}F]**23**:

$$\text{M(FAP)} = 86\ \text{kDa} \triangleq 86000\ \text{g/mol} \qquad \text{m(FAP)} = 0.2\ \mu\text{g} = 0.2 \bullet 10^{-6}\ \text{g}$$

$$\text{n(FAP)} = \frac{\text{m (FAP)}}{\text{M (FAP)}} = \frac{0.2 \bullet 10^{-6}\ \text{g}}{86000\ \text{g/mol}} = 2.3 \bullet 10^{-12}\ \text{mol} \tag{4}$$

$$\text{A([}^{18}\text{F]}\mathbf{23}\text{)} = 10\ \text{kBq} \qquad A_M([^{18}\text{F}]\mathbf{23}) = 40\ \text{GBq/µmol} \rightarrow 4 \bullet 10^{10}\ \text{Bq/µmol}$$

$$4 \bullet 10^{10}\ \text{Bq} \triangleq 1\ \mu\text{mol} = 10^{-6}\ \text{mol} \tag{5}$$

$$1\ \text{Bq} = 2.5 \bullet 10^{-17}\ \text{mol} \tag{6}$$

$$10\ \text{kBq} = 10000\ \text{Bq} = 2.5 \bullet 10^{-13}\ \text{mol} = n([^{18}\text{F}]\mathbf{23}) \quad (7)$$

$$\rightarrow n(\text{FAP}) = 2.3 \bullet 10^{-12}\ \text{mol} > n([^{18}\text{F}]\mathbf{23}) = 2.5 \bullet 10^{-13}\ \text{mol}$$

Each enzyme experiment was paralleled by a corresponding control experiment without enzyme to determine the baseline [^{18}F]fluoride content of the tracer. Traces of [^{18}F]fluoride were always present in the formulated tracer, likely due external factors such as the formulation conditions or interaction with fluorine-containing laboratory materials. Subtracting this background allowed precise quantification of enzyme-induced [^{18}F]fluoride release. In a preliminary trial, 10 kBq of [^{18}F]**23** was incubated with 0.2 µg FAP and 25 mg HA in a total volume of 500 µL. After 1 h of incubation and subsequent work-up, [^{18}F]fluoride release amounted to 3.3 ± 0.1%. Preincubation of FAP with a 1 µM solution of UAMC-1110 for 20 min almost completely suppressed this release, indicating that the reaction of [^{18}F]**23** with FAP occurs within the active site. When HA was omitted from the reaction solution, [^{18}F]fluoride release increased almost 5-fold to 16%, suggesting that HA reduces the enzyme activity. Consequently, all subsequent experiments were conducted without HA in the reaction solution. A new batch of enzyme was used to examine the effect of enzyme concentration on [^{18}F]fluoride release. The results demonstrated that doubling or quadrupling the amount of FAP from 0.2 µg to 0.4 or 0.8 µg results in a corresponding increase of [^{18}F]fluoride release (Figure 30, A). Subsequent experiments were conducted with 0.4 µg of FAP due to reduced activity of the new enzyme batch.

Self-inhibition experiments with 1 µM of the non-radioactive reference compound revealed a significant ($p < 0.0001$) suppression of [^{18}F]fluoride release (11 ± 0.5% without carrier vs. 0.8 ± 0.1% with carrier, Figure 30, B). Reaction kinetics were assessed by sampling after 10, 30, 60, 90 and 120 min. Parallel inhibition experiments were carried out using UAMC-1110 without pre-incubation. Due to the substantial number of samples, HA-based work-up was omitted and radio-TLC was used to determine [^{18}F]fluoride release. [^{18}F]Fluoride release followed an almost linear pattern over two hours, while the inhibitor consistently blocked enzyme activity throughout the measurement period (Figure 30, C). An initial slight increase in [^{18}F]fluoride release despite the presence of UAMC-1110 indicated good affinity of [^{18}F]**23** for FAP. After approximately 60 min, [^{18}F]fluoride release under these conditions ceased, indicating saturation of the enzyme by UAMC-1110.

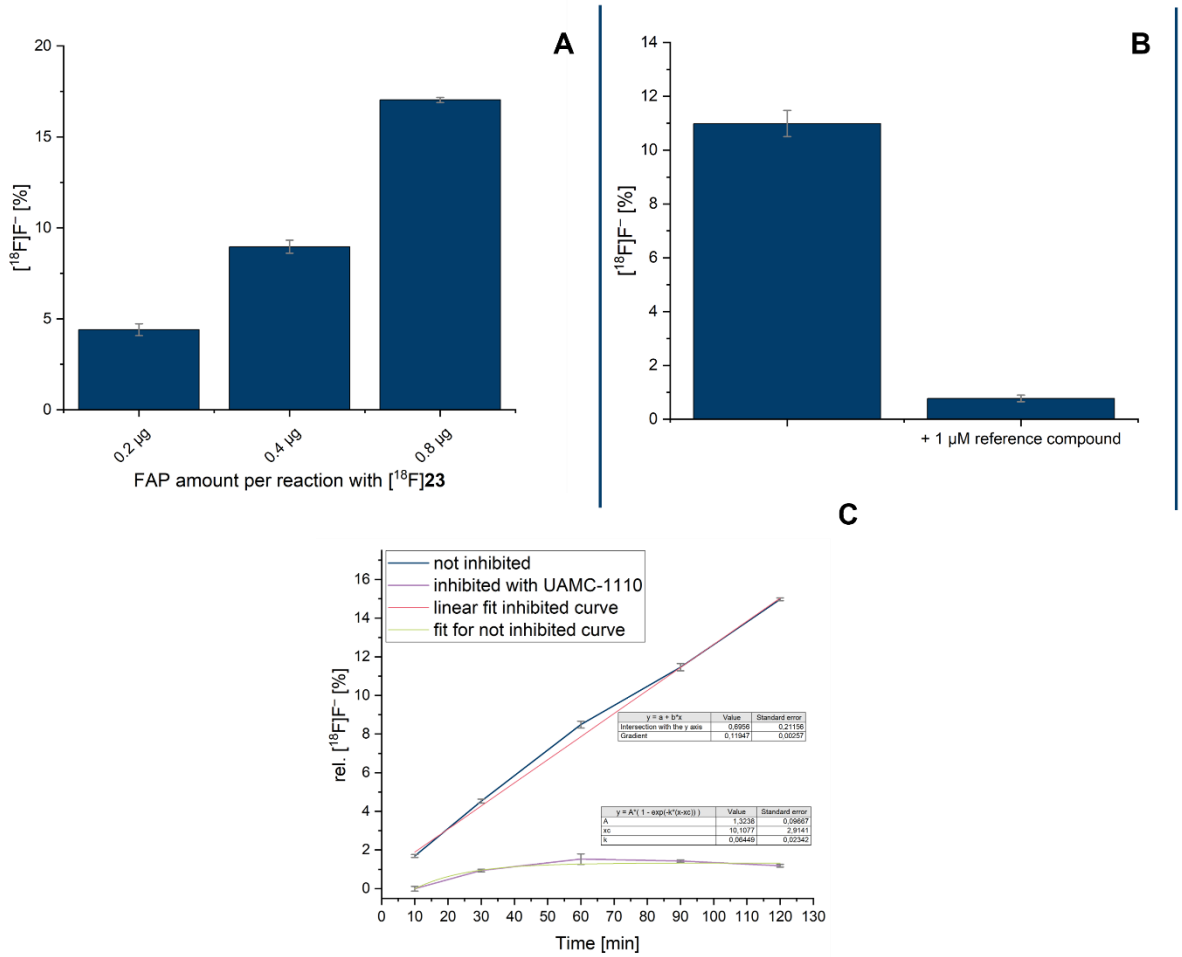

Figure 30: The graphics depict the release of [^{18}F]fluoride during reaction of FAP with [^{18}F]**23**. A: The enzyme's concentration dependence on [^{18}F]fluoride release. Reaction conditions: 0.2 µg / 0.4 µg / 0.8 µg of FAP, 10 kBq of [^{18}F]**23** (A_M 30 GBq/µmol), 500 µL reaction volume, one hour incubation at rt, triplicate determination; B: Comparison of the reaction of FAP with [^{18}F]**23** in the presence and absence of the non-radioactive reference compound. Reaction conditions: 0.4 µg of FAP, 10 kBq of [^{18}F]**23** (A_M 43 GBq/µmol), inhibition with a 1 µM solution of the non-radioactive reference compound, 500 µL reaction volume, incubation for one hour at rt, triplicate determination. C: Reaction kinetics with and without addition of UAMC-1110. Reaction conditions: 0.4 of µg FAP, 10 of kBq [^{18}F]**23** (A_M 80 GBq/µmol), inhibition with a 1 µM solution of UAMC-1110, 500 µL reaction volume, incubation at rt, triplicate determination.

Finally, to assess selectivity for FAP, [^{18}F]**23** was incubated with several FAP-related peptidases (PREP, DPP 2, DPP 4, and DPP 9). Prior to the experiments, the activity of the peptidases was confirmed using appropriate enzyme-specific fluorogenic substrates (FAP and PREP: *Z*-Gly-Pro-AMC; DPP 2: Lys-Pro-AMC; DPP 4 and DPP 9: GP-AMC). The individual experiments were designed so that the amount of each enzyme was equivalent, based on the purity specifications provided by the manufacturers. All buffers were utilized in accordance with the manufacturer's specifications for the individual peptidases. Parallel inhibition studies were performed with enzyme-specific inhibitors at a concentration of 0.1 µM (FAP: UAMC-1110; DPP 2: puromycin aminonucleoside; DPP 4 and DPP 9: anagliptin) or 10 µM (PREP: UAMC-1110). After incubation for 90 min at ambient temperature, analysis by radio-TLC showed no reaction of [^{18}F]**23** with DPP 2, DPP 4 and DPP 9. However, [^{18}F]**23** exhibited 62 ± 2%

[^{18}F]fluoride release in the presence of PREP, which could be inhibited by UAMC-1110 (Figure 31). This indicates that [^{18}F]**23** also reacts with the active site of PREP. Nevertheless, while [^{18}F]**23** exhibited even greater reactivity with PREP than with FAP, its potential for endoradiotherapy applications remains viable. Thus, although PREP activity has been detected in extracellular fluids or membranes, PREP is a soluble cytoplasmic peptidase and therefore primarily located within cells.[260] Conversely, FAP is a membrane-anchored protein, and as such, it is found outside of cells. Accordingly, it is plausible that [^{18}F]**23** derivatives, which lack significant cell-permeability, will primarily interact with FAP *in vivo*.

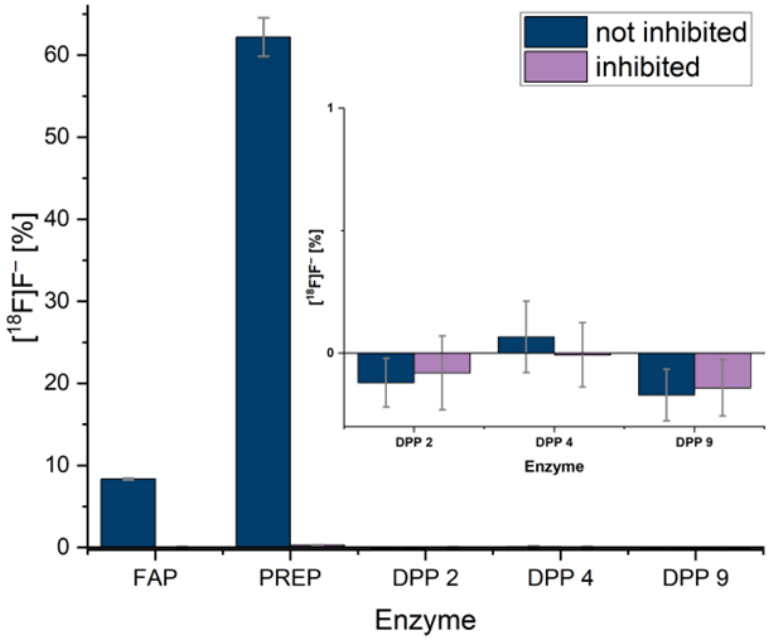

Figure 31: [^{18}F]Fluoride released through reaction of [^{18}F]**23** with various peptidases. Reaction conditions: 10 kBq of [^{18}F]**23** (A_M 101 GBq/µmol), inhibition with 0.1 µM inhibitor (10 µM for PREP), 500 µL reaction volume, incubation for 90 min at rt, triplicate determination.

To validate the selectivity of FAP for specific structural motifs, additional experiments were performed with [^{18}F]**25** as a negative control. As already described above, [^{18}F]**25** lacks the quinoline backbone responsible for the inhibitory effect of UAMC-1110, while retaining the phosphonofluoridate warhead. Experiments analogous to those with [^{18}F]**23** showed no [^{18}F]fluoride release after background correction during an incubation for 90 min at ambient temperature, indicating no reaction of [^{18}F]**25** with FAP. Due to instability of [^{18}F]**25** on NP-TLC (Normal-phase thin-layer chromatography), analysis of the reaction mixture was conducted using radio-RP-TLC (Reversed-phase thin-layer chromatography). These results confirmed that [^{18}F]**25** does not react with FAP, thus obviating the need for further kinetic analysis.

3.3.3 Conclusion

In this study, a covalent FAP inhibitor precursor with a diphenylphosphonate moiety was successfully synthesized over nine steps, with an overall yield of 14%. Subsequent radiofluorination using a “minimalist-like” approach afforded [^{18}F]**23** in RCYs and RCPs of 56 ± 9% and >95%, respectively. The corresponding reference compound was obtained in a total yield of 7% over 10 steps. [^{18}F]**23** exhibited good stability in aqueous solutions across a broad pH range (2−10) and in human blood plasma. Enzyme experiments confirmed that [^{18}F]**23** reacts with the active site of FAP. No interaction was observed with DPP 2, DPP 4 and DPP 9, whereas [^{18}F]**23** did react with PREP. Furthermore, a negative control compound was synthesized and radiofluorinated. It showed no reaction with FAP, thereby confirming the selective interaction of FAP with [^{18}F]**23**. Prospectively, [^{18}F]**23** could serve as a lead for radiotherapeutics for covalent FAP-targeting.

3.4 Synthesis and preliminary *in vitro* evaluation of an ^{18}F-labeled covalent FAP inhibitor containing a phosphono[^{18}F]fluoridodithioate functionality as warhead

3.4.1 Abstract

As previously demonstrated, a fibroblast activation protein inhibitor (FAPI) bearing a phosphonofluoridate warhead could covalently bond on the active site of FAP. Building upon these findings, a new labeled FAPI with phosphono[^{18}F]fluoridodithioate warhead was designed (Figure 32).

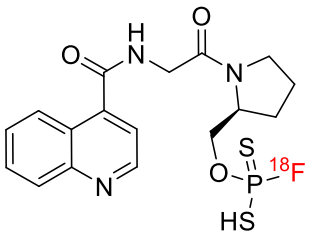

Figure 32: FAPI bearing a phosphono[^{18}F]fluoridodithioate warhead.

This compound was prepared from the corresponding oxydithiaphospholane 2-sulfide labeling precursors. Initially, a model phosphono[^{18}F]fluoridodithioate was produced and evaluated for its hydrolytic and blood plasma stability. Based on its high stability, the corresponding radiofluorinated FAPI candidate was produced and subjected to *in vitro* stability tests as well as to enzyme binding experiments

3.4.2 Results and Discussion

3.4.2.1 Chemistry

N,*N*-Diethyl-1,3,2-dithiaphospholan-2-amine (**26**) was synthesized according to the protocol of Yang *et al*.[171] by reacting (diethylamino)phosphine dichloride and ethane-1,2-dithiol in the presence of triethylamine. **26** was then allowed to react with Boc-L-prolinol in the presence of 5-(ethylthio)-1*H*-tetrazole affording the intermediate **27**. Subsequent oxidation of the latter with elemental sulfur yielded the dithiaphospholane **28**. The next step was intended to be deprotection of **28** to **29**, followed by coupling of this pyrrolidine derivative with 2,3,5,6-tetrafluorophenyl (quinoline-4-carbonyl)glycinate (**17**) to obtain the labeling precursor **30** (Scheme 51).

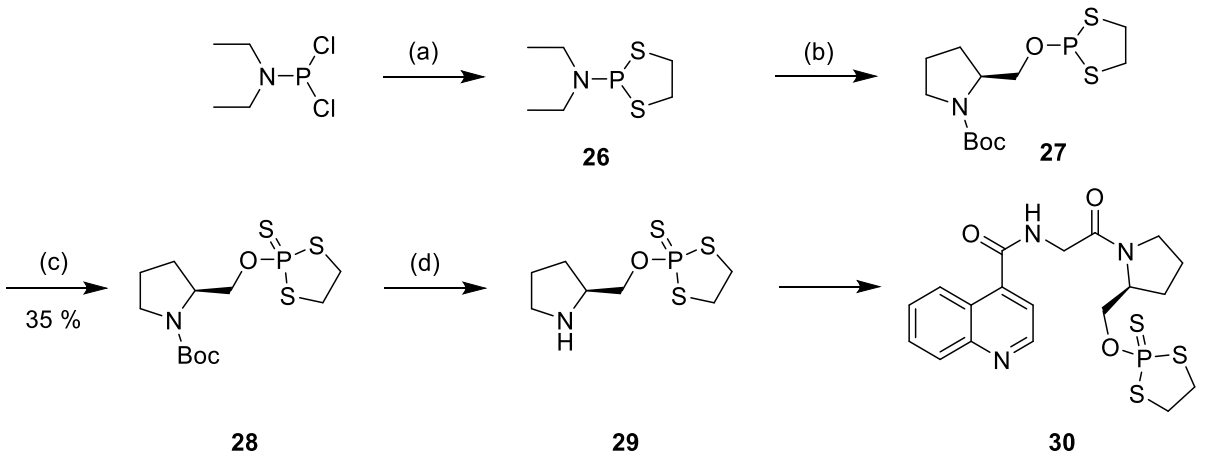

Scheme 51: Synthesis of **30** according to the protocol of Yang *et al*.[171] Reaction conditions: a) Ethane-1,2-dithiol, Et_3N, C_6H_6, 0 °C – rt, 2.5 h; b) 5-(Ethylthio)-1*H*-tetrazol, Boc-L-prolinol, CH_2Cl_2, rt, 3 h; c) S_8, CH_2Cl_2, rt, overnight; d) TFA, CH_2Cl_2, rt, overnight.

Unfortunately, the deprotection step did not deliver **29**. Therefore, an alternative route was pursued, in which amide **31** was synthesized through reaction of **17** with L-prolinol. This intermediate was then used as the alcohol in the phosphitylation reaction. After subsequent oxidation with elemental sulfur, the labeling precursor **30** was obtained in 37% yield (Scheme 52).

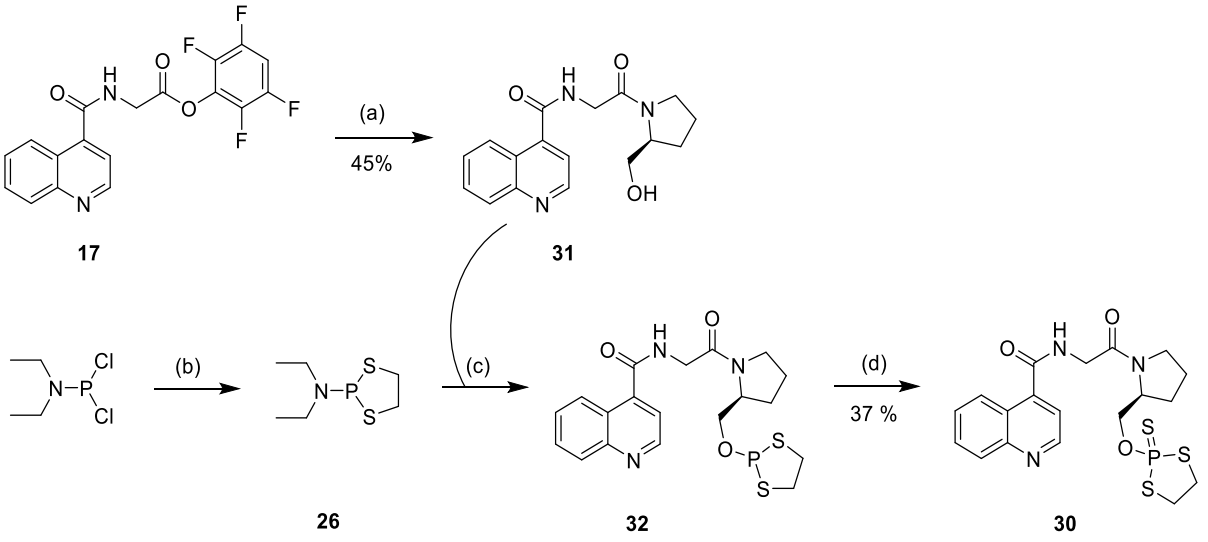

Scheme 52: Synthesis of **30** according to the protocol of Yang *et al*.[171] Reaction conditions: a) L-Prolinol, 2,6-lutidine, DMF, 55 °C, overnight; b) Ethane-1,2-dithiol, Et_3N, C_6H_6, 0 °C – rt, 2.5 h; c) 5-(Ethylthio)-1*H*-tetrazol, CH_2Cl_2, rt, 3 h; d) S_8, rt, overnight.

The non-radioactive radioactive reference compounds, **33** and **34**, were prepared from **28** and **30** by fluorination with TBAF in THF[171] in yields of 95% and 65%, respectively (Scheme 53).

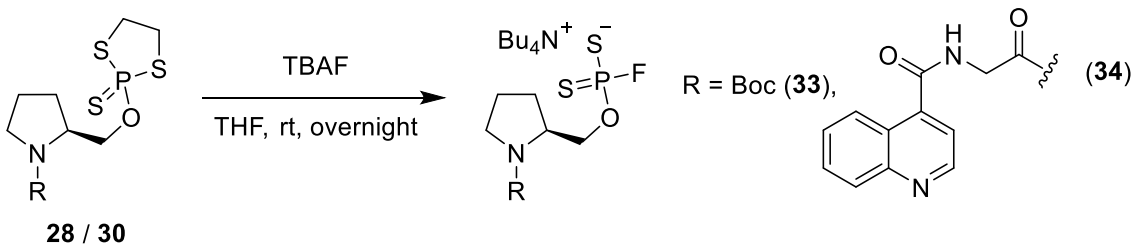

Scheme 53: Synthesis of the reference compounds by fluorination of **28** or **30** with TBAF.[171]

To determine the appropriate UV wavelength for HPLC analysis, an absorption spectrum of **33** was recorded, identifying a maximum absorption at 226 nm.

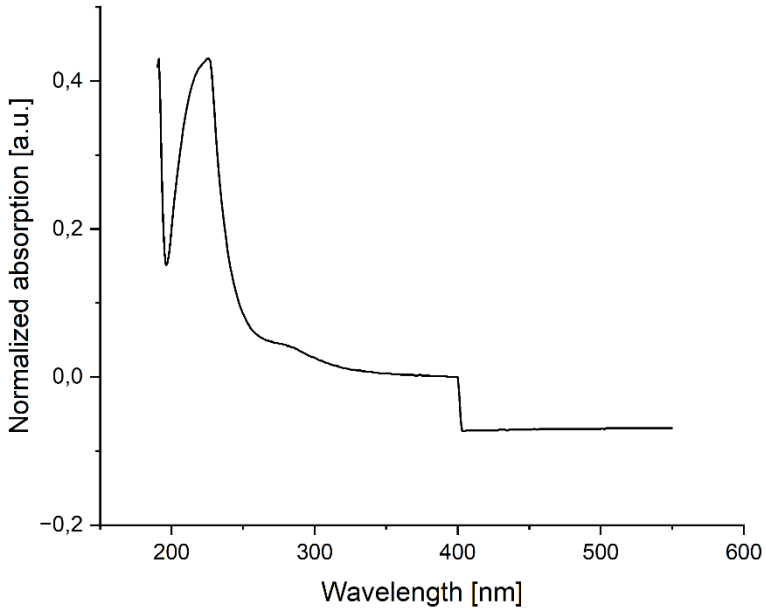

Figure 33: Absorption spectrum of **33** (0.1 mmol/L MeCN).

3.4.2.2 Radiochemistry

Radiosynthesis and isolation of intermediate (*S*)-*O*-((1-(*tert*-butoxycarbonyl)pyrrolidin-2-yl)methyl) phosphorofluoridodithioate ([^{18}F]**33**)

The radiosynthesis of [^{18}F]**33** from precursor **28** was initially performed according to the protocol of Yang *et al*.[171], except that the reaction was carried out with 0.18 µmol of precursor in DMF. Based on an subsequent optimization study (Table 10), higher RCCs were obtained using Et_4NHCO_3 in MeOH for the [^{18}F]fluoride elution (Table 10, entry 10). After removal of the solvent, a solution of **28** (0.4 µmol) in DMF was added and the reaction mixture was heated at 40 °C for 60 s without stirring. The radiolabeled product was isolated by semi-preparative

HPLC and further purified by solid-phase extraction with an HLB cartridge, which afforded [^{18}F]**33** in RCCs of 49 ± 10 (n=8), RCYs of 39 ± 2% (n=3) and RCPs of >90%. After solid-phase extraction, formation of a radioactive impurity that accounted for 4–8% of the total activity was detected. This by-product, which eluted prior to [^{18}F]**33** during HPLC separation, was not further characterized.

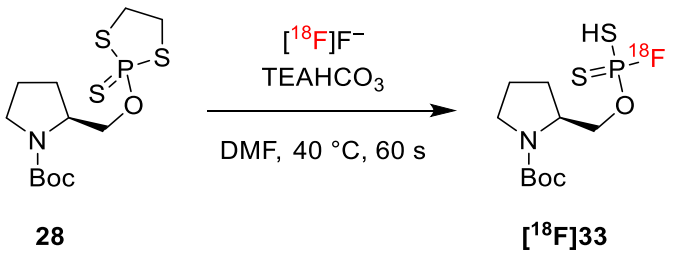

28 **[^{18}F]33**

Scheme 54: Radiosynthesis of [^{18}F]**33**.

Table 10: Optimization of the radiosynthesis of [^{18}F]**33**. All reactions were carried out in DMF. n=3.

Entry	Precursor amount [µmol]	Solvent amount [µL]	Elution solution (1.00 mg/mL)	Reaction temperature [°C]	Reaction time [s]	RCC [%]
1	0.18	90	K_{222}/K_2CO_3[a]	rt	30	30 ± 15
2	0.18	90	K_{222}/K_2CO_3[a]	rt	60	33 ± 8
3	0.18	90	K_{222}/K_2CO_3[a]	rt	300	25 ± 4*
4	0.18	90	K_{222}/K_2CO_3[a]	rt	600	34 ± 1*
5	0.38	190	K_{222}/K_2CO_3[a]	rt	300	37 ± 9*
6	0.18	90	K_{222}/K_2CO_3[a]	40	30	35 ± 4
7	0.18	90	K_{222}/K_2CO_3[a]	40	300	42 ± 2*
8	0.20	100	K_{222}/K_2CO_3[a]	40	60	25 ± 6*
9	0.40	200	K_{222}/K_2CO_3[a]	40	60	46 ± 8**
10	0.40	200	$TEAHCO_3$	40	60	49 ± 10***
11	0.40	200	$TEAHCO_3$	40	120	47 ± 1*

[a] K_{222} (8 mg)/K_2CO_3 (1 mg) in 1 mL MeCN:H_2O (4:1), * n=2; ** n=7; *** n=8.

Radiosynthesis and isolation of (*S*)-*O*-((1-((quinoline-4-carbonyl)glycyl)pyrrolidin-2-yl)methyl) phosphoro[^{18}F]fluoridodithioate ([^{18}F]**34**)

Radiolabeling of **30** was initially performed based on the optimized conditions for radiosynthesis of [^{18}F]**33**. During subsequent parameter optimization, the most favorable results were obtained using TEAOTf in MeOH for [^{18}F]fluoride elution (Table 11). After removal of the solvent, a solution of **30** (0.5 µmol) in MeCN was added and the reaction mixture was heated at 60 °C for 60 s (Scheme 55). The ^{18}F-labeled product was isolated by semi-preparative HPLC and the corresponding HPLC fraction was directly used for further experiments. Under these conditions, [^{18}F]**34** was obtained in RCCs of 62 ± 8% (n=13), RCPs of >98%, RCYs of 46 ± 11% (n=7), activity yields of 33 ± 7% (n=7), and molar activities of 86–164 GBq/µmol (216–408 MBq product activity, n=7).

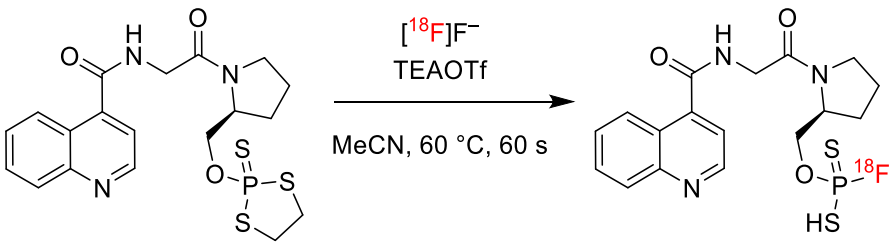

30 **[^{18}F]34**

Scheme 55: Radiosynthesis of [^{18}F]**34**.

Table 11: Optimization of the reaction conditions for radiosynthesis of [^{18}F]**34**. All reactions were carried out in 100 µL of solvent. n=3.

Entry	Precursor amount [µmol]	Solvent	Elution solution (1.00 mg/mL)	Reaction temperature [°C]	Reaction time [s]	RCC [%]
1	0.50	DMF	$TEAHCO_3$	40	60	30 ± 2
2	0.50	DMF	$TEAHCO_3$	50	60	36 ± 5*
3	0.25	DMF	$TEAHCO_3$	50	60	25 ± 8
4	0.25	DMF	$TEAHCO_3$	50	300	28 ± 5**
5	0.50	DMF	$TEAHCO_3$	60	60	49 ± 13*
6	0.50	DMF	$TEAHCO_3$	80	60	42 ± 9**
7	0.50	MeCN	$TEAHCO_3$	60	60	55 ± 12**
8	0.50	MeCN	TEAOTf	60	60	68 ± 9
9	0.25	MeCN	TEAOTf	60	60	62 ± 14
10	0.25	MeCN	TEAOTf	50	60	58 ± 24

* n=4, ** n=2.

3.4.2.3 Stability studies in aqueous media

Stability studies of [^{18}F]**33** in aqueous solutions

The stability of [^{18}F]**33** was investigated in H_2O, phosphate-buffered saline (PBS) at physiological pH (7.4), slightly acidic (pH 2–6) and slightly basic aqueous media (8–10) (Figure 34). Stability was monitored over a period of 3 h. Aliquots were taken and analyzed immediately after addition of [^{18}F]**33**, as well as 1, 2 and 3 h after addition. Furthermore, the stability of [^{18}F]**33** was investigated in aqueous solutions (pH 4) after heating to 100 °C for 5 and 10 min, both immediately after cooling and 1, 2 and 3 h later. The analysis was conducted using HPLC, as no suitable TLC system could be established for [^{18}F]**33**. Due to the single injection and statistical errors, minor deviations may occur.

[^{18}F]**33** remained stable throughout the 3 h period in both H_2O and 0.1 M NaOAc buffer (pH 4 and 6). In PBS (pH 7.4), a defluorination by approximately 5% was observed over the same period. In 0.1% TFA solution (pH 2), defluorination reached approximately 15% within 3 h. When heated to 100 °C for 5 or 10 min (pH 4) and subsequently cooled, [^{18}F]**33** showed 12–15% defluorination but remained stable during the remaining 3 h incubation period at ambient temperature. In slightly basic media, such 0.1 M $NaHCO_3$ solution (pH 8), approximately 10% defluorination occurred immediately upon addition of [^{18}F]**33**, with no significant further degradation during the remaining 3 h. Similarly, in NH_4Cl/NH_4OH buffer (pH 10), around 12% defluorination was detected immediately after addition, followed by a further 2% over the 3 h incubation. Overall, [^{18}F]**33** demonstrated sufficient stability across a range of aqueous media with different pH values for a duration of up to 3 h.

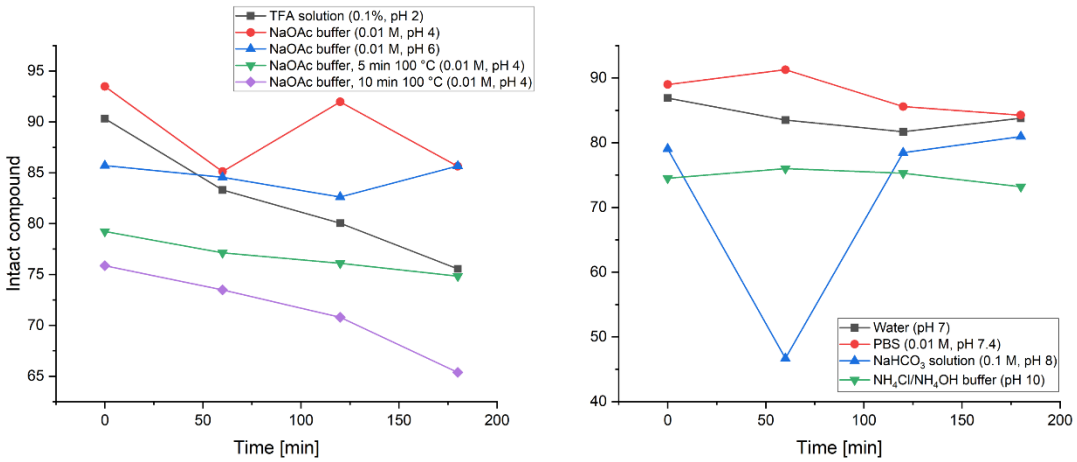

Figure 34: Hydrolytic stability of [^{18}F]**33**. Left: Acidic pH solutions, right: Neutral and basic solutions.

Stability studies of [^{18}F]**34** in aqueous solutions

The stability of [^{18}F]**34** was assessed in aqueous solutions with pH values ranging from 1 to 5, as well as in H_2O, PBS, and slightly basic solutions with pH values from 8 to 10 (Figure 35). Furthermore, [^{18}F]**34** was exposed to temperatures of 100 °C for 5 and 10 min in an aqueous solution with a pH of 4. After cooling, the compound was assessed for its stability. A 10% solution of [^{18}F]**34** (100 µL) was prepared for each of the solutions to be tested. The following solutions were used: 0.55% TFA (pH 1), 0.1% TFA (pH 2), NaOAc buffer (0.1 M, pH 4 and 5), H_2O, PBS, $NaHCO_3$ solution (0.1 M, pH 8) and NH_4OH/NH_4Cl buffer (pH 10). Stability was monitored over a period of 2 h and analyzed by HPLC. Due to the single injection and statistical errors, minor deviations may occur.

In acidic solutions at pH 1 and 2, [^{18}F]**34** exhibited slight defluorination in the range of 2−6%, while in mildly acidic media at pH 4 and 5, defluorination ranged from 3−9%. In H_2O, 10% defluorination was observed immediately after addition of [^{18}F]**34**, with no further degradation over 2 h. In PBS, defluorination reached 11% over the same period. In slightly basic media, defluorination amounted to 10% at pH 8 and increased to 20% at pH 10. Upon heating at 100 °C for 5 min, defluorination amounted to 8%, after which [^{18}F]**34** remained stable over 2 h at room temperature. After heating for 10 minutes, defluorination reached 10% and increased to 12% over the subsequent 2 h at room temperature.

In conclusion, [^{18}F]**34** demonstrated adequate stability in acidic media, whereas increased defluorination was observed in neutral and basic media. Nevertheless, the stability was deemed sufficient for further evaluation in human blood plasma.

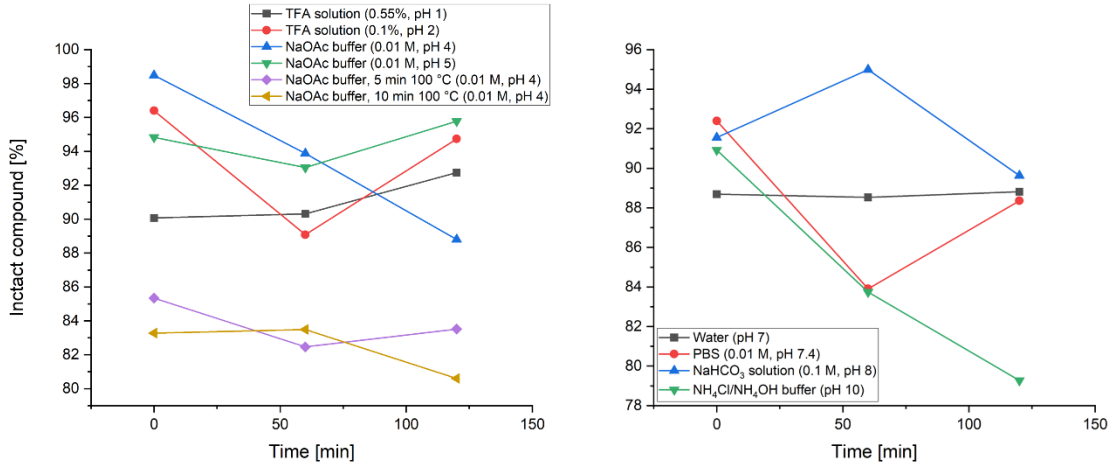

Figure 35: Hydrolytic stability of [^{18}F]**34**. Left: Acidic pH solutions, right: Neutral and basic pH

3.4.2.4 Stability studies in human blood plasma

Stability studies of [^{18}F]**33** in human blood plasma

For the assessment of stability in blood, [^{18}F]**33** was formulated in DMSO. The blood plasma was preheated at 37°C for 5 min and for each time point, a sample of [^{18}F]**33** (5 µL) was added to 95 µL plasma. After precipitation of proteins by addition of MeCN, the samples were analyzed by HPLC. During the measurement period of three hours, a defluorination of 5–9% was observed. These results indicated that the warhead exhibits sufficient stability to justify synthesis of the corresponding FAPI analogue for stability tests and FAP enzyme experiments.

Stability studies of [^{18}F]**34** in human blood plasma

To investigate the stability of [^{18}F]**34** in human blood plasma, the compound was isolated by semi-preparative HPLC and concentrated. To minimize the salt concentration, phosphate buffer (0.01 M, pH 7.1) was used in the HPLC solvent system instead of PBS. 40 µL of the concentrated HPLC fraction were added to 960 µL of pre-warmed (37 °C) human blood plasma and aliquots were taken after 5, 30, 60, 90 and 120 min. After protein precipitation and dilution with PBS, the samples were analyzed by HPLC. The results demonstrated that [^{18}F]**34** is stable in human blood plasma over a period of 2 h. A minor by-product amounting to 0.5% was detected, the formation of which did not increase over the measurement period.

3.4.2.5 Enzyme experiments

[The enzyme experiments were performed with the support of the radiopharmacology team at INM-5.]

Next, enzyme experiments were conducted to determine whether [^{18}F]**34** reacts with FAP. To this end, the release of [^{18}F]fluoride during incubation with FAP was measured at various time points. [^{18}F]**34** was synthesized and isolated by semi-preparative HPLC, and an aliquot of the HPLC fraction was added to FAP-buffer. Three samples were then prepared, each containing 50 kBq [^{18}F]**34** and 1 µg FAP (in 50 µL FAP buffer), diluted with an additional 400 µL FAP-buffer. After 10, 30, 60, 90, and 120 min, 90 µL aliquots were taken and added to 25 mg hydroxyapatite (HA) in 410 µL FAP buffer. Following three washing cycles with H_2O and separation of HA from the washing solution, no discernible [^{18}F]fluoride release was detected after correcting for the inherent [^{18}F]fluoride content of the tracer solution. These findings indicate that [^{18}F]**34** is not a substrate for FAP and thus does not form a covalent bond with the enzyme. Accordingly, no further experiments with [^{18}F]**34** were conducted.

3.4.3 Conclusion

In this study, a model compound ([^{18}F]**33**) and a FAPI ([^{18}F]**34**) with a phosphono[^{18}F]fluoridodithioate warhead were successfully prepared. The oxydithiaphospholane 2-sulfide-functionalized precursors were radiolabeled using a “minimalist” approach, achieving RCYs of 46 ± 11% (n=7) for [^{18}F]**34** and 39 ± 2% (n=3) for [^{18}F]**33**. The RCPs amounted to >98% for [^{18}F]**34** and >90% for [^{18}F]**33**, respectively. The corresponding non-radioactive reference compounds were obtained in yields of 65% and 95%, respectively. Both [^{18}F]**33** and [^{18}F]**34** demonstrated sufficient stability in aqueous solutions with pH values between 2 and 10 over a period of 2 h, as well as in human blood plasma. However, in enzyme experiments, [^{18}F]**34** showed no detectable reaction with FAP. Phosphonofluoridodithioate can not be used as a covalent warhead for the development of the novel FAPIs.

4 Summary and Outlook

Endoradiotherapy is a therapeutic approach that uses cytotoxic radiation to treat diseases from within the body. This method entails the injection of radiolabeled compounds that specifically bind to or accumulate at the disease site, thereby minimizing damage to healthy tissue. Fibroblast activation protein (FAP) is an attractive target for endoradiotherapy, as it is overexpressed in the microenvironment of malignant tumors but absent in healthy tissue or benign tumors. Several FAP inhibitors (FAPIs), derived from the potent inhibitor UAMC-1110, are currently undergoing clinical evaluation. However, their application for endoradiotherapy is limited by insufficient tumor retention due to rapid clearance from the tumor site.

The aim of this work was therefore to develop FAPIs capable of forming irreversible covalent bonds with the enzyme's active site. Building upon the structure of UAMC-1110, the nitrile group was replaced with three warheads designed to enable covalent binding. To allow for detection of covalent bond formation, the warheads were labeled with fluorine-18, which acts as a leaving group that undergoes nucleophilic attack by serine or an other residue in the active site of FAP. The release of [^{18}F]fluoride upon covalent bond formation was assessed indirectly via radio-TLC or hydroxyapatite adsorption.

The first compound synthesized was a FAPI featuring an alkyl sulfonyl [^{18}F]fluoride warhead ([^{18}F]**11**). The radiolabeling precursor, which also served as non-radioactive reference compound, was prepared over eight steps in 11% overall yield. Radiofluorination was achieved via SuFEx-based ^{18}F/^{19}F isotopic exchange, which afforded the ^{18}F-labeled FAPI in radiochemical conversions (RCCs) of 53 ± 12% and, after isolation by solid-phase extraction (SPE), radiochemical yields (RCYs) of 24 ± 3%. While [^{18}F]**11** was stable for 2 h in acidic aqueous media, it showed shorter half-lives in H_2O (117 min), PBS (124 min) and especially in human blood plasma (6 min), limiting its practical utility.

To initially evaluate the radiofluorination and stability of phosphonates, two model precursors (**12** and **15**) were synthesized and radiofluorinated. The first model precursor with a trityl group directly bound to the phosphorus atom of the phosphonate was obtained in 57% yield but showed low radiofluorination efficiency (RCCs ≤13%), presumably due to significant steric hindrance by the trityl group. In addition, poor solubility of the radiolabeled product ([^{18}F]**13**) precluded isolation and stability testing. The second model precursor was synthesized in 11% overall yield over two steps and could be radiofluorinated in RCCs of 45 ± 9%, RCYs of 26 ± 12% and radiochemical purities (RCPs) of 77–97%. Preliminary stability studies with the radiolabeled product ([^{18}F]**16**) conducted in H_2O, PBS, and TFA solution demonstrated sufficient stability for up to 2 h.

Subsequently, a FAPI with a phosphonofluoridate warhead ([^{18}F]**23**) was synthesized. The corresponding phosphonate precursor **22** was prepared in a total yield of 14% over nine steps. Subsequent radiofluorination of **22** by a minimalist-like approach afforded [^{18}F]**23** in RCCs of 61 ± 12%, RCYs of 38 ± 8%, RCPs of >95%, and molar activities of 30–237 GBq/µmol. [^{18}F]**23** demonstrated good stability for up to 2 h in PBS and human blood plasma, as well as in aqueous media with pH values ranging from 1 to 10. Enzyme experiments confirmed covalent binding to FAP, evidenced by the release of [^{18}F]fluoride, which could be inhibited by UAMC-1110 or the non-radioactive reference compound. No reaction was observed with the FAP-related peptidases DPP 2, DPP 4, and DPP 9, while higher [^{18}F]fluoride release occurred with PREP, suggesting greater affinity of [^{18}F]**23** for PREP compared to FAP. Future work could include difluorination of the pyrrolidine ring to enhance selectivity for FAP, as observed in the case of UAMC-1110.

A FAPI with a phosphonofluoridodithioate warhead ([^{18}F]**34**) was synthesized from precursor **30**, which was obtained via a one-pot reaction in 37% total yield. For initial proof-of-concept studies, the Boc-protected intermediate **28** was radiofluorinated, affording the model compound [^{18}F]**33** in RCCs of 49 ± 10%, RCYs of 39 ± 2%, and RCPs of >90%. Stability tests demonstrated sufficient stability over a period of 2 h in aqueous media across pH 2−10, as well as in PBS and human blood plasma. Subsequently, [^{18}F]**34** was prepared in RCCs of 62 ± 8%, RCYs of 46 ± 11%, RCPs of >98%, and molar activities of 86–164 GBq/µmol. Despite its favorable stability at different pH values and under physiological conditions, no reaction with FAP was observed in enzyme assays, indicating that [^{18}F]**34** is not a suitable candidate for covalent FAPI development.

To discover more selective covalent FAPIs, additional warheads should be explored in future studies. Among the compounds evaluated in the present work, [^{18}F]**23** displayed the most promising results. Furthermore, [^{18}F]**23** should be modified with a linker and chelator on the quinoline moiety to label it with a therapeutic nuclide.

In summary, three potential covalent FAPIs were synthesized, with [^{18}F]**23** emerging as the most promising candidate. Future research may refine these approaches and expand the scope of covalent inhibitors for molecular imaging and targeted therapy.

5 Experimental part

5.1 General

5.1.1 Organic synthesis

5.1.1.1 Reaction conditions

Unless stated otherwise, all reactions were carried out in round bottom flasks under an argon atmosphere and stirred with a magnetic stirring bar. The flasks were dried in an oven at 100 °C overnight or with a hot air dryer at 630 °C and filled with argon using a Schlenk line.

5.1.2 Solvents and chemicals

All solvents used were commercially available, of the highest accessible quality and were used without further purification. All commercially available chemicals were used without further purification.

5.1.3 Spectroscopy

5.1.3.1 Nuclear magnetic resonance (NMR) spectroscopy

^{1}H, ^{13}C, ^{19}F und ^{31}P NMR spectra and the 2D NMR experiments were performed on a Bruker Ascend™ 400 instrument (*Bruker BioSpin*, Ettlingen, Germany) at ambient temperature. The deuterated solvent used always served as the internal standard, and the shifts are given relative to the internal standard in ppm. Deuterated $CHCl_3$ ($CDCl_3$, d_H 7.26, d_C 77.16), dimethyl sulfoxide (DMSO-d_6, d_H 2.50, d_C 39.52), MeOH (CD_3OD, d_H 3.31, d_C 49.00) and H_2O (D_2O, d_H 4.79) were used. The spin multiplicities were noted as s (singlet), d (doublet), t (triplet), q (quartet), and m (multiplet). The ^{1}H NMR spectra were recorded at 400 MHz, ^{13}C NMR spectra at 101 MHz, ^{19}F NMR spectra at 376 MHz and ^{31}P NMR spectra at 162 MHz.

5.1.3.2 Mass spectrometry

Low-resolution mass spectra were recorded on a Thermo Scientific MSQ Plus mass spectrometer (*Thermo Fisher Scientific GmbH*, Dreieich, Germany) using the ESI ionization method (ESI positive or negative). High-resolution mass spectra were recorded at the Institute of Organic Chemistry in the Mass Spectrometry Department of the University of Cologne on a THERMO Scientific LTQ Orbitrap XL (*Thermo Fisher Scientific GmbH*, Dreieich, Germany) using the ESI ionization method (ESI positive or negative).

5.1.4 Chromatography

For thin-layer chromatography (TLC), silica gel-coated TLC aluminum foils with fluorescent markers (DC Kieselgel 60 F_{254} or DC Kieselgel 60 RP-18 F_{254}s) from *Merck* (Darmstadt, Germany) were used. Detection was performed using UV light (λ = 254 nm and λ = 365 nm) and/or by staining with iodine, potassium permanganate, or cerium molybdate phosphoric acid.

Preparative column chromatography was performed on a Pure C-815 Flash chromatography system from *Büchi* (Essen, Germany) with FlashPure cartridges as the stationary phase (silicon oxide, 25–50 µm particle size, 12–80 g). In the case of dry loading the crude products were adsorbed on Celite® 535 (*Roth*, Karlsruhe, Germany) or Kieselgel M60, particle size 0.04–0.063 mm, (*Macherey-Nagel*, Düren, Germany).

5.2 Radiochemistry

5.2.1 $[^{18}F]F^-$ production

No-carrier-added [^{18}F]fluoride ($[^{18}F]F^-$) was produced via the $^{18}O(p,n)^{18}F$ nuclear reaction by irradiating ^{18}O-enriched water on a JSW BC 1710 cyclotron (*The Japan Steel Works Ltd.*, Shinagawa, Japan) in a 1.3 mL titanium target or on a GE PETtrace (*General Electric,* Boston, USA) in a 1.6 mL silver target at the INM-5, FZJ, Jülich.

5.2.2 Materials

The following cartridges Sep-Pak® Accell Plus QMA Carbonate Plus Light cartridges (130 mg sorbent, pre-conditioned with 2 mL of ultrapure H_2O), Sep-Pak® Accell Plus QMA Plus Light cartridges (130 mg sorbent), Sep-Pak® C18 Plus Light cartridges (130 mg sorbent), Oasis HLB 1cc Vac (30 mg sorbent; all three from *Waters GmbH*, Eschborn, Germany) and Strata™-X 33 µm Polymeric Reversed Phase (60 mg sorbent; *Phenomenex*, Aschaffenburg, Germany) were used for solid-phase extraction. Anhydrous solvents were obtained from *Merck* (Darmstadt, Germany).

All reactions were carried out under argon in Wheaton V-Vials equipped with a PTFE magnetic stirring bar and a silicone septum. The reactors were heated in an aluminum block with matching drill holes on the magnetic stirrer, and the specified reaction temperatures correspond to those of the heating block. All chemicals were added using a syringe.

5.2.3 Chromatography

Analytical HPLC: The HPLC system consisted of a Dionex UltiMate 3000 Pump, a Dionex UltiMate 3000 Diode Array Detector (*Thermo Scientific*) and a HERM LB500 radio detector (*Berthold Technologies*, Bad Wildbad, Germany). The UV and radio detectors were coupled in series, resulting in a time delay of a few seconds between the corresponding responses. For analysis, an aliquot was injected into a Rheodyne-6-way valve with a 20 µL sample loop before and after the chromatography column.

Semi-preparative HPLC: The HPLC system consisted of a Knauer Pump 40P, a Knauer UVD 2.1S detector (both from Knauer, Berlin, Germany), a Rheodyne 6-way valve with a 2 mL sample loop, and a custom-built Geiger counter.

Radio-TLC: Radio-TLC was carried out using silica gel-coated TLC aluminum foils with fluorescent markers (DC Kieselgel 60 F_{254}) from *Merck* (Darmstadt, Germany). Detection was performed using a Perkin Elmer Cyclone® Plus Photoimager (*PerkinElmer*, Waltham, USA) or Fujifilm BAS-5000 (*Fujifilm*, Ratingen, Germany). To identify radiolabeled products, their R_f value was compared with that of the reference compound, or the reference compound was developed simultaneously, detected using UV light, and labeled with diluted activity solution. The frontline and baseline were also labeled with diluted activity solution after development of the TLC.

5.2.4 Characteristic parameters for describing radiolabeled substances

5.2.4.1 Radiochemical conversion (RCC)

Radiochemical conversions (RCCs) were determined by HLPC with post-column injection according to the protocol of Humpert *et al*.[241] To this end, an aliquot of the reaction solution, which had a least three times the volume of the sample loop, was injected before the column. The total activity of the aliquot was determined with a second injection into a second valve, which was connected behind the column, and was led directly into the radio detector. The RCC was calculated as the ratio of the decay-corrected area of the product peak to the decay-corrected area of the post-column injection peak expressed in %.

5.2.4.2 Radiochemical purity (RCP)

Radiochemical purity (RCP) was determined by HPLC according to the protocol of Humpert *et al.*[241] or by TLC. RCP is defined as the ratio of the isolated product to the total activity of the product and any by-products expressed in %.

5.2.4.3 Radiochemical yield (RCY)

The radiochemical yield (RCY) is defined as the decay-corrected activity of the isolated radiolabeled product divided by the starting activity and multiplied by 100. The activities were determined using a curiemeter. The product activity was decay-corrected to the measurement time of the starting activity.

5.2.4.4 Activity yield

The activity yield (AY) corresponds to the non-decay-corrected radiochemical yield. To calculate AYs, the activity of the isolated radiolabeled products was divided by the starting activity and multiplied by 100.

5.2.4.5 Molar Activity (A_M)

Molar activity (A_m) is defined as the ratio of the activity of the radiolabeled product to the sum of the amounts of the radioactive compound and the carrier, expressed in GBq/µmol. A calibration curve was prepared for the respective reference compound to determine the molar activity.

5.2.5 Radiosyntheses

5.2.5.1 Preprocessing of [^{18}F]fluoride

Irradiated [^{18}O]H_2O was diluted with H_2O (to 1.5 mL) and [^{18}F]F^- was loaded (from the male side) onto a QMA cartridge, which had been preconditioned (from the female side) with 2 mL of H_2O. The cartridge was rinsed with MeOH (1.5 mL) to remove residual H_2O and dried with air (20 mL) before the [^{18}F]F^- was eluted with a solution of the respective elution salt in MeOH or aqueous MeCN.

5.3 Supporting Information to chapter 3.1

5.3.1 Organic preparative syntheses

Quinoline-4-carbonyl chloride hydrochloride (**1**)[227]

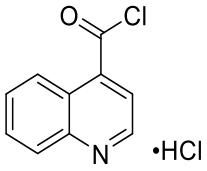

1

$C_{10}H_6ClNO•HCl$
[228.07]

Oxalyl chloride (713 µL, 8.30 mmol, 1.2 eq) and DMF (1–2 drops) were added dropwise to a pre-cooled (0 °C) suspension of 4-quinolinecarboxylic acid (1.2 g, 6.93 mmol, 1 eq) in dry CH_2Cl_2 (0.13 M). The reaction mixture was stirred for 5 min at 0 °C and then left to stir for another 18 h at ambient temperature. The solvent was removed under reduced pressure, and the product was used without further purification.

^{1}H NMR (400 MHz, DMSO) δ = 9.31 (d, J = 5.1, 1H), 8.75 (d, J = 8.6, 1H), 8.46 (d, J = 8.5, 1H), 8.23 (d, J = 5.1, 1H), 8.10 (t, J = 8.4, 1H), 7.95 (t, J = 8.3, 1H).

The analytical data corresponds to the literature.[227]

General procedure 1 (**GP 1**)[198]

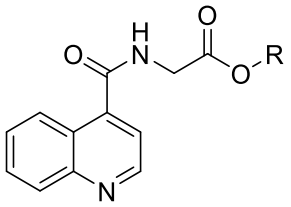

R = -Me, -Et

Triethylamine (1.2 eq) was added to a pre-cooled (0 °C) solution of the HCl salt of the corresponding amino ester (1 eq) in dry CH_2Cl_2. After stirring for 30 min at 0 °C, a second portion of triethylamine (2.3 eq) was added, followed by dropwise addition of a solution of quinoline-4-carbonyl chloride hydrochloride (**1**, 1 eq) in dry CH_2Cl_2. After complete addition, the reaction mixture was stirred for 30 min at 0 °C and then warmed to ambient temperature and stirred for another 24 h. The reaction was terminated by addition of 1 N citric acid and stirred for another 30 min. The aqueous phase was separated, neutralized with saturated Na_2CO_3 solution and extracted twice with CH_2Cl_2. The combined organic fractions were dried with Na_2SO_4, and the solvent was removed under reduced pressure.

Table 12: Experimental data of the synthesis of **2a** and **2b**.

Entry	Hydrochloride	Hydrochloride mg (mmol)	Acid chloride mmol	Triethylamine mL (mmol)	Compound	Yield (%)
1	Glycine methyl ester hydrochloride	628 (5.00)	5.00	0.83 (6) 1.7 (12)	**2a**	97
2	Glycine ethyl ester hydrochloride	698 (5.00)	5.00	0.83 (6) 1.7 (12)	**2b**	94

Methyl (quinoline-4-carbonyl)glycinate (**2a**)[198]

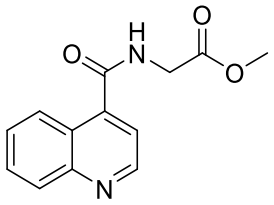

2a

$C_{13}H_{12}N_2O_3$
[244.25]

The synthesis was carried out according to **GP 1**. Glycine methyl ester hydrochloride was dissolved in CH_2Cl_2 (0.1 M). 1.19 g (4.87 mmol, 97%) of the title compound could be obtained as a red-brownish oil.

R_f (CH_2Cl_2:MeOH = 9:1) = 0.65.
^{1}H NMR (400 MHz, $CDCl_3$) δ = 8.86 (d, J = 4.3, 1H), 8.27 – 8.22 (m, 1H), 8.09 (dd, J = 8.4, 0.4, 1H), 7.73 (ddd, J = 8.4, 6.9, 1.4, 1H), 7.59 (ddd, J = 8.3, 6.9, 1.3, 1H), 7.42 (d, J = 4.3, 1H), 6.90 (s, 1H), 4.30 (d, J = 5.4, 2H), 3.81 (s, 3H).
^{13}C NMR (101 MHz, $CDCl_3$) δ = 170.11, 167.65, 149.83, 148.66, 141.28, 130.22, 129.89, 127.95, 125.36, 124.43, 118.74, 52.74, 41.69.
MS (**ESI**) calculated for $C_{13}H_{12}N_2O_3$ ($[M+H]^+$): 245.26; found: 245.24.

Ethyl (quinoline-4-carbonyl)glycinate (**2b**)[198]

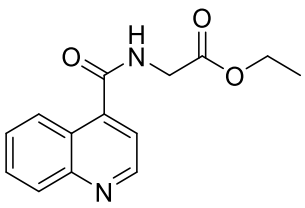

2b

$C_{14}H_{14}N_2O_3$
[258.28]

The synthesis was carried out according to **GP 1**. Glycine ethyl ester hydrochloride was dissolved in CH_2Cl_2 (0.2 M). 1.22 g (4.72 mmol, 94%) of the title compound could be obtained as a violet oil.

R_f (CH_2Cl_2:MeOH = 9:1) = 0.67.
^{1}H NMR (400 MHz, $CDCl_3$) δ = 8.88 (d, *J* = 4.3 Hz, 1H), 8.26 (dd, *J* = 8.4, 0.7 Hz, 1H), 8.11 (d, *J* = 8.4 Hz, 1H), 7.74 (ddd, *J* = 8.4, 6.9, 1.4 Hz, 1H), 7.59 (ddd, *J* = 8.2, 6.9, 1.2 Hz, 1H), 7.44 (d, *J* = 4.3 Hz, 1H), 6.84 (s, 1H), 4.32 – 4.19 (m, 4H), 1.33 (t, *J* = 7.1, 3H).
^{13}C NMR (101 MHz, $CDCl_3$) δ = 169.65, 167.59, 149.85, 148.67, 141.37, 130.23, 129.90, 127.94, 125.39, 124.46, 118.77, 61.99, 41.88, 14.30.
MS (**ESI**) calculated for $C_{14}H_{14}N_2O_3$ ($[M+H]^+$): 259.28; found: 259.23.

(Quinoline-4-carbonyl)glycine (**3**)[198]

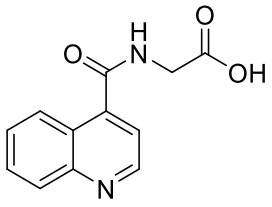

3

$C_{12}H_{10}N_2O_3$
[230.22]

NaOH (372 mg, 9.3 mmol, 2 eq) was added to a solution of ethyl-(quinoline-4-carbonyl)glycine (**2b**, 1.2 g, 4.64 mmol, 1 eq) in MeOH/H_2O (1:1; 0.37 M), and the reaction mixture was stirred for 18 h at ambient temperature. The solvent was removed under reduced pressure and the residue was dissolved in H_2O (15 mL). The aqueous phase was washed three times with CH_2Cl_2 (10 mL) and then acidified to pH 1 with 1 M HCl. The precipitate was recovered by filtration and dried azeotropically three times with MeCN to afford 775 mg (3.37 mmol, 73%) of the title compound as a violet solid.

^{1}H NMR (400 MHz, DMSO) δ = 12.78 (s, 1H), 9.15 (t, J = 5.9 Hz, 1H), 8.99 (d, J = 4.3 Hz, 1H), 8.33 – 8.24 (m, 1H), 8.09 (d, J = 8.3 Hz, 1H), 7.82 (ddd, J = 8.4, 6.9, 1.3 Hz, 1H), 7.67 (ddd, J = 8.2, 6.9, 1.1 Hz, 1H), 7.56 (d, J = 4.3 Hz, 1H), 4.03 (d, J = 6.0 Hz, 2H).
^{13}C NMR (101 MHz, DMSO) δ = 171.43, 167.67, 150.73, 148.38, 142.32, 130.35, 129.75, 127.75, 126.10, 124.64, 119.48, 41.57.
MS (**ESI**) calculated for $C_{12}H_{10}N_2O_3$ ($[M+H]^+$): 231.23; found 231.24.

Benzyl (*S*)-2-((acetylthio)methyl)pyrrolidine-1-carboxylate (**4**)[223]

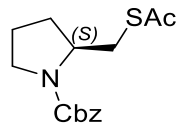

4

$C_{11}H_{19}NO_3S$
[293.28]

Triethylamine (2.1 mL, 15.2 mmol, 1.19 eq) was added to a solution of Z-L-prolinol (3 g, 12.8 mmol, 1 eq) in dry CH_2Cl_2 (0.2 M), and the reaction mixture was stirred for 1 h at 0 °C. Methane sulfonyl chloride (1.18 mL, 15.3 mmol, 1.2 eq) was then added dropwise at 0 °C and the reaction mixture was stirred for another 16.5 h at ambient temperature. Following addition of CH_2Cl_2 (60 mL), the organic phase was washed three times with 1 M $KHSO_4$ solution (60 mL), once with H_2O (60 mL), and once with saturated NaCl solution (60 mL). The organic phase was dried with anhydrous $MgSO_4$ and the solvent was removed under reduced pressure. The crude mesylate thus obtained was used in the next step without storage.
Thioacetic acid (1.35 mL, 19.1 mmol, 1.5 eq) was added to a solution of Cs_2CO_3 (3.12 g, 9.56 mmol, 0.75 eq) in dry DMF (0.2 M), and the reaction mixture was stirred for 5 min at ambient temperature. Using a cannula, the reaction mixture was then added to the crude mesylate, upon which the reaction mixture turned cloudy and developed an orange color. The reaction mixture was protected from light with aluminum foil and stirred for three nights at ambient temperature. EtOAc (140 mL) and H_2O (60 mL) were then added, and the aqueous phase was extracted with EtOAc (30 mL). The combined organic fractions were washed twice with saturated $NaHCO_3$ solution (60 mL), twice with 1 M $KHCO_3$ solution (60 mL) and once with saturated NaCl solution (20 mL). After drying with $MgSO_4$, the solvent was removed under reduced pressure. The crude product was adsorbed onto silica gel and after purification by column chromatography (cyclohexane:EtOAc = 9:1), 2.57 g (8.76 mmol, 69%) of the title compound could be obtained as an orange oil.

R_f (*n*-hexane:EtOAc = 8:2) = 0.42.
^{1}H NMR (400 MHz, $CDCl_3$) δ = 7.45 – 7.28 (m, 5H), 5.13 (m, 2H), 4.02 (m, 1H), 3.45 (m, 2H), 3.14 (m, 2H), 2.33 (d, *J* = 6.7, 1H), 2.07 – 1.63 (m, 4H).
MS (**ESI**) calculated for $C_{11}H_{19}NO_3S$ ($[M+H]^+$): 294.12; found: 294.17.

The analytical data corresponds to the literature.[223]

Sodium (*S*)-(1-((benzyloxy)carbonyl)pyrrolidin-2-yl)methanesulfonate (**5**)[223]

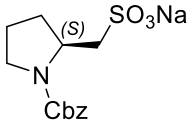

5
$C_{13}H_{16}NNaO_5S$
[321.32]

Aqueous H_2O_2 (30% w/w, 3.4 mL) was added to a solution of benzyl *(S)*-2-((acetylthio)methyl)pyrrolidine-1-carboxylate (**4**, 1 g, 3.41 mmol, 1 eq) in AcOH (0.33 M), and the reaction mixture was stirred for 17 h at ambient temperature. Sodium acetate trihydrate (463 mg, 3.4 mmol, 1 eq) was then added and the reaction mixture was stirred for another 20 min at ambient temperature. The reaction mixture was diluted with DMF (11.3 mL) and the volume was reduced to approximately half under reduced pressure before adding another portion of DMF (11.3 mL) and reducing the volume to one third under reduced pressure. The addition of DMF and subsequent reduction of the solution was repeated twice with 12 mL of DMF each time until no more peroxide could be detected using KI starch paper. The reaction mixture was then concentrated under reduced pressure, and the residue was taken up in H_2O (22.6 mL) and CH_2Cl_2 (11.3 mL). The aqueous phase was washed with CH_2Cl_2 (11.3 mL), the solvent was removed under reduced pressure, and the crude product was dissolved in H_2O (15 mL) before it was freeze-dried. 1.07 g (3.33 mmol, 98%) of the title compound could be obtained as a white solid.

^{1}H NMR (400 MHz, D_2O) δ = 7.53 – 7.32 (m, 5H), 5.29 – 5.07 (m, 2H), 4.34 – 4.10 (m, 1H), 3.50 – 3.21 (m, 3H), 3.00 – 2.86 (m, 1H), 2.23 – 1.98 (m, 2H), 1.98 – 1.83 (m, 2H).
MS (**ESI**) calculated for $C_{11}H_{19}NO_3S$ ($[M\text{-}H]^-$): 298.08; found: 298.13.

The analytical data corresponds to the literature.[223]

Benzyl (*S*)-2-((chlorosulfonyl)methyl)pyrrolidine-1-carboxylate (**6**)[230]

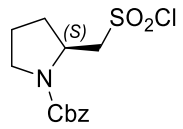

6
$C_{13}H_{16}ClNO_4S$
[317.78]

2 M HCl (1.6 mL) was added to a solution of *N*-chlorosuccinimide (1.07 g, 8 mmol, 4 eq) in MeCN (8 M) and the reaction mixture was cooled to 0 °C. A solution of benzyl-(*S*)-2-((acetylthio)methyl)pyrrolidine-1-carboxylate (**4**, 586 mg, 2 mmol, 1 eq) in MeCN (1 M) was then added dropwise and the reaction mixture was stirred for 80 min at 0 °C. After dilution of the reaction mixture with isopropyl ether (10 mL), the organic phase was separated and washed three times with a 12% solution of NaCl (10 mL). After drying with $MgSO_4$, the solvent was removed under reduced pressure. 572 mg (1.80 mmol, 90%) of the title compound could be obtained as a pale yellow solid, which was used in the next reaction without further purification.

Benzyl (*S*)-2-((fluorosulfonyl)methyl)pyrrolidine-1-carboxylate (**7**)[186,223]

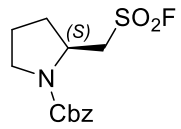

7
$C_{13}H_{16}FNO_4S$
[301.33]

A solution of KHF_2 (210 mg, 2.68 mmol, 2.3 eq) in H_2O (0.86 M) was stirred under air for 1 h at ambient temperature and then added to a solution of benzyl-(*S*)-2-((chlorosulfonyl)methyl)pyrrolidine-1-carboxylate (**6**, 370 mg, 1.16 mmol, 1 eq) in MeCN (0.15 M). The reaction mixture was vigorously stirred for 92 h at ambient temperature, before the aqueous phase was separated and extracted twice with EtOAc (7 mL). The combined organic fractions were washed three times with saturated NaCl solution (5 mL) and dried with anhydrous $MgSO_4$. The solvent was removed under reduced pressure, and the crude product was adsorbed onto silica gel. After purification by column chromatography (100% CH_2Cl_2), 258 mg (0.86 mmol, 73%) of the title compound could be obtained as a pale yellow solid.

R_f (*n*-hexane:EtOAc = 6:4) = 0.55.
^{1}H NMR (400 MHz, $CDCl_3$) δ = 7.43 – 7.29 (m, 5H), 5.24 – 5.09 (m, 2H), 4.36 (m, 1H), 4.17 (d, *J* = 14.3, 0.6H), 3.79 (d, *J* = 14.4, 0.3H), 3.64 – 3.18 (m, 3H), 2.24 (m, 1H), 2.12 (m, 1H), 1.96 (dd, *J* = 13.6, 7.2, 2H).
MS (**ESI**) calculated for $C_{13}H_{16}FNO_4S$ ($[M+H]^+$): 302.08; found: 302.20.

The analytical data corresponds to the literature.[223]

(*S*)-Pyrrolidin-2-ylmethanesulfonyl fluoride hydrochloride (**8**)[223]

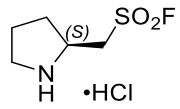

8

$C_5H_{10}FNO_2S$•HCl
[203.66]

HBr in AcOH (33 wt. %, 19.8 mL) was added to a solution of benzyl-(*S*)-2-((fluorosulfonyl)methyl)pyrrolidine-1-carboxylate (**7**, 1 g, 3.3 mmol, 1 eq) in CH_2Cl_2 (0.1 M) and the reaction mixture was stirred for 1 h at ambient temperature. The solvent was removed under reduced pressure, and the residue was taken up in H_2O (30 mL). The resulting solution was washed twice with EtOAc (30 mL). An anion exchange resin (AmberLite™ HPR 4100 Cl) was treated with HCl for 10 column volumes, then washed with H_2O until the pH was 7, then with MeOH for 10 column volumes, and then again with H_2O. 2.5 g of the pretreated resin was then added to the aqueous solution and stirred for 10 minutes at ambient temperature. The anion exchange resin was filtered off and the filtrate was freeze-dried. 619 mg (3.04 mmol, 92%) of the title compound could be obtained as a slightly yellowish, hygroscopic solid.

^{1}H NMR (400 MHz, D_2O) δ = 4.39 – 4.27 (m, 1H), 4.22 – 4.06 (m, 2H), 3.37 (m, 2H), 2.39 (m, 1H), 2.16 – 1.92 (m, 2H), 1.90 – 1.73 (m, 1H).
MS (**ESI**) calculated for $C_5H_{10}FNO_2S$ ($[M+H]^+$): 168.05; found: 168.08.

The analytical data corresponds to the literature.[223]

Methyl L-prolinate hydrochloride (**9**)[236]

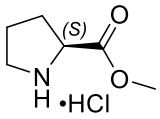

9

$C_6H_{11}NO_2$•HCl
[165.62]

Thionyl chloride (0.47 mL, 6.45 mmol, 1.49 eq) was added dropwise in a stream of argon to a pre-cooled (0 °C) solution of L-proline (500 mg, 4.34 mmol, 1 eq) in dry MeOH (0.59 M). The reaction mixture slowly warmed to ambient temperature and stirred for 21.5 h. The solvent and excess thionyl chloride were removed under reduced pressure, and the residue was triturated twice with diethyl ether (3 mL) and then stirred in diethyl ether. After removal of the diethyl ether and drying in a high vacuum, a white, hygroscopic solid was obtained in quantitative yield (712 mg, 4.30 mmol).

^{1}H NMR (400 MHz, D_2O) δ = 4.52 (dd, J = 8.5, 7.5 Hz, 1H), 3.87 (s, 3H), 3.53 – 3.38 (m, 2H), 2.55 – 2.39 (m, 1H), 2.26 – 2.14 (m, 1H), 2.14 – 2.02 (m, 2H).

The analytical data corresponds to the literature.[261]

General procedure 2 (**GP 2**)

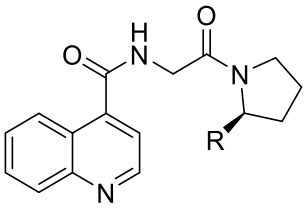

R = -$COOCH_3$, -CH_2SO_2F

Triethylamine (90 µL, 0.65 mmol, 1 eq) was added to a solution of the corresponding amine (1 eq) in dry DMF (0.1 M) and the reaction mixture was stirred for 15 min at ambient temperature. **3** (150 mg, 0.65 mmol, 1 eq) and EEDQ (322 mg, 1.30 mmol, 2 eq) were then added and the reaction mixture was stirred at ambient temperature for several nights. After completion of the reaction, the reaction mixture was poured into 70 mL ice H_2O and stirred. The resulting mixture was extracted twice with $CHCl_3$ or CH_2Cl_2. The combined organic fractions were washed five times with H_2O, then once with 1 N citric acid, H_2O and finally with saturated NaCl solution. The aqueous citric acid phase was adjusted to pH 7–8 with Na_2CO_3 and then extracted twice with $CHCl_3$ or CH_2Cl_2. The combined organic fractions were dried with Na_2SO_4 and the solvent was removed under reduced pressure. After purification by column chromatography (CH_2Cl_2 or $CHCl_3$/MeOH), the product was triturated with diethyl ether.

Table 13: Experimental data for the synthesis of **10** and **11**.

Entry	Amine	Amine mg (mmol)	Compound	Yield (%)
1	Methyl L-prolinate hydrochloride (**9**)	108 (0.65)	**10**	27
2	(*S*)-Pyrrolidine-2-ylmethanesulfonyl fluoride hydrochloride (**8**)	132 (0.65)	**11**	19

Methyl (quinoline-4-carbonyl)glycyl-L-prolinate (**10**)

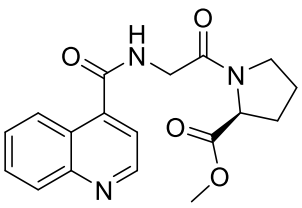

10

$C_{18}H_{19}N_3O_4$

[341.37]

The synthesis was carried out according to **GP 2**. The reaction mixture was stirred for 44.5 h. Deviating from **GP 2**, the product was purified by column chromatography (CH_2Cl_2:MeOH = 97:3), isolated by acid-base extraction and subsequently extracted with EtOAc. 60 mg (0.17 mmol, 27%) of a slightly yellowish oil were obtained.

R_f (CH_2Cl_2:MeOH = 95:5) = 0.63.

^{1}H NMR (400 MHz, $CDCl_3$) δ = 8.87 (d, *J* = 3.9, 1H), 8.24 (d, *J* = 8.5, 1H), 8.08 (d, *J* = 8.5, 1H), 7.70 (dd, *J* = 8.3, 7.0, 1H), 7.56 (q, *J* = 7.5, 1H), 7.46 (dd, *J* = 4.1, 2.8, 1H), 7.26 (s, 1H), 4.51 – 4.42 (m, 1H), 4.40 – 4.16 (m, 2H), 3.76 (s, 1H), 3.67 (s, 2H), 3.67 – 3.57 (m, 1H), 3.56 – 3.44 (m, 1H), 2.30 – 1.78 (m, 4H).

^{13}C NMR (101 MHz, $CDCl_3$) δ = 172.23, 167.27, 166.59, 149.80, 148.60, 141.23, 130.01, 129.76, 127.75, 125.39, 124.46, 118.90, 58.99, 58.65, 52.97, 52.45, 46.77, 46.10, 42.42, 42.21, 31.33, 29.05, 24.65, 22.21.

MS (**ESI**) calculated for $C_{18}H_{19}N_3O_4$ ($[M+H]^+$): 342.14; found: 342.20.

Due to rotamers, more signals are present in the ^{13}C-NMR.

(*S*)-(1-((Quinoline-4-carbonyl)glycyl)pyrrolidin-2-yl)methanesulfonyl fluoride (**11**)

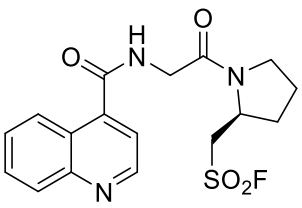

11

$C_{17}H_{18}FN_3O_4S$
[379.41]

The synthesis was carried out according to **GP 2**. The reaction mixture was stirred for 119 h. After purification by column chromatography ($CHCl_3$:MeOH = 98:2), the product was triturated twice with diethyl ether. 47 mg (0.11 mmol, 19%) of the title compound were obtained as a grayish solid.

R_f (CH_2Cl_2/MeOH = 98:2) = 0.15.
Mp: Decomposition from 156–158 °C.
^{1}H NMR (400 MHz, $CDCl_3$) δ = 8.97 (d, *J* = 4.0 Hz, 1H), 8.30 (d, *J* = 7.8 Hz, 1H), 8.17 (d, *J* = 8.4 Hz, 1H), 7.78 (ddd, *J* = 8.4, 6.9, 1.3 Hz, 1H), 7.63 (ddd, *J* = 8.2, 6.9, 1.1 Hz, 1H), 7.53 (d, *J* = 4.3 Hz, 1H), 7.03 (s, 1H), 4.57 (t, *J* = 8.2 Hz, 1H), 4.31 (qd, *J* = 17.8, 4.4 Hz, 2H), 4.07 (dt, *J* = 14.4, 3.0 Hz, 1H), 3.67 – 3.45 (m, 3H), 2.35 – 2.20 (m, 2H), 2.20 – 2.05 (m, 2H).
^{13}C NMR (101 MHz, $CDCl_3$) δ = 167.24, 149.55, 148.30, 141.65, 130.54, 129.66, 128.21, 125.44, 124.64, 119.00, 53.44, 52.13, 51.99, 46.27, 42.85, 29.14, 24.18.
^{19}F NMR (376 MHz, $CDCl_3$) δ = 60.50.
HRMS (**ESI**) calculated for $C_{17}H_{18}FN_3O_4S$ ($[M+H]^+$): 380.10748; found: 380.10768.

5.3.2 NMR spectra

^{1}H NMR of quinoline-4-carbonyl chloride hydrochloride (**1**)[227]

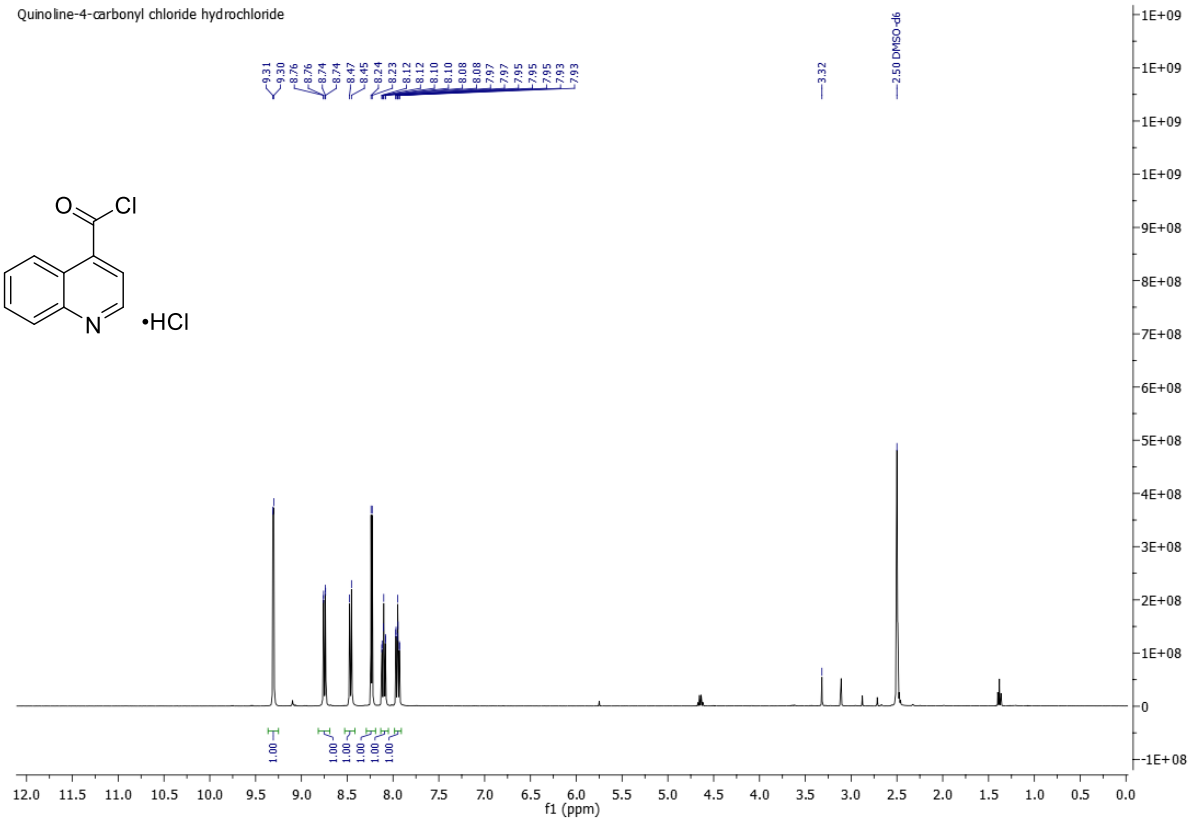

^{1}H and ^{13}C NMR of methyl (quinoline-4-carbonyl)glycinate (**2a**)

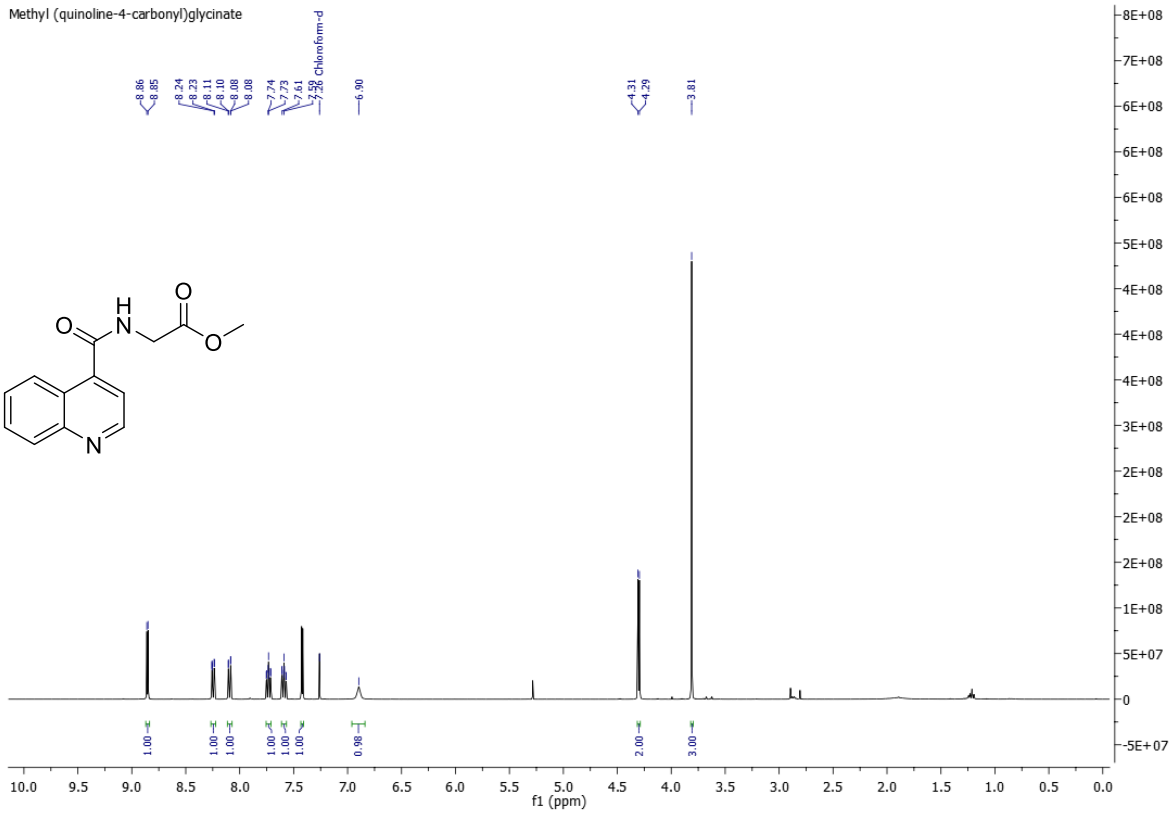

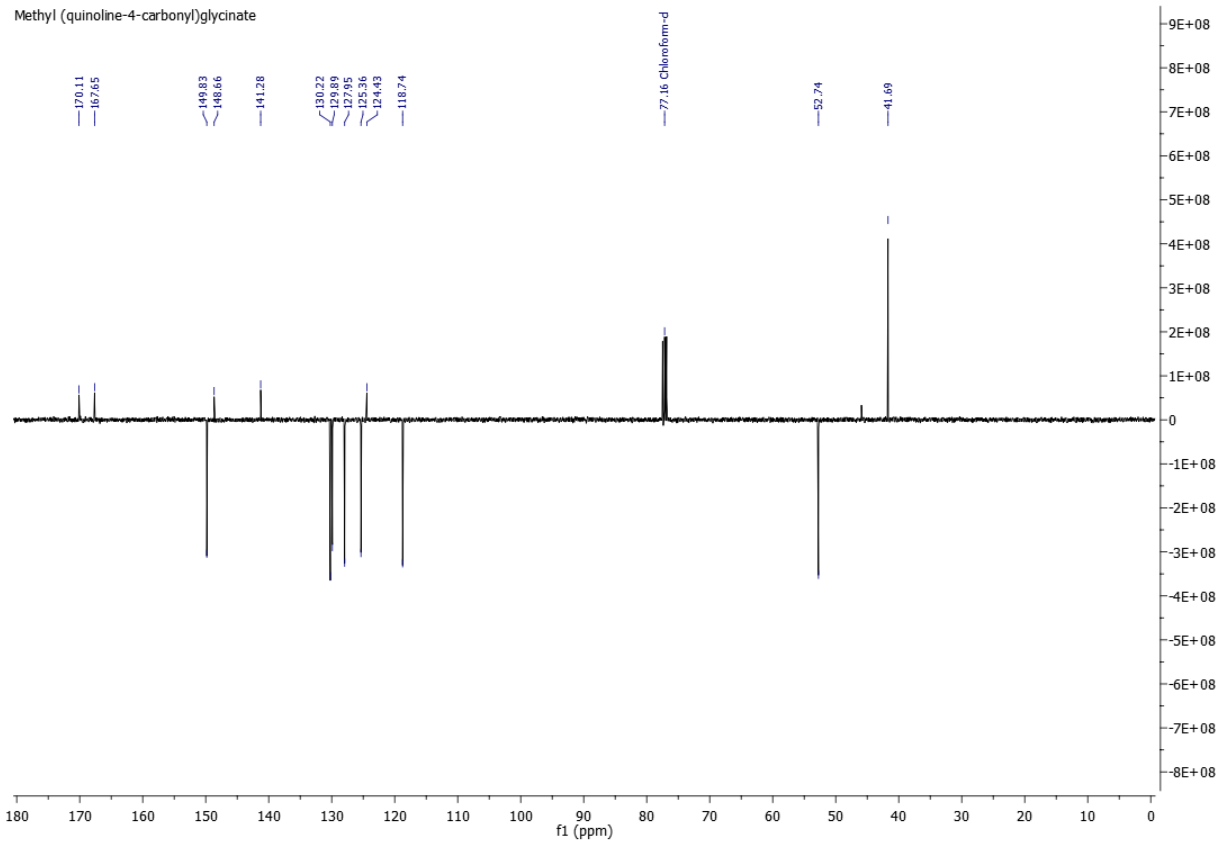

^{1}H and ^{13}C NMR of ethyl (quinoline-4-carbonyl)glycinate (**2b**)[198]

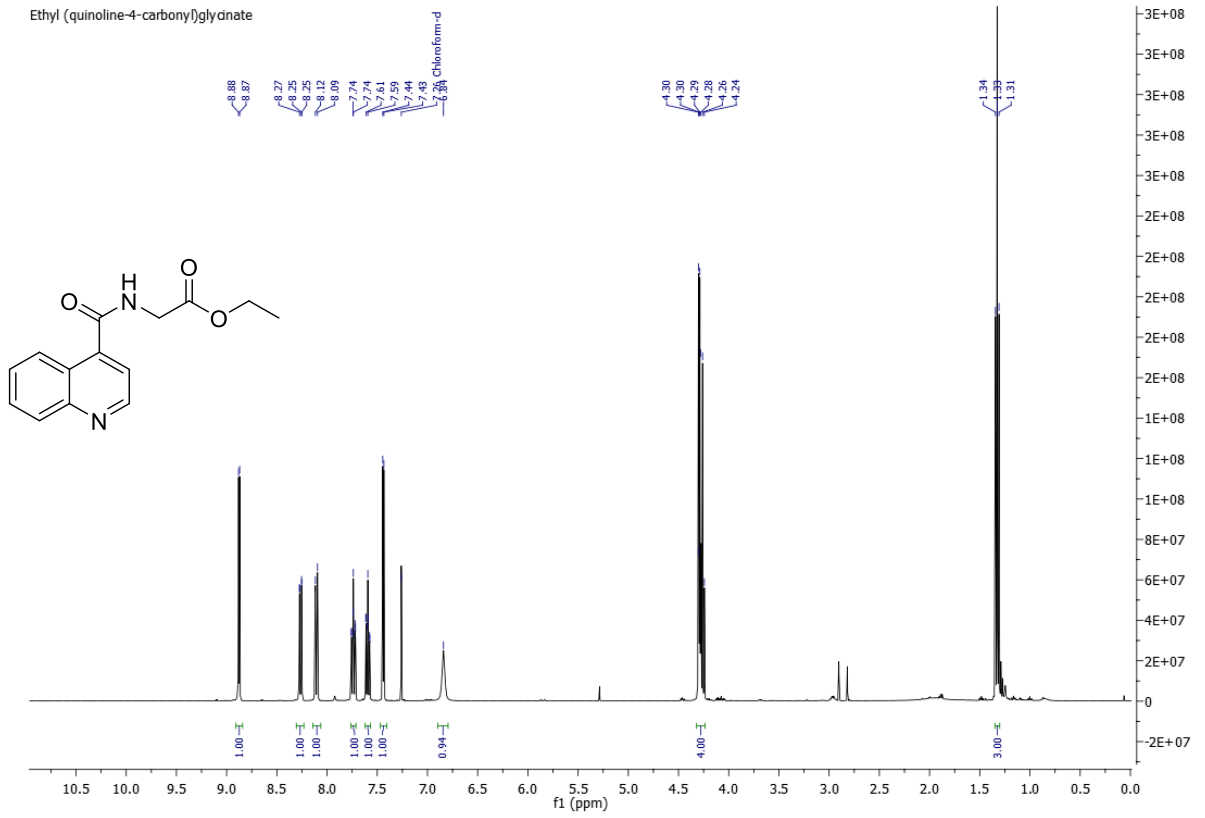

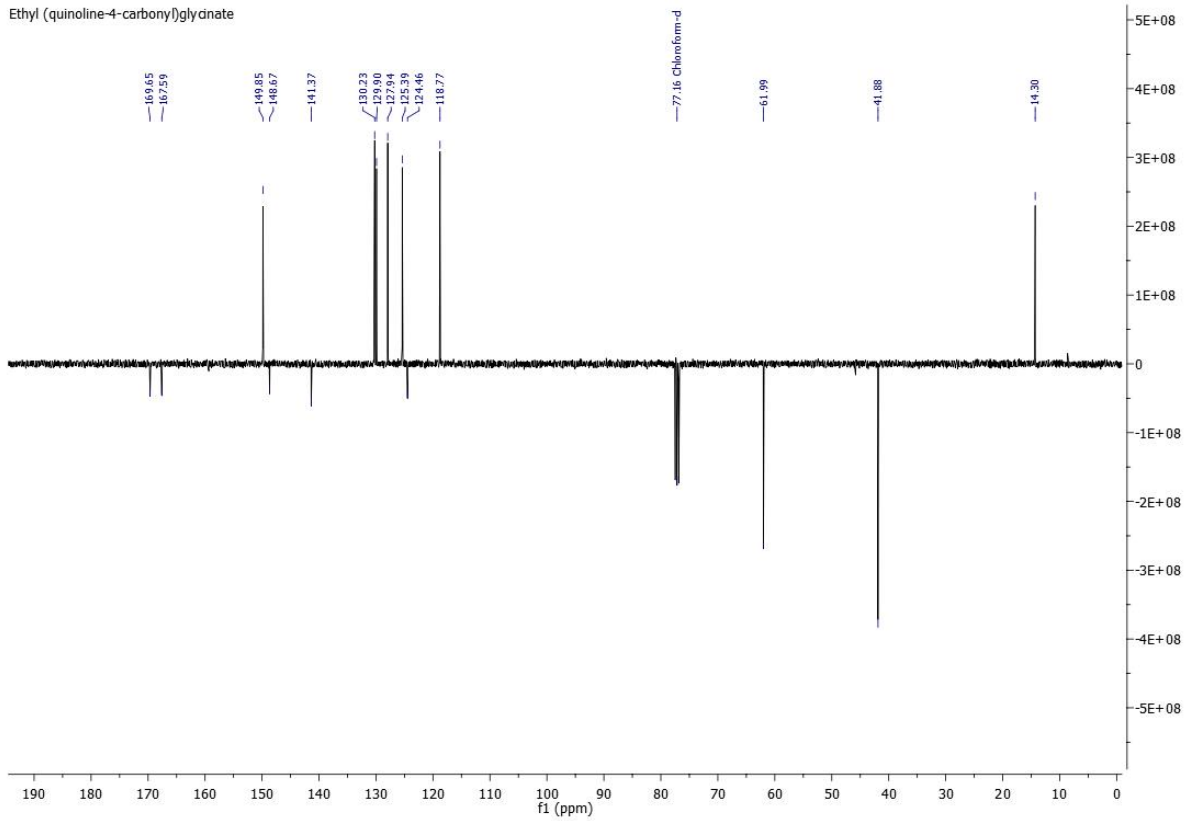

^{1}H and ^{13}C NMR of (quinoline-4-carbonyl)glycine (**3**)[198]

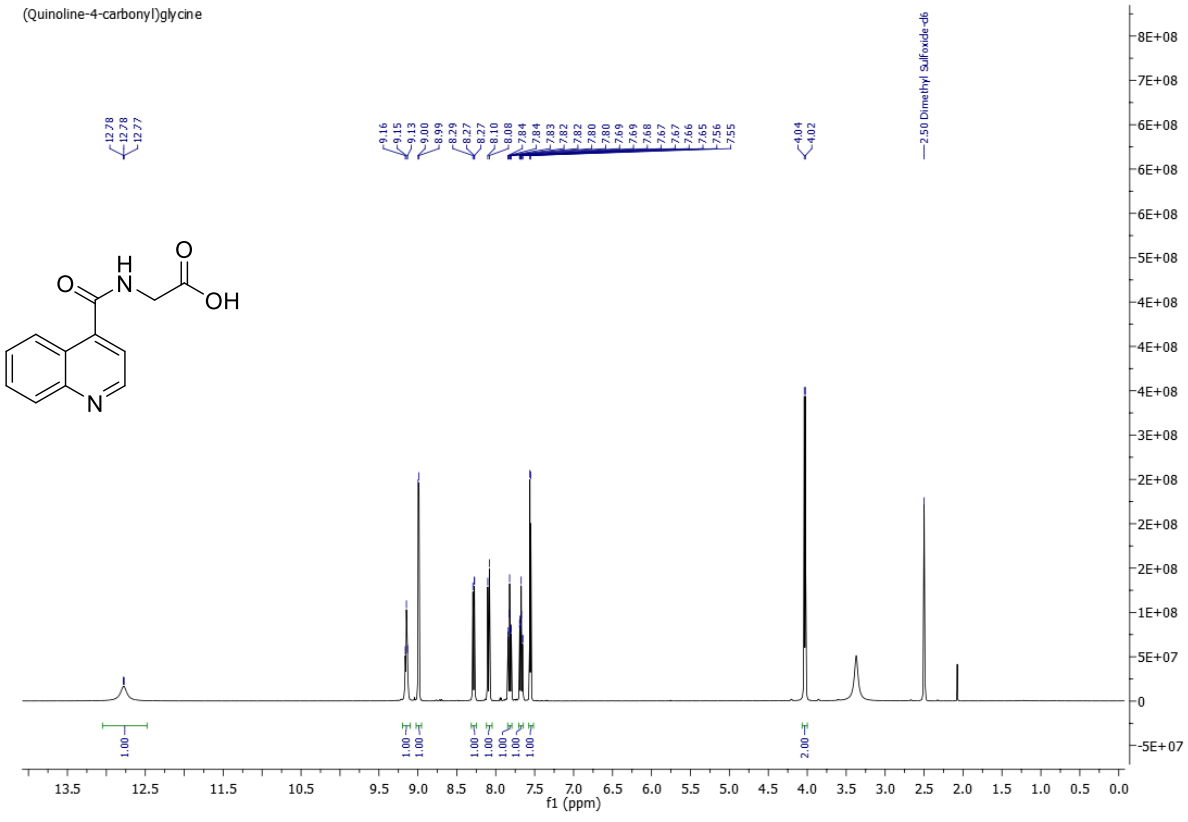

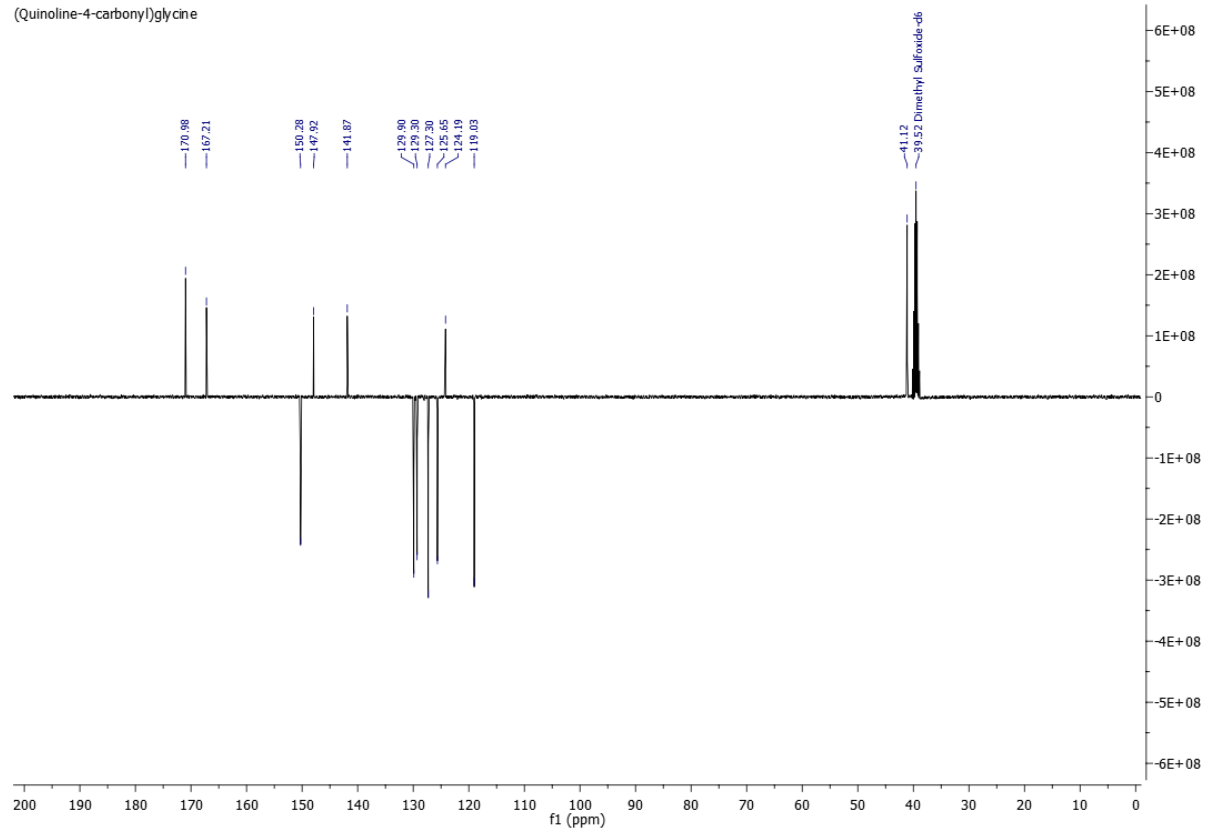

^{1}H NMR of benzyl (*S*)-2-((acetylthio)methyl)pyrrolidine-1-carboxylate (**4**)[223]

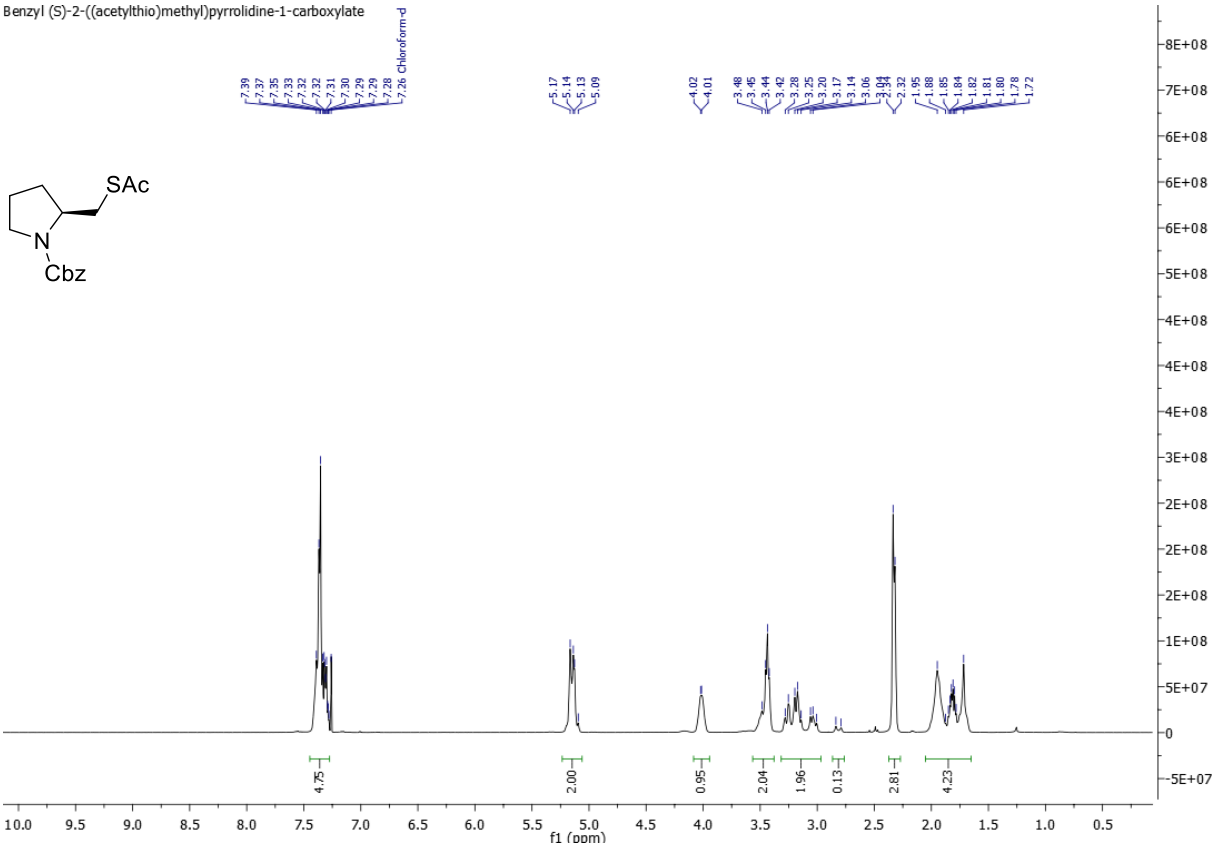

^{1}H NMR of sodium (*S*)-(1-((benzyloxy)carbonyl)pyrrolidin-2-yl)methanesulfonate (**5**)[223]

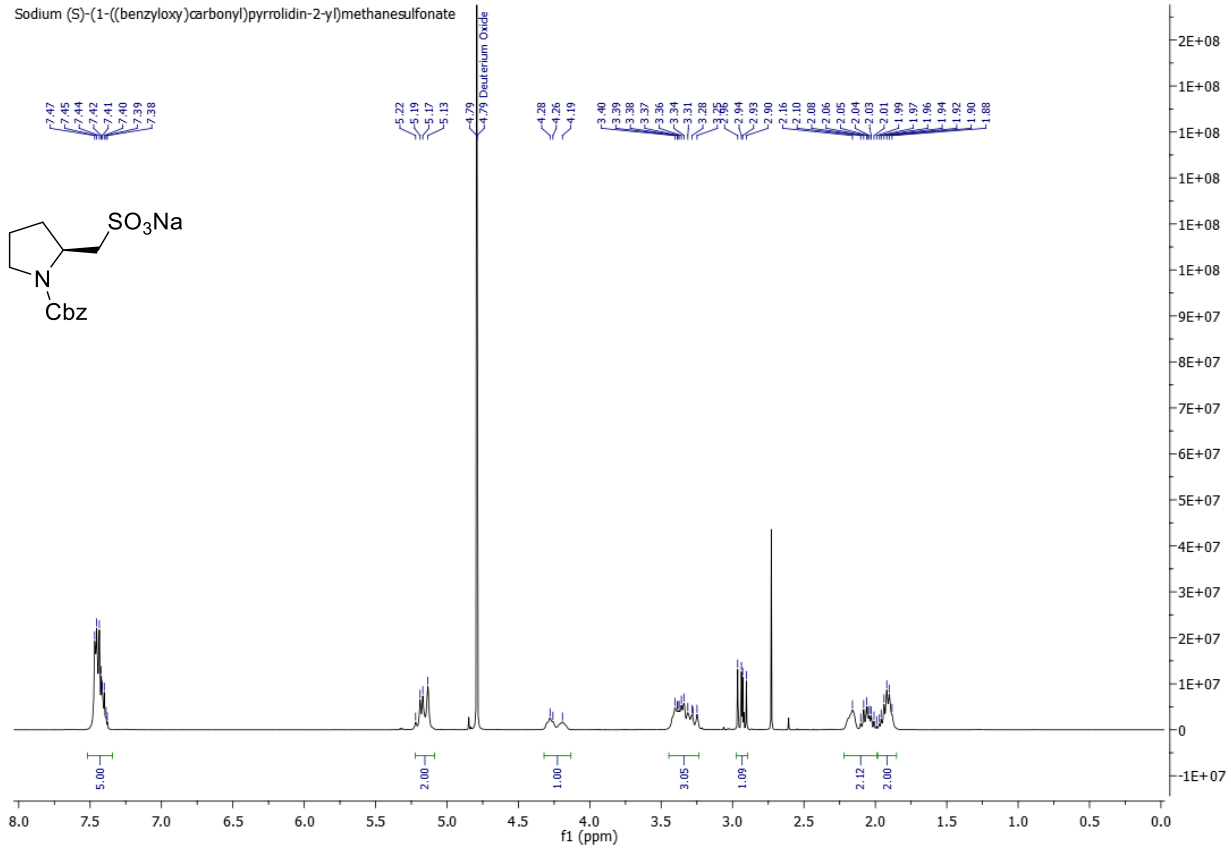

^{1}H NMR of benzyl (*S*)-2-((fluorosulfonyl)methyl)pyrrolidine-1-carboxylate (**7**)[223]

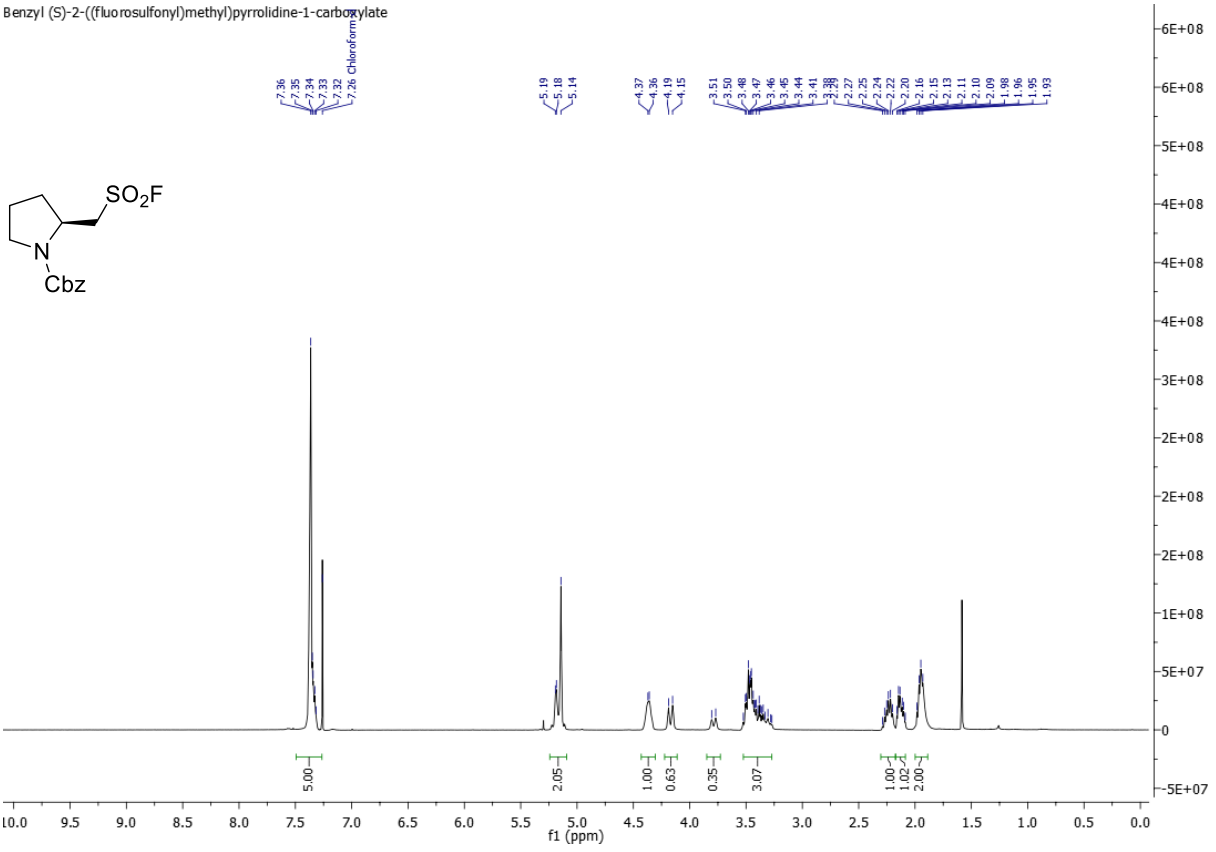

^{1}H NMR of (*S*)-pyrrolidin-2-ylmethanesulfonyl fluoride hydrochloride (**8**)[223]

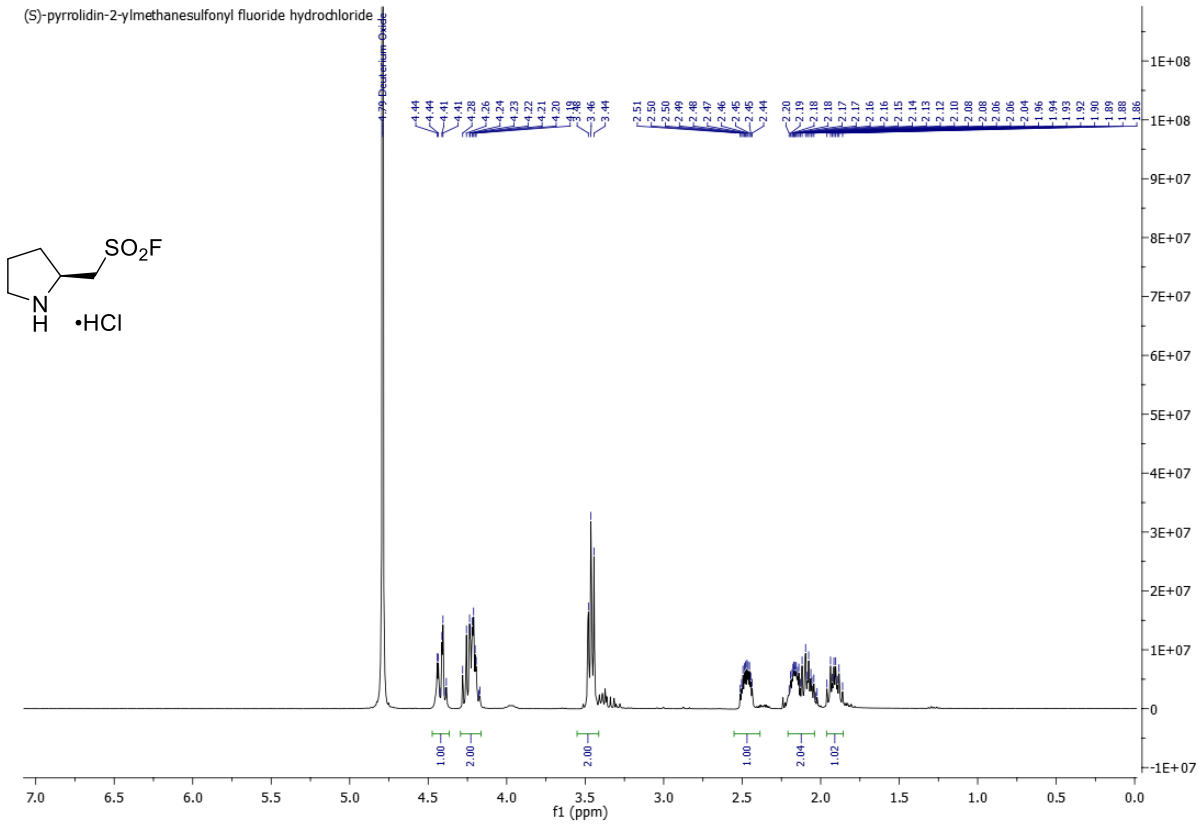

^{1}H NMR of methyl L-prolinate hydrochloride (**9**)[261]

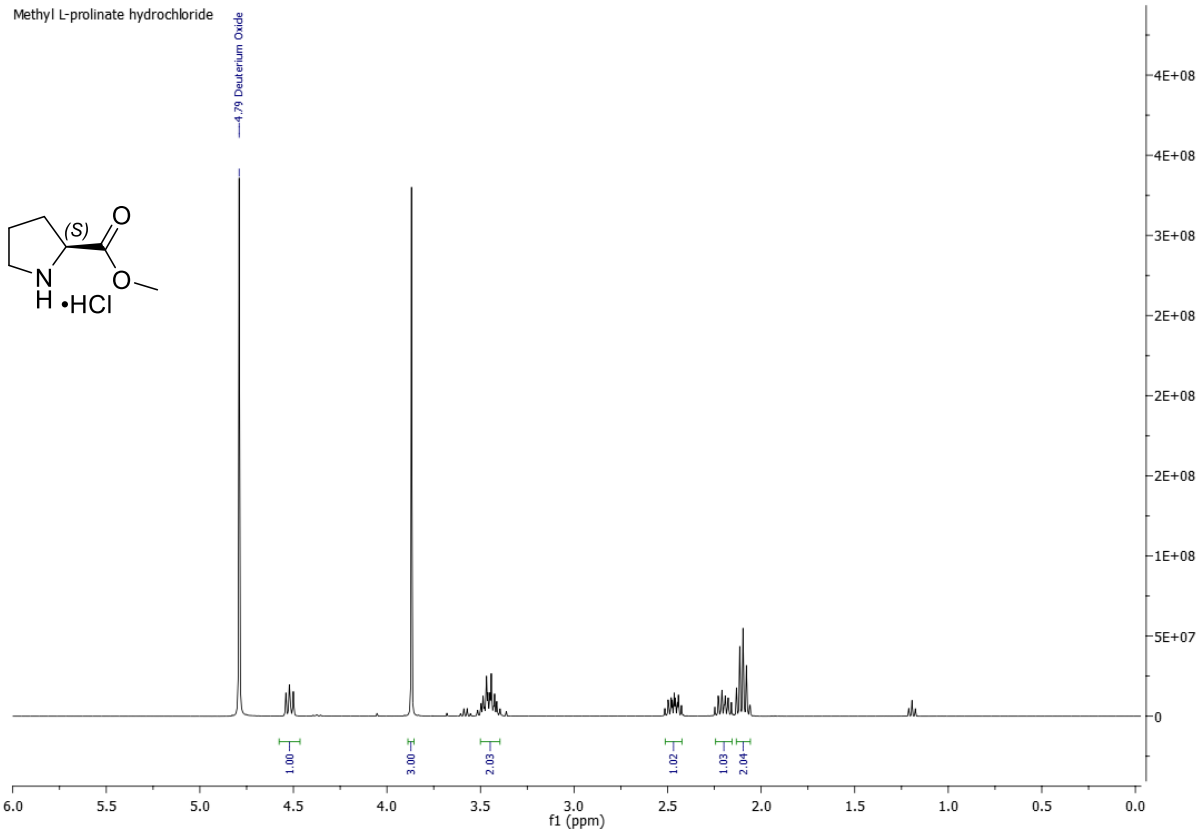

^{1}H, ^{13}C, COSY and HSQC NMR of methyl (quinoline-4-carbonyl)glycyl-L-prolinate (**10**)

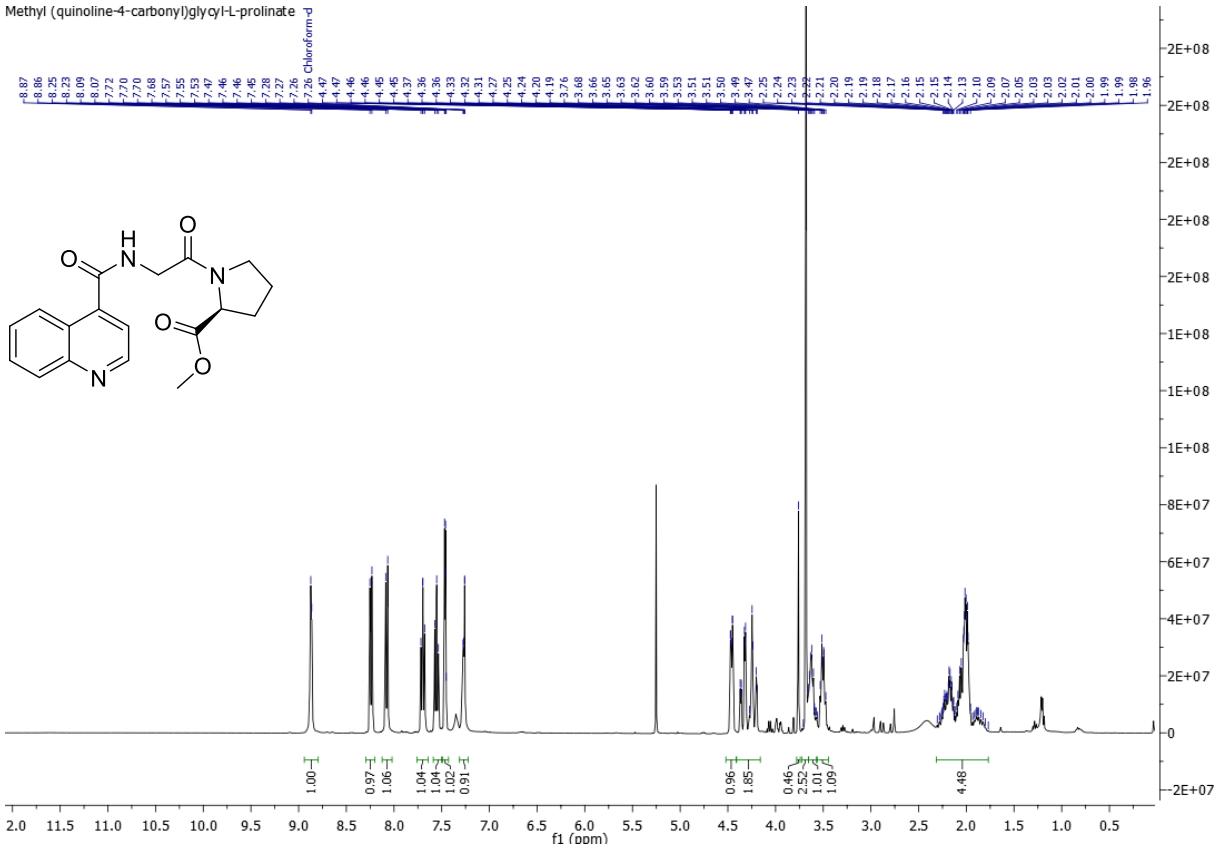

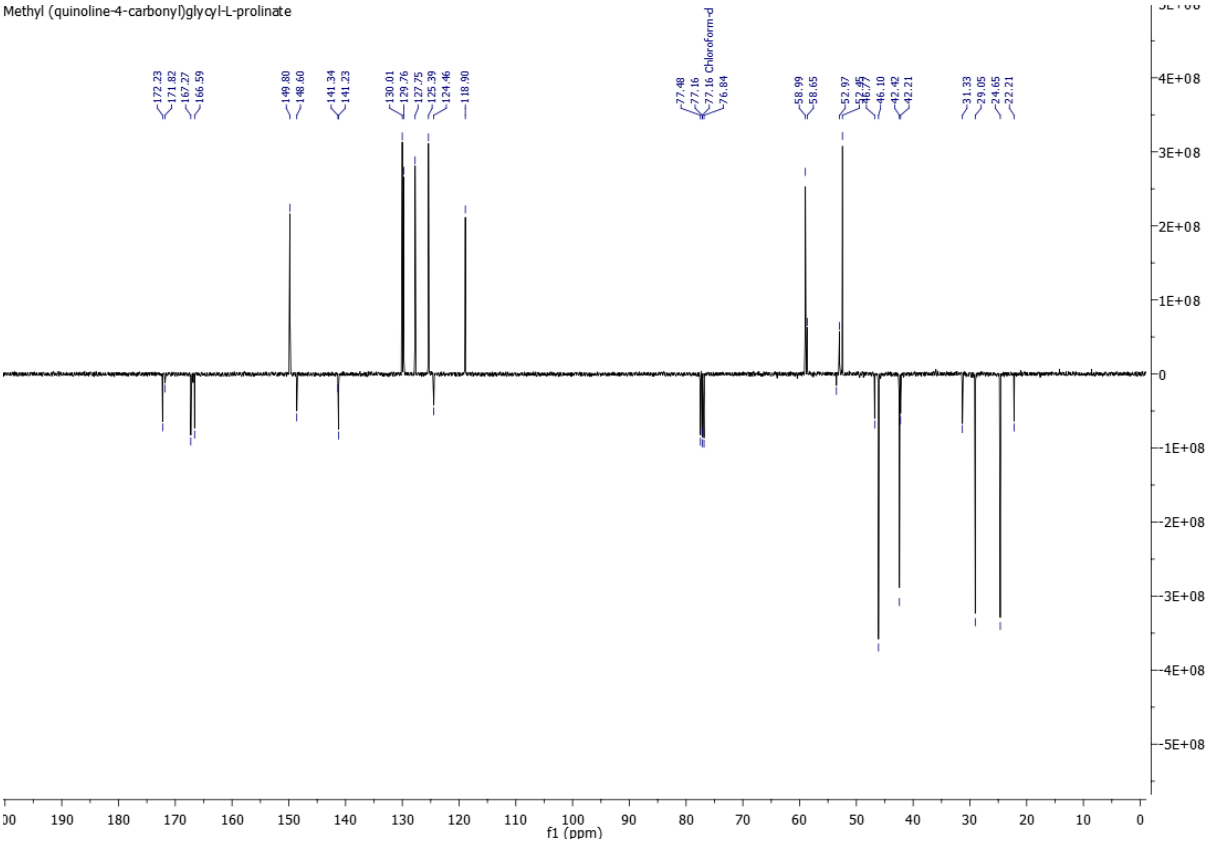

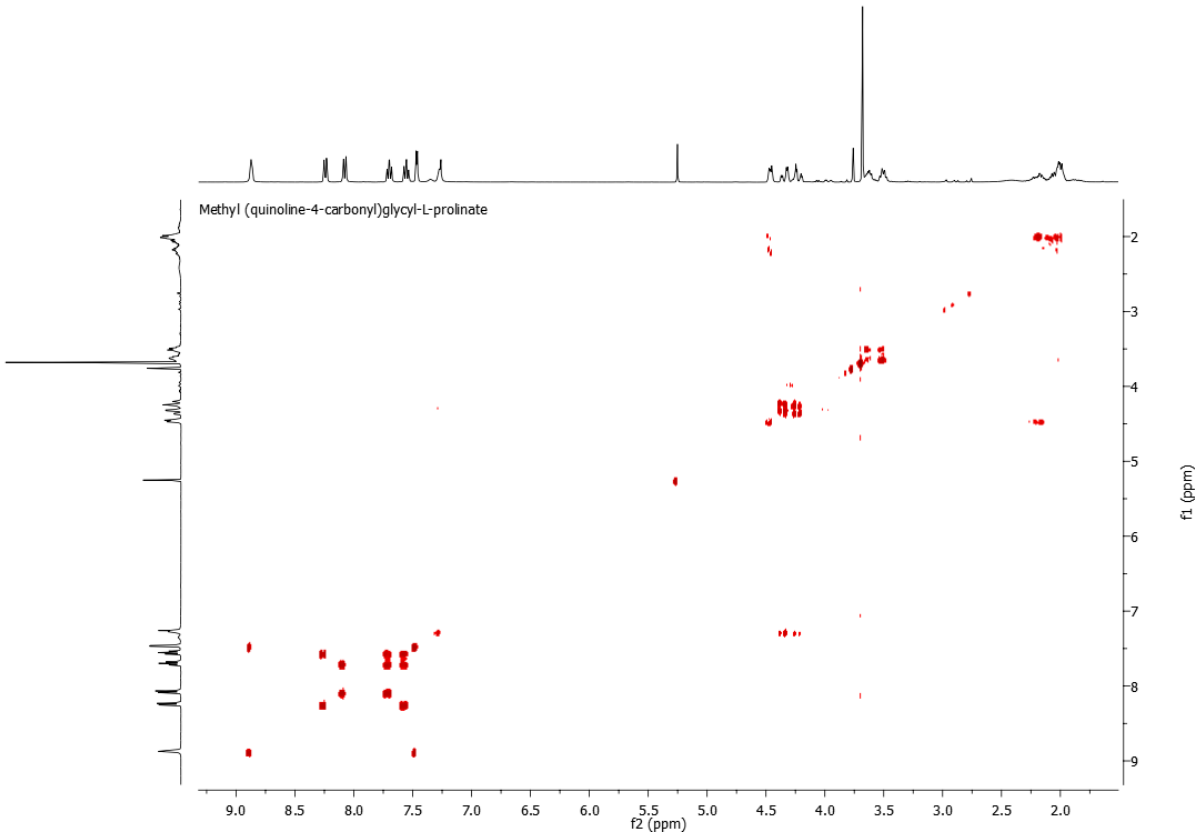
Methyl (quinoline-4-carbonyl)glycyl-L-prolinate
f2 (ppm)
f1 (ppm)

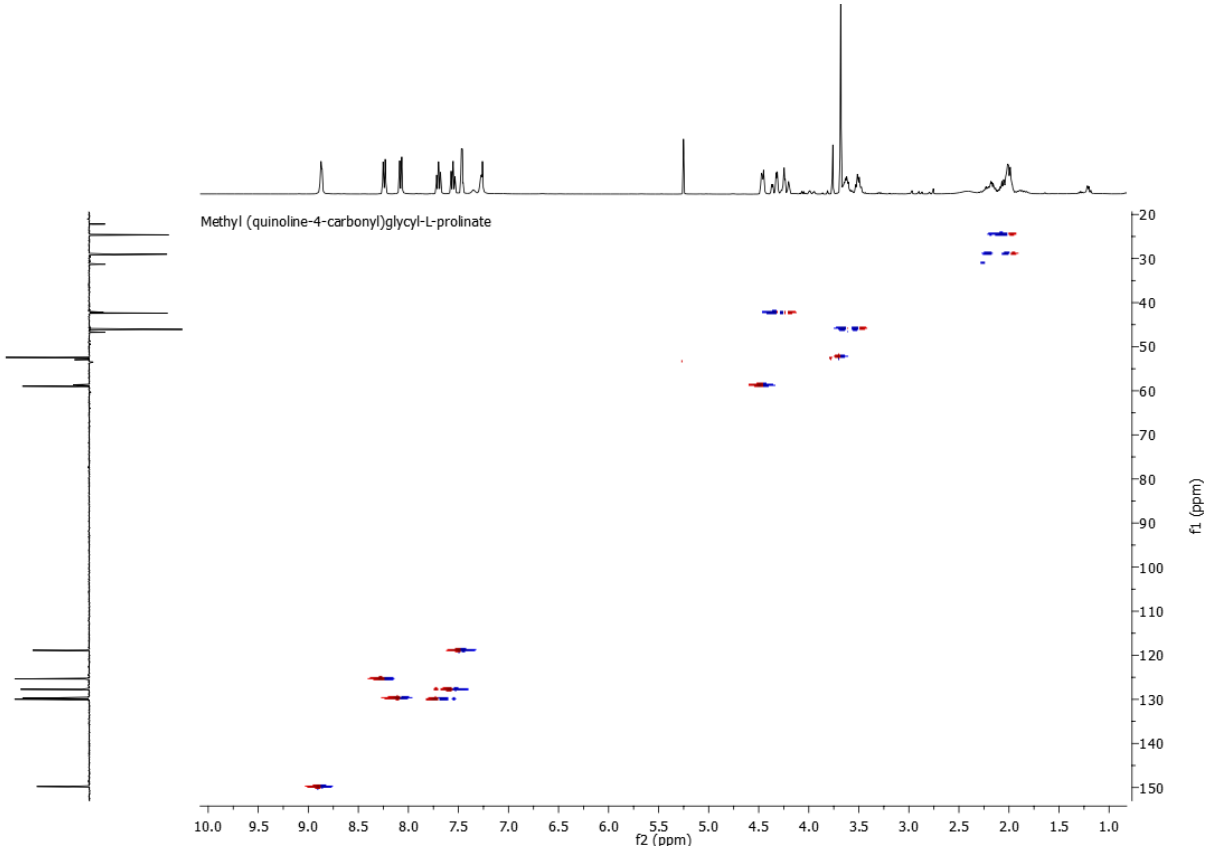
Methyl (quinoline-4-carbonyl)glycyl-L-prolinate
f2 (ppm)
f1 (ppm)

^{1}H, ^{13}C and ^{19}F NMR of (*S*)-(1-((quinoline-4-carbonyl)glycyl)pyrrolidin-2-yl)methanesulfonyl fluoride (**11**)

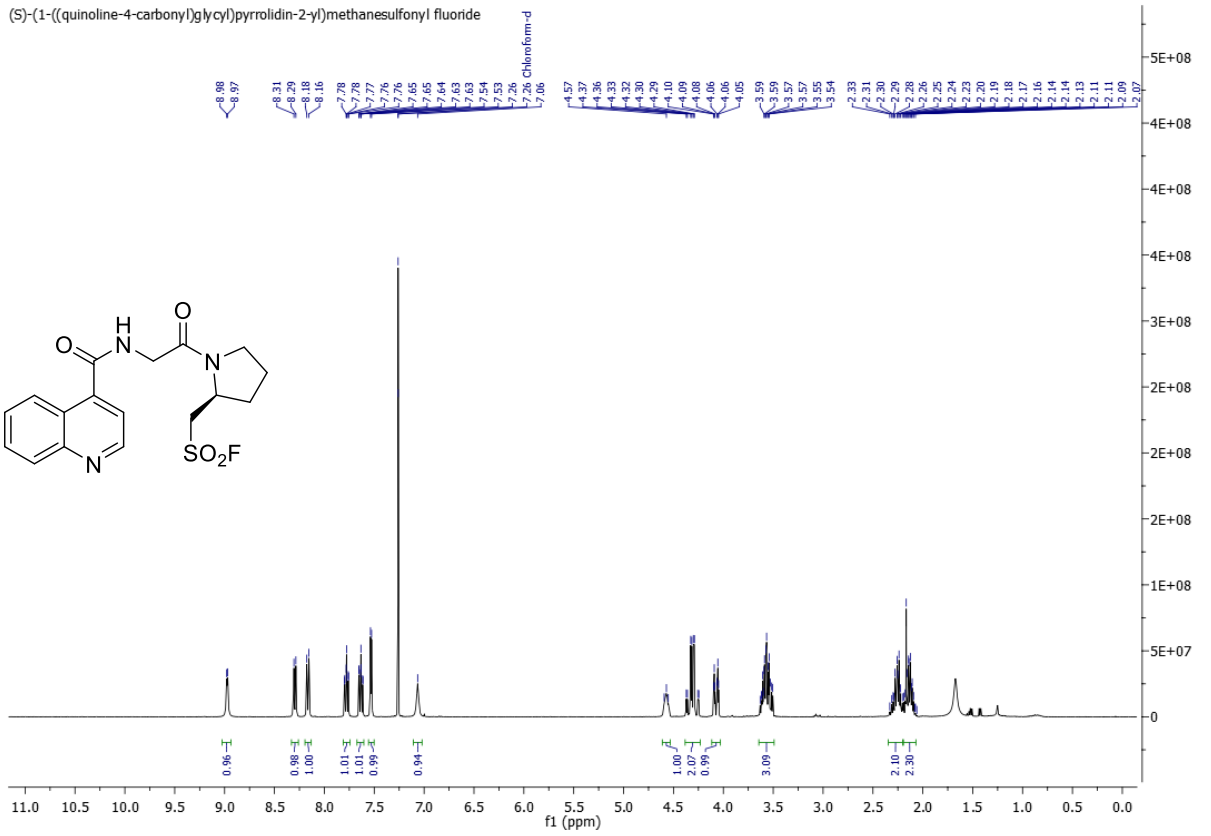

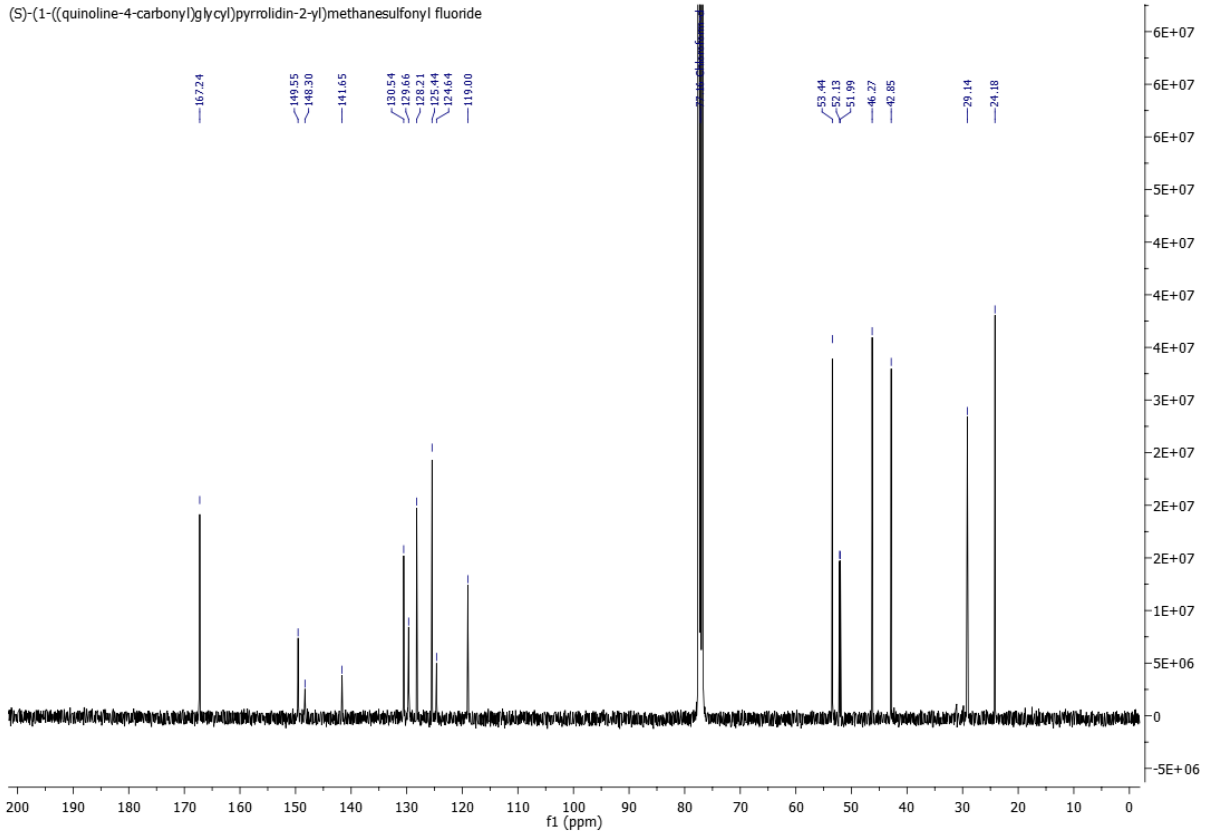

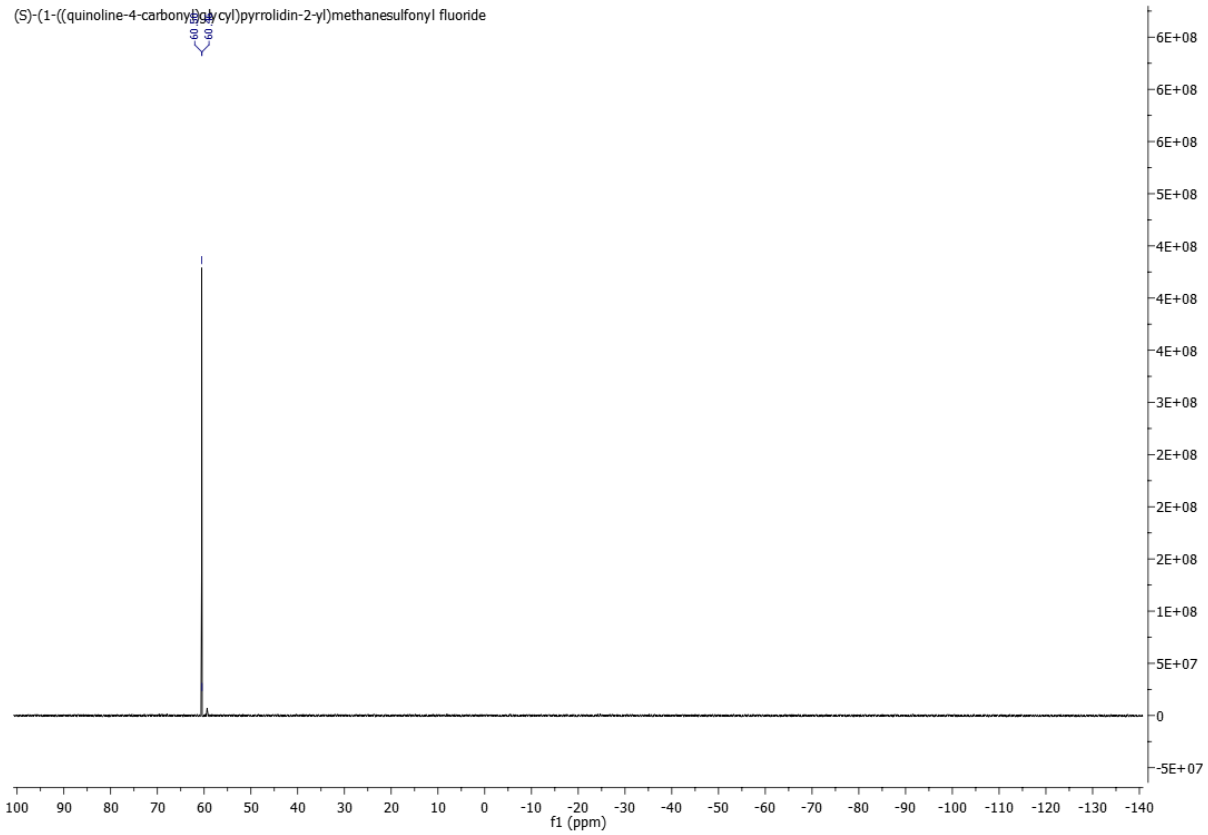

5.3.3 Radiosynthesis

*5.3.3.1 Radiosynthesis of (S)-(1-((quinoline-4-carbonyl)glycyl)pyrrolidin-2-yl)methanesulfonyl [^{18}F]fluoride ([^{18}F]**11**)*[84]

[^{18}F]F^- was eluted from the QMA cartridge with a solution of $BnEt_3Cl$ (0.35 mg) in MeOH (0.7 mL). After evaporation of the solvent and addition of (*S*)-(1-((quinoline-4-carbonyl)glycyl)pyrrolidin-2-yl)methanesulfonyl fluoride (**11**, 100 nmol) in MeCN (1 mL), the reaction mixture was incubated for 5 min at 0 °C under argon without stirring. The reaction was quenched by addition of H_2O (0.5 mL) and an aliquot was taken for determination of the RCC by HPLC analysis. The product was isolated by solid-phase extraction on a Strata™-X 33 µm Polymeric Reversed Phase cartridge (pre-conditioned with 1 mL EtOH). The product was eluted with EtOH (500 µL) and an aliquot of the eluate was used for determination of the RCP by HPLC analysis.

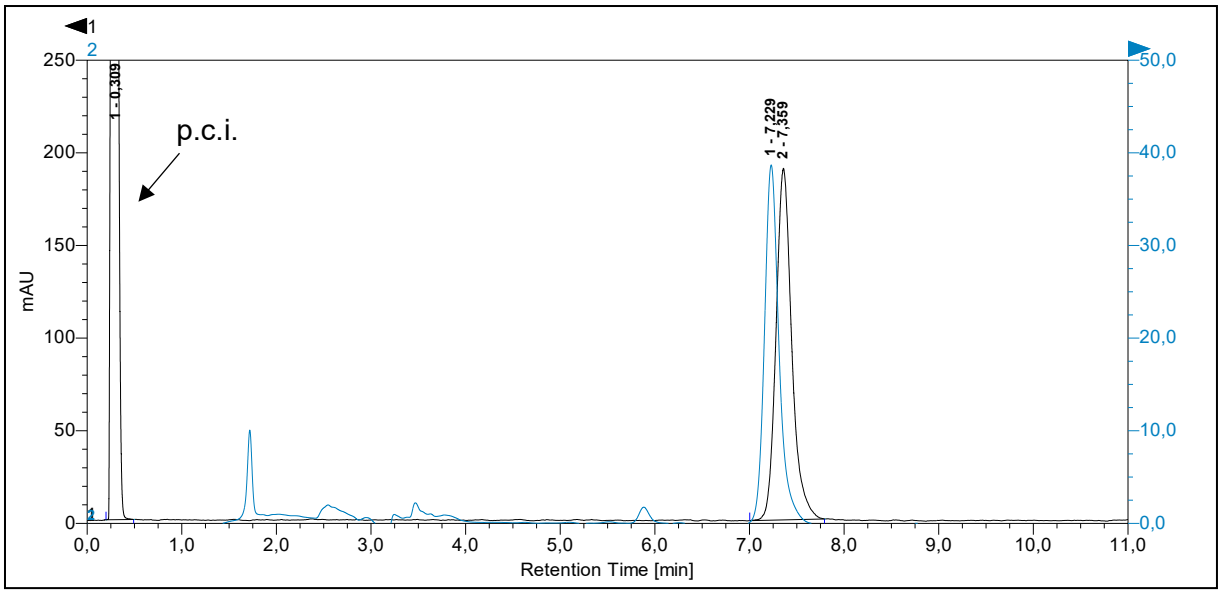

Figure 36: HPLC trace of [^{18}F]**11** co-injected with the non-radioactive reference compound **11** (Black: radio chromatogram; blue: UV chromatogram at 254 nm). Column: Phenomenex Luna® 5µm PFP(2) 100 Å LC column 250×4.6 mm; eluent: 40% MeCN. Flow rate: 1 mL/min. Abbreviation: p.c.i. – post-coloumn injection.

5.3.4 Stability studies in aqueous media

[^{18}F]**11** was synthesized and formulated in EtOH. Subsequently, up to 10 vol% of the tracer (~ 2 MBq, see Table 14) was added to the respective test medium to obtain a total volume of 1 mL. Immediately after adding the tracer to the test solution and after 1 and 2 h, an aliquot was removed and 1 µL of this aliquot was spotted on a TLC plate in single determination together with the non-radioactive reference compound **11**. The TLC plate was developed in a solvent mixture of 4% MeOH in CH_2Cl_2. The baseline, frontline and the reference compound, previously detected under UV light, were marked with a diluted aqueous [^{18}F]F^- solution and the TLC plate was developed with a phosphor imager. The spots were integrated, the background was subtracted, and [^{18}F]**11** was identified by comparison with **11**.

For the stability test in a heated, acidic solution, an aliquot was added to 1 mL of sodium acetate buffer (pH 4), which was heated at 100 °C for five minutes and then cooled to ambient temperature. From the time of cooling, the stability was monitored over a period of 2 h according to the protocol described above.

Table 14: Concentration of [^{18}F]**11** in the test solutions examined. The tracer was filled up to 1.00 mL with the test medium.

Entry	Test medium	Amount [^{18}F]11 [µL]
1	H_2O	100
2	Phosphate-buffered saline	70
3	Sodium acetate buffer (0.1 M, pH 4)	70

4	Sodium acetate buffer (0.1 M, pH 5)	70
5	0.10% TFA solution (pH 2)	45
6	Sodium acetate buffer (0.1 M, pH 4), heating for 10 minutes at 100 °C	80

5.3.5 Stability study in human blood plasma

1 mL of human blood plasma was placed in a 2 mL vial and pre-warmed to 37 °C in a thermoshaker for 5 min before 1 µL of the tracer formulated in DMSO was added. After 5, 15, 30, and 60 min, 80 µL aliquots were removed and 2.5 µL of these aliquots were spotted onto a paper strip with a polymer-coated backing to determine the recovery rate. 60 µL of the aliquots were added to 120 µL of MeCN to precipitate plasma proteins. The mixture was vortexed for 2 min and then centrifuged for 2 min. 2.5 µL of the supernatant were then spotted onto a TLC plate in triplicate and the radio-TLC was developed in a solvent mixture of 4% MeOH in CH_2Cl_2. The baseline and frontline were marked with a diluted aqueous $[^{18}F]F^-$ solution. The radio-TLC was visualized with a phosphor imager, the spots were integrated, and the background was subtracted.

5.3.6 Radio-TLC

(*S*)-(1-((Quinoline-4-carbonyl)glycyl)pyrrolidin-2-yl)methanesulfonyl $[^{18}F]$fluoride ($[^{18}F]$**11**)

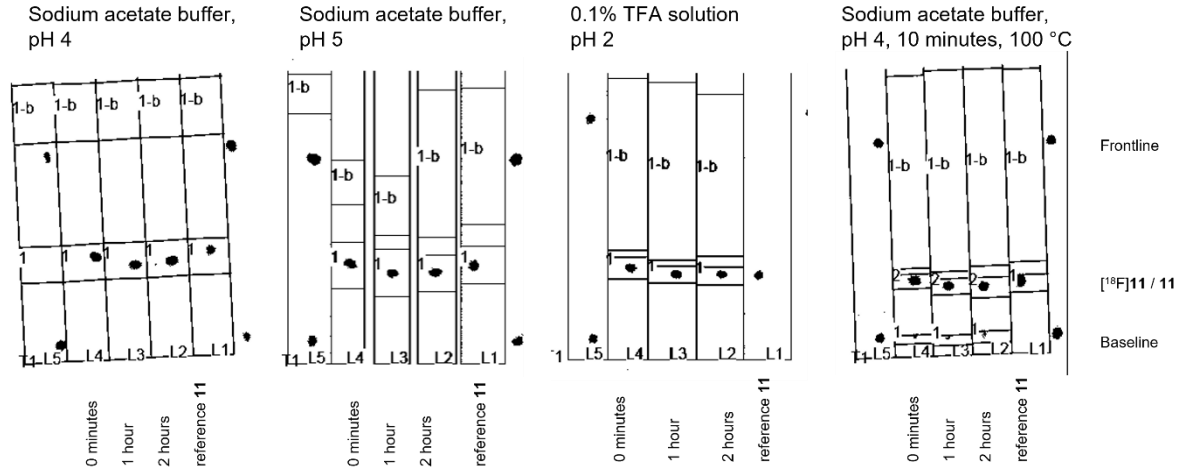

Figure 37: Stability test of $[^{18}F]$**11** in sodium acetate buffer (pH 4 and 5), 0.1% TFA solution (pH 2), and sodium acetate buffer (pH 4) after heating for 10 minutes at 100 °C; detected by radio-TLC. Solvent mixture: 4% MeOH in CH_2Cl_2.

5.4 Experimental part to chapter 3.2

5.4.1 Organic preparative syntheses

Diphenyl tritylphosphonate (**12**)[262]

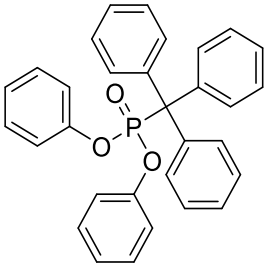

12

$C_{31}H_{25}O_3P$
[476.51]

DBU (1.07 mL, 7.18 mmol, 2 eq) was added to a solution of trityl chloride (1 g, 3.59 mmol, 1 eq) and diphenyl phosphite (730 µL, 3.83 mmol, 1.07 eq) in dry MeCN (0.14 M), and the reaction mixture was stirred for 18.5 h at ambient temperature. The solvent was removed under reduced pressure and the crude product was adsorbed on Celite®. After purification by column chromatography (cyclohexane:EtOAc = 95:5), 971 mg (2.04 mmol, 57%) of the title compound could be obtained as a white solid.

R_f (*n*-hexane:EtOAc = 8:2) = 0.42.
Mp: 112.9 °C.
^{1}H NMR (400 MHz, MeOD) δ = 7.45 – 7.38 (m, 6H), 7.35 (q, *J* = 3.7, 9H), 7.23 – 7.16 (m, 4H), 7.15 – 7.08 (m, 2H), 6.73 – 6.66 (m, 4H).
^{13}C NMR (101 MHz, MeOD) δ = 151.79 (d, *J* = 11.6), 141.75 (d, *J* = 5.7), 131.94 (d, *J* = 6.8), 130.63 (d, *J* = 0.9), 129.36 (d, *J* = 1.2), 128.82 (d, *J* = 1.8), 126.55 (s), 121.78 (d, *J* = 3.9).
^{31}P NMR (162 MHz, MeOD) δ = 19.35.
MS (**ESI**) calculated for $C_{31}H_{25}O_3P$ ($[M+H]^+$): 477.16; found: 477.10.

The analytical data corresponds to the literature.[262]

The aliphatic quaternary carbon atom is not visible in the ^{13}C NMR.

tert-Butyl 3-methylbut-2-enoate (**14**)[238]

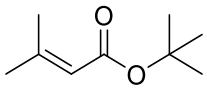

14

$C_9H_{16}O_2$

[156.23]

n-BuLi (1.6 M in *n*-hexane, 7 mL, 11.2 mmol, 1.12 eq) was added dropwise over a period of 10 min to a solution of *tert*-BuOH (938 µL, 10 mmol, 1 eq) in dry THF (0.5 M), and the reaction mixture was stirred for 40 min at ambient temperature. A solution of 3,3-dimethylacryloyl chloride (1.1 mL, 10 mmol, 1 eq) in 8 mL of dry THF was then added dropwise over a period of 10 min. The reaction mixture was heated to reflux for 1 h, then allowed to warm to ambient temperature over a period of 1.5 h and then cooled to 0 °C. The reaction was quenched by slow addition of H_2O (20 mL) at 0 °C, and the aqueous phase was extracted three times with diethyl ether (10 mL). The combined organic fractions were dried with Na_2SO_4 and the solvent was removed under reduced pressure. The reddish-yellow clear residue was distilled using a *Kugelrohrdestille* (80 °C, 19 mbar) and 500 mg (3.20 mmol, 32%) of the title compound could be obtained as a colorless oil.

^{1}H NMR (400 MHz, $CDCl_3$) δ = 5.60 (dt, *J* = 2.6, 1.3, 1H), 2.12 (d, *J* = 1.2, 3H), 1.85 (d, *J* = 1.2, 3H), 1.47 (s, 9H).

The analytical data corresponds to the literature.[263]

tert-Butyl 3-(diphenoxyphosphoryl)-3-methylbutanoate (**15**)[240]

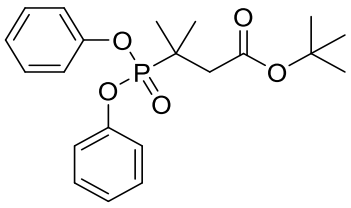

15

$C_{21}H_{27}O_5P$

[390.42]

Trimethylaluminum (2 M in toluene, 1.44 mL, 2.88 mmol, 1 eq) was added dropwise to a pre-cooled (0 °C) solution of diphenyl phosphite (549 µL, 2.88 mmol, 1 eq) in dry CH_2Cl_2 (0.2 M), and the reaction mixture was stirred for 20 min at 0 °C. After adding **14** (450 mg, 2.88 mmol, 1 eq), the reaction mixture was stirred for another 22 hours at ambient temperature. The reaction was quenched by slow addition of 1 N HCl solution (30 mL) and stirring for 10 min. The aqueous phase was extracted twice with CH_2Cl_2 (15 mL), the combined organic fractions were dried with Na_2SO_4 and the solvent was removed under reduced pressure. The crude product was dissolved in CH_2Cl_2, adsorbed on Celite®, and after double purification by column chromatography (cyclohexane:EtOAc = 1:0 – 8:2), 421 mg (1.09 mmol, 37%) of a beige solid were obtained.

^{1}H NMR (400 MHz, $CDCl_3$) δ = 7.28 (m, *J* = 7.4, 4H), 7.13 (m, *J* = 8.1, 6H), 2.71 (d, *J* = 10.3, 2H), 1.57 (s, 3H), 1.53 (s, 3H), 1.47 (s, 9H).
^{13}C NMR (101 MHz, $CDCl_3$) δ = 169.74 (d, *J* = 22.0), 150.91 (d, *J* = 10.6), 129.78, 125.10, 120.71 (d, *J* = 4.0), 81.27, 64.72, 41.79 (d, *J* = 1.0), 28.29, 21.49, 21.46.
^{31}P NMR (162 MHz, $CDCl_3$) δ = 27.56.
HRMS (**ESI**) calculated for $C_{21}H_{27}O_5P$ ($[M+H]^+$): 391.16689; found: 391.16742.

General procedure 3 (**GP 3**)[169]

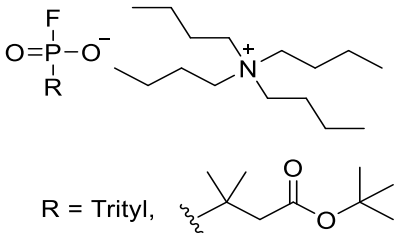

TBAF (1 M in THF, 2 eq) was added to a solution of the corresponding phosphonate in dry THF (0.1 M), and the reaction mixture was stirred overnight at ambient temperature. The solvent was removed under reduced pressure and the crude product was purified by column chromatography (CH_2Cl_2/MeOH).

Table 15: Experimental data for the synthesis of phosphonofluoridates with TBAF as fluorinating reagent.

Entry	Phosphonate	Phosphonate mg (mmol)	TBAF µL (mmol)	Compound	Yield (%)
1	**12**	200 (0.42)	840 (0.84)	**13**	61
2	**15**	100 (0.26)	510 (0.51)	**16**	96

Tritylphosphonofluoridate tetrabutylammonium salt (**13**)[169]

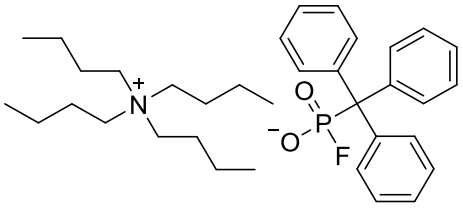

13

$C_{19}H_{15}FO_2P^-•C_{16}H_{36}N^+$

[567.77]

The synthesis was carried out according to **GP 3**. After purification by column chromatography (CH_2Cl_2:MeOH = 100:0 – 9:1), 146 mg (0.26 mmol, 61%) of the title compound could be obtained as a yellowish solid.

^{1}H NMR (400 MHz, MeOD) δ = 7.32 (m, 6H), 7.26 – 7.19 (m, 9H), 3.28 – 3.20 (m, 2H), 1.72 – 1.61 (m, 2H), 1.42 (dq, *J* = 14.6, 7.4, 2H), 1.02 (dd, *J* = 12.6, 5.2, 3H).
^{13}C NMR (101 MHz, MeOD) δ = 145.06 (d, *J* = 5.4), 131.85 (d, *J* = 5.3), 128.64, 127.46, 59.90 – 59.00 (m), 24.78, 20.71, 13.93.
^{19}F NMR (376 MHz, MeOD) δ = -56.60 (d, *J* = 1029.7).
^{31}P NMR (162 MHz, MeOD) δ = 18.57 (d, *J* = 1030.4).
MS (**ESI**) calculated for $C_{19}H_{15}FO_2P^-$ ($[M-H]^-$): 325.08; found: 325.06.

The aliphatic quaternary carbon atom is not visible in the ^{13}C NMR. Only ¼ of the tetrabutylammonium signals can be seen in the ^{1}H NMR.

(4-(*tert*-Butoxy)-2-methyl-4-oxobutan-2-yl)phosphonofluoridate tetrabutylammonium salt (**16**)[169]

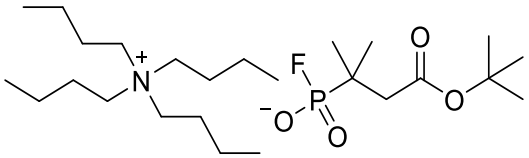

16

$C_9H_{17}FO_4P^-•C_{16}H_{36}N^+$

[481.67]

The synthesis was carried out according to **GP 3**. After purification by column chromatography (CH_2Cl_2:MeOH = 96:4 – 9:1), 120 mg (0.25 mmol, 95%) of the title compound could be obtained as a pale yellow oil.

^{1}H NMR (400 MHz, $CDCl_3$) δ = 3.26 – 3.13 (m, 8H), 2.42 (d, J = 9.1, 2H), 1.63 – 1.49 (m, 8H), 1.42 – 1.30 (m, 17H), 1.22 (s, 6H), 0.92 (t, J = 7.3, 12H).
^{13}C NMR (101 MHz, $CDCl_3$) δ = 171.78 (d, J = 20.9), 80.14, 58.65, 42.71, 29.65, 28.12, 23.91, 22.08 (d, J = 3.1), 19.63, 13.62.
^{19}F NMR (376 MHz, $CDCl_3$) δ = –77.47 (d, J = 1007.7).
^{31}P NMR (162 MHz, $CDCl_3$) δ = 27.48 (d, J = 1007.6), 27,14 (d, J = 1006.0).
HRMS (**ESI**) calculated for $C_9H_{17}FO_4P^-$ ([M-H]$^-$): 239.08540; found: 239.08576.

5.4.2 NMR spectra

^{1}H, ^{13}C and ^{31}P NMR of diphenyl tritylphosphonate (**12**)[262]

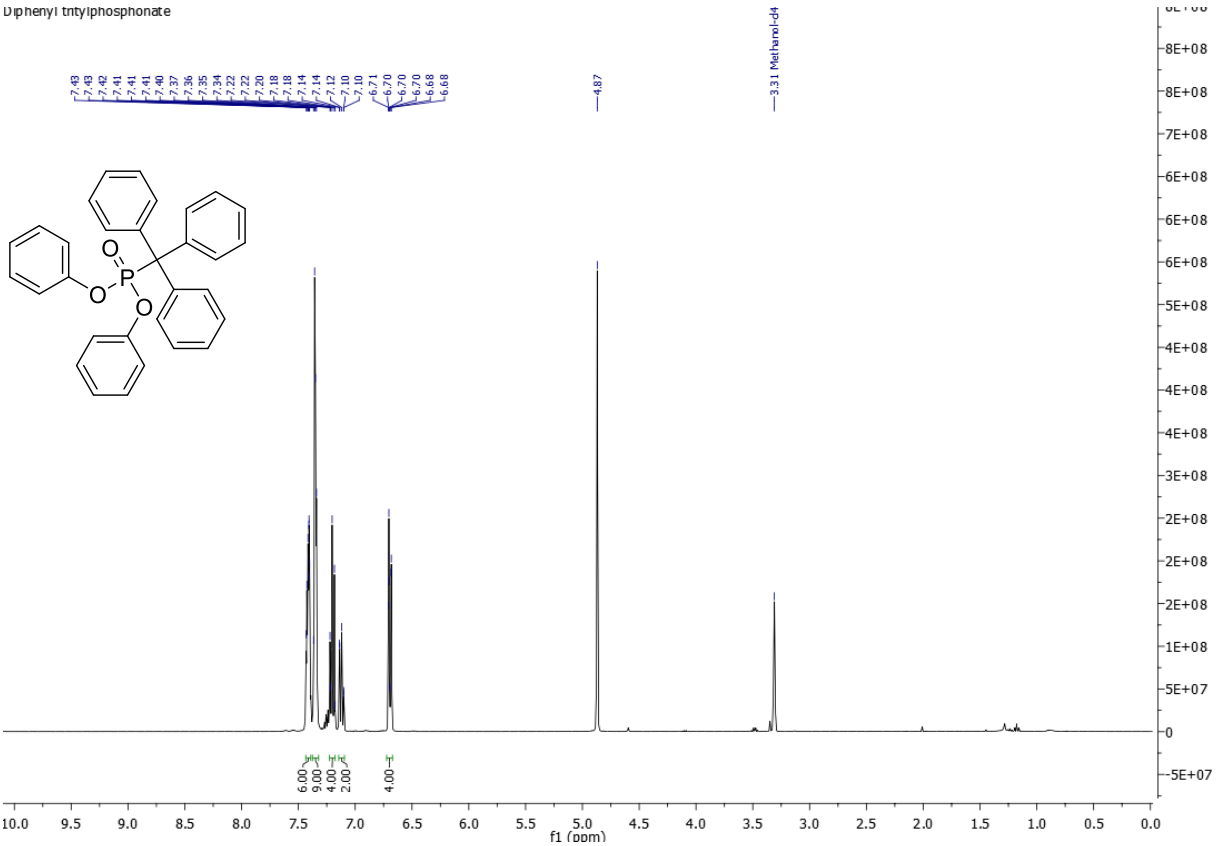

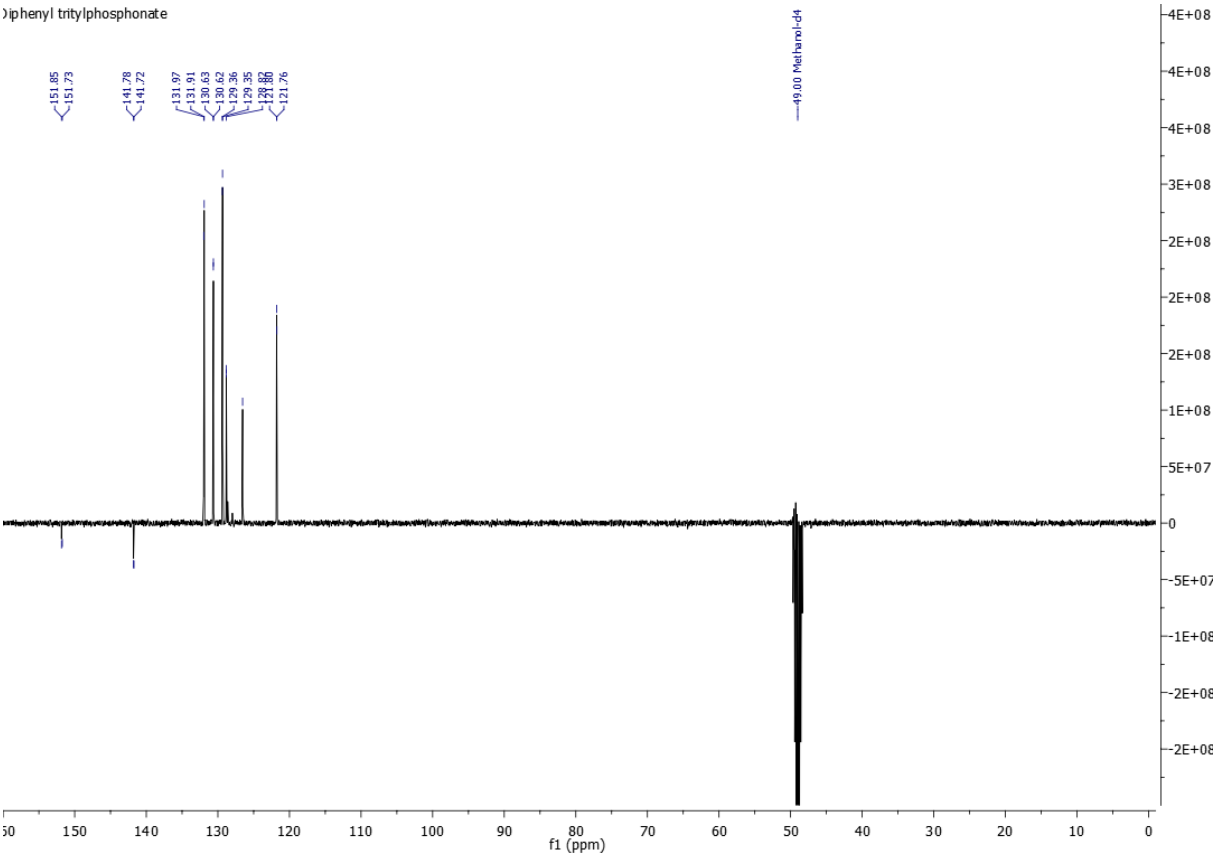

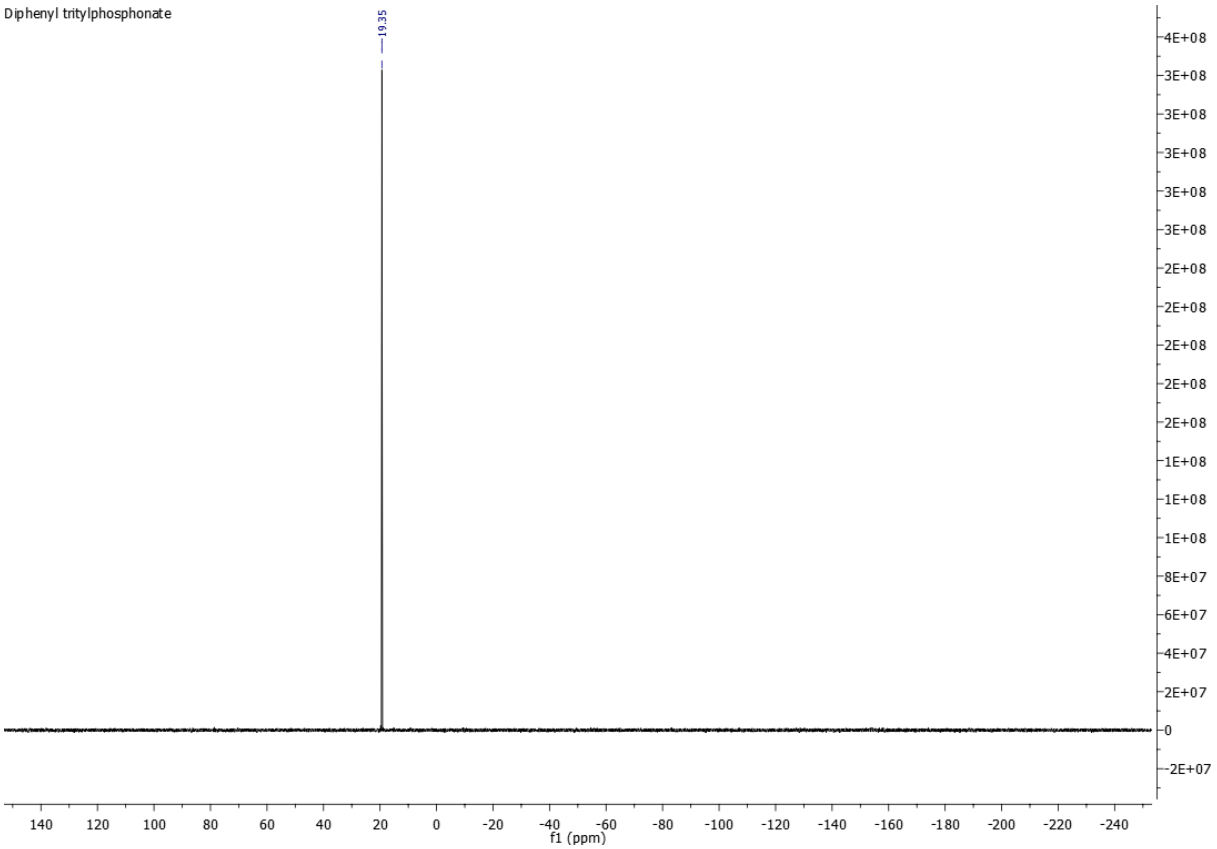

^{1}H NMR of *tert*-butyl 3-methylbut-2-enoate (**14**)

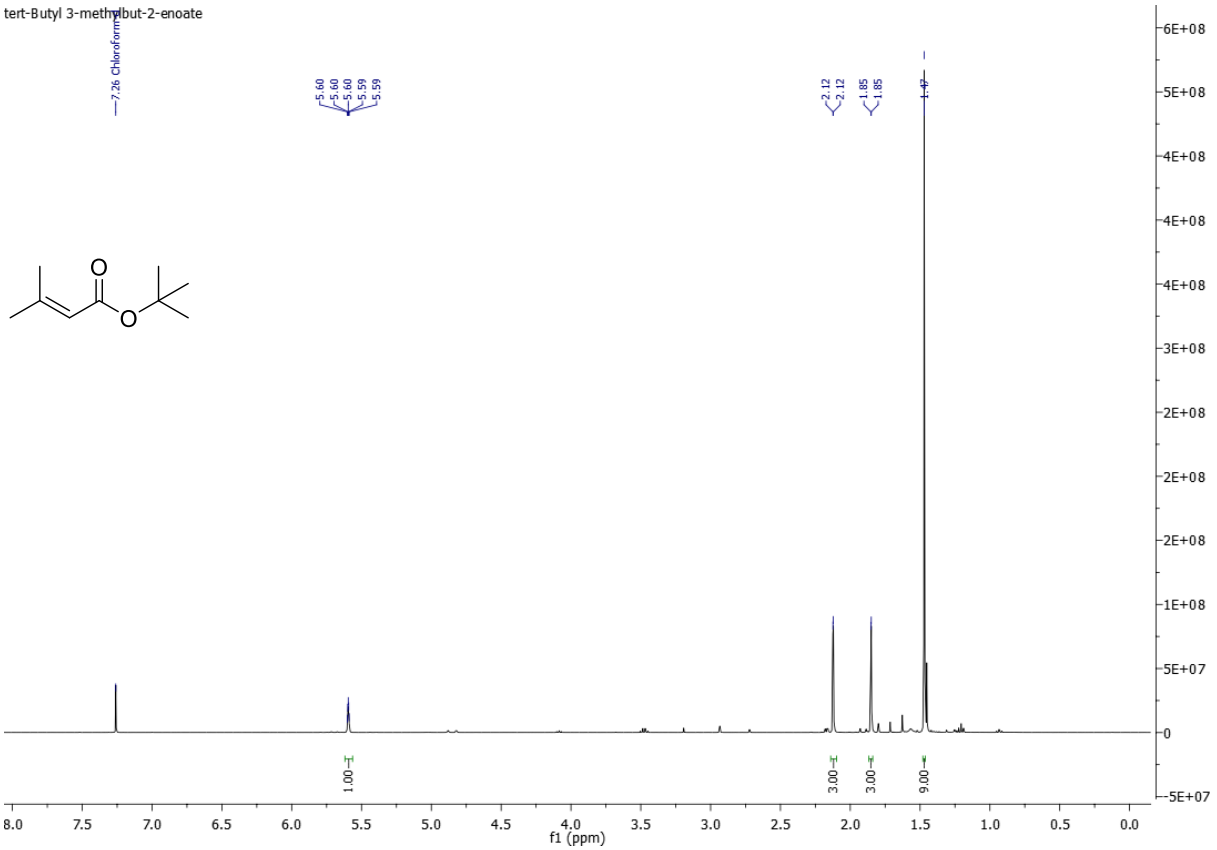

^{1}H, ^{13}C and ^{31}P NMR of *tert*-butyl 3-(diphenoxyphosphoryl)-3-methylbutanoate (**15**)

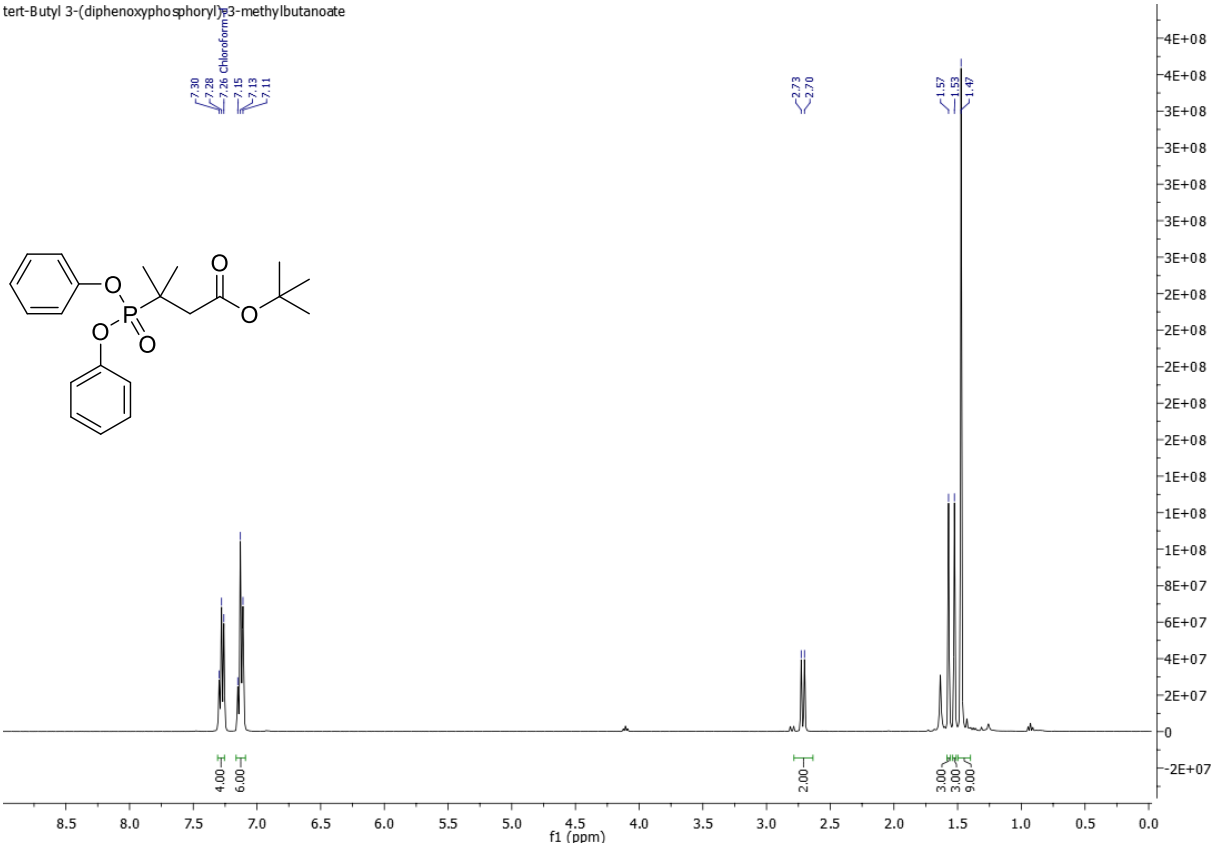

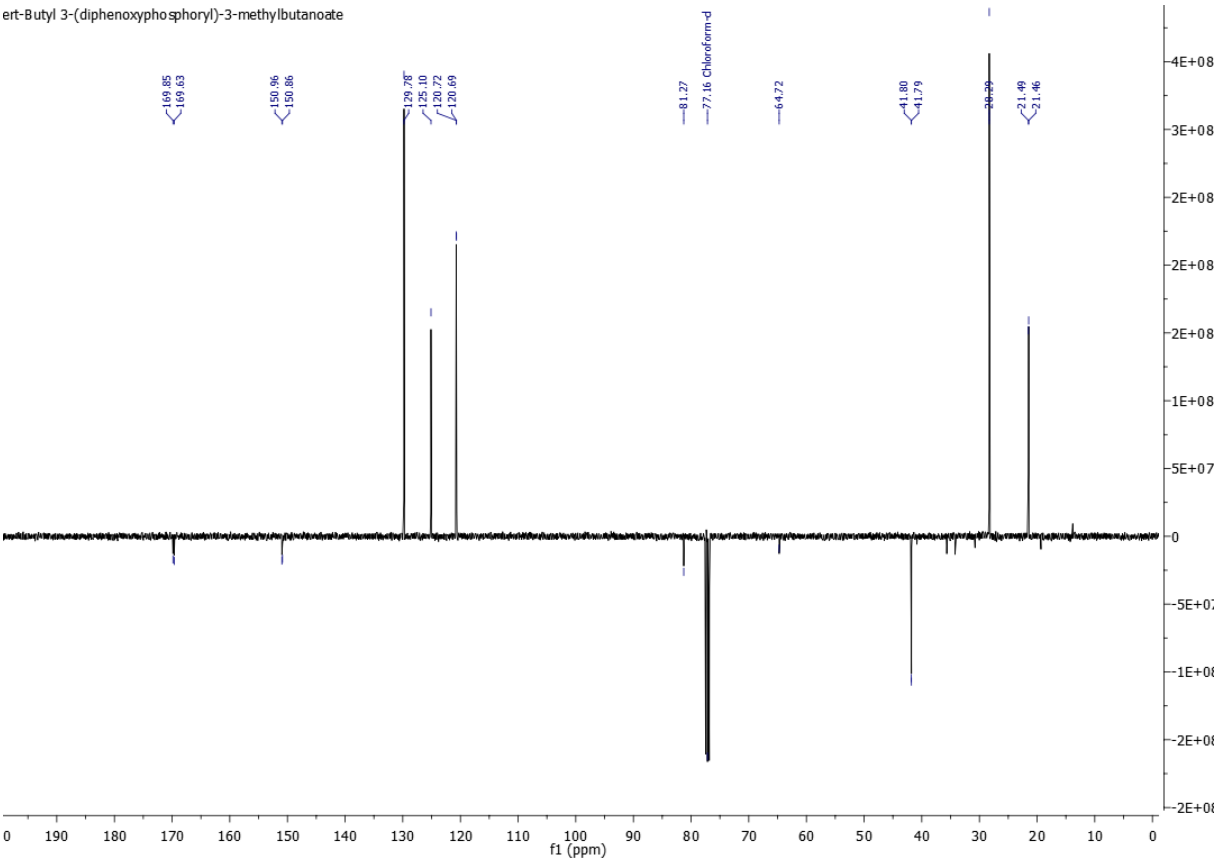

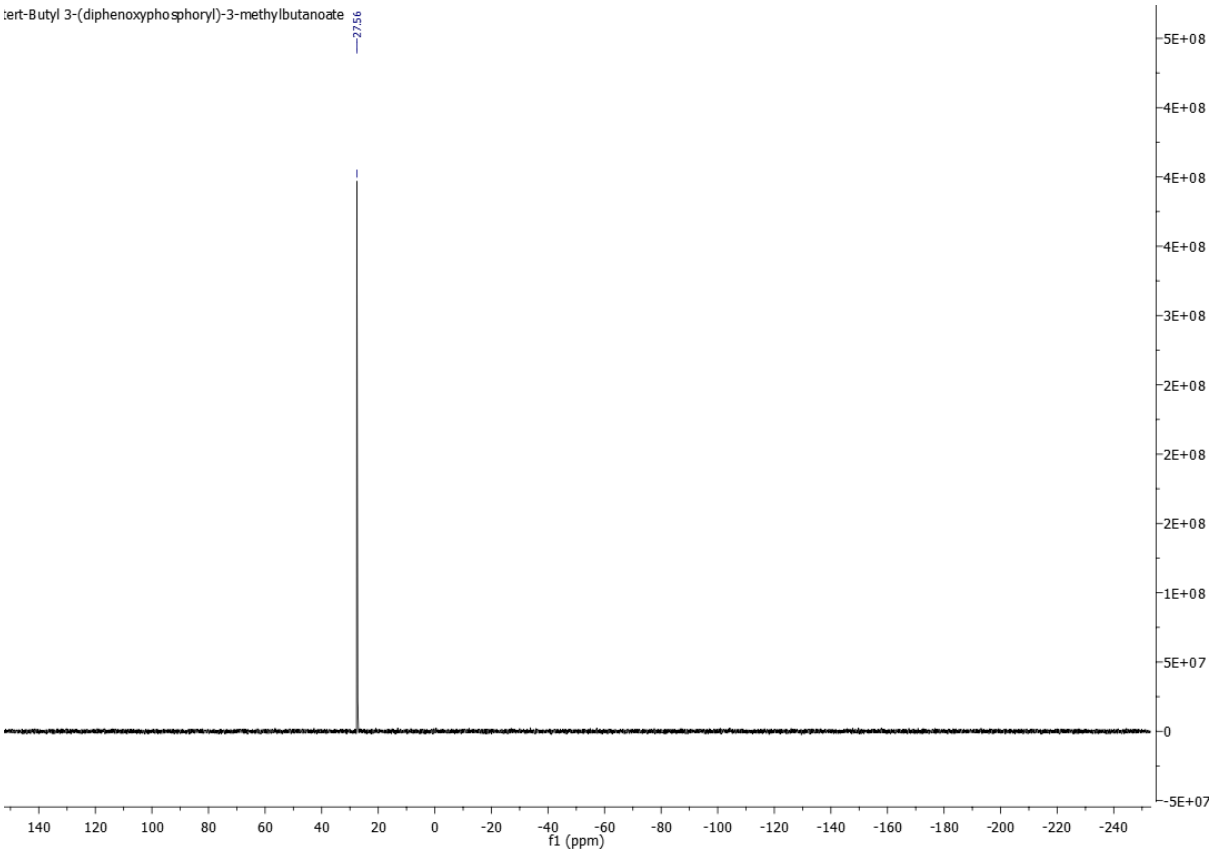

^{1}H, ^{13}C, ^{19}F and ^{31}P NMR of tritylphosphonofluoridate tetrabutylammonium salt (**13**)

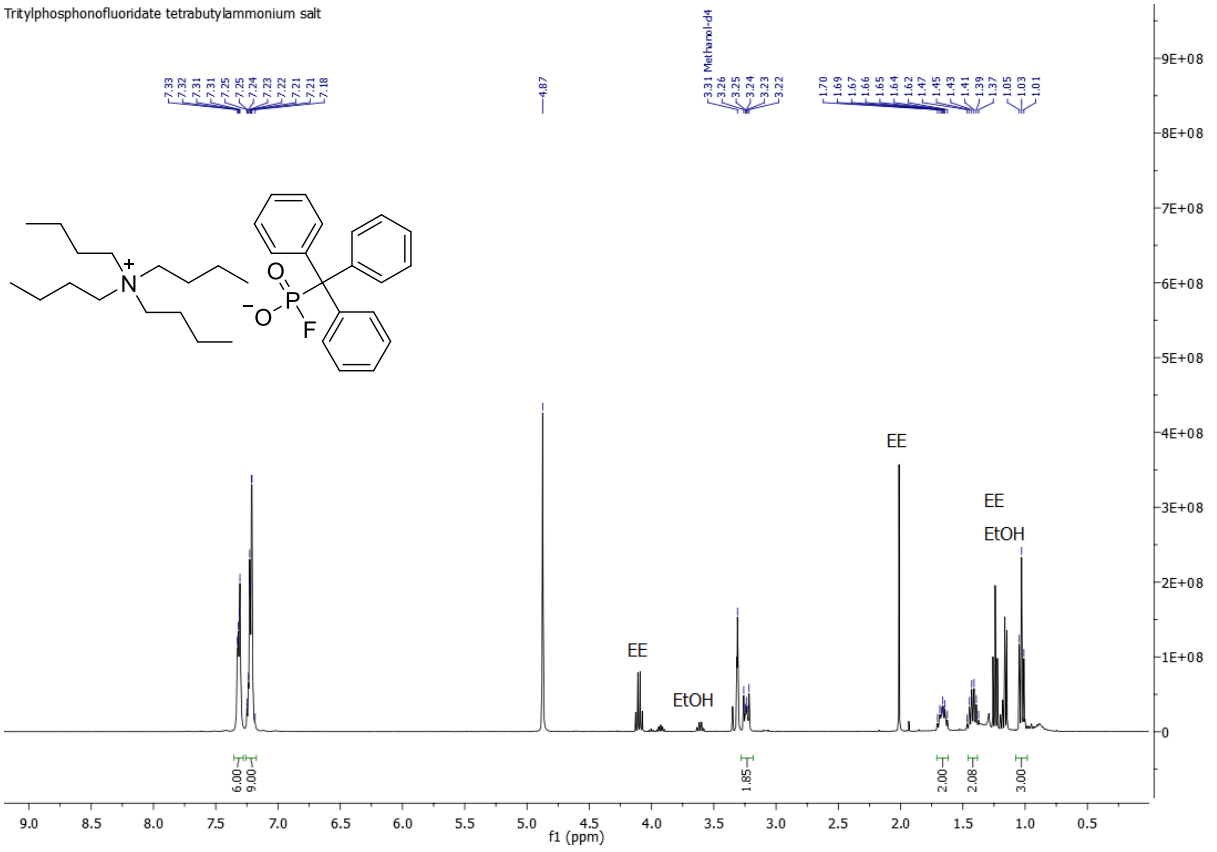

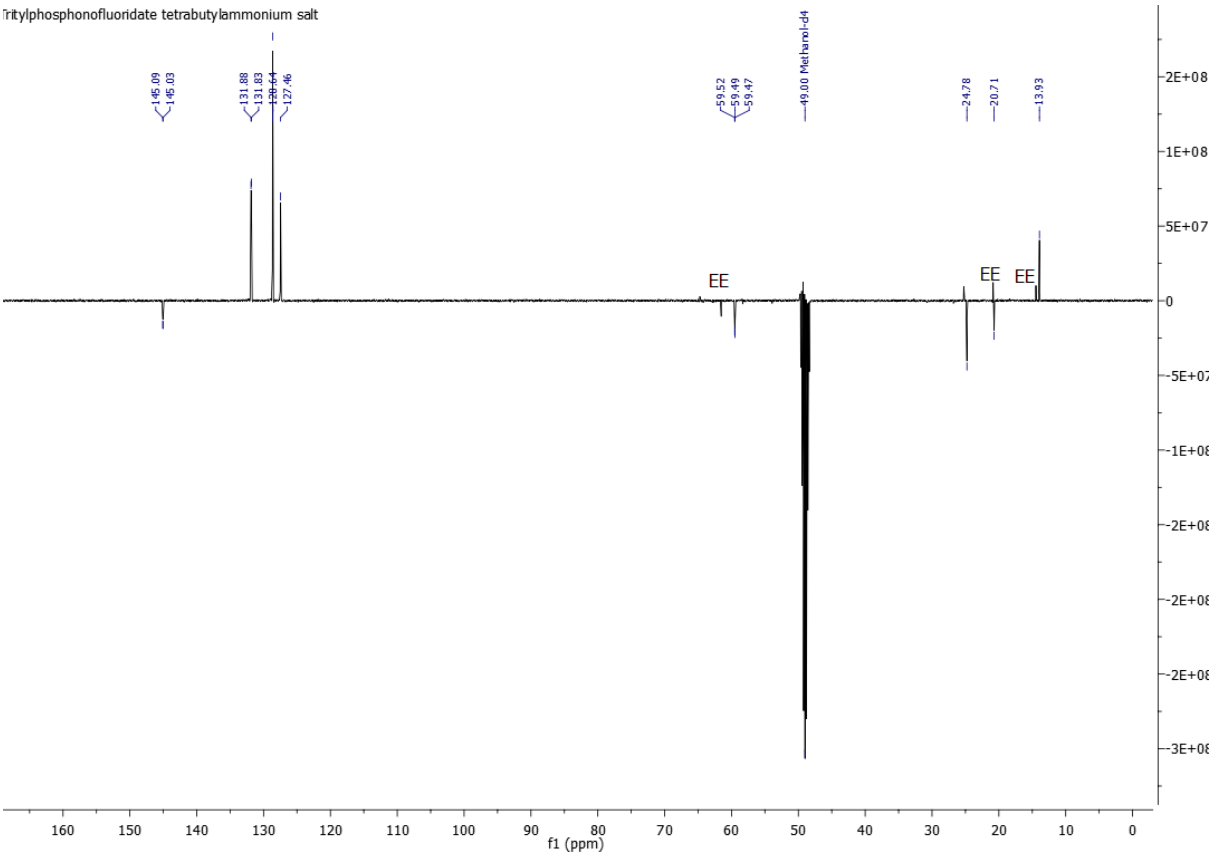
Tritylphosphonofluoridate tetrabutylammonium salt
145.09
145.03
131.88
131.83
128.64
127.46
59.52
59.49
59.47
49.00 Methanol-d4
24.78
20.71
13.93
EE
EE
EE
f1 (ppm)

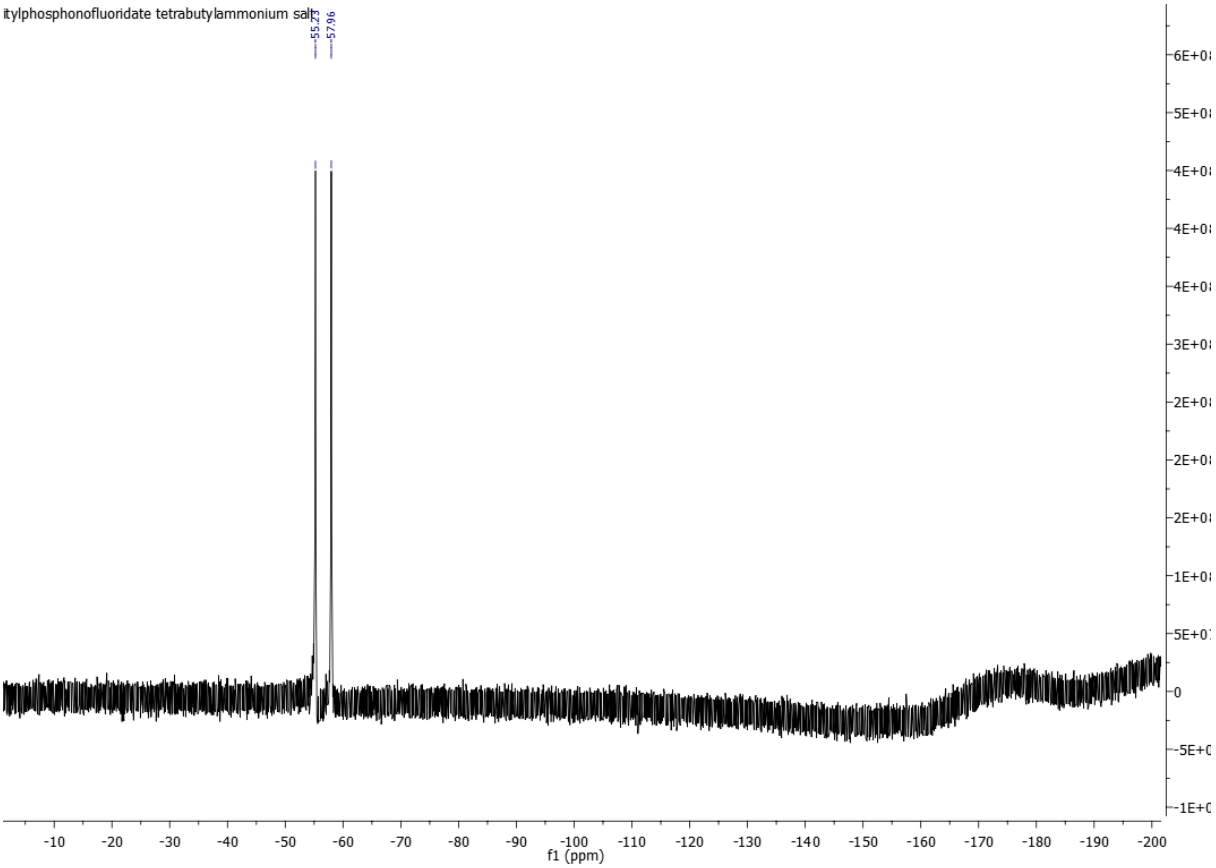
itylphosphonofluoridate tetrabutylammonium salt
55.22
57.96
f1 (ppm)

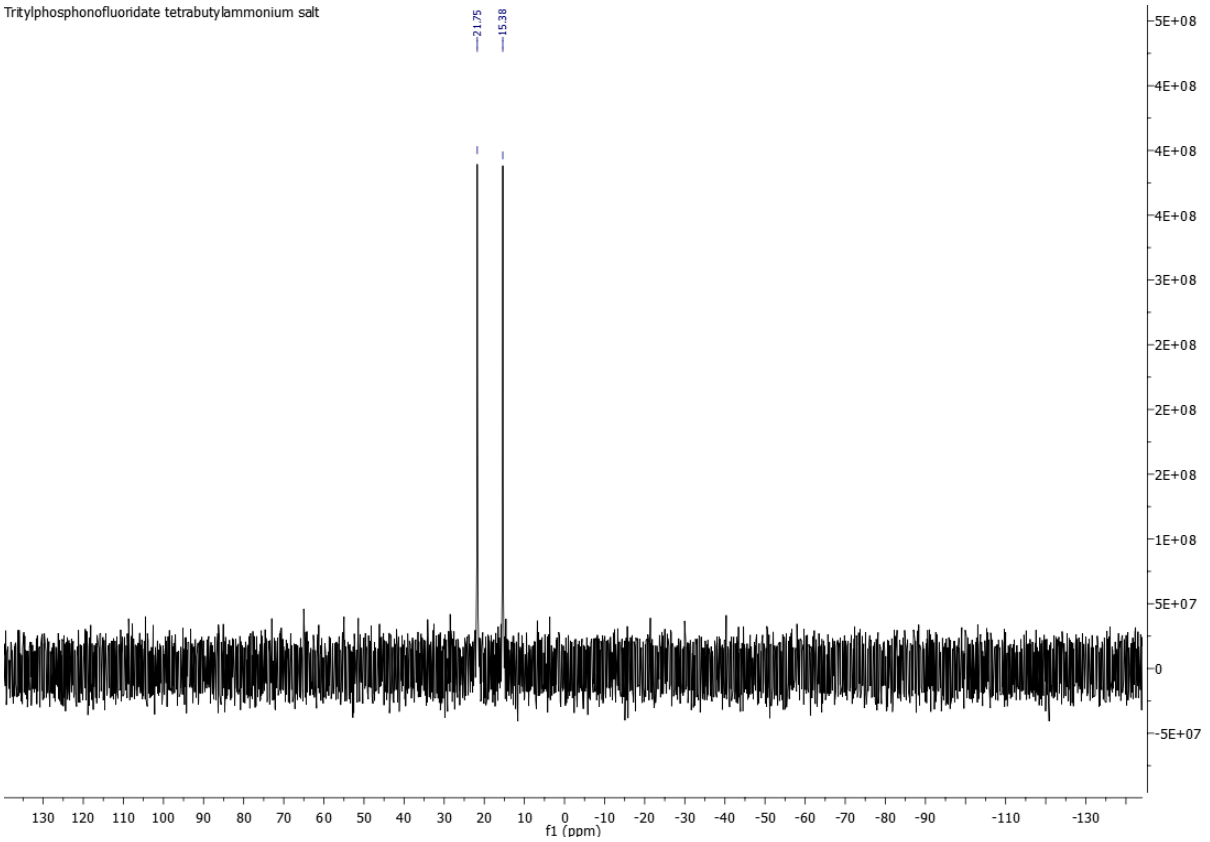

^{1}H, ^{13}C, ^{19}F and ^{31}P NMR of (4-(*tert*-butoxy)-2-methyl-4-oxobutan-2-yl)phosphonofluoridate tetrabutylammonium salt (**16**)

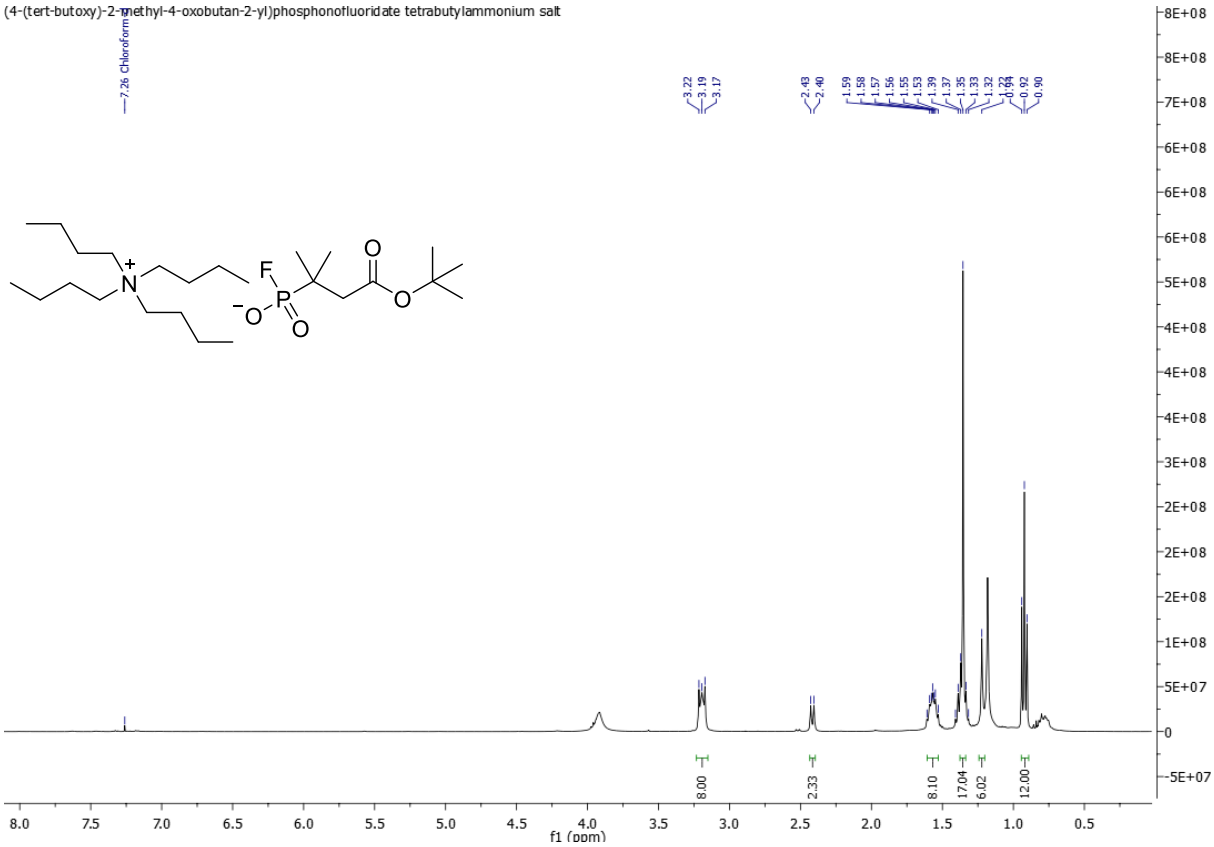

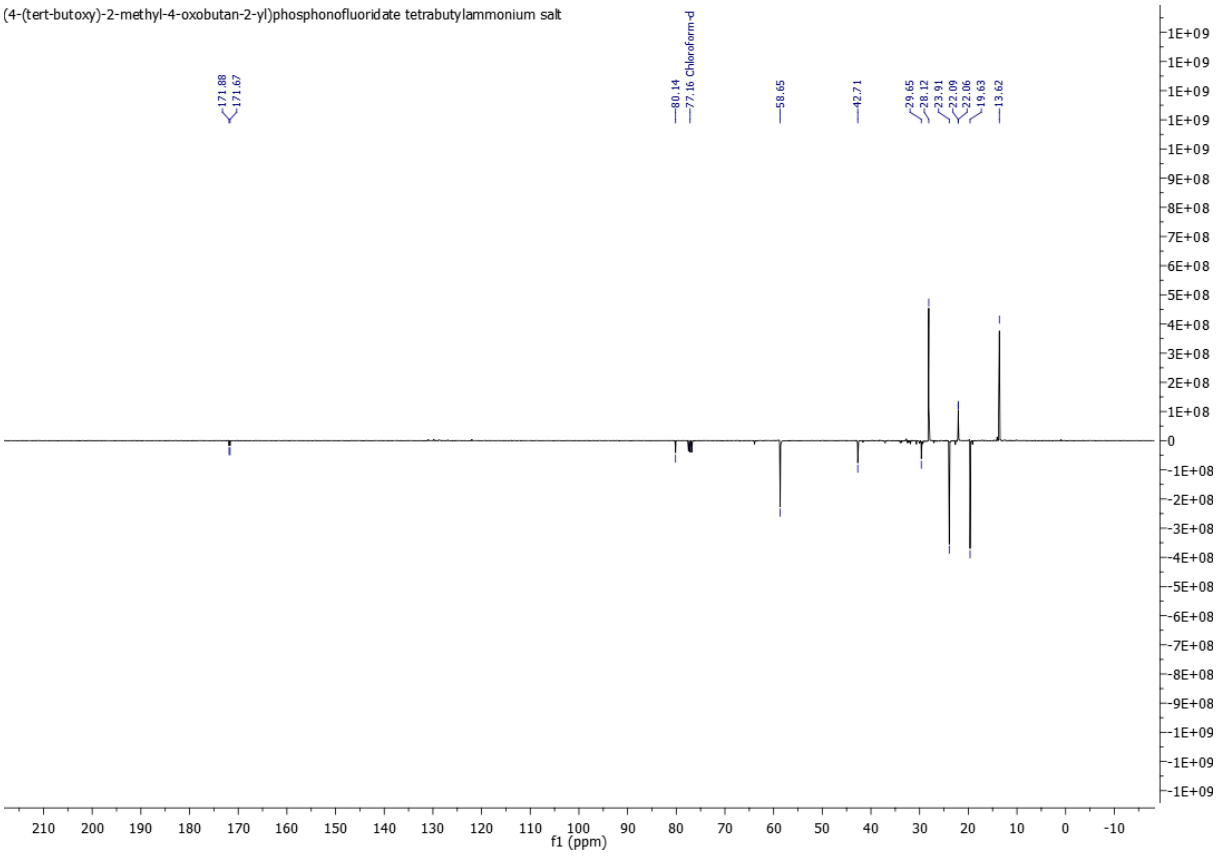
(4-(tert-butoxy)-2-methyl-4-oxobutan-2-yl)phosphonofluoridate tetrabutylammonium salt
171.88
171.67
80.14
77.16 Chloroform-d
58.65
42.71
29.65
26.12
23.91
22.09
22.06
19.63
13.62
f1 (ppm)

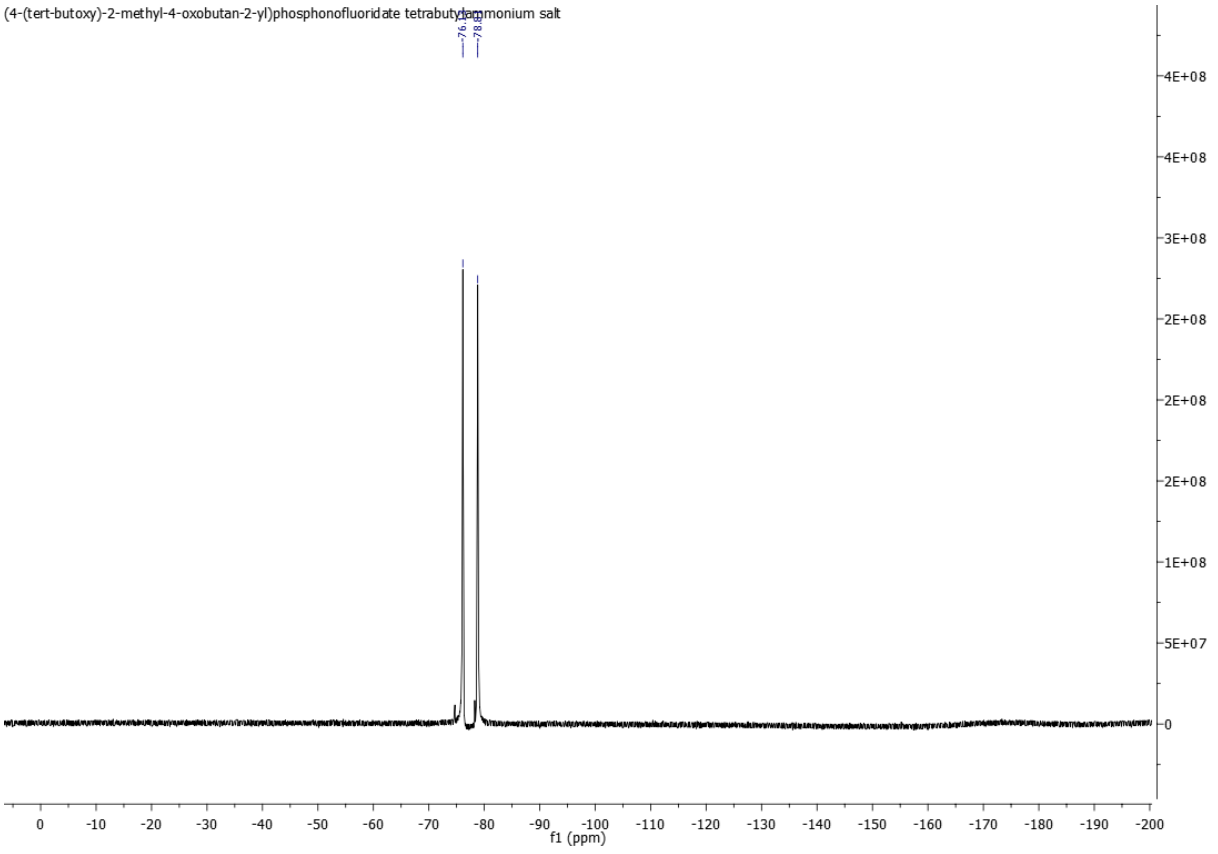
(4-(tert-butoxy)-2-methyl-4-oxobutan-2-yl)phosphonofluoridate tetrabutylammonium salt
f1 (ppm)

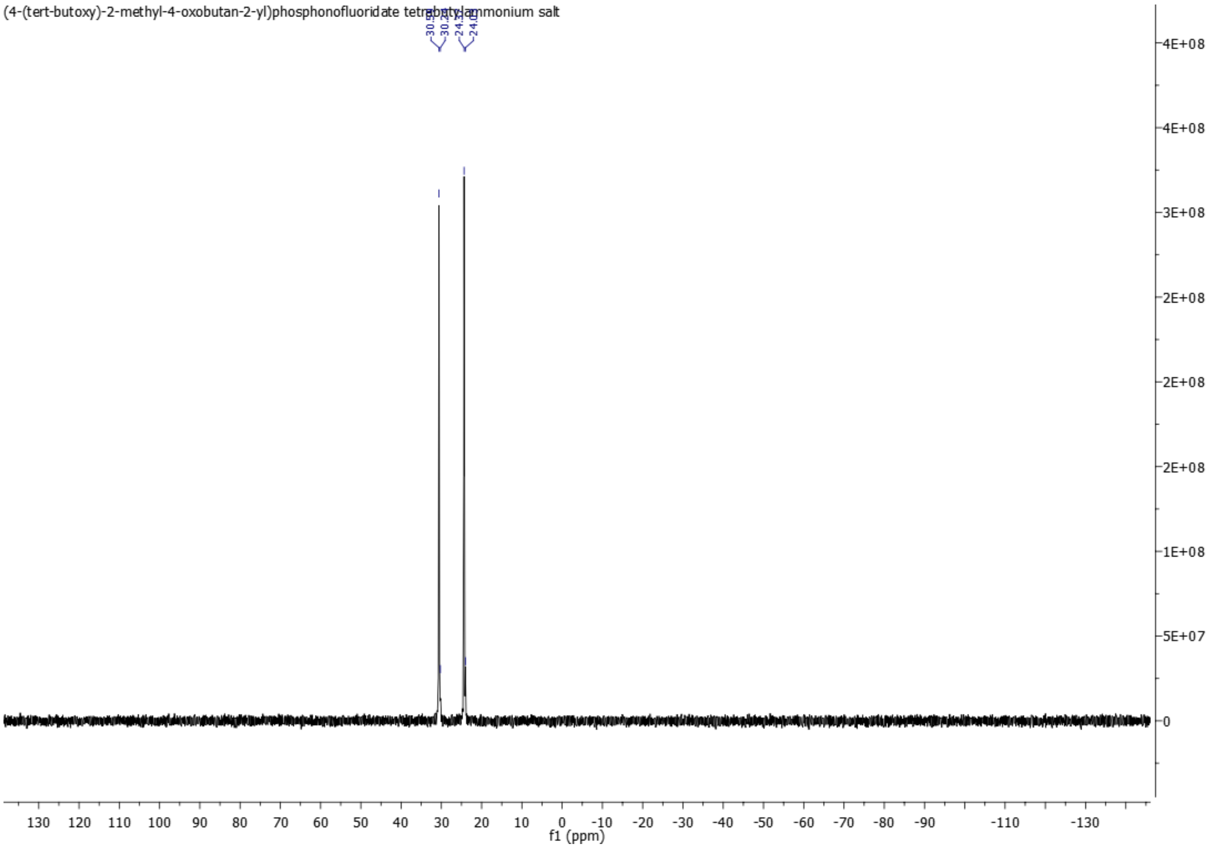
(4-(tert-butoxy)-2-methyl-4-oxobutan-2-yl)phosphonofluoridate tetrabutylammonium salt
f1 (ppm)

5.4.3 Radiosyntheses

*5.4.3.1 Radiosynthesis of tritylphosphono[^{18}F]fluoridate ([^{18}F]**13**)*

[^{18}F]F^- was eluted from the QMA cartridge with a solution of Et_4NOTf (1 mg) in MeOH (1 mL). After evaporation of the solvent and addition of diphenyl tritylphosphonate (**12**, 0.5 µmol) in DMF (100 µL), the reaction mixture was stirred for 15 min at 80 °C under argon. The reaction was quenched by addition of H_2O (0.5 µL) and an aliquot was taken and diluted with MeCN to determine the RCC by HPLC analysis.

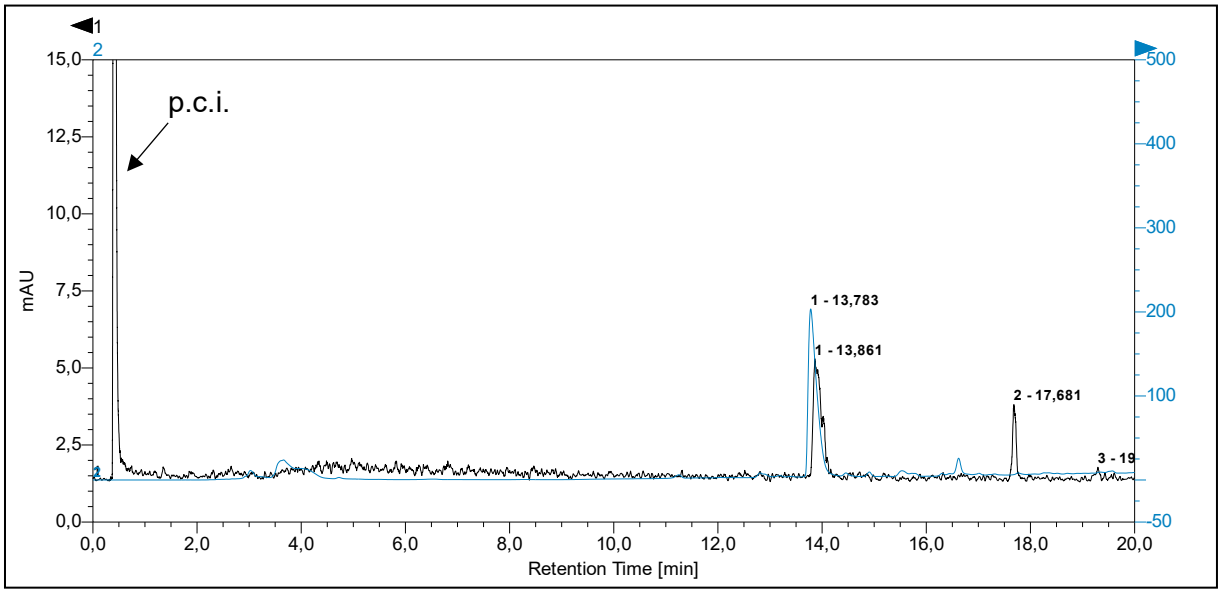

Figure 38: HPLC trace of [^{18}F]**13** co-injected with the non-radioactive reference compound **13** (Black: radio chromatogram; blue: UV chromatogram at 254 nm). Column: MultoKrom® 100-5 C18 AQ LC column 250×4.6 mm; eluent: 0–5 min 20% MeCN (0.1% TFA), 5–20 min: 20→90% MeCN (0.1% TFA). Flow rate: 1 mL/min. Abbreviation: p.c.i. – post-column injection.

*5.4.3.2 Radiosynthesis of (4-(tert-butoxy)-2-methyl-4-oxobutan-2-yl)phosphono[^{18}F]fluoridate ([^{18}F]**16**)*

[^{18}F]F^- was eluted from the QMA cartridge with a solution of Et_4NOTf (1 mg) in MeOH (1 mL). After evaporation of the solvent and addition of *tert*-butyl 3-(diphenoxyphosphoryl)-3-methylbutanoate (**15**, 0.5 µmol) in MeCN (100 µL), the reaction mixture was stirred for 15 min at 100 °C under argon. The reaction was quenched by addition of H_2O (0.5 mL) and an aliquot was taken to determine the RCC by HPLC analysis. The remaining reaction solution was diluted with H_2O (0.8 mL) and the product was isolated by semi-preparative HPLC. The product fraction was diluted with H_2O (20 mL) and fixed on a Sep-Pak® Accell Plus QMA Plus Light cartridge. The cartridge was rinsed with H_2O (3 mL) and dried with air (10 mL) before the product was eluted with isotonic NaCl solution (0.9%, 500 µL) and the RCP determined by HPLC analysis.

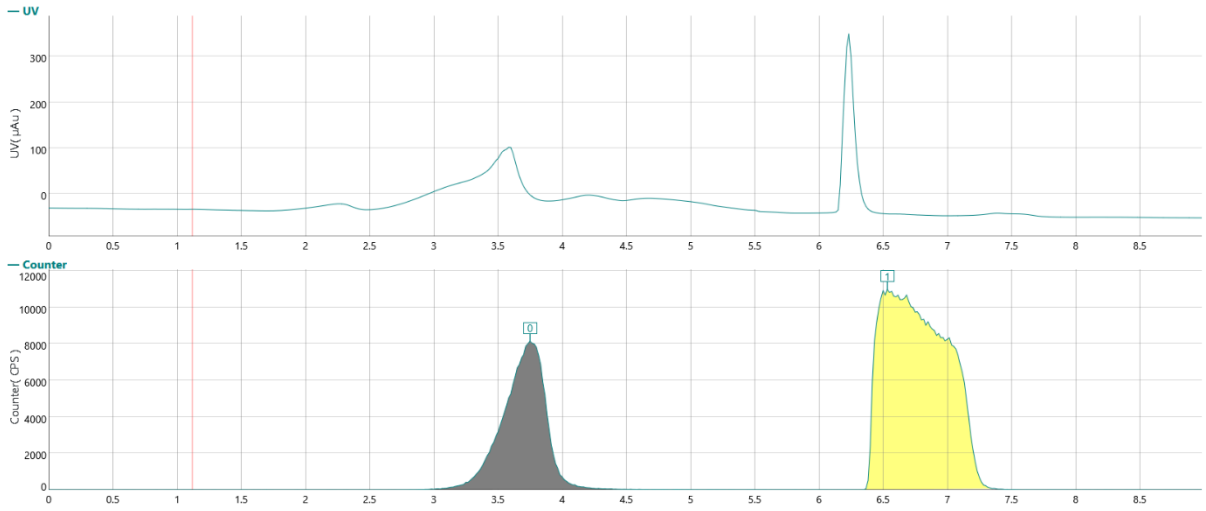

Figure 39: HPLC trace of the isolation of [^{18}F]**16**. (Top: UV chromatogram at 210 nm; bottom: radio chromatogram). Column: Phenomenex Synergi 10 µm Hydro-RP 80 Å, LC column 250×10 mm; eluent: 15% MeCN. Flow rate: 3.5 mL/min.

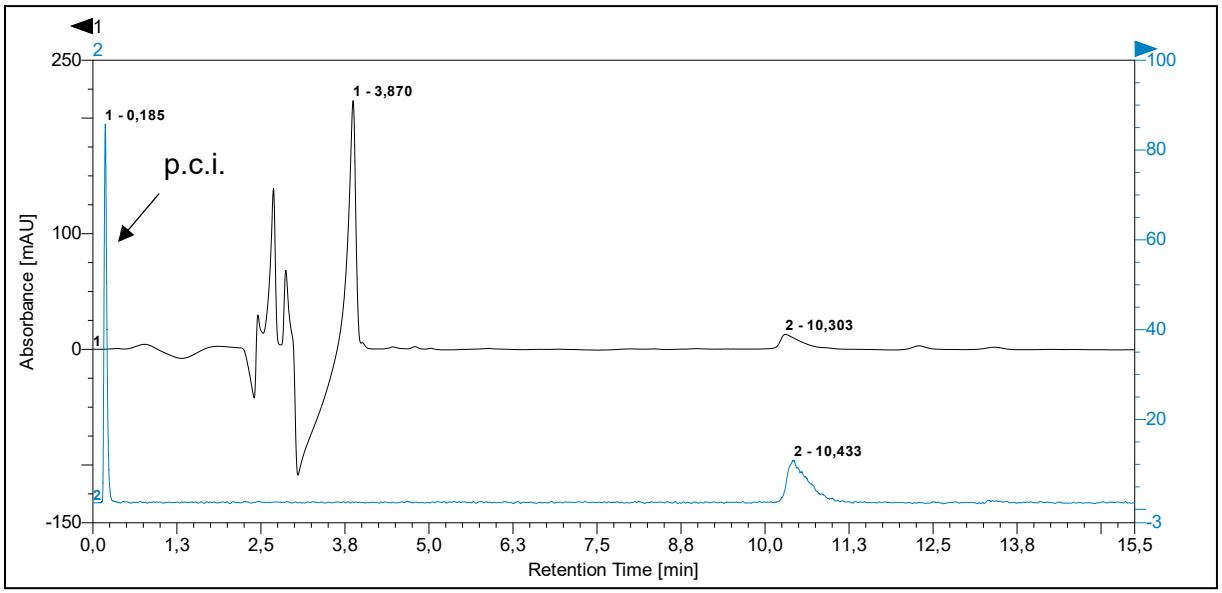

Figure 40: HPLC trace of [^{18}F]**16** co-injected with the non-radioactive reference compound **16** (Blue: radio chromatogram; black: UV chromatogram at 210 nm). Column: MultoKrom® 100-5 C18 AQ LC column 250×4.6 mm; eluent: 20% MeCN (0.1% TFA). Flow rate: 1 mL/min. Abbreviation: p.c.i. – post-column injection.

5.5 Supporting Information to chapter 3.3

5.5.1 Organic preparative syntheses

2,3,5,6-Tetrafluorophenyl (quinoline-4-carbonyl)glycinate (**17**)

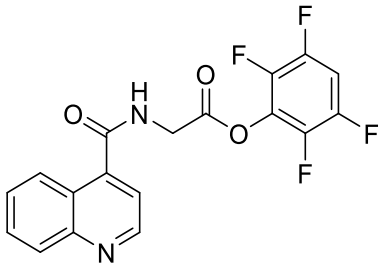

17

$C_{18}H_{10}F_4N_2O_3$

[378.28]

A solution of dicyclohexylcarbodiimide (458 mg, 2.22 mmol, 1.02 eq) in DMF (0.19 M) was added dropwise to a pre-cooled (0 °C) solution of (quinoline-4-carbonyl)glycine (**3**, 500 mg, 2.17 mmol, 1 eq) and 2,3,5,6-tetrafluorophenol (432 mg, 2.60 mmol, 1.2 eq) in DMF (0.07 M). The reaction mixture was stirred for 5 min at 0 °C and for 17.5 h at ambient temperature. The solid was removed by filtration, and the filtrate was concentrated under reduced pressure. The residue was dissolved in EtOAc and the crude product was adsorbed on Celite®. After purification by column chromatography (cyclohexane:EtOAc = 8:2 – 3:7) the product was trituated twice with diethyl ether and washed with diethyl ether. 211 mg (0.56 mmol, 26%) of the title compound could be obtained as a pale pink solid.

R_f (*n*-hexane:EtOAc = 4:6) = 0.19.

Mp: Decomposition from 155 °C

^{1}H NMR (400 MHz, DMSO) δ = 9.57 (t, *J* = 5.7 Hz, 1H), 9.01 (d, *J* = 4.3 Hz, 1H), 8.22 (dd, *J* = 8.4, 0.8 Hz, 1H), 8.10 (d, *J* = 8.0 Hz, 1H), 8.00 (tt, *J* = 10.9, 7.4 Hz, 1H), 7.83 (ddd, *J* = 8.4, 6.9, 1.4 Hz, 1H), 7.68 (ddd, *J* = 8.3, 6.9, 1.2 Hz, 1H), 7.60 (d, *J* = 4.3 Hz, 1H), 4.62 (d, *J* = 5.8 Hz, 2H).

^{13}C NMR (101 MHz, DMSO) δ = 167.62, 166.62, 150.30, 147.93, 141.03, 129.98, 129.40, 127.48, 125.29, 124.02, 119.13, 104.63 – 104.40 (m), 40.80.

^{19}F NMR (376 MHz, DMSO) δ = -139.02 (dd, *J* = 23.1, 9.8 Hz), -153.00 (dd, *J* = 23.2, 9.8 Hz).

MS (**ESI**) calculated for $C_{18}H_{10}F_4N_2O_3$ ($[M+H]^+$): 379.29; found 378.96.

Three quaternary carbon atoms are not visible in the ^{13}C NMR and are overlapped by other signals.

4,4-Dimethoxybutanal[246,247]

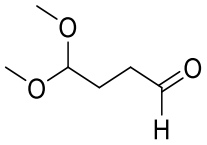

18
$C_6H_{12}O$
[132.16]

DIBAL-H (0.1 M in THF, 8 mL, 8 mmol, 1.2 eq) was added to a pre-cooled (–78 °C) solution of 4.4-dimethoxybutanenitrile (866 mg, 6.7 mmol, 1 eq) in CH_2Cl_2 (0.25 M). The reaction mixture was stirred for 3 h at –78 °C and then warmed to ambient temperature over 18 h. The reaction solution was then diluted with diethyl ether (13.4 mL) and cooled to 0 °C. Next, H_2O (0.32 mL) was slowly added, then a 15% NaOH solution (0.32 mL) was added to the reaction mixture before adding H_2O (0.8 mL). The reaction mixture was allowed to warm to ambient temperature and stirred for 15 min. Na_2SO_4 was then added and stirred for another 15 min. The salts were removed by filtration before saturated Rochelle salt solution (13.4 mL) and saturated NH_4Cl solution (13.4 mL) were added. After phase separation, the aqueous phase was extracted twice with CH_2Cl_2 (13.4 mL) and the combined organic fractions were washed once with saturated NaCl solution (13.4 mL). The organic phase was dried with Na_2SO_4 and the solvents were removed under reduced pressure. 818 mg (6.20 mmol, 92%) of the title compound could be obtained as a clear oil.

^{1}H NMR (400 MHz, $CDCl_3$) δ = 9.73 (t, J = 1.4, 1H), 4.35 (t, J = 5.5, 1H), 3.30 (s, 6H), 2.48 (td, J = 7.1, 1.4, 2H), 1.91 (td, J = 7.1, 5.5, 2H).
^{13}C NMR (101 MHz, $CDCl_3$) δ 201.81, 103.89, 53.50, 38.92, 25.45.

The analytical data corresponds to the literature.[264]

(*S*,*E*)-*N*-(4,4-Dimethoxybutylidene)-2-methylpropane-2-sulfinamide [(*S*)-**19**][244]

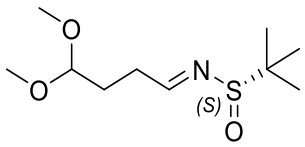

(*S*)-**19**

$C_{10}H_{21}NO_3S$

[235.34]

$Ti(OEt)_4$ (9.6 mL, 45.4 mmol, 6 eq) was added to a solution of 4,4-dimethoxybutanal (**18**, 1 g, 7.6 mmol, 1 eq) in dry CH_2Cl_2 (0.12 M) and the reaction mixture was stirred for 30 min at ambient temperature. (*S*)-(–)-^{t}Butylsulfinamide (1.1 g, 9.1 mmol, 1.2 eq) was then added and the mixture was stirred for another 65.5 h at ambient temperature. After completion, the reaction mixture was cooled (0 °C), diluted with H_2O (23 mL), stirred vigorously, and the precipitate was filtered off over a pad of Celite®. The organic phase was washed with saturated NaCl solution (25 mL), dried with Na_2SO_4 and the crude product mixture was adsorbed on Celite®. After purification by column chromatography (cyclohexane: EtOAc = 8:2), 852 mg (3.62 mmol, 48%) of the title compound could be obtained as a slightly yellowish oil.

R_f (cyclohexane:EtOAc = 6:4) = 0.43.

^{1}H NMR (400 MHz, $CDCl_3$) δ = 8.08 (t, *J* = 4.1, 1H), 4.42 (t, *J* = 5.6, 1H), 3.31 (s, 6H), 2.57 (ddd, *J* = 8.2, 7.0, 4.1, 2H), 1.97 – 1.89 (m, 2H), 1.17 (s, 9H).

^{13}C NMR (101 MHz, $CDCl_3$) δ = 168.84, 103.78, 56.69, 53.25 (d, *J* = 11.7), 31.31, 28.31, 22.43.

MS (**ESI**) calculated for $C_{10}H_{21}NO_3S$ ($[M+H]^+$): 236.35; found: 236.25.

(*R*,*E*)-*N*-(4,4-Dimethoxybutylidene)-2-methylpropane-2-sulfinamide [(*R*)-**19**][244]

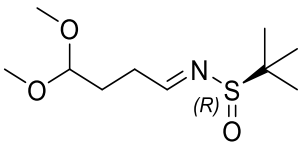

(*R*)-**19**

$C_{10}H_{21}NO_3S$

[235.34]

$Ti(OEt)_4$ (7.7 mL, 36.6 mmol, 6 eq) was added to a solution of 4,4-dimethoxybutanal (**18**, 806 mg, 6.1 mmol, 1 eq) in dry CH_2Cl_2 (0.12 M) and the reaction mixture was stirred for 30 min at ambient temperature . (*R*)-(–)-^{t}Butylsulfinamide (1.85 g, 15.3 mmol, 2.5 eq) was then added and the mixture was stirred for another 113 h at ambient temperature. After completion, the reaction mixture was diluted with EtOAc (50 mL), poured onto ice H_2O (18 mL), stirred vigorously, and the precipitate was filtered off over a pad of Celite®. The organic phase was dried with Na_2SO_4, and the crude product mixture was adsorbed on Celite®. After purification by column chromatography (cyclohexane:EtOAc = 8:2), 527 mg (2.24 mmol, 37%) of the title compound could be obtained as a slightly yellowish oil.

R_f (cyclohexane:EtOAc = 6:4) = 0.43.

^{1}H NMR (400 MHz, $CDCl_3$) δ = 8.09 (t, *J* = 4.1, 1H), 4.43 (t, *J* = 5.6, 1H), 3.33 (s, 6H), 2.58 (ddd, *J* = 8.2, 6.9, 4.2, 2H), 1.94 (m, 2H), 1.18 (s, 9H).

^{13}C NMR (101 MHz, $CDCl_3$) δ = 168.89, 103.81, 56.74, 53.30 (d, *J* = 11.8), 31.35, 28.34, 22.47.

Diphenyl [(*R*)-1-([(*S*)-*tert*-butylsulfinyl]amino)-4,4-dimethoxybutyl]phosphonate [(*S,R*)-**20**][244]

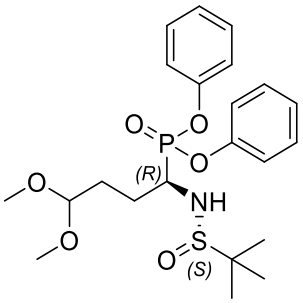

(*S,R*)-**20**
$C_{22}H_{32}NO_6PS$
[469.53]

(*S*)-**19** (780 mg, 3.31 mmol, 1 eq) was dissolved in dry THF (0.08 M) and cooled to –78 °C. In a second flask, diphenyl phosphite (1.4 mL, 6.99 mmol, 2.11 eq) was dissolved in dry THF (0.17 M) and cooled to –78 °C. LiHMDS (1 M in THF, 6.7 mL, 6.7 mmol, 2 eq) was then added dropwise to the diphenyl phosphite solution and the mixture was stirred for 15 min at –78 °C before it was added (via a cannula) to the solution of (*S*)-**19**. The resulting mixture was stirred for 2.5 h at –78 °C, after which the reaction was quenched by addition of saturated NH_4Cl solution (6.7 mL). The reaction mixture was diluted with EtOAc (39 mL), and the organic phase was washed twice with H_2O (13 mL) and once with saturated NaCl solution (13 mL). The organic phase was dried with Na_2SO_4, and the solvent was removed under reduced pressure. After purification by column chromatography (cyclohexane:acetone = 85:15) and precipitation of the product from a solution in EtOAc with *n*-hexane, 1.14 g (2.43 mmol, 74%) of a slightly bleached solid were obtained.

R_f (cyclohexane:EtOAc = 6:4) = 0.84.
Mp: 72.4 °C.
^{1}H NMR (400 MHz, $CDCl_3$) δ = 7.34 – 7.27 (m, 4H), 7.26 – 7.13 (m, 6H), 4.39 (t, *J* = 5.4, 1H), 3.95 (m, 2H), 3.32 (d, *J* = 0.9, 6H), 2.26 – 2.09 (m, 1H), 2.08 – 1.92 (m, 2H), 1.92 – 1.79 (m, 1H), 1.26 (s, 9H).
^{13}C NMR (101 MHz, $CDCl_3$) δ = 150.25 – 150.14 (m), 129.93, 125.52 (d, *J* = 6.6), 120.80 (dd, *J* = 9.4, 4.2), 104.27, 57.05, 53.70 – 52.75 (m), 51.54, 29.02 (d, *J* = 10.0), 26.30, 22.77.
^{31}P NMR (162 MHz, $CDCl_3$) δ = 18.02.
HRMS (**ESI**) calculated for $C_{22}H_{32}NO_6PS$ ($[M+H]^+$): 470.17607; found: 470.17653.

Diphenyl [(*S*)-1-([(*R*)-*tert*-butylsulfinyl]amino)-4,4-dimethoxybutyl]phosphonate [(*R*,*S*)-**20**][244]

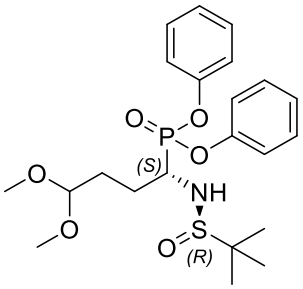

(*R*,*S*)-**20**
$C_{22}H_{32}NO_6PS$
[469.53]

(*R*)-**19** (477 mg, 2.03 mmol, 1 eq) was dissolved in dry THF (0.07 M) and cooled to –78 °C. In a second flask, diphenyl phosphite (804 µL, 4.2 mmol, 2.07 eq) was dissolved in dry THF (0.17 M) and cooled to –78 °C. LiHMDS (1 M in THF, 4 mL, 4 mmol, 1.97 eq) was then added dropwise to the diphenyl phosphite solution and the mixture was stirred for 15 min at –78 °C before it was added (via a cannula) to the solution of (*R*)-**19**. The resulting mixture was stirred for 3.5 h at –78 °C, after which the reaction was quenched by addition of saturated NH_4Cl solution (4 mL). The reaction mixture was diluted with EtOAc (24 mL), and the organic phase was washed twice with H_2O (9 mL) and once with saturated NaCl solution (8 mL). The organic phase was dried with Na_2SO_4, and the solvent was removed under reduced pressure. After purification by column chromatography (cyclohexane:acetone = 85:15) and precipitation of the product from a solution in EtOAc with *n*-hexane, 564 mg (1.20 mmol, 59%) of a slightly bleached solid were obtained.

R_f (cyclohexane:EtOAc = 6:4) = 0.84.
^{1}H NMR (400 MHz, $CDCl_3$) δ = 7.34 – 7.27 (m, 4H), 7.26 – 7.12 (m, 6H), 4.39 (t, *J* = 5.4, 1H), 4.04 – 3.85 (m, 2H), 3.32 (d, *J* = 0.8, 6H), 2.25 – 2.09 (m, 1H), 2.09 – 1.92 (m, 2H), 1.92 – 1.78 (m, 1H), 1.27 (s, 9H).
^{13}C NMR (101 MHz, $CDCl_3$) δ = 129.74, 125.33 (d, *J* = 6.5), 120.61 (dd, *J* = 9.4, 4.3), 104.10, 53.29 – 52.71 (m), 51.37 (s), 28.84 (d, *J* = 10.0), 26.11, 22.58.
^{31}P NMR (162 MHz, $CDCl_3$) δ = 18.03.
MS (**ESI**) calculated for $C_{22}H_{32}NO_6PS$ ($[M+H]^+$): 470.18; found: 470.05.

Two quaternary carbon atoms are not visible due to the recording mode (DEPT 135).

Diphenyl (*R*)-pyrrolidin-2-ylphosphonate [(*R*)-**21**][256]

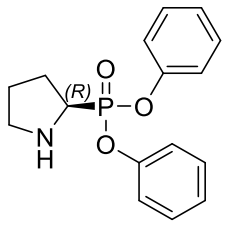

(*R*)-**21**
$C_{16}H_{18}NO_3P$
[303.30]

A solution of (*S,R*)-**20** (1.03 g, 2.19 mmol, 1 eq) in TFA/H_2O (95:5; 0.1 M) was stirred for 30 min at ambient temperature before triethylsilane (3.5 mL, 21.9 mmol, 10 eq) was added. After stirring for 25 h, the solvent was removed under reduced pressure, and the residue was dried azeotropically three times with toluene (5 mL). After purification by column chromatography (CH_2Cl_2/MeOH = 96:4), 408 mg (1.35 mmol, 62%) of a brownish, oily solid were obtained.

R_f (CH_2Cl_2:MeOH = 93:7) = 0.48.
^{1}H NMR (400 MHz, $CDCl_3$) δ = 7.31 – 7.23 (m, 4H), 7.22 – 7.12 (m, 6H), 4.23 (dt, *J* = 11.0, 8.7, 1H), 3.45 (dd, *J* = 13.7, 5.9, 2H), 2.52 – 2.28 (m, 2H), 2.21 – 1.97 (m, 2H).
^{13}C NMR (101 MHz, $CDCl_3$) δ = 149.74 – 149.47 (m), 130.13 (d, *J* = 2.0), 126.14, 120.63 – 120.43 (m), 53.01 (d, *J* = 160.8), 47.16 (d, *J* = 6.2), 26.84 (s), 24.44 (d, *J* = 8.8).
^{31}P NMR (162 MHz, $CDCl_3$) δ = 12.14.
HRMS (**ESI**) calculated for $C_{16}H_{18}NO_3P$ ($[M+H]^+$): 304.10971; found: 304.10975.

Diphenyl (*S*)-pyrrolidin-2-ylphosphonate [(*S*)-**21**][256]

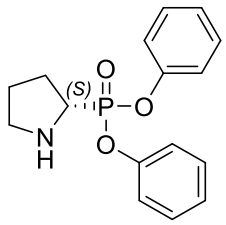

(*S*)-**21**
$C_{16}H_{18}NO_3P$
[303.30]

A solution of (*R*,*S*)-**20** (330 mg, 0.7 mmol, 1 eq) in TFA/H_2O (95:5; 0.1 M) was stirred for 30 min at ambient temperature before triethylsilane (1.12 mL, 7 mmol, 10 eq) was added. After stirring for 18 h, the solvent was removed under reduced pressure, and the residue was dried azeotropically three times with toluene (4 mL). After purification by column chromatography (CH_2Cl_2/MeOH = 96:4), 169 mg (0.56 mmol, 80%) of a beige solid were obtained.

R_f (CH_2Cl_2:MeOH = 93:7) = 0.48.
^{1}H NMR (400 MHz, $CDCl_3$) δ 7.30 – 7.22 (m, 4H), 7.21 – 7.10 (m, 6H), 4.20 (dt, *J* = 11.0, 8.7 Hz, 1H), 3.40 (dd, *J* = 10.6, 4.4 Hz, 2H), 2.53 – 2.25 (m, 1H), 2.22 – 1.93 (m, 2H).
^{13}C NMR (101 MHz, $CDCl_3$) δ = 149.83 – 149.29 (m), 130.06 (d, *J* = 1.9 Hz), 126.03, 120.73 – 120.34 (m), 52.91 (d, *J* = 160.8 Hz), 47.00 (d, *J* = 6.4 Hz), 26.78, 24.39 (d, *J* = 8.9 Hz).
^{31}P NMR (162 MHz, $CDCl_3$) δ = 12.12.
MS (**ESI**) calculated for $C_{16}H_{18}NO_3P$ ($[M+H]^+$): 304.11; found: 304.14.

Diphenyl (*R*)-(1-((quinoline-4-carbonyl)glycyl)pyrrolidin-2-yl)phosphonate (**22**)

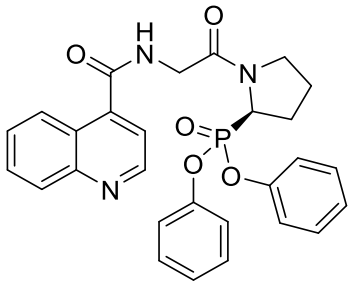

22

$C_{28}H_{26}N_3O_5P$
[515.51]

2,6-Lutidine (45 µL, 0.39 mmol, 1.11 eq) was added to a solution of (*R*)-**21** (106 mg, 0.35 mmol, 1.35 eq) in dry DMF (0.1 M), and the reaction mixture was stirred for 10 min at ambient temperature. 2,3,5,6-Tetrafluorophenyl (quinoline-4-carbonyl)glycinate (**17**, 100 mg, 0.26 mmol, 1 eq) was then added and the reaction mixture was stirred overnight at ambient temperature and poured into ice H_2O (20 mL). The aqueous phase was extracted three times with CH_2Cl_2. The combined organic fractions were washed three times with H_2O and once with saturated NaCl solution. The organic phase was dried with Na_2SO_4, and the crude product was adsorbed on Celite®. After purification by column chromatography (CH_2Cl_2/MeOH), the product was triturated with *n*-hexane and 55 mg (0.11 mmol, 41%) of a slightly yellowish solid were obtained.

R_f (CH_2Cl_2:MeOH = 96:4) = 0.28.
Mp: Melting range 38.6 – 49 °C
^{1}H NMR (400 MHz, MeOD) δ = 8.93 (d, *J* = 4.4 Hz, 1H), 8.39 (d, *J* = 8.5 Hz, 1H), 8.09 (d, *J* = 8.5 Hz, 1H), 7.83 (ddd, *J* = 8.4, 6.1, 2.7 Hz, 1H), 7.74 – 7.55 (m, 2H), 7.44 – 7.29 (m, 4H), 7.29 – 7.11 (m, 6H), 5.16 – 5.02 (m, 1H), 4.65 (d, *J* = 4.1 Hz, 0.5H), 4.36 (ddd, *J* = 60.6, 16.9, 1.5 Hz, 1,5H), 3.96 – 3.68 (m, 2H), 2.74 – 2.05 (m, 5H).
^{13}C NMR (101 MHz, MeOD) δ = 170.15, 169.76, 150.98, 149.16, 144.13, 131.54, 131.17, 130.99, 130.91, 129.57, 128.89, 127.09, 126.71, 126.54, 126.05, 121.80 (d, *J* = 4.0 Hz), 121.65 (d, *J* = 4.2 Hz), 121.55 – 121.44 (m), 120.36, 56.53, 54.91, 47.62, 43.25, 29.13, 28.72 (m), 27.48, 25.84, 23.20.
^{31}P NMR (162 MHz, MeOD) δ = 17.55, 17.10.
HRMS (**ESI**) calculated for $C_{28}H_{26}N_3O_5P$ ($[M+H]^+$): 516.16828; found: 516.16879.

Diphenyl (*R*)-(1-benzylpyrrolidin-2-yl)phosphonate (**24**)[257]

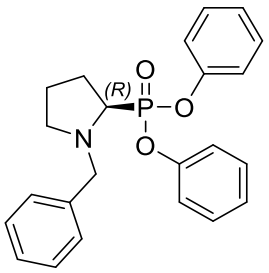

24

$C_{23}H_{24}NO_3P$
[393.42]

Triethylamine (126 µL, 0.91 mmol, 2.4 eq) was added to a pre-cooled (0 °C) solution of (*R*)-**21** (160 mg, 0.38 mmol, 1 eq) in dry CH_2Cl_2 (0.1 M) and the reaction mixture was stirred for 30 min at 0 °C, after which benzyl bromide (68 µL, 0.57 mmol, 1.5 eq) was added dropwise. After warming to ambient temperature, the reaction mixture was stirred for 40 h at ambient temperature. The reaction mixture was diluted with CH_2Cl_2 (5 mL), and the organic phase was washed twice with H_2O (10 mL). The aqueous phase was then extracted twice with CH_2Cl_2 (5 mL). The combined organic fractions were washed once with saturated NaCl solution (10 mL), dried with Na_2SO_4 and the solvent was removed under reduced pressure. After purification by column chromatography (cyclohexane:EtOAc = 9:1), 70 mg (0.18 mmol, 47%) of the title compound could be obtained as a beige solid.

R_f (cyclohexane:EtOAc = 7:3) = 0.52.
Mp: 65.5 °C.
^{1}H NMR (400 MHz, $CDCl_3$) δ = 7.26 (s, 15H), 4.51 (d, J = 12.9, 1H), 3.53 (d, J = 12.2, 1H), 3.46 – 3.38 (m, 1H), 2.98 (d, J = 25.0, 1H), 2.50 – 2.18 (m, 3H), 1.91 (dd, J = 25.2, 16.5, 2H).
^{13}C NMR (101 MHz, $CDCl_3$) δ = δ = 151.22 – 150.93 (m), 150.70, 139.24 – 138.90 (m), 129.77 (d, J = 13.4 Hz), 129.20, 128.28, 127.10, 125.06 (d, J = 13.0 Hz), 121.53 – 120.38 (m), 60.73, 60.35, 58.98, 54.30 (d, J = 15.1 Hz), 27.45, 24.66.
^{31}P NMR (162 MHz, $CDCl_3$) δ = 19.72.
HRMS (**ESI**) calculated for $C_{23}H_{24}NO_3P$ ($[M+H]^+$): 394.15666; found: 394.15718.

General procedure 4 (**GP 4**)[170]

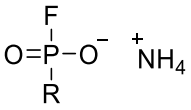

R =

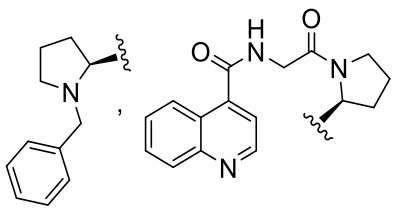

Ammonium fluoride (10 eq) was added to a solution of the corresponding phosphonate in dry MeCN, and the reaction mixture was stirred overnight at 60 °C. The solvent was removed under reduced pressure, and the crude product was purified by semi-preparative column chromatography (H_2O/MeCN).

Table 16: Experimental data for the synthesis of phosphonofluoridates with NH_4F as fluorinating reagent.

Entry	Phosphonate	Phosphonate mg (mmol)	NH_4F mg (mmol)	Compound	Yield (%)
1	**22**	20.3 (0.04)	14.0 (0.39)	**23**	50
2	**24**	25.0 (0.06)	24 (0.60)	**25**	58

(*R*)-(1-((Quinoline-4-carbonyl)glycyl)pyrrolidin-2-yl)phosphonofluoridate ammonium salt (**23**)[170]

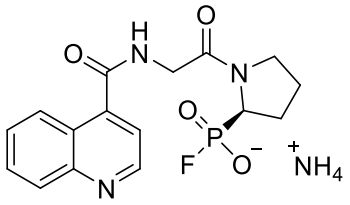

23

$C_{16}H_{16}FN_3O_4P^-\bullet NH_4^+$

[382.33]

The synthesis was carried out according to **GP 4**. The phosphonate was dissolved in MeCN (0.04 M), and the reaction mixture was stirred for 14 h at 60 °C. The crude product was dissolved in H_2O/MeCN (93:7, 1 mL) and the non-soluble residue was removed by centrifugation. The dissolved crude product was purified by semi-preparative column chromatography (Column: Phenomenex Synergi 10 µm Hydro-RP, 250×100 mm: 7% MeCN. Flow rate: 4.5 mL/min) and the solvent was removed under reduced pressure. The title compound could be obtained as a hygroscopic white solid of 7.20 mg (0.02 mmol, 50%).

^{1}H NMR (400 MHz, MeOD) δ = 9.03 – 8.98 (m, 1H), 8.52 – 8.40 (m, 1H), 8.13 (d, *J* = 8.5, 1H), 7.94 – 7.86 (m, 1H), 7.80 – 7.71 (m, 2H), 4.59 (d, *J* = 3.4, 1H), 4.56 – 4.44 (m, 1H), 4.41 – 4.35 (m, 0.6H), 4.17 (d, *J* = 17.0, 0.4H), 3.78 – 3.66 (m, 1.4H), 3.55 (m, 0.6H), 2.47 – 2.12 (m, 3H), 2.13 – 1.90 (m, 1H).

^{13}C NMR (101 MHz, MeOD) δ = 170.08 – 169.07 (m), 168.91 – 168.02 (m), 150.15, 147.42, 146.09, 132.49, 129.49 (d, *J* = 5.6), 128.13 (d, *J* = 5.6), 127.39 (d, *J* = 11.2), 126.32 (d, *J* = 5.8), 120.56 (d, *J* = 11.1), 56.82 – 54.73 (m), 56.29 – 54.24 (m), 47.49 (d, *J* = 45.7), 43.79 – 42.78 (m), 28.49 (d, *J* = 178.6), 24.43 (d, *J* = 241.8).

^{19}F NMR (376 MHz, MeOD) δ = -64.24 (d, *J* = 1029.0), -67.15 (d, *J* = 1017.4).

^{31}P NMR (162 MHz, MeOD) δ = 17.83 (d, *J* = 1017.4).

HRMS (**ESI**) calculated for $C_{16}H_{16}FN_3O_4P^-$ ([M-H]$^-$): 364.08679; found: 364.08717.

(*R*)-(1-Benzylpyrrolidin-2-yl)phosphonofluoridate ammonium salt (**25**)[170]

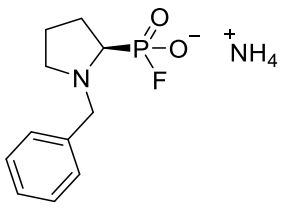

25

$C_{11}H_{14}FNO_2P^-\bullet NH_4^+$

[260.25]

The synthesis was carried out according to **GP 4**. The phosphonate was dissolved in MeCN (0.03 M), and the reaction mixture was stirred for 17 h at 60 °C. The crude product was dissolved in H_2O/MeCN (93:7, 1.5 mL) and purified by semi-preparative column chromatography (Column: Phenomenex Synergi 10 µm Hydro-RP, 250×100 mm; eluent: 7% MeCN. Flow rate: 4.5 mL/min). The product fraction was concentrated and freeze-dried. The title compound could be obtained as a white, hygroscopic solid of 9 mg (0.03 mmol, 58%).

^{1}H NMR (400 MHz, MeOD) δ = 7.59 – 7.53 (m, 2H), 7.51 – 7.43 (m, 3H), 4.21 (d, *J* = 12.2, 1H), 3.67 (dd, *J* = 17.5, 8.6, 1H), 3.42 – 3.29 (m, 2H), 3.23 (m, 1H), 2.49 – 2.34 (m, 1H), 2.34 – 2.17 (m, 1H), 2.16 – 2.05 (m, 1H), 2.04 – 1.85 (m, 1H).
^{13}C NMR (101 MHz, MeOD) δ = 132.11, 131.08, 130.29, 63.93 (d, *J* = 39.7), 62.43 (d, *J* = 39.8), 59.76, 55.71, 27.44, 23.14 (d, *J* = 8.2 Hz).
^{19}F NMR (376 MHz, MeOD) δ = -62.21 (d, *J* = 988.0 Hz).
^{31}P NMR (162 MHz, MeOD) δ = 9.36 (d, *J* = 985.9 Hz).
HRMS (**ESI**) calculated for $C_{11}H_{14}FNO_2P^-$ ([M-H]$^-$): 242.07517; found: 242.07557.

The quaternary carbon atom is not visible in the ^{13}C NMR.

5.5.2 NMR-spectra

^{1}H, ^{13}C and ^{19}F NMR of 2,3,5,6-tetrafluorophenyl (quinoline-4-carbonyl)glycinate (**17**)

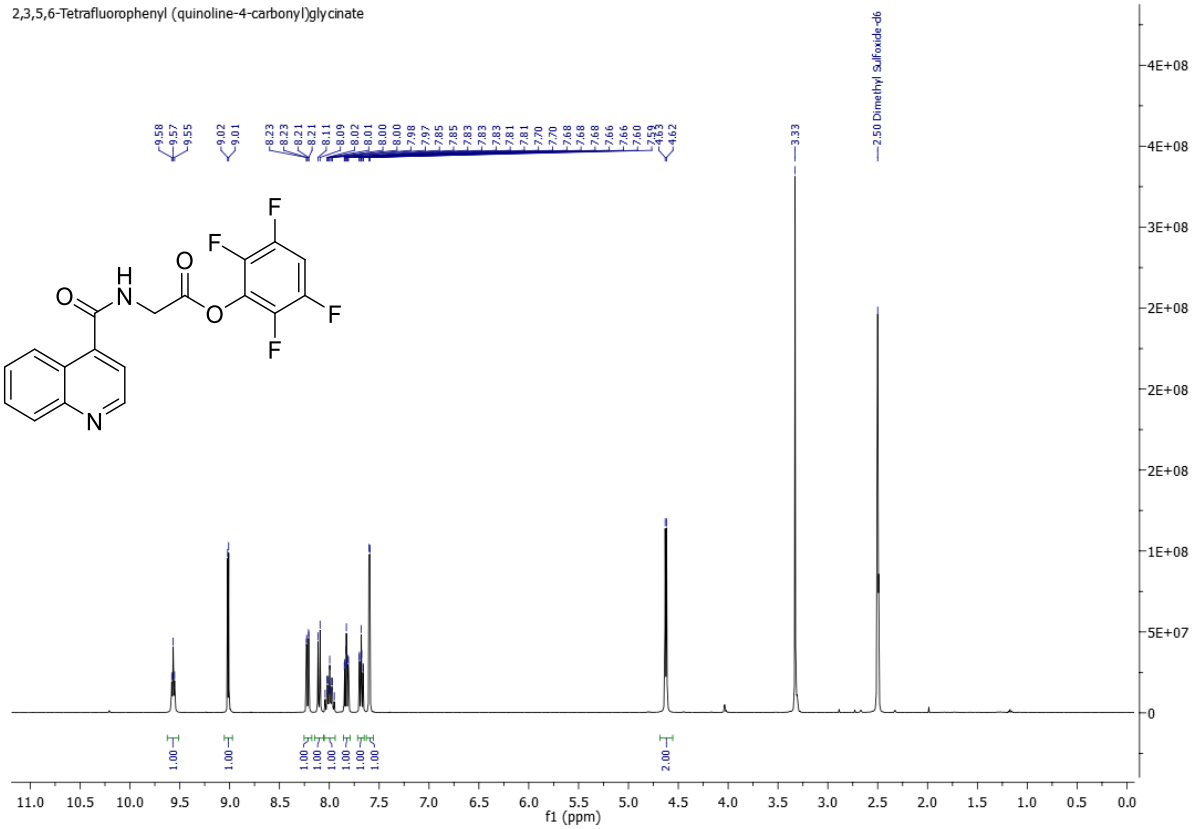

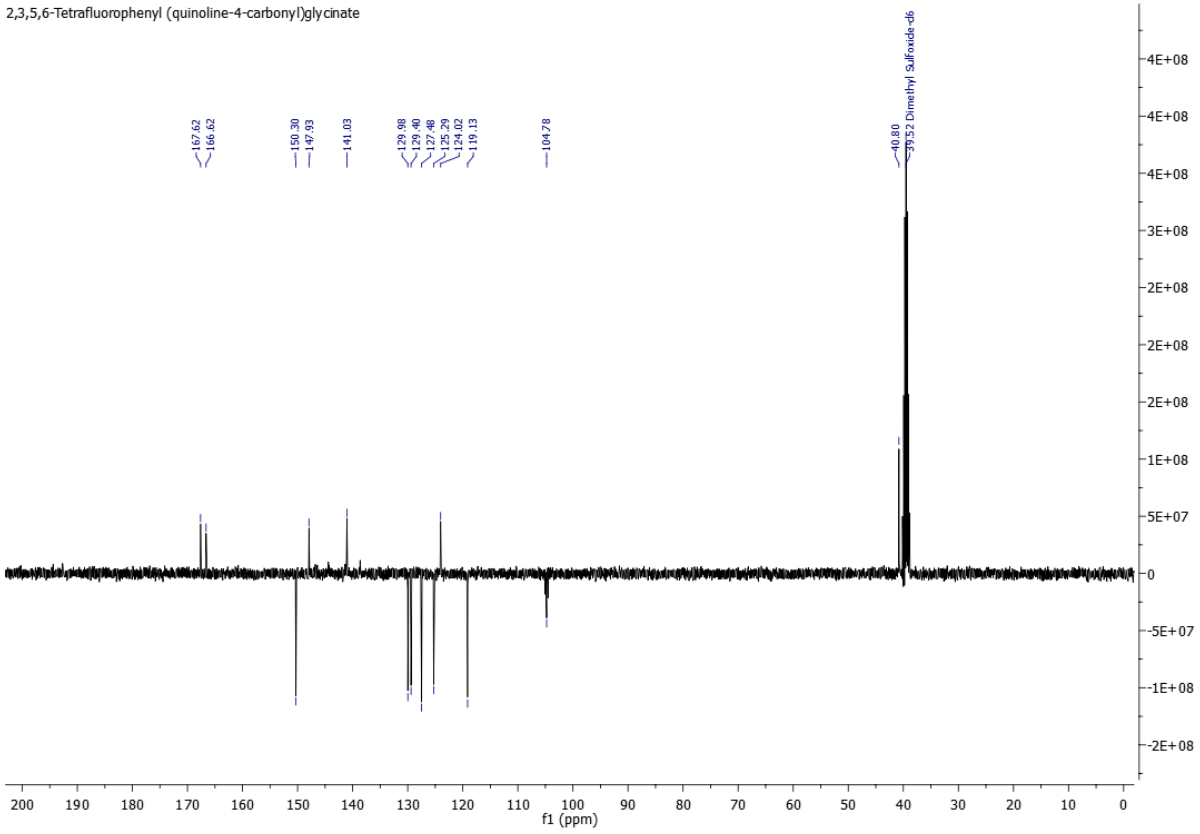

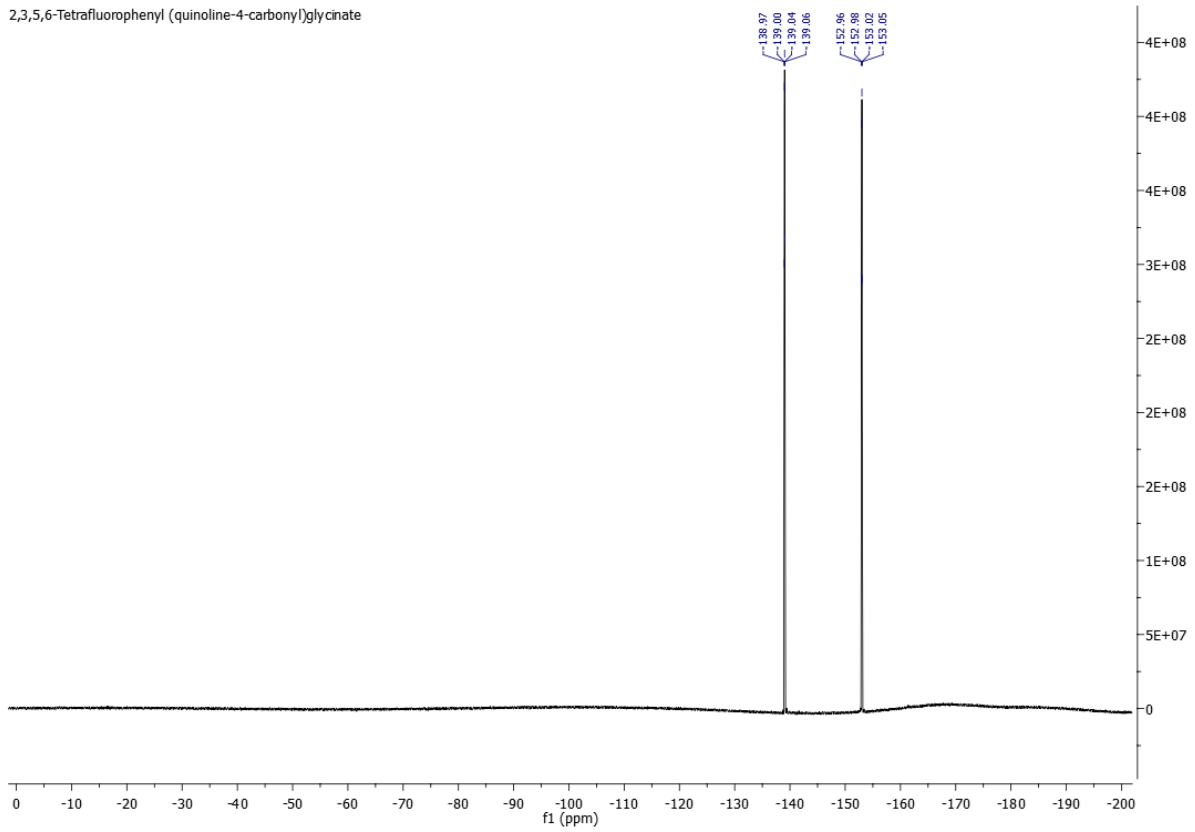

^{1}H und ^{13}C NMR of 4,4-dimethoxybutanal[264]

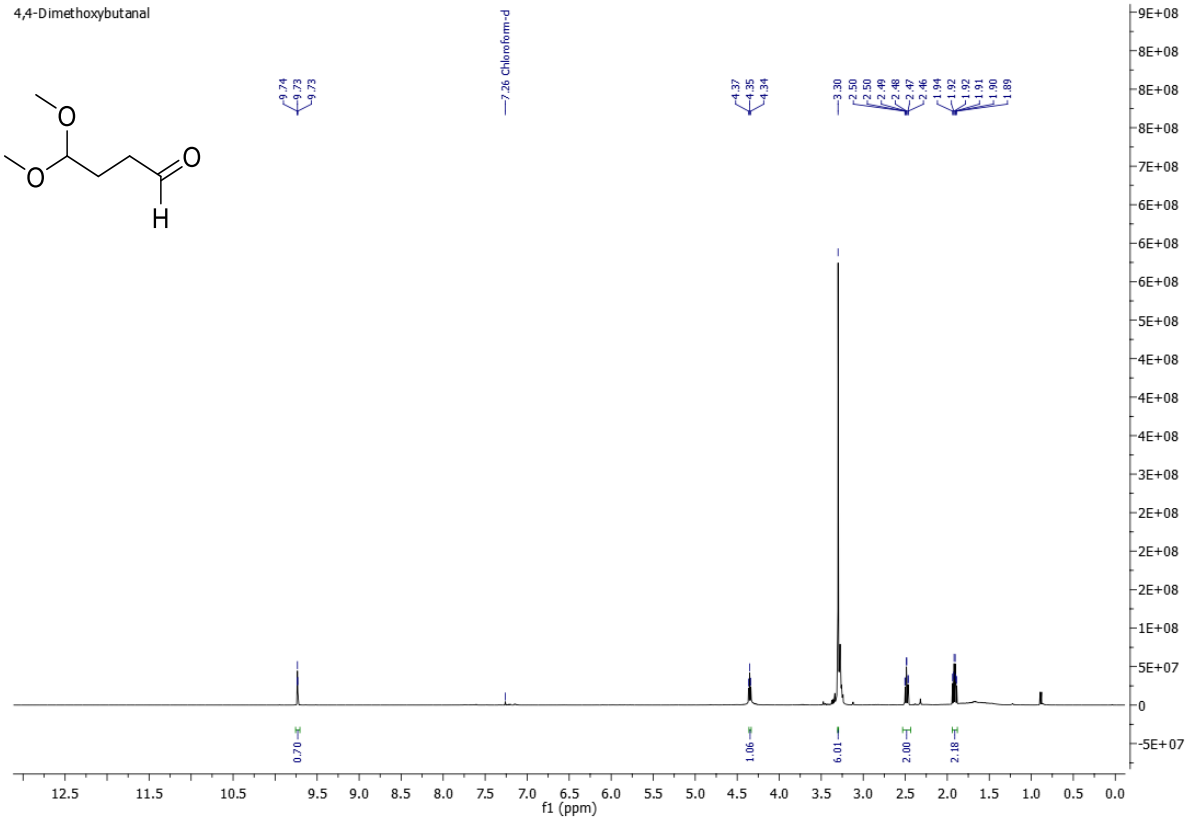

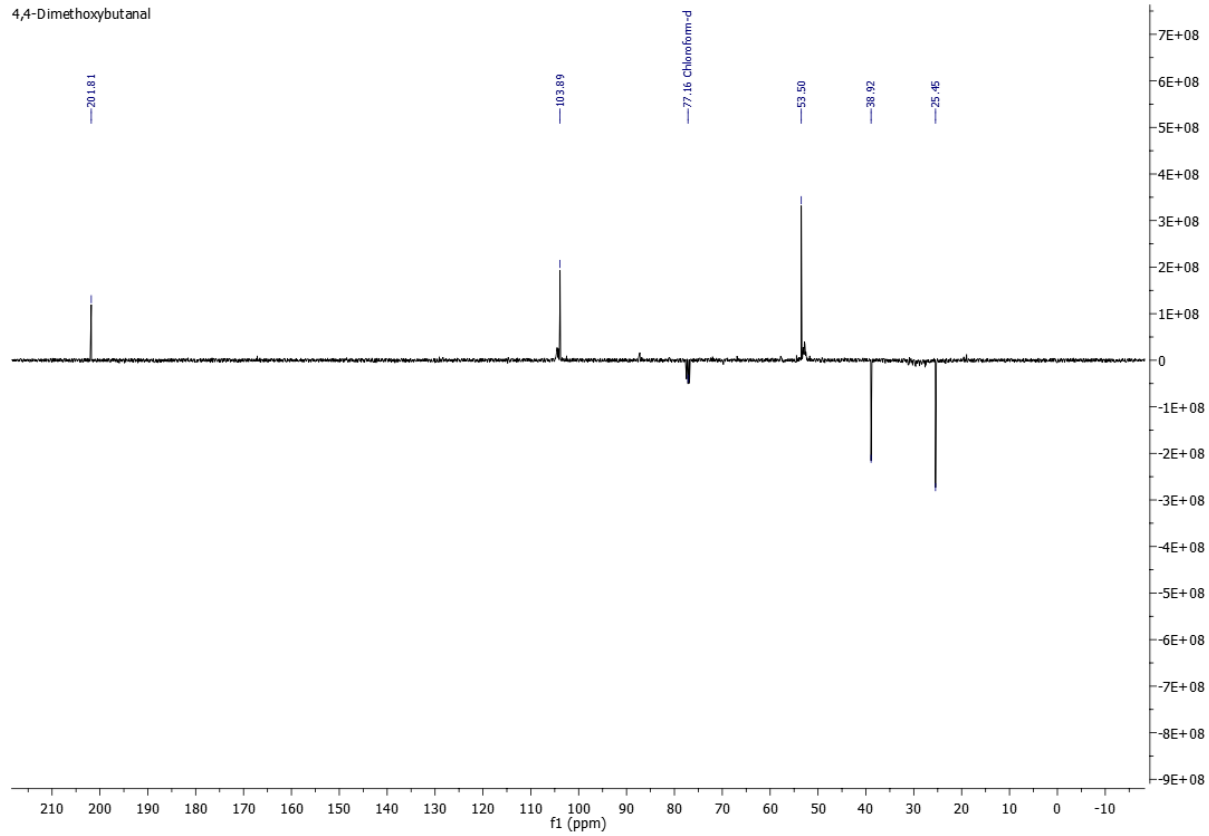

^{1}H and ^{13}C NMR of (*S,E*)-*N*-(4,4-dimethoxybutyliden)-2-methylpropan-2-sulfinamide [(*S*)-**19**]

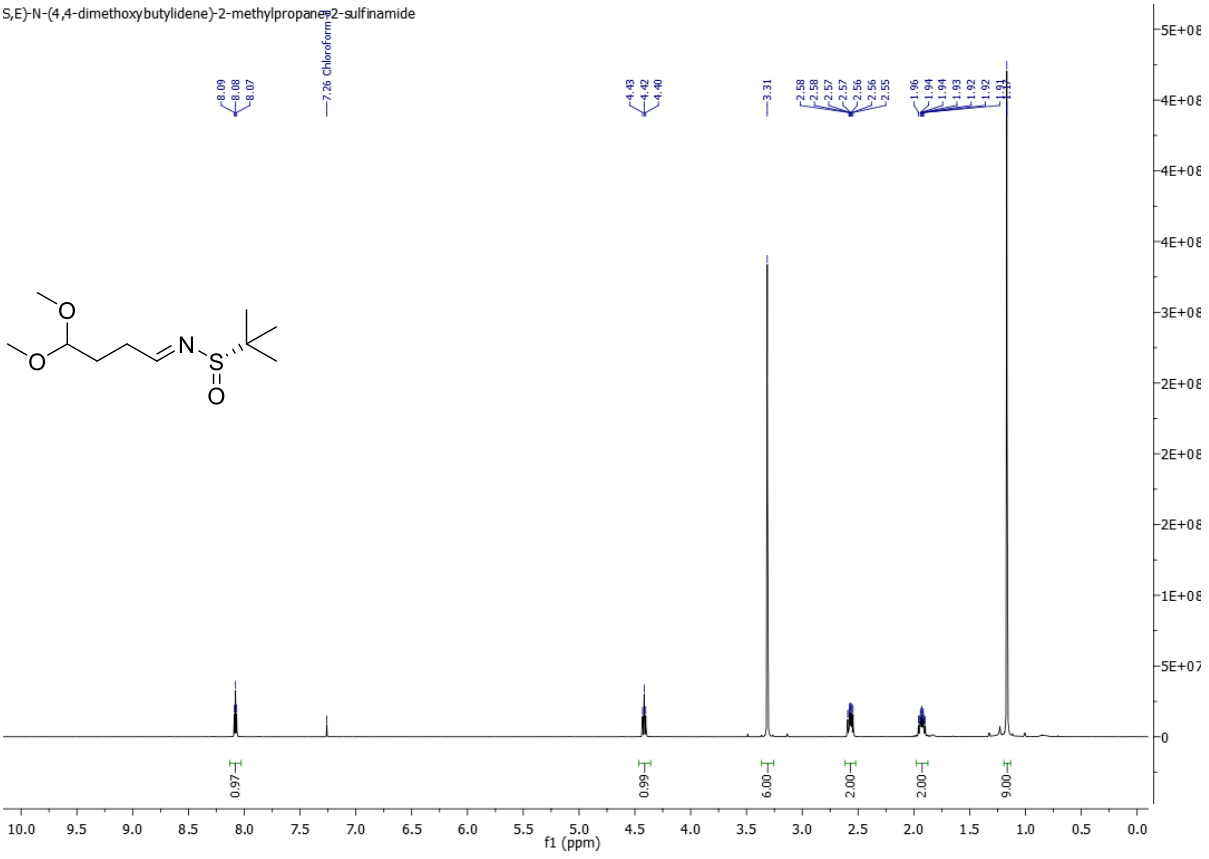

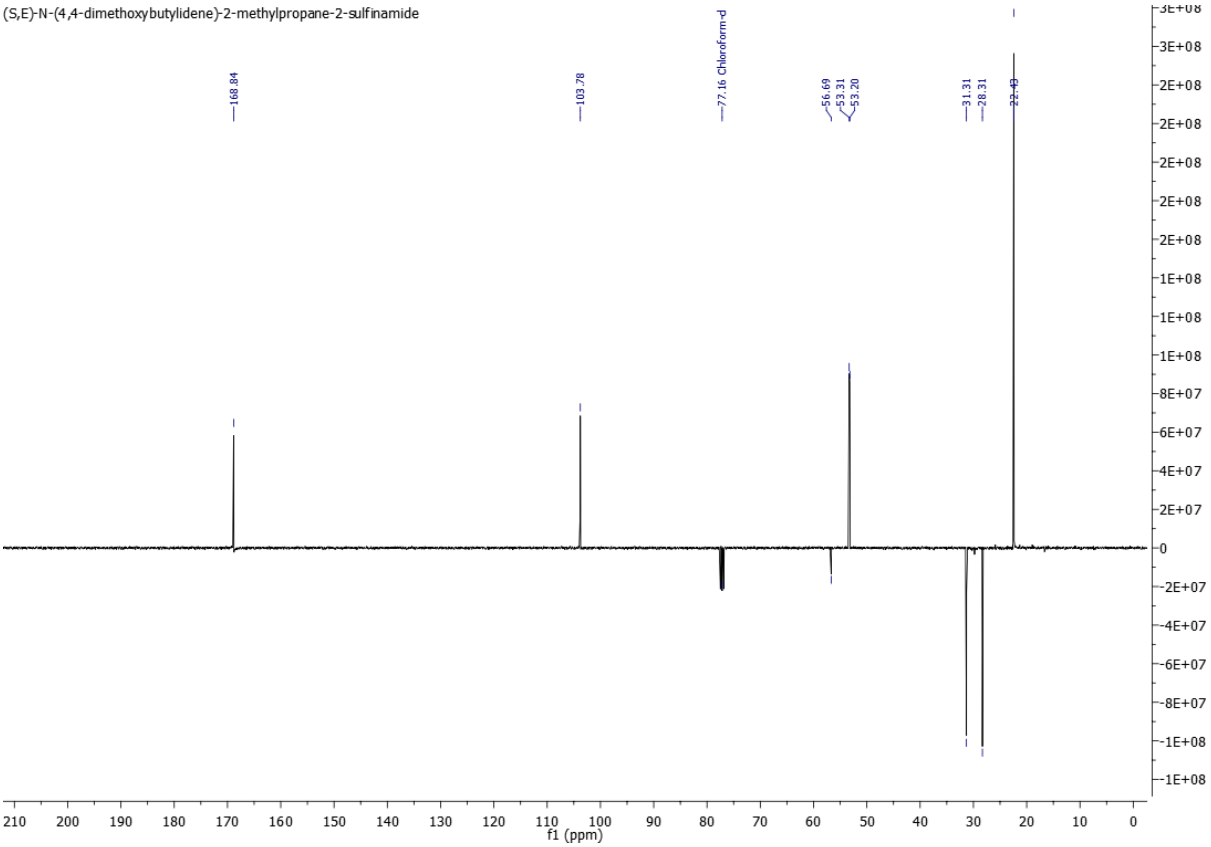

^{1}H and ^{13}C NMR of (*R*,*E*)-*N*-(4,4-dimethoxybutylidene)-2-methylpropane-2-sulfinamide [(*R*)-**19**]

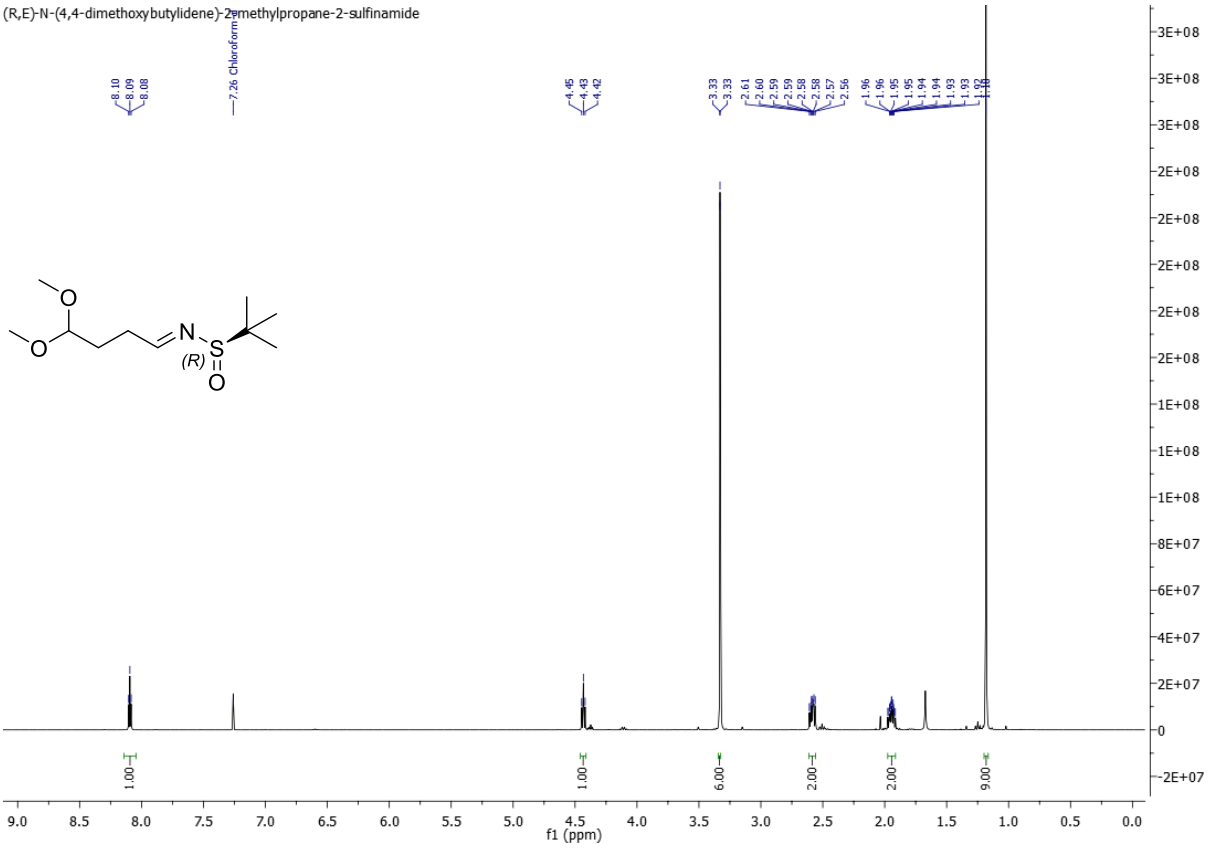

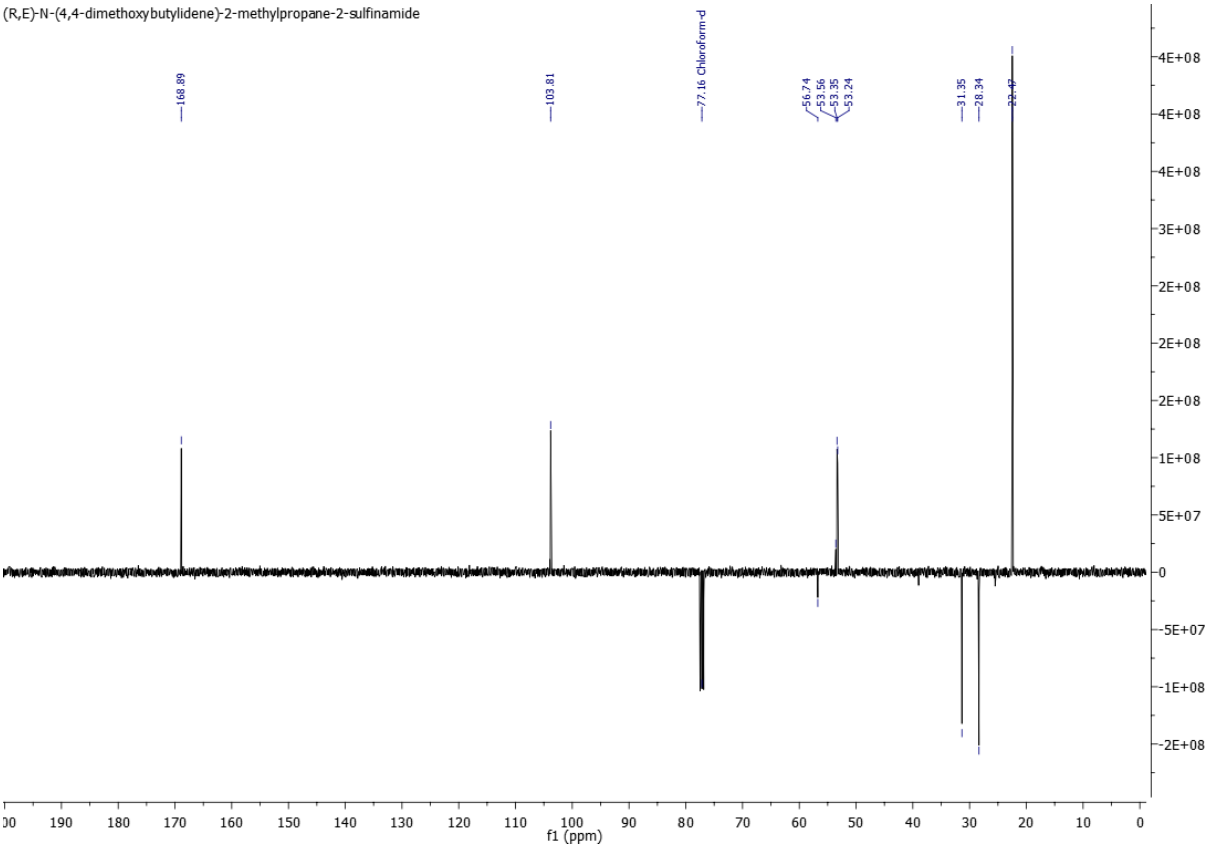

^{1}H, ^{13}C, ^{31}P, COSY, HSQC and HMBC NMR of diphenyl [(*R*)-1-([(*S*)-*tert*-butylsulfinyl]amino)-4,4-dimethoxybutyl]phosphonate [(*S,R*)-**20**]

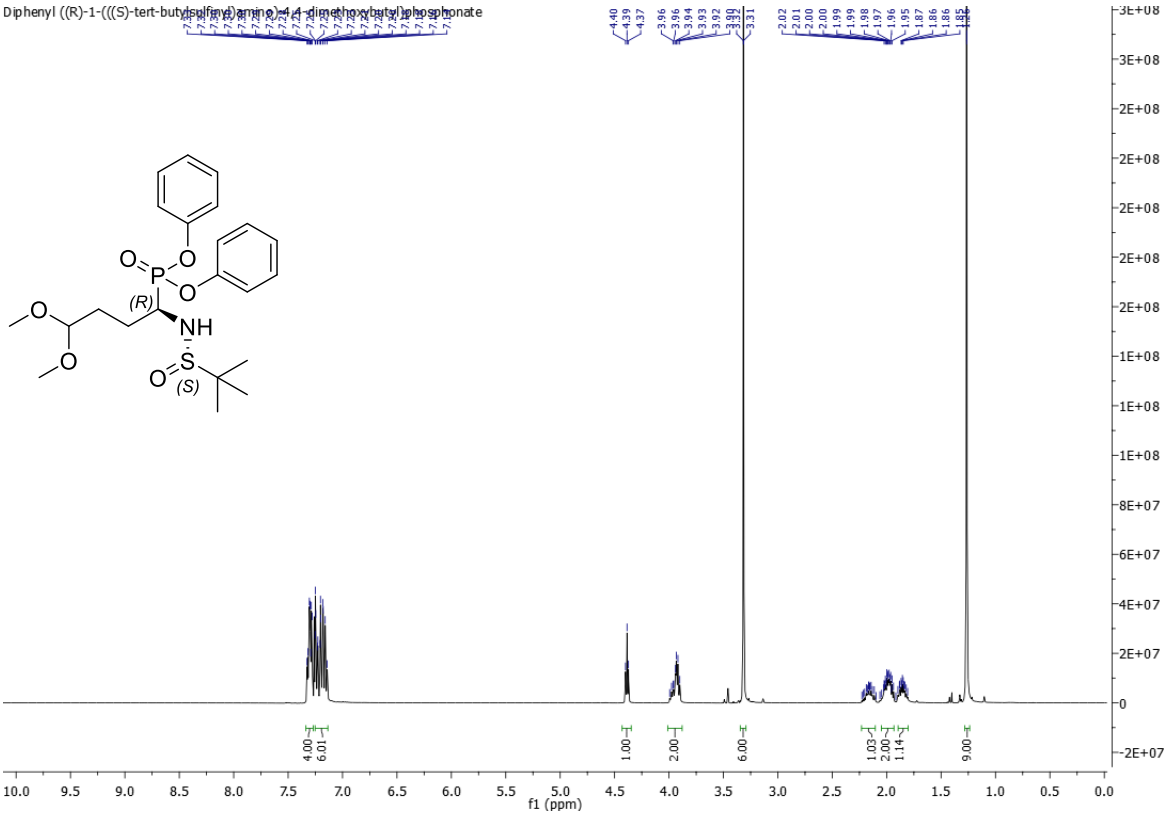

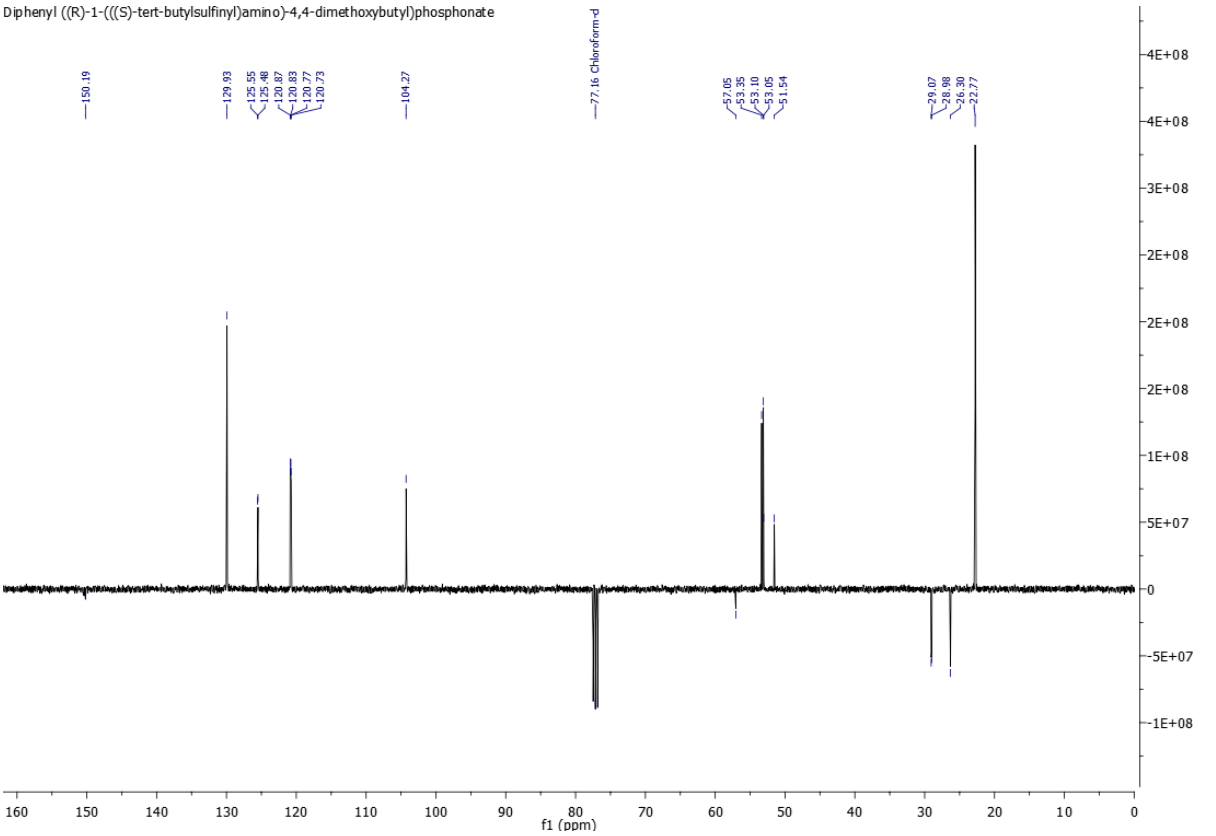
Diphenyl ((R)-1-(((S)-tert-butylsulfinyl)amino)-4,4-dimethoxybutyl)phosphonate
150.19
129.93
125.55
125.48
120.87
120.83
120.77
120.73
104.27
77.16 Chloroform-d
67.05
53.35
53.10
53.05
51.54
29.07
28.98
26.30
22.77
f1 (ppm)

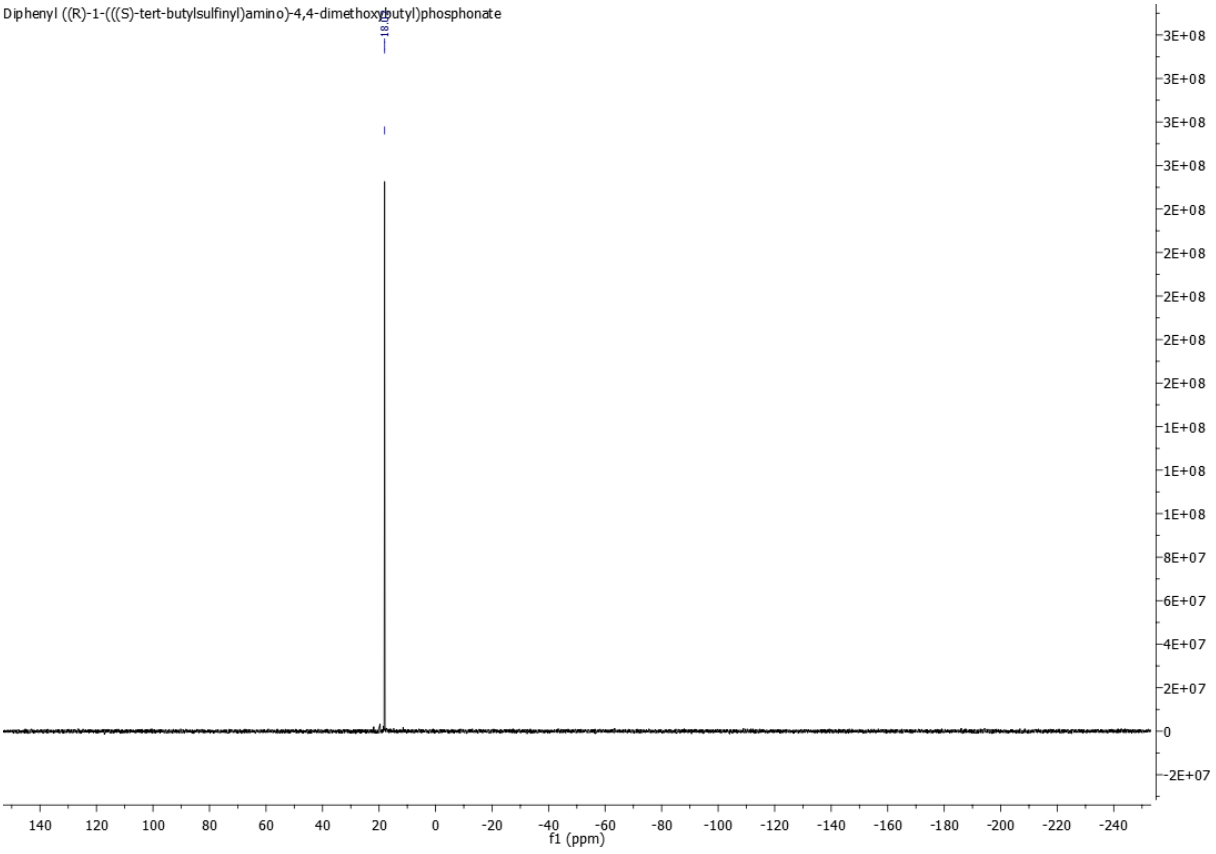
Diphenyl ((R)-1-(((S)-tert-butylsulfinyl)amino)-4,4-dimethoxybutyl)phosphonate
18.15
f1 (ppm)

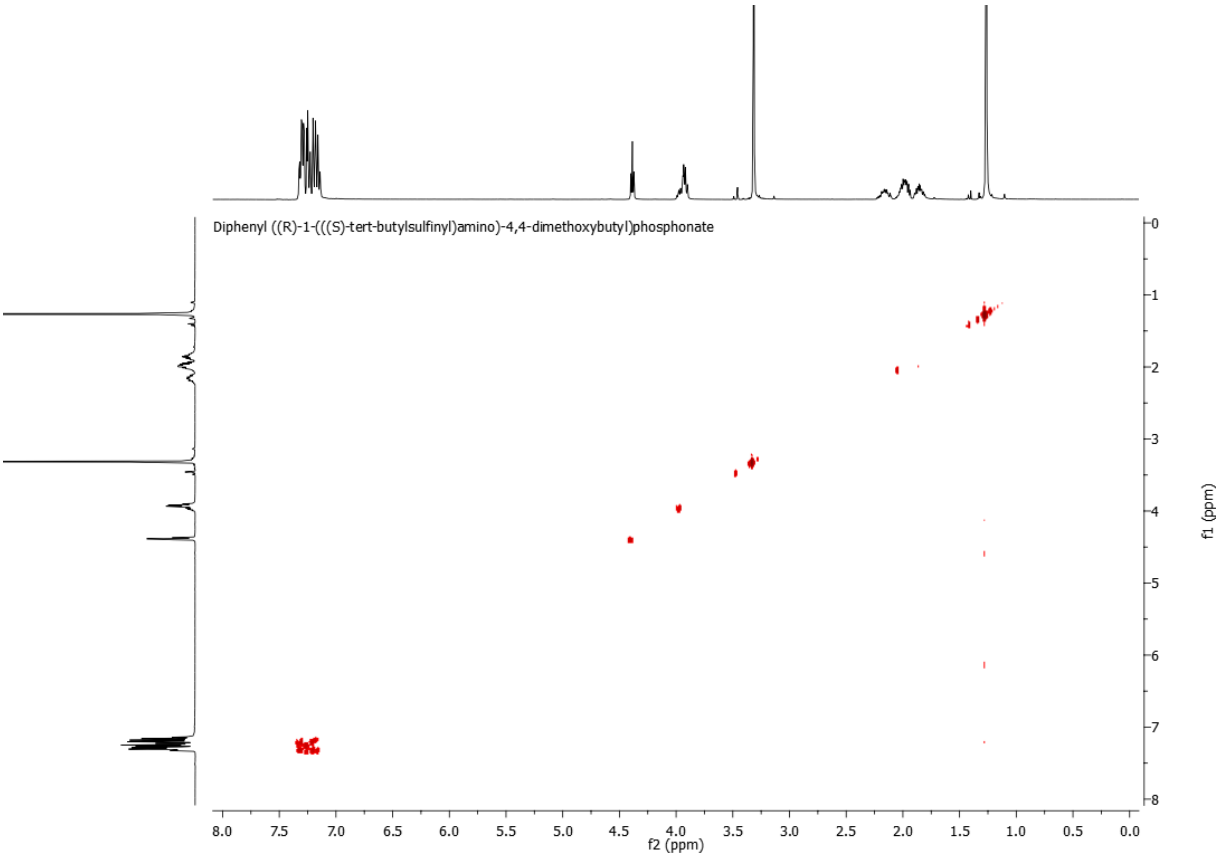
Diphenyl ((R)-1-(((S)-tert-butylsulfinyl)amino)-4,4-dimethoxybutyl)phosphonate
f2 (ppm)
f1 (ppm)

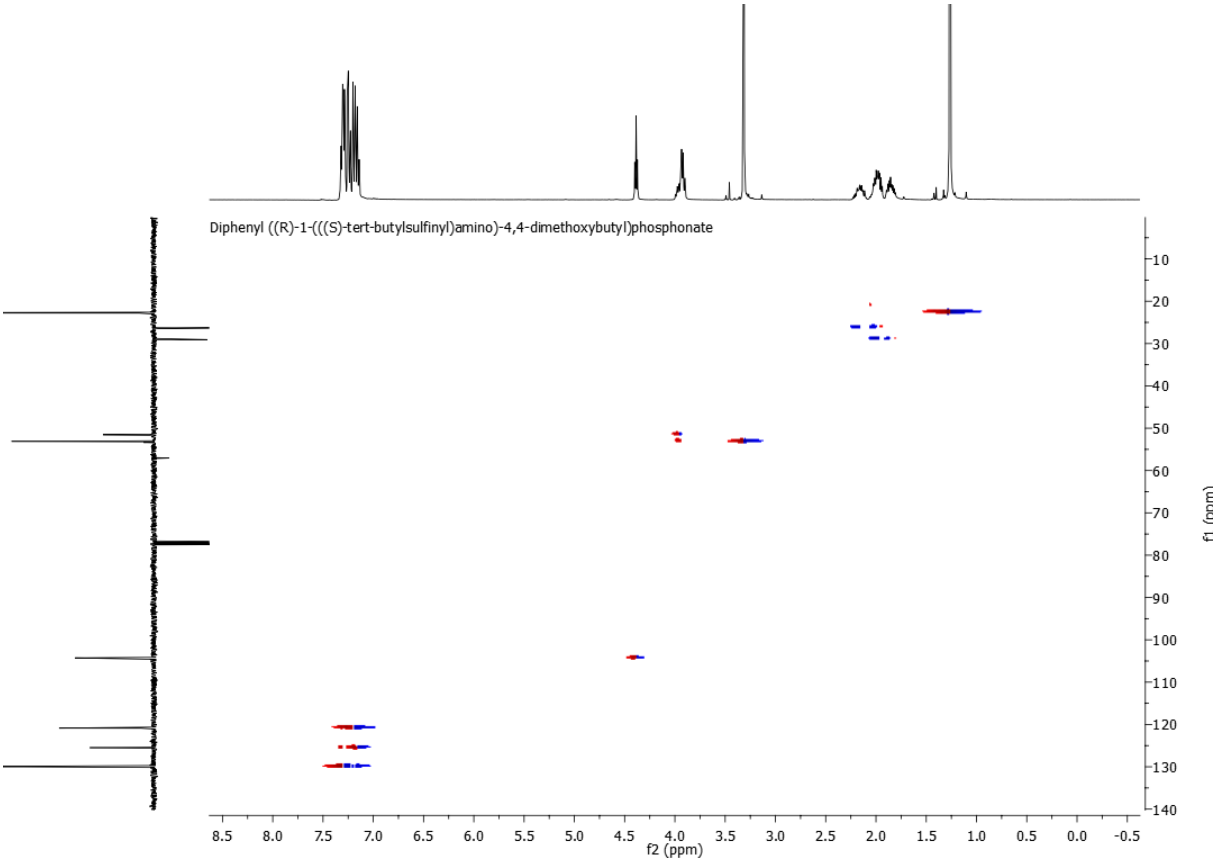
Diphenyl ((R)-1-(((S)-tert-butylsulfinyl)amino)-4,4-dimethoxybutyl)phosphonate
f2 (ppm)
f1 (ppm)

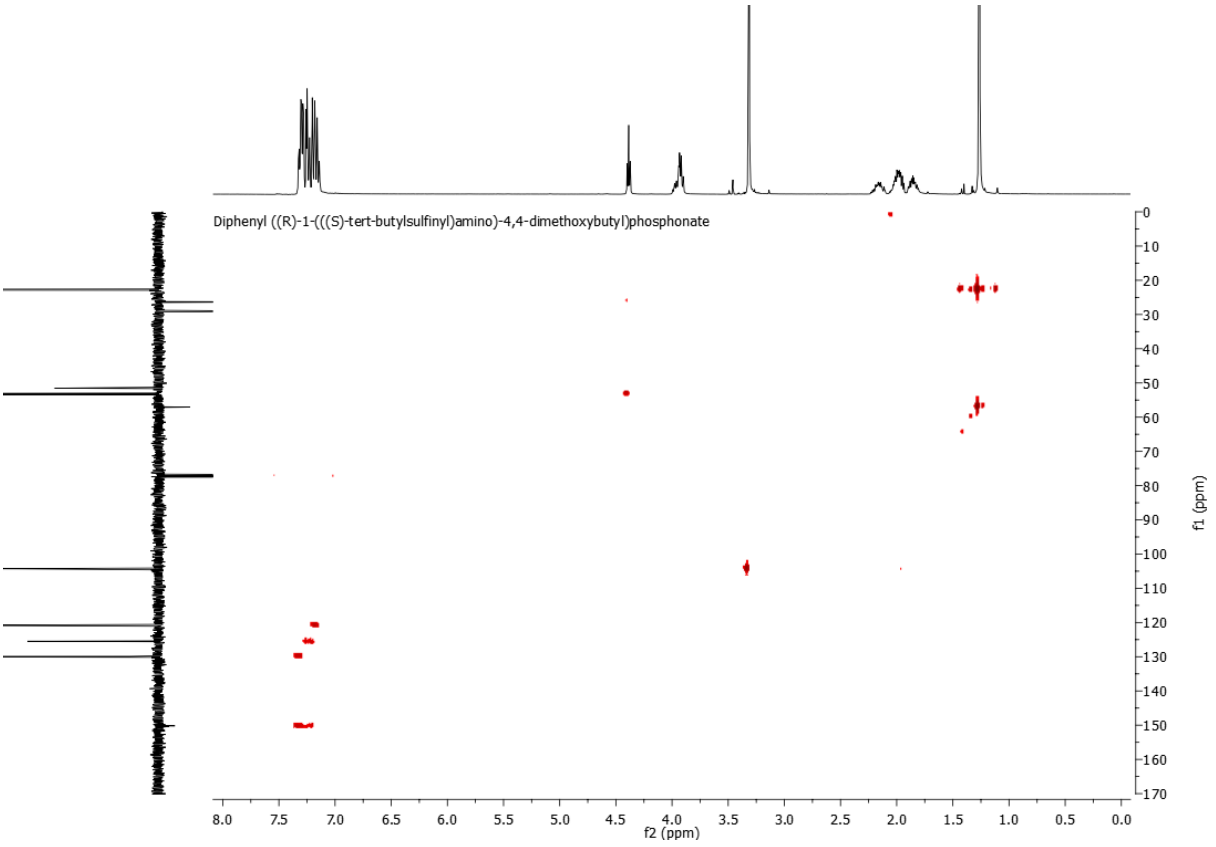

^{1}H, ^{13}C, ^{31}P and HSQC NMR of diphenyl [(*S*)-1-([(*R*)-*tert*-butylsulfinyl]amino)-4,4-dimethoxybutyl]phosphonate [(*R*,*S*)-**20**]

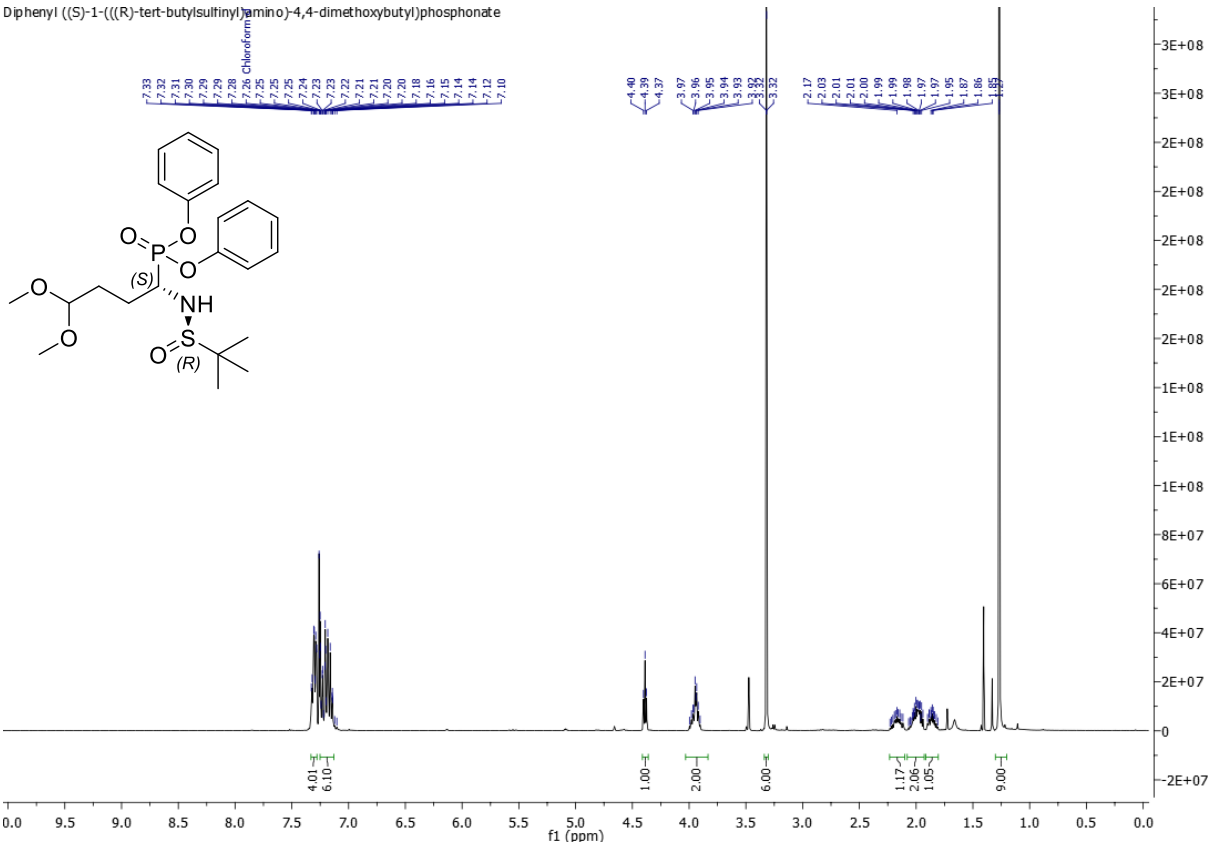

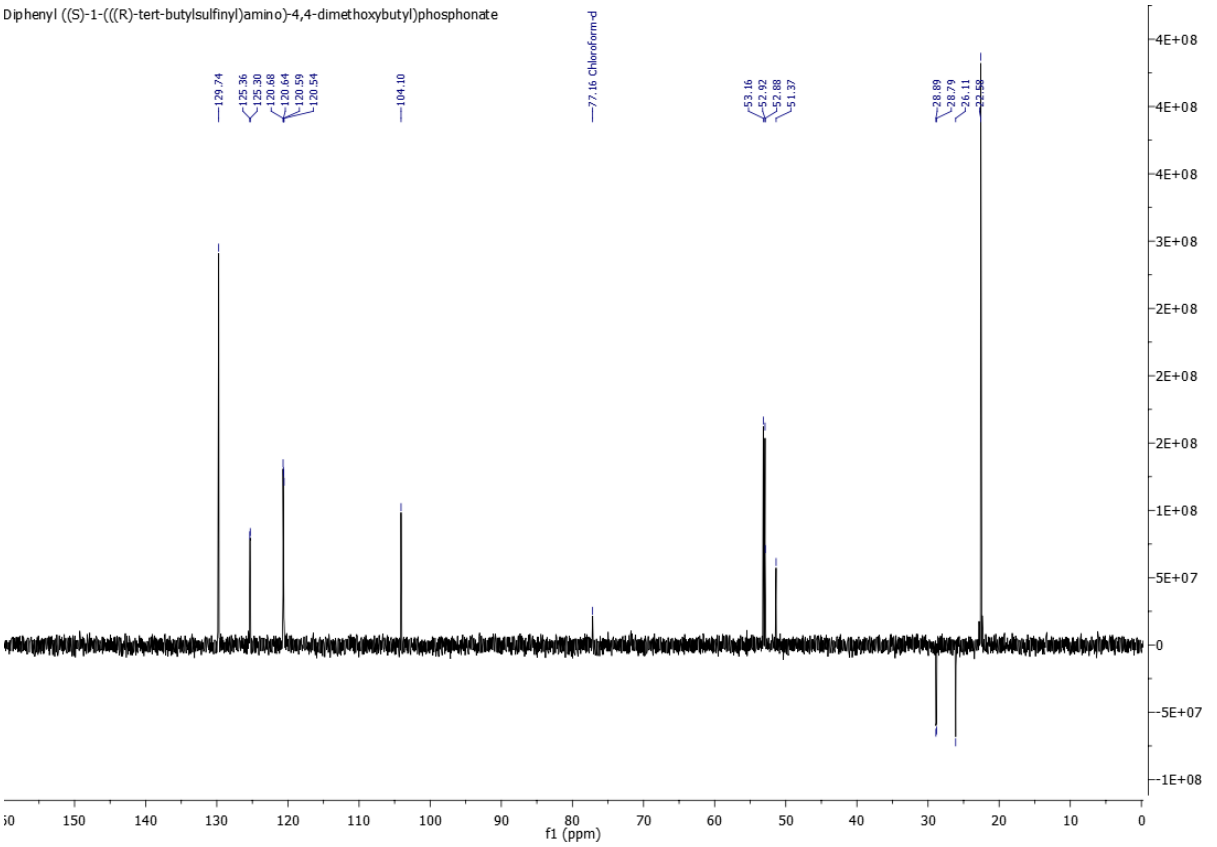
Diphenyl ((S)-1-(((R)-tert-butylsulfinyl)amino)-4,4-dimethoxybutyl)phosphonate
129.74
125.36
125.30
120.68
120.64
120.59
120.54
104.10
77.16 Chloroform-d
53.16
52.92
52.88
51.37
28.89
28.79
26.11
22.88
f1 (ppm)

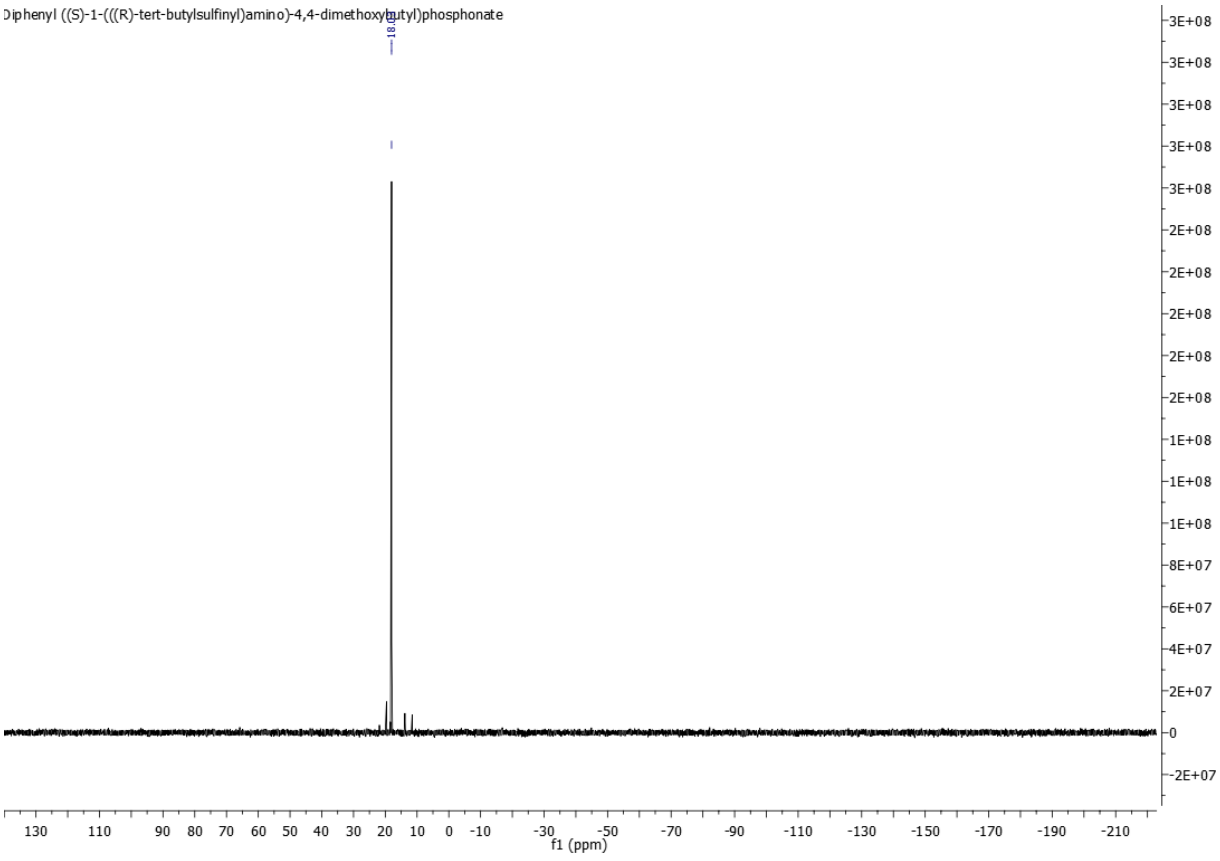
Diphenyl ((S)-1-(((R)-tert-butylsulfinyl)amino)-4,4-dimethoxybutyl)phosphonate
18.07
f1 (ppm)

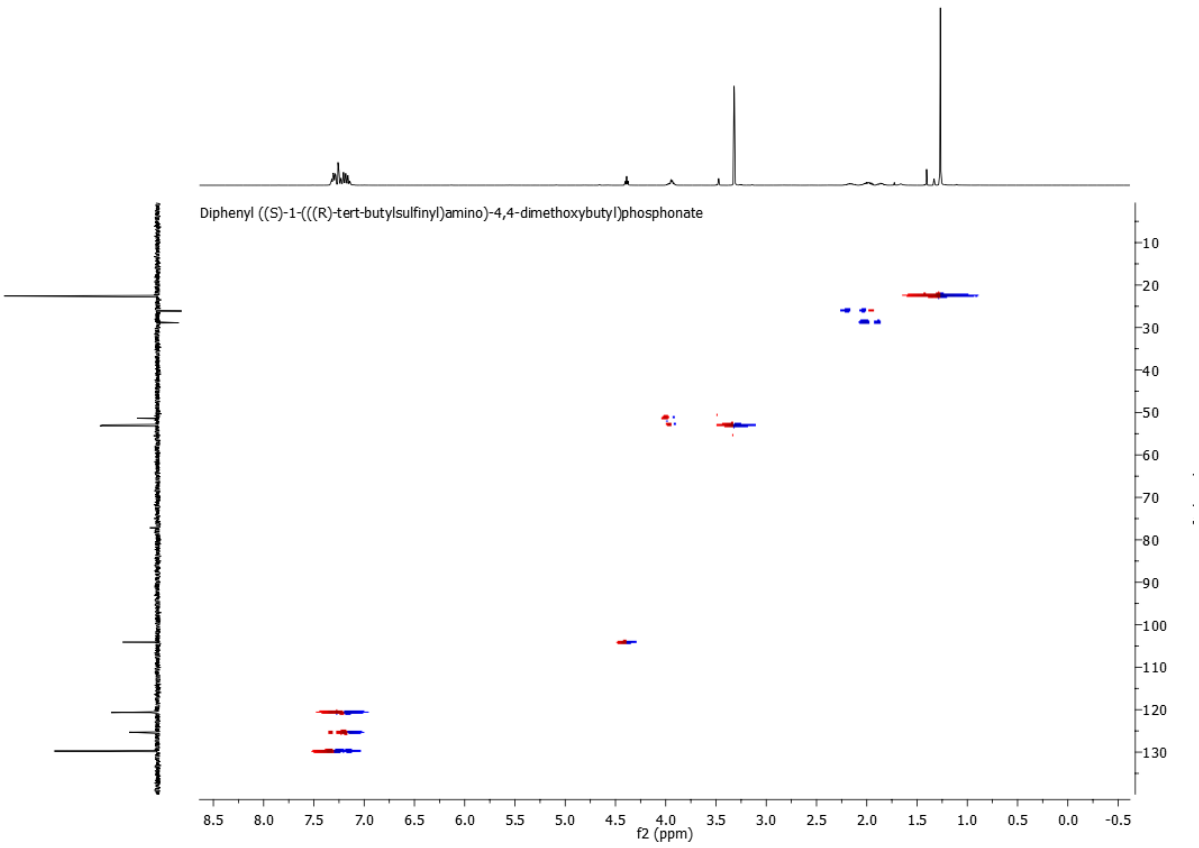

^{1}H, ^{13}C and ^{31}P NMR of diphenyl (*R*)-pyrrolidin-2-ylphosphonate [(*R*)-**21**]

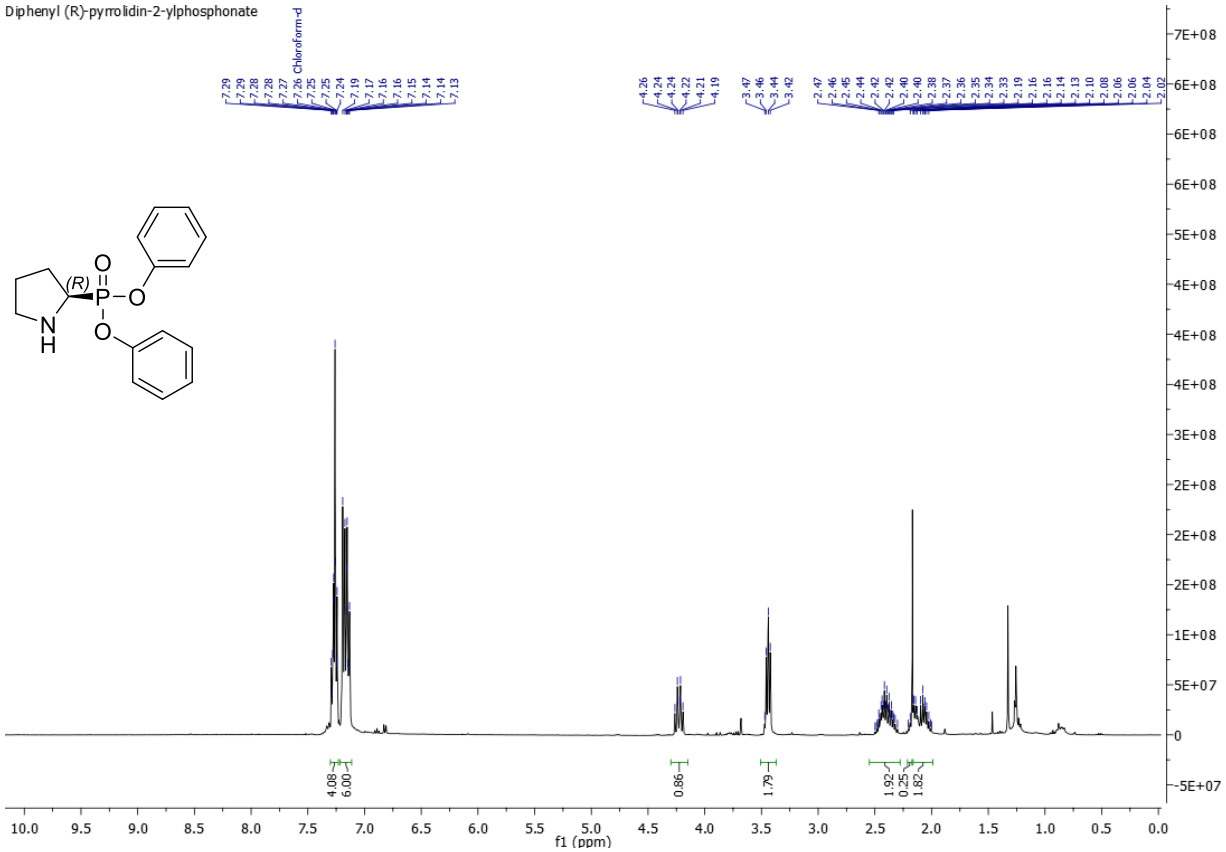

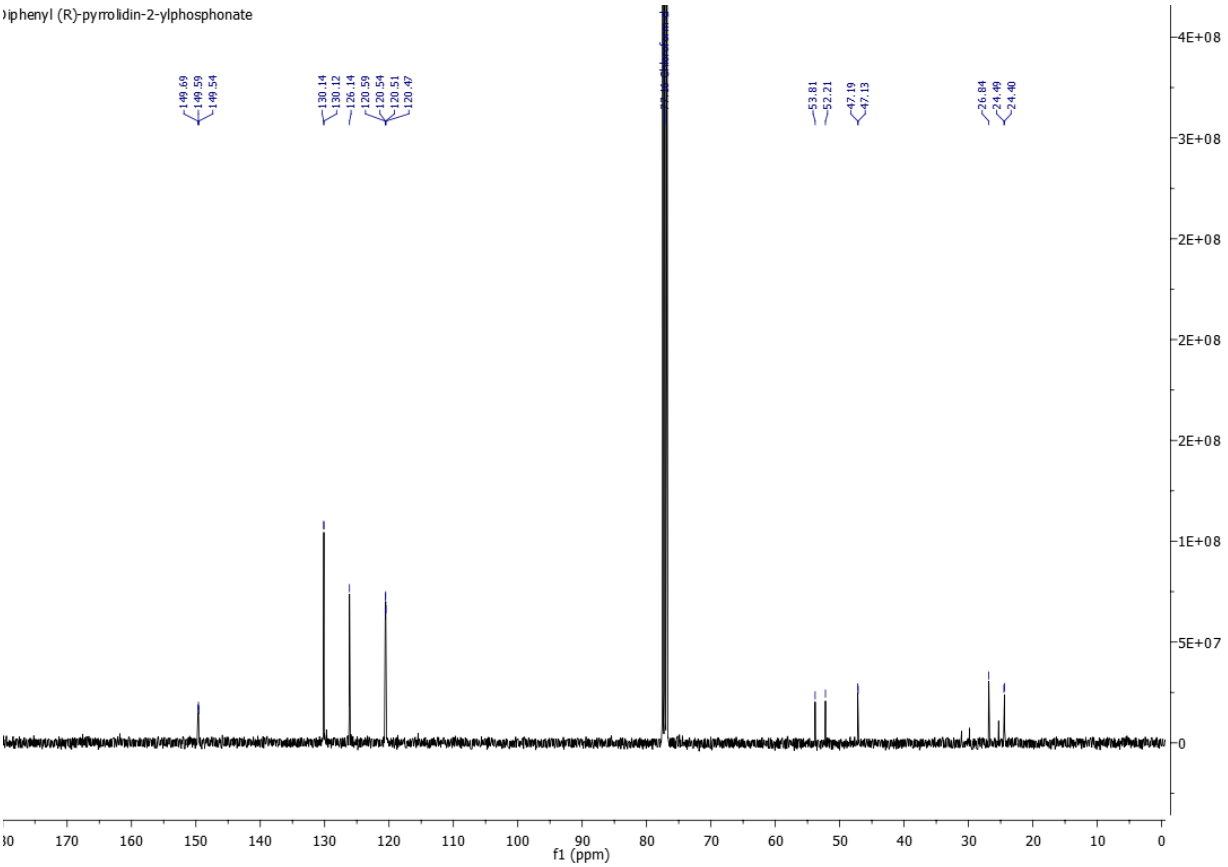
iphenyl (R)-pyrrolidin-2-ylphosphonate
149.69
149.59
149.54
130.14
130.12
126.14
120.59
120.54
120.51
120.47
53.81
52.21
47.19
47.13
26.84
24.49
24.40
4E+08
3E+08
2E+08
2E+08
2E+08
1E+08
5E+07
0
f1 (ppm)

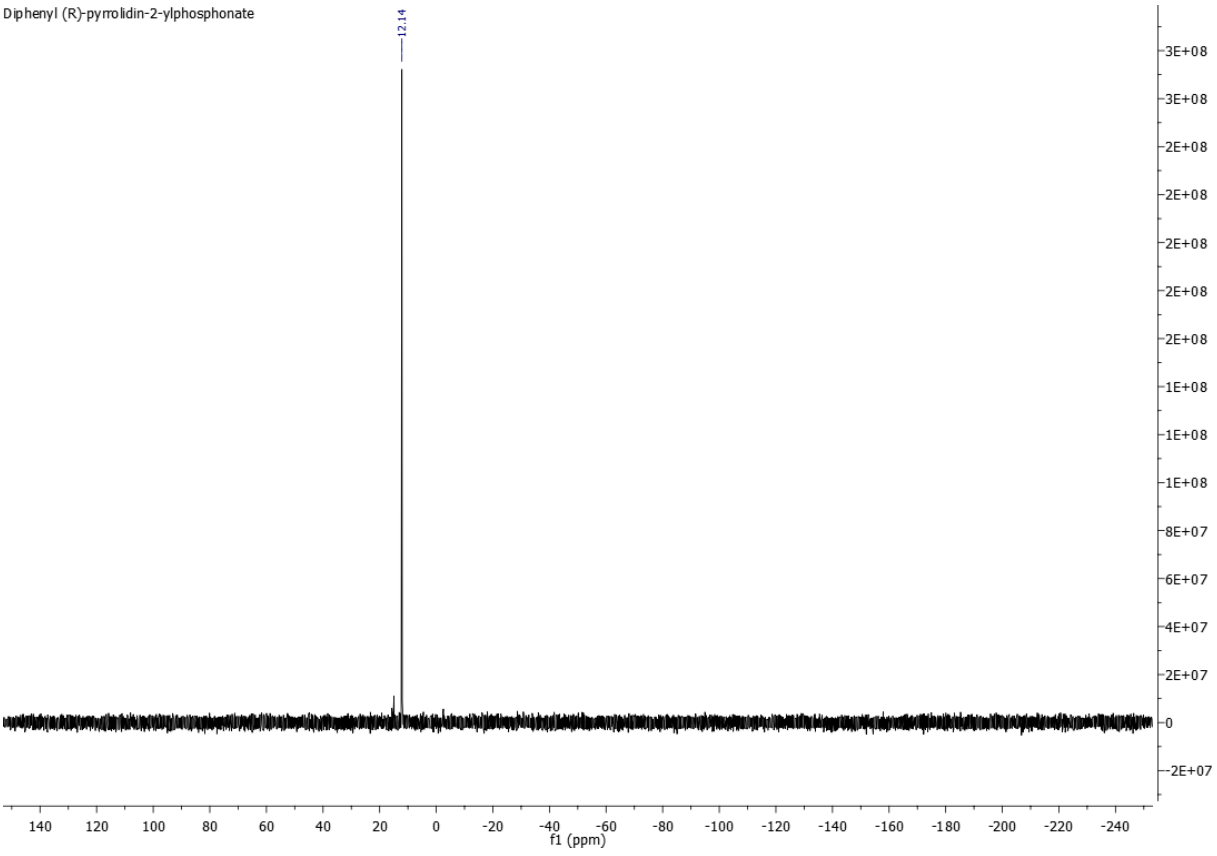
Diphenyl (R)-pyrrolidin-2-ylphosphonate
12.14
3E+08
3E+08
2E+08
2E+08
2E+08
2E+08
2E+08
2E+08
1E+08
1E+08
1E+08
8E+07
6E+07
4E+07
2E+07
0
-2E+07
f1 (ppm)

^{1}H, ^{13}C and ^{31}P NMR of diphenyl (*S*)-pyrrolidin-2-ylphosphonate [(*S*)-**21**]

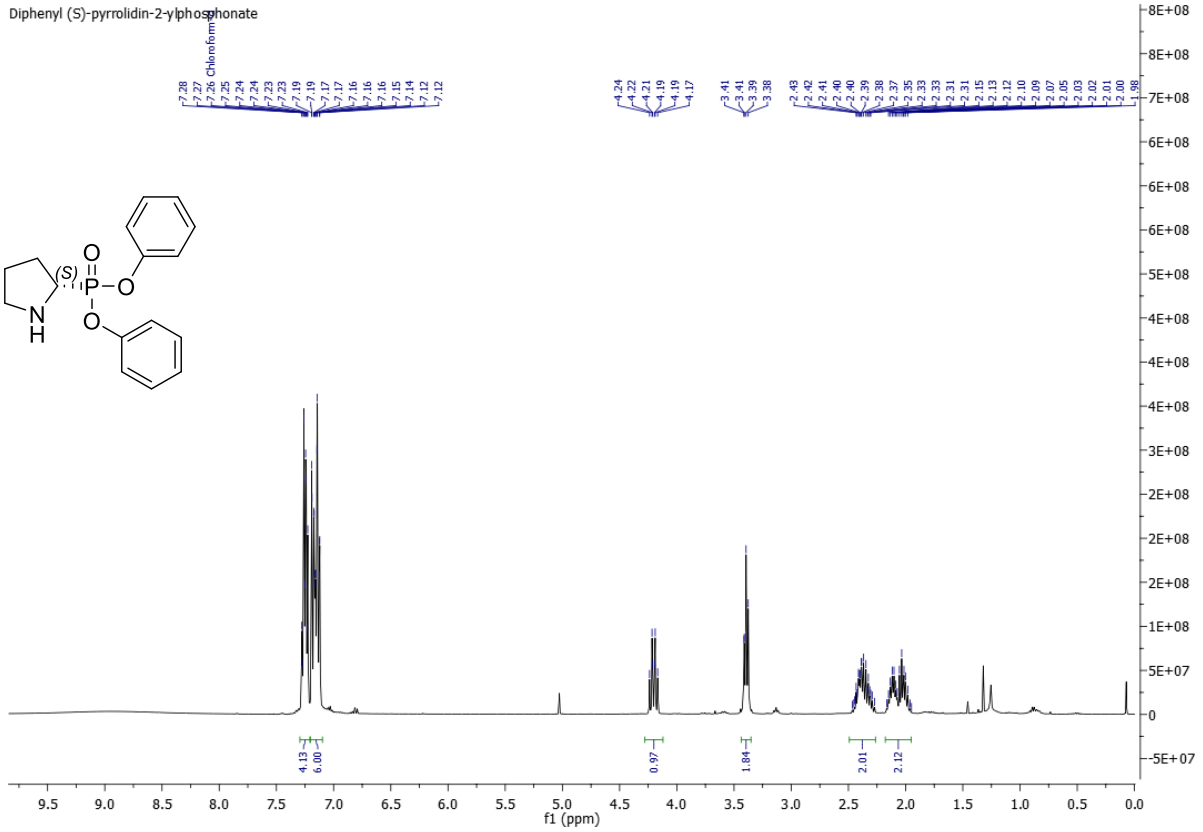

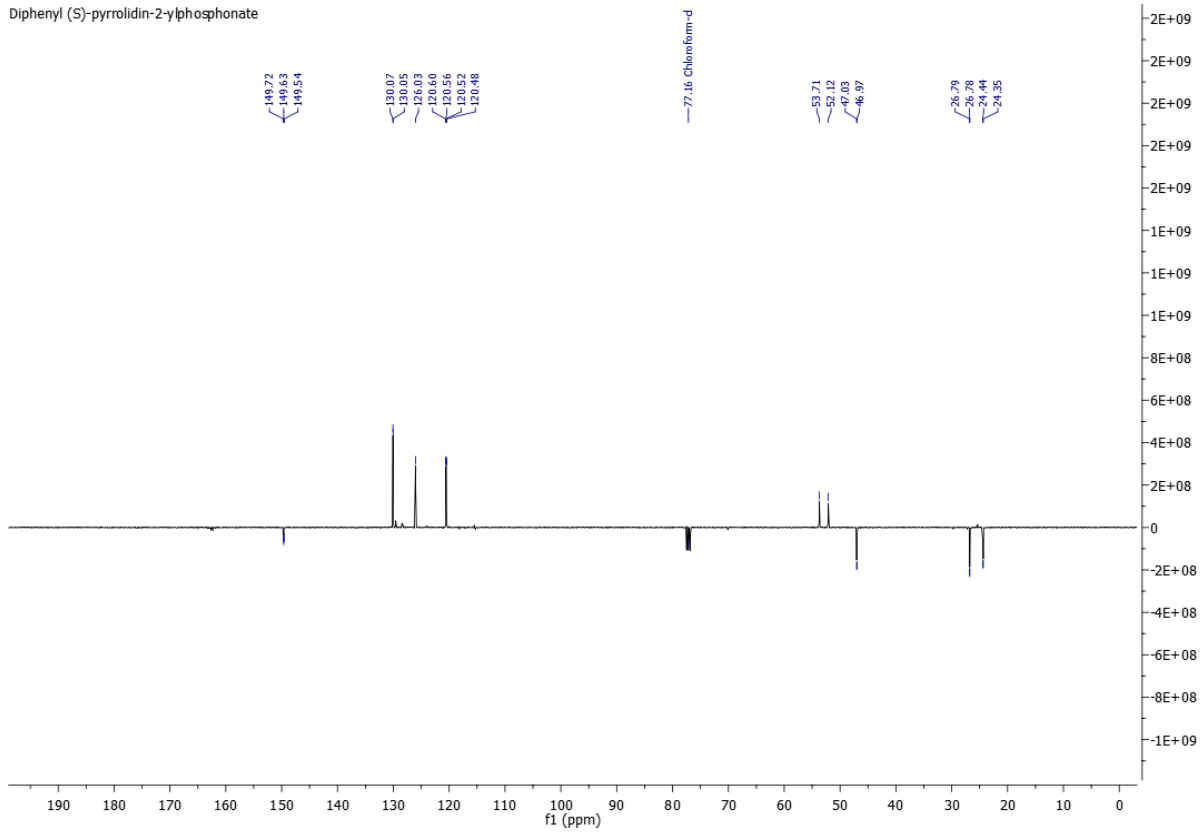

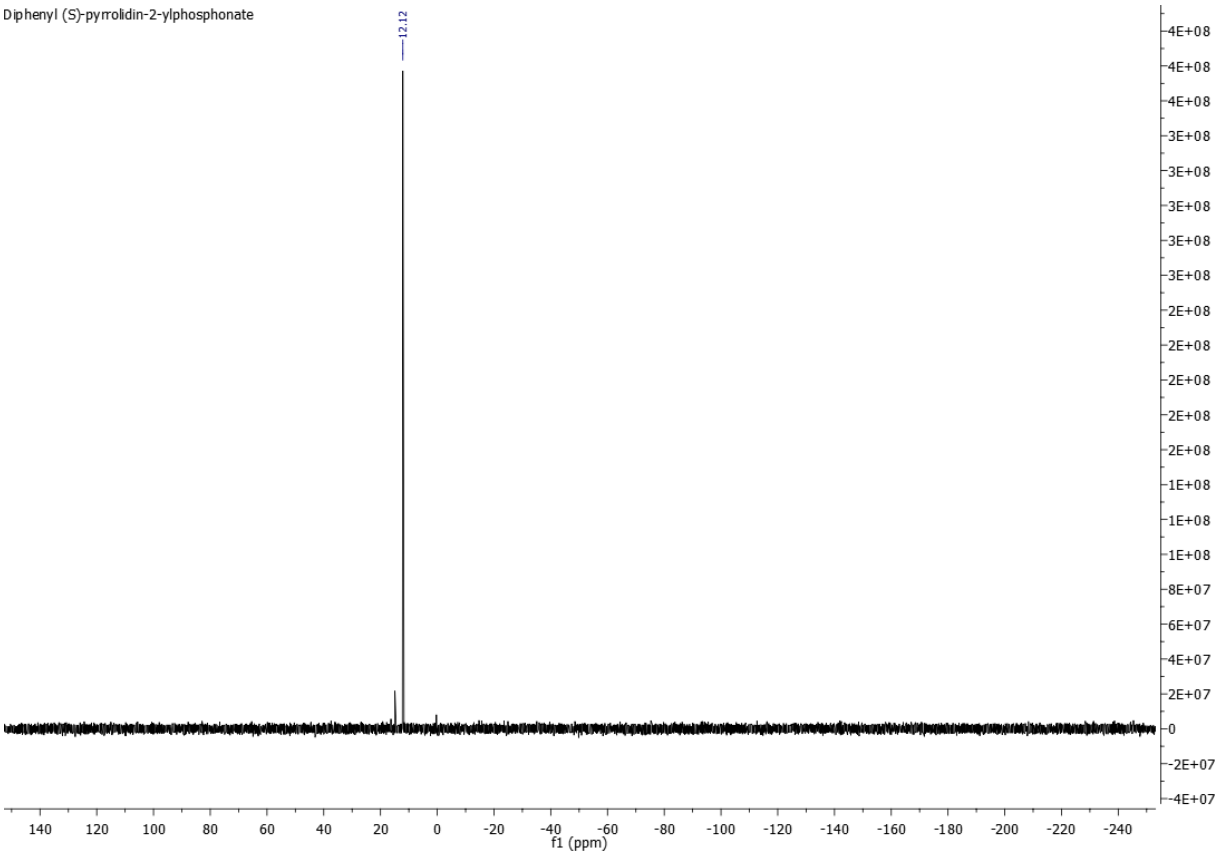

^{1}H, ^{13}C and ^{19}F NMR of diphenyl (*R*)-(1-((quinoline-4-carbonyl)glycyl)pyrrolidin-2-yl)phosphonate (**22**)

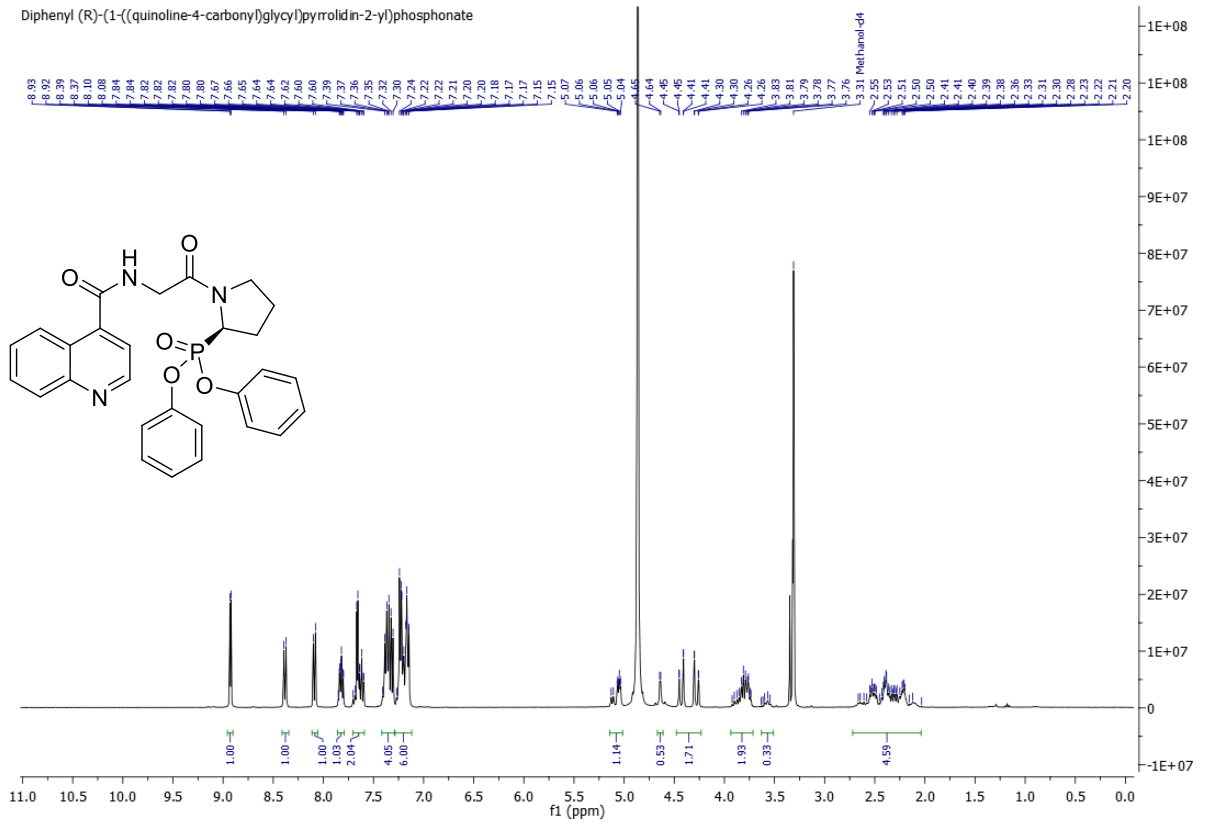

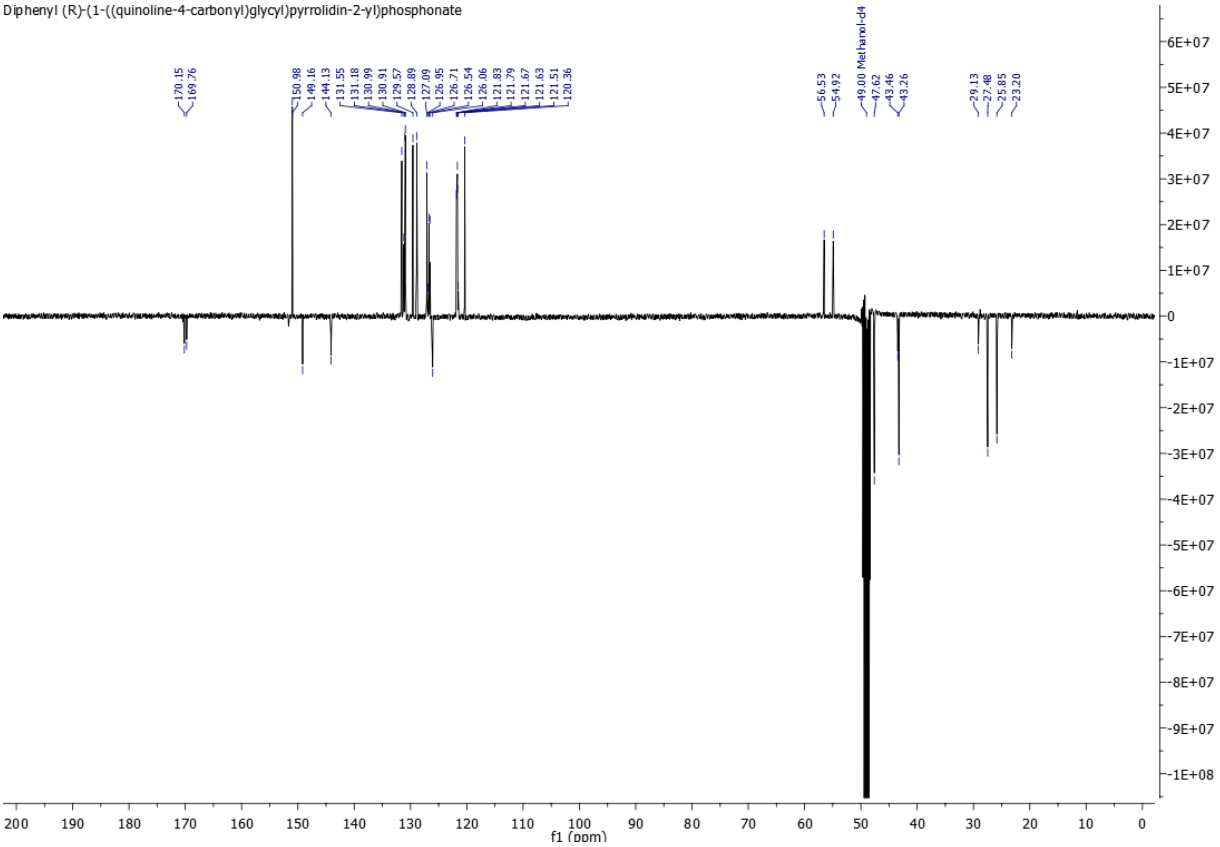
Diphenyl (R)-(1-((quinoline-4-carbonyl)glycyl)pyrrolidin-2-yl)phosphonate
170.15
169.76
150.98
149.16
144.13
131.55
131.18
130.99
130.91
129.57
128.89
127.09
126.95
126.71
126.54
126.06
121.83
121.79
121.67
121.63
121.51
120.36
56.53
54.92
49.00 Methanol-d4
47.62
43.46
43.26
29.13
27.48
25.85
23.20
f1 (ppm)

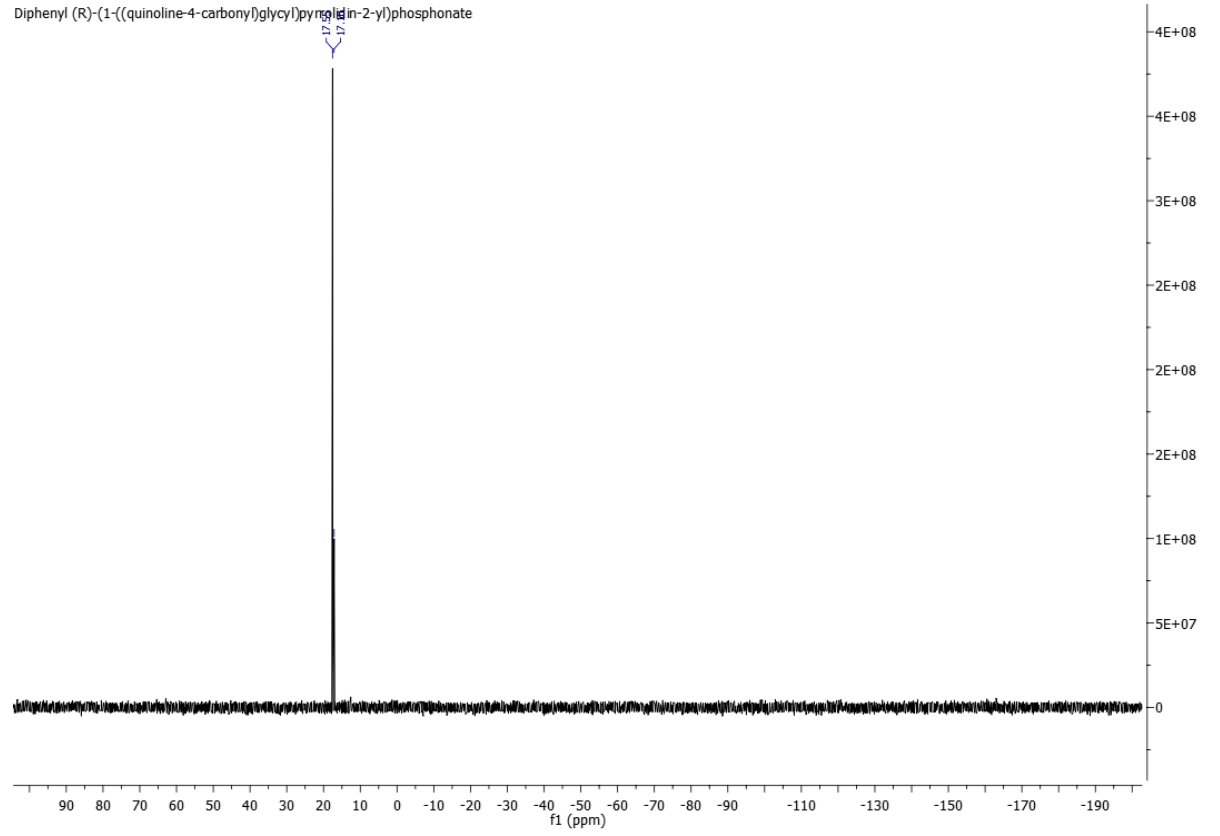
Diphenyl (R)-(1-((quinoline-4-carbonyl)glycyl)pyrrolidin-2-yl)phosphonate
f1 (ppm)

^{1}H, ^{13}C and ^{31}P NMR of diphenyl (*R*)-(1-benzylpyrrolidin-2-yl)phosphonate (**24**)

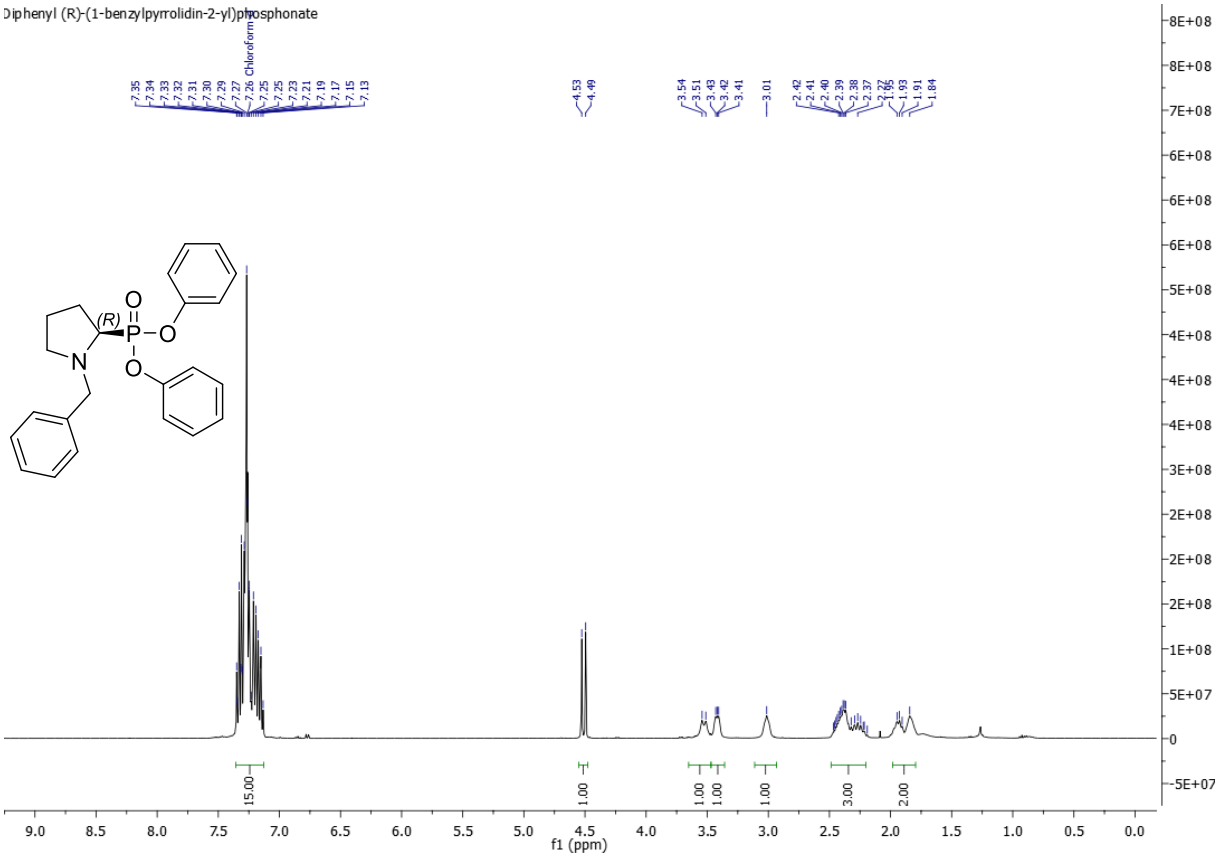

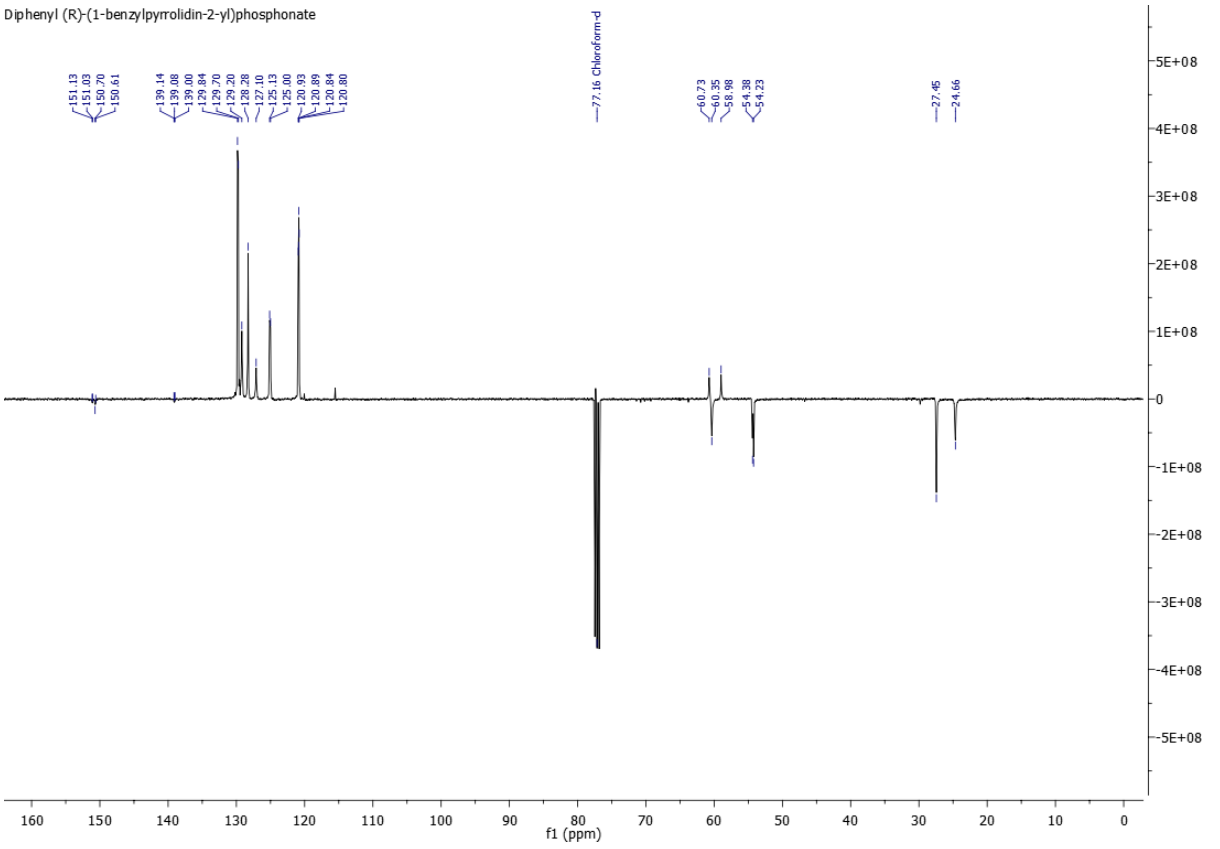

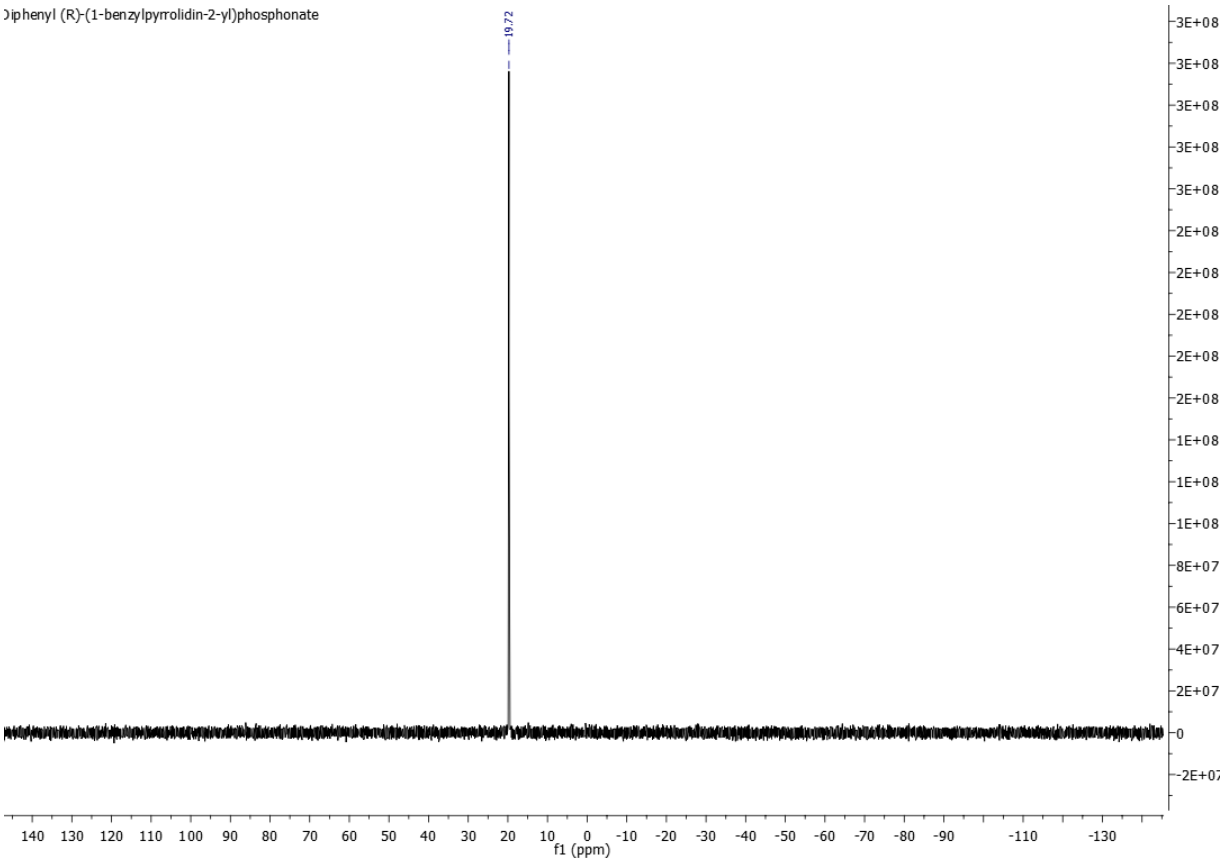

^{1}H, ^{13}C, ^{19}F and ^{31}P NMR of (*R*)-(1-benzylpyrrolidin-2-yl)phosphonofluoridate ammonium salt (**25**)

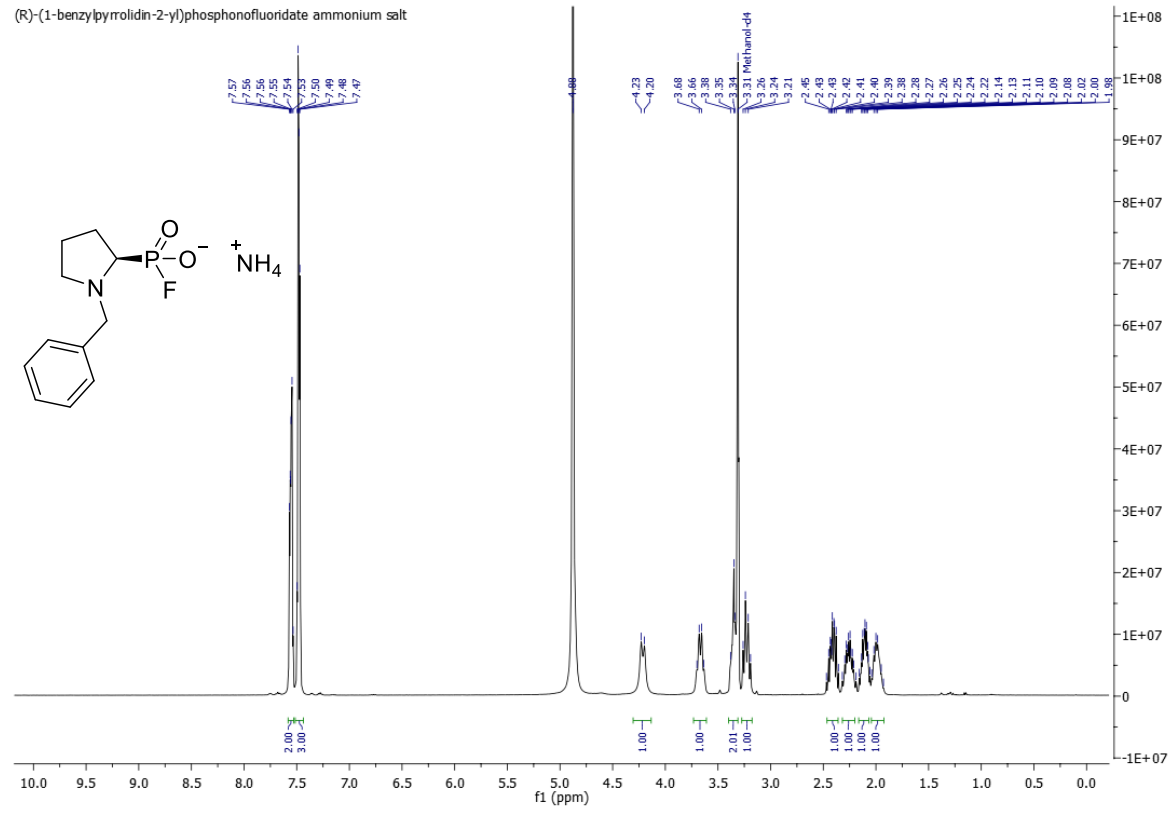

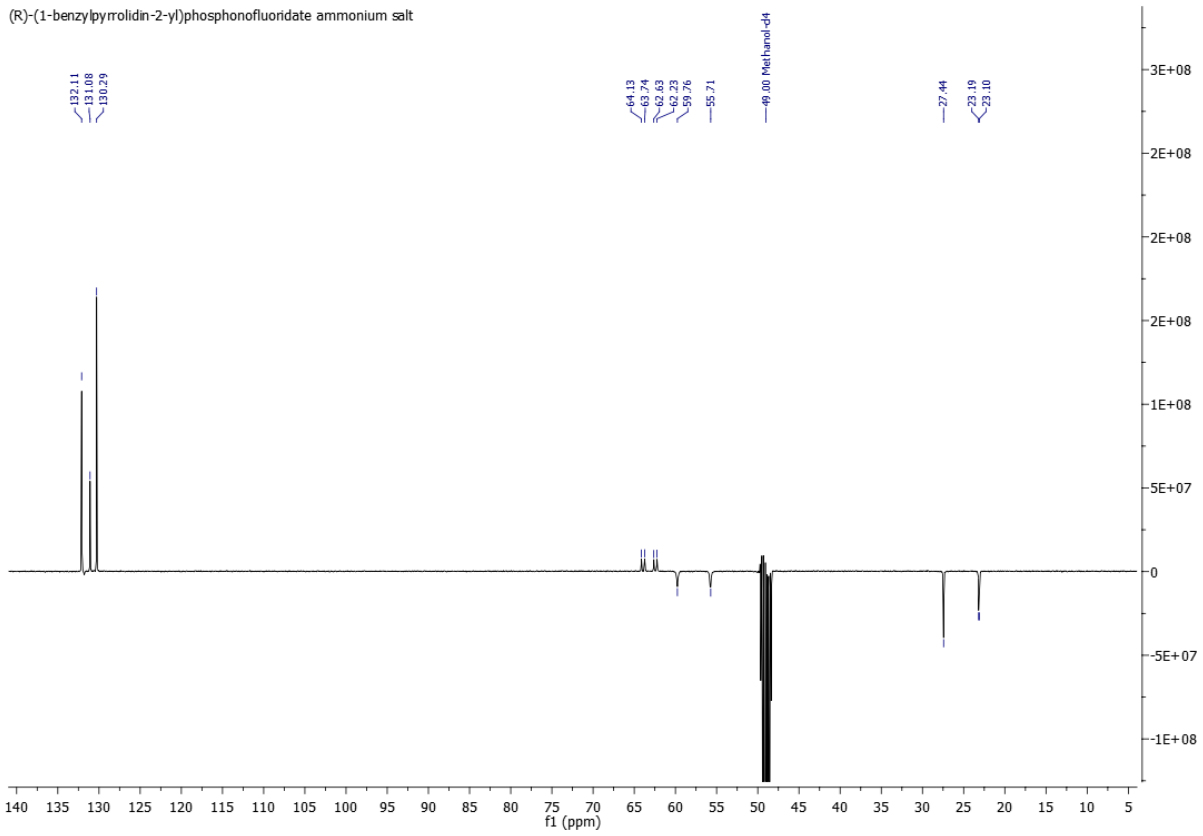
(R)-(1-benzylpyrrolidin-2-yl)phosphonofluoridate ammonium salt
132.11
131.08
130.29
64.13
63.74
62.63
62.23
59.76
55.71
49.00 Methanol-d4
27.44
23.19
23.10
f1 (ppm)

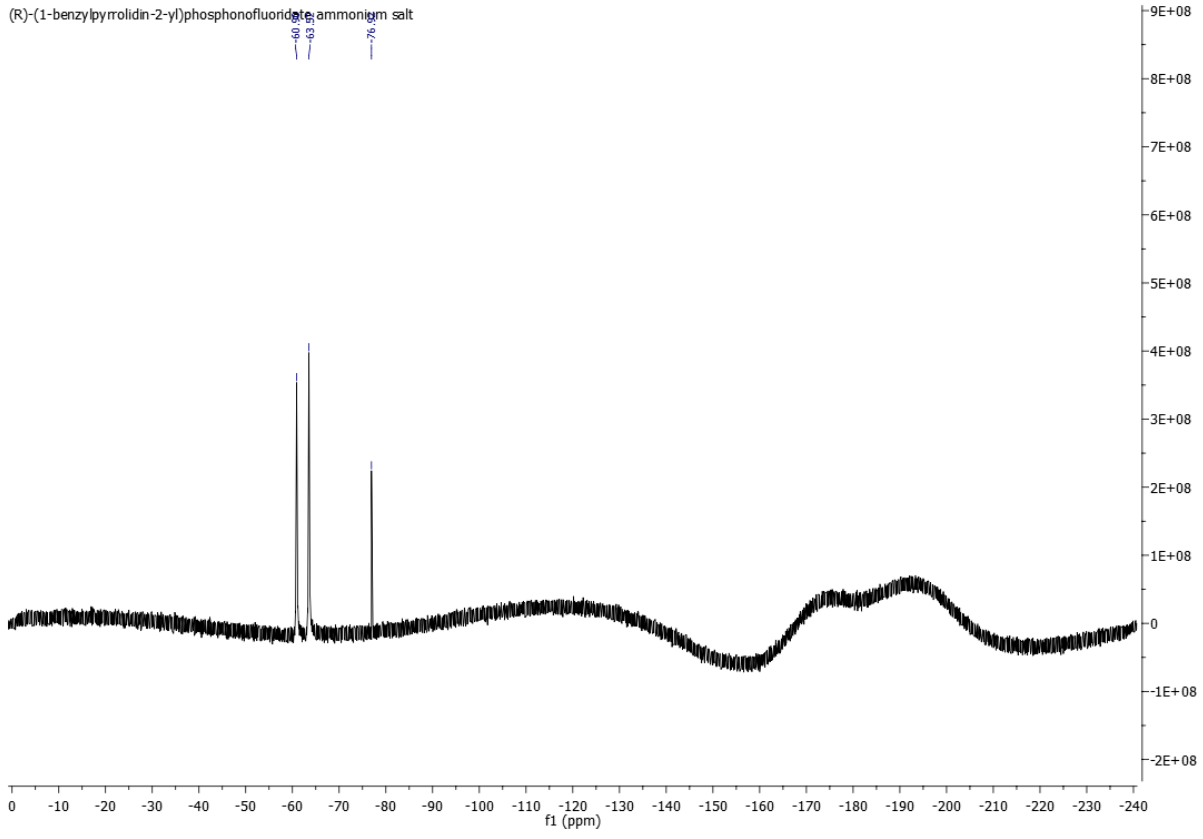
(R)-(1-benzylpyrrolidin-2-yl)phosphonofluoridate ammonium salt
f1 (ppm)

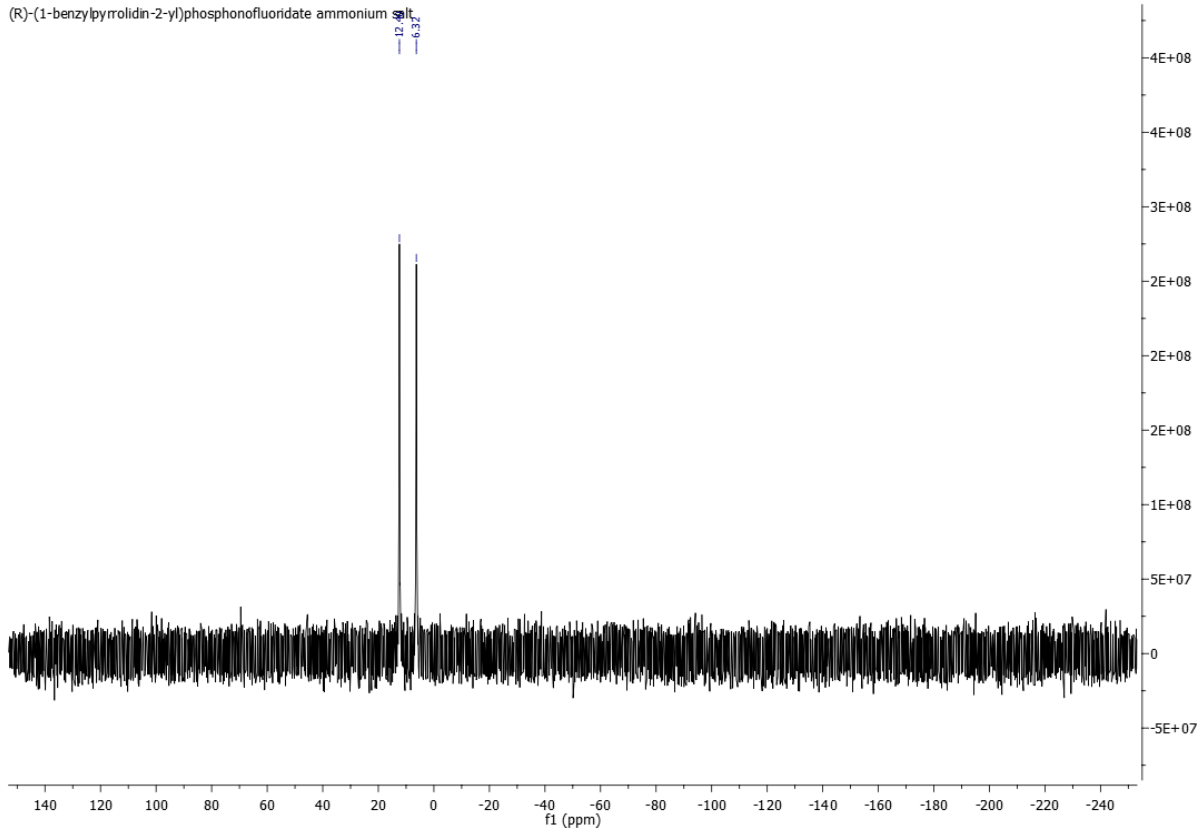

^{1}H, ^{13}C, ^{19}F and ^{31}P NMR of (*R*)-(1-((quinoline-4-carbonyl)glycyl)pyrrolidin-2-yl)phosphonofluoridate ammonium salt (**23**)

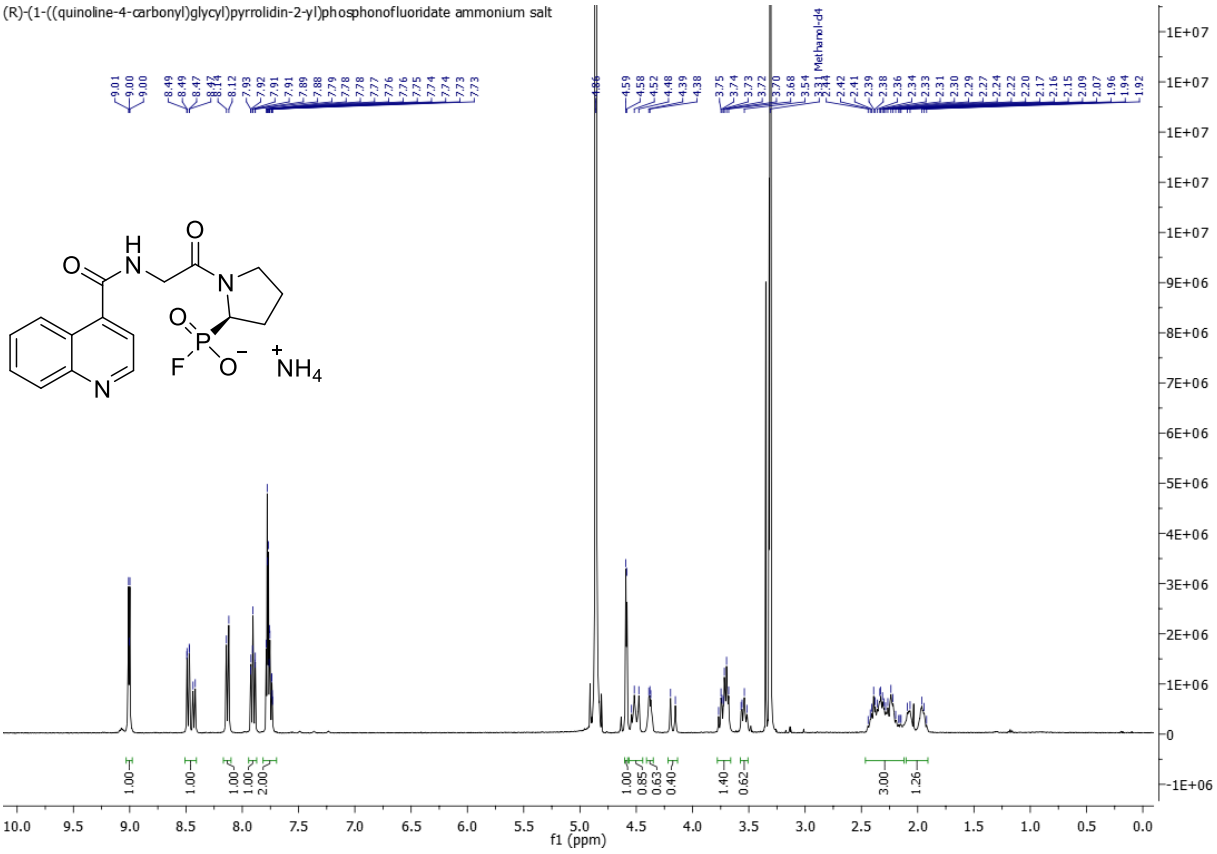

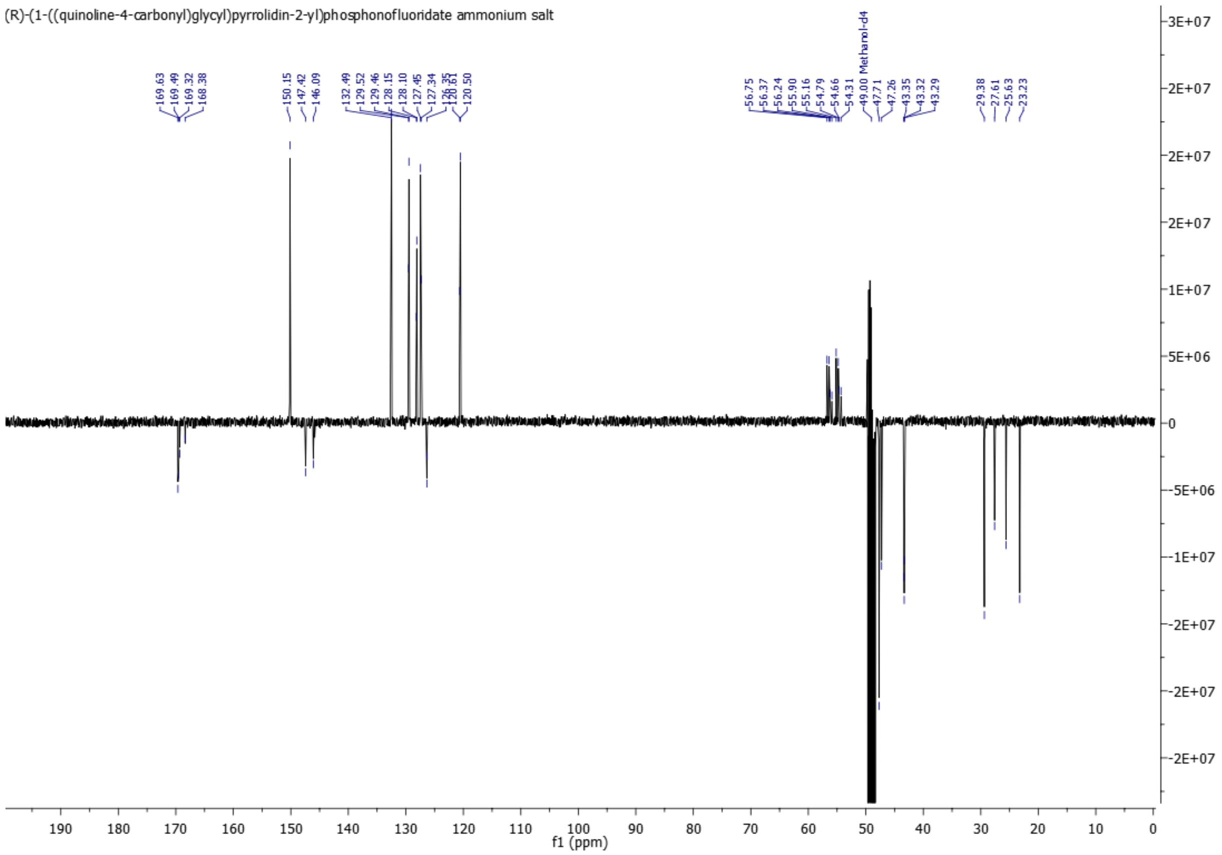
(R)-(1-((quinoline-4-carbonyl)glycyl)pyrrolidin-2-yl)phosphonofluoridate ammonium salt
169.63 169.49 169.32 168.38
150.15 147.42 146.09
132.49 129.52 129.46 128.15 128.10 127.45 127.34 126.35 120.61 120.50
56.75 56.37 56.24 55.90 55.16 54.79 54.66 54.31 49.00 Methanol-d4 47.71 47.26 43.35 43.32 43.29
29.38 27.61 25.63 23.23
f1 (ppm)

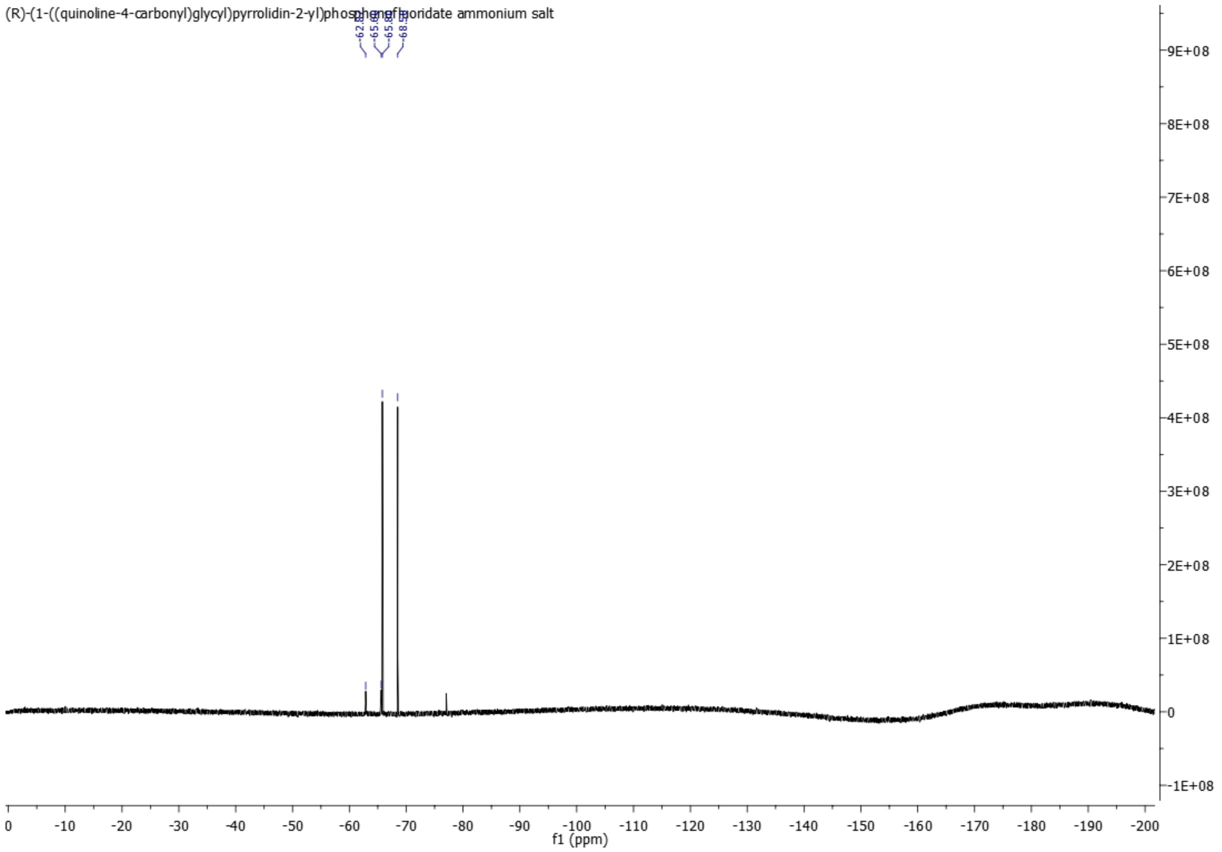
(R)-(1-((quinoline-4-carbonyl)glycyl)pyrrolidin-2-yl)phosphonofluoridate ammonium salt
f1 (ppm)

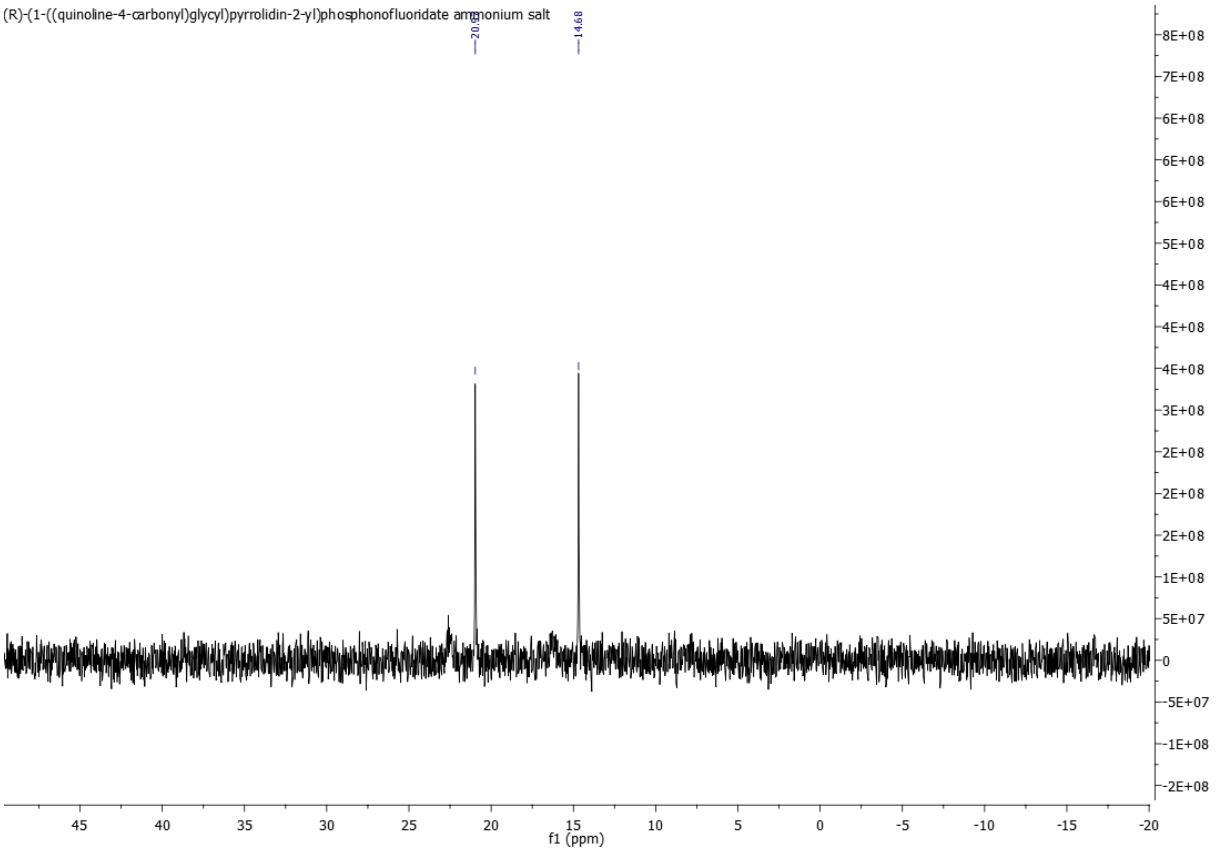
(R)-(1-((quinoline-4-carbonyl)glycyl)pyrrolidin-2-yl)phosphonofluoridate ammonium salt
20.63
14.68
8E+08
7E+08
6E+08
6E+08
6E+08
5E+08
4E+08
4E+08
4E+08
3E+08
2E+08
2E+08
2E+08
1E+08
5E+07
0
-5E+07
-1E+08
-2E+08
45
40
35
30
25
20
15
10
5
0
-5
-10
-15
-20
f1 (ppm)

5.5.3 Determination of enantiomeric excess

5.5.3.1 Determination of the specific rotation angle

The specific rotation angle was calculated for compound (*R*)-**21** and (*S*)-**21**. First, the optical rotation angles were measured with a polarimeter. Before measuring the optical rotation angles, a blank measurement was performed with $CHCl_3$. (*R*)-**21** and (*S*)-**21** were each dissolved at ~1 mg/mL in $CHCl_3$ and injected into the measuring cell of the polarimeter to measure the optical rotation angle and calculate the specific rotation angle (Table 17).

Table 17: Optical rotations of (*R*)-**21** and (*S*)-**21**.

Entry	Compound	Temperature [°C]	N (mg/mL)	Optical rotation	Specific rotation
1	(*R*)-**21**	20.1	0.1728	–0,0087	–5.2
2	(*S*)-**21**	20.1	0.1458	0,0105	7.2

5.5.3.2 Determination of enantiomeric excess via chiral HPLC

To determine the enantiomeric excess, a racemic mixture of 1:1 (*R*)-**21** and (*S*)-**21** was injected onto a Daicel CHIRALPAK AD 10 µm (80 Å) 250×4.6 mm column with a solvent mixture of 10% isopropyl alcohol in *n*-hexane and a flow rate of 1 mL/min. The (*R*)- and (*S*)-enantiomers were then injected separately onto the chiral HPLC column to determine the retention time and enantiomeric purity.

Table 18: Data from the measurement using chiral HPLC for (*R*)-**21** and (*S*)-**21**.

Entry	Compound	Retention time [min]	ee (%)
1	(*R*)-**21**	24.8	>99
2	(*S*)-**21**	30.5	>99

The enantiomeric purity for both enantiomers was ee >99%.

5.5.4 Radiosyntheses

*5.5.4.1 Radiosynthesis of (R)-(1-((quinoline-4-carbonyl)glycyl)pyrrolidin-2-yl)phosphono[^{18}F]fluoridate ([^{18}F]**23**)*

[^{18}F]F$^-$ was eluted from the QMA cartridge with a solution of $Et_4N(HCO_3)$ (1 mg) in MeOH (1 mL). After evaporation of the solvent and addition of diphenyl (*R*)-(1-((quinoline-4-carbonyl)glycyl)pyrrolidin-2-yl)phosphonate (**22**, 0.5 µmol) in MeCN (100 µL), the reaction mixture was stirred for 20 min at 50 °C under argon. The reaction was quenched by adding H_2O (0.5 mL) and an aliquot was taken to determine the RCC by HPLC analysis. The remaining reaction solution was diluted with H_2O (0.8 mL) and the product was isolated by semi-preparative HPLC. The product fraction was diluted with H_2O (20 mL) and fixed on a Sep-Pak® Accell Plus QMA Plus Light cartridge. The cartridge was rinsed with H_2O (3 mL) and dried with air (10 mL) before the product was eluted with isotonic NaCl solution (0.9%, 500 µL) and the RCP determined by TLC or HPLC analysis.

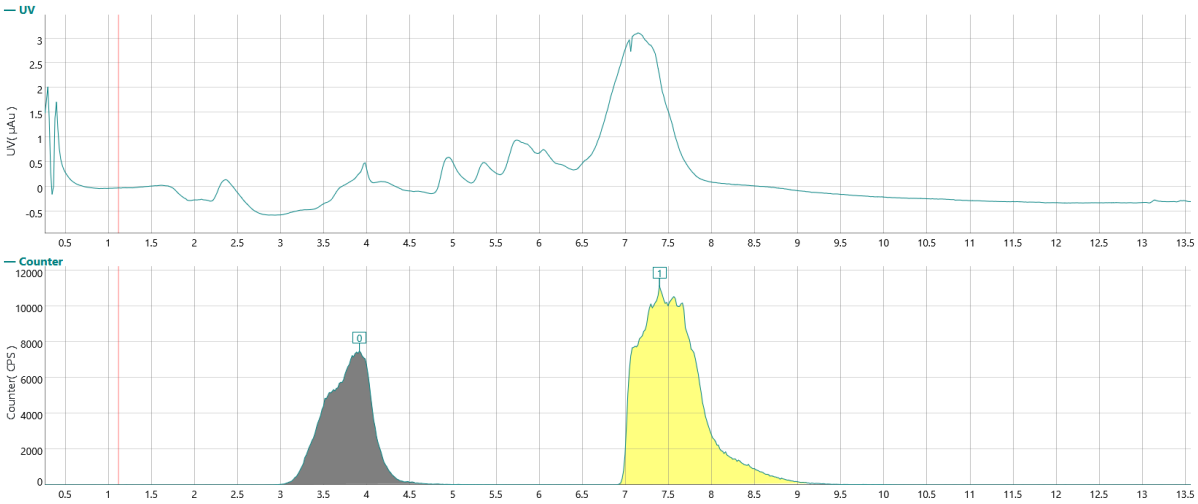

Figure 41: Trace of the isolation of [^{18}F]**23**. (Top: UV chromatogram at 254 nm; bottom: radio chromatogram). Column: Phenomenex Synergi 10 µm Hydro-RP 80 Å, LC column 250×10 mm; eluent: 7% MeCN. Flow rate: 4.5 mL/min.

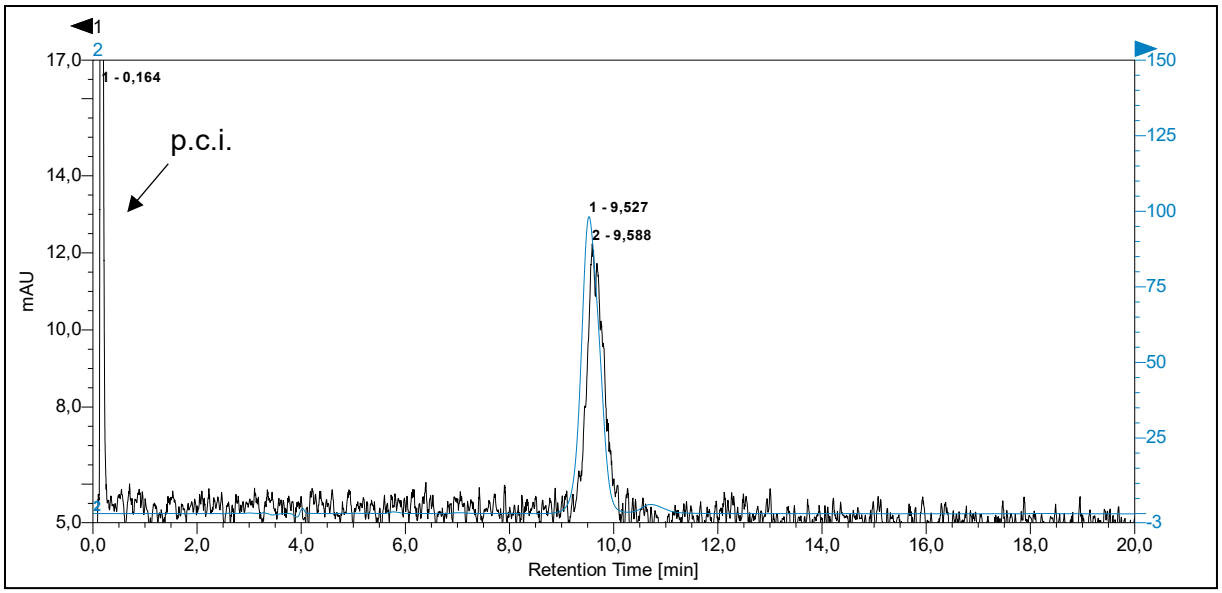

Figure 42: HPLC trace of [^{18}F]**23** co-injected with the non-radioactive reference compound **23** (Black: radio chromatogram; blue: UV chromatogram at 254 nm). Column: MultoKrom® 100-5 C18 AQ LC column 250×4.6 mm; eluent: 7% MeCN (0.1% TFA). Flow rate: 1 mL/min. Abbreviation: p.c.i. − post-column injection.

The calibration curve for calculating the molar activity of [^{18}F]**23** was measured at 254 nm.

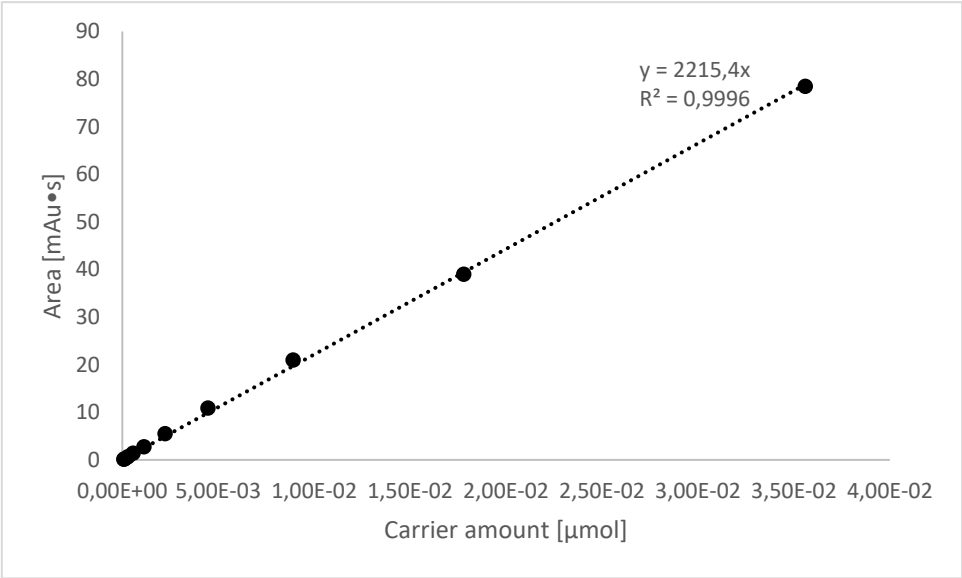

Figure 43: Calibration curve for calculating the molar activity of [^{18}F]**23**.

Table 19: Data for generating the calibration curve for determining the molar activity of [^{18}F]**23**.

Entry	mg/mL	mg/20 µL	g/20 µL	mol (g/365,3 g/mol)	µmol	Area
1	0.65	1.30E-02	1.30E-05	3.56E-08	3.56E-02	78.536
2	0.325	6.50E-03	6.50E-06	1.78E-08	1.78E-02	39.0147
3	0.1625	3.25E-03	3.25E-06	8.90E-09	8.90E-03	21.0012

Entry	mg/mL	mg/20 µL	g/20 µL	mol (g/365,3 g/mol)	µmol	Area
4	0.08125	1.63E-03	1.63E-06	4.45E-09	4.45E-03	10.8961
5	0.040625	8.13E-04	8.13E-07	2.22E-09	2.22E-03	5.5247
6	0.0203125	4.06E-04	4.06E-07	1.11E-09	1.11E-03	2.8139
7	0.01015625	2.03E-04	2.03E-07	5.56E-10	5.56E-04	1.4403
8	0.00507813	1.02E-04	1.02E-07	2.78E-10	2.78E-04	0.7076
9	0.00253906	5.08E-05	5.08E-08	1.39E-10	1.39E-04	0.326
10	0.00126953	2.54E-05	2.54E-08	6.95E-11	6.95E-05	0.188

*5.5.4.2 Radiosynthesis of (R)-(1-benzylpyrrolidin-2-yl)phosphono[^{18}F]fluoridate ([^{18}F]**25**)*

[^{18}F]F^- was eluted from the QMA cartridge with a solution of $Et_4N(HCO_3)$ (1 mg) in MeOH (1 mL). After evaporation of the solvent and addition of diphenyl (*R*)-(1-benzylpyrrolidin-2-yl)phosphonate (**24**, 0.5 µmol) in MeCN (100 µL), the reaction mixture was stirred for 15 min at 60 °C under argon. The reaction was quenched by addition of H_2O (0.5 µL) and an aliquot was taken to determine the RCC by HPLC analysis. The remaining reaction solution was diluted with H_2O (0.8 µL) and the product was isolated by semi-preparative HPLC. The product fraction was used for further experiments without further isolation, and an aliquot was taken to determine the RCP by HPLC analysis.

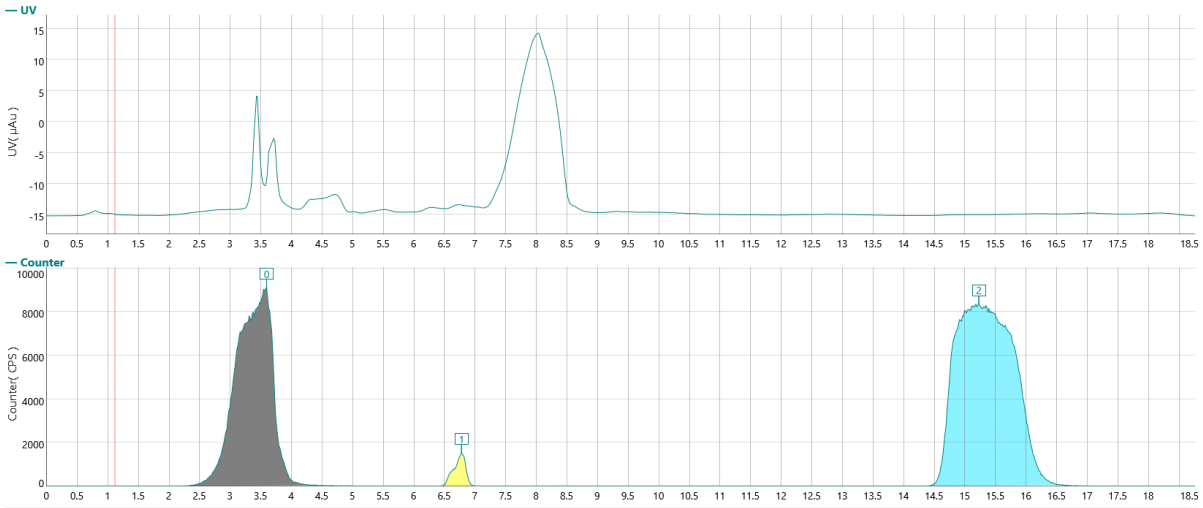

Figure 44: HPLC trace of the isolation of [^{18}F]**25**. (Top: UV chromatogram at 254 nm; bottom: radio chromatogram). Column: Phenomenex Synergi 10 µm Hydro-RP 80 Å, LC column 250×10 mm; eluent: 7% MeCN. Flow rate: 4.5 mL/min.

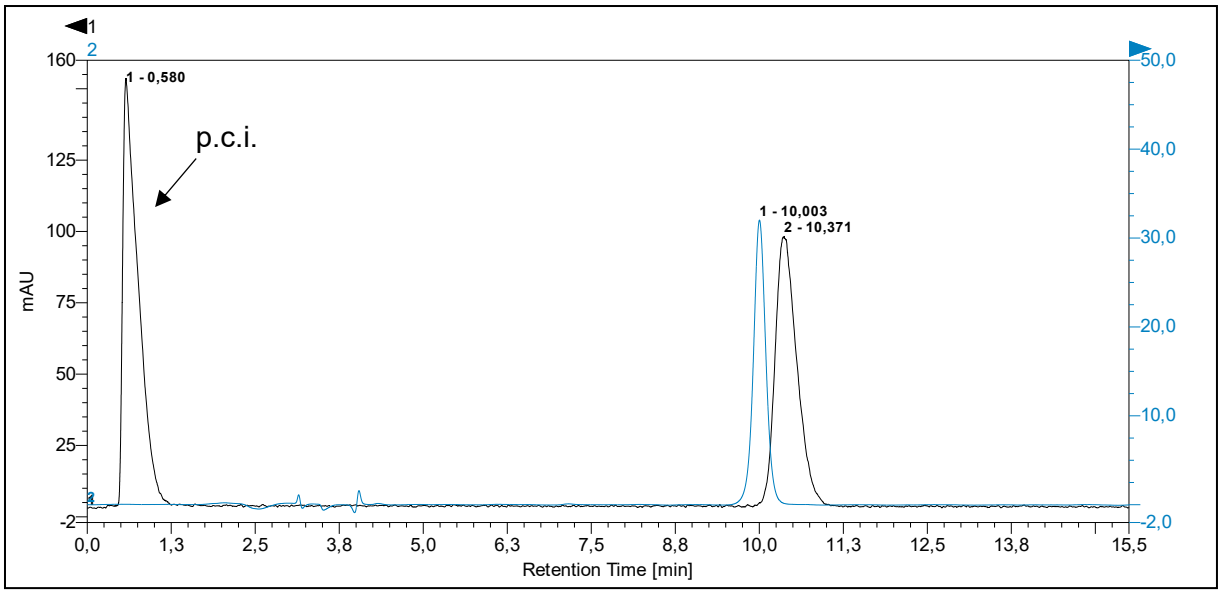

Figure 45: HPLC trace of [^{18}F]**25** co-injected with the non-radioactive reference compound **25** (black: radio chromatogram; blue: UV chromatogram at 254 nm). Column: MultoKrom® 100-5 C18 AQ LC column 250×4.6 mm; eluent: 10% MeCN (0.1% TFA). Flow rate: 1 mL/min. Abbreviation: p.c.i. – post-column injection.

The calibration curve for calculating the molar activity of [^{18}F]**25** was measured at 254 nm.

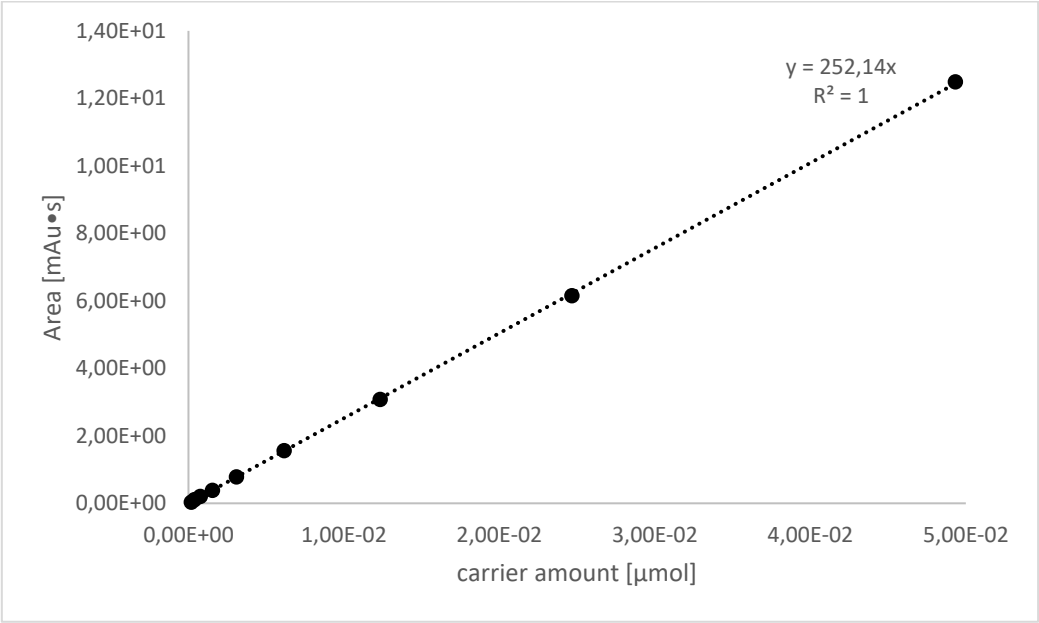

Figure 46: Calibration curve for calculating the molar activity of [^{18}F]**25**.

Table 20: Data for generating the calibration curve for determining the molar activity of [^{18}F]**25**.

Entry	mg/mL	mg/20 µL	g/20 µL	mol (g/243,2 g/mol)	µmol	Area
1	0.6	1.20E-02	1.20E-05	4.93E-08	4.93E-02	1.25E+01
2	0.3	6.00E-03	6.00E-06	2.47E-08	2.47E-02	6.15E+00
3	0.15	3.00E-03	3.00E-06	1.23E-08	1.23E-02	3.08E+00
4	0.075	1.50E-03	1.50E-06	6.17E-09	6.17E-03	1.56E+00
5	0.0375	7.50E-04	7.50E-07	3.08E-09	3.08E-03	7.75E-01
6	0.01875	3.75E-04	3.75E-07	1.54E-09	1.54E-03	3.75E-01
7	0.009375	1.88E-04	1.88E-07	7.71E-10	7.71E-04	2.00E-01
8	0.0046875	9.38E-05	9.38E-08	3.85E-10	3.85E-04	1.04E-01
9	0.00234375	4.69E-05	4.69E-08	1.93E-10	1.93E-04	3.20E-02

5.5.5 Stability studies in aqueous media

[^{18}F]**23** was synthesized and purified by semi preparative HPLC. To investigate its stability, 20 µL of the HPLC fraction (~1 MBq) were added to 980 µL of the test medium. Exceptions were made for the investigation of [^{18}F]**23** in FAP-buffer (50 mM TRIS buffer (pH 7.5, 1 M NaCl, 0.1% BSA) and in phosphate buffer (pH 4) with subsequent heating to 100 °C. In these cases, [^{18}F]**23** was formulated in isotonic saline and 5 µL or 2 µL of the resulting tracer solution were added to 995 µL FAP-buffer or 998 µL phosphate buffer, respectively. For the FAP-buffer, 750 µL of the solution thus obtained were further diluted with 250 µL buffer. For the analysis, 1 µL aliquots of each sample were spotted in triplicate on NP-TLC plates. The TLC plates were developed with a mobile phase of 7% MeCN in H_2O +0.1% TFA or 70% MeOH in CH_2Cl_2 in case of FAP-buffer. If the non-radioactive reference compound **23** was also spotted, it was detected under UV light after development of the TLC and marked with a diluted activity solution, as well as the baseline and frontline. The TLC was developed with a phosphor imager, the spots were integrated, the background was subtracted and [^{18}F]**23** was identified by comparison with **23**.

[^{18}F]**25** was synthesized and purified by semi preparative HPLC. To determine the stability in H_2O and PBS, 40 µL of the HPLC fraction were added to 960 µL of test medium. For the FAP-buffer, 50 µL of the HPLC fraction were dissolved in 950 µL of the FAP-buffer, and 363 µL of this was diluted in 637 µL of the buffer. Furthermore, the first aliquot was taken after 10 minutes of incubation for the determination of the stability in FAP-buffer and was subsequently analyzed. The NP-TLC for determining stability in H_2O and PBS was developed in a mobile phase of 50% MeOH in CH_2Cl_2, for the FAP-buffer, the RP-TLC was developed in 30% MeCN in H_2O.

5.5.6 Stability studies in human blood plasma for [^{18}F]**23**

1 mL of human blood plasma was placed in a 2 mL vial and pre-warmed to 37 °C in a thermoshaker for five min before 1 µL of the tracer formulated in isotonic saline was added. After 5, 15, 30, and 60 min, 80 µL aliquots were removed and 60 µL of these aliquots were added to 120 µL of MeCN to precipitate plasma proteins. The mixture was vortexed for 2 min and then centrifuged for 2 min. 2.5 µL of the supernatant and the non-radioactive reference compound were spotted onto a TLC plate in triplicate. The radio-NP-TLC was developed in a solvent mixture of 70% MeOH in CH_2Cl_2. The reference compound was detected under UV light and marked together with the baseline and frontline with a diluted aqueous [^{18}F]F^- solution. The radio-TLC was visualized with a phosphor imager, the spots were integrated, the background was subtracted, and the radiolabeled product was identified by comparison with the reference compound.

5.5.7 Evaluation in FAP experiments

General procedure A (**GP A**) for carrying out enzyme experiments

All enzyme experiments were performed with either 0.2 µg (10-fold enzyme excess) or 0.4 µg (20-fold enzyme excess) FAP [Recombinant Human FAP His-tag (Mammalian) Protein, CF, *Bio-Techne GmbH,* Wiesbaden, Germany]. 10 kBq of [^{18}F]**23** or [^{18}F]**25** were used in 50 µL of FAP-buffer (50 mM TRIS buffer [pH 7.5, 1 M NaCl, 0.1% BSA]) and a total reaction volume of 500 µL. The enzyme was inhibited with UAMC-1110 or the non-radioactive reference compound **23** (for [^{18}F]**23**) at a concentration of 1 µM. The samples were either incubated for 1 h at 21 °C with 550 rpm on a thermoshaker or at ambient temperature without shaking. To determine the reaction kinetics, aliquots were taken and analyzed at the corresponding time points. In addition to the enzyme experiments, samples containing only the tracer in buffer were also prepared to determine the baseline amount of [^{18}F]F^- in the tracer solutions.
If [^{18}F]F^- release was determined with hydroxyapatite, the samples were vortexed for 2 min and then centrifuged for 10 min at 20817 rfc and 4 °C. The supernatant was pipetted into an empty Eppendorf tube (wash solution) and 500 µL of H_2O was added. The samples were vortexed for 2 min and centrifuged for 5 min at 4 °C before the supernatant added to the wash solution. The process was repeated with another 500 µl of H_2O and centrifuged again for 10 min at 4 °C. After final removal of the supernatant, the samples were measured individually in a gamma counter (Hidex AMG Automatic Gamma Counter (*Hidex Deutschland Vertrieb GmbH*, Mainz, Germany). Samples for determining the background consisted of 500 µL FAP-buffer.

If [^{18}F]F^- release was determined by radio-TLC, radio-NP-TLC was developed for [^{18}F]**23** with a solvent mixture of 70% MeOH in CH_2Cl_2 and radio-RP-TLC was developed for [^{18}F]**25** with a solvent mixture of 30% MeCN in H_2O. 2.5 µL of the aliquots were spotted onto the radio-TLC plates. The radio-TLC was visualized with a phosphor imager, the spots were integrated, and the background was subtracted. The released [^{18}F]F^- was quantified using 2D densitometry, whereby the activity spots were marked on the TLC plate and the background was subtracted by marking an empty field of the TLC plate.

Preliminary tests to determine the amount of hydroxyapatite (HA) required

Four series of measurements were carried out with solutions of 5, 10, and 20 kBq ([^{18}F]F^- or [^{18}F]**23**) each in 500 µL H_2O. In two series of measurements, 50 mg of HA were used per sample and in the other two series of measurements, 25 mg HA were used per sample.
For this purpose, 50 mg (measurement series 1) or 25 mg (measurement series 2) HA were weighed into each of six Eppendorf tubes. For each series of measurements, 5, 10 and 20 kBq [^{18}F]F^- or [^{18}F]**23** were pipetted in three Eppendorf tubes and made up to a volume of 500 µL with H_2O. The work-up was according to **GP A**.

FAP enzyme experiments with [^{18}F]**23** and hydroxyapatite in the reaction solution

The enzyme experiments were performed according to **GP A** as preliminary tests. 0.2 µg FAP were used, and the samples were shaken for one hour at 21 °C and 550 rpm on a thermoshaker. 25 mg of HA were used per sample. In the second experiment, the enzyme was pre-incubated with UAMC-1110 for 20 min.

Table 21: Pipetting protocols for the two preliminary experiments with HA in the reaction solution and observed [^{18}F]F^- release.

Entry	FAP [µL]	[^{18}F]23 [µL] (A_M [GBq/µmol])	UAMC-1110 [µL]	FAP-buffer [µL]	HA [mg]	Released [^{18}F]F^- [%]
Preliminary test - Reaction of FAP with [^{18}F]23 (n=1)						
1	-		-	450	-	-
2	-	50 (39)	-	450	25	-
3	50		-	400	25	3.3
Preliminary test - Reaction of FAP and [^{18}F]23 and inhibition with UAMC-1110 (n=3)						
1	-		-	450	-	-
2	-	50 (47)	-	450	25	-
3	50		-	400	25	3.4 ± 0.3

4	50		1	400	25	0.4	± 0.4

Preliminary test to determine the enzyme kinetics with [^{18}F]**23**

To determine the enzyme kinetics, 1 µg FAP was added to 400 µL buffer in an Eppendorf tube (n=1). After addition of 50 kBq [^{18}F]**23** in 50 µL buffer, the reaction solution was shaken at 21 °C and 550 rpm. After 5, 10, 30 and 60 min, 100 µL aliquots were removed and added to a second Eppendorf tube containing 25 mg HA and 400 µL buffer. The work-up was carried out analogously to **GP A**.

Table 22: Released [^{18}F]F$^-$ by the reaction of [^{18}F]**23** with FAP (n=1).

Entry	Time [min]	Released [^{18}F]F$^-$ [%]
1	5	2.7
2	10	3.1
3	30	9.9
4	60	16.1

Enzyme concentration and self-inhibition of the reaction of [^{18}F]**23** with FAP

The enzyme experiments were performed according to **GP A**. 0.4 µg FAP were used for the self-inhibition experiment due to a new enzyme batch, and the samples were incubated at ambient temperature. For the enzyme concentration series, 0.2, 0.4 and 0.8 µg of FAP were used. After incubation for 1 h, 450 µL aliquots were removed and added to another Eppendorf vial containing 50 µL buffer and 25 mg HA. The reference samples were treated in the same manner.

Table 23: Pipetting protocols and observed [^{18}F]F$^-$ release.

Entry	FAP [µL] (m [µg])	[^{18}F]23 [µL] (A_M [GBq/µmol])	23 [µL]	FAP-buffer [µL]	Released [^{18}F]F$^-$ [%]
Enzyme concentration experiment (n=3)					
1	-		-	450	-
2	-		-	450	-
3	10 (0.20)	50 (30)	-	440	4.4 ± 0.3
4	20 (0.40)		-	430	9 ± 0.4
5	40 (0.80)		-	410	17 ± 0.1

Entry	FAP [µL] (m [µg])	[^{18}F]23 [µL] (A_M [GBq/µmol])	23 [µL]	FAP-buffer [µL]	Released [^{18}F]F^- [%]
Self-inhibition (n=3)					
1	-		-	451	-
3	40	49 (43)	-	411	11 ± 0.5
4	40		1	410	0.8 ± 0.1

Enzyme kinetics and inhibition with UAMC-1110 over 2 h of the reaction of [^{18}F]**23** with FAP

The enzyme experiments were performed according to **GP A**. 0.4 µg FAP were used, and the samples were incubated at ambient temperature for 2 h. After 10, 30, 60, 90 and 120 min, 2.5 µL aliquots were removed and spotted onto a NP-TLC-plate.

Table 24: Pipetting protocols and observed [^{18}F]F^- release.

Entry	FAP [µL]	[^{18}F]23 [µL] (A_M [GBq/µmol])	UAMC-1110 [µL]	FAP-buffer [µL]
Enzyme kinetic and inhibition with UAMC-1110 (n=3)				
1	-		-	450
2	40	50 (80)	-	410
3	40		1	409

Entry	Time [min]	Rel. released [^{18}F]F^- [%] without UAMC-1110	Rel. released [^{18}F]F^- [%] without UAMC-1110
1	10	1.7 ± 0.1	0 ± 0.1
2	30	4.5 ± 0.1	0.9 ± 0.1
3	60	8.5 ± 0.2	1.5 ± 0.3
4	90	11 ± 0.2	1.4 ± 0.1
5	120	15 ± 0.1	1.2 ± 0.1

Enzyme experiments of [^{18}F]**23** with FAP-related peptidases

The enzyme experiments were performed according to **GP A**. In relation to the amount of FAP, all peptidases (PREP [Recombinant Human Prolyl Oligopeptidase/PREP Protein, CF], DPP 2 [Recombinant Human DPPII/QPP/DPP7 Protein, CF], DPP 4 [Recombinant Human DPPIV/CD26 Fc Chimera Protein, CF] and DPP 9 [Recombinant Human DPP9 Protein, CF], all from *Bio-Techne GmbH,* Wiesbaden, Germany) were used in the same amount of substance. For each enzyme, the buffer and substrate specified by the manufacturer were

used. The substrate was used for determination of the enzyme activity. In addition, enzyme-specific inhibitors were used for inhibition. In deviation from **GP A**, the experiment with PREP was inhibited with UAMC-1110 at a concentration of 10 µM and the four other peptidases were inhibited with inhibitors at a concentration of 0.1 µM. The reactions were incubated at ambient temperature for 90 min before 2.5 µL aliquots were removed and spotted onto a radio-TLC plate in triplicate.

Table 25: Overview of the enzyme-specific buffer systems, inhibitors and substrates used.

Entry	Enzyme	Buffer	Inhibitor	Substrate
1	FAP	50 mM Tris, 1 M NaCl, 0.1% BSA (pH 7.5)	UAMC-1110	*Z*-Gly-Pro-AMC
2	PREP	25 mM Tris, 250 mM NaCl, 2.5 mM DTT (pH 7.5)	UAMC-1110	*Z*-Gly-Pro-AMC
3	DPP 2	25 mM MES (pH 6.0)	Puromycin Aminonucleoside	Lys-Pro-AMC
4	DPP 4	25 mM Tris (pH 8.0)	Anagliptin	GP-AMC
5	DPP 9	25 mM Tris (pH 8.0)	Anagliptin	GP-AMC

To determine the [^{18}F]F^- content of the tracer solution, 50 µL (10 kBq) of [^{18}F]**23** was added to 450 µL of buffer for each buffer system.

Table 26: Pipetting protocols for each enzyme experiment.

Entry	Component [µL]	FAP		PREP		DPP 2		DPP 4		DPP 9	
		–	+	–	+	–	+	–	+	–	+
1	Buffer	430	429	431	430.2	437	436	424	423	247	426
2	Enzyme	20	20	18.8	18.8	12.4	12.4	26	26	23	23
3	Inhibitor	-	1	-	1	-	1	-	1	-	1
4	[^{18}F]**23** (101 GBq/µmol)	50	50	50	50	50	50	50	50	50	50

–: without inhibitor, +: with inhibitor

FAP enzyme experiment with [^{18}F]**25**

The enzyme experiments were performed according to **GP A**. 0.4 µg FAP was used, and the samples were incubated at ambient temperature. After incubation for 1 h, 2.5 µL aliquots were removed and spotted in triplicate onto a radio-NP-TLC plate. In addition, 450 µL aliquots were removed and added to another Eppendorf vial containing 50 µL buffer and 25 mg HA. The reference samples were treated in the same manner. FAP was inhibited with a 10 µM UAMC-1110 solution.

Entry	FAP [µL]	[^{18}F]25 [µL] (A_M [GBq/µmol])	UAMC-1110 [µL]	FAP-buffer [µL]	Released [^{18}F]F^- [%]
1	-		-	450	-
2	20	50 (18)	-	430	0.1
3	20		1	429	0.1

5.5.7 Radio-TLC

(R)-(1-((quinoline-4-carbonyl)glycyl)pyrrolidin-2-yl)phosphono[^{18}F]fluoridate ([^{18}F]**23**)

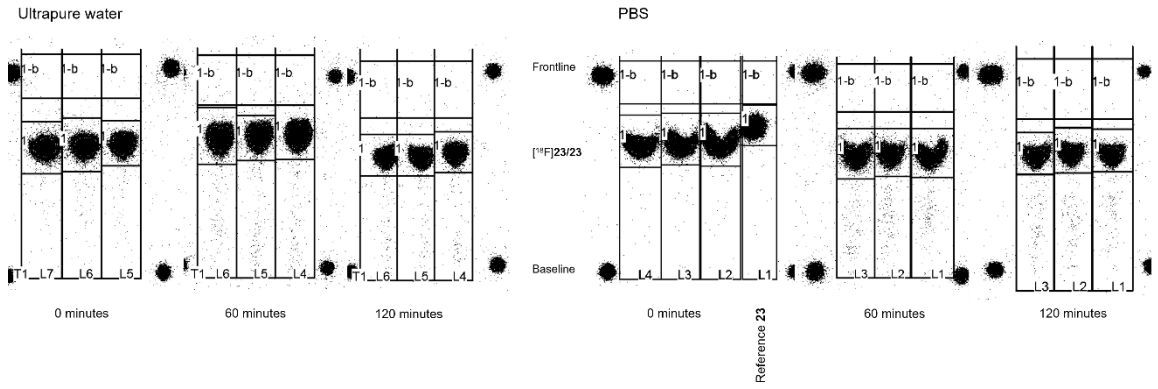

Figure 47: NP-Radio-TLCs of stability tests in H_2O (left) and PBS (right).

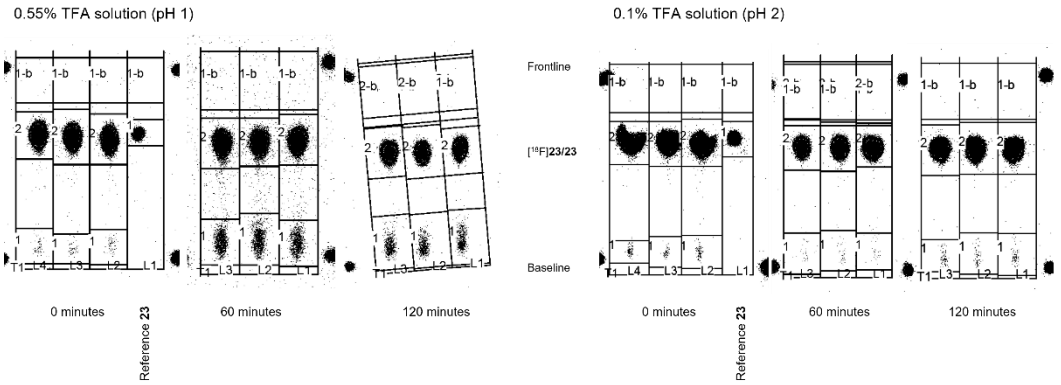

Figure 48: NP-Radio-TLCs of stability tests at pH 1 (left) and pH 2 (right).

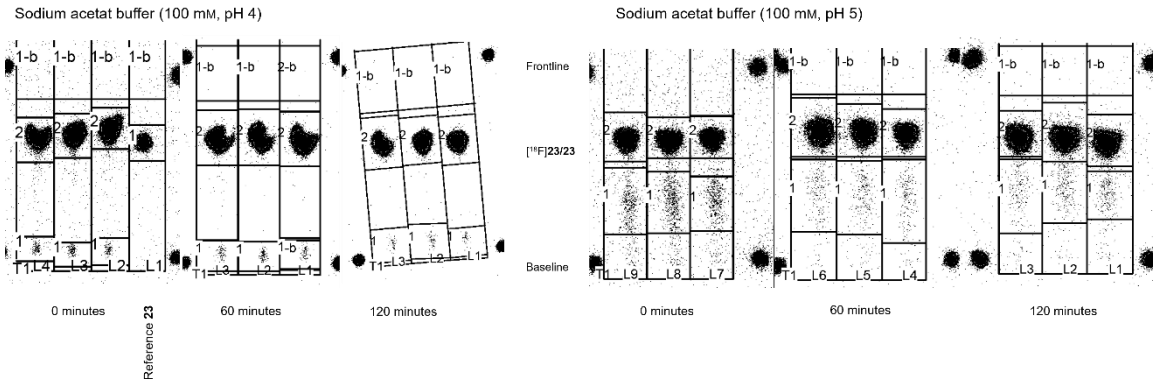

Figure 49: NP-Radio-TLCs of stability tests at pH 4 (left) and pH 5 (right).

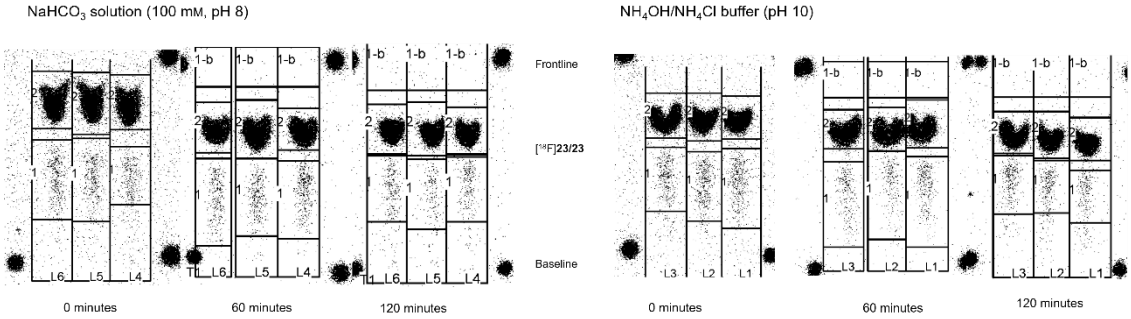

Figure 50: NP-Radio-TLCs of stability tests at pH 8 (left) and pH 10 (right).

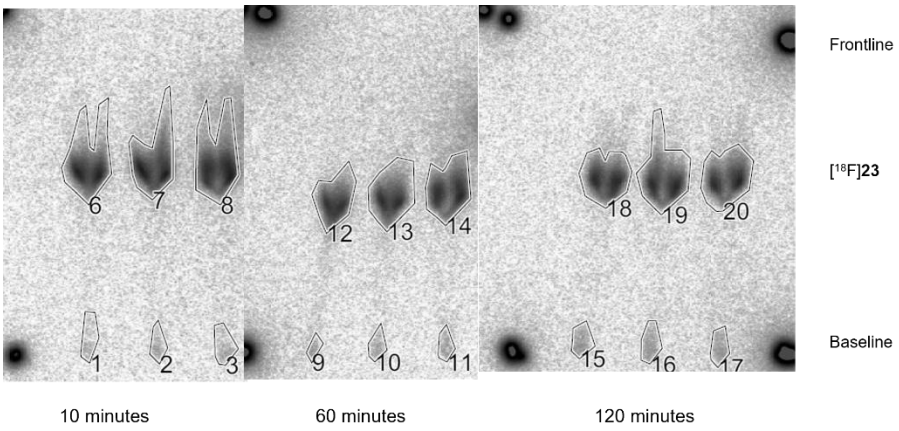

Figure 51: NP-Radio-TLCs of stability tests in FAP-buffer.

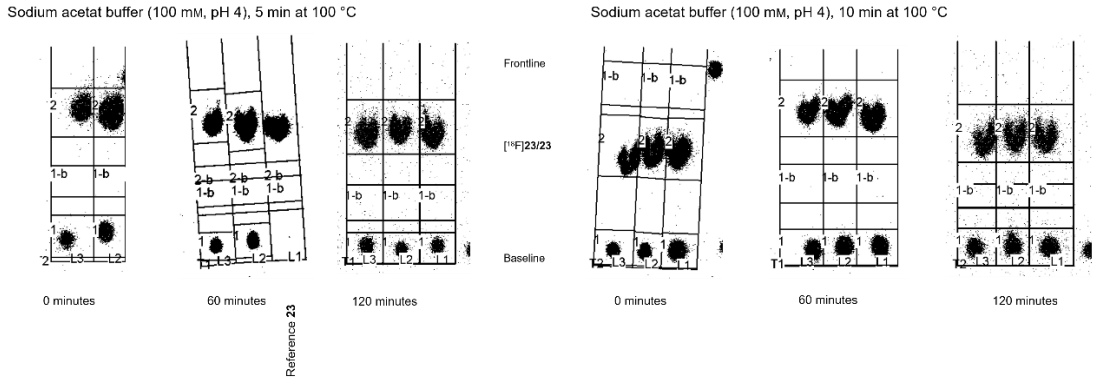

Figure 52: NP-Radio-TLCs of stability tests at pH 4, 5 minutes heating at 100 °C (left) and 10 minutes heating at 100 °C (right).

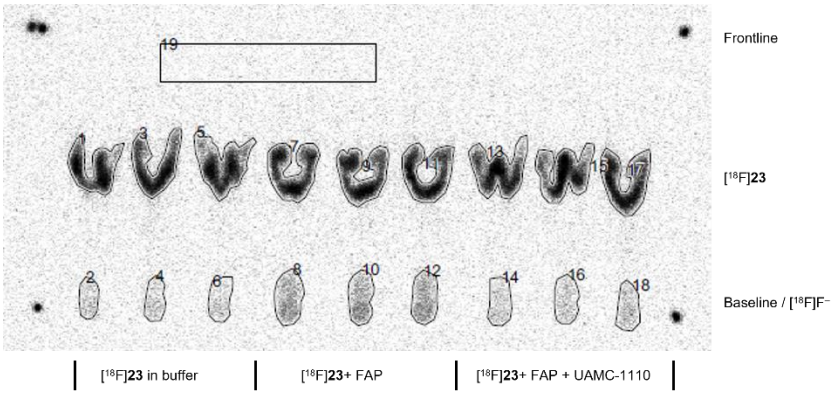

Figure 53: Radio-TLC from a FAP enzyme experiment.

(*R*)-(1-benzylpyrrolidin-2-yl)phosphono[^{18}F]fluoridate ([^{18}F]**25**)

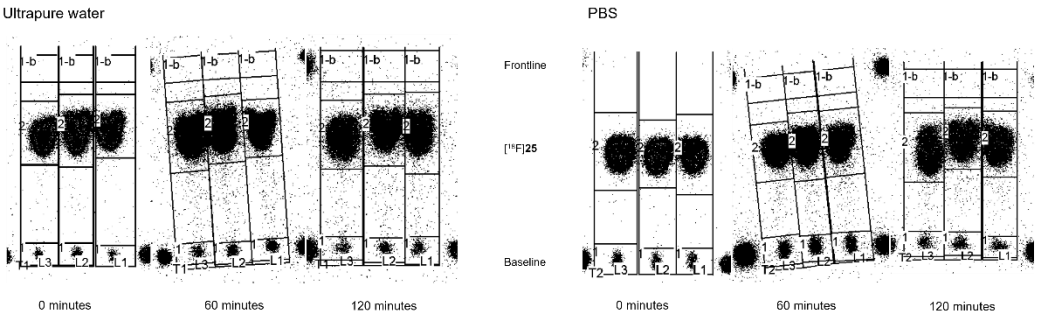

Figure 54: NP-Radio-TLCs of stability tests in H_2O (left) and PBS (right).

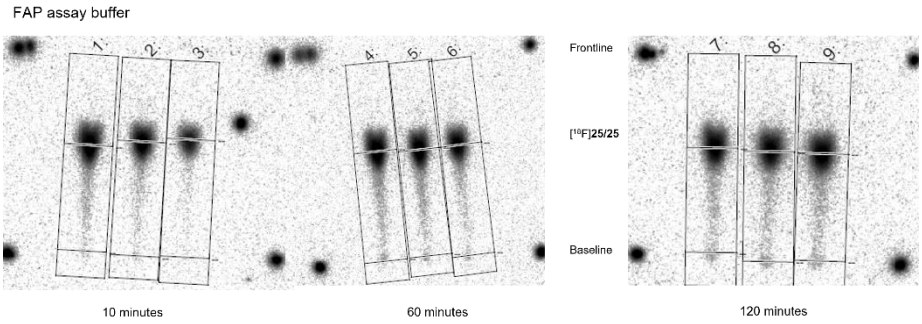

Figure 55: NP-Radio-TLCs of stability tests in FAP-buffer.

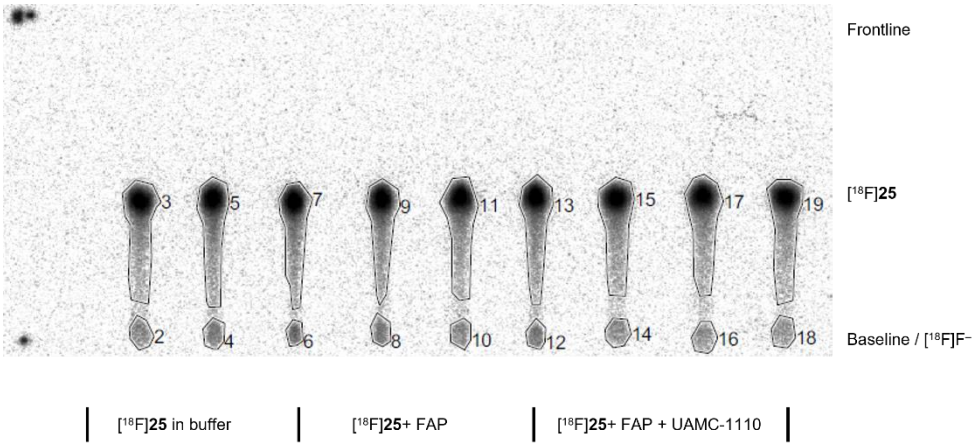

Figure 56: Radio-TLC from a FAP enzyme experiment.

5.6 Supporting Information to chapter 3.4

5.6.1 Organic preparative syntheses

(*S*)-*N*-(2-(2-(Hydroxymethyl)pyrrolidin-1-yl)-2-oxoethyl)quinoline-4-carboxamide (**31**)

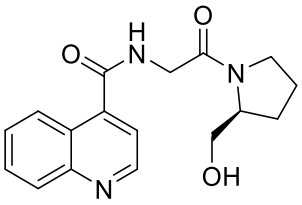

31

$C_{17}H_{19}N_3O_3$
[313.14]

2,6-Lutidine (264 µL, 2.3 mmol, 2 eq) was added to a solution of L-prolinol (246 mg, 2.4 mmol, 2.1 eq) in dry DMF (0.2 M), and the reaction mixture was stirred for 10 min at ambient temperature. 2,3,5,6-Tetrafluorophenyl (quinoline-4-carbonyl)glycinate (**17**, 1 eq) was then added, the reaction mixture was stirred overnight at 55 °C, cooled and poured into 110 mL ice H_2O. The aqueous phase was extracted three times with CH_2Cl_2 (55 mL). The combined organic fractions were washed three times with H_2O (55 mL) and once with saturated NaCl solution (30 mL). The organic phase was dried with Na_2SO_4, and the crude product was adsorbed on Celite®. After purification by column chromatography (CH_2Cl_2/MeOH), the product was triturated with diethyl ether. After stirring in ether, 162 mg (0.52 mmol, 45%) of a white solid were obtained.

R_f (CH_2Cl_2:MeOH = 96:4) = 0.25.
Mp: 134.5 °C.
^{1}H NMR (400 MHz, MeOD) δ = 8.94 (dd, *J* = 4.4, 2.0 Hz, 1H), 8.40 (dd, *J* = 8.5, 0.7 Hz, 1H), 8.10 (d, *J* = 8.5 Hz, 1H), 7.88 – 7.78 (m, 1H), 7.74 – 7.64 (m, 2H), 4.44 (q, *J* = 16.5 Hz, 0.6H), 4.37 – 4.12 (m, 2.4H), 3.72 – 3.43 (m, 4H), 2.20 – 1.89 (m, 4H).
^{13}C NMR (101 MHz, MeOD) δ = 170.08, 169.23, 150.97, 149.15, 144.11, 131.53, 129.58, 128.88, 127.00, 126.03, 120.36 (d, *J* = 4.2 Hz), 64.45, 63.23, 61.12, 60.39, 47.85, 47.16, 43.25 (d, *J* = 10.4 Hz), 29.18, 28.07, 25.11, 22.55.
HRMS (**ESI**) calculated for $C_{17}H_{16}N_3O_3$ ($[M+H]^+$): 314.14992; found: 314.14987.

General procedure 5 (**GP 5**)[171]

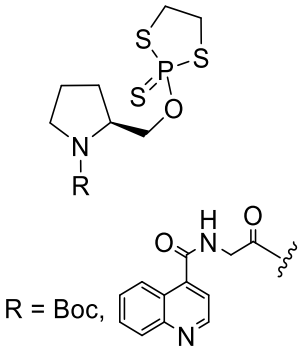

A solution of ethane-1,2-dithiol (1.1 eq) and triethylamine (2.07 eq) in dry benzene (0.63 M) was added dropwise to a pre-cooled (0 °C) solution of diethylphosphoramidous dichloride in benzene (0.13 M), and the reaction mixture was stirred for 30 min at 0 °C. The reaction mixture was allowed to warm to ambient temperature over 2 h. The resulting solid was filtered off under inert conditions and the solvent was removed under reduced pressure under inert conditions. The residue was dissolved in dry CH_2Cl_2 (0.5 M) and a solution of 5-(ethylthio)-1*H*-tetrazole (1.05 eq) and the corresponding alcohol (1.05 eq) in dry CH_2Cl_2 (0.14 M) was added dropwise. The reaction mixture was stirred for 3 h at ambient temperature before elemental sulfur (3 eq) was added and the reaction mixture stirred overnight at ambient temperature. After completion, the solvent was removed under reduced pressure until the remaining sulfur precipitated. The sulfur was filtered off and the solvent was removed under reduced pressure. After purification by column chromatography, the product was triturated with CH_2Cl_2 and diethyl ether.

Table 27: Experimental data for the synthesis of **28** and **30**.

Entry	Alcohol	µL (mmol)			mg (mmol)		Compound	Yield (%)
		Diethylphosphoramidous dichloride	Ethane-1,2-dithiol	Et_3N	5-(Ethylthio)-1*H*-tetrazole	Sulfur		
1	Boc-L-Prolinol	209 (1.44)	132 (1.58)	412 (2.97)	197 (1.51)	139 (4.32)	**28**	35
2	**31**	74 (0.51)	48 (0.57)	148 (1.07)	70 (0.54)	50 (1.55)	**30**	37

tert-Butyl (*S*)-2-(((2-sulfido-1,3,2-dithiaphospholan-2-yl)oxy)methyl)pyrrolidine-1-carboxylate (**28**)[171]

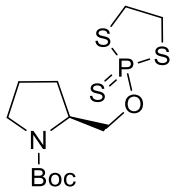

28

$C_{12}H_{22}NO_3PS_3$
[355.47]

The synthesis was carried out according to **GP 5**. After purification by column chromatography (*n*-hexane:EtOAc = 7:3 – 1:1), 177 mg (0.50 mmol, 35%) of a colorless oil were obtained.

R_f (*n*-hexane:EtOAc = 1:1) = 0.71.
^{1}H NMR (400 MHz, $CDCl_3$) δ = 4.09 (dd, *J* = 55.4, 11.1, 9H), 3.79 – 3.49 (m, 4H), 3.35 (dd, *J* = 16.6, 10.0, 2H), 2.06 – 1.70 (m, 4H), 1.47 (s, 3H).
^{13}C NMR (101 MHz, $CDCl_3$) δ = 68.55 – 67.49 (m), 56.41 (d, *J* = 10.3), 46.81, 41.65, 28.67, 24.63 – 23.53 (m), 23.53 – 22.06 (m).
^{31}P NMR (162 MHz, $CDCl_3$) δ = 121.76 (d, *J* = 19.2).
HRMS (**ESI**) calculated for $C_{12}H_{22}NO_3PS_3$ ($[M+H]^+$): 356.05722; found: 356.05746.

Two quaternary carbon atoms are not visible in the ^{13}C NMR.

(*S*)-*N*-(2-Oxo-2-(2-(((2-sulfido-1,3,2-dithiaphospholan-2-yl)oxy)methyl)pyrrolidin-1-yl)ethyl)quinoline-4-carboxamide (**30**)[171]

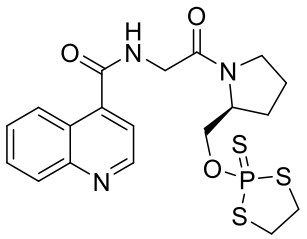

30

$C_{19}H_{22}N_3O_3PS_3$
[467.56]

The synthesis was carried out according to **GP 5**. Deviating from **GP 5**, 7.84 mL/mmol and 1.94 mL/mmol of solvent were used for the first and second reaction step. After double purification by column chromatography (CH_2Cl_2:MeOH = 100:0 – 96:4) and repeated trituration with CH_2Cl_2/diethyl ether, 88 mg (0.19 mmol, 37%) of a white foam were obtained.

R_f (CH_2Cl_2:MeOH = 96:4) = 0.38.
Mp: Shrinkage from 50 °C, melting from 78 °C, decomposition from 150 °C.
^{1}H NMR (400 MHz, $CDCl_3$) δ = 8.97 (d, *J* = 4.3, 1H), 8.30 (dd, *J* = 8.5, 0.7, 1H), 8.15 (d, *J* = 8.0, 1H), 7.76 (ddd, *J* = 8.4, 6.9, 1.4, 1H), 7.62 (ddd, *J* = 8.3, 6.9, 1.3, 1H), 7.53 (dd, *J* = 4.3, 2.7, 1H), 7.15 (s, 1H), 4.46 – 4.23 (m, 4H), 4.18 (td, *J* = 9.6, 3.0, 0.8H), 4.12 – 4.04 (m, 0.2H), 3.75 – 3.44 (m, 6H), 2.25 – 1.96 (m, 4H).
^{13}C NMR (101 MHz, $CDCl_3$) δ = 13C NMR (101 MHz, CDCl3) δ = 167.37, 166.78, 150.00, 148.88, 141.33, 130.12 (d, *J* = 9.5), 127.92, 125.44, 124.59, 118.99, 67.79 (d, *J* = 9.6), 67.02 (d, *J* = 9.7), 57.13 (d, *J* = 9.4), 56.59 (d, *J* = 9.5), 46.47, 46.15, 42.83 (d, *J* = 9.5), 41.95 (d, *J* = 13.8), 41.79 (d, *J* = 8.1), 29.83, 28.63, 27.26, 24.29, 21.75.
^{31}P NMR (162 MHz, $CDCl_3$) δ = 123.09 (d, *J* = 146.5).
HRMS (**ESI**) calculated for $C_{19}H_{22}N_3O_3PS_3$ ($[M+H]^+$): 468.06337; found: 468.06404.

Due to rotamers, more signals are present in the ^{13}C-NMR.

General procedure 6 (**GP 6**)[171]

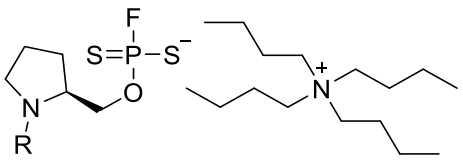

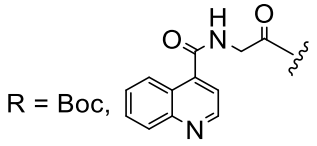

TBAF (1 M in THF) was added to a solution of the corresponding dithiaphospholan in dry THF, and the reaction mixture was stirred overnight at ambient temperature. The solvent was removed under reduced pressure, and the crude product was purified by column chromatography (CH_2Cl_2/MeOH) after filtering off the solid.

Table 28: Experimental data for the synthesis of phosphorofluoridodithioates with TBAF as the fluorination reagent.

Entry	Oxydithiaphospholane 2-sulfide	Oxydithiaphospholane 2-sulfide mg (mmol)	TBAF µL (mmol)	Compound	Yield (%)
1	**28**	25 (0.07)	110 (0.11)	**33**	95
2	**30**	98 (0.21)	420 (0.42)	**34**	65

(*S*)-*O*-((1-(*tert*-Butoxycarbonyl)pyrrolidin-2-yl)methyl) phosphorofluoridodithioate tetrabutylammonium salt (**33**)[171]

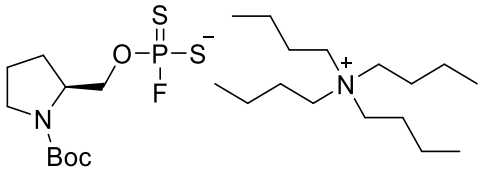

33

$C_{10}H_{18}FNO_3PS_2^-•C_{16}H_{36}N^+$

[556.82]

The synthesis was carried out according to **GP 6**. **28** was dissolved in THF (0.07 M, 1 mL). After purification by column chromatography (CH_2Cl_2:MeOH = 93:7), 37 mg (0.07 mmol, 95%) of a colorless oil were obtained.

R_f (CH_2Cl_2:MeOH = 9:1) = 0.57.

^{1}H NMR (400 MHz, $CDCl_3$) *δ* = 4.24 – 4.04 (m, 1H), 4.03 – 3.76 (m, 2H), 3.37 – 3.22 (m, 9H), 2.13 (s, 1H), 2.03 – 1.71 (m, 4H), 1.70 – 1.59 (m, 8H), 1.49 – 1.36 (m, 17H), 1.03 – 0.93 (m, 12H).

^{13}C NMR (101 MHz, $CDCl_3$) *δ* = 66.15, 58.98, 56.86 (d, *J* = 10.4), 46.84, 46.45, 28.60, 28.40, 23.88 (d, *J* = 67.0), 23.55, 22.70, 19.82, 13.78.

^{19}F NMR (376 MHz, $CDCl_3$) δ = -8.13 (d, *J* = 1101.7).

^{31}P NMR (162 MHz, $CDCl_3$) δ = 119.32 (d, *J* = 1100.4).

HRMS (**ESI**) calculated for $C_{10}H_{18}FNO_3PS_2^-$ ([M-H]$^-$): 314.04552; found: 314.04488.

The two quaternary carbon atoms are not visible in the ^{13}C NMR.

(*S*)-*O*-((1-((Quinoline-4-carbonyl)glycyl)pyrrolidin-2-yl)methyl) phosphorofluoridodithioate tetrabutylammonium salt (**34**)[171]

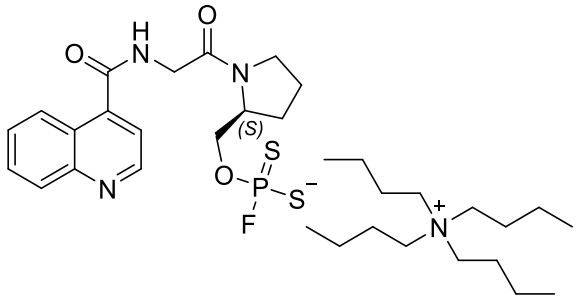

34

$C_{17}H_{18}FN_3O_3PS_2^-•C_{16}H_{36}N^+$

[668.91]

The synthesis was carried out according to **GP 6**. **30** was dissolved in THF (0.10 M, 2.1 mL). After purification by column chromatography (CH_2Cl_2:MeOH = 98:2 – 92:8), 91 mg (0.14 mmol, 65%) of the title compound could be obtained as a slightly yellowish solid.

R_f (CH_2Cl_2:MeOH = 96:4) = 0.47.

^{1}H NMR (400 MHz, MeOD) δ = 8.93 (t, *J* = 4.1, 1H), 8.41 (t, *J* = 8.2, 1H), 8.09 (d, *J* = 8.4, 1H), 7.84 (ddd, *J* = 8.5, 6.9, 1.4, 1H), 7.73 – 7.66 (m, 2H), 4.66 – 4.00 (m, 5.7H), 3.76 – 3.46 (m, 2.3H), 3.29 – 3.18 (m, 8H), 2.38 – 1.91 (m, 4H), 1.74 – 1.60 (m, 8H), 1.46 – 1.36 (m, 8H), 1.02 (t, *J* = 7.4, 12H).

^{13}C NMR (101 MHz, MeOD) δ = 170.00, 168.87, 150.96 (d, *J* = 3.7), 149.09, 144.49 – 144.14 (m), 131.56, 129.46 (d, *J* = 6.0), 128.93 (d, *J* = 6.6), 127.16 (d, *J* = 10.8), 126.08, 120.45 (d, *J* = 7.6), 67.43 (dd, *J* = 117.5, 8.2), 59.70 – 59.36 (m), 58.76 (dd, *J* = 30.8, 9.0), 47.46 (d, *J* = 52.9), 43.40 (d, *J* = 12.2), 28.63 (d, *J* = 132.8), 24.82, 23.86 (d, *J* = 269.7), 20.71, 13.95.

^{19}F NMR (376 MHz, MeOD) δ = -10.23 (d, *J* = 1109.2), -10.91 (d, *J* = 1106.4).

^{31}P NMR (162 MHz, MeOD) δ = 119.98 (d, *J* = 1106.5), 119.70 (d, *J* = 1109.7).

HRMS (**ESI**) calculated for $C_{17}H_{18}FN_3O_3PS_2^-$ ([M-H]$^-$): 426.05167; found: 426.05230.

5.6.2 NMR-spectra

^{1}H and ^{13}C NMR of (*S*)-*N*-(2-(2-(hydroxymethyl)pyrrolidin-1-yl)-2-oxoethyl)quinoline-4-carboxamide (**31**)

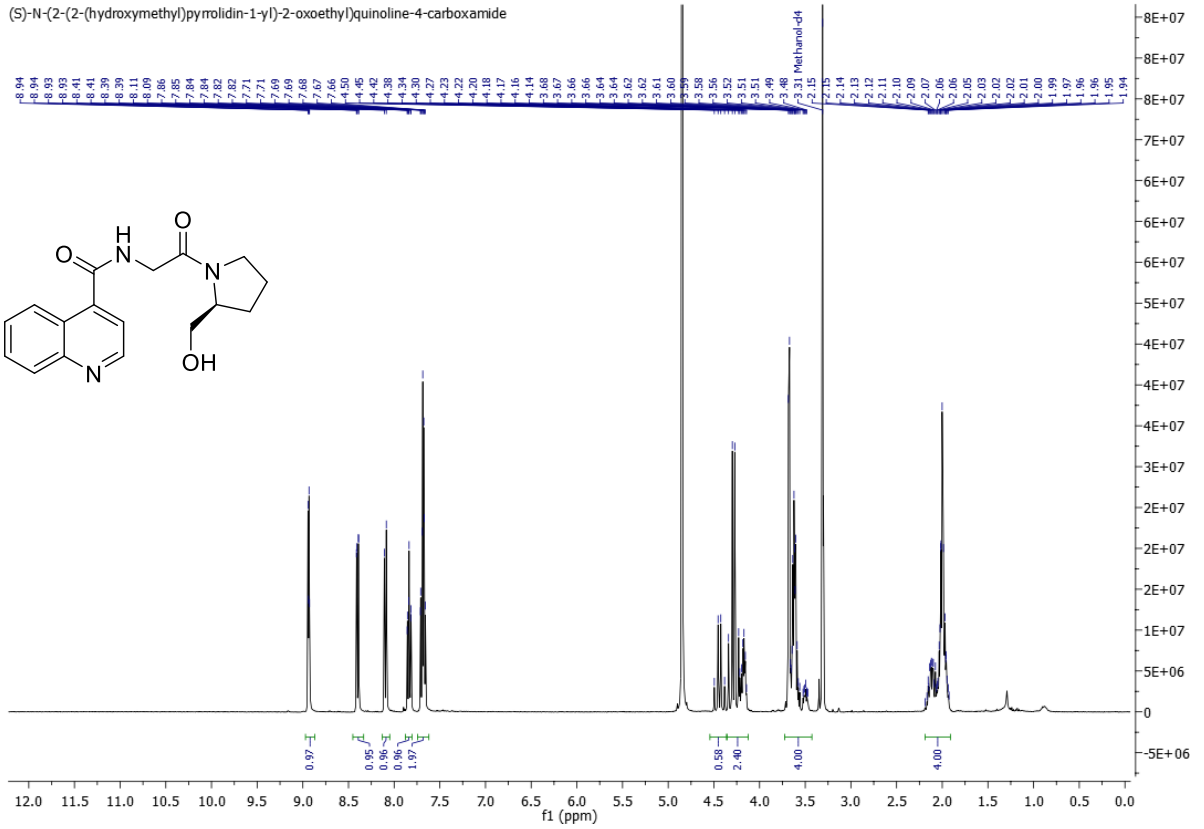

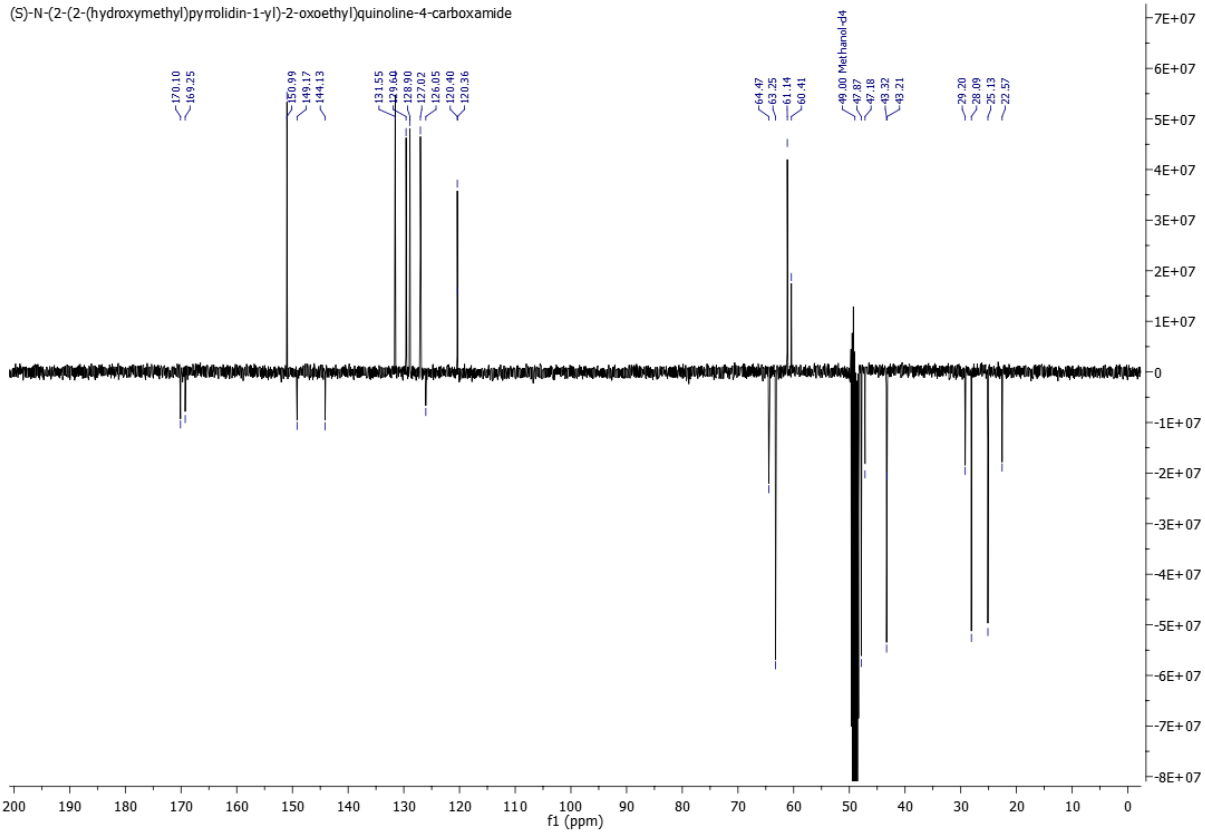

^{1}H, ^{13}C and ^{31}P NMR of *tert*-butyl (*S*)-2-(((2-sulfido-1,3,2-dithiaphospholan-2-yl)oxy)methyl)pyrrolidine-1-carboxylate (**28**)

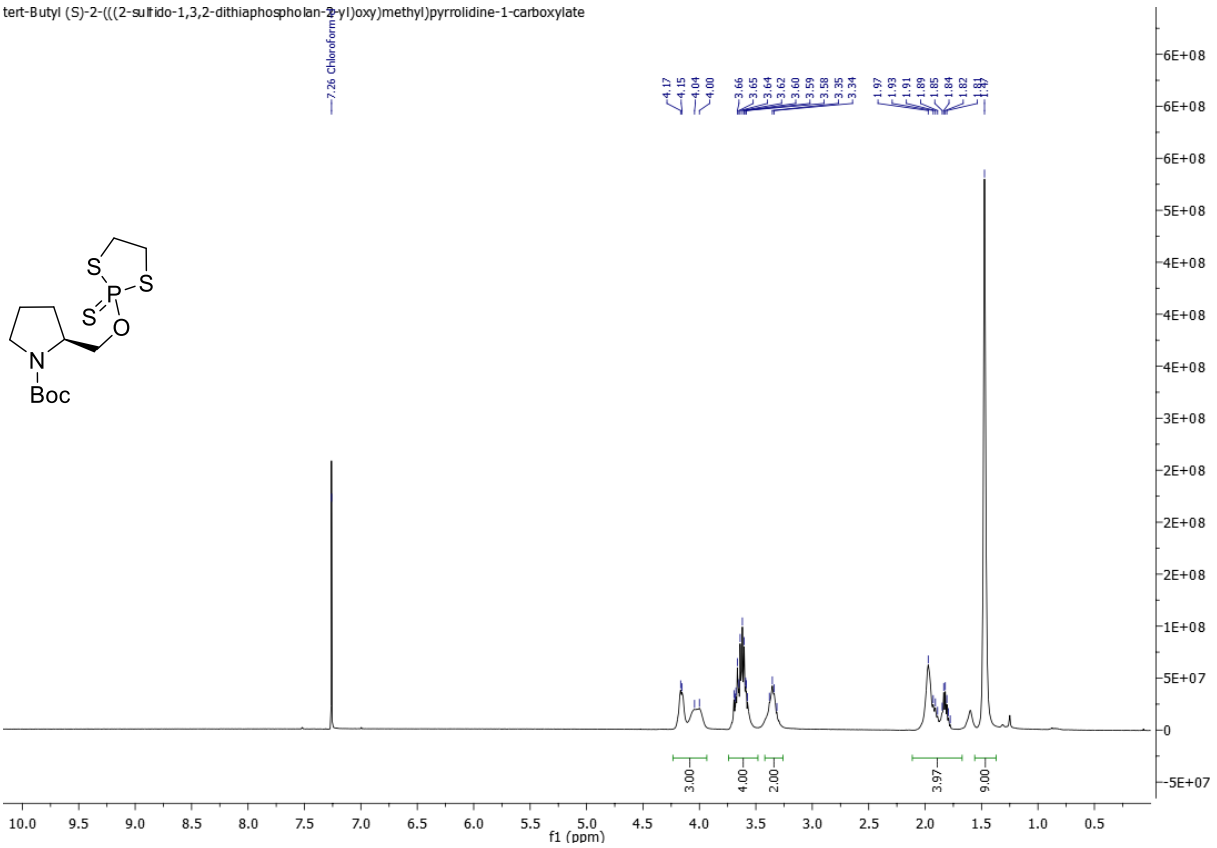

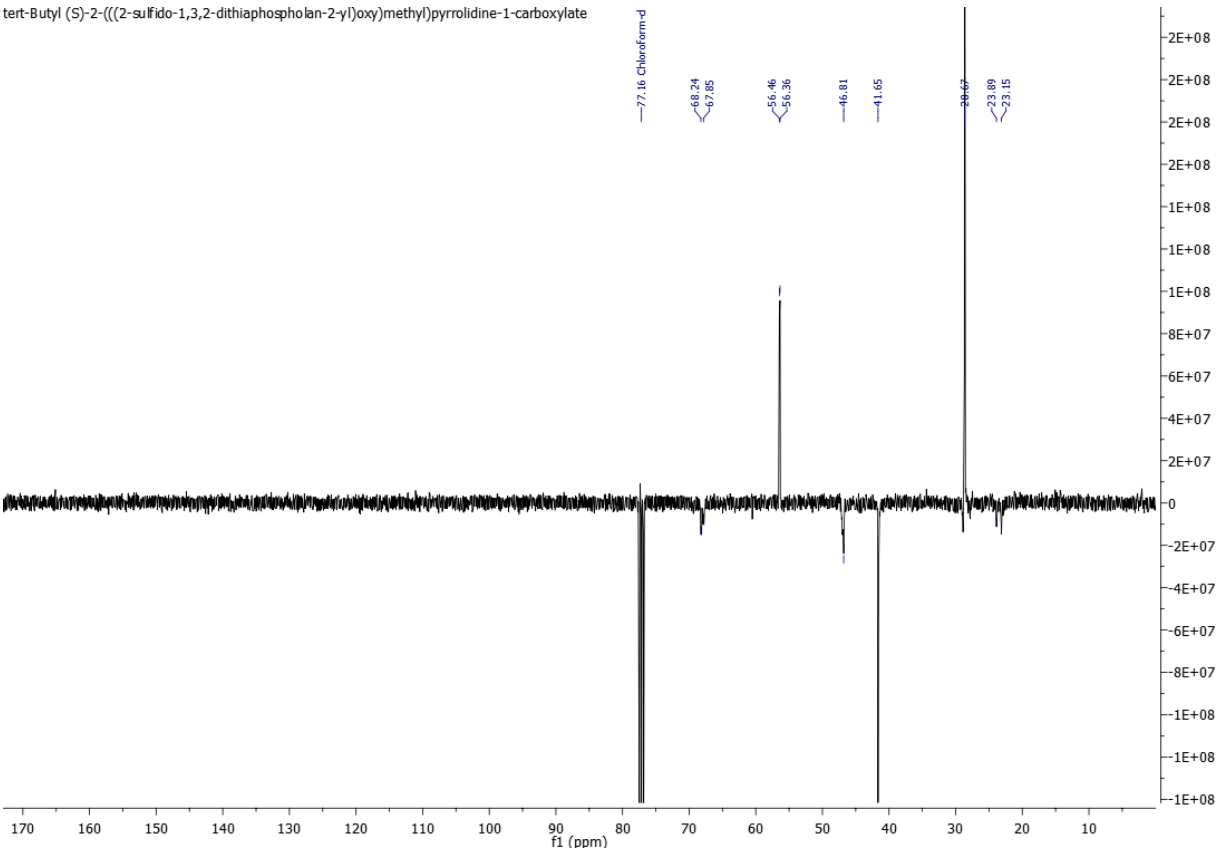

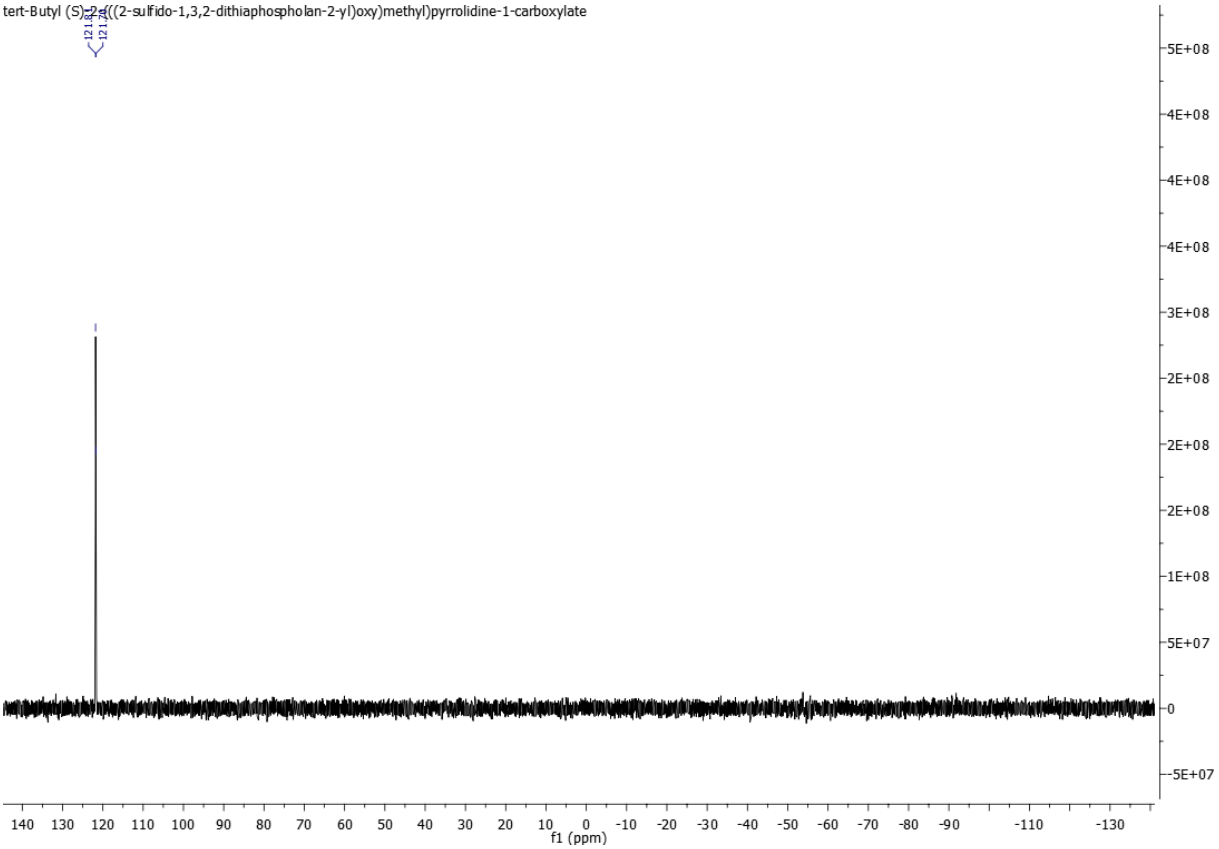

^{1}H, ^{13}C and ^{31}P NMR of (*S*)-*N*-(2-oxo-2-(2-(((2-sulfido-1,3,2-dithiaphospholan-2-yl)oxy)methyl)pyrrolidin-1-yl)ethyl)quinoline-4-carboxamide (**30**)

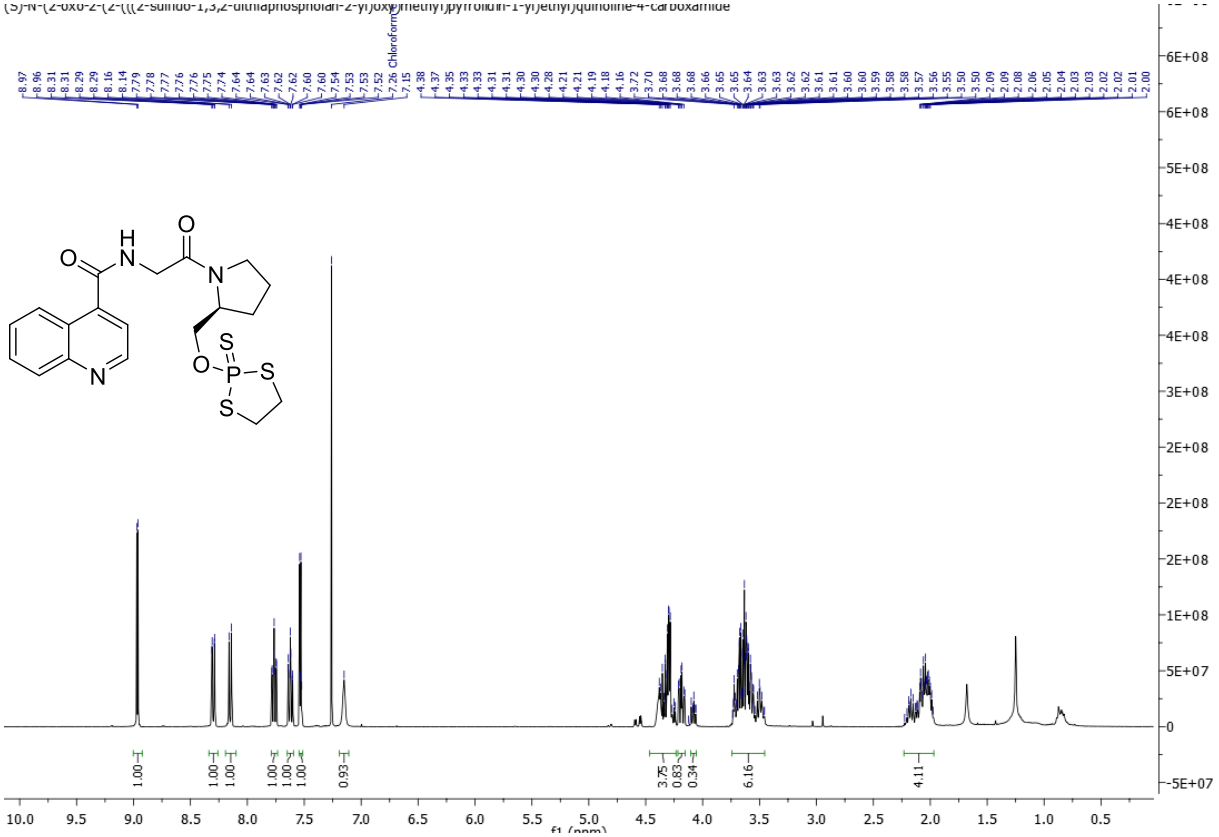

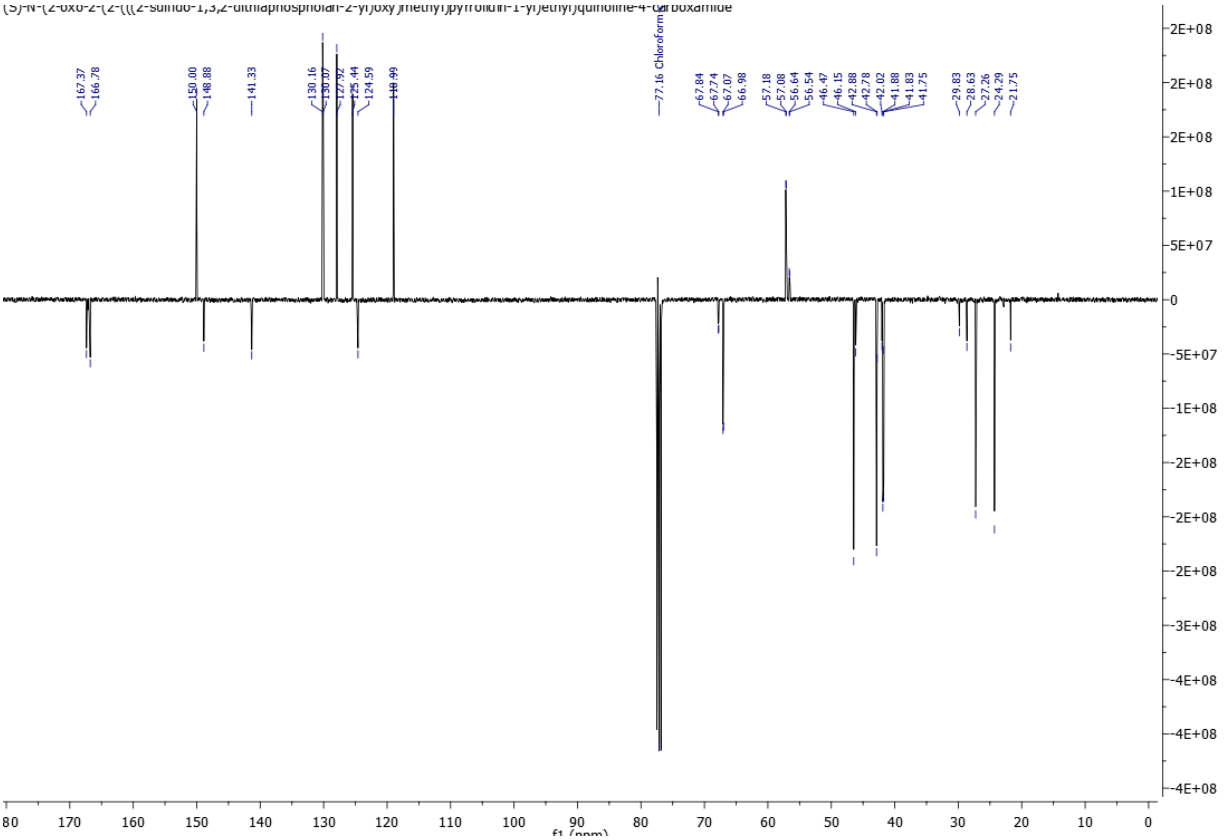
167.37
166.78
150.00
149.88
141.33
130.16
130.07
127.92
125.44
124.59
118.99
77.16 Chloroform
67.84
67.74
67.07
66.98
57.18
57.08
56.64
56.54
46.47
46.15
42.88
42.78
42.02
41.88
41.83
41.75
29.83
28.63
27.26
24.29
21.75
f1 (ppm)

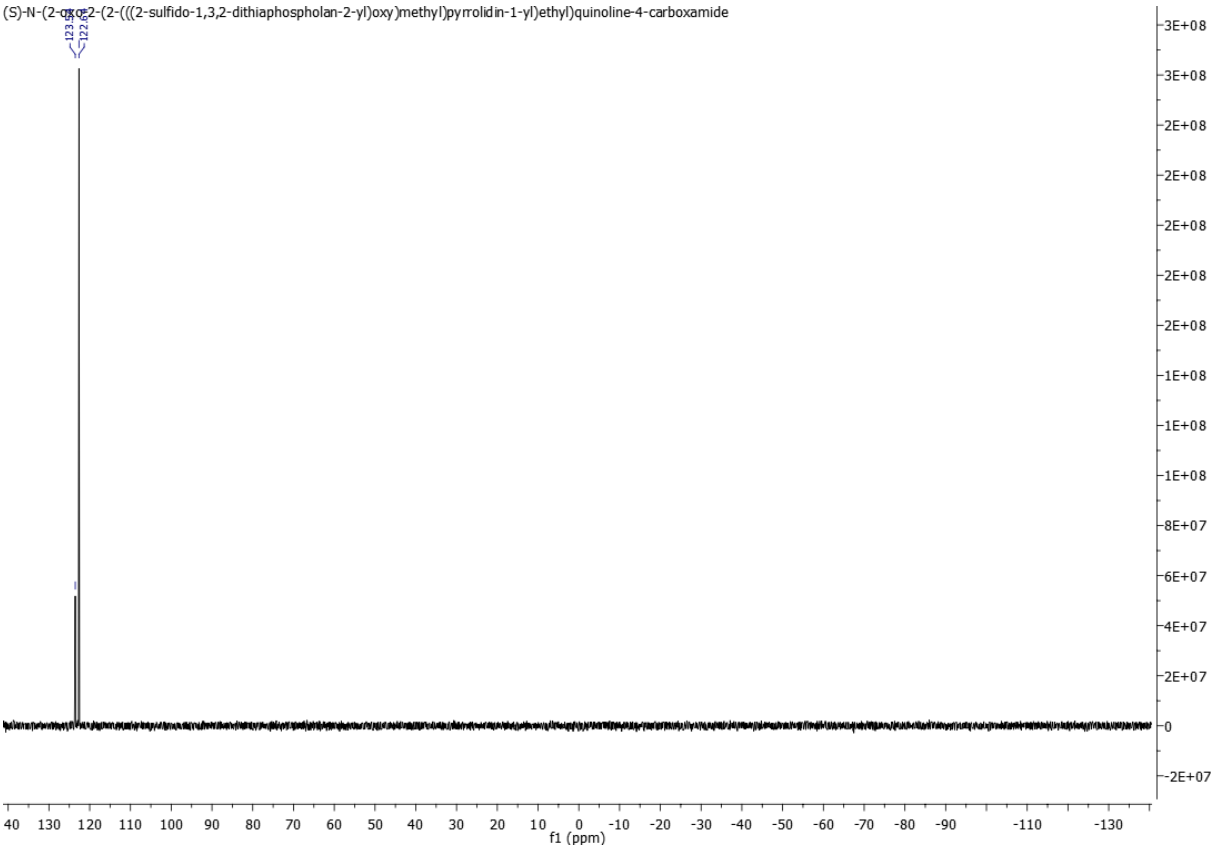
(S)-N-(2-oxo-2-(2-(((2-sulfido-1,3,2-dithiaphospholan-2-yl)oxy)methyl)pyrrolidin-1-yl)ethyl)quinoline-4-carboxamide
123.32
122.82
f1 (ppm)

^{1}H, ^{13}C, ^{19}F and ^{31}P NMR of (*S*)-*O*-((1-(*tert*-butoxycarbonyl)pyrrolidin-2-yl)methyl) phosphorofluoridodithioate tetrabutylammonium salt (**33**)

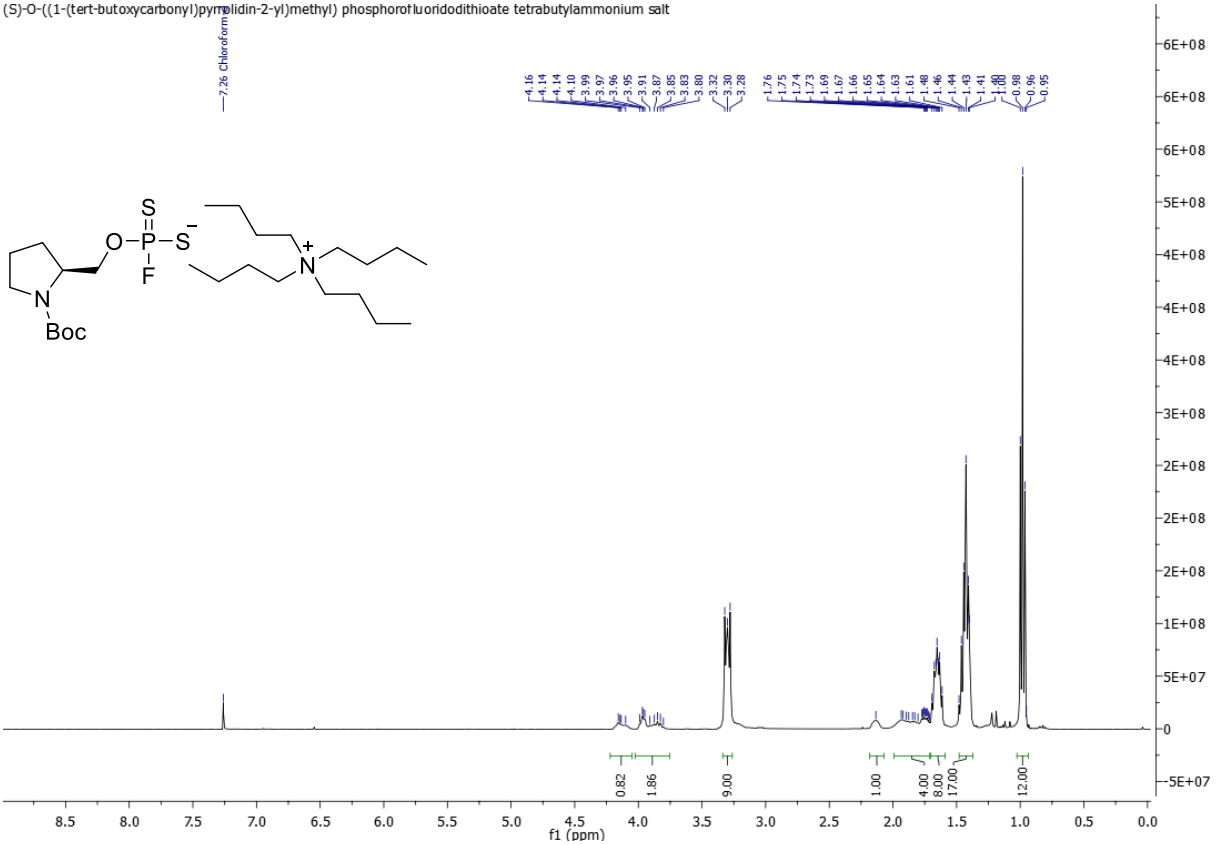

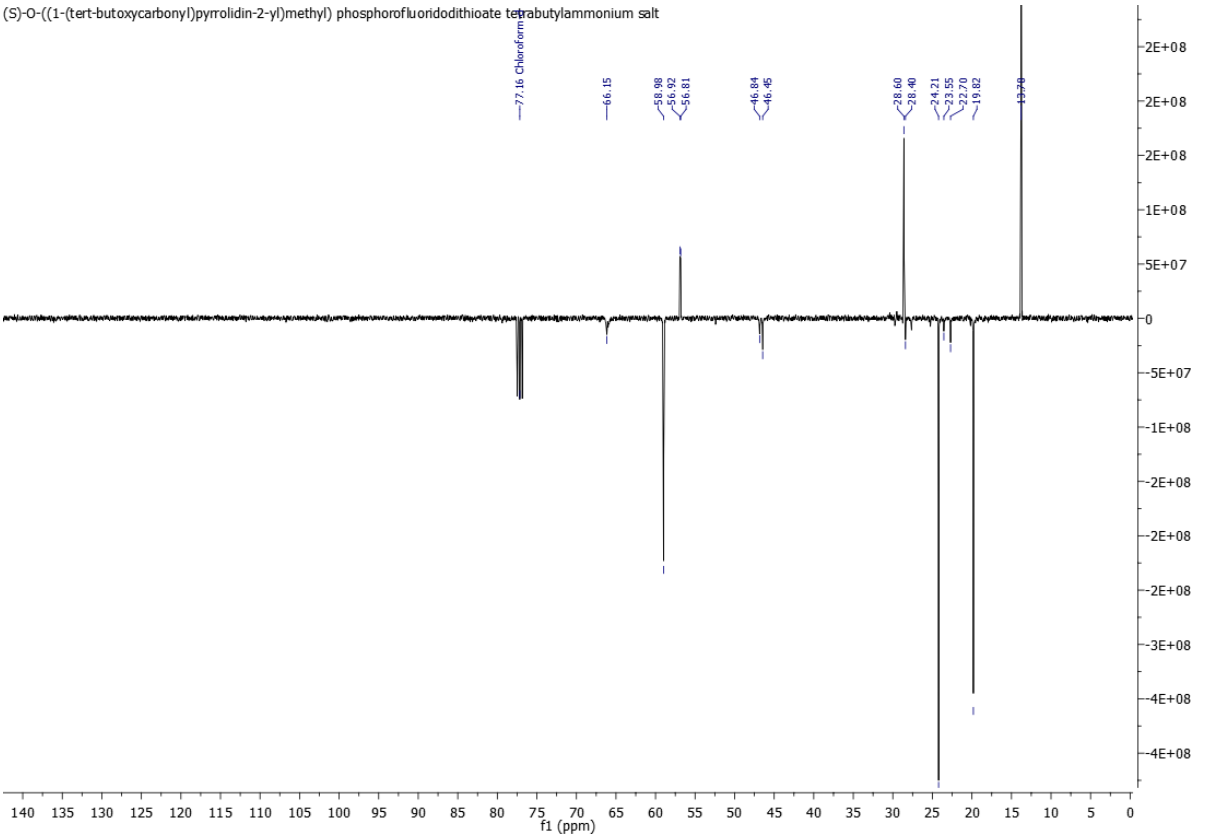

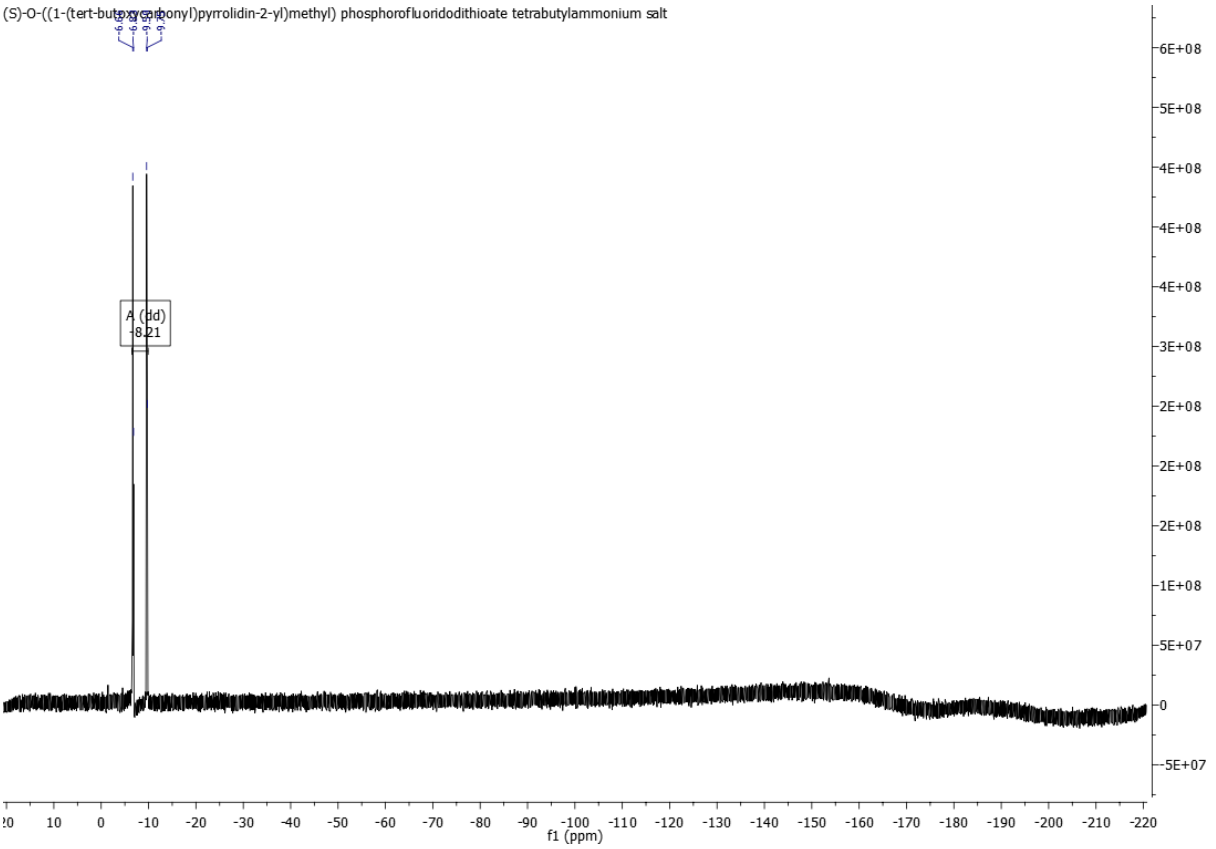
(S)-O-((1-(tert-butoxycarbonyl)pyrrolidin-2-yl)methyl) phosphorofluoridodithioate tetrabutylammonium salt
A (dd)
-8.21
f1 (ppm)

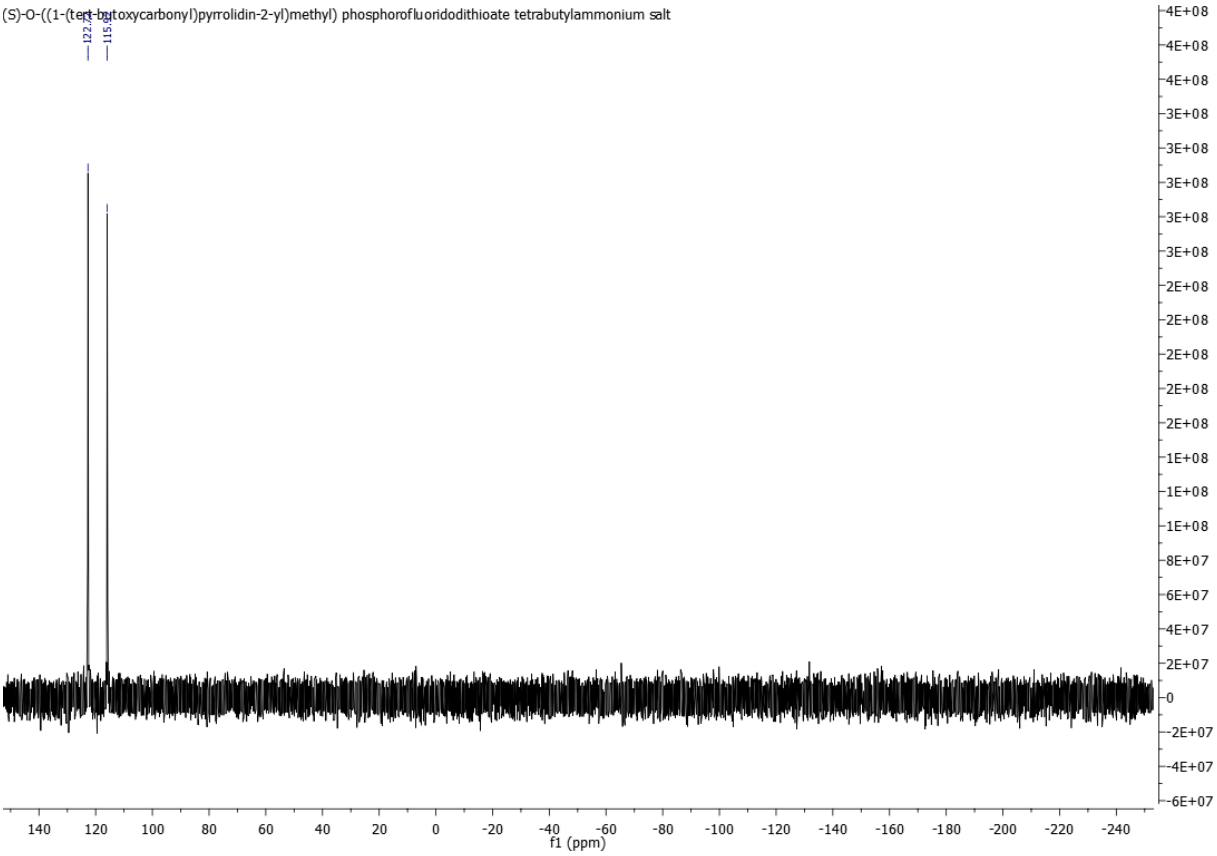
(S)-O-((1-(tert-butoxycarbonyl)pyrrolidin-2-yl)methyl) phosphorofluoridodithioate tetrabutylammonium salt
f1 (ppm)

^{1}H, ^{13}C, ^{19}F and ^{31}P NMR of (*S*)-*O*-((1-((quinoline-4-carbonyl)glycyl)pyrrolidin-2-yl)methyl) phosphorofluoridodithioate tetrabutylammonium salt (**34**)

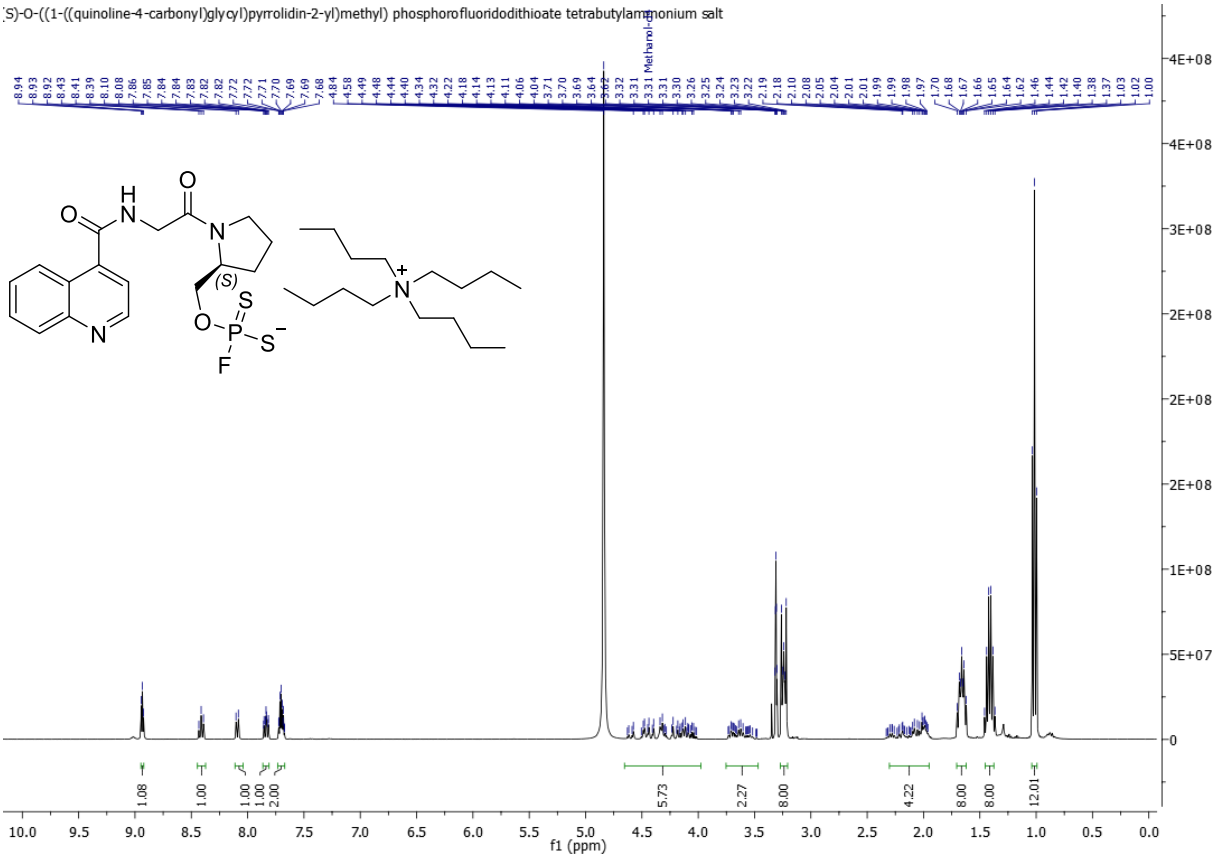

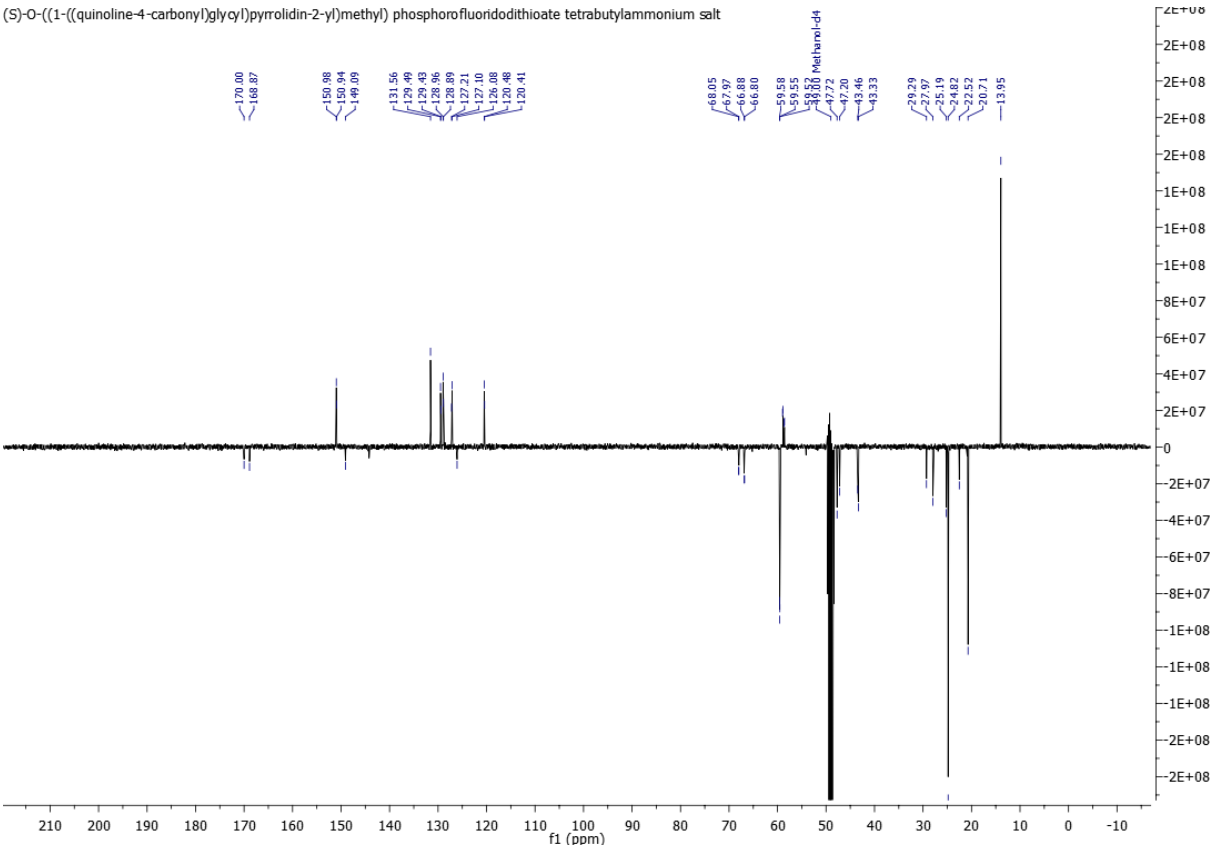

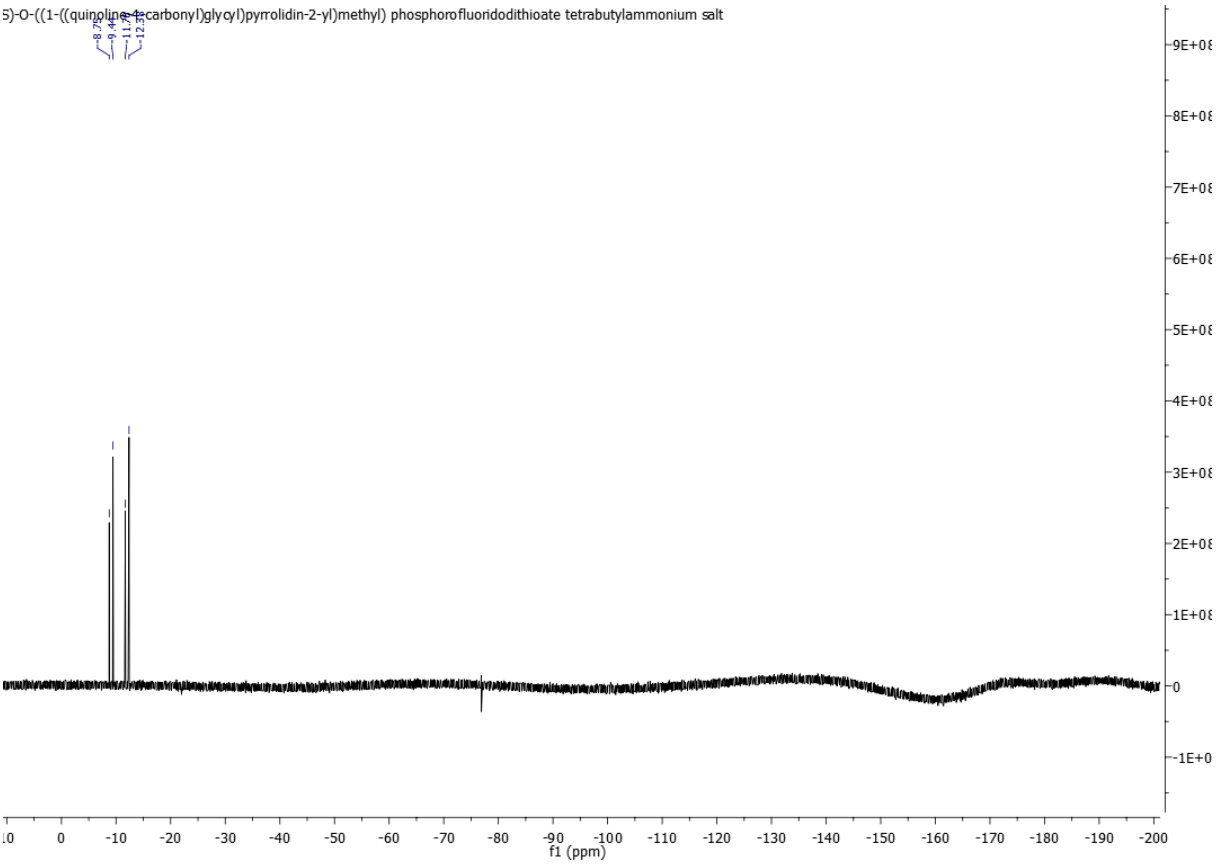
S)-O-((1-((quinoline-4-carbonyl)glycyl)pyrrolidin-2-yl)methyl) phosphorofluoridodithioate tetrabutylammonium salt
f1 (ppm)

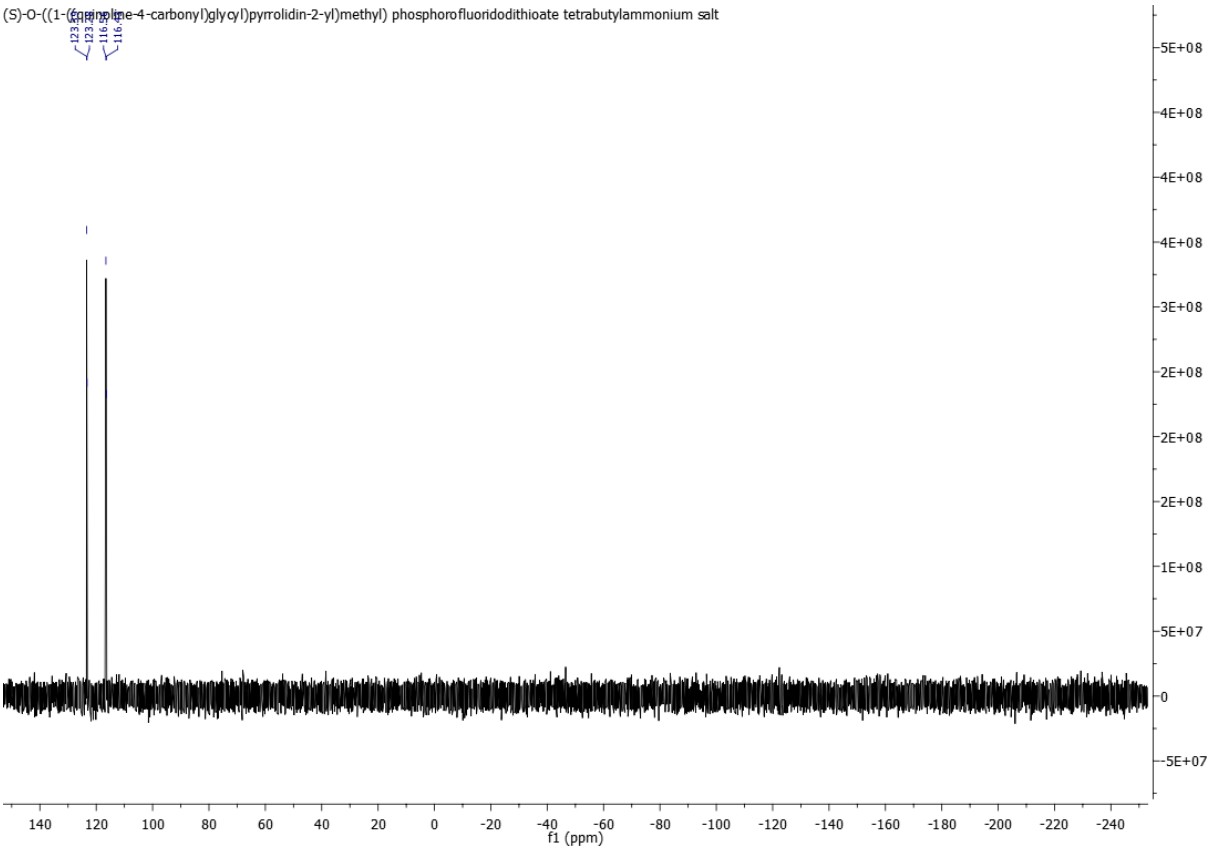
(S)-O-((1-((quinoline-4-carbonyl)glycyl)pyrrolidin-2-yl)methyl) phosphorofluoridodithioate tetrabutylammonium salt
f1 (ppm)

5.6.3 Radiosyntheses

*5.6.3.1 Radiosynthesis of (S)-O-((1-(tert-butoxycarbonyl)pyrrolidin-2-yl)methyl) phosphorofluoridodithioate ([^{18}F]**33**)*

[^{18}F]F$^-$ was eluted from the QMA cartridge with a solution of $Et_4N(HCO_3)$ (1 mg) in MeOH (1 mL). After evaporation of the solvent and addition of *tert*-butyl (*S*)-2-(((2-sulfido-1,3,2-dithiaphospholan-2-yl)oxy)methyl)pyrrolidine-1-carboxylate (**28**, 0.4 µmol) in DMF (100 µL), the reaction mixture was heated for 60 s at 40 °C under argon without stirring. The reaction was quenched by addition of H_2O (0.5 mL) and an aliquot was taken to determine the RCC by HPLC analysis. The remaining reaction solution was diluted with PBS (0.8 mL), and the product was isolated by semi-preparative HPLC. The product fraction was diluted with H_2O (20 mL) and fixed on an Oasis HLB 1cc Vac cartridge (30 mg sorbent, pre-conditioned with 1 mL EtOH and 1 mL H_2O). The cartridge was rinsed with H_2O (10 mL) and dried with air (10 mL) before the product was eluted with DMSO (500 µL) and the RCP determined by HPLC analysis.

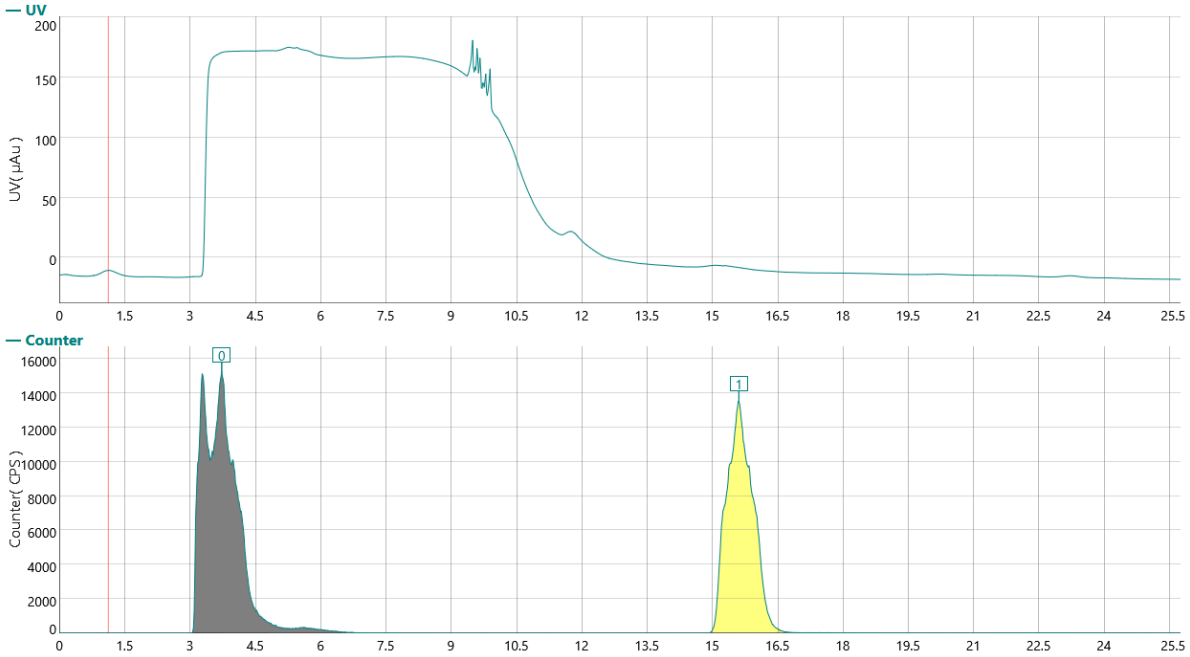

Figure 57: HPLC trace of the isolation of [^{18}F]**33**. (Top: UV chromatogram at 210 nm; bottom: radio chromatogram). Column: Phenomenex Gemini 5 µm C18 110 Å, LC column 250×10 mm; eluent: 40% MeCN in PBS (0.01 M, pH 7.4). Flow rate: 4.5 mL/min.

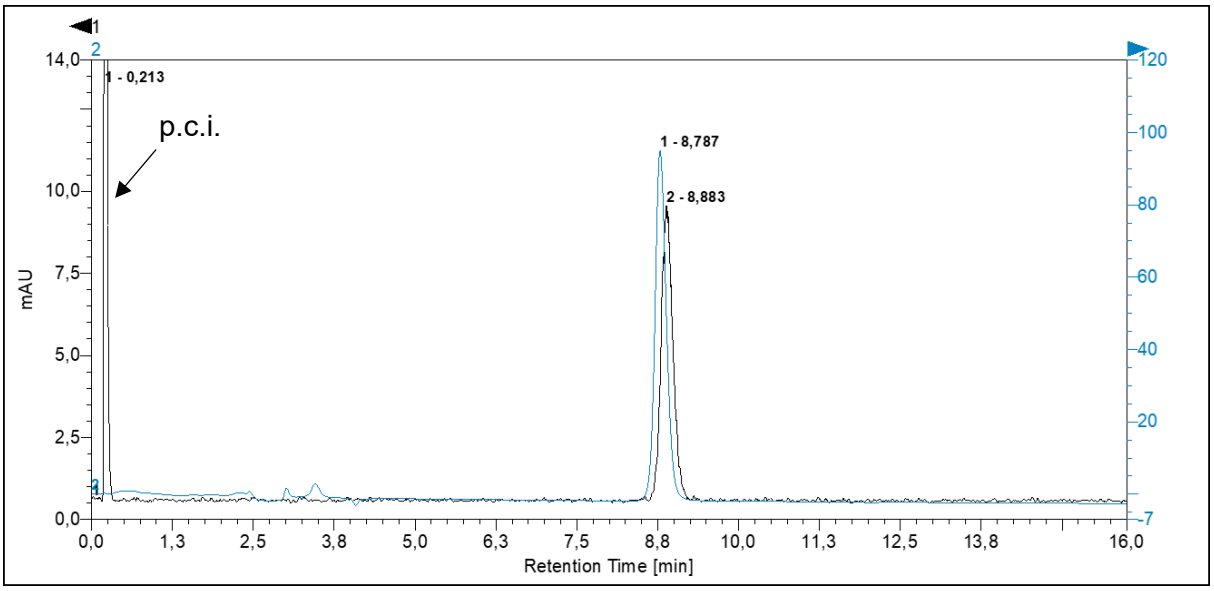

Figure 58: HPLC chromatogram of [^{18}F]**33** co-injected with the non-radioactive reference compound **33** (Black: radio chromatogram; blue: UV chromatogram at 226 nm). Column: Phenomenex Luna® 5µm PFP(2) 100 Å LC column 250×4.6 mm; eluent: 30% MeCN in PBS (0.01 M, pH 7.4). Flow rate: 1 mL/min. Abbreviation: p.c.i. – post-column injection.

*5.6.3.2 Radiosynthesis of (S)-O-((1-((quinoline-4-carbonyl)glycyl)pyrrolidin-2-yl)methyl) phosphoro[^{18}F]fluoridodithioate ([^{18}F]**34**)*

[^{18}F]F^- was eluted from the QMA cartridge with a solution of Et_4NOTf (1 mg) in MeOH (1 mL). After evaporation of the solvent and addition of (*S*)-*N*-(2-oxo-2-(2-(((2-sulfido-1,3,2-dithiaphospholan-2-yl)oxy)methyl)pyrrolidin-1-yl)ethyl)quinoline-4-carboxamide (**30**, 0.5 µmol) in MeCN (100 µL), the reaction mixture was heated for 60 s at 60 °C under argon without stirring. The reaction was quenched by addition of H_2O (0.5 mL) and an aliquot was taken to determine the RCC by HPLC analysis. The remaining reaction solution was diluted with PBS (0.8 mL) and the product was isolated by semi-preparative HPLC. The product fraction was used for experiments without further isolation, and an aliquot was taken to determine the RCP by HPLC analysis.

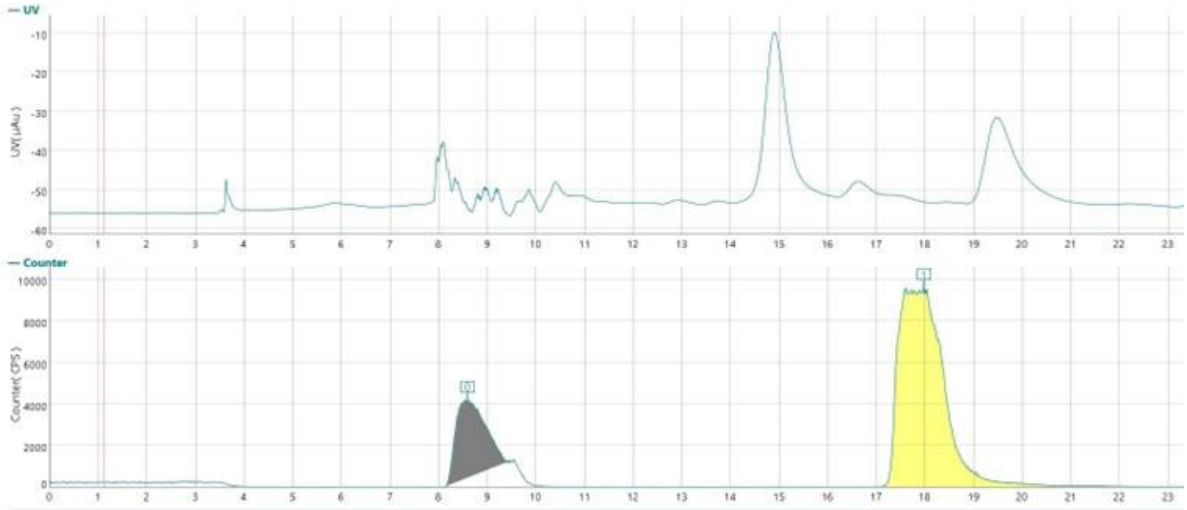

Figure 59: HPLC trace of the isolation of [^{18}F]**34**. (Top: UV chromatogram at 254 nm; bottom: radio chromatogram). Column: Phenomenex Gemini 5 µm C18 110 Å, LC column 250×10 mm; eluent: 30% EtOH in PBS (0.01 M, pH 7.4). Flow rate: 3.5 mL/min.

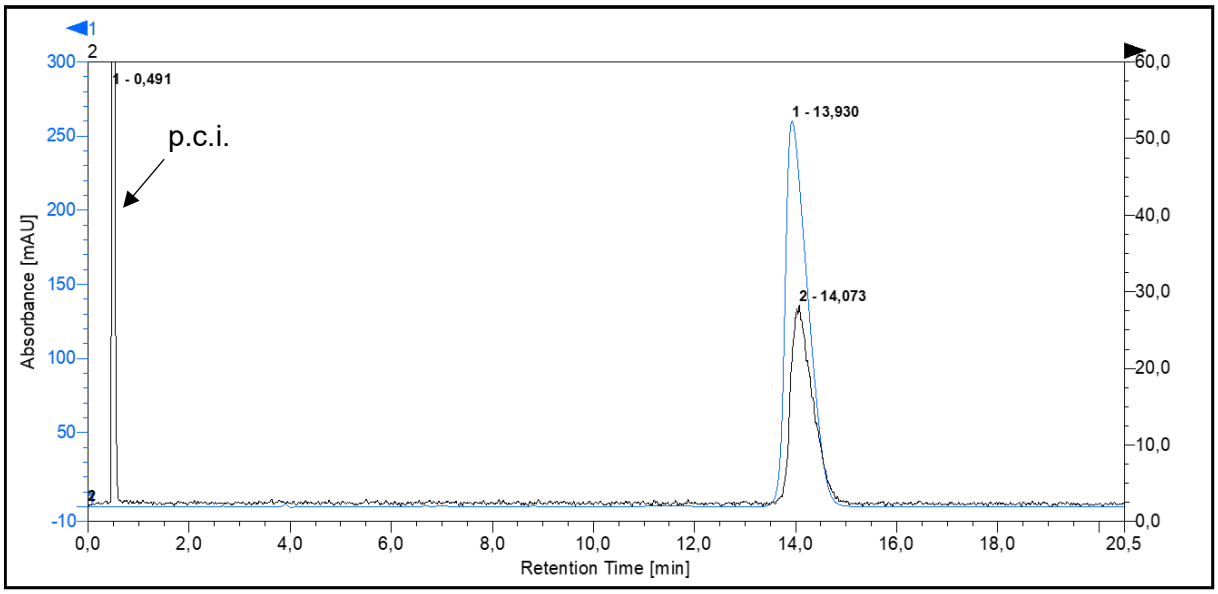

Figure 60: HPLC chromatogram of [^{18}F]**34** co-injected with the non-radioactive reference compound **34** (Black: radio chromatogram; blue: UV chromatogram at 254 nm). Column: Phenomenex Luna® 5µm PFP(2) 100 Å LC column 250×4.6 mm; eluent: 20% MeCN in PBS (0.01 M, pH 7.4). Flow rate: 1 mL/min. Abbreviation: p.c.i. – post-column injection.

The calibration curve for calculating the molar activity of [^{18}F]**34** was measured at 280 nm.

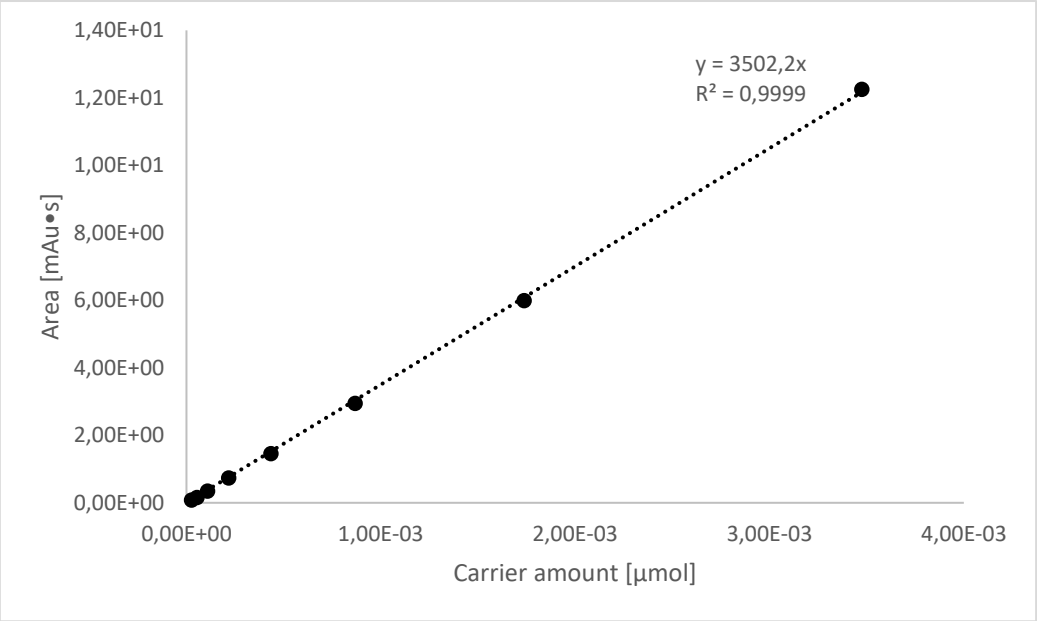

Figure 61: Calibration curve for calculating the molar activity of [^{18}F]**34**.

Table 29: Data for generating the calibration curve for determining the molar activity of [^{18}F]**34**.

Entry	mg/mL	mg/20 µL	g/20 µL	mol (g/668,9 g/mol)	µmol	Area
1	0.11625	2.33E-03	2.33E-06	4.93E-08	3.48E-03	1.23E+01
2	0.058125	1.16E-03	1.16E-06	2.47E-08	1.74E-03	6.00E+00
3	0.0290625	5.81E-04	5.81E-07	1.23E-08	8.69E-04	2.95E+00
4	0.01453125	2.91E-04	2.91E-07	6.17E-09	4.34E-04	1.46E+00
5	0.007265625	1.45E-04	1.45E-07	3.08E-09	2.17E-04	7.43E-01
6	0.003632813	7.27E-05	7.27E-08	1.54E-09	1.09E-04	3.54E-01
7	0.001816406	3.63E-05	3.63E-08	7.71E-10	5.43E-05	1.59E-01
8	0.000908203	1.82E-05	1.82E-08	3.85E-10	2.72E-05	8.80E-02

5.6.4 Stability studies in aqueous solutions

[^{18}F]**33** was synthesized and formulated in DMSO. To determine the stability in different aqueous solutions, 20 µL of [^{18}F]**33** in DMSO were brought to 1 mL with the respective test solution. At selected time points, an aliquot was taken and analyzed by analytical HPLC.
[^{18}F]**34** was synthesized and isolated by semi-preparative HPLC. After concentration of the HPLC fraction at 40 °C under semi-vacuum in a stream of argon, 100 µL were brought to 1 mL with the respective test solution. At selected time points, an aliquot was taken and analyzed by analytical HPLC.

5.6.5 Stability studies in human blood plasma

[^{18}F]**33** was synthesized and formulated in DMSO. For each measurement time point, a sample of 5.00 µL [^{18}F]**33** in 95.0 µL human blood plasma was prepared. The plasma was pre-warmed for five minutes at 37 °C on a thermoshaker. After the corresponding time points, 100 µL MeCN was added to the corresponding sample to precipitate the blood proteins. The sample was vortexed for two minutes and then centrifuged for two minutes at 20000 rcp. The supernatant was analyzed by analytical HPLC.
960 µL of human blood plasma was placed in a 2.00 mL vial and pre-warmed to 37 °C in a thermoshaker for five minutes before adding 40.0 µL of [^{18}F]**34** synthesized, isolated by semi-preparative HPLC and concentrated. After five, 30, 60, 90 and 120 minutes, an aliquot of 80.0 µL was taken and 60.0 µL were added to 120 µL of acetonitrile to precipitate the proteins. The mixture was vortexed for two minutes and then centrifuged for two minutes. The supernatant was analyzed by analytical HPLC.

5.6.6 Enzyme experiments

The reaction kinetics were determined in triplicate. To this end, 1.00 µg of FAP (Recombinant Human FAP His-tag (Mammalian) Protein, CF, *Bio-Techne GmbH,* Wiesbaden, Germany) in 50.0 µL FAP-buffer and 50 kBq of [^{18}F]**34** in 50.0 µL FAP-buffer (A_M 91 GBq/µmol) were added to FAP-buffer (50 mM TRIS buffer (pH 7.5, 1.0 M NaCl, 0.1% BSA), yielding a total volume of 500 µL. The reaction mixtures were incubated at ambient temperature without shaking, and aliquots of 90.0 µL were taken after 10, 30, 60, 90, and 120 minutes. The aliquots were added to 410 µL acetonitrile and 25.0 mg hydroxyapatite. The samples were then vortexed for 2 min, centrifuged for 10 minutes, and the supernatant was transferred to a second Eppendorf tube. 500 µL of H_2O was added to the hydroxyapatite. After 2 minutes on the vortex and 5 min of centrifugation, the supernatant was added to the second Eppendorf tube. The procedure was repeated with 500 µL of H_2O and centrifugation for 10 minutes. To determine the [^{18}F]fluoride content in the tracer, three samples, each containing 50 kBq of [^{18}F]**34** (50.0 µL in FAP-buffer) in 450 µL FAP-buffer, were prepared and treated identically to the reaction samples. In addition, three samples, each containing 50 kBq of [^{18}F]**34** (in 50.0 µL Fap-buffer) in 450 µL FAP-buffer, were prepared and processed identically without hydroxyapatite to determine the 100% value of the activity. The samples were measured individually with a gamma counter (*Hidex Deutschland Vertrieb GmbH*, Mainz, Germany). Samples for determining the background consisted of 500 µL FAP-buffer.

5.6.7 Chromatograms

Stability study of [^{18}F]**33** in various aqueous solutions and human blood plasma

The peaks at t_R = 0.2 minutes are the injections behind the column to quantify the activity on the chromatography column (post-column injection). Peaks at 2.6–3.8 minutes are assigned to [^{18}F]F$^-$. Peaks at ~ 5 minutes belong to the unidentified by-product. [^{18}F]**33** elutes at 8.8 – 10.1 min.

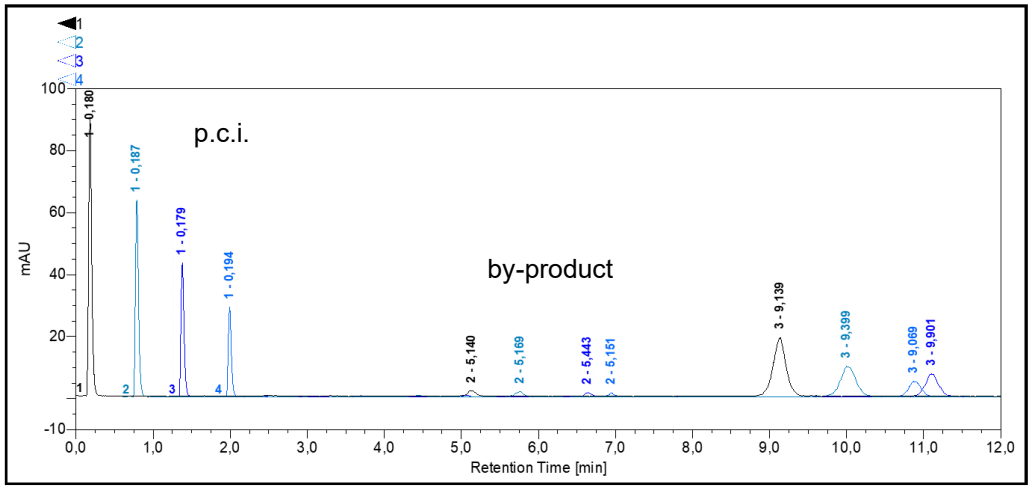

Figure 62: Radio-HPLC chromatogram of [^{18}F]**33** to determine the stability in TFA solution (0.1%, pH 2). Column: Phenomenex Luna® 5 µm PFP(2) 100 Å LC column 250×4.6 mm; eluent: 30% MeCN in PBS (0.01 M, pH 7.4). Flow rate: 1 mL/min. Abbreviation: p.c.i. – post-column injection.

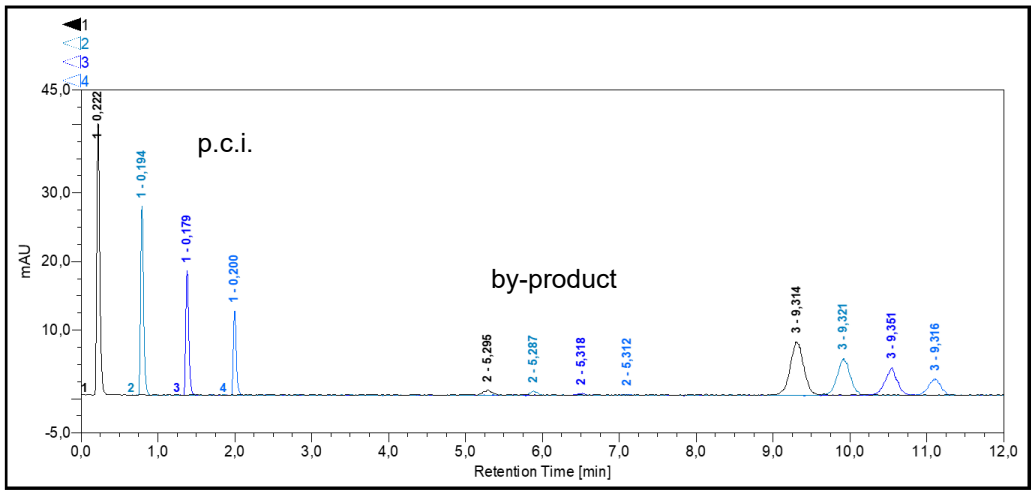

Figure 63: Radio-HPLC chromatogram of [^{18}F]**33** to determine the stability in NaOAc buffer (0.1 M, pH 4). Column: Phenomenex Luna® 5 µm PFP(2) 100 Å LC column 250×4.6 mm; eluent: 30% MeCN in PBS (0.01 M, pH 7.4). Flow rate: 1 mL/min. Abbreviation: p.c.i. – post-column injection.

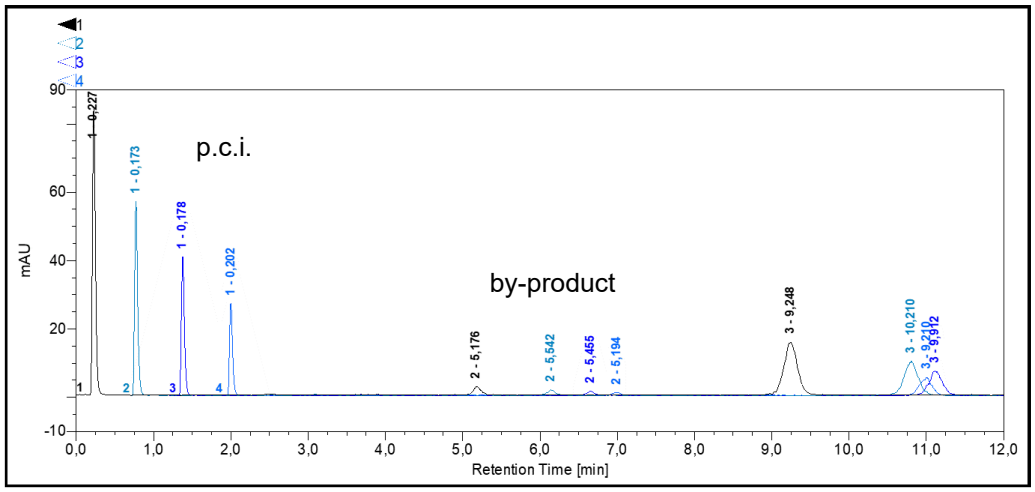

Figure 64: Radio-HPLC chromatogram of [^{18}F]**33** to determine the stability in NaOAc buffer (0.1 M, pH 6). Column: Phenomenex Luna® 5 µm PFP(2) 100 Å LC column 250×4.6 mm; eluent: 30% MeCN in PBS (0.01 M, pH 7.4). Flow rate: 1 mL/min. Abbreviation: p.c.i. – post-column injection.

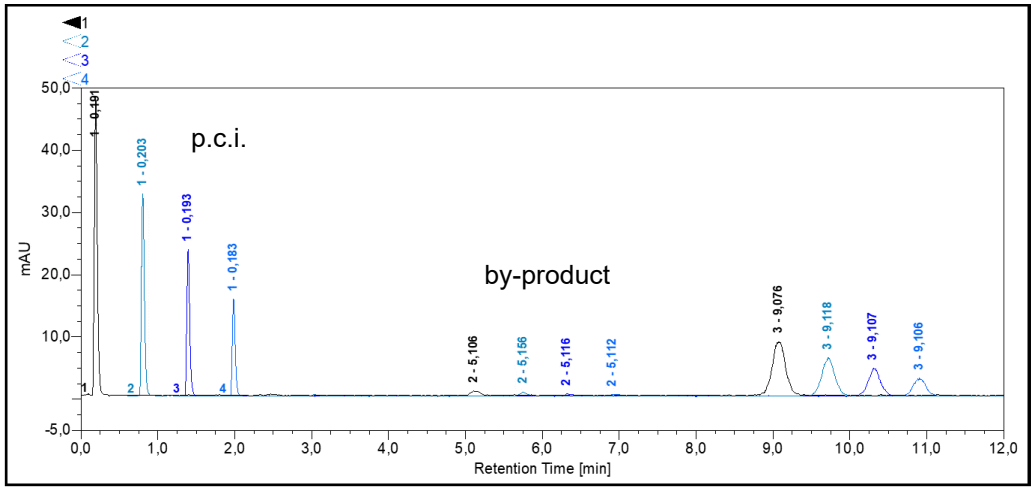

Figure 65: Radio-HPLC chromatogram of [^{18}F]**33** to determine the stability in H_2O. Column: Phenomenex Luna® 5 µm PFP(2) 100 Å LC column 250×4.6 mm; eluent: 30% MeCN in PBS (0.01 M, pH 7.4). Flow rate: 1 mL/min. Abbreviation: p.c.i. – post-column injection.

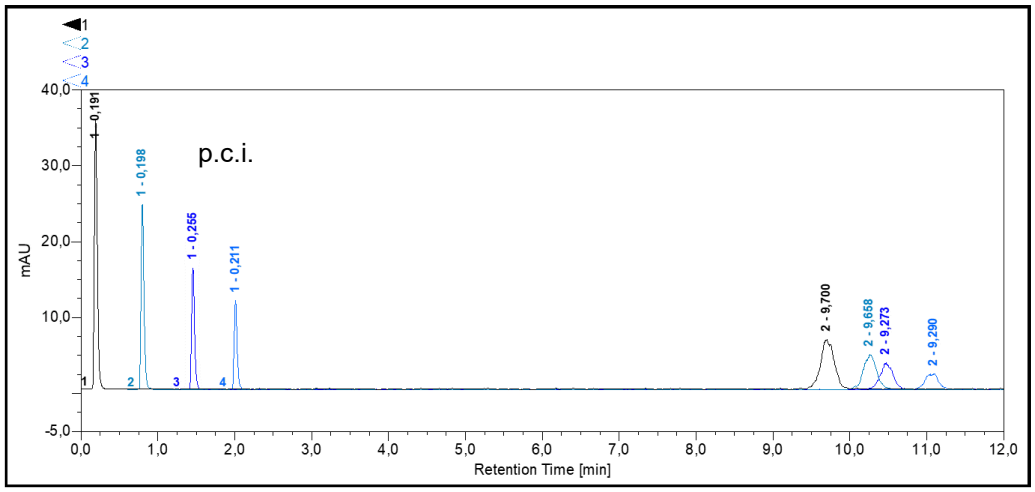

Figure 66: Radio-HPLC chromatogram of [^{18}F]**33** to determine the stability in PBS buffer (0.01 M, pH 7.4). Column: Phenomenex Luna® 5 µm PFP(2) 100 Å LC column 250×4.6 mm; eluent: 30% MeCN in PBS (0.01 M, pH 7.4). Flow rate: 1 mL/min. Abbreviation: p.c.i. – post-column injection.

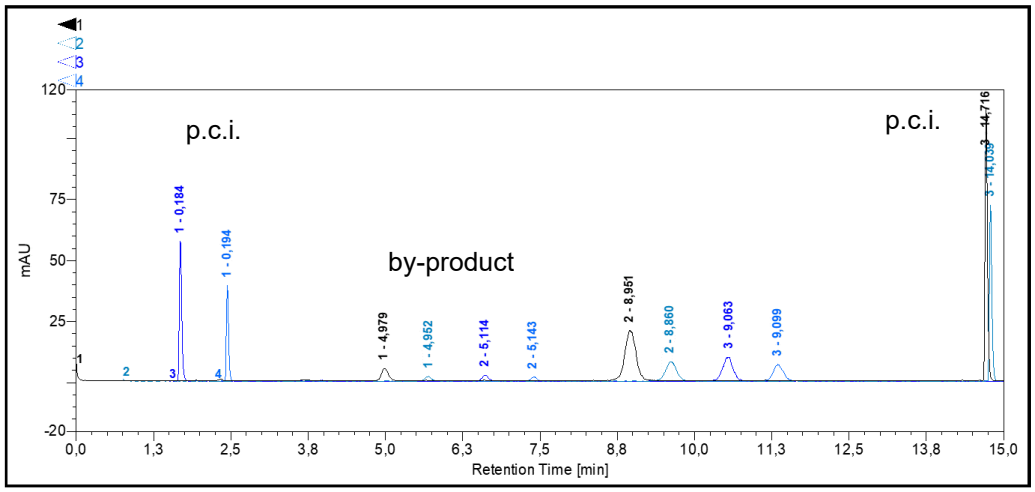

Figure 67: Radio-HPLC chromatogram of [^{18}F]**33** to determine the stability in $NaHCO_3$ solution (0.1 M, pH 8). Column: Phenomenex Luna® 5 µm PFP(2) 100 Å LC column 250×4.6 mm; eluent: 30% MeCN in PBS (0.01 M, pH 7.4). Flow rate: 1 mL/min. Abbreviation: p.c.i. – post-column injection.

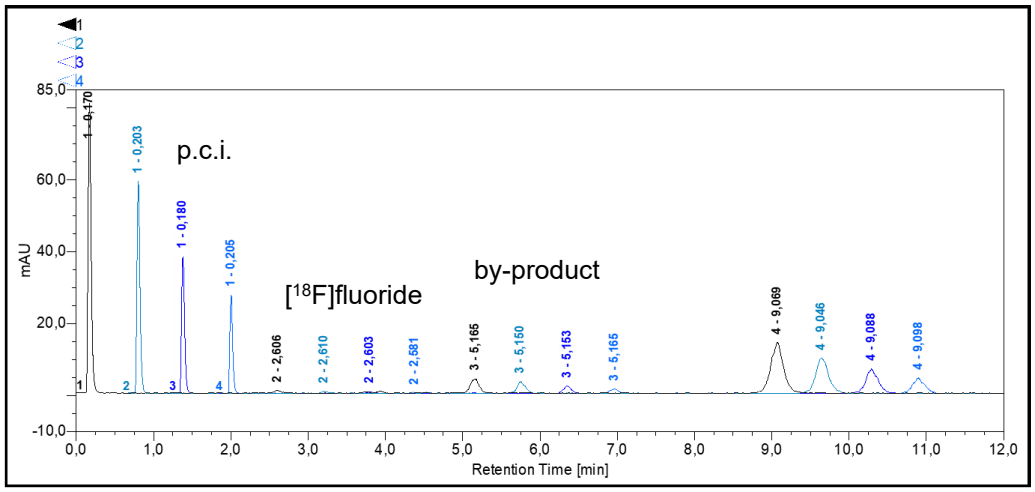

Figure 68: Radio-HPLC chromatogram of [^{18}F]**33** to determine the stability in NH_4Cl/NH_4OH buffer (pH 10). Column: Phenomenex Luna® 5 µm PFP(2) 100 Å LC column 250×4.6 mm; eluent: 30% MeCN in PBS (0.01 M, pH 7.4). Flow rate: 1 mL/min. Abbreviation: p.c.i. – post-column injection.

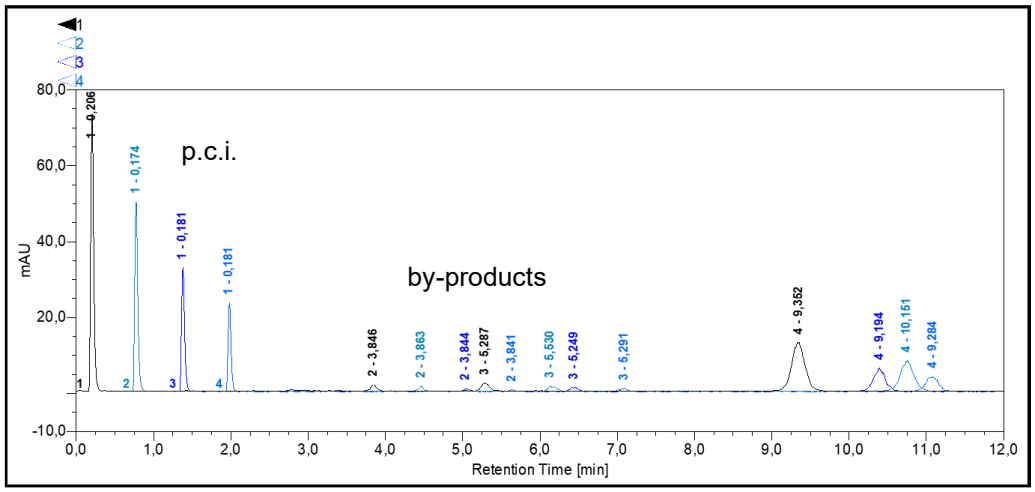

Figure 69: Radio-HPLC chromatogram of [^{18}F]**33** to determine the stability in NaOAc buffer (0.1 M, pH 4) after heating for 5 min at 100 °C. Column: Phenomenex Luna® 5 µm PFP(2) 100 Å LC column 250×4.6 mm; eluent: 30% MeCN in PBS (0.01 M, pH 7.4). Flow rate: 1 mL/min. Abbreviation: p.c.i. – post-column injection.

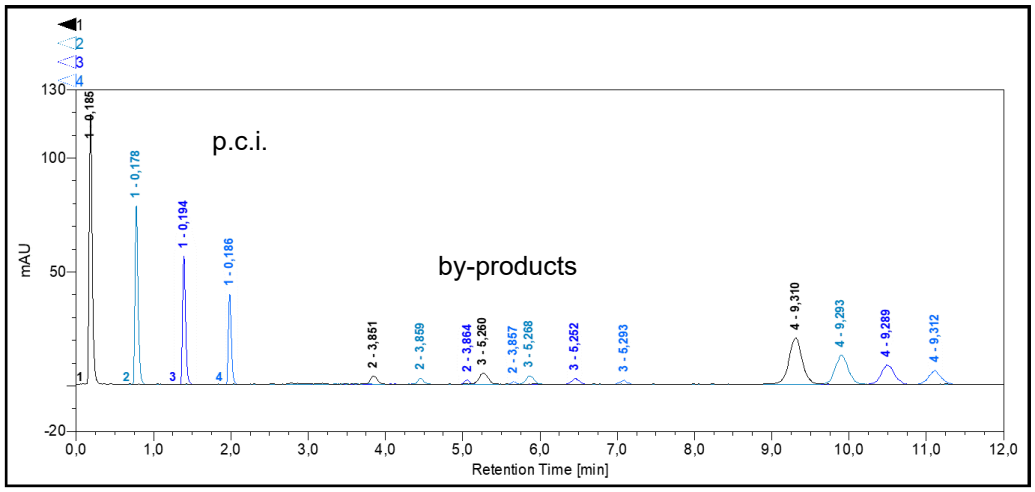

Figure 70: Radio-HPLC chromatogram of [^{18}F]**33** to determine the stability in NaOAc buffer (0.1 M, pH 4) after heating for 10 min at 100 °C. Column: Phenomenex Luna® 5 µm PFP(2) 100 Å LC column 250×4.6 mm; eluent: 30% MeCN in PBS (0.01 M, pH 7.4). Flow rate: 1 mL/min. Abbreviation: p.c.i. – post-column injection.

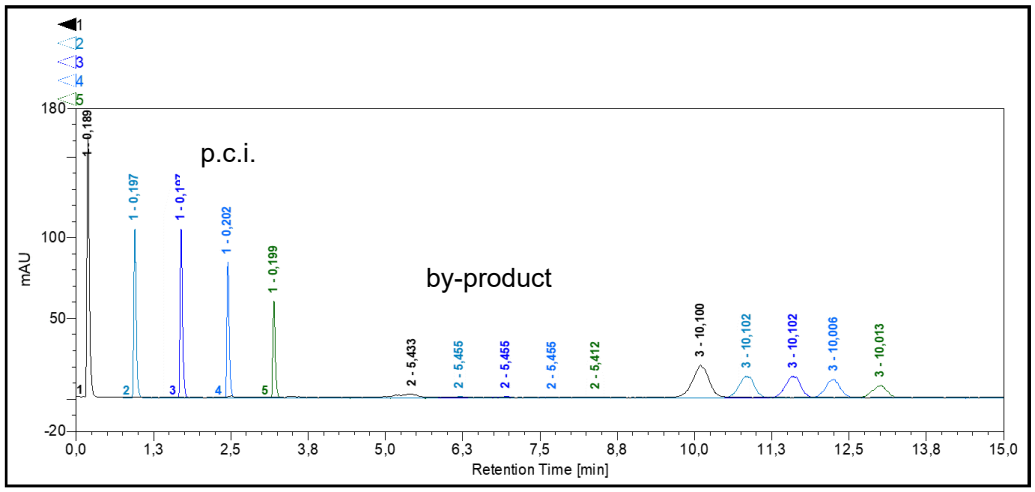

Figure 71: Radio-HPLC chromatogram of [^{18}F]**33** to determine the stability in human blood plasma. Column: Phenomenex Luna® 5 µm PFP(2) 100 Å LC column 250×4.6 mm; eluent: 30% MeCN in PBS (0.01 M, pH 7.4). Flow rate: 1 mL/min. Abbreviation: p.c.i. – post-column injection.

Stability study of [^{18}F]**34** in various aqueous solutions and human blood plasma

The peaks at t_R = 0.4–0.5 minutes are the injections behind the column to quantify the activity on the chromatography column (post-column injection). [^{18}F]**34** elutes at 10.0–11.3 minutes.

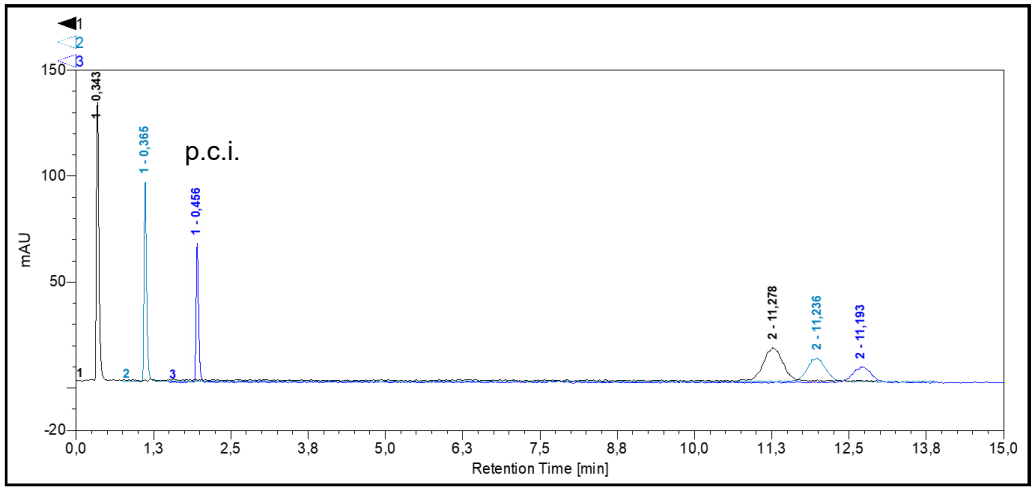

Figure 72: Radio-HPLC chromatogram of [^{18}F]**34** to determine the stability in TFA solution (0.55%, pH 1). Column: Phenomenex Luna® 5 µm PFP(2) 100 Å LC column 250×4.6 mm; eluent: 20% MeCN in PBS (0.01 M, pH 7.4). Flow rate: 1 mL/min. Abbreviation: p.c.i. – post-column injection.

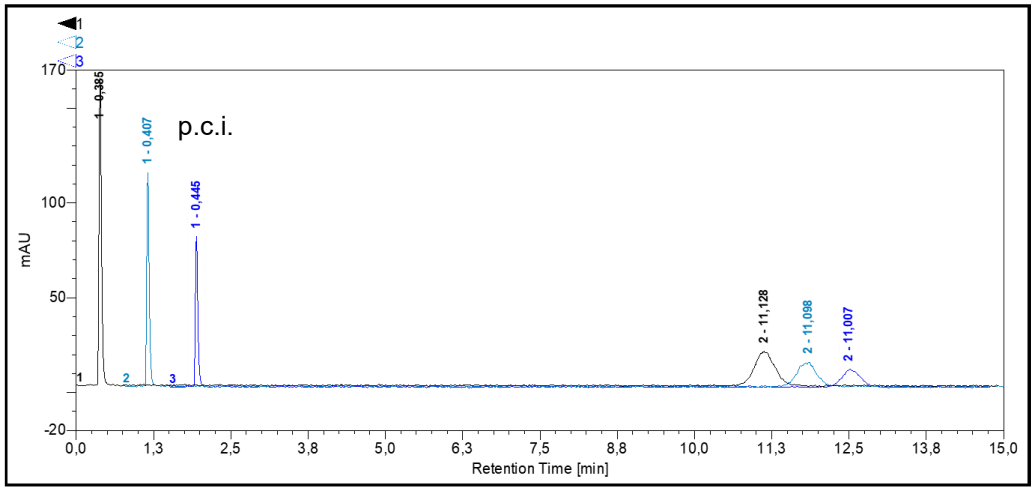

Figure 73: Radio-HPLC chromatogram of [^{18}F]**34** to determine the stability in TFA solution (0.1%, pH 2). Column: Phenomenex Luna® 5 µm PFP(2) 100 Å LC column 250×4.6 mm; eluent: 20% MeCN in PBS (0.01 M, pH 7.4). Flow rate: 1 mL/min. Abbreviation: p.c.i. – post-column injection.

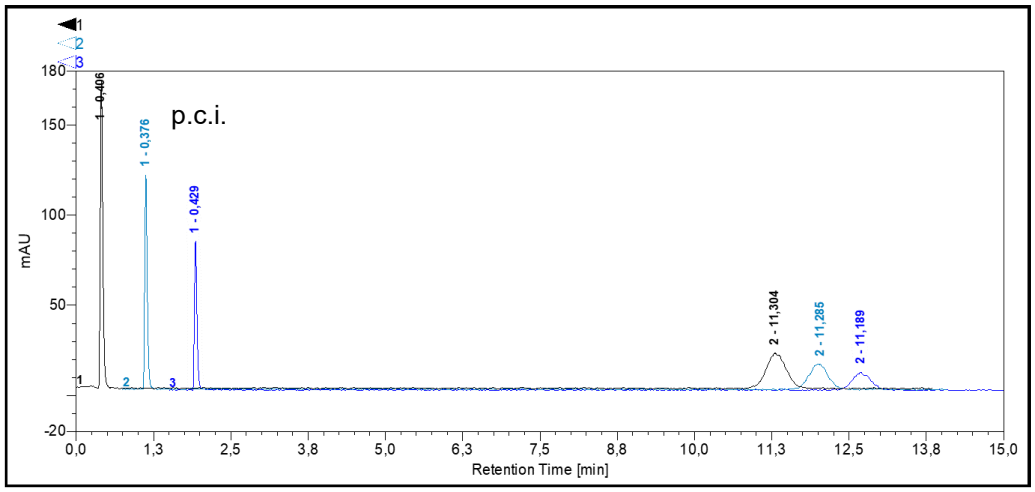

Figure 74: Radio-HPLC chromatogram of [^{18}F]**34** to determine the stability in NaOAc buffer (0.1 M, pH 4). Column: Phenomenex Luna® 5 µm PFP(2) 100 Å LC column 250×4.6 mm; eluent: 20% MeCN in PBS (0.01 M, pH 7.4). Flow rate: 1 mL/min. Abbreviation: p.c.i. – post-column injection.

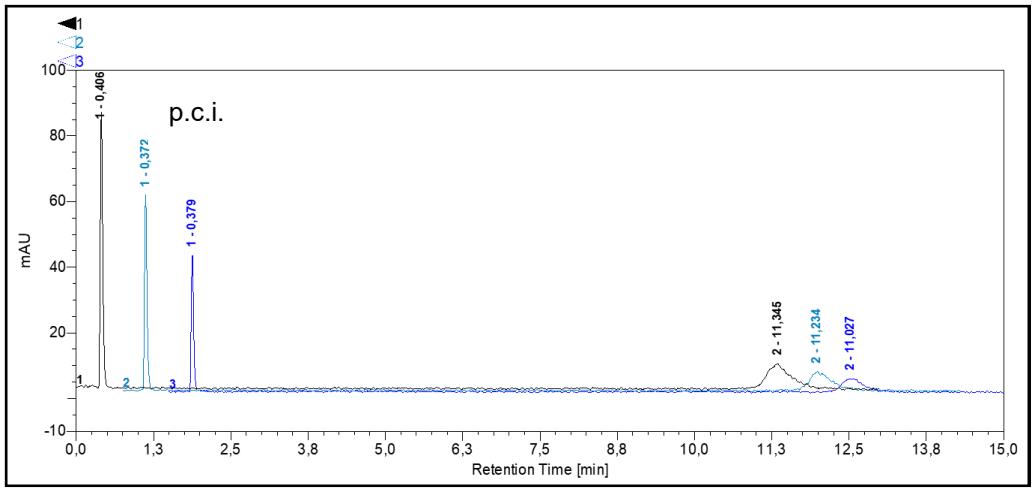

Figure 75: Radio-HPLC chromatogram of [^{18}F]**34** to determine the stability in NaOAc buffer (0.1 M, pH 5). Column: Phenomenex Luna® 5 µm PFP(2) 100 Å LC column 250×4.6 mm; eluent: 20% MeCN in PBS (0.01 M, pH 7.4). Flow rate: 1 mL/min. Abbreviation: p.c.i. – post-column injection.

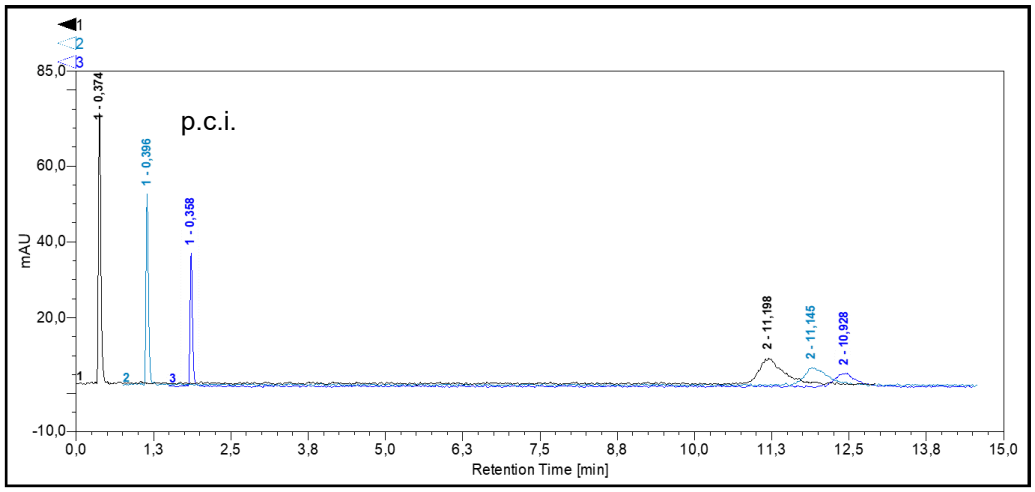

Figure 76: Radio-HPLC chromatogram of [^{18}F]**34** to determine the stability in H_2O. Column: Phenomenex Luna® 5 µm PFP(2) 100 Å LC column 250×4.6 mm; eluent: 20% MeCN in PBS (0.01 M, pH 7.4). Flow rate: 1 mL/min. Abbreviation: p.c.i. – post-column injection.

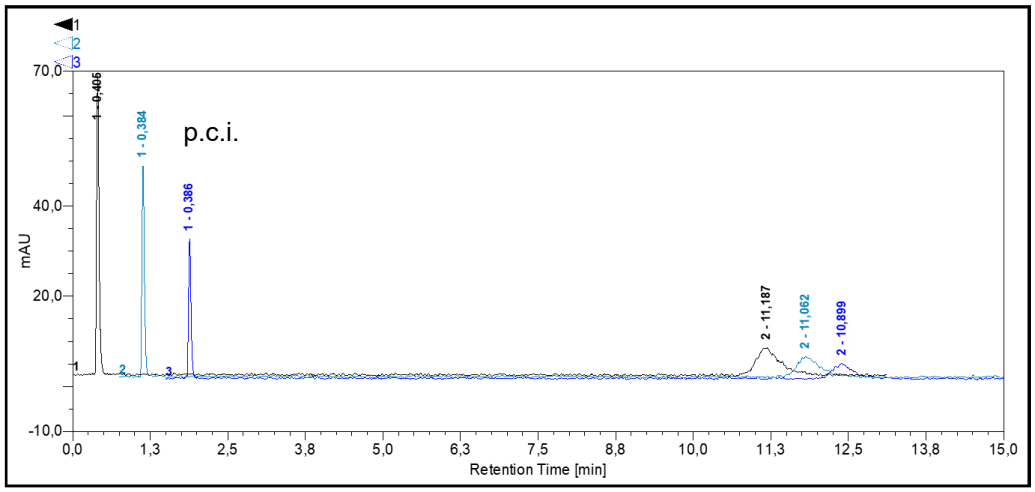

Figure 77: Radio-HPLC chromatogram of [^{18}F]**34** to determine the stability in PBS (0.01 M, pH 7.4). Column: Phenomenex Luna® 5 µm PFP(2) 100 Å LC column 250×4.6 mm; eluent: 20% MeCN in PBS (0.01 M, pH 7.4). Flow rate: 1 mL/min. Abbreviation: p.c.i. – post-column injection.

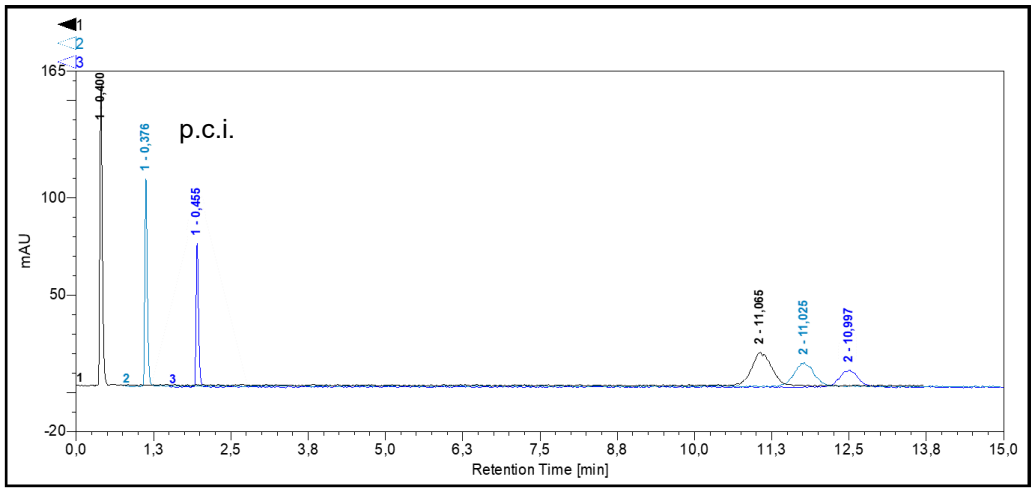

Figure 78: Radio-HPLC chromatogram of [^{18}F]**34** to determine the stability in $NaHCO_3$ solution (0.1 M, pH 8). Column: Phenomenex Luna® 5 µm PFP(2) 100 Å LC column 250×4.6 mm; eluent: 20% MeCN in PBS (0.01 M, pH 7.4). Flow rate: 1 mL/min. Abbreviation: p.c.i. – post-column injection.

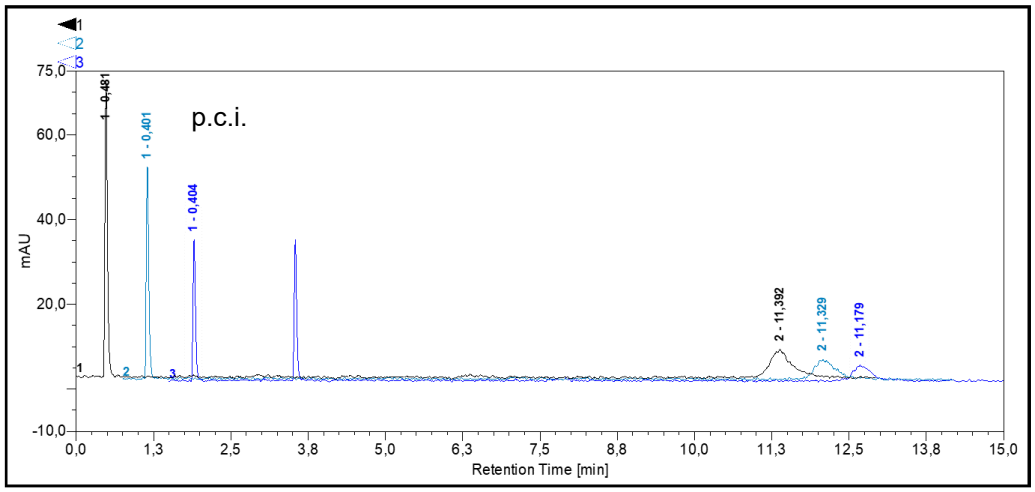

Figure 79: Radio-HPLC chromatogram of [^{18}F]**34** to determine the stability in NH_4OH/NH_4Cl buffer (pH 10). Column: Phenomenex Luna® 5 µm PFP(2) 100 Å LC column 250×4.6 mm; eluent: 20% MeCN in PBS (0.01 M, pH 7.4). Flow rate: 1 mL/min. Abbreviation: p.c.i. – post-column injection.

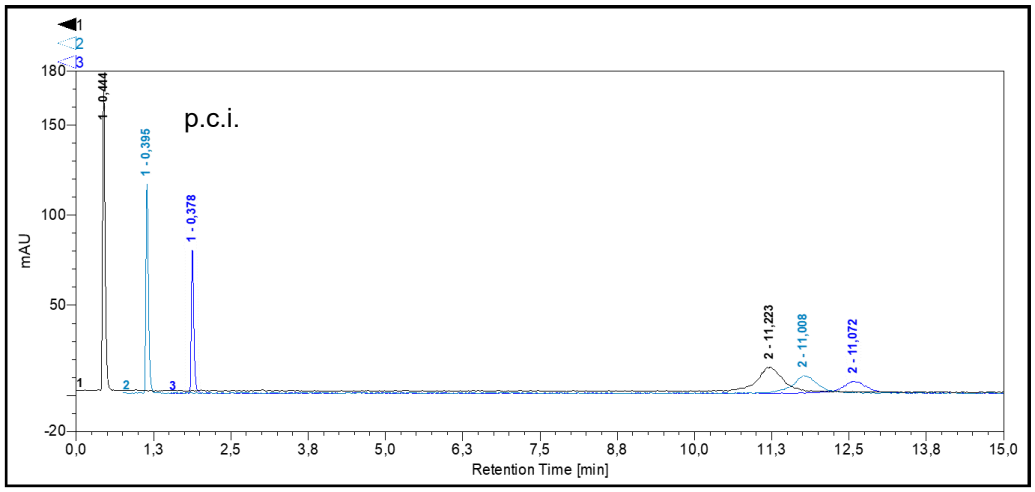

Figure 80: Radio-HPLC chromatogram of [^{18}F]**34** to determine the stability in NaOAc buffer (0.1 M, pH 4) after heating for 5 min at 100 °C. Column: Phenomenex Luna® 5 µm PFP(2) 100 Å LC column 250×4.6 mm; eluent: 20% MeCN in PBS (0.01 M, pH 7.4). Flow rate: 1 mL/min. Abbreviation: p.c.i. – post-column injection.

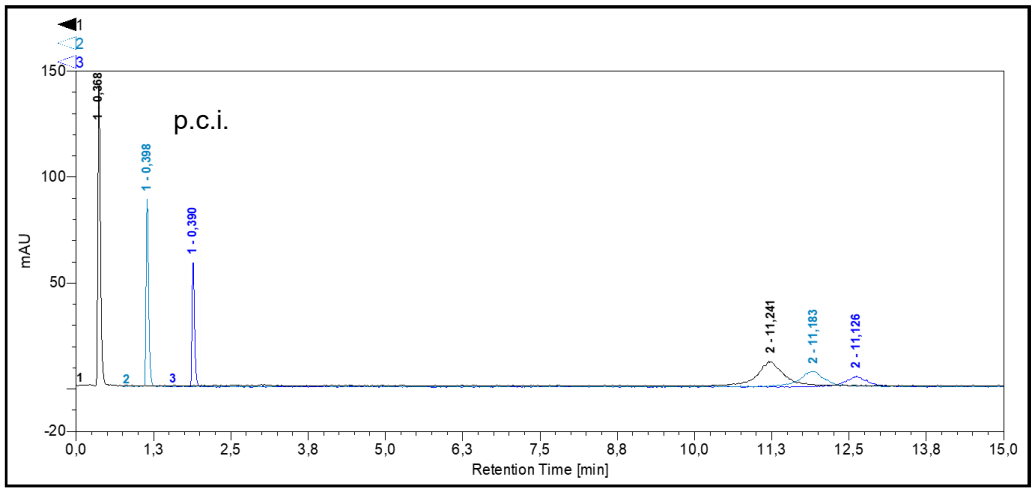

Figure 81: Radio-HPLC chromatogram of [^{18}F]**34** to determine the stability in NaOAc buffer (0.1 M, pH 4) after heating for 10 min at 100 °C. Column: Phenomenex Luna® 5 µm PFP(2) 100 Å LC column 250×4.6 mm; eluent: 20% MeCN in PBS (0.01 M, pH 7.4). Flow rate: 1 mL/min. Abbreviation: p.c.i. – post-column injection.

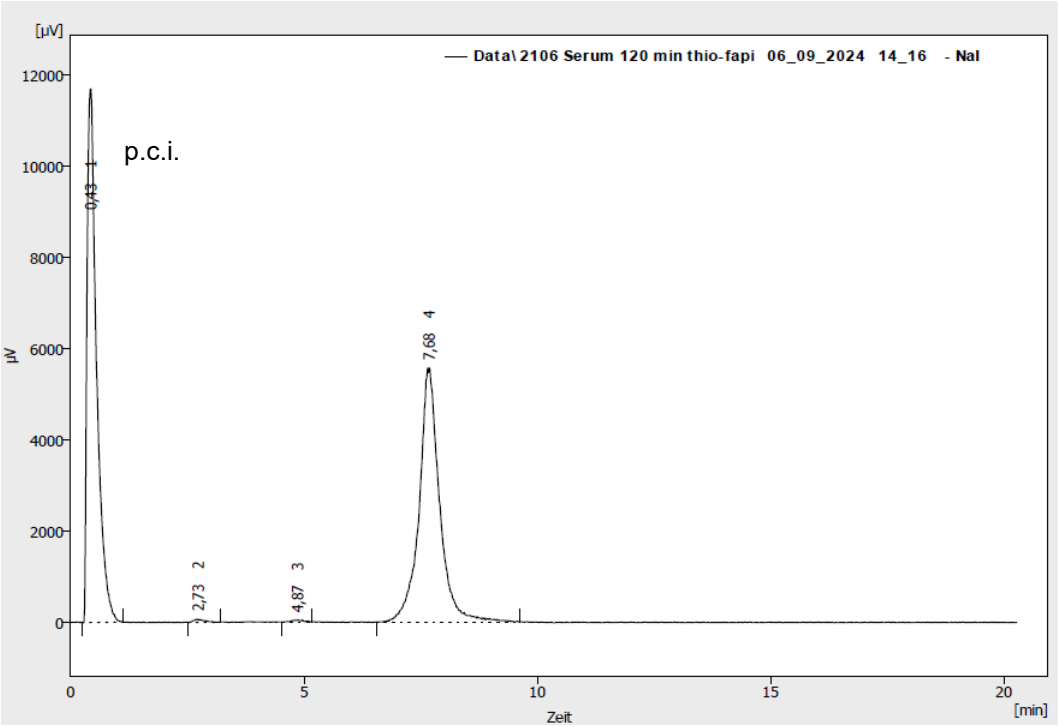

Figure 82: Radio-HPLC chromatogram of [^{18}F]**34** to determine the stability in human blood plasma after 120 min. Column: Phenomenex Luna® 5 µm PFP(2) 100 Å LC column 250×4.6 mm; eluent: 20% MeCN in PBS (0.01 M, pH 7.4). Flow rate. 1 mL/min. Shifting the retention time of [^{18}F]**34** by using a different HPLC. Abbreviation: p.c.i. – post-column injection.

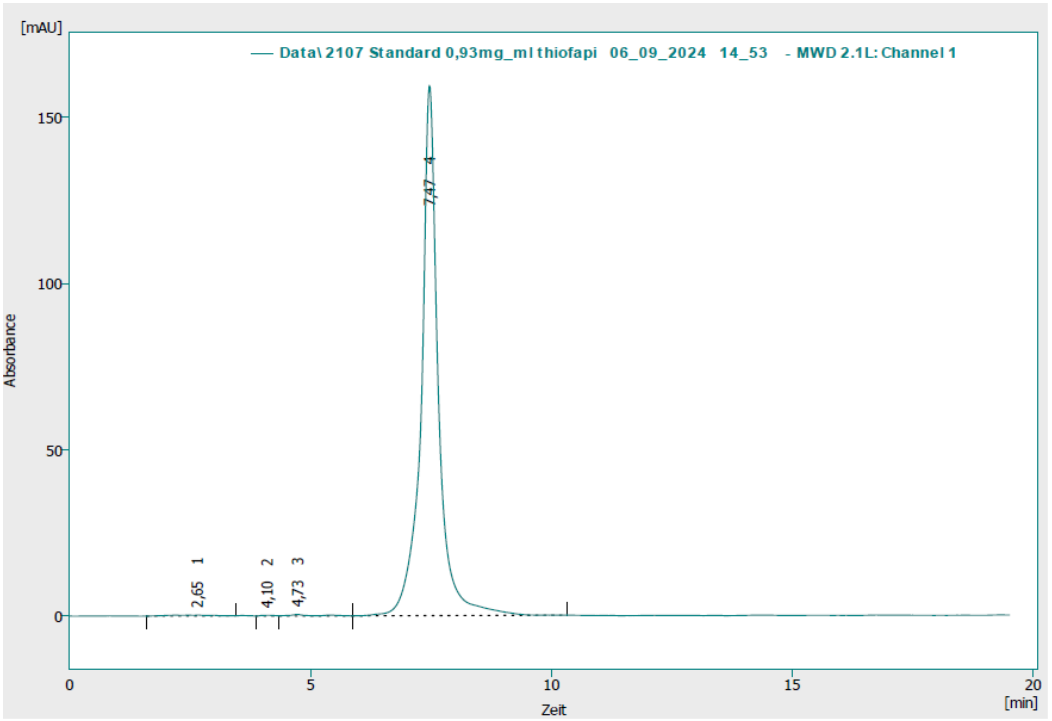

Figure 83: HPLC chromatogram of the non-radioactive reference compound **34**. UV chromatogram at 254 nm. Column: Phenomenex Luna® 5 µm PFP(2) 100 Å LC column 250×4.6 mm; eluent: 20% MeCN in PBS (0.01 M, pH 7.4). Flow rate. 1 mL/min.Confirmation of the retention time of [^{18}F]**34** due to the use of a different HPLC system for the reference compound.

6 References

[1] NobelPrize.org, "George de Hevesy – Facts - NobelPrize.org", can be found under https://www.nobelprize.org/prizes/chemistry/1943/hevesy/facts/, **2025**.

[2] G. Hevesy, *The Biochemical journal* **1923**, *17*. 439–445.

[3] S. Hoberück, K. Zöphel, M. G. Pomper, S. P. Rowe, A. Gafita, *J Nucl Med* **2023**, *64*. 1998–2000.

[4] Rutherford, E, Geiger, H., *Proceedings of the Royal Society of London. Series A, Containing Papers of a Mathematical and Physical Character* **1908**, *81*. 141–161.

[5] Feld, M., de Roo, M. (Ed.) *Geschichte der Nuklearmedizin in Europa*. *Mit 11 Tabellen*, Schattauer, Stuttgart, New York, **2000**.

[6] E. Rutherford, *The London, Edinburgh, and Dublin Philosophical Magazine and Journal of Science* **1911**, *21*. 669–688.

[7] a) D. Petroni, L. Menichetti, *J Radioanal Nucl Chem* **2024**, *333*. 4471–4484; b) I. J. Pruis, G. A. M. S. van Dongen, S. E. M. van Veldhuijzen Zanten, *International journal of molecular sciences* **2020**, *21*.

[8] D. E. Kuhl, R. Q. Edwards, *Radiology* **1963**, *80*. 653–662.

[9] H. Herzog, F. Rösch, *Pharmazie in unserer Zeit* **2005**, *34*. 468–473.

[10] G. Crișan, N. S. Moldovean-Cioroianu, D.-G. Timaru, G. Andrieș, C. Căinap, V. Chiș, *International journal of molecular sciences* **2022**, *23*.

[11] S. M. Qaim, *Nuclear Medicine and Biology* **2017**, *44*. 31–49.

[12] S. Rankowitz, J. S. Robertson, W. A. Higinbotham, M. J. Rosenblum, *POSITRON SCANNER FOR LOCATING BRAIN TUMORS*, **1961**.

[13] M. M. Ter-Pogossian, M. E. Phelps, E. J. Hoffman, N. A. Mullani, *Radiology* **1975**, *114*. 89–98.

[14] K. H. Lieser, *Nuclear and Radiochemistry*. *Fundamentals and applications*, Wiley, Berlin, New York, **2001**.

[15] P. Moskal, D. Kisielewska, C. Curceanu, E. Czerwiński, K. Dulski, A. Gajos, M. Gorgol, B. Hiesmayr, B. Jasińska, K. Kacprzak et al., *Physics in medicine and biology* **2019**, *64*. 55017.

[16] P. Moskal, B. Jasińska, E. Ł. Stępień, S. D. Bass, *Nat Rev Phys* **2019**, *1*. 527–529.

[17] M. D. Harpen, *Medical physics* **2004**, *31*. 57–61.

[18] Y. Keuthen, Dissertation Universität zu Köln, **2025**.

[19] a) A. Kasbollah, P. Eu, S. Cowell, P. Deb, *Journal of nuclear medicine technology* **2013**, *41*. 35–41; b) G. A. M. S. van Dongen, G. W. M. Visser, M. N. Lub-de Hooge, E. G. de Vries, L. R. Perk, *The oncologist* **2007**, *12*. 1379–1389.

[20] W. G. Kuhle, G. Porenta, S. C. Huang, D. Buxton, S. S. Gambhir, H. Hansen, M. E. Phelps, H. R. Schelbert, *Circulation* **1992**, *86*. 1004–1017.

[21] B. A. Herzog, L. Husmann, I. Valenta, O. Gaemperli, P. T. Siegrist, F. M. Tay, N. Burkhard, C. A. Wyss, P. A. Kaufmann, *Journal of the American College of Cardiology* **2009**, *54*. 150–156.

[22] P. Herscovitch, J. Markham, M. E. Raichle, *J Nucl Med* **1983**, *24*. 782–789.

[23] T. Maaniitty, J. Knuuti, A. Saraste, *Seminars in Nuclear Medicine* **2020**, *50*. 238–247.

[24] M. E. Raichle, W. R. Martin, P. Herscovitch, M. A. Mintun, J. Markham, *J Nucl Med* **1983**, *24*. 790–798.

[25] A. P. Fan, H. Jahanian, S. J. Holdsworth, G. Zaharchuk, *Journal of cerebral blood flow and metabolism : official journal of the International Society of Cerebral Blood Flow and Metabolism* **2016**, *36*. 842–861.

[26] G. D. Rabinovici, A. J. Furst, J. P. O'Neil, C. A. Racine, E. C. Mormino, S. L. Baker, S. Chetty, P. Patel, T. A. Pagliaro, W. E. Klunk et al., *Neurology* **2007**, *68*. 1205–1212.

[27] A. W. J. M. Glaudemans, R. H. Enting, M. A. A. M. Heesters, R. A. J. O. Dierckx, R. W. J. van Rheenen, A. M. E. Walenkamp, R. H. J. A. Slart, *European journal of nuclear medicine and molecular imaging* **2013**, *40*. 615–635.

[28] N. Ginovart, A. A. Wilson, J. H. Meyer, D. Hussey, S. Houle, *Synapse (New York, N.Y.)* **2003**, *47*. 123–133.

[29] X. Deng, J. Rong, L. Wang, N. Vasdev, L. Zhang, L. Josephson, S. H. Liang, *Angewandte Chemie (International ed. in English)* **2019**, *58*. 2580–2605.

[30] O. Jacobson, D. O. Kiesewetter, X. Chen, *Bioconjugate chemistry* **2015**, *26*. 1–18.

[31] N. A. Meanwell, *Journal of medicinal chemistry* **2018**, *61*. 5822–5880.

[32] B. K. Park, N. R. Kitteringham, *Drug metabolism reviews* **1994**, *26*. 605–643.

[33] D. Barnes-Seeman, J. Beck, C. Springer, *Current topics in medicinal chemistry* **2014**, *14*. 855–864.

[34] N. Sheikhi, M. Bahraminejad, M. Saeedi, S. S. Mirfazli, *European journal of medicinal chemistry* **2023**, *260*. 115758.

[35] A. Dash, F. F. R. Knapp, M. R. A. Pillai, *Current Radiopharmaceuticals* **2013**, *6*. 152–180.

[36] F. Zoller, M. Eisenhut, U. Haberkorn, W. Mier, *European journal of pharmacology* **2009**, *625*. 55–62.

[37] F. Rösch, *Radiochimica Acta* **2007**, *95*. 303–311.

[38] A. I. Kassis, S. J. Adelstein, *J Nucl Med* **2005**, *46 Suppl 1*. 4S-12S.

[39] W. A. Volkert, W. F. Goeckeler, G. J. Ehrhardt, A. R. Ketring, *J Nucl Med* **1991**, *32*. 174–185.

[40] D. Ersahin, I. Doddamane, D. Cheng, *Cancers* **2011**, *3*. 3838–3855.

[41] C. Wängler, I. Buchmann, M. Eisenhut, U. Haberkorn, W. Mier, *Protein and peptide letters* **2007**, *14*. 273–279.

[42] E. J. Hall, *Health physics* **2003**, *85*. 31–35.

[43] S. M. Qaim, B. Scholten, B. Neumaier, *J Radioanal Nucl Chem* **2018**, *318*. 1493–1509.

[44] W. D. Erwin, S. M. Spies, M. E. Kelly, P. Rao, T. E. Eckersberg-Rhodes, M. Nannapaneni, M. W. Groch, *Nuclear medicine communications* **2001**, *22*. 247–255.

[45] B. Brans, M. Monsieurs, G. Laureys, J.-M. Kaufman, H. Thierens, R. A. Dierckx, *Medical and pediatric oncology* **2002**, *38*. 41–46.

[46] G. A. Kaltsas, D. Papadogias, P. Makras, A. B. Grossman, *Endocrine-related cancer* **2005**, *12*. 683–699.

[47] S. Salih, A. Alkatheeri, W. Alomaim, A. Elliyanti, *Molecules (Basel, Switzerland)* **2022**, *27*.

[48] G. Kramer-Marek, J. Capala, *Tumor Biol.* **2012**, *33*. 629–640.

[49] C.-H. Yeong, M. Cheng, K.-H. Ng, *Journal of Zhejiang University. Science. B* **2014**, *15*. 845–863.

[50] S. M. Qaim, *Radiochimica Acta* **2001**, *89*. 297–304.

[51] S. Zhang, X. Wang, X. Gao, X. Chen, L. Li, G. Li, C. Liu, Y. Miao, R. Wang, K. Hu, *Signal transduction and targeted therapy* **2025**, *10*. 1.

[52] a) M. T. Ercan, M. Caglar, *Current pharmaceutical design* **2000**, *6*. 1085–1121; b) M. Gabriel, *Wiener medizinische Wochenschrift (1946)* **2012**, *162*. 430–439.

[53] A. Elliyanti in *Graves' Disease* (Ed.: R. Gensure), IntechOpen, **2021**.

[54] M. Luster, A. Pfestroff, H. Hänscheid, F. A. Verburg, *Seminars in Nuclear Medicine* **2017**, *47*. 126–134.

[55] D. A. Meier, D. R. Brill, D. V. Becker, S. E. M. Clarke, E. B. Silberstein, H. D. Royal, H. R. Balon, *J Nucl Med* **2002**, *43*. 856–861.

[56] D. Kayano, S. Kinuya, *Nuclear medicine and molecular imaging* **2018**, *52*. 254–265.

[57] a) L. Filippi, O. Schillaci, R. Cianni, O. Bagni, *Future oncology (London, England)* **2018**, *14*. 809–818; b) Z. Jia, W. Wang, *European Journal of Radiology* **2018**, *100*. 23–29.

[58] S. Navalkissoor, A. Grossman, *Neuroendocrinology* **2019**, *108*. 256–264.

[59] a) L. Nisa, G. Savelli, R. Giubbini, *Annals of nuclear medicine* **2011**, *25*. 75–85; b) A. L. Oei, R. H. Verheijen, M. V. Seiden, B. B. Benigno, A. Lopes, J. T. Soper, A. A. Epenetos, L. F. Massuger, *International journal of cancer* **2007**, *120*. 2710–2714; c) G. Sgouros, L. Bodei, M. R. McDevitt, J. R. Nedrow, *Nat Rev Drug Discov* **2020**, *19*. 589–608; d) T. A. Waldmann, J. D. White, J. A. Carrasquillo, J. C. Reynolds, C. H. Paik, O. A. Gansow, M. W. Brechbiel, E. S. Jaffe, T. A. Fleisher, C. K. Goldman et al., *Blood* **1995**, *86*. 4063–4075.

[60] a) K. P. Maresca, S. M. Hillier, F. J. Femia, D. Keith, C. Barone, J. L. Joyal, C. N. Zimmerman, A. P. Kozikowski, J. A. Barrett, W. C. Eckelman et al., *Journal of medicinal chemistry* **2009**, *52*. 347–357; b) F. Nan, T. Bzdega, S. Pshenichkin, J. T. Wroblewski, B.

Wroblewska, J. H. Neale, A. P. Kozikowski, *Journal of medicinal chemistry* **2000**, *43*. 772–774; c) E. O'Neill, V. Kersemans, P. D. Allen, S. Y. A. Terry, J. B. Torres, M. Mosley, S. Smart, B. Q. Lee, N. Falzone, K. A. Vallis et al., *Journal of nuclear medicine : official publication, Society of Nuclear Medicine* **2020**, *61*. 743–750; d) J. Strosberg, E. Wolin, B. Chasen, M. Kulke, D. Bushnell, M. Caplin, R. P. Baum, P. Kunz, T. Hobday, A. Hendifar et al., *Journal of clinical oncology : official journal of the American Society of Clinical Oncology* **2018**, *36*. 2578–2584.

[61] U. Hennrich, K. Kopka, *Pharmaceuticals (Basel, Switzerland)* **2019**, *12*.

[62] U. Hennrich, M. Eder, *Pharmaceuticals (Basel, Switzerland)* **2022**, *15*.

[63] S. Ahenkorah, I. Cassells, C. M. Deroose, T. Cardinaels, A. R. Burgoyne, G. Bormans, M. Ooms, F. Cleeren, *Pharmaceutics* **2021**, *13*.

[64] M. Silindir-Gunay, M. Karpuz, A. Y. Ozer, *Cancer biotherapy & radiopharmaceuticals* **2020**, *35*. 446–458.

[65] F. Rosar, J. Krause, M. Bartholomä, S. Maus, T. Stemler, I. Hierlmeier, J. Linxweiler, S. Ezziddin, F. Khreish, *Pharmaceutics* **2021**, *13*.

[66] C. Kratochwil, F. Bruchertseifer, F. L. Giesel, M. Weis, F. A. Verburg, F. Mottaghy, K. Kopka, C. Apostolidis, U. Haberkorn, A. Morgenstern, *Journal of nuclear medicine : official publication, Society of Nuclear Medicine* **2016**, *57*. 1941–1944.

[67] J. Kleynhans, M. Sathekge, T. Ebenhan, *Materials (Basel, Switzerland)* **2021**, *14*.

[68] D. Zuo, H. Wang, B. Yu, Q. Li, L. Gan, W. Chen, *Acta biochimica et biophysica Sinica* **2024**, *57*. 327–343.

[69] D. R. CORSON, K. R. MACKENZIE, E. SEGRÈ, *Nature* **1947**, *159*. 24.

[70] a) R. M. Lambrecht, S. Mirzadeh, *The International Journal of Applied Radiation and Isotopes* **1985**, *36*. 443–450; b) Y. Feng, M. R. Zalutsky, *Nuclear Medicine and Biology* **2021**, *100-101*. 12–23.

[71] M. R. Zalutsky, D. A. Reardon, G. Akabani, R. E. Coleman, A. H. Friedman, H. S. Friedman, R. E. McLendon, T. Z. Wong, D. D. Bigner, *J Nucl Med* **2008**, *49*. 30–38.

[72] H. Andersson, E. Cederkrantz, T. Bäck, C. Divgi, J. Elgqvist, J. Himmelman, G. Horvath, L. Jacobsson, H. Jensen, S. Lindegren et al., *J Nucl Med* **2009**, *50*. 1153–1160.

[73] G. Blessing, H. H. Coenen, K. Franken, S. M. Qaim, *International Journal of Radiation Applications and Instrumentation. Part A. Applied Radiation and Isotopes* **1986**, *37*. 1135–1139.

[74] T. J. RUTH, A. P. WOLF, *Radiochimica Acta* **1979**, *26*. 21–24.

[75] H. H. Coenen, *Ernst Schering Research Foundation workshop* **2007**. 15–50.

[76] E. Hess, G. Blessing, H. H. Coenen, S. M. Qaim, *Applied radiation and isotopes : including data, instrumentation and methods for use in agriculture, industry and medicine* **2000**, *52*. 1431–1440.

[77] T. Ido, C.-N. Wan, V. Casella, J. S. Fowler, A. P. WOLF, M. Reivich, D. E. Kuhl, *Journal of Labelled Compounds and Radiopharmaceuticals* **1978**, *14*. 175–183.

[78] a) G. W. M. Visser, B. W. v. Halteren, J. D. M. Herscheid, G. A. Brinkman, A. Hoekstra, *J. Chem. Soc., Chem. Commun.* **1984**. 655; b) R. Chirakal, G. Firnau, G. J. Schrobilgen, J. Mckay, E. S. Garnett, *The International Journal of Applied Radiation and Isotopes* **1984**, *35*. 401–404; c) M. Constantinou, F. I. Aigbirhio, R. G. Smith, C. A. Ramsden, V. W. Pike, *J. Am. Chem. Soc.* **2001**, *123*. 1780–1781; d) H. Teare, E. G. Robins, A. Kirjavainen, S. Forsback, G. Sandford, O. Solin, S. K. Luthra, V. Gouverneur, *Angewandte Chemie (International ed. in English)* **2010**, *49*. 6821–6824.

[79] a) M. J. Adam, B. F. Abeysekera, T. J. RUTH, S. Jivan, B. D. Pate, *TRIUMF, Vancouver, BC* **1983**, *25:5*; b) H. H. Coenen, S. M. Moerlein, *Journal of Fluorine Chemistry* **1987**, *36*. 63–75.

[80] J. M. Gillies, N. Najim, J. Zweit, *Applied radiation and isotopes : including data, instrumentation and methods for use in agriculture, industry and medicine* **2006**, *64*. 431–434.

[81] H. H. Coenen, M. Colosimo, M. Schüller, G. Stöcklin, *Journal of Labelled Compounds and Radiopharmaceuticals* **1986**, *23*. 587–595.

[82] R. Richarz, P. Krapf, F. Zarrad, E. A. Urusova, B. Neumaier, B. D. Zlatopolskiy, *Organic & biomolecular chemistry* **2014**, *12*. 8094–8099.

[83] F. Zarrad, B. D. Zlatopolskiy, P. Krapf, J. Zischler, B. Neumaier, *Molecules (Basel, Switzerland)* **2017**, *22*.

[84] N. Walter, J. Bertram, B. Drewes, V. Bahutski, M. Timmer, M. B. Schütz, F. Krämer, F. Neumaier, H. Endepols, B. Neumaier et al., *European journal of medicinal chemistry* **2022**, *237*. 114383.

[85] T. A. Hamlin, M. Swart, F. M. Bickelhaupt, *Chemphyschem : a European journal of chemical physics and physical chemistry* **2018**, *19*. 1315–1330.

[86] J. Ermert, B. Neumaier in *Radiopharmaceutical Chemistry* (Eds.: J. S. Lewis, A. D. Windhorst, B. M. Zeglis), Springer International Publishing, Cham, **2019**, pp. 273–283.

[87] K. Hamacher, H. H. Coenen, G. Stöcklin, *J Nucl Med* **1986**, *27*. 235–238.

[88] O. Rahman, M. Erlandsson, E. Blom, B. Långström, *Journal of Labelled Compounds and Radiopharmaceuticals* **2010**, *53*. 169–171.

[89] K. Bratteby, V. Shalgunov, M. M. Herth, *ChemMedChem* **2021**, *16*. 2612–2622.

[90] a) J. P. Holland, *Chemistry (Weinheim an der Bergstrasse, Germany)* **2018**, *24*. 16472–16483; b) Z. Li, H. Cai, M. Hassink, M. L. Blackman, R. C. D. Brown, P. S. Conti, J. M. Fox, *Chemical communications (Cambridge, England)* **2010**, *46*. 8043–8045.

[91] M. Suehiro, S. Vallabhajosula, S. J. Goldsmith, D. J. Ballon, *Applied radiation and isotopes : including data, instrumentation and methods for use in agriculture, industry and medicine* **2007**, *65*. 1350–1358.

[92] S.-J. Lee, S.-J. Oh, D.-Y. Chi, D.-H. Moon, J.-S. Ryu, *Bulletin of the Korean Chemical Society* **2012**, *33*. 2177–2180.

[93] S. J. Lee, S. J. Oh, W. Y. Moon, M. S. Choi, J. S. Kim, D. Y. Chi, D. H. Moon, J. S. Ryu, *Nuclear Medicine and Biology* **2011**, *38*. 593–597.

[94] a) S. J. Lee, M. T. Morales-Colón, A. F. Brooks, J. S. Wright, K. J. Makaravage, P. J. H. Scott, M. S. Sanford, *J. Org. Chem.* **2021**, *86*. 14121–14130; b) R. N. Krasikova, V. V. Orlovskaya, *Applied Sciences* **2022**, *12*. 321.

[95] E. E. Kwan, Y. Zeng, H. A. Besser, E. N. Jacobsen, *Nature chemistry* **2018**, *10*. 917–923.

[96] a) S. Rohrbach, A. J. Smith, J. H. Pang, D. L. Poole, T. Tuttle, S. Chiba, J. A. Murphy, *Angewandte Chemie International Edition* **2019**, *58*. 16368–16388; b) J. Meisenheimer, *Justus Liebigs Ann. Chem.* **1902**, *323*. 205–246.

[97] K. Hamacher, H. H. Coenen, *Applied radiation and isotopes : including data, instrumentation and methods for use in agriculture, industry and medicine* **2006**, *64*. 989–994.

[98] B. B. Quednow, V. Treyer, F. Hasler, N. Dörig, M. T. Wyss, C. Burger, K. M. Rentsch, G. Westera, P. A. Schubiger, A. Buck et al., *NeuroImage* **2012**, *59*. 3922–3932.

[99] V. W. Pike, F. I. Aigbirhio, *J. Chem. Soc., Chem. Commun.* **1995**. 2215–2216.

[100] a) F. Basuli, H. Wu, G. L. Griffiths, *Journal of Labelled Compounds and Radiopharmaceuticals* **2011**, *54*. 224–228; b) B. C. Lee, K. C. Lee, H. Lee, R. H. Mach, J. A. Katzenellenbogen, *Bioconjugate chemistry* **2007**, *18*. 514–523.

[101] a) L. Cai, S. Lu, V. W. Pike, *Eur J Org Chem* **2008**, *2008*. 2843; b) M. Tredwell, V. Gouverneur, *Angewandte Chemie (International ed. in English)* **2012**, *51*. 11426–11437.

[102] T. L. Ross, J. Ermert, C. Hocke, H. H. Coenen, *J. Am. Chem. Soc.* **2007**, *129*. 8018–8025.

[103] E. D. Hostetler, S. D. Jonson, M. J. Welch, J. A. Katzenellenbogen, *J. Org. Chem.* **1999**, *64*. 178–185.

[104] M. S. Yusubov, D. Y. Svitich, M. S. Larkina, V. V. Zhdankin, *Arkivoc* **2013**, *2013*. 364–395.

[105] B. H. Rotstein, N. A. Stephenson, N. Vasdev, S. H. Liang, *Nature communications* **2014**, *5*. 4365.

[106] L. Mu, C. R. Fischer, J. P. Holland, J. Becaud, P. A. Schubiger, R. Schibli, S. M. Ametamey, K. Graham, T. Stellfeld, L. M. Dinkelborg et al., *Eur J Org Chem* **2012**, *2012*. 889–892.

[107] T. Gendron, K. Sander, K. Cybulska, L. Benhamou, P. K. B. Sin, A. Khan, M. Wood, M. J. Porter, E. Årstad, *J. Am. Chem. Soc.* **2018**, *140*. 11125–11132.

[108] J. Han, Z.-M. Zhang, *Eur J Org Chem* **2024**, *27*.

[109] P. Xu, Da Zhao, F. Berger, A. Hamad, J. Rickmeier, R. Petzold, M. Kondratiuk, K. Bohdan, T. Ritter, *Angewandte Chemie (International ed. in English)* **2020**, *59*. 1956–1960.

[110] T. G. Luu, H.-K. Kim, *Org. Chem. Front.* **2023**, *10*. 5746–5781.

[111] Z. Liu, Y. Sun, T. Liu, *Frontiers in chemistry* **2022**, *10*. 883866.

[112] a) R. Halder, T. Ritter, *J. Org. Chem.* **2021**, *86*. 13873–13884; b) C. Wang, R. Lin, S. Yao, *Pharmaceutics* **2022**, *14*.

[113] E. Lee, A. S. Kamlet, D. C. Powers, C. N. Neumann, G. B. Boursalian, T. Furuya, D. C. Choi, J. M. Hooker, T. Ritter, *American Association for the Advancement of Science* **2011**.

[114] E. Lee, J. M. Hooker, T. Ritter, *J. Am. Chem. Soc.* **2012**, *134*. 17456–17458.

[115] N. Ichiishi, A. F. Brooks, J. J. Topczewski, M. E. Rodnick, M. S. Sanford, P. J. H. Scott, *Organic letters* **2014**, *16*. 3224–3227.

[116] M. Tredwell, S. M. Preshlock, N. J. Taylor, S. Gruber, M. Huiban, J. Passchier, J. Mercier, C. Génicot, V. Gouverneur, *Angewandte Chemie (International ed. in English)* **2014**, *53*. 7751–7755.

[117] A. V. Mossine, A. F. Brooks, K. J. Makaravage, J. M. Miller, N. Ichiishi, M. S. Sanford, P. J. H. Scott, *Organic letters* **2015**, *17*. 5780–5783.

[118] K. J. Makaravage, A. F. Brooks, A. V. Mossine, M. S. Sanford, P. J. H. Scott, *Organic letters* **2016**, *18*. 5440–5443.

[119] S. J. Lee, K. J. Makaravage, A. F. Brooks, P. J. H. Scott, M. S. Sanford, *Angewandte Chemie International Edition* **2019**, *58*. 3119–3122.

[120] L. S. Sharninghausen, A. F. Brooks, W. P. Winton, K. J. Makaravage, P. J. H. Scott, M. S. Sanford, *J. Am. Chem. Soc.* **2020**, *142*. 7362–7367.

[121] B. D. Zlatopolskiy, J. Zischler, P. Krapf, F. Zarrad, E. A. Urusova, E. Kordys, H. Endepols, B. Neumaier, *Chemistry (Weinheim an der Bergstrasse, Germany)* **2015**, *21*. 5972–5979.

[122] J. Zischler, N. Kolks, D. Modemann, B. Neumaier, B. D. Zlatopolskiy, *Chemistry (Weinheim an der Bergstrasse, Germany)* **2017**, *23*. 3251–3256.

[123] C. Hoffmann, N. Kolks, D. Smets, A. Haseloer, B. Gröner, E. A. Urusova, H. Endepols, F. Neumaier, U. Ruschewitz, A. Klein et al., *Chemistry (Weinheim an der Bergstrasse, Germany)* **2023**, *29*. e202202965.

[124] D. Block, H. H. Coenen, G. Stöcklin, *Journal of Labelled Compounds and Radiopharmaceuticals* **1988**, *25*. 201–216.

[125] M. Kuchar, M. Pretze, T. Kniess, J. Steinbach, J. Pietzsch, R. Löser, *Amino acids* **2012**, *43*. 1431–1443.

[126] N. Malik, H.-J. Machulla, C. Solbach, G. Winter, S. N. Reske, B. Zlatopolskiy, *Applied radiation and isotopes : including data, instrumentation and methods for use in agriculture, industry and medicine* **2011**, *69*. 1014–1018.

[127] S. Guhlke, H. H. Coenen, G. Stöcklin, *Applied radiation and isotopes : including data, instrumentation and methods for use in agriculture, industry and medicine* **1994**, *45*. 715–727.

[128] W. Cai, X. Zhang, Y. Wu, X. Chen, *J Nucl Med* **2006**, *47*. 1172–1180.

[129] D. O. Kiesewetter, O. Jacobson, L. Lang, X. Chen, *Applied radiation and isotopes : including data, instrumentation and methods for use in agriculture, industry and medicine* **2011**, *69*. 410–414.

[130] K. Kettenbach, H. Schieferstein, T. L. Ross, *BioMed research international* **2014**, *2014*. 361329.

[131] J. Marik, J. L. Sutcliffe, *Tetrahedron Letters* **2006**, *47*. 6681–6684.

[132] a) R. D. Carpenter, S. H. Hausner, J. L. Sutcliffe, *ACS medicinal chemistry letters* **2011**, *2*. 885–889; b) V. Bouvet, M. Wuest, F. Wuest, *Organic & biomolecular chemistry* **2011**, *9*. 7393–7399.

[133] Z. Gao, V. Gouverneur, B. G. Davis, *J. Am. Chem. Soc.* **2013**, *135*. 13612–13615.

[134] J. D. Way, C. Bergman, F. Wuest, *Chemical communications (Cambridge, England)* **2015**, *51*. 3838–3841.

[135] N. A. Lange, *Lange's handbook of chemistry*, McGraw-Hill Education, New York, **2013**.

[136] K. R. Scroggie, M. V. Perkins, J. M. Chalker, *Frontiers in chemistry* **2021**, *9*. 687678.

[137] H. M. ASKENASY, M. ANBAR, Y. LAOR, Z. LEWITUS, I. Z. KOSARY, S. GUTTMANN, *The American journal of roentgenology, radium therapy, and nuclear medicine* **1962**, *88*. 350–354.

[138] W. ENTZIAN, S. ARONOW, A. H. SOLOWAY, W. H. SWEET, *J Nucl Med* **1964**, *5*. 542–550.

[139] R. Ting, M. J. Adam, T. J. Ruth, D. M. Perrin, *J. Am. Chem. Soc.* **2005**, *127*. 13094–13095.

[140] V. Bernard-Gauthier, M. L. Lepage, B. Waengler, J. J. Bailey, S. H. Liang, D. M. Perrin, N. Vasdev, R. Schirrmacher, *Journal of nuclear medicine : official publication, Society of Nuclear Medicine* **2018**, *59*. 568–572.

[141] a) R. Ting, C. W. Harwig, J. Lo, Y. Li, M. J. Adam, T. J. Ruth, D. M. Perrin, *J. Org. Chem.* **2008**, *73*. 4662–4670; b) Z. Liu, D. Chao, Y. Li, R. Ting, J. Oh, D. M. Perrin, *Chemistry (Weinheim an der Bergstrasse, Germany)* **2015**, *21*. 3924–3928.

[142] a) Y. Li, J. Guo, S. Tang, L. Lang, X. Chen, D. M. Perrin, *American journal of nuclear medicine and molecular imaging* **2013**, *3*. 44–56; b) Y. Li, Z. Liu, C. W. Harwig, M. Pourghiasian, J. Lau, K.-S. Lin, P. Schaffer, F. Benard, D. M. Perrin, *American journal of*

nuclear medicine and molecular imaging **2013**, *3*. 57–70; c) Y. Li, Z. Liu, J. Lozada, M. Q. Wong, K.-S. Lin, D. Yapp, D. M. Perrin, *Nuclear Medicine and Biology* **2013**, *40*. 959–966.

[143] Z. Liu, Y. Li, J. Lozada, P. Schaffer, M. J. Adam, T. J. Ruth, D. M. Perrin, *Angewandte Chemie (International ed. in English)* **2013**, *52*. 2303–2307.

[144] Z. Liu, M. Pourghiasian, M. A. Radtke, J. Lau, J. Pan, G. M. Dias, D. Yapp, K.-S. Lin, F. Bénard, D. M. Perrin, *Angewandte Chemie (International ed. in English)* **2014**, *53*. 11876–11880.

[145] M. S. Rosenthal, A. L. Bosch, R. J. Nickles, S. J. Gatley, *The International Journal of Applied Radiation and Isotopes* **1985**, *36*. 318–319.

[146] U. Choudhry, K. E. Martin, S. Biagini, P. J. Blower, *Nuclear medicine communications* **2006**, *27*. 293.

[147] R. Schirrmacher, G. Bradtmöller, E. Schirrmacher, O. Thews, J. Tillmanns, T. Siessmeier, H. G. Buchholz, P. Bartenstein, B. Wängler, C. M. Niemeyer et al., *Angewandte Chemie (International ed. in English)* **2006**, *45*. 6047–6050.

[148] W. J. McBride, R. M. Sharkey, H. Karacay, C. A. D'Souza, E. A. Rossi, P. Laverman, C.-H. Chang, O. C. Boerman, D. M. Goldenberg, *J Nucl Med* **2009**, *50*. 991–998.

[149] S. J. Archibald, L. Allott, *EJNMMI radiopharmacy and chemistry* **2021**, *6*. 30.

[150] a) G. E. Smith, H. L. Sladen, S. C. G. Biagini, P. J. Blower, *Dalton transactions (Cambridge, England : 2003)* **2011**, *40*. 6196–6205; b) E. Farkas, T. Fodor, F. K. Kálmán, G. Tircsó, I. Tóth, *Reac Kinet Mech Cat* **2015**, *116*. 19–33.

[151] a) R. Bruce Martin, *Biochemical and Biophysical Research Communications* **1988**, *155*. 1194–1200; b) W. J. McBride, R. M. Sharkey, D. M. Goldenberg, *EJNMMI research* **2013**, *3*. 36.

[152] J. Šimeček, P. Hermann, H.-J. Wester, J. Notni, *ChemMedChem* **2013**, *8*. 95–103.

[153] C. A. D'Souza, W. J. McBride, R. M. Sharkey, L. J. Todaro, D. M. Goldenberg, *Bioconjugate chemistry* **2011**, *22*. 1793–1803.

[154] C. Da Pieve, L. Allott, C. D. Martins, A. Vardon, D. M. Ciobota, G. Kramer-Marek, G. Smith, *Bioconjugate Chem.* **2016**, *27*. 1839–1849.

[155] F. Cleeren, J. Lecina, E. M. F. Billaud, M. Ahamed, A. Verbruggen, G. M. Bormans, *Bioconjugate Chem.* **2016**, *27*. 790–798.

[156] F. Cleeren, J. Lecina, M. Ahamed, G. Raes, N. Devoogdt, V. Caveliers, P. McQuade, D. J. Rubins, W. Li, A. Verbruggen et al., *Theranostics* **2017**, *7*. 2924–2939.

[157] L. Russelli, J. Martinelli, F. de Rose, S. Reder, M. Herz, M. Schwaiger, W. Weber, L. Tei, C. D'Alessandria, *ChemMedChem* **2020**, *15*. 284–292.

[158] C. Anderson, J. Freeman, L. H. Lucas, M. Farley, H. Dalhoumi, T. S. Widlanski, *Biochemistry* **1997**, *36*. 2586–2594.

[159] a) A. L. Green, G. L. Sainsbury, B. Saville, M. Stansfield, *J. Chem. Soc.* **1958**. 1583; b) Y. Ashani, H. Leader, N. Rothschild, C. Dosoretz, *Biochemical pharmacology* **1998**, *55*. 159–168.

[160] M. Ghorab, J. M. Winfield, *Journal of Fluorine Chemistry* **1990**, *49*. 367–383.

[161] A. R. Studenov, M. J. Adam, J. S. Wilson, T. J. Ruth, *Journal of Labelled Compounds and Radiopharmaceuticals* **2005**, *48*. 497–500.

[162] Y. Hayakawa, M. Uchiyama, R. Noyori, *Tetrahedron Letters* **1986**, *27*. 4191–4194.

[163] R. P. Iyer, W. Egan, J. B. Regan, S. L. Beaucage, *J. Am. Chem. Soc.* **1990**, *112*. 1253–1254.

[164] B. Vabre, K. Chansaenpak, M. Wang, H. Wang, Z. Li, F. P. Gabbaï, *Chemical communications (Cambridge, England)* **2017**, *53*. 8657–8659.

[165] H. Jiang, A. Bansal, R. Goyal, K.-W. Peng, S. J. Russell, T. R. DeGrado, *Bioorganic & medicinal chemistry* **2018**, *26*. 225–231.

[166] H. Hong, L. Zhang, F. Xie, R. Zhuang, D. Jiang, H. Liu, J. Li, H. Yang, X. Zhang, L. Nie et al., *Nature communications* **2019**, *10*. 989.

[167] Z. Mou, X. Chen, C. Wang, T. Wang, H. Yang, Z. Li, *Tetrahedron Letters* **2021**, *68*. 152917.

[168] X. Tang, S. Lv, Z. Mou, X. Liu, Z. Li, *EJNMMI radiopharmacy and chemistry* **2024**, *9*. 4.

[169] Chao Wang, Lei Zhang, Zhaobiao Mou, Wanru Feng, Zhongjing Li, Hongzhang Yang, Xueyuan Chen, Shengji Lv, and Zijing Li, *Organic letters* **2021**, *23*. 4261–4266.

[170] F. B. d'Andrea, C. A. Townsend, *Cell chemical biology* **2019**, *26*. 878-884.e8.

[171] H. Yang, L. Zhang, H. Liu, Y. Zhang, Z. Mou, X. Chen, J. Li, F. He, Z. Li, *Theranostics* **2023**, *13*. 472–482.

[172] X. Deng, X. Zhu, *ACS omega* **2023**, *8*. 37720–37730.

[173] a) A. J. Brouwer, A. Jonker, P. Werkhoven, E. Kuo, N. Li, N. Gallastegui, J. Kemmink, B. I. Florea, M. Groll, H. S. Overkleeft et al., *Journal of medicinal chemistry* **2012**, *55*. 10995–11003; b) N. P. Grimster, S. Connelly, A. Baranczak, J. Dong, L. B. Krasnova, K. B. Sharpless, E. T. Powers, I. A. Wilson, J. W. Kelly, *J. Am. Chem. Soc.* **2013**, *135*. 5656–5668; c) C. Gu, D. A. Shannon, T. Colby, Z. Wang, M. Shabab, S. Kumari, J. G. Villamor, C. J. McLaughlin, E. Weerapana, M. Kaiser et al., *Chemistry & biology* **2013**, *20*. 541–548; d) A. Narayanan, L. H. Jones, *Chemical science* **2015**, *6*. 2650–2659; e) D. A. Shannon, C. Gu, C. J. McLaughlin, M. Kaiser, R. A. L. van der Hoorn, E. Weerapana, *Chembiochem : a European journal of chemical biology* **2012**, *13*. 2327–2330; f) Q. Zheng, J. L. Woehl, S. Kitamura, D. Santos-Martins, C. J. Smedley, G. Li, S. Forli, J. E. Moses, D. W. Wolan, K. B. Sharpless, *Proceedings of the National Academy of Sciences of the United States of America* **2019**, *116*. 18808–18814.

[174] G. Pascali, L. Matesic, B. Zhang, A. T. King, A. J. Robinson, A. T. Ung, B. H. Fraser, *EJNMMI radiopharmacy and chemistry* **2017**, *2*. 9.

[175] a) J. P. de Kleijn, H. J. Meeuwissen, B. van Zanten, *Vrije Univ., Amsterdam* **1975**; b) J. P. de Kleijn, B. van Zantan, *LABELING WITH REACTOR-PRODUCED F-18/RINE-18*, **1977**.

[176] T. R. Neal, S. Apana, M. S. Berridge, *Journal of Labelled Compounds and Radiopharmaceuticals* **2005**, *48*. 557–568.

[177] J. A. H. Inkster, K. Liu, S. Ait-Mohand, P. Schaffer, B. Guérin, T. J. Ruth, T. Storr, *Chemistry (Weinheim an der Bergstrasse, Germany)* **2012**, *18*. 11079–11087.

[178] L. Matesic, N. A. Wyatt, B. H. Fraser, M. P. Roberts, T. Q. Pham, I. Greguric, *J. Org. Chem.* **2013**, *78*. 11262–11270.

[179] E. Al-Momani, I. Israel, A. K. Buck, S. Samnick, *Applied radiation and isotopes : including data, instrumentation and methods for use in agriculture, industry and medicine* **2015**, *104*. 136–142.

[180] Q. Chen, P. Mayer, H. Mayr, *Angewandte Chemie (International ed. in English)* **2016**, *55*. 12664–12667.

[181] B. Zhang, G. Pascali, N. Wyatt, L. Matesic, M. A. Klenner, T. R. Sia, A. J. Guastella, M. Massi, A. J. Robinson, B. H. Fraser, *Journal of Labelled Compounds and Radiopharmaceuticals* **2018**, *61*. 847–856.

[182] B. Zhang, B. H. Fraser, M. A. Klenner, Z. Chen, S. H. Liang, M. Massi, A. J. Robinson, G. Pascali, *Chemistry (Weinheim an der Bergstrasse, Germany)* **2019**, *25*. 7613–7617.

[183] P. K. Chinthakindi, P. I. Arvidsson, *Eur J Org Chem* **2018**, *2018*. 3648–3666.

[184] H. Mukherjee, J. Debreczeni, J. Breed, S. Tentarelli, B. Aquila, J. E. Dowling, A. Whitty, N. P. Grimster, *Organic & biomolecular chemistry* **2017**, *15*. 9685–9695.

[185] A. Khoshnevisan, K. Chuamsaamarkkee, M. Boudjemeline, A. Jackson, G. E. Smith, A. D. Gee, G. O. Fruhwirth, P. J. Blower, *Journal of nuclear medicine : official publication, Society of Nuclear Medicine* **2017**, *58*. 156–161.

[186] J. Dong, L. Krasnova, M. G. Finn, K. B. Sharpless, *Angewandte Chemie (International ed. in English)* **2014**, *53*. 9430–9448.

[187] Q. Zheng, H. Xu, H. Wang, W.-G. H. Du, N. Wang, H. Xiong, Y. Gu, L. Noodleman, K. B. Sharpless, G. Yang et al., *J. Am. Chem. Soc.* **2021**, *143*. 3753–3763.

[188] M. H. Jeon, Y.-D. Kwon, M. P. Kim, G. B. Torres, J. K. Seo, J. Son, Y. H. Ryu, S. Y. Hong, J.-H. Chun, *Organic letters* **2021**, *23*. 2766–2771.

[189] M. P. Kim, H. Cho, S. Kayal, M. H. Jeon, J. K. Seo, J. Son, J. Jeong, S. Y. Hong, J.-H. Chun, *J. Org. Chem.* **2023**, *88*. 6263–6273.

[190] A. A. Fitzgerald, L. M. Weiner, *Cancer Metastasis Rev* **2020**, *39*. 783–803.

[191] a) A. Aoyama, W. T. Chen, *Proceedings of the National Academy of Sciences of the United States of America* **1990**, *87*. 8296–8300; b) M. L. Piñeiro-Sánchez, L. A. Goldstein, J. Dodt, L. Howard, Y. Yeh, H. Tran, W. S. Argraves, W. T. Chen, *Journal of Biological Chemistry* **1997**, *272*. 7595–7601; c) S. Mathew, M. J. Scanlan, B. K. Mohan Raj, V. V. Murty, P. Garin-Chesa, L. J. Old, W. J. Rettig, R. S. Chaganti, *Genomics* **1995**, *25*. 335–337.

[192] W. L. Monsky, C.-Y. Lin, A. Aoyama, T. Kelly, S. K. Akiyama, S. C. Mueller, W.-T. Chen, *Cancer Res* **1994**, *54*. 5702–5710.

[193] a) S. Iwasa, X. Jin, K. Okada, M. Mitsumata, A. Ooi, *Cancer letters* **2003**, *199*. 91–98; b) T. Kelly, S. Kechelava, T. L. Rozypal, K. W. West, S. Korourian, *Mod Pathol* **1998**, *11*. 855–863; c) Y. Mori, K. Kono, Y. Matsumoto, H. Fujii, T. Yamane, M. Mitsumata, W.-T. Chen, *Oncology* **2004**, *67*. 411–419.

[194] A. Lo, C.-P. Li, E. L. Buza, R. Blomberg, P. Govindaraju, D. Avery, J. Monslow, M. Hsiao, E. Puré, *JCI Insight* **2017**, *2*.

[195] J. N. Arnold, L. Magiera, M. Kraman, D. T. Fearon, *Cancer Immunology Research* **2014**, *2*. 121–126.

[196] K. N. Lee, K. W. Jackson, V. J. Christiansen, C. S. Lee, J.-G. Chun, P. A. McKee, *Blood* **2006**, *107*. 1397–1404.

[197] K. Aertgeerts, I. Levin, L. Shi, G. P. Snell, A. Jennings, G. S. Prasad, Y. Zhang, M. L. Kraus, S. Salakian, V. Sridhar et al., *Journal of Biological Chemistry* **2005**, *280*. 19441–19444.

[198] K. Jansen, L. Heirbaut, R. Verkerk, J. D. Cheng, J. Joossens, P. Cos, L. Maes, A.-M. Lambeir, I. de Meester, K. Augustyns et al., *Journal of medicinal chemistry* **2014**, *57*. 3053–3074.

[199] L. A. Goldstein, G. Ghersi, M. L. Piñeiro-Sánchez, M. Salamone, Y. Yeh, D. Flessate, W. T. Chen, *Biochimica et biophysica acta* **1997**, *1361*. 11–19.

[200] J. S. Rosenblum, J. W. Kozarich, *Current opinion in chemical biology* **2003**, *7*. 496–504.

[201] P. J. Collins, G. McMahon, P. O'Brien, B. O'Connor, *The International Journal of Biochemistry & Cell Biology* **2004**, *36*. 2320–2333.

[202] A. Altmann, U. Haberkorn, J. Siveke, *Journal of nuclear medicine : official publication, Society of Nuclear Medicine* **2021**, *62*. 160–167.

[203] P. Gascard, T. D. Tlsty, *Genes & development* **2016**, *30*. 1002–1019.

[204] L. Bu, H. Baba, N. Yoshida, K. Miyake, T. Yasuda, T. Uchihara, P. Tan, T. Ishimoto, *Oncogene* **2019**, *38*. 4887–4901.

[205] F. Liu, L. Qi, B. Liu, J. Liu, H. Zhang, D. Che, J. Cao, J. Shen, J. Geng, Y. Bi et al., *PloS one* **2015**, *10*. e0116683.

[206] A. Šimková, P. Bušek, A. Šedo, J. Konvalinka, *Biochimica et biophysica acta. Proteins and proteomics* **2020**, *1868*. 140409.

[207] Y. Hu, L. Ma, M. Wu, M. S. Wong, B. Li, S. Corral, Z. Yu, T. Nomanbhoy, S. Alemayehu, S. R. Fuller et al., *Bioorganic & medicinal chemistry letters* **2005**, *15*. 4239–4242.

[208] a) K. Narra, S. R. Mullins, H.-O. Lee, B. Strzemkowski-Brun, K. Magalong, V. J. Christiansen, P. A. McKee, B. Egleston, S. J. Cohen, L. M. Weiner et al., *Cancer biology & therapy* **2007**, *6*. 1691–1699; b) R. M. Eager, C. C. Cunningham, N. N. Senzer, J. Stephenson, S. P. Anthony, S. J. O'Day, G. Frenette, A. C. Pavlick, B. Jones, M. Uprichard et al., *BMC cancer* **2009**, *9*. 263.

[209] K. Jansen, L. Heirbaut, J. D. Cheng, J. Joossens, O. Ryabtsova, P. Cos, L. Maes, A.-M. Lambeir, I. de Meester, K. Augustyns et al., *ACS medicinal chemistry letters* **2013**, *4*. 491–496.

[210] a) C. Y. Edosada, C. Quan, C. Wiesmann, T. Tran, D. Sutherlin, M. Reynolds, J. M. Elliott, H. Raab, W. Fairbrother, B. B. Wolf, *Journal of Biological Chemistry* **2006**, *281*. 7437–7444; b) T. Tran, C. Quan, C. Y. Edosada, M. Mayeda, C. Wiesmann, D. Sutherlin, B. B. Wolf, *Bioorganic & medicinal chemistry letters* **2007**, *17*. 1438–1442; c) T.-Y. Tsai, T. Hsu, C.-T. Chen, J.-H. Cheng, M.-C. Chiou, C.-H. Huang, Y.-J. Tseng, T.-K. Yeh, C.-Y. Huang, K.-C. Yeh et al., *Bioorganic & medicinal chemistry letters* **2009**, *19*. 1908–1912; d) T.-Y. Tsai, T.-K. Yeh, X. Chen, T. Hsu, Y.-C. Jao, C.-H. Huang, J.-S. Song, Y.-C. Huang, C.-H. Chien, J.-H. Chiu et al., *Journal of medicinal chemistry* **2010**, *53*. 6572–6583; e) O. Ryabtsova, K. Jansen, S. van Goethem, J. Joossens, J. D. Cheng, A.-M. Lambeir, I. de Meester, K. Augustyns, P. van der Veken, *Bioorganic & medicinal chemistry letters* **2012**, *22*. 3412–3417; f) S. E. Poplawski, J. H. Lai, Y. Li, Z. Jin, Y. Liu, W. Wu, Y. Wu, Y. Zhou, J. L. Sudmeier, D. G. Sanford et al., *Journal of medicinal chemistry* **2013**, *56*. 3467–3477.

[211] A. Loktev, T. Lindner, W. Mier, J. Debus, A. Altmann, D. Jäger, F. Giesel, C. Kratochwil, P. Barthe, C. Roumestand et al., *Journal of nuclear medicine : official publication, Society of Nuclear Medicine* **2018**, *59*. 1423–1429.

[212] T. Lindner, A. Loktev, A. Altmann, F. Giesel, C. Kratochwil, J. Debus, D. Jäger, W. Mier, U. Haberkorn, *Journal of nuclear medicine : official publication, Society of Nuclear Medicine* **2018**, *59*. 1415–1422.

[213] A. Loktev, T. Lindner, E.-M. Burger, A. Altmann, F. Giesel, C. Kratochwil, J. Debus, F. Marmé, D. Jäger, W. Mier et al., *Journal of nuclear medicine : official publication, Society of Nuclear Medicine* **2019**, *60*. 1421–1429.

[214] K. R. Chandekar, A. Prashanth, S. Vinjamuri, R. Kumar, *Diagnostics (Basel, Switzerland)* **2023**, *13*.

[215] C. Kratochwil, P. Flechsig, T. Lindner, L. Abderrahim, A. Altmann, W. Mier, S. Adeberg, H. Rathke, M. Röhrich, H. Winter et al., *Journal of nuclear medicine : official publication, Society of Nuclear Medicine* **2019**, *60*. 801–805.

[216] M. Li, M. H. Younis, Y. Zhang, W. Cai, X. Lan, *Eur J Nucl Med Mol Imaging* **2022**, *49*. 2844–2868.

[217] E. S. Moon, F. Elvas, G. Vliegen, S. de Lombaerde, C. Vangestel, S. de Bruycker, an Bracke, E. Eppard, L. Greifenstein, B. Klasen et al., *EJNMMI radiopharmacy and chemistry* **2020**, *5*. 19.

[218] E. S. Moon, S. Ballal, M. P. Yadav, C. Bal, Y. van Rymenant, S. Stephan, an Bracke, P. van der Veken, I. de Meester, F. Roesch, *American journal of nuclear medicine and molecular imaging* **2021**, *11*. 476–491.

[219] S. Ballal, M. P. Yadav, E. S. Moon, F. Roesch, S. Kumari, S. Agarwal, M. Tripathi, R. K. Sahoo, B. S. Mangu, A. Tupalli et al., *Thyroid : official journal of the American Thyroid Association* **2022**, *32*. 65–77.

[220] Y. Pang, L. Zhao, J. Fang, J. Chen, L. Meng, L. Sun, H. Wu, Z. Guo, Q. Lin, H. Chen, *Journal of nuclear medicine : official publication, Society of Nuclear Medicine* **2023**, *64*. 1449–1455.

[221] F. L. Giesel, S. Adeberg, M. Syed, T. Lindner, L. D. Jiménez-Franco, E. Mavriopoulou, F. Staudinger, E. Tonndorf-Martini, S. Regnery, S. Rieken et al., *Journal of nuclear medicine : official publication, Society of Nuclear Medicine* **2021**, *62*. 201–207.

[222] X.-Y. Cui, Z. Li, Z. Kong, Y. Liu, H. Meng, Z. Wen, C. Wang, J. Chen, M. Xu, Y. Li et al., *Nature* **2024**, *630*. 206–213.

[223] S. Guardiola, R. Prades, L. Mendieta, A. J. Brouwer, J. Streefkerk, L. Nevola, T. Tarragó, R. M. J. Liskamp, E. Giralt, *Cell chemical biology* **2018**, *25*. 1031-1037.e4.

[224] T. Yoshimoto, T. Nishimura, T. Kita, D. Tsuru, *Journal of biochemistry* **1983**, *94*. 1179–1190.

[225] a) E. Di Daniel, C. P. Glover, E. Grot, M. K. Chan, T. H. Sanderson, J. H. White, C. L. Ellis, K. T. Gallagher, J. Uney, J. Thomas et al., *Molecular and cellular neurosciences* **2009**, *41*. 373–382; b) M. J. Hannula, T. T. Myöhänen, J. Tenorio-Laranga, P. T. Männistö, J. A. Garcia-Horsman, *Neuroscience* **2013**, *242*. 140–150.

[226] A. López, T. Tarragó, E. Giralt, *Expert opinion on therapeutic patents* **2011**, *21*. 1023–1044.

[227] C. P. Wilson, S. J. Webb, *Chemical communications (Cambridge, England)* **2008**. 4007–4009.

[228] A. J. Brouwer, M. C. F. Monnee, R. M. J. Liskamp, *Synthesis* **2000**.

[229] J. Coulomb, V. Certal, M.-H. Larraufie, C. Ollivier, J.-P. Corbet, G. Mignani, L. Fensterbank, E. Lacôte, M. Malacria, *Chemistry (Weinheim an der Bergstrasse, Germany)* **2009**, *15*. 10225–10232.

[230] S. Kakaei, J. Xu, *Tetrahedron* **2013**, *69*. 9068–9075.

[231] B. Belleau, R. Martel, G. Lacasse, M. Ménard, N. L. Weinberg, Y. G. Perron, *Journal of the American Chemical Society* **1968**, *90*. 823–824.

[232] B. Belleau, G. Malek, *Journal of the American Chemical Society* **1968**, *90*. 1651–1652.

[233] 현명호, 진종성, 유재정, *Bulletin of the Korean Chemical Society* **1998**, *19*. 1392–1395.

[234] B. Zacharie, T. P. Connolly, C. L. Penney, *J. Org. Chem.* **1995**, *60*. 7072–7074.

[235] M. M. Joullie, K. M. Lassen, *Arkivoc* **2010**, *2010*. 189–250.

[236] A. Boruah, I. N. Rao, J. P. Nandy, S. K. Kumar, A. C. Kunwar, J. Iqbal, *J. Org. Chem.* **2003**, *68*. 5006–5008.

[237] J. J. Rojas, J. A. Bull, *Trends in Chemistry* **2025**, *7*. 124–133.

[238] K. M. Gillespie, C. J. Sanders, P. O'Shaughnessy, I. Westmoreland, C. P. Thickitt, P. Scott, *J. Org. Chem.* **2002**, *67*. 3450–3458.

[239] K. Green, *Tetrahedron Letters* **1989**, *30*. 4807–4810.

[240] P. F. Jackson, D. C. Cole, B. S. Slusher, S. L. Stetz, L. E. Ross, B. A. Donzanti, D. A. Trainor, *Journal of medicinal chemistry* **1996**, *39*. 619–622.

[241] S. Humpert, C. Hoffmann, F. Neumaier, B. D. Zlatopolskiy, B. Neumaier, *Journal of chromatography. B, Analytical technologies in the biomedical and life sciences* **2023**, *1228*. 123847.

[242] A. R. Katritzky, X.-L. Cui, B. Yang, P. J. Steel, *J. Org. Chem.* **1999**, *64*. 1979–1985.

[243] a) M. I. Bruce, G. Shaw, F. G. A. Stone, *J. Chem. Soc., Dalton Trans.* **1973**. 1667; b) A. R. Katritzky, B. V. Rogovoy, A. Y. Mitrokhin, *Arkivoc* **2003**, *2002*. 17–27; c) Z. Xu, M. Cen, Z. Chen, L. Yao, C. Li, B. Tang, L. Liu, T. Huang, T. Chen, L.-B. Han, *Organic letters* **2024**, *26*. 7004–7009.

[244] F. A. Davis, S. H. Lee, H. Xu, *J. Org. Chem.* **2004**, *69*. 3774–3781.

[245] F. A. Davis, H. Zhang, S. H. Lee, *Organic letters* **2001**, *3*. 759–762.

[246] L. Pache, S. K. Chanda, M. D. Vamos, N. D. P. Cosford, P. Teriete, J. Marlett, A. Diaz, J. A. T. Young, WO2015187998 (A2), **2015**.

[247] M. A. Larsen, E. T. Hennessy, M. C. Deem, Y.-H. Lam, J. Saurí, A. C. Sather, *Journal of the American Chemical Society* **2020**, *142*. 726–732.

[248] G. Liu, D. A. Cogan, J. A. Ellman, *J. Am. Chem. Soc.* **1997**, *119*. 9913–9914.

[249] D. A. Cogan, J. A. Ellman, *J. Am. Chem. Soc.* **1999**, *121*. 268–269.

[250] G. Liu, D. A. Cogan, T. D. Owens, T. P. Tang, J. A. Ellman, *J. Org. Chem.* **1999**, *64*. 1278–1284.

[251] T. Mukade, D. R. Dragoli, J. A. Ellman, *J. Comb. Chem.* **2003**, *5*. 590–596.

[252] J. T. Reeves, M. D. Visco, M. A. Marsini, N. Grinberg, C. A. Busacca, A. E. Mattson, C. H. Senanayake, *Organic letters* **2015**, *17*. 2442–2445.

[253] S. Higashibayashi, H. Tohmiya, T. Mori, K. Hashimoto, M. Nakata, *Synlett* **2004**. 457–460.

[254] F. A. Davis, S. Lee, H. Yan, D. D. Titus, *Organic letters* **2001**, *3*. 1757–1760.

[255] D. F. Bocian, H. M. Pickett, T. C. Rounds, H. L. Strauss, *J. Am. Chem. Soc.* **1975**, *97*. 687–695.

[256] K. M. Brinner, J. A. Ellman, *Organic & biomolecular chemistry* **2005**, *3*. 2109–2113.

[257] J. Vargas-Caporali, A. van der Lee, G. Dewynter, E. Juaristi, *LOC* **2018**, *15*. 352–358.

[258] a) M. Mourabet, A. El Rhilassi, H. El Boujaady, M. Bennani-Ziatni, R. El Hamri, A. Taitai, *Journal of Saudi Chemical Society* **2015**, *19*. 603–615; b) A. Bhatnagar, E. Kumar, M. Sillanpää, *Chemical Engineering Journal* **2011**, *171*. 811–840; c) X. Fan, D. J. Parker, M. D. Smith, *Water research* **2003**, *37*. 4929–4937; d) S. Gao, J. Cui, Z. Wei, *Journal of Fluorine Chemistry* **2009**, *130*. 1035–1041; e) M. Jiménez-Reyes, M. Solache-Ríos, *Journal of Hazardous Materials* **2010**, *180*. 297–302; f) J. Lin, S. Raghavan, D. W. Fuerstenau, *Colloids and Surfaces* **1981**, *3*. 357–370; g) Z. Mou, Y. Zhu, L. Zhang, M. Ma, Z. Li, Y. Guo, J. Zheng, Z. Zhao, K. Zhang, X. Chen et al., *J. Am. Chem. Soc.* **2024**, *146*. 17517–17529.

[259] an Bracke, R. van Elzen, P. van der Veken, K. Augustyns, I. de Meester, A.-M. Lambeir, *Clinica chimica acta; international journal of clinical chemistry* **2019**, *495*. 154–160.

[260] J. Tenorio-Laranga, J. I. Venäläinen, P. T. Männistö, J. A. García-Horsman, *The FEBS journal* **2008**, *275*. 4415–4427.

[261] J.-M. Vatèle, *Tetrahedron* **2004**, *60*. 4251–4260.

[262] A. Kers, J. Stawiński, L. Dembkowski, A. Kraszewski, *Tetrahedron* **1997**, *53*. 12691–12698.

[263] H. Mayr, U. von der Brüggen, *Chem. Ber.* **1988**, *121*. 339–345.

[264] P. Li, J. Wang, K. Zhao, *J. Org. Chem.* **1998**, *63*. 3151–3152.

7 Annex

7.1 Prostate-specific membrane antigen (PSMA) as biological target

Prostate-specific membrane antigen (PSMA) was first identified in 1987 by Horoszewicz *et al*. on the cell membrane of the prostate cancer (PCa) cell line LNCaP.[1] It is a type II transmembrane glycoprotein that exhibits both folate hydrolase and *N*-acetyl-α-linked acid dipeptidase activity. PSMA is involved in the regulation of intestinal folate uptake and catalyzes the hydrolysis of *N*-acetyl-*L*-aspartyl-*L*-glutamate (NAAG) to *N*-acetyl-*L*-aspartame and *L*-glutamate, the latter being an important neurotransmitter in the central nervous system.[2,3] The PSMA protein consists of 750 amino acids and is structurally divided into three domains: an intracellular domain composed of 19 amino acids, a transmembrane domain composed of 24 amino acids, and an extracellular domain composed of the remaining 707 amino acids.[1,4] PSMA expression is typically low in normal prostate tissue, the lacrimal glands, the duodenum, and the nervous system. In contrast, its expression is 100- to 1000-fold higher in metastatic, castration-resistant, and poorly differentiated prostate cancer tissues.[1,5] Due to this significant overexpression in malignant tissues, PSMA has emerged as a prominent target for the diagnosis and treatment of prostate cancer, which was the second most frequent cancer in men in 2022.[1,6]

7.1.1 PSMA inhibitors

PSMA-targeting ligands can be separated into three categories, which comprise aptamers, monoclonal antibodies, and small molecule inhibitors.[1] Small molecule PSMA inhibitors interact with the binuclear zinc active site of PSMA, which is essential for the hydrolytic activity[2] and formed by the amino acids His377, Asp387, Glu425, Asp435, and His553.[2,7] These inhibitors can be further classified into three distinct categories: sulfur compounds, including sulfhydryl and mercaptan derivatives; urea derivatives; and phosphorus compounds, comprising phosphate and phosphoramides.[1] Although sulfur compounds exhibit favorable oral bioavailability and membrane permeability, their clinical application is limited by a poor stability and the inability to bind specifically to PSMA. Urea compounds, composed of two amino acids linked by an urea group, are rapidly internalized by PSMA-expressing cells and exhibit high affinity and specificity for PSMA. Consequently, they are the most widely used PSMA inhibitors for the diagnosis and treatment of prostate cancer.[1,8] As of 2022, phosphorus-based compounds have not progressed beyond the preclinical research phase, showing low tumor uptake and relatively slow kinetics.[1]

The interest in ^{18}F-labeled radiotracers for PSMA imaging has grown significantly in recent years due to the advantages of ^{18}F.[9] Among the most studied ^{18}F-labeled PSMA tracers are [^{18}F]PSMA-1007[10,11] and [^{18}F]CDFPyL[12], both of which have recently been introduced into clinical practice.[3] [^{18}F]PSMA-1007 can be prepared in high RCYs, is not excreted via the urinary tract, and shows higher tumor uptake than other PSMA radioligands.[3] In 2019, Zlatopolskiy *et al*. developed the radiotracer [^{18}F]JK-PSMA-7, which has proven particularly suitable for the detection of small PSMA-positive lesions.[13] This tracer has undergone successfully evaluation in two clinical trials involving patients with biochemically recurrent prostate cancer.[3,14]

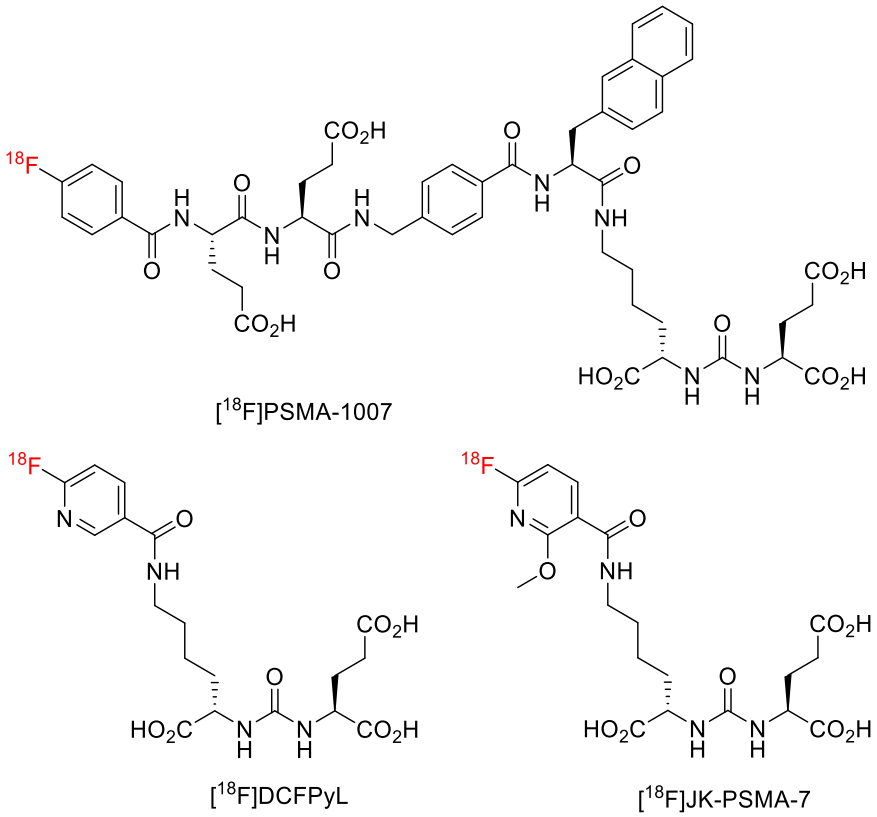

Figure 84: Structures of the urea-based PSMA inhibitors [^{18}F]PSMA-1007[10,11], [^{18}F]DCFPyL[12] and [^{18}F]JK-PSMA-7[13].

The first PSMA inhibitor with subnanomolar affinity identified was 2-PMPA (Figure 85)[15,16], which remains the reference standard for determining the binding affinity of PSMA inhibitors *in vitro*. However, it was not investigated for radiochemical applications until 2019, since it was long assumed that modification of the pentanedioic acid group or its substituents would result in a significant loss of affinity.[15] Nevertheless, Pomper *et al*. demonstrated that highly effective PSMA inhibitors could still be obtained by modifying the glutamate group.[17] Graham *et al*. introduced fluorine into the pentanedioic acid group (Figure 85) and synthesized various fluorinated stereoisomer derivatives of 2-PMPA. In addition, a mixture of stereoisomers was labeled with ^{18}F, enabling the acquisition of promising PET images in tumor-bearing mice.[15]

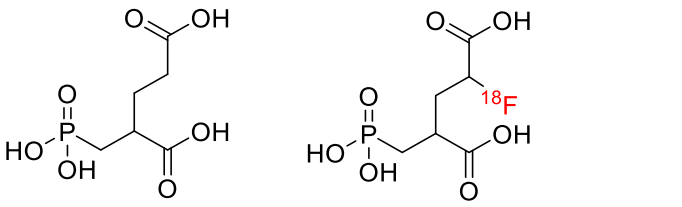

2-PMPA

rac-2-[^{18}F]Fluoro-4-(phosphonomethyl)pentanedioic acid

Figure 85: Structures of 2-PMPA[16] and *rac*-2-[^{18}F]fluoro-4-(phosphonomethyl)pentanedioic acid.[15]

7.2 Aim

2-(Phosphonomethyl)-pentandioic acid (2-PMPA, Figure 85) is a nanomolar PSMA inhibitor, which is widely used in preclinical studies. While 4-^{18}F-fluorinated 2-PMPA derivatives were prepared and evaluated on their suitability for prostate carcinoma PET-imaging[15], 2-PMPA analog with [^{18}F]fluorophosphonate instead of phosphonate group has not been synthesized yet (Figure 86). Therefore, a fluorine-18-labeled derivative of 2-PMPA would potentially be suitable for PET imaging. The aim of this subproject was to synthesize the [^{18}F]fluorophosphonate analog of 2-PMPA and to investigate its properties.

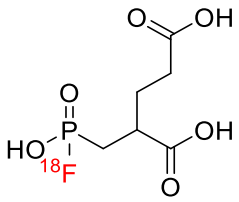

[^{18}F]39

Figure 86: Structure of the novel 2-PMPA analog.

7.3 Results and discussion

7.3.1 Preliminary work on the synthesis of the novel ^{18}F-labeled 2-PMPA analog

*7.3.1.1 Synthesis of the precursor di-tert-butyl 2-[(diphenoxyphosphoryl)methyl]pentanedioate (**36**) and the non-radioactive reference compound (5-(tert-butoxy)-2-(tert-butoxycarbonyl)-5-oxopentyl)phosphonofluoridate ammonium salt (**37**)*

The synthesis of **36** was performed in two steps. In the first step, *tert*-butyl acrylate was dimerized with tributylphosphine to afford the intermediate **35** in 73% yield (lit. 75%).[18] Subsequently, **36** was obtained from **35** by trimethylaluminum-mediated conjugate addition of diphenylphosphite, resulting in a yield of 32% (Scheme 56).[16]

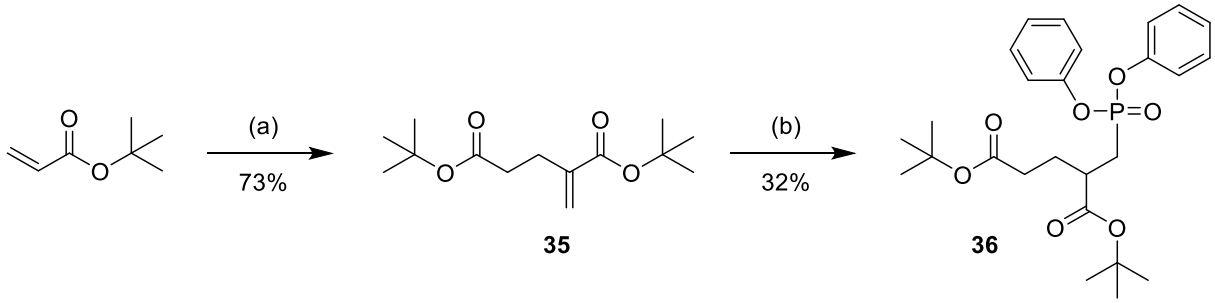

Scheme 56: Synthesis of **36**. Reaction conditions: a) tributylphosphine, rt, 2.5 h[18]; b) diphenylphosphite, trimethylaluminum, CH_2Cl_2, 0 °C–rt, overnight.[16]

Next, the protected non-radioactive reference compound (5-(*tert*-butoxy)-2-(*tert*-butoxycarbonyl)-5-oxopentyl)phosphonofluoridate ammonium salt (**37**) was synthesized as follows. **36** was dissolved in MeCN and fluorinated with NH_4F (Scheme 57).[19] After purification by semi-preparative HPLC and subsequent freeze-drying, the reference compound **37** was obtained in 25% yield.

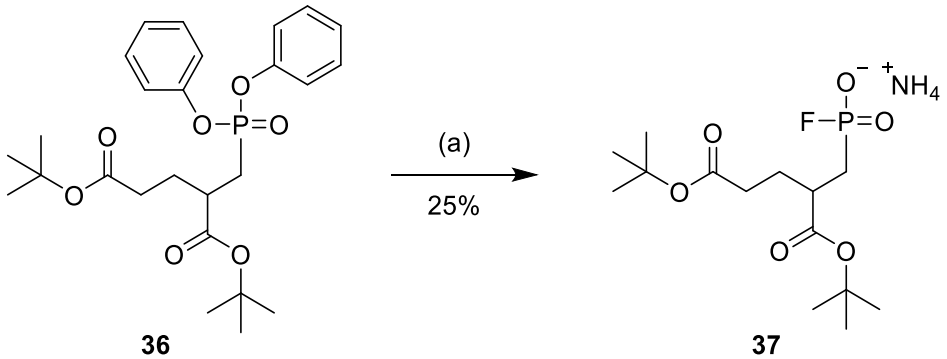

Scheme 57: Synthesis of the protected non-radioactive reference compound **37**. Reaction conditions: NH_4F, MeCN, 60 °C, 15 h.[19]

*7.3.1.2 Radiosynthesis of (5-(tert-butoxy)-2-(tert-butoxycarbonyl)-5-oxopentyl)phosphono[^{18}F]fluoridate ([^{18}F]**37**)*

The radiolabeling conditions for di-*tert*-butyl 2-[(diphenoxyphosphoryl)methyl]pentanedioate (**36**) were selected based on the optimized protocol previously established for the radiosynthesis of (4-(*tert*-butoxy)-2-methyl-4-oxobutan-2-yl)phosphono[^{18}F]fluoridate ([^{18}F]**16**, section 3.2.2.2). Specifically, [^{18}F]fluoride was fixed on a QMA cartridge and eluted with a solution of TEAOTf (1 mg) in MeOH (1 mL). After removal of the solvent, a solution of precursor **36** (0.5 µmol) in MeCN (100 µL) was added and the reaction mixture was stirred for 15 min at 90 °C before it was quenched with H_2O (500 µL). The radiochemical conversions (RCCs) thus obtained were 69 ± 10% (n=5), so that no further optimization of the reaction conditions was necessary. [^{18}F]**37** was isolated by semi-preparative HPLC followed by solid-phase extraction on a C18 Plus Light cartridge. After formulation in EtOH (0.5–1.0 mL), the protected intermediate was obtained in radiochemical yields (RCYs) of 33 ± 5% (n=2), activity yields (AYs) of 23 ± 6% (n=2), and radiochemical purities (RCPs) of >85%.

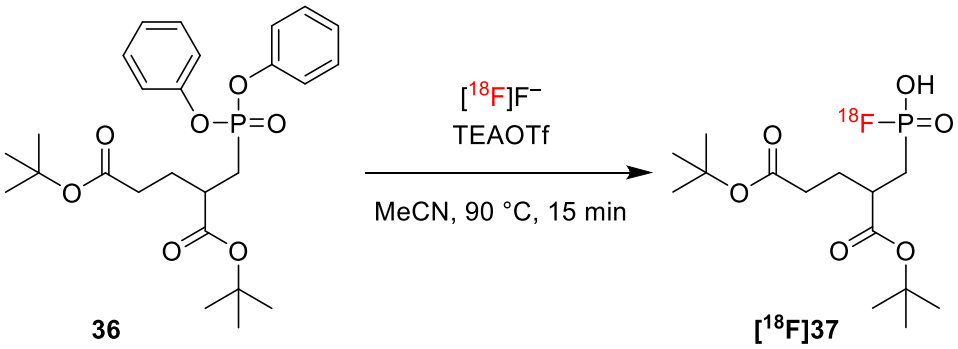

Scheme 58: Radiosynthesis of [^{18}F]**37**

Although the non-radioactive reference compound for the [^{18}F]2-PMPA analog (2,4-dicarboxybutyl)phosphono[^{18}F]fluoridate ([^{18}F]**39**, Figure 86) had not yet been synthesized, initial attempt were made to deprotect the radiolabeled intermediate [^{18}F]**37**.

In the first trial, after formulation of [^{18}F]**37** in EtOH, the solvent was evaporated and 6 M HCl (100 µL) was added. The reaction mixture was heated to 90 °C for 10 min, after which the remaining acid was evaporated. Upon dissolving the residue in EtOH (500 µL) and transferring the solution to another vessel, it was determined that only 4% of the radioactivity was dissolved. A further 23% was retained in the reactor, while 55% adhered to the septum. These findings suggest significant defluorination, likely with formation and volatilization of H[^{18}F]F, during the process.

In a second attempt, TFA (50 µL) was used instead of HCl and the reaction mixture was heated to 60 °C for 10 min. After an aliquot of the reaction mixture was taken for TLC analysis prior to

deprotection (Figure 87, lane 5), the acid was evaporated, the residue was dissolved in PBS (1 mL), and the resulting solution was transferred to a second vessel. Subsequent analysis revealed that 25% of the activity remained in the vessel, while only 8% was detected in the PBS fraction. The vessel containing the remaining 25% of the activity was then rinsed with EtOH (500 µL), which was transferred to another vessel. Of the remaining activity, 41% was recovered in the EtOH, while 56% remained in the vessel. TLC analysis of all fractions revealed a spot in the EtOH fraction that did not correspond to [^{18}F]fluoride (Figure 87, lane 2). In contrast, only [^{18}F]fluoride was detected in the PBS and TFA fractions (Figure 87, lanes 1 and 4). The absence of a second spot in the TFA fraction indicates that the unidentified spot in the EtOH fraction was not the desired product. However, its exact identity could not be elucidated due to the lack of a non-radioactive reference compound.

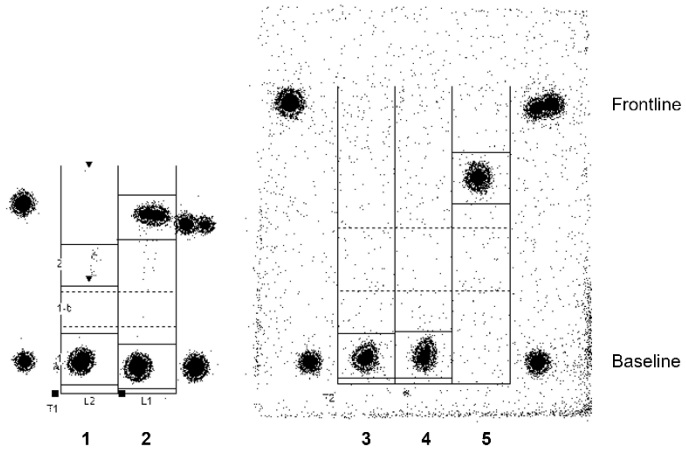

Figure 87: TLC analysis of the second attempt of deprotection of [^{18}F]**37**. TLC solvent mixture: *n*-BuOH:H_2O:HAc = 5:1:1. Lanes: 1: PBS fraction; 5: EtOH fraction; 3: Diluted [^{18}F]fluoride solution in H_2O; 4: TFA fraction; 5: Diluted solution of [^{18}F]**37** in H_2O.

*7.3.1.3 Attempt to synthesize the non-radioactive reference compound **39** from **36***

The synthesis of the non-radioactive reference compound (2,4-dicarboxybutyl)phosphonofluoridate (**39**) can be accomplished via two distinct reaction pathways (Scheme 59). In the first approach, the *tert*-butyl protecting groups in **36** are cleaved prior to fluorination of the diphenylphosphonic acid group. In the second, the two reaction steps are reversed.

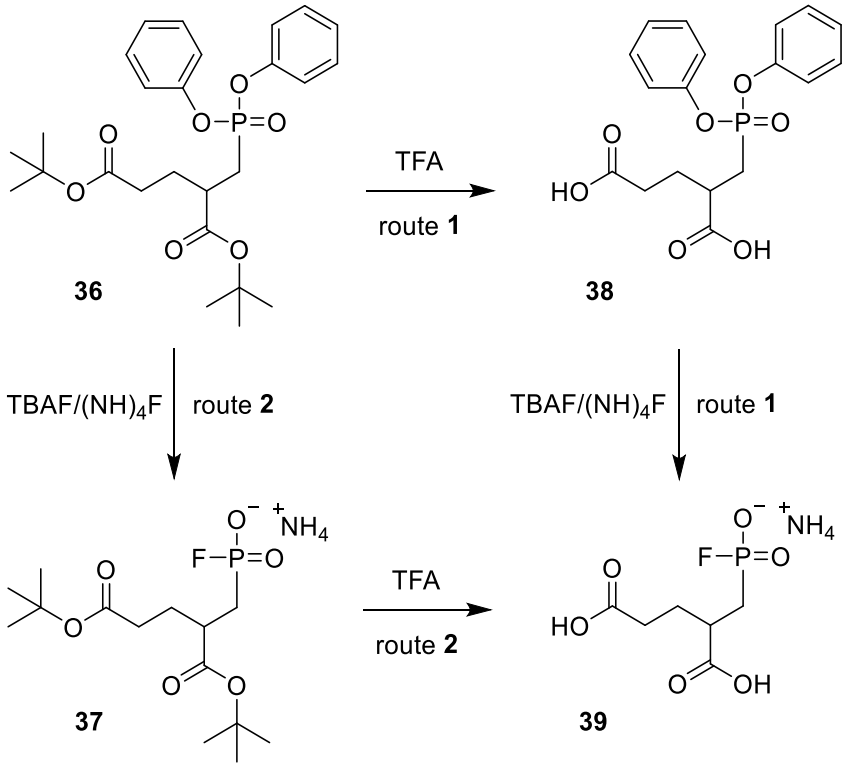

Scheme 59: Reaction pathways for the synthesis of **39**. Route 1 involves initial deprotection of the carboxylic acids followed by fluorination, while route 2 performs the two steps in reverse order.

Initially, route 1 was employed for the synthesis of **39**. The deprotection of **36** was performed using TFA in CH_2Cl_2. Following concentration of the reaction mixture, compound **38** was obtained, but it was not pure as determined by ^{1}H-NMR. Several purification attempts were carried out. First, the product was isolated by column chromatography, using a mobile phase composed of EtOAc in cyclohexane with 1% acetic acid as additive. Despite this, the product remained impure in ^{1}H-NMR. Next, an attempt was made to isolate the product by semi-preparative HPLC using a mobile phase composed of MeCN in H_2O with 0.1% TFA as additive. A sample was taken from the HPLC fraction before the MeCN was evaporated, and the aqueous phase was freeze-dried. Analytical HPLC was used to monitor the product immediately after removal, and again 30 and 60 min after the first injection. These analyses revealed that the product (t_R = 8.8–9.0 min, Figure 88) gradually decomposed in the mobile phase at ambient temperature, resulting in the formation of a by-product (t_R = 7.3–7.4 min, Figure 88). The declining concentration of the product and concurrent rise in by-product levels indicate a time-dependent degradation, most likely caused by the acidic hydrolysis.[20] The ^{1}H-NMR spectrum of the freeze-dried sample confirmed the presence of the product, albeit with impurities likely attributable to the by-product. Finally, the HPLC fraction containing the product was frozen immediately after collection using liquid nitrogen and subsequently freeze-dried. This approach enabled the isolation of an ^{1}H-NMR pure product, with a yield of 24%.

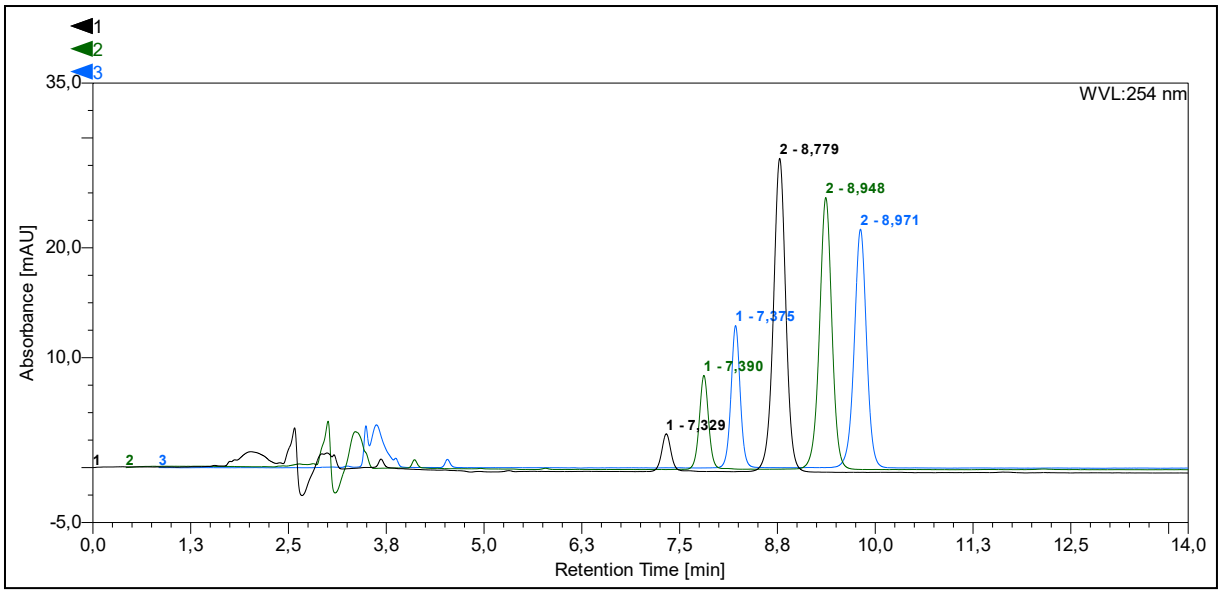

Figure 88: HPLC traces showing degradation of **38** in the semi-preparative HPLC mobile phase. Retention time of the product: t_R = 8.8–9.0 min; retention time of the by-product: t_R = 7.3–7.4 min. Black: injection close to HPLC cut; green: 30 minutes later; blue: 60 minutes later. Column: MultoKrom® 100-5 C18 AQ LC column 250×4.6 mm; eluent: 40% MeCN (0.1% TFA). Flow rate: 1 mL/min.

Fluorination was attempted using both ammonium fluoride[19] in MeCN and TBAF[21] in THF. In both cases, the product peak was detected in the negative mass spectrum, but the product could not be isolated.

Subsequently, the second reaction pathway was explored. In this route, **36** was fluorinated first, followed by deprotection of the carboxylic acid groups in the intermediate product **37**. Initial attempts to fluorinate diphenylphosphonate **36** with TBAF in THF[21] failed. In contrast, fluorination with ammonium fluoride[19] was successful, as confirmed by analytical HPLC. After isolation by semi-preparative HPLC, **37** was obtained in 25% yield. However, subsequent deprotection with TFA did not result in formation of the desired reference compound **39**. It is important to note that **39** is expected to be highly hydrophilic and not UV-active, which significantly limits detection by UV-based HPLC systems. An alternative approach would involve using an evaporative light scattering detector (ELSD) for detection of **39**. However, while suitable for the non-radioactive reference compound, this method is incompatible with radiolabeled compounds. Due to their hydrophilic nature, **39** and its ^{18}F-labeled isotopolog may also elute close to the solvent front in RP chromatography, potentially co-eluting with unreacted [^{18}F]fluoride. Therefore, prior to radiolabeling, the reference compound should be tested on various HPLC columns to determine an optimal separation profile.

*7.3.1.4 Synthesis of the labeling precursor bis(dicyclopropylmethyl) 2-[(diphenoxyphosphoryl)methyl]pentanedioate (**43**) and attempt to synthesize the non-radioactive reference compound (5-(dicyclopropylmethoxy)-2-[(dicyclopropylmethoxy)carbonyl]-5-oxopentyl)phosphonofluoridate ammonium salt (**44**)*

Due to the sensitivity of **38** after semi-preparative HPLC and the harsh reaction conditions required for removing *tert*-butyl groups, an alternative protecting group strategy was employed. The dicyclopropyl group was selected to protect the carboxylic acids, as it can be removed under milder acidic conditions compared to the *tert*-butyl group.

For precursor synthesis, dicyclopropylmethanol (**40**) was first prepared from dicyclopropyl ketone in 79% yield (Scheme 60).[22] **40** was then reacted with acryloyl chloride in the presence of triethylamine and DMAP,[23,24] to form dicyclopropylmethyl acrylate (**41**) in 57% yield. Subsequent dimerization of **41** with tributylphosphine[18] yielded **42** in 63% yield. Finally, trimethylaluminum-mediated conjugate addition of diphenylphosphite[16,25] to **42** afforded the desired precursor **43**, albeit in a yield of only 13%. The reaction formed a viscous material that complicated extraction and required acidic quenching, potentially leading to partial removal of the acid-labile protecting groups. To mitigate this, milder quenching agents like 0.01 N HCl or saturated NH_4Cl solution were used. Mass spectrometry and ^{1}H-NMR analysis identified diphenyl (dicyclopropylmethyl)phosphonate (Scheme 61) as a by-product. Due to the low yield and the required acidic processing, alternative reaction conditions were sought.

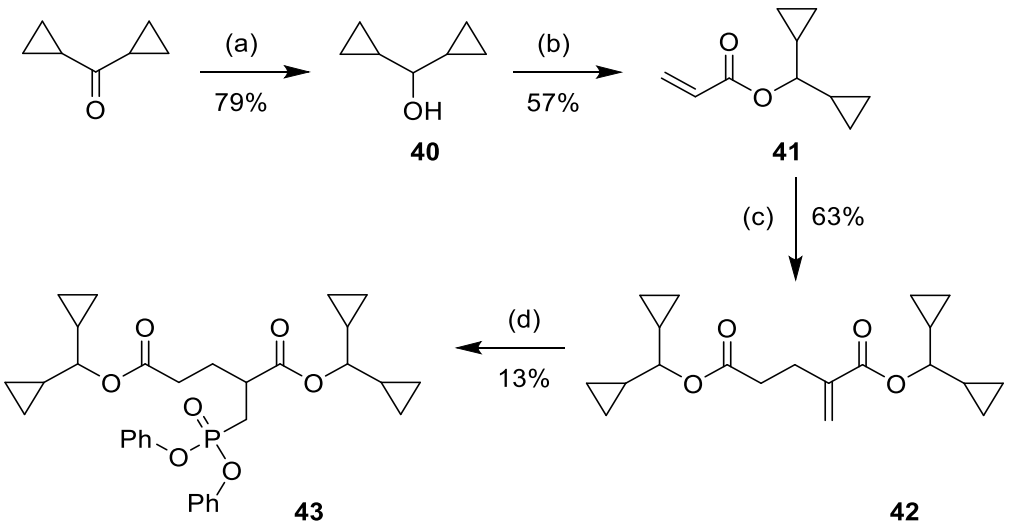

Scheme 60: Reaction route for the synthesis of precursor **43**. Reaction conditions: a) $NaBH_4$, MeOH, 0 °C–rt, 3 h[22]; b) acryloyl chloride, Et_3N, DMAP, CH_2Cl_2, 0 °C–rt, overnight[23,24]; c) tributylphosphine, rt, 2 h[18]; d) diphenyl phosphite, Me_3Al, CH_2Cl_2, 0 °C–rt, overnight.[16]

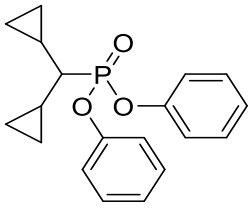

Scheme 61: Diphenyl (dicyclopropylmethyl)phosphonate was identified as a by-product in the synthesis of **43** with Me_3Al by ESI-LRMS and ^1H-NMR spectroscopy.

One alternative method explored, the Pudovik reaction with tributylphosphine,[26] did not afford the desired product. In contrast, a phospho-Michael addition using K_2CO_3 as a base[15] furnished **43** in albeit in a fair 27% yield.

Mass spectrometry using ESI(+)-LRMS at standard conditions (MeOH/H_2O +0.2% AcOH, 50 V cone voltage) revealed, in addition to the expected product peak at m/z = 567.12 (74) and its NH_4^+ adduct at m/z = 584.17 (45), signals corresponding to the monocarboxylic acid (m/z = 473.10 [33]) and dicarboxylic acid (m/z = 379.09 [100]). To determine whether this was a mass effect, mass spectra were recorded under different cone voltages and with and without acetic acid in the mobile phase.
At a cone voltage of 20 V, the product peak's relative intensity decreased (from 74% to 41%) while that of the NH_4^+ adduct increased (from 45% to 66%) and those of the mono- and dicarboxylic acids did not change significantly. At 100 V, the product peak became predominant (relative frequency of 100%), while the signals of the acids decreased (to 32% for the dicarboxylic acid and 23% for the monocarboxylic acid). In the absence of 0.2% acetic acid, the mono- and dicarboxylic acid adducts disappeared. These observations confirm that **43** is present as a dicyclopropyl-protected derivative and that the acidic conditions in the ESI-LRMS solvent cause partial deprotection.

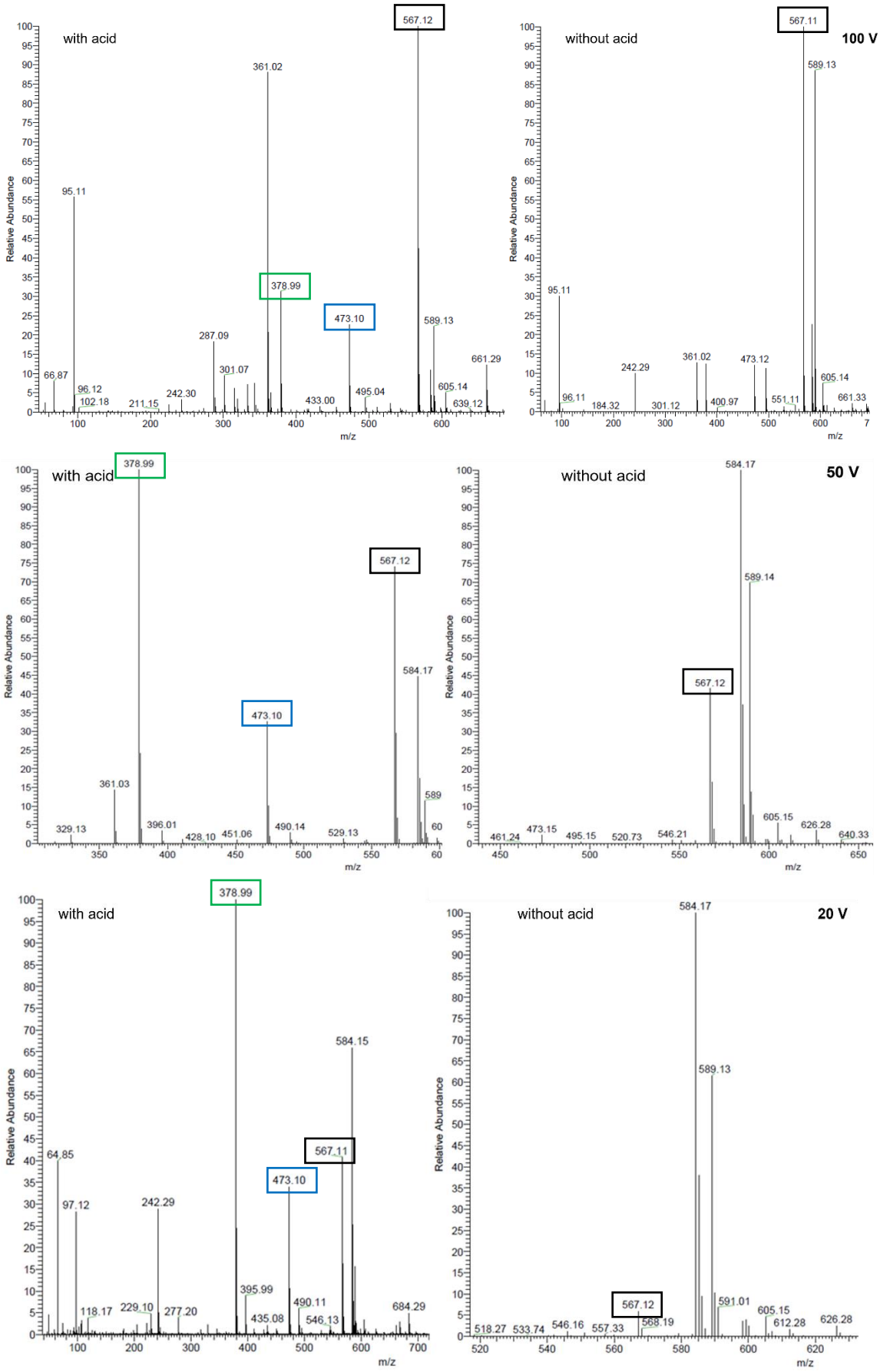

Figure 89: Mass spectra of **43** at different cone voltages and with and without acid in the solvent. From top to bottom: cone voltage of 100 V, 50 V, and 20 V. Black: Mass of **43** (m/z = 567.12), blue: mass of the monocarboxylic acid (m/z = 473.10), green: mass of the dicarboxylic acid (m/z = 379.09).

To enable identification of the radiolabeled product, an attempt was made to prepare the non-radioactive reference compound **44** by reacting **43** with ammonium fluoride (Scheme 62). The product peak was detected in the ESI-LRMS of the crude product solution. Using semi-preparative HPLC, the product was isolated together with the corresponding monocarboxylic acid and detected by ESI-LRMS. The amount of the HPLC fraction was insufficient for recording a ^{1}H-NMR spectrum. It is possible that the monocarboxylic acid identified in the MS spectrum is also a mass adduct, but this was not investigated further.

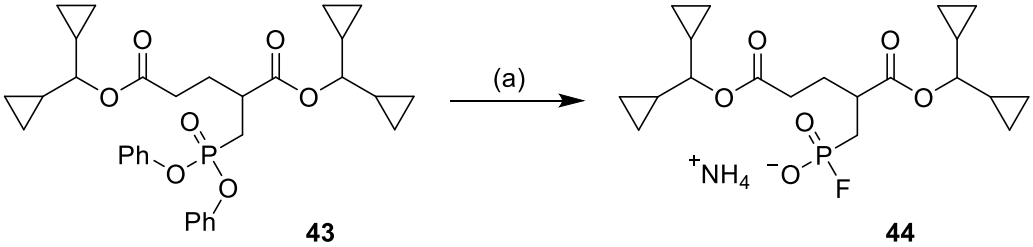

43 **44**

Scheme 62: Synthesis of **44** from **43**. Reaction conditions: NH_4F, MeCN, 60 °C, overnight.[19]

Due to time constraints and the absence of a pure, well-characterized reference compound, precursor **43** was not radiofluorinated. It is important to note that the dicyclopropyl protecting group is acid-labile and may decompose in an HPLC mobile phase containing TFA, which must be considered when analyzing any future radioproducts.

*7.3.1.5 Attempt to synthesize the non-radioactive reference compound **39** from **43***

Compound **43** was used in an attempt to synthesize the non-radioactive compound of the 2-PMPA analogue **39**. The intended approach involved removing the dicyclopropyl protecting groups using either HCl in 1,4-dioxane or TFA in CH_2Cl_2, followed by fluorination (Scheme 63). However, in both deprotection attempts, the desired product could not be obtained. In the reaction involving HCl in 1,4-dioxane, a by-product, identified as 2-PMPA, was detected by ESI-LRMS. The formation of this by-product may be attributable to traces of water in the reaction mixture.

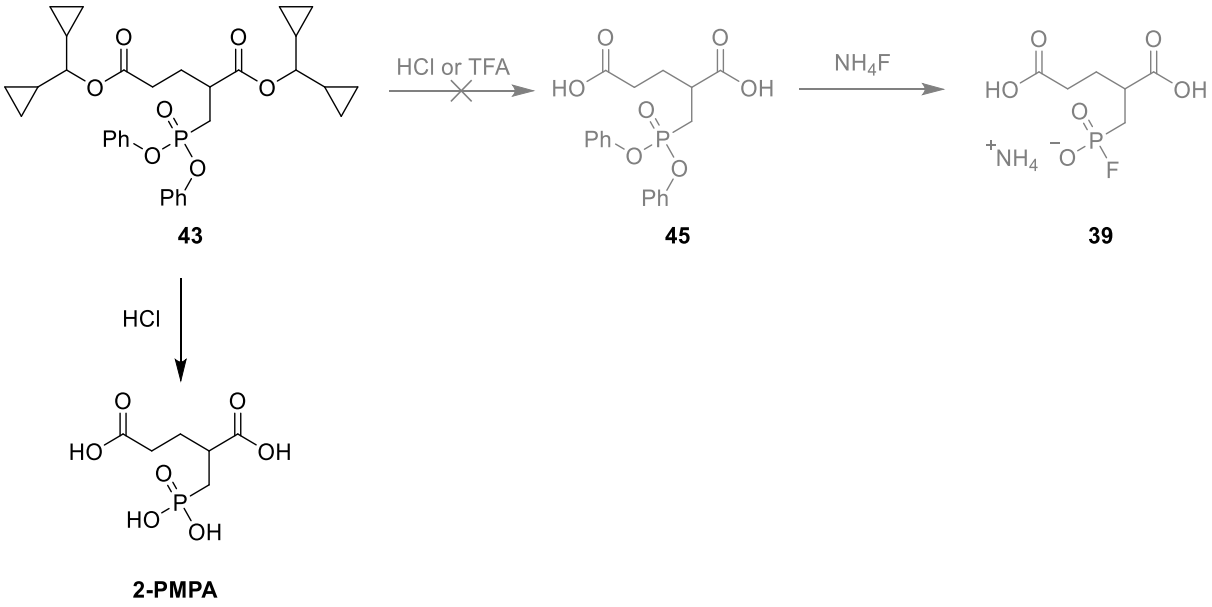

Scheme 63: Planned route for the synthesis of **39** from **43**. Instead, 2-PMPA was identified as a by-product from the reaction of **43** with HCl in 1,4-dioxane.

In summary, preliminary efforts towards the synthesis of **39** have been undertaken. Future investigations may involve exploring alternative protecting group strategies to overcome the current limitations.

7.4 Summary

Preliminary works on the synthesis of a P-^{18}F-labeled 2-PMPA analog were conducted, but completion was not achieved within the available timeframe.

7.5 Experimental part

7.5.1 Organic preparative syntheses

Di-*tert*-butyl 2-methylenepentanedioate (**35**)[18]

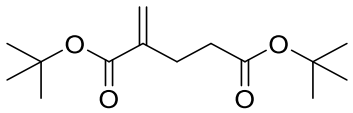

35

$C_{14}H_{24}O_4$

[256.34]

A mixture of *tert*-butyl acrylate (5.68 mL, 39 mmol, 1 eq) and tributylphosphine (1.07 mL, 4.29 mmol, 11 mol%) was stirred for 2.5 h at ambient temperature. After purification by distillation (1–3 mbar, 95–110 °C bp), 3.66 g (14.3 mmol, 73%) of a slightly yellowish oil were obtained.

^{1}H NMR (400 MHz, $CDCl_3$) δ = 6.16 – 5.95 (m, 1H), 5.48 (q, *J* = 1.4, 1H), 2.54 (dd, *J* = 7.8, 7.2, 2H), 2.47 – 2.33 (m, 2H), 1.48 (s, 9H), 1.43 (s, 9H).
^{13}C NMR (101 MHz, $CDCl_3$) *δ* = 172.33, 166.17, 140.87, 124.51, 80.63 (d, *J* = 33.2), 34.48, 28.21 (d, *J* = 4.1), 27.70.

The analytical data corresponds to the literature.[18]

Di-*tert*-butyl 2-[(diphenoxyphosphoryl)methyl]pentanedioate (**36**)[16]

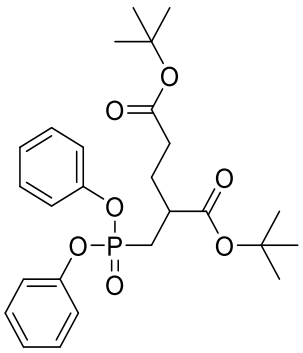

36

$C_{26}H_{35}O_7P$

[490.53]

Trimethylaluminum (2 mL in toluene, 7 mL, 14 mmol, 1 eq) was added dropwise to a pre-cooled (0 °C) solution of diphenyl phosphite (2.8 mL, 14.7 mmol, 1.05 eq) in CH_2Cl_2 (0.21 M), and the reaction mixture was stirred for 20 min at 0 °C. A solution of **35** (3.6 g, 14 mmol, 1 eq) in dry CH_2Cl_2 (1.6 M) was then added and the mixture was stirred overnight at ambient temperature. The reaction was quenched by addition of 1 N HCl solution (120 mL) and stirred for 10 min. The aqueous phase was extracted twice with CH_2Cl_2 (40 mL), the combined organic fractions were dried with Na_2SO_4, and the solvent was removed under reduced pressure. The crude product was adsorbed on Celite® and, after double purification by column chromatography (cyclohexane:EtOAc = 95:5 – 8:2), 2.23 g (4.5 mmol, 32%) of a white solid were obtained.

R_f (cyclohexane:EtOAc = 8:2) = 0.34.

Mp: 54,8 °C.

^{1}H NMR (400 MHz, $CDCl_3$) δ = 7.35 – 7.25 (m, 4H), 7.20 – 7.12 (m, 6H), 3.01 – 2.87 (m, 1H), 2.58 (ddd, *J* = 18.2, 15.6, 8.8, 1H), 2.38 – 2.21 (m, 2H), 2.13 (ddd, *J* = 18.6, 15.6, 4.9, 1H), 2.06 – 1.91 (m, 2H), 1.44 – 1.42 (m, 18H).

^{13}C NMR (101 MHz, $CDCl_3$) δ = 173.02 (d, *J* = 8.1), 171.92, 150.30 (d, *J* = 5.8), 129.87 (d, *J* = 1.8), 125.33, 120.79 (d, *J* = 4.3), 81.65, 80.73, 40.14 (d, *J* = 4.0), 32.79, 29.42 – 28.91 (m), 28.21, 28.13, 27.61.

^{31}P NMR (162 MHz, $CDCl_3$) δ = 22.55.

HRMS (**ESI**) calculated for $C_{26}H_{35}O_7P$ ($[M+H]^+$): 491.21932; found: 491.22039.

2-[(Diphenoxyphosphoryl)methyl]pentanedioic acid (**38**)

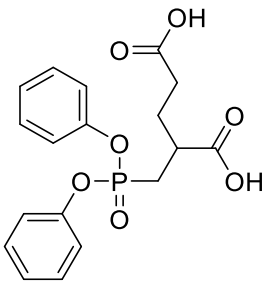

38

$C_{18}H_{19}O_7P$

[378.32]

TFA (4 mL) was added to a solution of **37** (400 mg, 0.82 mmol) in dry CH_2Cl_2 (0.20 M), and the reaction mixture was stirred at ambient temperature for three nights. The solvent was removed under reduced pressure, and the crude product was dissolved in EtOAc and adsorbed on Celite®. After purification by column chromatography (cyclohexane:EtOAc + 1% AcOH = 8:2 – 4:6) and subsequent triple azeotropic drying with 5 mL toluene each, 73 mg (0.19 mmol, 24%) of an oil were obtained. Alternatively, the crude product can be purified by semi-preparative column chromatography (Column: Phenomenex Synergi 10 µm Hydro-RP, 250×100 mm; eluent: 25% MeCN (0.1% TFA). Flow rate: 4.5 mL/min) and direct freeze drying.

R_f (cyclohexane:EtOAc = 8:2 + 1% acetic acid) = 0.40.

^{1}H NMR (400 MHz, MeOD) δ = 7.36 (ddd, *J* = 8.1, 6.6, 3.0, 4H), 7.26 – 7.13 (m, 6H), 3.00 (tdd, *J* = 14.0, 8.8, 5.2, 1H), 2.64 (ddd, *J* = 18.1, 15.8, 9.0, 1H), 2.51 – 2.29 (m, 3H), 2.12 – 1.96 (m, 2H).

^{13}C NMR (101 MHz, MeOD) δ = 176.88 (d, *J* = 7.3), 176.20, 151.47 (dd, *J* = 9.3, 5.8), 130.87 (t, *J* = 14.9), 126.88 – 126.14 (m), 121.73 (t, *J* = 4.4), 40.43 (d, *J* = 4.2), 32.02, 30.26 – 28.95 (m), 28.04.

^{31}P NMR (162 MHz, MeOD) δ = 23.44.

HRMS (**ESI**) calculated for $C_{18}H_{19}O_7P$ ($[M+H]^+$): 379.09412; found: 379.09470.

Dicyclopropylmethanol (**40**)[22]

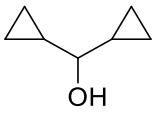

40

$C_7H_{12}O$

[112.17]

$NaBH_4$ (3.43 g, 90.4 mmol, 1 eq) was added in portions to a pre-cooled (0 °C) solution of dicyclopropyl ketone (9.96 g, 90.4 mmol, 1 eq) in dry MeOH (0.9 M), after which the reaction mixture was warmed to ambient temperature and stirred for 3 h. The solvent was then removed under reduced pressure, and the residue was treated with pure H_2O (100 mL). The aqueous phase was extracted three times with EtOAc (100 mL), and the combined organic fractions were washed once with H_2O (100 mL) and saturated NaCl solution (100 mL). The organic phase was dried with Na_2SO_4, and the solvent was removed under reduced pressure. 8 g (71.3 mmol, 79%) of a colorless oil were obtained.

^{1}H NMR (400 MHz, $CDCl_3$) δ = 2.42 (t, J = 7.9 Hz, 1H), 1.07 – 0.95 (m, 2H), 0.58 – 0.41 (m, 4H), 0.35 – 0.22 (m, 4H).
^{13}C NMR (101 MHz, $CDCl_3$) δ = 80.14, 17.06, 2.27, 2.12.

The analytical data corresponds to the literature.[27]

Dicyclopropylmethyl acrylate (**41**)[23,24]

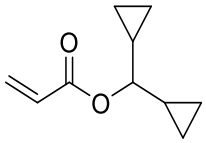

41

$C_{10}H_{14}O_2$

[166.22]

Acryloyl chloride (4.84 g, 53.5 mmol, 1.2 eq) was added dropwise to a pre-cooled (0 °C) solution of **40** (5 g, 44.6 mmol, 1 eq), triethylamine (6.77 g, 66.9 mmol, 1.5 eq) and DMAP (817 mg, 6.7 mmol, 15 mol%) in dry CH_2Cl_2 (0.3 M), and the reaction mixture was stirred overnight at ambient temperature. The resulting solid was filtered off, and the organic phase was washed twice with H_2O (150 mL) and once with saturated NaCl solution (150 mL). The organic phase was dried with Na_2SO_4, and the solvent was removed under reduced pressure. The crude product was fractionally distilled under reduced pressure (0.85 mbar, 53–56 °C bp). 4.24 g (25.5 mmol, 57%) of a colorless oil were obtained.

^{1}H NMR (400 MHz, $CDCl_3$) δ = 6.39 (dd, J = 17.3, 1.6 Hz, 1H), 6.14 (dd, J = 17.3, 10.4 Hz, 1H), 5.81 (dd, J = 10.4, 1.6 Hz, 1H), 4.00 (t, J = 8.2 Hz, 1H), 1.11 (qt, J = 8.2, 5.0 Hz, 2H), 0.56 (tdd, J = 8.4, 5.6, 4.0 Hz, 2H), 0.50 – 0.30 (m, 6H).
^{13}C NMR (101 MHz, $CDCl_3$) δ = 166.15, 130.42, 129.18, 81.91, 14.86, 2.93, 2.68.

Bis(dicyclopropylmethyl) 2-methylenepentanedioate (**42**)[18]

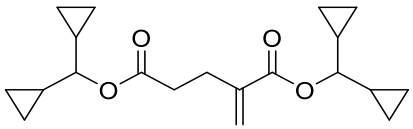

42

$C_{20}H_{28}O_4$

[332.44]

A mixture of **41** (4.1 g, 24.7 mmol, 1 eq) and tributylphosphine (0.67 mL, 549 mg, 2.7 mmol, 11 mol%) was stirred for 2 h at ambient temperature and then diluted with cyclohexane. After purification by column chromatography (100% cyclohexane + 3% Et_3N), 2.59 g (7.8 mmol, 63%) of the title compound could be obtained as a colorless oil.

^{1}H NMR (400 MHz, $CDCl_3$) δ = 6.19 (dd, *J* = 3.6, 3.0, 1H), 5.61 – 5.55 (m, 1H), 4.03 (t, *J* = 8.1, 1H), 3.91 (t, *J* = 8.2, 1H), 2.71 – 2.62 (m, 2H), 2.58 – 2.51 (m, 2H), 1.17 – 1.00 (m, 4H), 0.60 – 0.50 (m, 4H), 0.50 – 0.27 (m, 12H).
^{13}C NMR (101 MHz, $CDCl_3$) δ = 172.64, 166.57, 139.63, 125.39, 81.87, 81.79, 33.55, 27.76, 14.84, 2.95, 2.85, 2.66, 2.64.

Bis(dicyclopropylmethyl) 2-[(diphenoxyphosphoryl)methyl]pentanedioate (**43**)[15]

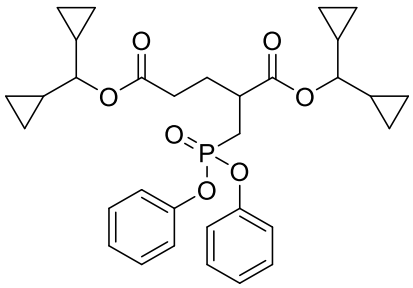

43

$C_{32}H_{39}O_7P$

[566.63]

A solution of **42** (200 mg, 0.6 mmol, 1 eq), diphenyl phosphite (148 µL, 0.77 mmol, 1.25 eq) and K_2CO_3 (124 mg, 0.9 mmol, 1.5 eq) in DMF (0.16 M) was stirred for 2 h at 90 °C and 3.6 d at ambient temperature. The solvent was removed under reduced pressure, the residue was dissolved in EtOAc (10 mL), and the resulting solution washed with saturated NH_4Cl solution (10 mL). The organic phase was washed twice with semi-concentrated NaCl solution (10 mL) and dried with Na_2SO_4. The solvent was removed under reduced pressure. After purification by column chromatography (cyclohexane:EtOAc = 95:5 – 85:15), whereby the silica gel was pre-conditioned (cyclohexane:EtOAc + 3% Et_3N [95:5]), 91 mg (0.16 mmol, 27%) of a colorless oil were obtained.

R_f (cyclohexane:EtOAc + 3% Et_3N) = 0.47.
^{1}H NMR (400 MHz, $CDCl_3$) δ = 7.34 – 7.27 (m, 4H), 7.20 – 7.11 (m, 6H), 3.96 – 3.87 (m, 2H), 3.17 – 3.06 (m, 1H), 2.66 (ddd, *J* = 18.4, 15.6, 8.3, 1H), 2.53 – 2.38 (m, 2H), 2.26 – 2.02 (m, 3H), 1.15 – 1.00 (m, 4H), 0.60 – 0.27 (m, 16H).
^{13}C NMR (101 MHz, $CDCl_3$) δ = 173.55 (d, *J* = 9.3), 172.32, 150.41 – 150.30 (m), 150.28 – 150.18 (m), 129.88 (d, *J* = 1.8), 125.37, 120.81 (d, *J* = 4.3), 83.40, 81.96, 39.60 (d, *J* = 3.8), 31.82, 29.55 – 28.65 (m), 27.51, 15.03 – 14.71 (m), 14.66, 3.22 – 2.86 (m), 2.70 (d, *J* = 10.7).
^{31}P NMR (162 MHz, $CDCl_3$) δ = 22.29.
HRMS (**ESI**) calculated for $C_{32}H_{39}O_7P$ ($[M+H]^+$): 567.25062; found: 567.25116.

General procedure 7 (**GP 7**)[19]

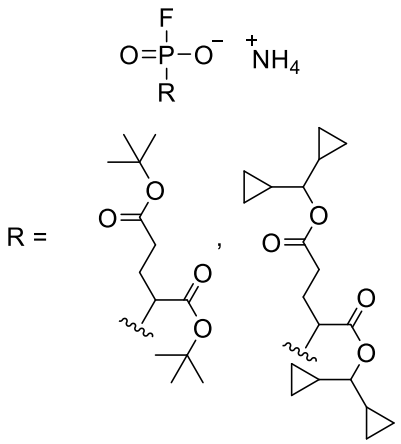

Ammonium fluoride (10 eq) was added to a solution of the corresponding phosphonate in dry MeCN, and the reaction mixture was stirred overnight at 60 °C. The solvent was removed under reduced pressure, and the crude product was purified by semi-preparative column chromatography (H_2O/MeCN).

Table 30: Experimental data for the synthesis of phosphonofluoridates with NH_4F as fluorinating reagent.

Entry	Phosphonate	Phosphonate mg (mmol)	NH_4F mg (mmol)	Compound	Yield (%)
1	**36**	200 (0.41)	151 (4.10)	**37**	25
2	**43**	30 (0.05)	19.6 (0.53)	**44**	traces

(5-(*tert*-Butoxy)-2-(*tert*-butoxycarbonyl)-5-oxopentyl)phosphonofluoridate ammonium salt (**37**)[19]

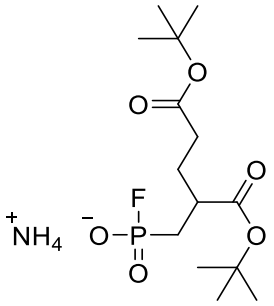

37

$C_{14}H_{25}FO_6P^-\bullet NH_4^+$

[357.36]

The synthesis was carried out according to **GP 7**. The phosphonate was dissolved in MeCN (0.05 M), and the reaction was stirred for 15 h at 60 °C. The crude product was dissolved in H_2O/MeCN (7:3, 4 mL) and the non-soluble residue was removed by centrifugation. The dissolved crude product was purified by semi-preparative column chromatography (Column: Phenomenex Synergi 10 µm Hydro-RP, 250×100 mm; eluent: 30% MeCN. Flow rate: 4.5 mL/min). The product fraction was concentrated under reduced pressure and freeze-dried. The title compound could be obtained as hygroscopic, colorless oil of 36 mg (0.1 mmol, 25%).

^{1}H NMR (400 MHz, MeOD) δ = 2.73 – 2.59 (m, 1H), 2.33 – 2.17 (m, 2H), 2.14 – 2.01 (m, 1H), 1.95 (dddd, *J* = 14.0, 9.1, 7.0, 5.1, 1H), 1.87 – 1.67 (m, 2H), 1.46 (d, *J* = 6.6, 18H).
^{13}C NMR (101 MHz, MeOD) δ = 175.77, 175.68, 173.89, 81.99, 81.59, 42.24 (d, *J* = 3.4), 33.84, 29.96 (d, *J* = 11.7), 30.71 – 28.63 (m), 28.31 (d, *J* = 5.6).
^{19}F NMR (376 MHz, MeOD) δ = -60.10 (d, *J* = 983.2).
^{31}P NMR (162 MHz, MeOD) δ = 23.00 (d, *J* = 983.4).
HRMS (**ESI**) calculated for $C_{14}H_{25}FO_6P^-$ ([M-H]$^-$): 339.13783; found: 339.13772.

Attempt to synthesize (5-(Dicyclopropylmethoxy)-2-[(dicyclopropylmethoxy)carbonyl]-5-oxopentyl)phosphonofluoridate ammonium salt (**44**)[19]

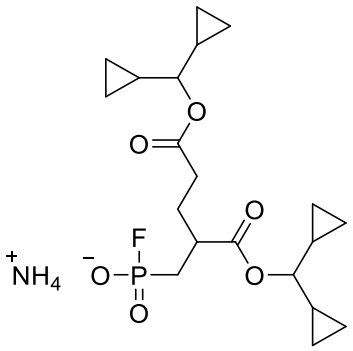

44

$C_{20}H_{29}FO_6P^-\bullet NH_4^+$

[433.46]

The synthesis was carried out according to **GP 7**. The phosphonate was dissolved in MeCN (0.03 M), and the reaction was stirred for 18.5 h at 60 °C. The product could not be purified and isolated.

MS (**ESI**) calculated for $C_{20}H_{29}FO_6P^-$ ($[M\text{-}H]^-$): 415.17; found: 415.03.

Attempt to synthesize (2,4-Dicarboxybutyl)phosphonofluoridate tetrabutylammonium salt (**39**)[28]

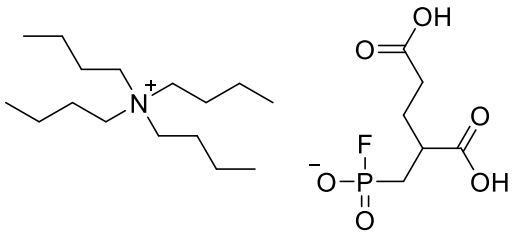

45

$C_6H_9FO_6P^-•C_{16}H_{36}N^+$

[227.10]

TBAF (1 M in THF, 200 µL, 2 eq) was added to a solution of 2-([diphenoxyphosphoryl]methyl)pentanedioic acid (**38**, 38 mg, 0.1 mmol, 1 eq) in dry THF (0.1 M), and the reaction mixture was stirred for 3 h at ambient temperature. The solvent was removed under reduced pressure, but the product could not be purified and isolated.

MS (**ESI**) calculated for $C_6H_9FO_6P^-$ ($[M\text{-}H]^-$): 227.10; found: 227.12.

7.5.2 NMR-spectra

^{1}H NMR of di-*tert*-butyl 2-methylenepentanedioate (**35**)[29]

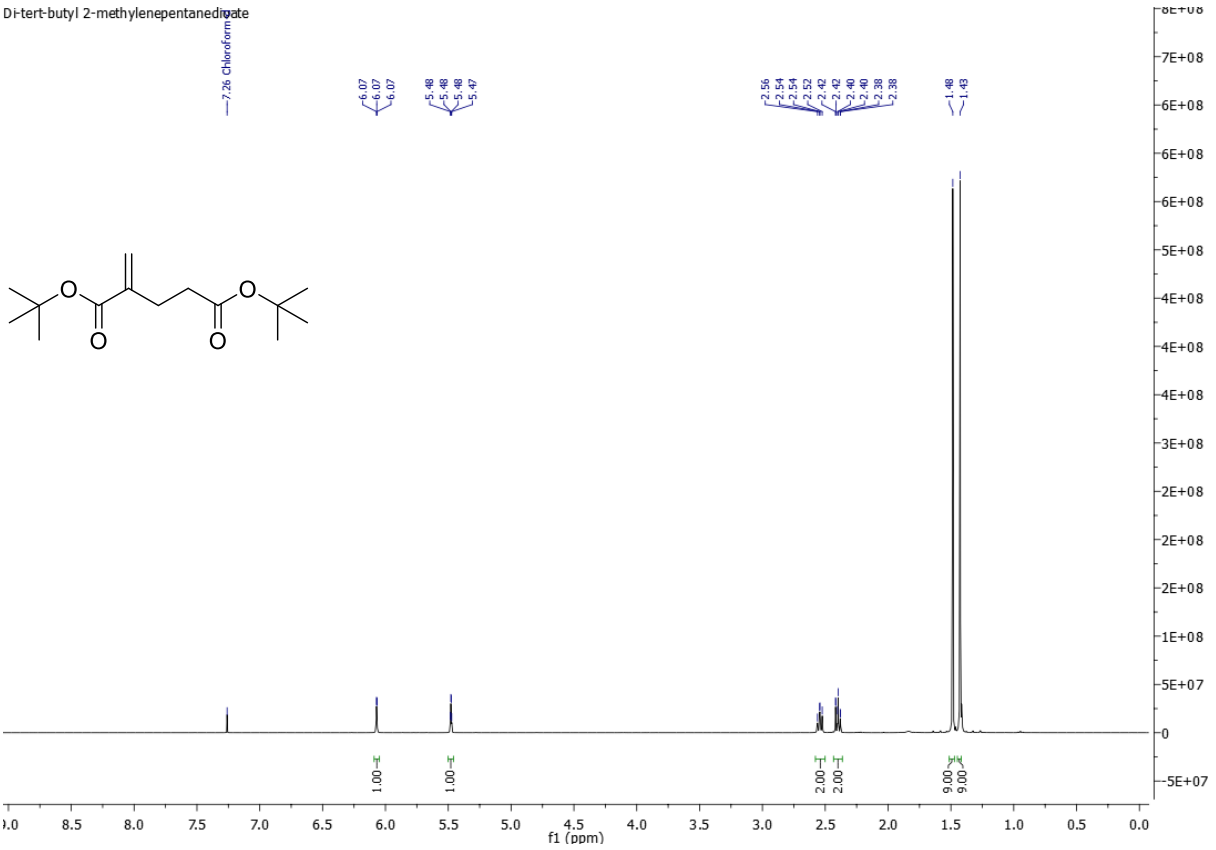

^{1}H, ^{13}C and ^{31}P NMR of di-*tert*-butyl 2-[(diphenoxyphosphoryl)methyl]pentanedioate (**36**)

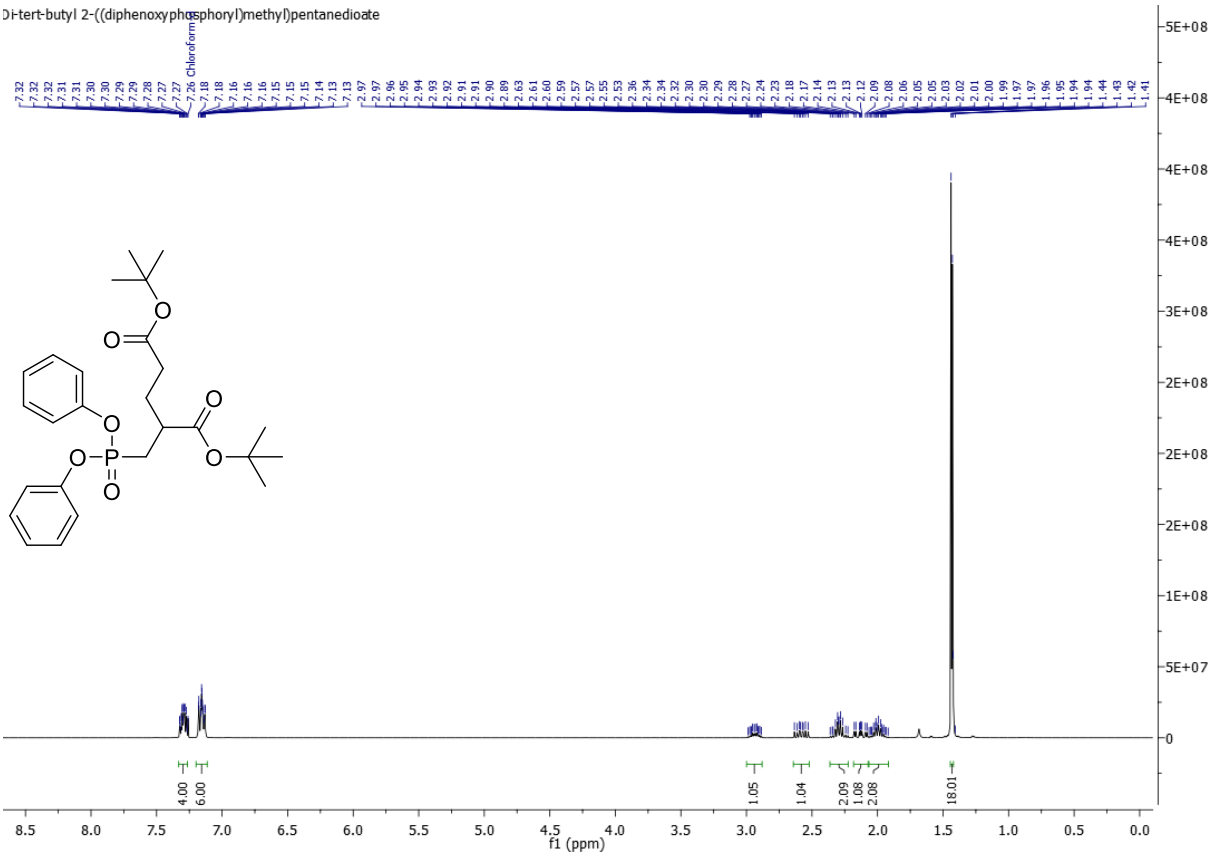

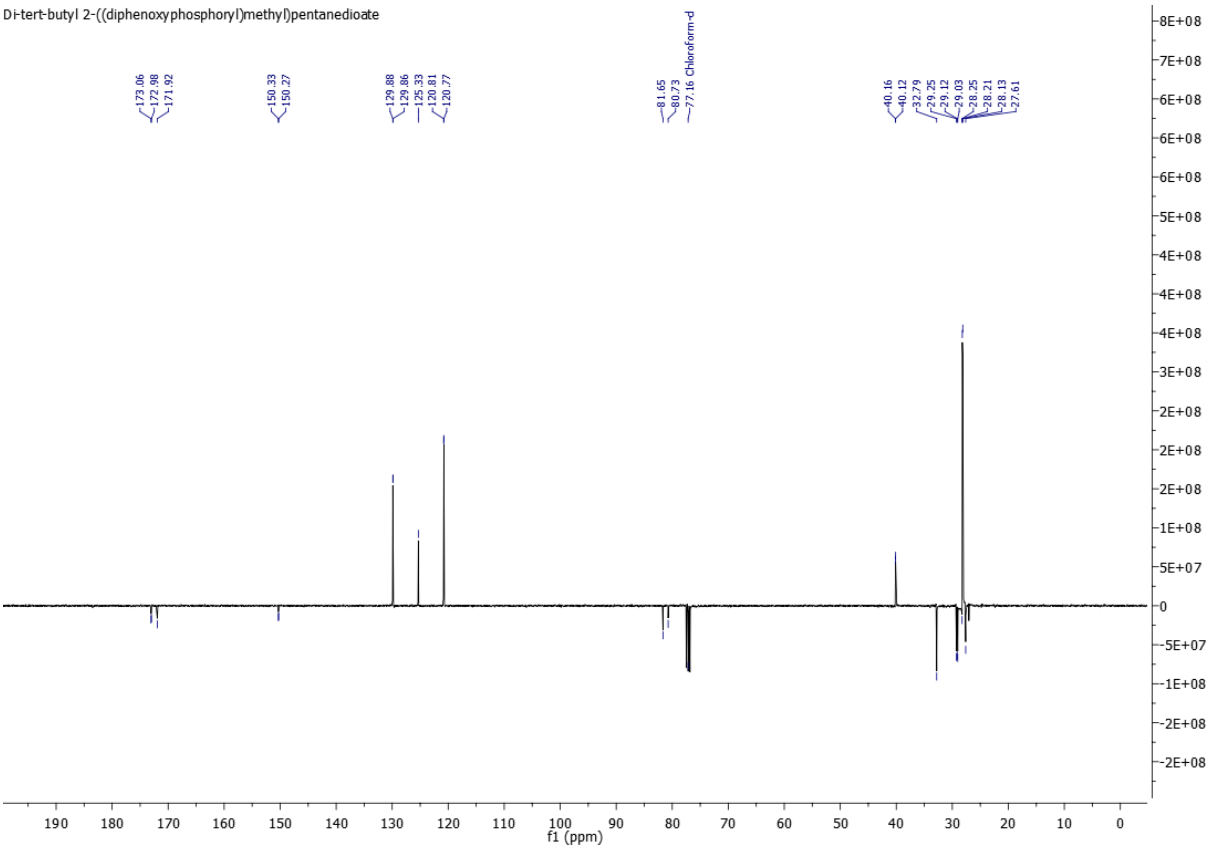
Di-tert-butyl 2-((diphenoxyphosphoryl)methyl)pentanedioate
173.06
172.98
171.92
150.33
150.27
129.88
129.86
125.33
120.81
120.77
81.65
80.73
77.16 Chloroform-d
40.16
40.12
32.79
29.25
29.12
29.03
28.25
28.21
28.13
27.61
f1 (ppm)

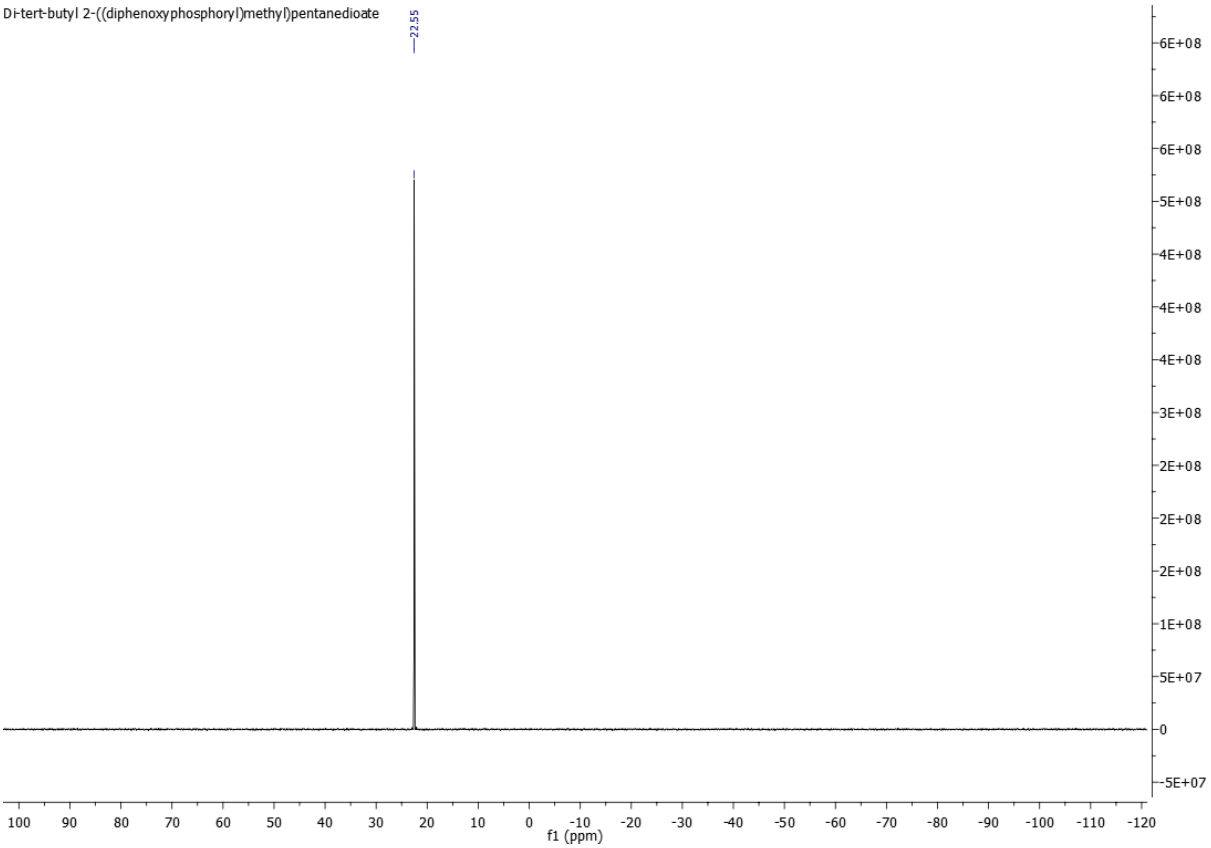
Di-tert-butyl 2-((diphenoxyphosphoryl)methyl)pentanedioate
22.55
f1 (ppm)

^{1}H, ^{13}C and ^{31}P NMR of 2-[(diphenoxyphosphoryl)methyl]pentanedioic acid (**38**)

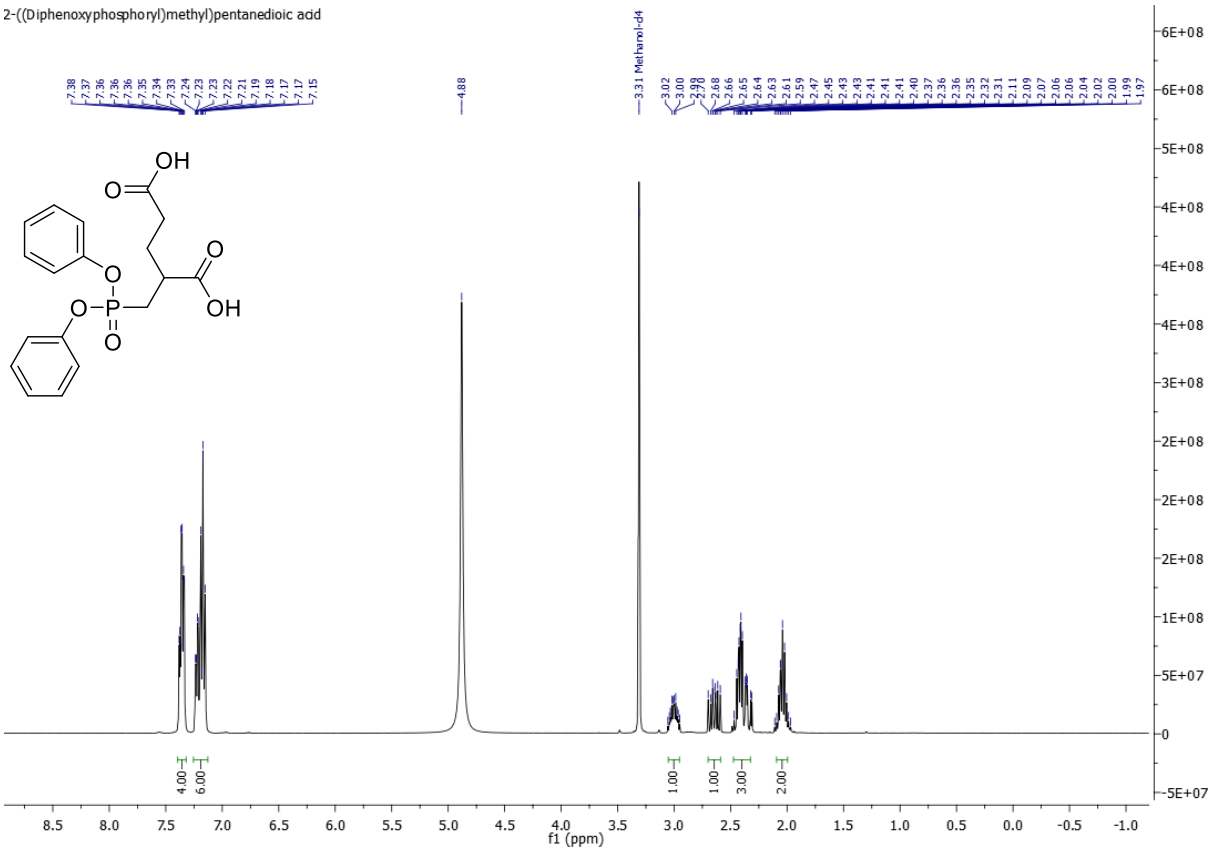

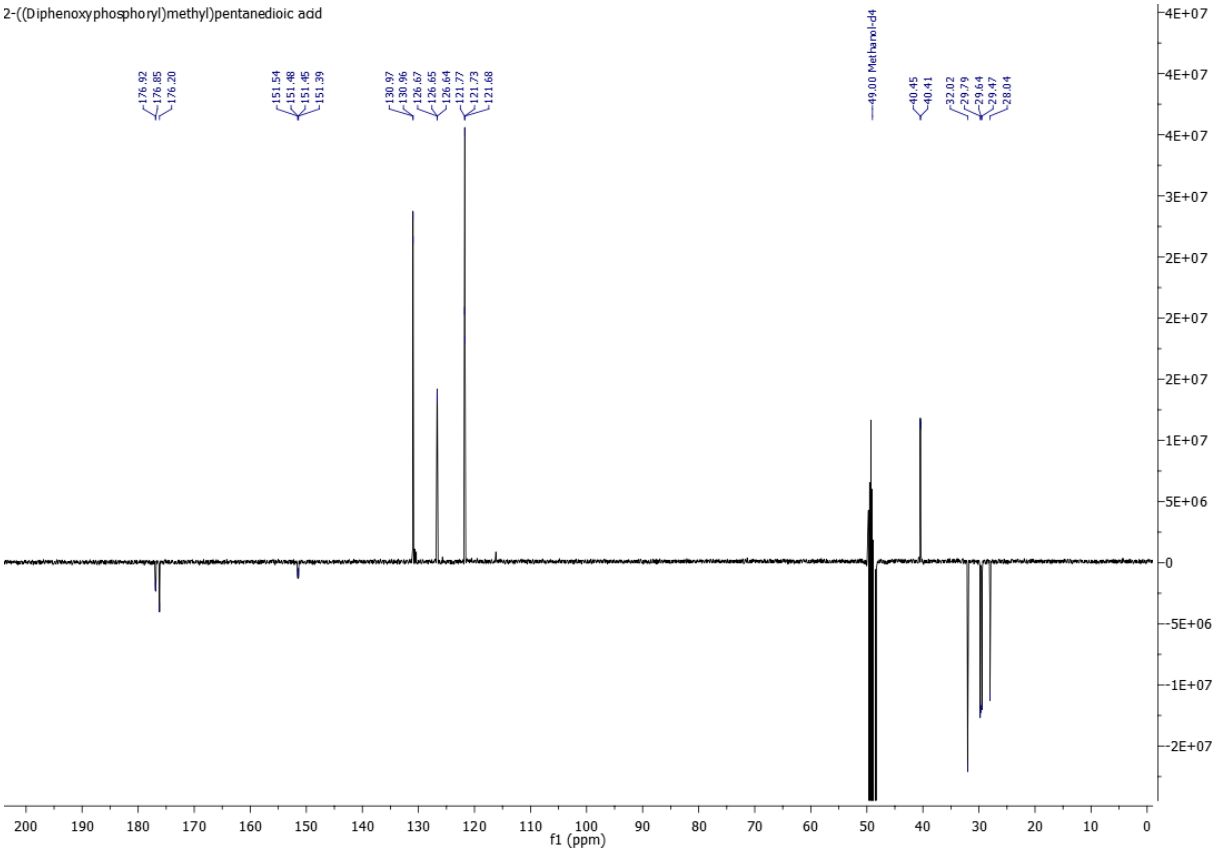

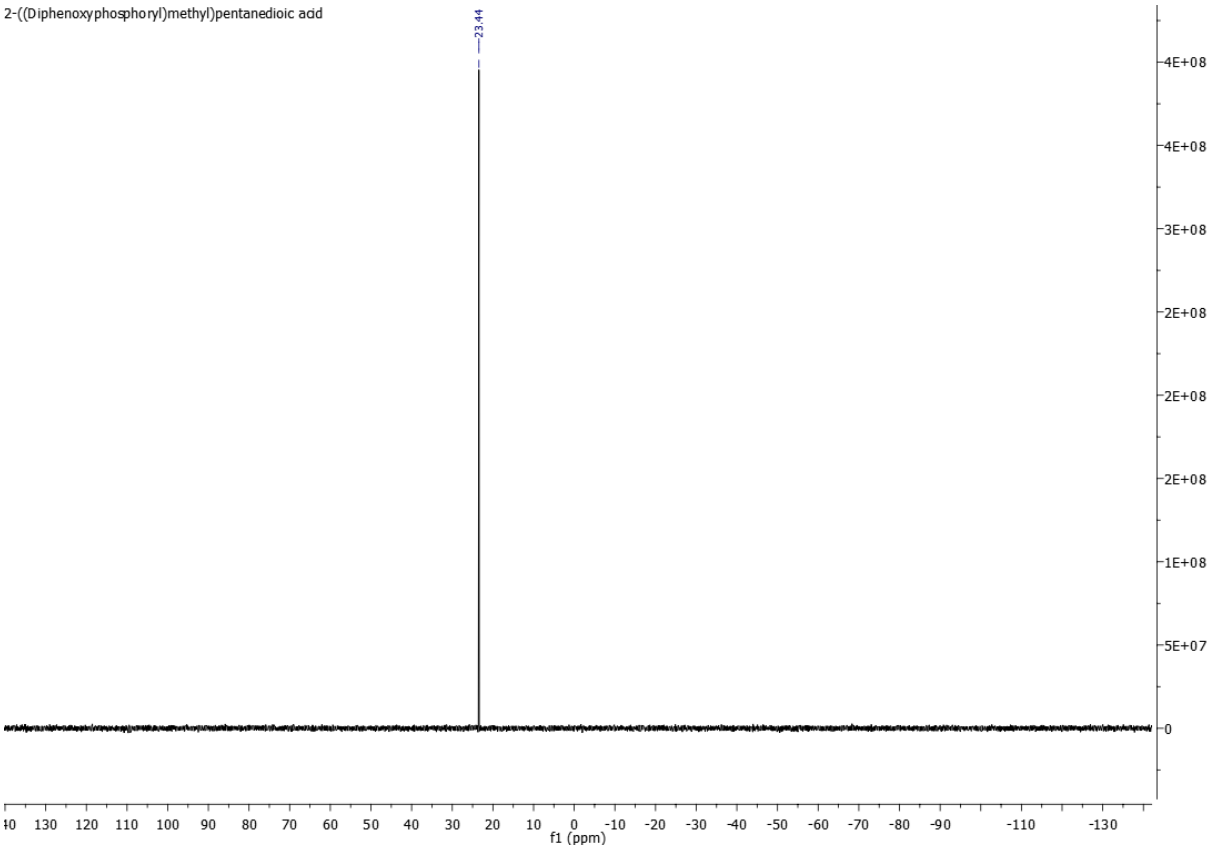

^{1}H NMR of dicyclopropylmethanol (**40**)[18]

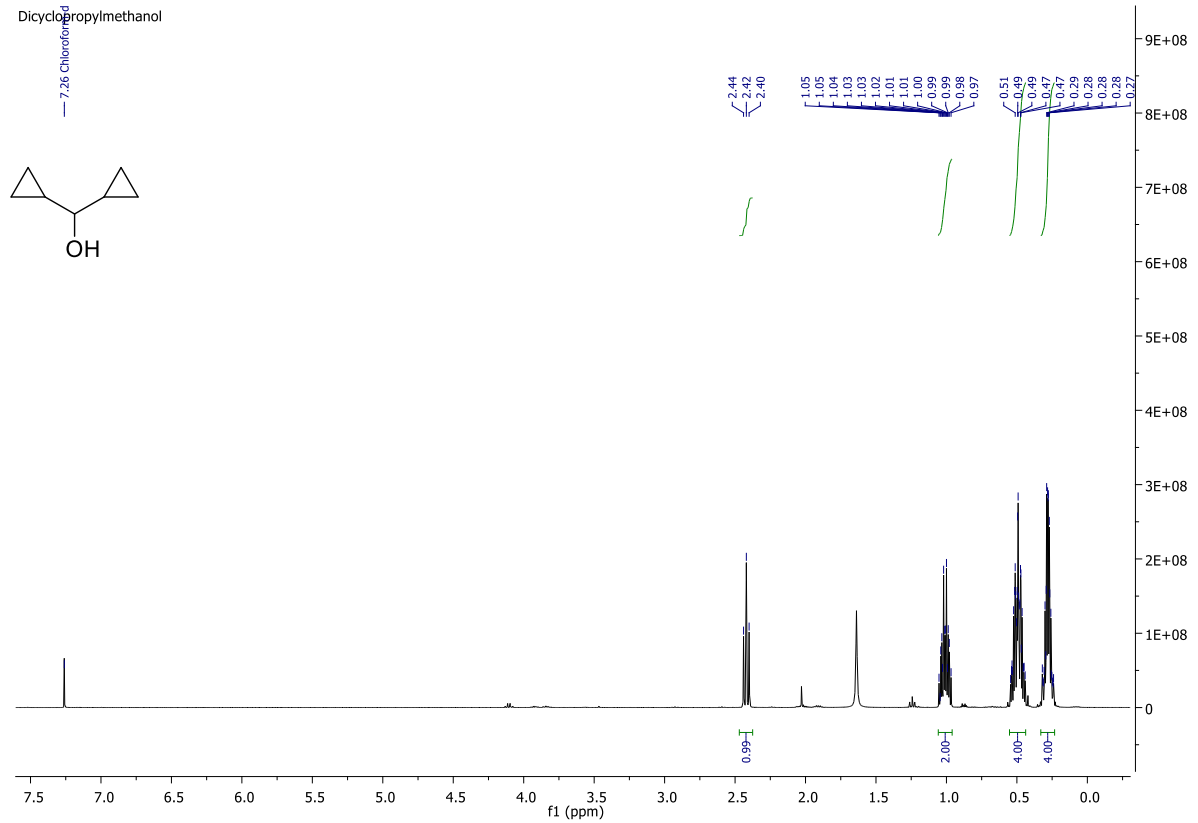

^{1}H and ^{13}C NMR of dicyclopropylmethyl acrylate (**41**)

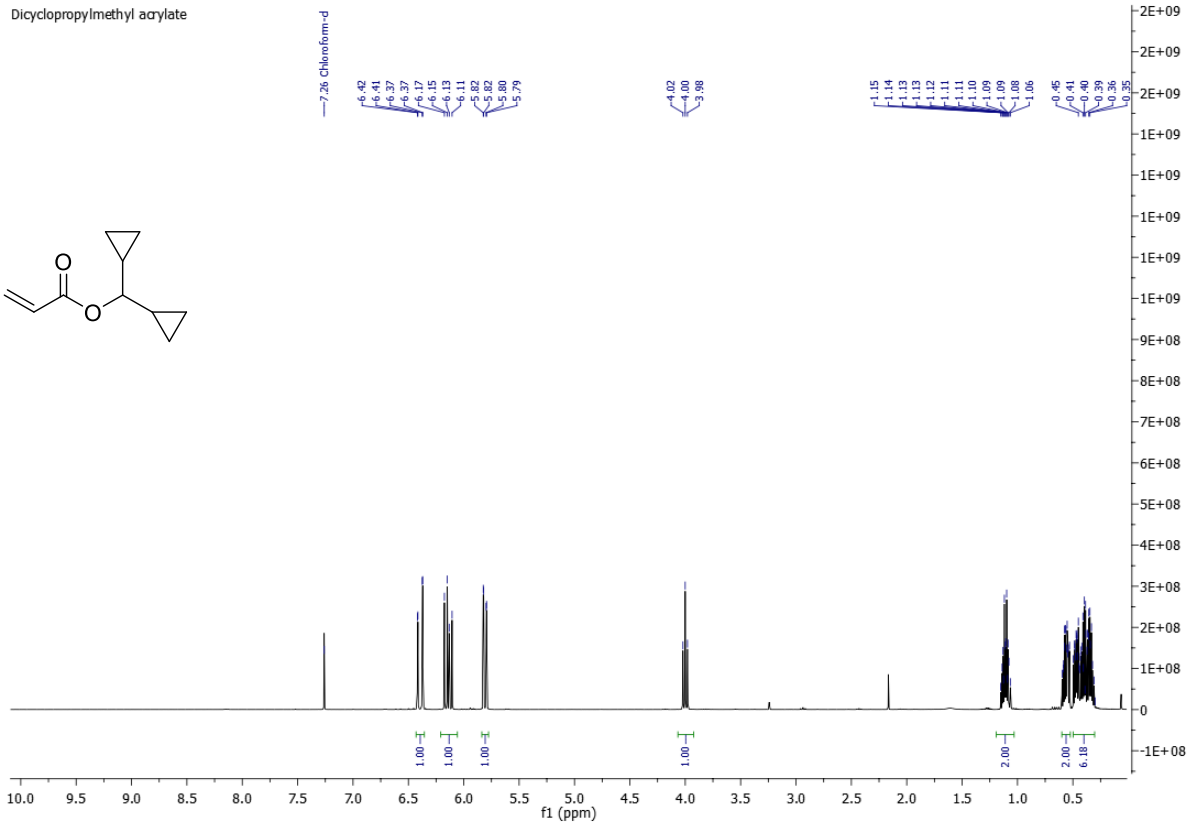

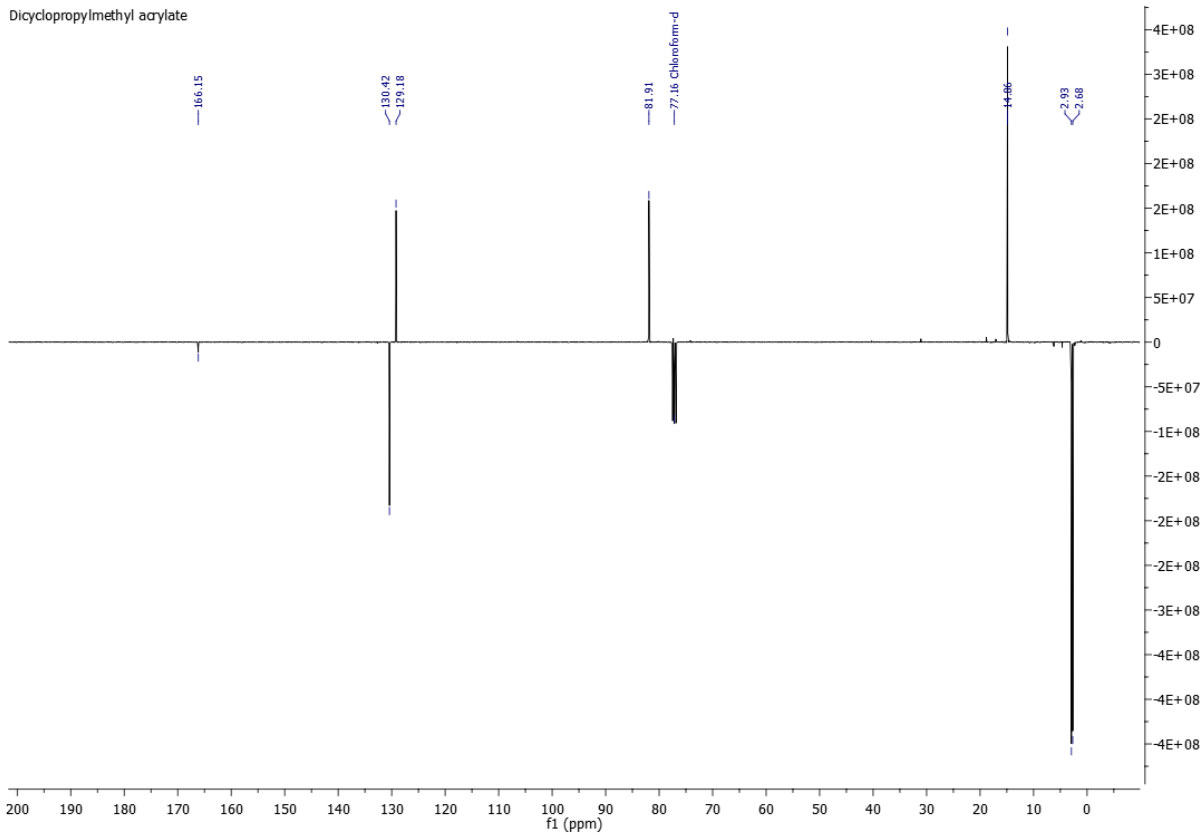

^{1}H and ^{13}C NMR of bis(dicyclopropylmethyl) 2-methylenepentanedioate (**42**)

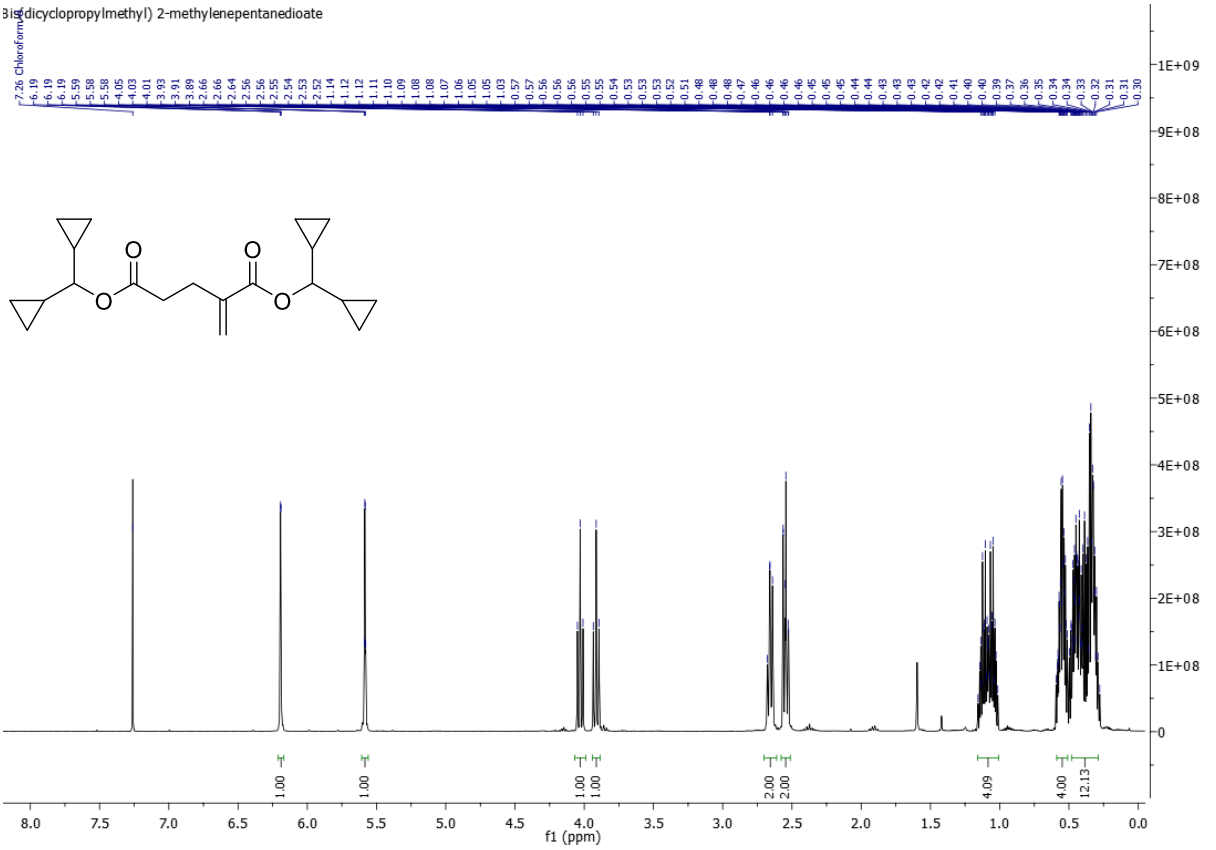

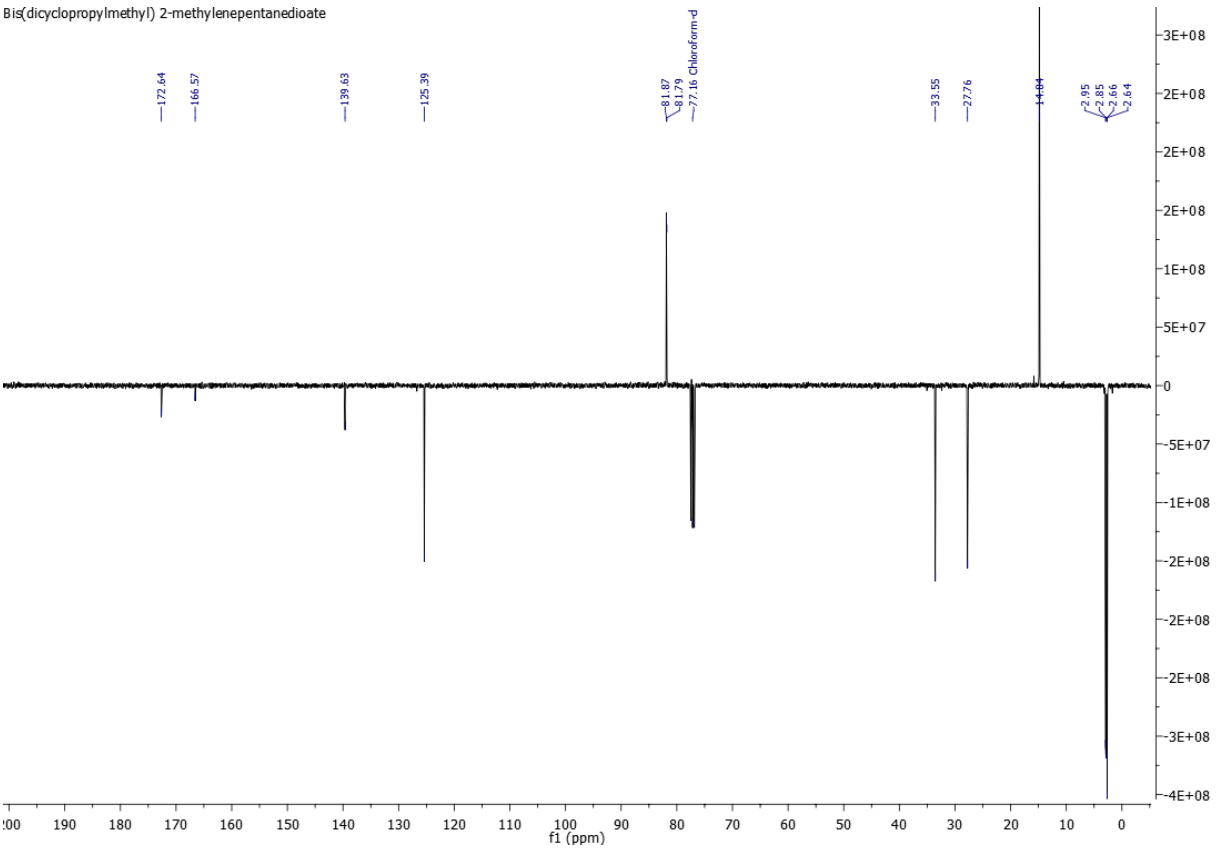

^{1}H, ^{13}C and ^{31}P NMR of bis(dicyclopropylmethyl) 2-[(diphenoxyphosphoryl)methyl]pentanedioate (**43**)

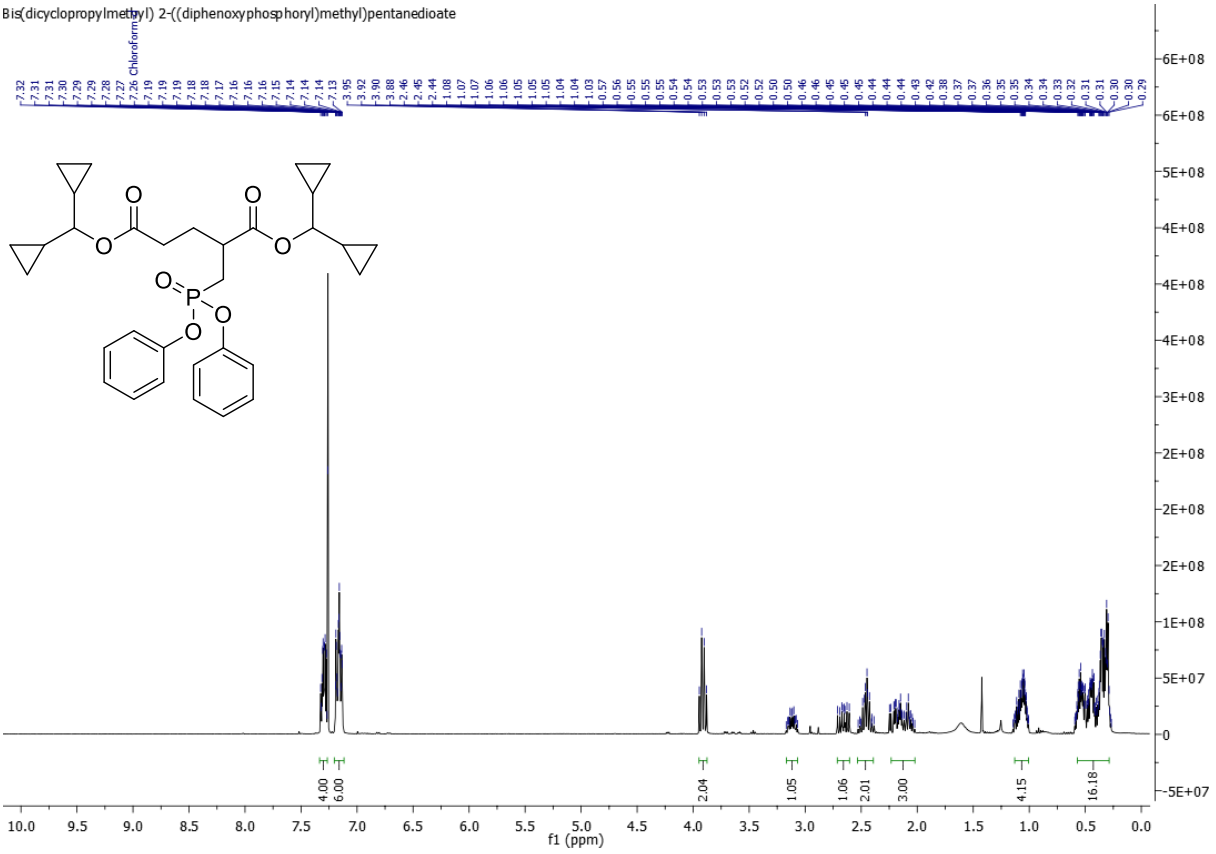

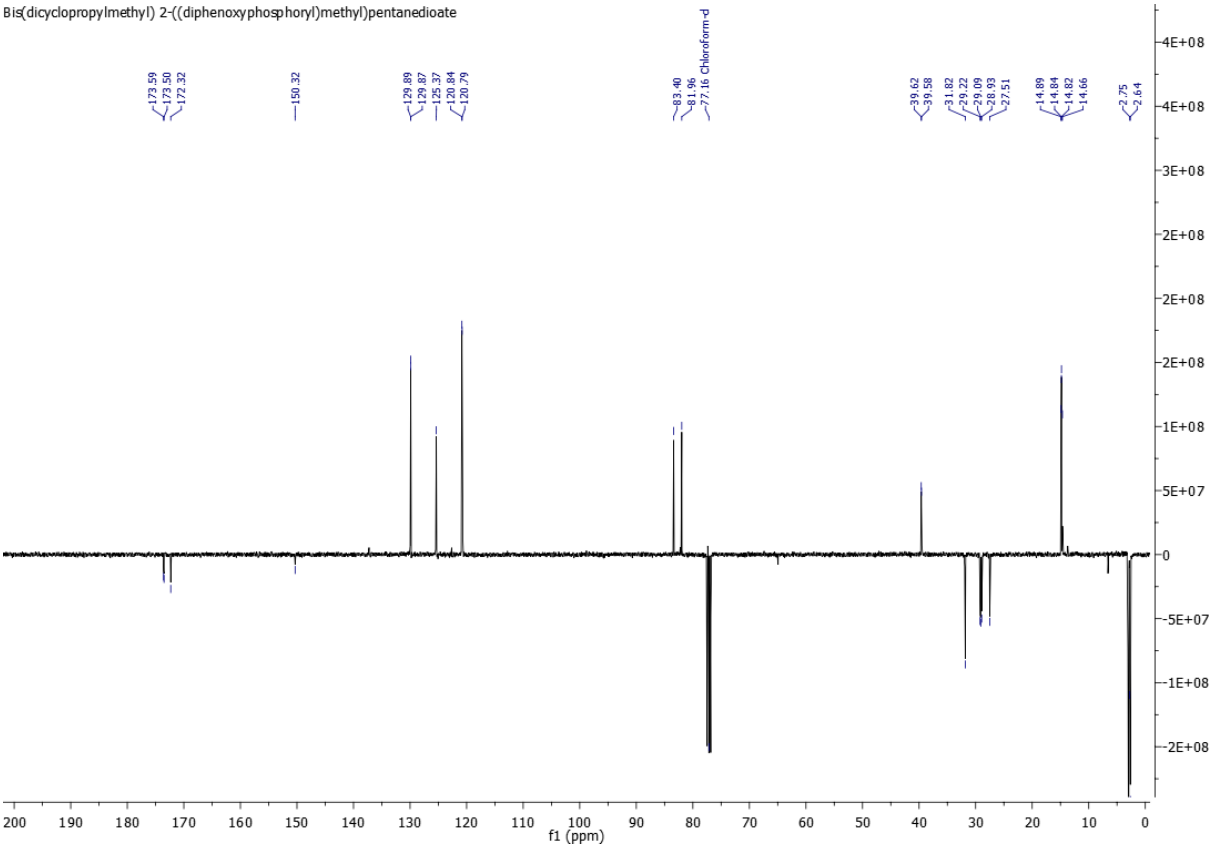

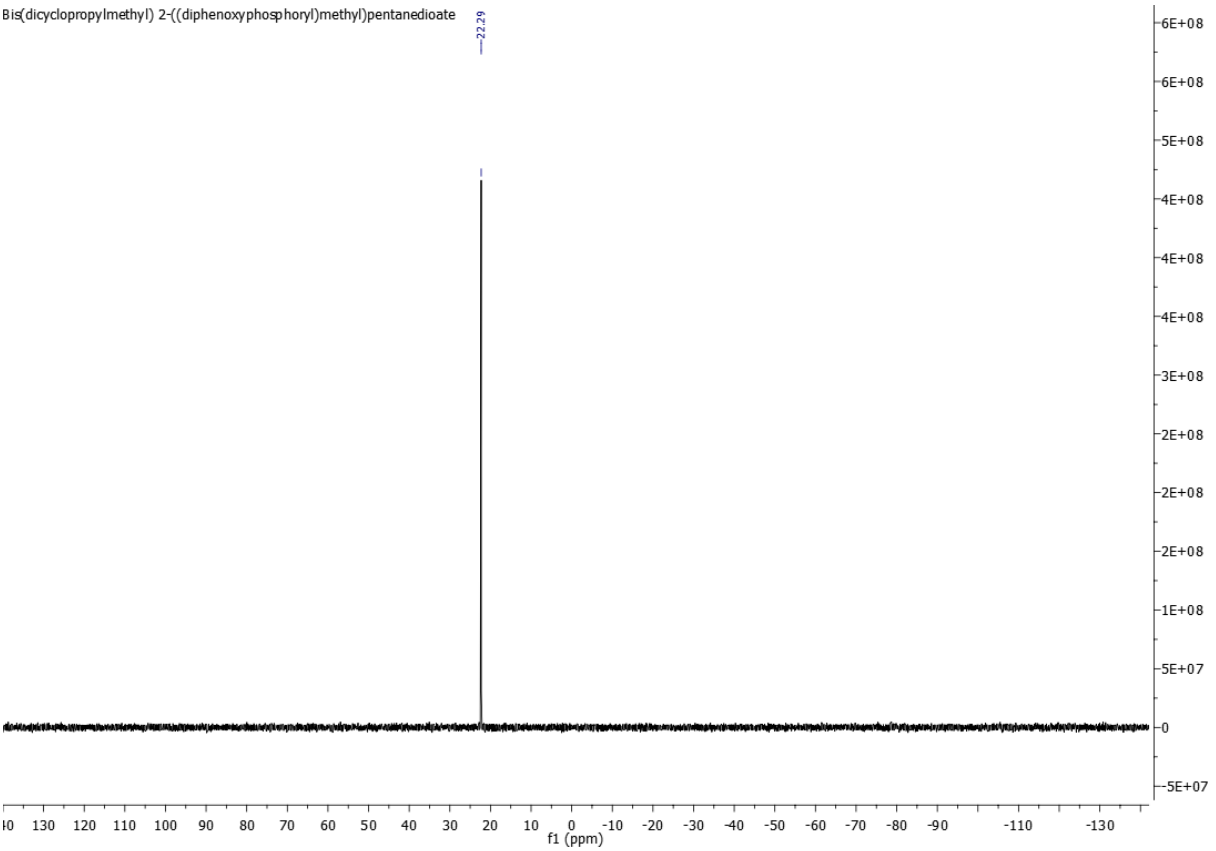

^{1}H, ^{13}C, ^{19}F and ^{31}P NMR of (5-(*tert*-butoxy)-2-(*tert*-butoxycarbonyl)-5-oxopentyl)phosphonofluoridate ammonium salt (**37**)

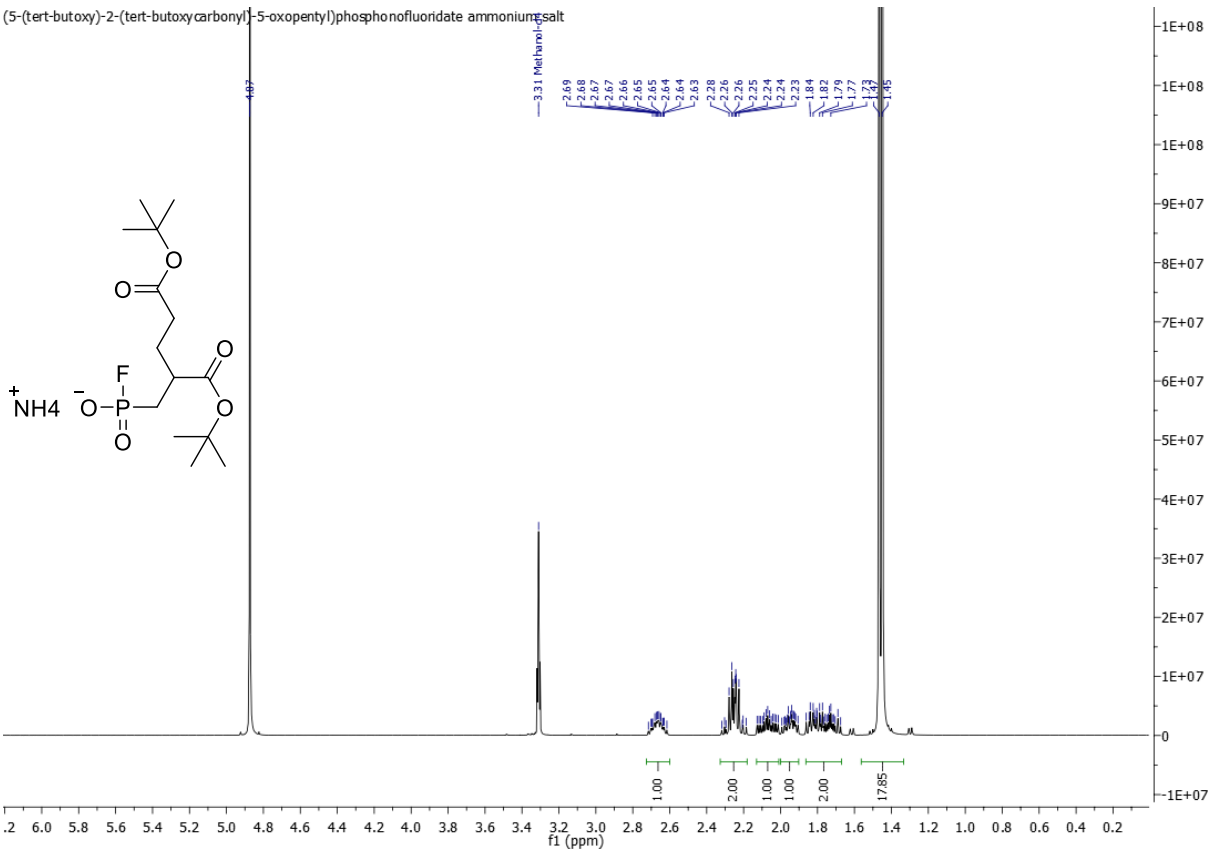

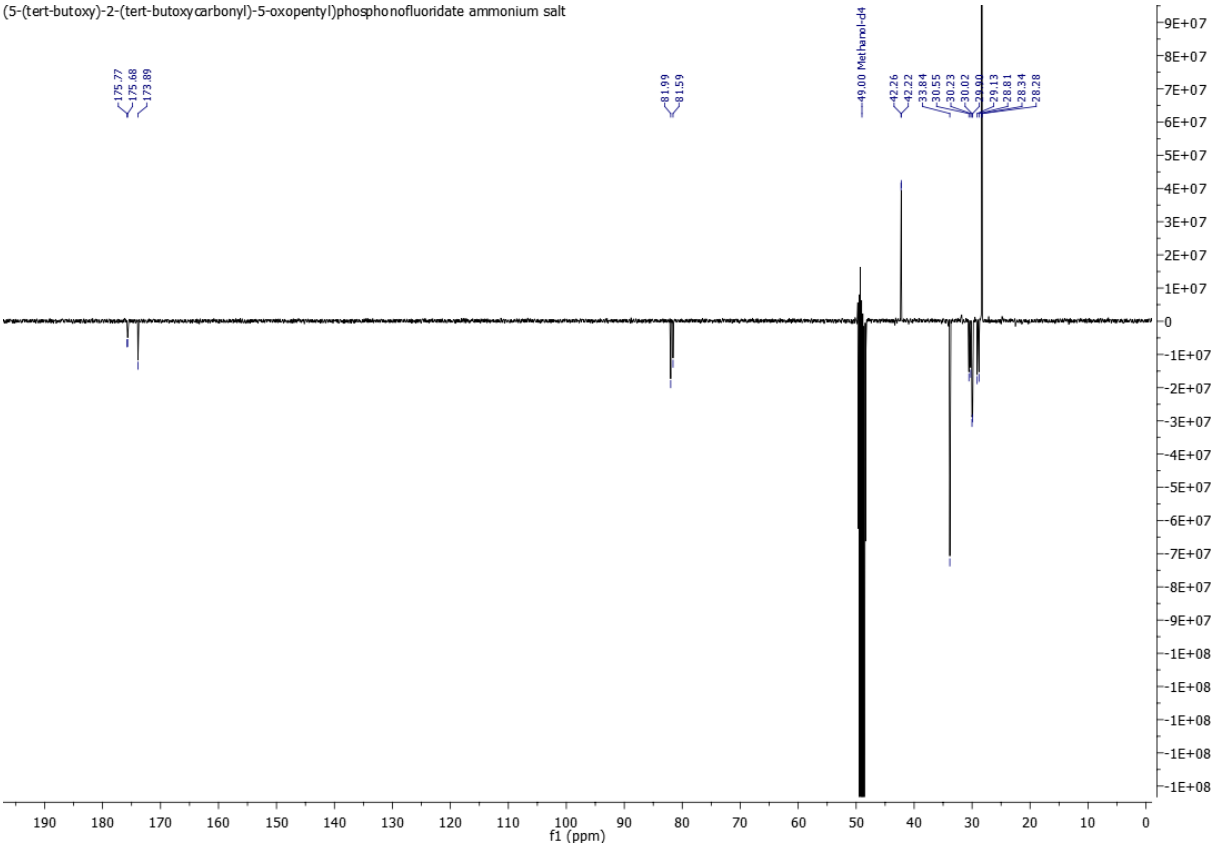
(5-(tert-butoxy)-2-(tert-butoxycarbonyl)-5-oxopentyl)phosphonofluoridate ammonium salt
175.77
175.68
173.89
81.99
81.59
49.00 Methanol-d4
42.26
42.22
33.84
30.55
30.23
30.02
29.13
28.81
28.34
28.28
f1 (ppm)

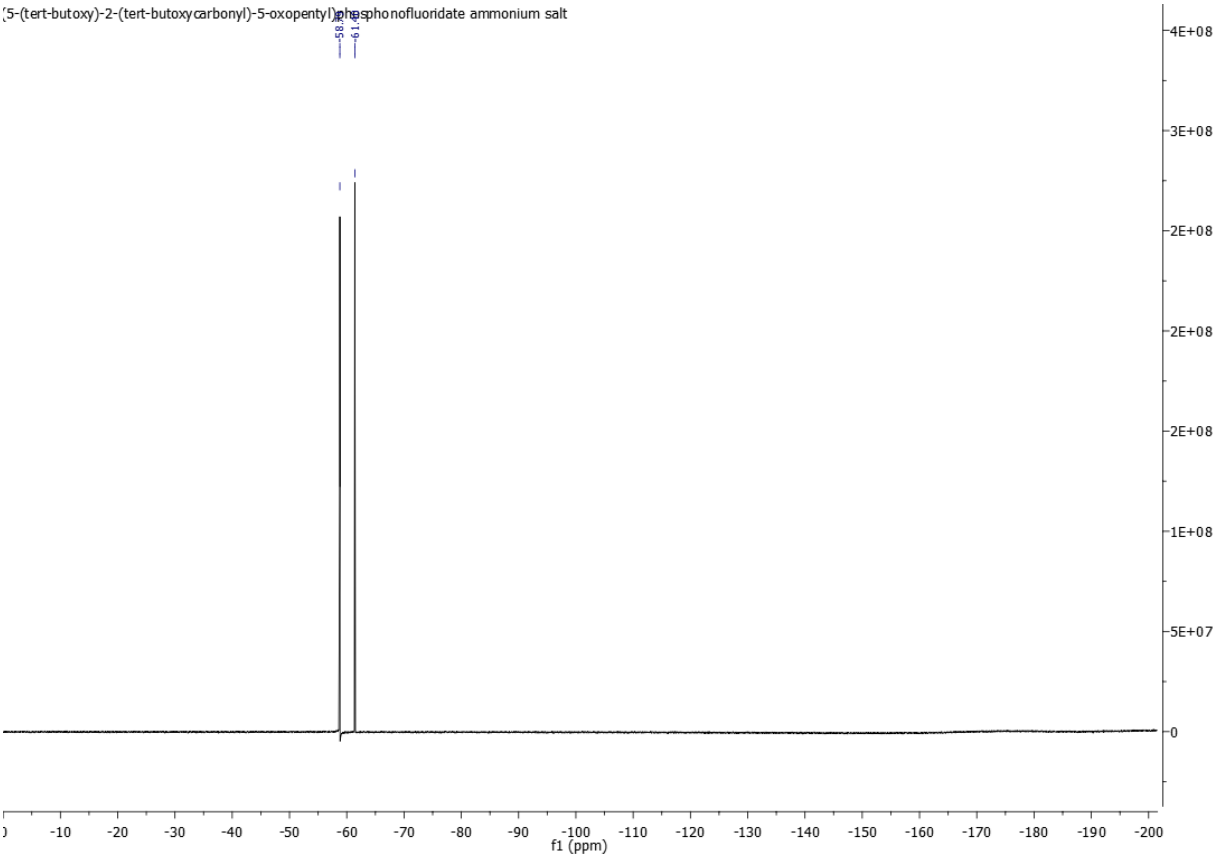
(5-(tert-butoxy)-2-(tert-butoxycarbonyl)-5-oxopentyl)phosphonofluoridate ammonium salt
f1 (ppm)

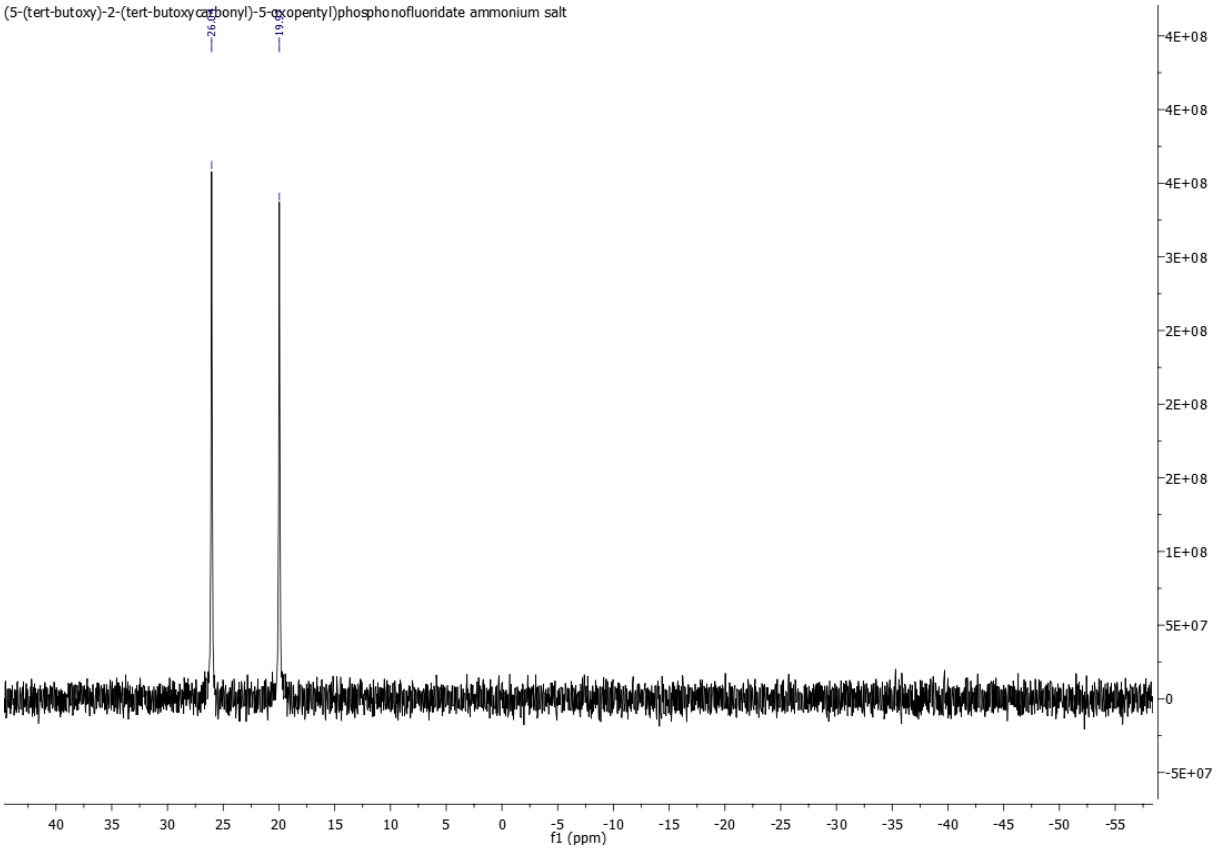
(5-(tert-butoxy)-2-(tert-butoxycarbonyl)-5-oxopentyl)phosphonofluoridate ammonium salt
26.0
19.8
4E+08
4E+08
4E+08
3E+08
2E+08
2E+08
2E+08
1E+08
5E+07
0
-5E+07
40 35 30 25 20 15 10 5 0 -5 -10 -15 -20 -25 -30 -35 -40 -45 -50 -55
f1 (ppm)

7.5.3 Radiosyntheses

*7.5.3.1 Radiosynthesis of (5-(tert-butoxy)-2-(tert-butoxycarbonyl)-5-oxopentyl)phosphono[^{18}F]fluoridate ([^{18}F]**37**)*

[^{18}F]F$^-$ was eluted from the QMA cartridge with a solution of Et_4NOTf (1 mg) in MeOH (1 mL). After evaporation of the solvent and addition of di-*tert*-butyl 2-[(diphenoxyphosphoryl)methyl]pentanedioate (**36**, 0.5 µmol) in MeCN (100 µL), the reaction mixture was stirred for 15 min at 90 °C under argon. The reaction was quenched by addition of H_2O (0.5 mL) and an aliquot was removed to determine the RCC by HPLC analysis. The remaining reaction was diluted with H_2O (0.8 mL) and the product was isolated by semi-preparative HPLC. The product fraction was diluted with H_2O (40 mL) and fixed on a Sep-Pak® C18 Plus Light cartridge (130 mg sorbent, pre-conditioned with 1 mL EtOH and 1 mL H_2O). The cartridge was rinsed with H_2O (3 mL) and dried with air (10 mL) before the product was eluted with EtOH (1 mL) and the RCP determined by HPLC analysis.

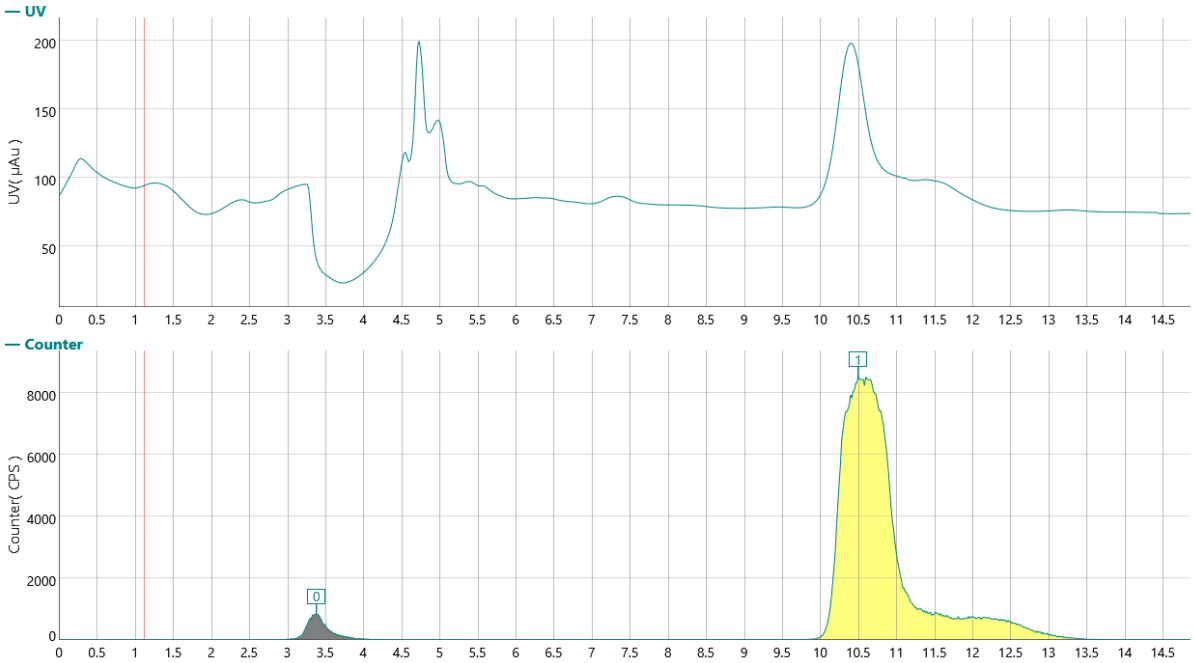

Figure 90: HPLC trace of the isolation of [^{18}F]**37**. (Top: UV chromatogram at 220 nm; bottom: radio chromatogram). Column: Phenomenex Synergi 10 µm Hydro-RP 80 Å, LC column 250×10 mm; eluent: 35% MeCN (0.1% TFA). Flow rate: 4.5 mL/min.

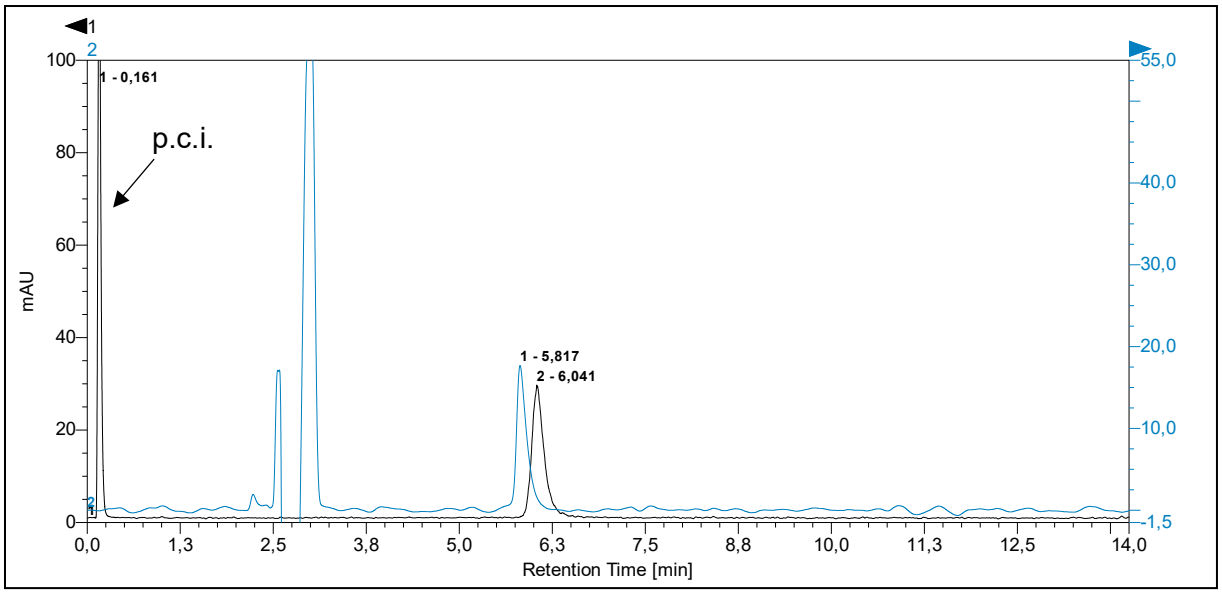

Figure 91: HPLC trace of [^{18}F]**37** co-injected with the non-radioactive reference compound **37** (Black: radio chromatogram; blue: UV chromatogram at 220 nm). Column: MultoKrom® 100-5 C18 AQ LC column 250×4.6 mm; eluent: 40% MeCN (0.1% TFA). Flow rate: 1 mL/min. Abbreviation: p.c.i. – post-column injection.

7.6 References

[1] F. Wang, Z. Li, X. Feng, D. Yang, M. Lin, *Prostate cancer and prostatic diseases* **2022**, *25*. 11–26.

[2] H.-J. Wester, M. Schottelius, *Seminars in Nuclear Medicine* **2019**, *49*. 302–312.

[3] G. Capasso, A. Stefanucci, A. Tolomeo, *European journal of medicinal chemistry* **2024**, *263*. 115966.

[4] M. Czerwińska, A. Bilewicz, M. Kruszewski, A. Wegierek-Ciuk, A. Lankoff, *Molecules (Basel, Switzerland)* **2020**, *25*.

[5] Y. Kinoshita, K. Kuratsukuri, S. Landas, K. Imaida, P. M. Rovito, C. Y. Wang, G. P. Haas, *World journal of surgery* **2006**, *30*. 628–636.

[6] a) A. Cimadamore, M. Cheng, M. Santoni, A. Lopez-Beltran, N. Battelli, F. Massari, A. B. Galosi, M. Scarpelli, R. Montironi, *Frontiers in oncology* **2018**, *8*. 653; b) F. Bray, M. Laversanne, H. Sung, J. Ferlay, R. L. Siegel, I. Soerjomataram, A. Jemal, *CA: a cancer journal for clinicians* **2024**, *74*. 229–263.

[7] K. Hlouchová, C. Barinka, V. Klusák, P. Sácha, P. Mlcochová, P. Majer, L. Rulísek, J. Konvalinka, *Journal of neurochemistry* **2007**, *101*. 682–696.

[8] S. Pastorino, M. Riondato, L. Uccelli, G. Giovacchini, E. Giovannini, V. Duce, A. Ciarmiello, *Current Radiopharmaceuticals* **2020**, *13*. 63–79.

[9] L. Schweiger, I. Virgolini, *memo* **2025**. 1–4.

[10] F. L. Giesel, J. Cardinale, M. Schäfer, O. Neels, M. Benešová, W. Mier, U. Haberkorn, K. Kopka, C. Kratochwil, *Eur J Nucl Med Mol Imaging* **2016**, *43*. 1929–1930.

[11] J. Cardinale, M. Schäfer, M. Benešová, U. Bauder-Wüst, K. Leotta, M. Eder, O. C. Neels, U. Haberkorn, F. L. Giesel, K. Kopka, *Journal of nuclear medicine : official publication, Society of Nuclear Medicine* **2017**, *58*. 425–431.

[12] Y. Chen, M. Pullambhatla, C. A. Foss, Y. Byun, S. Nimmagadda, S. Senthamizhchelvan, G. Sgouros, R. C. Mease, M. G. Pomper, *Clinical cancer research : an official journal of the American Association for Cancer Research* **2011**, *17*. 7645–7653.

[13] B. D. Zlatopolskiy, H. Endepols, P. Krapf, M. Guliyev, E. A. Urusova, R. Richarz, M. Hohberg, M. Dietlein, A. Drzezga, B. Neumaier, *Journal of nuclear medicine : official publication, Society of Nuclear Medicine* **2019**, *60*. 817–823.

[14] a) F. Dietlein, M. Hohberg, C. Kobe, B. D. Zlatopolskiy, P. Krapf, H. Endepols, P. Täger, J. Hammes, A. Heidenreich, B. Neumaier et al., *Journal of nuclear medicine : official publication, Society of Nuclear Medicine* **2020**, *61*. 202–209; b) F. Dietlein, P. Mueller, C. Kobe, H. Endepols, M. Hohberg, B. D. Zlatopolskiy, P. Krapf, A. Heidenreich, B. Neumaier, A. Drzezga et al., *Mol Imaging Biol* **2021**, *23*. 277–286; c) M. Hohberg, C. Kobe, P. Krapf, P. Täger, J. Hammes, F. Dietlein, B. D. Zlatopolskiy, H. Endepols, M. Wild, S. Neubauer et al., *EJNMMI research* **2019**, *9*. 66; d) I. Vierasu, N. Trotta, S. Albisinni, C. Mathey, G.

Leurquin-Sterk, S. Lacroix, G. van Simaeys, T. Quackels, T. Roumeguère, S. Goldman, *European J Hybrid Imaging* **2022**, *6*. 6.

[15] K. Graham, R. Lesche, A. V. Gromov, N. Böhnke, M. Schäfer, J. Hassfeld, L. Dinkelborg, G. Kettschau, *Journal of medicinal chemistry* **2012**, *55*. 9510–9520.

[16] P. F. Jackson, D. C. Cole, B. S. Slusher, S. L. Stetz, L. E. Ross, B. A. Donzanti, D. A. Trainor, *Journal of medicinal chemistry* **1996**, *39*. 619–622.

[17] H. Wang, Y. Byun, C. Barinka, M. Pullambhatla, H. C. Bhang, J. J. Fox, J. Lubkowski, R. C. Mease, M. G. Pomper, *Bioorganic & medicinal chemistry letters* **2010**, *20*. 392–397.

[18] Y. Feng, J. K. Coward, *Journal of medicinal chemistry* **2006**, *49*. 770–788.

[19] F. B. d'Andrea, C. A. Townsend, *Cell chemical biology* **2019**, *26*. 878-884.e8.

[20] C. M. Sevrain, M. Berchel, H. Couthon, P.-A. Jaffrès, *Beilstein journal of organic chemistry* **2017**, *13*. 2186–2213.

[21] H. Yang, L. Zhang, H. Liu, Y. Zhang, Z. Mou, X. Chen, J. Li, F. He, Z. Li, *Theranostics* **2023**, *13*. 472–482.

[22] Y. Shinagawa, T. Inoue, T. Kiguchu, T. Ikenogami, N. Ogawa, T. Nakagawa, M. Shindo, Y. Soejima, EP1630157 (A1), **2004**.

[23] S. Tanimoto, A. Kita, M. Okano, R. Oda, *J. Syn. Org. Chem., Jpn.* **1969**, *27*. 444–447.

[24] H. Sindhe, A. Kamble, M. M. Reddy, A. Singh, S. Sharma, *Organic & biomolecular chemistry* **2024**, *22*. 1162–1166.

[25] K. Green, *Tetrahedron Letters* **1989**, *30*. 4807–4810.

[26] A. Il'in, A. Gubaev, A. Antonova, A. Khannanov, V. Galkin, *Synthetic Communications* **2020**, *50*. 3287–3297.

[27] N. L. Fifer, J. M. White, *Organic & biomolecular chemistry* **2005**, *3*. 1776–1780.

[28] Chao Wang, Lei Zhang, Zhaobiao Mou, Wanru Feng, Zhongjing Li, Hongzhang Yang, Xueyuan Chen, Shengji Lv, and Zijing Li, *Organic letters* **2021**, *23*. 4261–4266.

[29] H. Mayr, U. von der Brüggen, *Chem. Ber.* **1988**, *121*. 339–345.

8 List of abbreviations

%	Percent
$[M+/-H]^+$	Molecule mass plus/minus one proton
®	Registered trademark
°C	Degrees celsius
2-PMPA	2-(Phosphonomethyl)-pentandioic acid
Å	Angstrom
Ac	Acetyl group
AcOH	Acetic acid
AEC	Anion exchange cartridge
Ah	Ampere-hour
A_M	Molar activity
AMP	2-Aminomethylpiperidine
Asp	Aspartaic acid
Bneo	Neopentyl glycol boronate
Boc	*tert*-Butyloxycarbonyl protecting group
Bp	Boiling point
Bpin	Pinacol boronate
Bq	Becquerel
Cat	Catalyst
Cbz	Benzyloxycarbonyl protecting group
CD	Cluster of differentiation
$CDCl_3$	Deuterated chloroform
CIT	2β-Carbomethoxy-3β-4-iodophenyl nortropane
COSY	Correlation Spectroscopy
CT	Computed Tomography
D	Deuterium
d	Doublet
d	Day
Da	Dalton
DBU	1,8-Diazabicyclo[5.4.0]undec-7-ene
DCE	1,2-Dichloroethane
DEPT 135	Distortionless Enhancement by Polarization Transfer
DIBAL-H	Diisobutylaluminium hydride
DIPEA	N,N-Diisopropylethylamine

DMAP	4-(Dimethylamino)pyridine
DMF	Dimethylformamide
DMI	1,3-Dimethyl-2-imidazolidinon
DMSO	Dimethyl sulfoxide
DNA	Deoxyribonucleic acid
DOPA	3,4-Dihydroxyphenylalanine
DOTA	2,2′,2″,2‴-(1,4,7,10-Tetraazacyclododecane-1,4,7,10-tetrayl)tetraacetic acid
DOTAGA	2,2',2''-(10-(2,6-Dioxotetrahydro-2H-pyran-3-yl)-1,4,7,10-tetraazacyclododecane-1,4,7-triyl)triacetic acid
DOTATOC	Edotreotide
DPP	Dipeptidyl peptidase
DTPA	Diethylenetriaminepentaacetic acid
DTT	Dithiothreitol
e	Electron
e.g.	“exempli gratia” (lat.)/ “for example”
EEDQ	*N*-Ethoxycarbonyl-2-ethoxy-1,2-dihydroquinoline
ELSD	Evaporative light scattering detector
EN	Electronegativity
eq	Equivalent
ESF	Ethenesulfonyl fluoride
ESI	Electrospray ionization
Et	Ethyl (-CH_2CH_3)
EtOAc	Ethyl acetate
eV	Electronvolt
EWG	Electron withdrawing group
FAP	Fibroblast activation protein
FAPI	Fibroblast activation protein inhibitor
FBEM	*N*-[2-(4-Fluorobenzoamido)ethyl]maleimide
FDA	Food and Drug Administration
FDG	2-Fluoro-deoxy-2-glucose
FDM	2-Fluoro-2-deoxy-mannose
FES	Fluoroestradiol
FETos	Fluoroethyl tosylate
FIB	1-Fluoro-4-iodobenzene
fig	Figure
FP-CIT	*N*-(3-Fluoropropyl)-2ß-carbomethoxy-3ß-(4-iodophenyl)nortropane

FPEB	3-Fluoro-5-[(pyridin-3-yl)ethynyl]benzonitrile
FPy-TFP	2,3,5,6-Tetrafluorophenyl-6-fluorodnicotinate
FS-PTAD	4-(*p*-(Fluorosulfonyl)phenyl)-1,2,4-triazoline-3,5-dione
FTP	Fluorothiophosphate
Glu	Glutamic acid
Gly	Glycine
GP	General procedure
h	Hour
HA	Hydroxyapatite
HER2	Human epidermal growth factor receptor-2
HFP	Hexyfluorophosphate
His	Histidine
HLB	Hydrophilic-lipophilic balance
HMBC	Heteronuclear Multiple Bond Correlation
HPLC	High performance liquid chromatography
HRMS	High Resolution Mass Spectrometry
HSQC	Heteronuclear Single Quantum Coherence
Hz	Hertz
i.e.	“id est” (lat.) / “that is”
*i*Pr	Isopropyl group
J	Coupling constant (Hertz)
K222	Kryptofix®222
kcal/mol	Kilocalorie per mol
kJ	Kilojoule
L	Liter
LET	Linear energy transfer
LG	Leaving group
LiHMDS	Lithium bis(trimethylsilyl)amide
Lit	Literature
LRMS	Low Resolution Mass Spectrometry
m	Meter
M	Molar (mol/L)
m	Multiplet
Me	Methyl (-CH_3)
MeCN	Acetonitrile
MeOH	Methanol
MES	2-(*N*-morpholino)ethanesulfonic acid

Met	Methionine
min	Minute
mol	Mole
Mp	Melting point
MRI	Magnetic resonance imaging
MS	Mass spectrometry
Ms	Mesyl
n	Neutron
N	Normality of a solution (1N = 1 mol/L)
NAAG	*N*-acetyl-*L*-aspartyl-*L*-glutamate
NaPi 2b	Sodium-dependent phosphate transport protein 2B
NCS	*N*-Chlorosuccinimide
NETs	Neuroendocrine tumors
NIS	Sodium Iodide Symporter
NMR	Nuclear magnetic resonance
NODA	1,4,7-Triazacyclononane-1,4-diacetic acid
NOTA	Triazacyclononane-1,4,7-triacetic acid
NP-TLC	Normal-phase thin-layer chromatography
Nu	Nucleophile
OAc	Acetoxy group
OBn	Benzyl group
OTos	Tosyl group
p	Proton
p	p-value (probability value)
p.c.i.	Post column injection
PBS	Phosphate-buffered saline
PCa	Prostata cancer
PEB	3-Fluoro-5-[(pyridin-3-yl)ethynyl]benzonitrile
PEP/POP/PREP	Prolyl endopeptidase/prolyl oligopeptidase/post-proline cleaving enzyme
PET	Positron emission tomography
PFAs	Phosphonofluoridic acids
pH	Potential of hydrogen (lat. pondus hydrogenii or potentia hydrogenii)
Phe	Phenylalanine
PPTS	Pyridinium *p*-toluenesulfonate
Pro	Proline
PSMA	Prostate-specific membrane antigen

QMA	Quarternary methyl ammonium
R	Rest
RCA	Radiochemische Ausbeute (engl. radiochemical yield (RCY))
RCC	Radiochemical conversion
RCP	Radiochemical purity
RCU	Radiochemischer Umsatz (engl. radiochemical conversion (RCC))
RCY	Radiochemical yield
R_f	Retardation factor
RP-TLC	Reversed-phase thin-layer chromatography
rt	Ambient temperature
s	Second
SA	Squaric acid
S_EAr	Electrophilic aromatic substitution
SFB	Fluorobenzoate
S_N1	Nucleophilic substitution 1
S_N2	Nucleophilic substitution 2
S_NAr	Nucleophilic aromatic substitution
SPECT	Single photon emission computed tomography
SuFEx	Sulfur(VI) fluoride exchange
T	Temperature
t	Triplet
^{t}/tert	tertiary
$t_{1/2}$	Half-life
TAT	Targeted alpha particle therapy
TATE	(Tyr^3)-octreotate
TBAF	Tetra-*n*-butylammonium fluoride
TBAP	Tetrabutylammonium perchlorate
TEAF	Tetraethylammonium fluoride
$TEAHCO_3$	Tetraethylammonium bicarbonate
TEAOTf	Tetraethylammonium triflate
TEMPO	2,2,6,6-Tetramethylpiperidine-1-oxyl
Tf	Triflyl group ($CF_3SO_3^-$)
TFA	Trifluoroacetic acid
TFP	2,3,5,6-Tetrafluorphenol
THF	Tetrahydrofuran
TLC	Thin layer chromatography
Tris	Tris(hydroxymethyl)aminomethane

TTIP	Titanium isopropoxide
™	Trademark
Val	Valine
wt	Mass percentage by weight
Z	Atomic number
Z-Gly-Pro-AMC	Benzyloxycarbonyl-Glycine-Proline-7-amino-4-methylcoumarin
γ	Gamma quant
δ	Chemical shift
ε	Electron capture

9 List of figures

Figure 1: Schematic presentation of a radiotracer consisting of a pharmacophore, a linker, and a radionuclide. 2
Figure 2: Schematic illustration of ß$^+$ decay (**A**[18]) and a PET scan (**B**). 4
Figure 3: ^{11}C-labeled radiotracers.[26–29] 6
Figure 4: Schematic representation of the ranges of various β$^-$-emitters, including the crossfire effect (left). 9
Figure 5: Chemical structures of [^{177}Lu]Lu-DOTA-TATE (left)[61] and [^{177}Lu]Lu-PSMA-617 (right)[62]. 12
Figure 6: Prosthetic groups for the indirect radiofluorination of biomolecules.[125,126,128,129] 25
Figure 7: Zwitterionic trifluoroborates suitable as precursors of radiolabeled prosthetic groups for click conjugation.[144] 27
Figure 8: Structures of Al[^{18}F]F chelating chelators, proposed complexes and labeling conditions.[148,149,154] 29
Figure 9: Structure of chelators for Al[^{18}F]F chelation, the resulting complexes and labeling conditions.[149,156,157] 30
Figure 10: Preparation of ^{18}F-labeled organofluorophosphines via ^{18}F/^{19}F isotopic exchange as described by Hong et al.[166] 32
Figure 11: ^{18}F-labeled organofluorophosphates described by Mou et al.[167] 32
Figure 12: Biologically relevant molecules functionalized with [^{18}F]phosphonofluoridic acids by Wang et al.[169] 34
Figure 13: A: [^{18}F]Sulfonyl fluorides synthesized by Inkster et al.[177]; B: Radiofluorination of sulfonyl chlorids in a microreactor as described by Matesic et al.[178]; C: [^{18}F]FS-Tyrosine synthesized by Al-Momani et al.[179] 35
Figure 14: Structure of UAMC-1110.[198] 41
Figure 15: Structures of FAPI-01 and FAPI-02.[211] 41
Figure 16: Structures of FAPI-04 and FAPI-46.[212,213] 42
Figure 17: Structures of DOTAGA.(SA.FAPI)$_2$ and DOTA.SA.FAPI.[217,218] 42
Figure 18: A: Structure of FAPI-SF, a covalent FAPI that binds via the sulfonyl fluoride group; B: Scheme of proximity-based SuFEx ligation on FAP.[222] 43
Figure 19: Structures of the target compounds with the corresponding warhead; A: sulfonyl [^{18}F]fluorides; B: phosphono[^{18}F]fluoridates; C: [^{18}F]fluoridodithioates 44
Figure 20: Structures of POP inhibitors described by Guardiola et al.[223] 46
Figure 21: Target compound with a sulfonyl [^{18}F]fluoride warhead. 46
Figure 22: Radio-NP-TLC of stability tests with [^{18}F]**11** in H_2O and PBS, solvent mixture: 4% MeOH in CH_2Cl_2. 52

Figure 23: A) Stability of [^{18}F]**11** in human blood plasma and the recovery rate. B) Radio-NP-TLC of the stability test in human blood plasma, solvent mixture: 4% MeOH in CH_2Cl_2. 52
Figure 24: Radiofluorinated phosphonate model compounds. 54
Figure 25: Example HPLC chromatograms of the various radiofluorination reactions of **12**. A) HPLC trace of [^{18}F]**13**. Reaction conditions: Kryptofix® 222 & K_2CO_3 at 80 °C for 15 minutes in MeCN. [^{18}F]**13** elutes at 14.1 min, the radioactive by-products elute later. Column: MultoKrom® 100-5 C18 AQ LC column 250×4.6 mm; eluent: 0–5 min: 20% MeCN (0.1% TFA), 5–17 min: 20→90% MeCN (0.1% TFA), 17–22 min: 90% MeCN (0.1% TFA). Flow rate: 1 mL/min. B) HPLC trace of [^{18}F]**13**. Reaction conditions: $TEAHCO_3$ at 80 °C for 15 min in DMF. [^{18}F]**13** elutes at 16.9 min, the radioactive by-products elute earlier. Column: MultoKrom® 100-5 C18 AQ LC column 2504.6 mm; eluent: 0–5 min: 20% MeCN (0.1% TFA), 5–20 min: 20→80% MeCN (0.1% TFA). The product elutes later under the conditions of B) due to the flatter gradient compared to A). Abbreviation: p.c.i. – post-column injection.....56
Figure 26: Stability of [^{18}F]**16** in H_2O (blue), PBS (pH 7.4, pink) and 0.1% TFA in H_2O (pH 2, green).....59
Figure 27: FAPI derivative with a phosphono[^{18}F]fluoridate warhead. 60
Figure 28: Structure of the second derivative without the quinolone backbone. 60
Figure 29: Chiral HPLC of (R)-**21** and (S)-**21**. HPLC conditions: Column: Daicel CHIRALPAK AD 10 µm (80 Å) 250×4.6 mm; eluent: 10% isopropyl alcohol in n-hexane. Flow rate: 1 mL/min. A) Racemic mixture (1:1); B) Chiral HPLC of (R)-**21**, t_R = 24.8 min; C) Chiral HPLC of (S)-**21**, t_R = 30.5 min.....65
Figure 30: The graphics depict the release of [^{18}F]fluoride during reaction of FAP with [^{18}F]**23**. A: The enzyme's concentration dependence on [^{18}F]fluoride release. Reaction conditions: 0.2 µg / 0.4 µg / 0.8 µg of FAP, 10 kBq of [^{18}F]**23** (A_M 30 GBq/µmol), 500 µL reaction volume, one hour incubation at rt, triplicate determination; B: Comparison of the reaction of FAP with [^{18}F]**23** in the presence and absence of the non-radioactive reference compound. Reaction conditions: 0.4 µg of FAP, 10 kBq of [^{18}F]**23** (A_M 43 GBq/µmol), inhibition with a 1 µM solution of the non-radioactive reference compound, 500 µL reaction volume, incubation for one hour at rt, triplicate determination. C: Reaction kinetics with and without addition of UAMC-1110. Reaction conditions: 0.4 of µg FAP, 10 of kBq [^{18}F]**23** (A_M 80 GBq/µmol), inhibition with a 1 µM solution of UAMC-1110, 500 µL reaction volume, incubation at rt, triplicate determination. ..72
Figure 31: [^{18}F]Fluoride released through reaction of [^{18}F]**23** with various peptidases. Reaction conditions: 10 kBq of [^{18}F]**23** (A_M 101 GBq/µmol), inhibition with 0.1 µM inhibitor (10 µM for PREP), 500 µL reaction volume, incubation for 90 min at rt, triplicate determination. 73
Figure 32: FAPI bearing a phosphono[^{18}F]fluoridodithioate warhead. 75
Figure 33: Absorption spectrum of **33** (0.1 mmol/L MeCN). 77

Figure 34: Hydrolytic stability of [^{18}F]**33**. Left: Acidic pH solutions, right: Neutral and basic solutions. 80
Figure 35: Hydrolytic stability of [^{18}F]**34**. Left: Acidic pH solutions, right: Neutral and basic pH 81
Figure 36: HPLC trace of [^{18}F]**11** co-injected with the non-radioactive reference compound **11** (Black: radio chromatogram; blue: UV chromatogram at 254 nm). Column: Phenomenex Luna® 5µm PFP(2) 100 Å LC column 250×4.6 mm; eluent: 40% MeCN. Flow rate: 1 mL/min. Abbreviation: p.c.i. – post-coloumn injection. 114
Figure 37: Stability test of [^{18}F]**11** in sodium acetate buffer (pH 4 and 5), 0.1% TFA solution (pH 2), and sodium acetate buffer (pH 4) after heating for 10 minutes at 100 °C; detected by radio-TLC. Solvent mixture: 4% MeOH in CH_2Cl_2. 115
Figure 38: HPLC trace of [^{18}F]**13** co-injected with the non-radioactive reference compound **13** (Black: radio chromatogram; blue: UV chromatogram at 254 nm). Column: MultoKrom® 100-5 C18 AQ LC column 250×4.6 mm; eluent: 0–5 min 20% MeCN (0.1% TFA), 5–20 min: 20→90% MeCN (0.1% TFA). Flow rate: 1 mL/min. Abbreviation: p.c.i. – post-column injection. 130
Figure 39: HPLC trace of the isolation of [^{18}F]**16**. (Top: UV chromatogram at 210 nm; bottom: radio chromatogram). Column: Phenomenex Synergi 10 µm Hydro-RP 80 Å, LC column 250×10 mm; eluent: 15% MeCN. Flow rate: 3.5 mL/min. 131
Figure 40: HPLC trace of [^{18}F]**16** co-injected with the non-radioactive reference compound **16** (Blue: radio chromatogram; black: UV chromatogram at 210 nm). Column: MultoKrom® 100-5 C18 AQ LC column 250×4.6 mm; eluent: 20% MeCN (0.1% TFA). Flow rate: 1 mL/min. Abbreviation: p.c.i. – post-column injection. 131
Figure 41: Trace of the isolation of [^{18}F]**23**. (Top: UV chromatogram at 254 nm; bottom: radio chromatogram). Column: Phenomenex Synergi 10 µm Hydro-RP 80 Å, LC column 250×10 mm; eluent: 7% MeCN. Flow rate: 4.5 mL/min. 166
Figure 42: HPLC trace of [^{18}F]**23** co-injected with the non-radioactive reference compound **23** (Black: radio chromatogram; blue: UV chromatogram at 254 nm). Column: MultoKrom® 100-5 C18 AQ LC column 250×4.6 mm; eluent: 7% MeCN (0.1% TFA). Flow rate: 1 mL/min. Abbreviation: p.c.i. − post-column injection. 167
Figure 43: Calibration curve for calculating the molar activity of [^{18}F]**23**. 167
Figure 44: HPLC trace of the isolation of [^{18}F]**25**. (Top: UV chromatogram at 254 nm; bottom: radio chromatogram). Column: Phenomenex Synergi 10 µm Hydro-RP 80 Å, LC column 250×10 mm; eluent: 7% MeCN. Flow rate: 4.5 mL/min. 168
Figure 45: HPLC trace of [^{18}F]**25** co-injected with the non-radioactive reference compound **25** (black: radio chromatogram; blue: UV chromatogram at 254 nm). Column: MultoKrom® 100-5 C18 AQ LC column 250×4.6 mm; eluent: 10% MeCN (0.1% TFA). Flow rate: 1 mL/min. Abbreviation: p.c.i. – post-column injection. 169

Figure 46: Calibration curve for calculating the molar activity of [^{18}F]**25**. 169
Figure 47: NP-Radio-TLCs of stability tests in H_2O (left) and PBS (right). 176
Figure 48: NP-Radio-TLCs of stability tests at pH 1 (left) and pH 2 (right). 177
Figure 49: NP-Radio-TLCs of stability tests at pH 4 (left) and pH 5 (right). 177
Figure 50: NP-Radio-TLCs of stability tests at pH 8 (left) and pH 10 (right). 177
Figure 51: NP-Radio-TLCs of stability tests in FAP-buffer. 178
Figure 52: NP-Radio-TLCs of stability tests at pH 4, 5 minutes heating at 100 °C (left) and 10 minutes heating at 100 °C (right). 178
Figure 53: Radio-TLC from a FAP enzyme experiment. 178
Figure 54: NP-Radio-TLCs of stability tests in H_2O (left) and PBS (right). 179
Figure 55: NP-Radio-TLCs of stability tests in FAP-buffer. 179
Figure 56: Radio-TLC from a FAP enzyme experiment. 179
Figure 57: HPLC trace of the isolation of [^{18}F]**33**. (Top: UV chromatogram at 210 nm; bottom: radio chromatogram). Column: Phenomenex Gemini 5 µm C18 110 Å, LC column 250×10 mm; eluent: 40% MeCN in PBS (0.01 M, pH 7.4). Flow rate: 4.5 mL/min. 195
Figure 58: HPLC chromatogram of [^{18}F]**33** co-injected with the non-radioactive reference compound **33** (Black: radio chromatogram; blue: UV chromatogram at 226 nm). Column: Phenomenex Luna® 5µm PFP(2) 100 Å LC column 250×4.6 mm; eluent: 30% MeCN in PBS (0.01 M, pH 7.4). Flow rate: 1 mL/min. Abbreviation: p.c.i. – post-column injection. 196
Figure 59: HPLC trace of the isolation of [^{18}F]**34**. (Top: UV chromatogram at 254 nm; bottom: radio chromatogram). Column: Phenomenex Gemini 5 µm C18 110 Å, LC column 250×10 mm; eluent: 30% EtOH in PBS (0.01 M, pH 7.4). Flow rate: 3.5 mL/min. 197
Figure 60: HPLC chromatogram of [^{18}F]**34** co-injected with the non-radioactive reference compound **34** (Black: radio chromatogram; blue: UV chromatogram at 254 nm). Column: Phenomenex Luna® 5µm PFP(2) 100 Å LC column 250×4.6 mm; eluent: 20% MeCN in PBS (0.01 M, pH 7.4). Flow rate: 1 mL/min. Abbreviation: p.c.i. – post-column injection. 197
Figure 61: Calibration curve for calculating the molar activity of [^{18}F]**34**. 198
Figure 62: Radio-HPLC chromatogram of [^{18}F]**33** to determine the stability in TFA solution (0.1%, pH 2). Column: Phenomenex Luna® 5 µm PFP(2) 100 Å LC column 250×4.6 mm; eluent: 30% MeCN in PBS (0.01 M, pH 7.4). Flow rate: 1 mL/min. Abbreviation: p.c.i. – post-column injection. 200
Figure 63: Radio-HPLC chromatogram of [^{18}F]**33** to determine the stability in NaOAc buffer (0.1 M, pH 4). Column: Phenomenex Luna® 5 µm PFP(2) 100 Å LC column 250×4.6 mm; eluent: 30% MeCN in PBS (0.01 M, pH 7.4). Flow rate: 1 mL/min. Abbreviation: p.c.i. – post-column injection. 200
Figure 64: Radio-HPLC chromatogram of [^{18}F]**33** to determine the stability in NaOAc buffer (0.1 M, pH 6). Column: Phenomenex Luna® 5 µm PFP(2) 100 Å LC column 250×4.6 mm;

eluent: 30% MeCN in PBS (0.01 M, pH 7.4). Flow rate: 1 mL/min. Abbreviation: p.c.i. – post-column injection.....201
Figure 65: Radio-HPLC chromatogram of [^{18}F]**33** to determine the stability in H_2O. Column: Phenomenex Luna® 5 µm PFP(2) 100 Å LC column 250×4.6 mm; eluent: 30% MeCN in PBS (0.01 M, pH 7.4). Flow rate: 1 mL/min. Abbreviation: p.c.i. – post-column injection.....201
Figure 66: Radio-HPLC chromatogram of [^{18}F]**33** to determine the stability in PBS buffer (0.01 M, pH 7.4). Column: Phenomenex Luna® 5 µm PFP(2) 100 Å LC column 250×4.6 mm; eluent: 30% MeCN in PBS (0.01 M, pH 7.4). Flow rate: 1 mL/min. Abbreviation: p.c.i. – post-column injection.....202
Figure 67: Radio-HPLC chromatogram of [^{18}F]**33** to determine the stability in $NaHCO_3$ solution (0.1 M, pH 8). Column: Phenomenex Luna® 5 µm PFP(2) 100 Å LC column 250×4.6 mm; eluent: 30% MeCN in PBS (0.01 M, pH 7.4). Flow rate: 1 mL/min. Abbreviation: p.c.i. – post-column injection.....202
Figure 68: Radio-HPLC chromatogram of [^{18}F]**33** to determine the stability in NH_4Cl/NH_4OH buffer (pH 10). Column: Phenomenex Luna® 5 µm PFP(2) 100 Å LC column 250×4.6 mm; eluent: 30% MeCN in PBS (0.01 M, pH 7.4). Flow rate: 1 mL/min. Abbreviation: p.c.i. – post-column injection.....203
Figure 69: Radio-HPLC chromatogram of [^{18}F]**33** to determine the stability in NaOAc buffer (0.1 M, pH 4) after heating for 5 min at 100 °C. Column: Phenomenex Luna® 5 µm PFP(2) 100 Å LC column 250×4.6 mm; eluent: 30% MeCN in PBS (0.01 M, pH 7.4). Flow rate: 1 mL/min. Abbreviation: p.c.i. – post-column injection.....203
Figure 70: Radio-HPLC chromatogram of [^{18}F]**33** to determine the stability in NaOAc buffer (0.1 M, pH 4) after heating for 10 min at 100 °C. Column: Phenomenex Luna® 5 µm PFP(2) 100 Å LC column 250×4.6 mm; eluent: 30% MeCN in PBS (0.01 M, pH 7.4). Flow rate: 1 mL/min. Abbreviation: p.c.i. – post-column injection. 204
Figure 71: Radio-HPLC chromatogram of [^{18}F]**33** to determine the stability in human blood plasma. Column: Phenomenex Luna® 5 µm PFP(2) 100 Å LC column 250×4.6 mm; eluent: 30% MeCN in PBS (0.01 M, pH 7.4). Flow rate: 1 mL/min. Abbreviation: p.c.i. – post-column injection.....204
Figure 72: Radio-HPLC chromatogram of [^{18}F]**34** to determine the stability in TFA solution (0.55%, pH 1). Column: Phenomenex Luna® 5 µm PFP(2) 100 Å LC column 250×4.6 mm; eluent: 20% MeCN in PBS (0.01 M, pH 7.4). Flow rate: 1 mL/min. Abbreviation: p.c.i. – post-column injection.....205
Figure 73: Radio-HPLC chromatogram of [^{18}F]**34** to determine the stability in TFA solution (0.1%, pH 2). Column: Phenomenex Luna® 5 µm PFP(2) 100 Å LC column 250×4.6 mm; eluent: 20% MeCN in PBS (0.01 M, pH 7.4). Flow rate: 1 mL/min. Abbreviation: p.c.i. – post-column injection.....205

Figure 74: Radio-HPLC chromatogram of [^{18}F]**34** to determine the stability in NaOAc buffer (0.1 M, pH 4). Column: Phenomenex Luna® 5 µm PFP(2) 100 Å LC column 250×4.6 mm; eluent: 20% MeCN in PBS (0.01 M, pH 7.4). Flow rate: 1 mL/min. Abbreviation: p.c.i. – post-column injection.....206
Figure 75: Radio-HPLC chromatogram of [^{18}F]**34** to determine the stability in NaOAc buffer (0.1 M, pH 5). Column: Phenomenex Luna® 5 µm PFP(2) 100 Å LC column 250×4.6 mm; eluent: 20% MeCN in PBS (0.01 M, pH 7.4). Flow rate: 1 mL/min. Abbreviation: p.c.i. – post-column injection.....206
Figure 76: Radio-HPLC chromatogram of [^{18}F]**34** to determine the stability in H_2O. Column: Phenomenex Luna® 5 µm PFP(2) 100 Å LC column 250×4.6 mm; eluent: 20% MeCN in PBS (0.01 M, pH 7.4). Flow rate: 1 mL/min. Abbreviation: p.c.i. – post-column injection. 207
Figure 77: Radio-HPLC chromatogram of [^{18}F]**34** to determine the stability in PBS (0.01 M, pH 7.4). Column: Phenomenex Luna® 5 µm PFP(2) 100 Å LC column 250×4.6 mm; eluent: 20% MeCN in PBS (0.01 M, pH 7.4). Flow rate: 1 mL/min. Abbreviation: p.c.i. – post-column injection. 207
Figure 78: Radio-HPLC chromatogram of [^{18}F]**34** to determine the stability in $NaHCO_3$ solution (0.1 M, pH 8). Column: Phenomenex Luna® 5 µm PFP(2) 100 Å LC column 250×4.6 mm; eluent: 20% MeCN in PBS (0.01 M, pH 7.4). Flow rate: 1 mL/min. Abbreviation: p.c.i. – post-column injection.....208
Figure 79: Radio-HPLC chromatogram of [^{18}F]**34** to determine the stability in NH_4OH/NH_4Cl buffer (pH 10). Column: Phenomenex Luna® 5 µm PFP(2) 100 Å LC column 250×4.6 mm; eluent: 20% MeCN in PBS (0.01 M, pH 7.4). Flow rate: 1 mL/min. Abbreviation: p.c.i. – post-column injection.....208
Figure 80: Radio-HPLC chromatogram of [^{18}F]**34** to determine the stability in NaOAc buffer (0.1 M, pH 4) after heating for 5 min at 100 °C. Column: Phenomenex Luna® 5 µm PFP(2) 100 Å LC column 250×4.6 mm; eluent: 20% MeCN in PBS (0.01 M, pH 7.4). Flow rate: 1 mL/min. Abbreviation: p.c.i. – post-column injection. 209
Figure 81: Radio-HPLC chromatogram of [^{18}F]**34** to determine the stability in NaOAc buffer (0.1 M, pH 4) after heating for 10 min at 100 °C. Column: Phenomenex Luna® 5 µm PFP(2) 100 Å LC column 250×4.6 mm; eluent: 20% MeCN in PBS (0.01 M, pH 7.4). Flow rate: 1 mL/min. Abbreviation: p.c.i. – post-column injection. 209
Figure 82: Radio-HPLC chromatogram of [^{18}F]**34** to determine the stability in human blood plasma after 120 min. Column: Phenomenex Luna® 5 µm PFP(2) 100 Å LC column 250×4.6 mm; eluent: 20% MeCN in PBS (0.01 M, pH 7.4). Flow rate. 1 mL/min. Shifting the retention time of [^{18}F]**34** by using a different HPLC. Abbreviation: p.c.i. – post-column injection.....210
Figure 83: HPLC chromatogram of the non-radioactive reference compound **34**. UV chromatogram at 254 nm. Column: Phenomenex Luna® 5 µm PFP(2) 100 Å LC column

250×4.6 mm; eluent: 20% MeCN in PBS (0.01 M, pH 7.4). Flow rate. 1 mL/min.Confirmation of the retention time of [^{18}F]**34** due to the use of a different HPLC system for the reference compound. 210
Figure 84: Structures of the urea-based PSMA inhibitors [^{18}F]PSMA-1007[10,11], [^{18}F]DCFPyL[12] and [^{18}F]JK-PSMA-7[13].....228
Figure 85: Structures of 2-PMPA[15] and rac-2-[^{18}F]fluoro-4-(phosphonomethyl)pentanedioic acid.[16].....229
Figure 86: Structure of the novel 2-PMPA analog.....230
Figure 87: TLC analysis of the second attempt of deprotection of [^{18}F]**37**. TLC solvent mixture: n-BuOH:H_2O:HAc = 5:1:1. Lanes: 1: PBS fraction; 5: EtOH fraction; 3: Diluted [^{18}F]fluoride solution in H_2O; 4: TFA fraction; 5: Diluted solution of [^{18}F]**37** in H_2O.....233
Figure 88: HPLC traces showing degradation of **38** in the semi-preparative HPLC mobile phase. Retention time of the product: t_R = 8.8–9.0 min; retention time of the by-product: t_R = 7.3–7.4 min. Black: injection close to HPLC cut; green: 30 minutes later; blue: 60 minutes later. Column: MultoKrom® 100-5 C18 AQ LC column 250×4.6 mm; eluent: 40% MeCN (0.1% TFA). Flow rate: 1 mL/min. 235
Figure 89: Mass spectra of **43** at different cone voltages and with and without acid in the solvent. From top to bottom: cone voltage of 100 V, 50 V, and 20 V. Black: Mass of **43** (m/z = 567.12), blue: mass of the monocarboxylic acid (m/z = 473.10), green: mass of the dicarboxylic acid (m/z = 379.09).....238
Figure 90: HPLC trace of the isolation of [^{18}F]**37**. (Top: UV chromatogram at 220 nm; bottom: radio chromatogram). Column: Phenomenex Synergi 10 µm Hydro-RP 80 Å, LC column 250×10 mm; eluent: 35% MeCN (0.1% TFA). Flow rate: 4.5 mL/min. 262
Figure 91: HPLC trace of [^{18}F]**37** co-injected with the non-radioactive reference compound **37** (Black: radio chromatogram; blue: UV chromatogram at 220 nm). Column: MultoKrom® 100-5 C18 AQ LC column 250×4.6 mm; eluent: 40% MeCN (0.1% TFA). Flow rate: 1 mL/min. Abbreviation: p.c.i. – post-column injection. 263

10 List of schemes

Scheme 1: Synthesis of [^{18}F]FDG via electrophilic radiofluorination of 3,4,6-tri-O-acetyl-D-glucal as described by Ido et al.[77] 14
Scheme 2: S_N2 reaction mechanism. Nu = nucleophile, LG = leaving group.[85] 16
Scheme 3: Synthesis of [^{18}F]FDG via aliphatic nucleophilic radiofluorination.[86,87] 16
Scheme 4: The various mechanisms of the SNAr reaction described by Meisenheimer (A)[96] and Kwan *et al*.[95] 18
Scheme 5: Synthesis of [^{18}F]altanserin described by Hamacher et al.[97] 18
Scheme 6: Radiofluorination by nucleophilic aromatic substitution of various iodonium precursors: A: diaryliodonium salts;[99] B: aryl(2-theinyl)iodonium salts;[102] C: iodonium ylides.[105] 19
Scheme 7: Radiofluorination of triarylsulfonium salts described by A: Mu et al.[106]; B: Årstad and co-workers;[107] C: Ritter and co-workers.[109] 20
Scheme 8: Pd-mediated electrophilic radiofluorination of aryl boronate described by Ritter and co-workers.[113] 21
Scheme 9: Ni-mediated oxidative radiofluorination described by Ritter and co-workers.[114] .21
Scheme 10: Various copper-mediated radiofluorinations. A: Radiolabeling of diaryliodonium salts described by Scott and co-workers[115]; B: Radiofluorination of aryl boronate esters described by Gouverneur and co-workers[116]; C: Radiofluorination of aryl boronic acids described by Scott and co-workers[117]; D: Radiofluorination of trialkylstannanes described by Scott and co-workers[118]; E: Cu-catalyzed C-H radiofluorination of aromatic carboxylic acids described by Sanford and co-workers[119]; F: NHC-Copper mediated ligand directed 18F-fluorination of aryl halogenides described by Sanford and co-workers.[120] 23
Scheme 11: Proposed mechanism of Cu-mediated radiofluorination described by Zarrad et al.[83] 24
Scheme 12: Optimized radiofluorination of different labeling precursors for the synthesis of ^{18}F-labeled aromatics.[123] 24
Scheme 13: Cu-catalyzed 1,3-dipolar cycloaddition between an azide-functionalized peptide and an ^{18}F-labeled alkyne.[131] 25
Scheme 14: Indirect radiofluorination via Suzuki-Miyaura cross-coupling (A)[133] and Sonogashira cross-coupling (B).[134] 26
Scheme 15: Synthesis of [^{18}F]aryltrifluoroborate from arylboronic acid pinacol esters as described by Ting et al. (A)[139] and from arylborimides as described by Liu et al. (B).[143] 27
Scheme 16: Preparation of radiolabeled compounds containing Si−^{18}F bonds by Rosenthal et al.[145] and Ting et al.[139] 28

Scheme 17: Radiolabeling of Try^3-octreotate via $^{18}F/^{19}F$ isotopic exchange. Method A: [^{18}F]KF/Kryptofix 222, MeCN, rt, 10-15 min; Method B: [^{18}F]F$^-$/[^{18}O]H_2O, MeCN (15-20% total volume), 95 °C, 30 min.[147] 29
Scheme 18: Radiosynthesis of [^{18}F]Dimefox described by Studenov et al.[161] 31
Scheme 19: Radiolabeling of a 1,3-dimethylimidazol-2-ylidene-PF5 derivative via $^{18}F/^{19}F$ isotopic exchange as described by Vabre et al.[164] 31
Scheme 20: Cu(II)-mediated direct ^{18}F-dehydrofluorination of a model compound (A); Proposed reaction mechanism for Cu(II)-mediated dehydrofluorination (B).[168] 33
Scheme 21: Proposed fluorination hydrolysis reaction mechanism by d'Andrea et al.[170] (A) and Wang et al.[169] (B). 33
Scheme 22: General reaction equation for the synthesis of [^{18}F]FTPs described by Yang et al.[171] 34
Scheme 23: [^{18}F]ESF as a fluorination reagent.[172,182] 36
Scheme 24: Synthesis of [^{18}F]fluorosulfate.[172,185] 36
Scheme 25: Synthesis of arylfluorosulfates via SuFEx-based $^{18}F/^{19}F$ isotopic exchange described by Zheng et al.[187]; B: Optimized protocol developed by Walter et al.[84] 37
Scheme 26: Radiosynthesis of sulfamoyl [^{18}F]fluorides described by Jeon et al.[188] 37
Scheme 27: Synthesis of sulfamoyl [^{18}F]fluorides by direct radiofluorosulfurylation of amines.[172,189] 38
Scheme 28: Synthesis of (S)-(1-((quinoline-4-carbonyl)glycyl)pyrrolidin-2-yl)methanesulfonyl fluoride (**11**). 47
Scheme 29: Synthesis of **3** according to protocols by Wilson et al.[227] and Jansen et al.[198] Reaction conditions: a) Oxalyl chloride, DMF, CH_2Cl_2, 0 °C – rt, 18 h; b) Glycine methyl ester hydrochloride (**2a**) or Gylcine ethyl ester hydrochloride (**2b**), Et_3N, CH_2Cl_2, 0 °C – rt, 24,5 h; c) NaOH, MeOH/H_2O (1:1), rt, 18 h, then: HCl. 47
Scheme 30: Synthesis of **8** according to protocols of Guardiola et al.[223] Reaction conditions: a) Et_3N, methanesulfonyl chloride, CH_2Cl_2, 0 °C – rt, 17,5 h, then: Cs_2CO_3, thioacetic acid, DMF, rt, 3 d; b) H_2O_2, AcOH, rt, 17 h, then: NaOAc•3H_2O, 20 min, rt; c) XtalFluor-M®, Et_3N•HF, reflux, 4d; d) HBr in AcOH, CH_2Cl_2, rt, 1 h. 48
Scheme 31: Synthesis of **7** by alternative reaction routes. Reaction conditions: a) $(COCl)_2$, DMF, C_6H_6, 0 °C – rt, 35 min[229]; b) NCS, HCl, MeCN, 0 °C, 80 min[230], 90%; c) KHF_2, MeCN/H_2O, rt, 92 h[186], 65% via **6** from a), 73% via **6** from b. 48
Scheme 32: Formation of mixed anhydrides by EEDQ and subsequent amide formation.[232,234,235] 49
Scheme 33: Synthesis route for the preparation of **10**. Reaction conditions: a) $SOCl_2$, MeOH, 0 °C – rt, 24 h [236]; b) Et_3N, EEDQ, DMF, rt, 45 h. 49
Scheme 34: Radiofluorination of **11** via $^{18}F/^{19}F$ isotopic exchange. 50

Scheme 35: Reaction scheme for the synthesis of diphenyl tritylphosphonate (**12**) and subsequent synthesis of the non-radioactive reference compound **13**. Reaction conditions: a) diphenyl phosphite, DBU, acetone, 18.5 h, rt; b) TBAF, THF, overnight, rt. 54
Scheme 36: Radiosynthesis of [^{18}F]**13** from **12**. 55
Scheme 37: Synthesis of the labeling precursor **15**. Reaction conditions: a) ^{t}BuOH, n-BuLi, THF, reflux, 1 h; b) diphenyl phosphite, Me_3Al, CH_2Cl_2, rt, overnight. 57
Scheme 38: Fluorination of **15** to obtain the non-radioactive reference compound **16**. Reaction conditions: a) TBAF, THF, rt, overnight.....57
Scheme 39: Radiosynthesis of [^{18}F]**16** from **15**. 58
Scheme 40: Synthesis of precursor **22**. 61
Scheme 41: Synthesis of **17** from **3** and TFP. 61
Scheme 42: Reaction route for the synthesis of diethyl (R)-pyrrolidin-2-ylphosphonate [(R)-**21**] according to Katritzky et al.[242] Reaction conditions: i) 0.1 N HCl, 50 °C, 0.5 h; ii) CH_2Cl_2, rt, 12 h; iii) $P(OEt)_3$, $ZnBr_2$, CH_2Cl_2, rt; iii) Pd/C, H_2.....62
Scheme 43: Synthesis of **18** from 4,4-dimethoxybutanenitrile and subsequent condensation to (S)-**19**. Reaction conditions: a) DIBAL-H, CH_2Cl_2, –78 °C to rt, 18 h[246,247]; b) (S)-(–)-^{t}butylsulfinamide, $Ti(OEt)_4$, CH_2Cl_2, rt, 65.5 h[244]. 62
Scheme 44: Synthesis of (R)-**21** via (S,R)-**20**. Reaction conditions: a) Diphenyl phosphite, LiHMDS, THF, –78 °C, 2.5 h[244]; b) Et_3SiH, TFA, H_2O, rt, 25 h.[256] 64
Scheme 45: Synthesis route for preparation of (S)-**21**. Reaction conditions: a) (R)-(–)-^{t}butylsulfinamide, $Ti(OEt)_4$, CH_2Cl_2, rt, 113 h[244]; b) diphenyl phosphite, LiHMDS, THF, –78 °C, 3.5 h[244]; c) Et_3SiH, TFA, H_2O, rt, 18 h[256]. 64
Scheme 46: Overview of the synthesis sequence for precursor **22** and reference compound **23**. 66
Scheme 47: Synthesis of **24** and **25**. Reaction conditions: a) Benzyl bromide, Et_3N, CH_2Cl_2, 0 °C – rt, 16 h[257]; b) NH_4F, MeCN, 60 °C, 17 h[170]. 66
Scheme 48: Radiosynthesis of [^{18}F]**23** from **22**. 67
Scheme 49: Radiosynthesis of [^{18}F]**25** from **24**. 68
Scheme 50: Hydrolysis of Z-Gly-Pro-AMC to 7-amino-4-methylcoumarin by prolyl endopeptidases.[259] 70
Scheme 51: Synthesis of **30** according to the protocol of Yang et al.[171] Reaction conditions: a) Ethane-1,2-dithiol, Et_3N, C_6H_6, 0 °C – rt, 2.5 h; b) 5-(Ethylthio)-1H-tetrazol, Boc-L-prolinol, CH_2Cl_2, rt, 3 h; c) S_8, CH_2Cl_2, rt, overnight; d) TFA, CH_2Cl_2, rt, overnight. 76
Scheme 52: Synthesis of **30** according to the protocol of Yang et al.[171] Reaction conditions: a) L-Prolinol, 2,6-lutidine, DMF, 55 °C, overnight; b) Ethane-1,2-dithiol, Et_3N, C_6H_6, 0 °C – rt, 2.5 h; c) 5-(Ethylthio)-1H-tetrazol, CH_2Cl_2, rt, 3 h; d) S_8, rt, overnight.....76

Scheme 53: Synthesis of the reference compounds by fluorination of **28** or **30** with TBAF.[171] 77
Scheme 54: Radiosynthesis of [^{18}F]**33**. 78
Scheme 55: Radiosynthesis of [^{18}F]**34**. 79
Scheme 56: Synthesis of **36**. Reaction conditions: a) tributylphosphine, rt, 2.5 h[18]; b) diphenylphosphite, trimethylaluminum, CH_2Cl_2, 0 °C–rt, overnight.[15] 231
Scheme 57: Synthesis of the protected non-radioactive reference compound **37**. Reaction conditions: NH_4F, MeCN, 60 °C, 15 h.[19] 231
Scheme 58: Radiosynthesis of [^{18}F]**37** 232
Scheme 59: Reaction pathways for the synthesis of **39**. Route 1 involves initial deprotection of the carboxylic acids followed by fluorination, while route 2 performs the two steps in reverse order. 234
Scheme 60: Reaction route for the synthesis of precursor **43**. Reaction conditions: a) $NaBH_4$, MeOH, 0 °C–rt, 3 h[22]; b) acryloyl chloride, Et_3N, DMAP, CH_2Cl_2, 0 °C–rt, overnight[23,24]; c) tributylphosphine, rt, 2 h[18]; d) diphenyl phosphite, Me_3Al, CH_2Cl_2, 0 °C–rt, overnight.[15] 236
Scheme 61: Diphenyl (dicyclopropylmethyl)phosphonate was identified as a by-product in the synthesis of **43** with Me_3Al by ESI-LRMS and ^{1}H-NMR spectroscopy. 237
Scheme 62: Synthesis of **44** from **43**. Reaction conditions: NH_4F, MeCN, 60 °C, overnight.[19] 239
Scheme 63: Planned route for the synthesis of **39** from **43**. Instead, 2-PMPA was identified as a by-product from the reaction of **43** with HCl in 1,4-dioxane. 240

11 List of tables

Table 1: Data of the most common PET nuclides.[11,19] 5
Table 2: Overview of selected radionuclides used for endoradiotherapy.[36] 10
Table 3: Screening (n=1) of reaction conditions for radiofluorination of **11** with TBAP as elution salt. 50
Table 4: Screening (n=1) of reaction conditions for the radiofluorination of **11** using 2.50 µmol $BnEt_3NCl$ in MeOH (0.7 mL) as elution salt.....51
Table 5: Optimization of the reaction conditions for radiofluorination of **12** (n=3). 55
Table 6: Optimization of the reaction conditions for radiofluorination of [^{18}F]**16**. 58
Table 7: Optimization of the reaction conditions for synthesis of (S)-**19** from 4,4-dimethoxybutanal and (S)-(–)-^{t}butylsulfinamide. 63
Table 8: Optimization of the reaction conditions for radiolabeling of **22** (n=3).....67
Table 9: Optimization of the reaction conditions for radiolabeling of **24**. Unchanged parameters: 0.5 µmol precursor in 100 µL MeCN. n=3. 68
Table 10: Optimization of the radiosynthesis of [^{18}F]**33**. All reactions were carried out in DMF. n=3. 78
Table 11: Optimization of the reaction conditions for radiosynthesis of [^{18}F]**34**. All reactions were carried out in 100 µL of solvent. n=3. 79
Table 12: Experimental data of the synthesis of **2a** and **2b**. 91
Table 13: Experimental data for the synthesis of **10** and **11**. 101
Table 14: Concentration of [^{18}F]**11** in the test solutions examined. The tracer was filled up to 1.00 mL with the test medium. 114
Table 15: Experimental data for the synthesis of phosphonofluoridates with TBAF as fluorinating reagent. 119
Table 16: Experimental data for the synthesis of phosphonofluoridates with NH_4F as fluorinating reagent. 142
Table 17: Optical rotations of (R)-**21** and (S)-**21**.....165
Table 18: Data from the measurement using chiral HPLC for (R)-**21** and (S)-**21**. 165
Table 19: Data for generating the calibration curve for determining the molar activity of [^{18}F]**23**. 167
Table 20: Data for generating the calibration curve for determining the molar activity of [^{18}F]**25**. 170
Table 21: Pipetting protocols for the two preliminary experiments with HA in the reaction solution and observed [^{18}F]F^- release. 172
Table 22: Released [^{18}F]F^- by the reaction of [^{18}F]**23** with FAP (n=1). 173
Table 23: Pipetting protocols and observed [^{18}F]F^- release. 173

Table 24: Pipetting protocols and observed [^{18}F]F^- release. 174
Table 25: Overview of the enzyme-specific buffer systems, inhibitors and substrates used. 175
Table 26: Pipetting protocols for each enzyme experiment. 175
Table 27: Experimental data for the synthesis of **28** and **30**. 181
Table 28: Experimental data for the synthesis of phosphorofluoridodithioates with TBAF as the fluorination reagent. 184
Table 29: Data for generating the calibration curve for determining the molar activity of [^{18}F]**34**. 198
Table 30: Experimental data for the synthesis of phosphonofluoridates with NH_4F as fluorinating reagent. 248

Teilpublikationen:

1. Humpert, S.; **Elsner, A.-L.**; Zlatopolskiy, B.; Neumaier, B.
   Towards covalent fibroplast activation protein (FAP) inhibitors for delivery of therapeutic radionuclides into FAP-positive tumors (Poster), 25th International Symposium on Radiopharmaceutical Sciences, iSRS 2023, 22. – 26. Mai 2023, Honolulu, USA. Conference Presentation (After Call).

2. **Elsner, A.-L.**; Zlatopolskiy, B.; Neumaier, B.
   Auf dem Weg zu kovalenten FAP-Inhibitoren für die Endoradiotherapie (Vortrag), 29. Jahrestagung der Arbeitsgemeinschaft Radiochemie / Radiopharmazie, 1. Jahrestagung der grpw e.V., 28. – 30. September 2023, Bad Salzuflen.

3. **A. Elsner**, B. D. Zlatopolskiy, B. Neumaier
   Synthese und Stabilitätsuntersuchung eines potenziellen kovalenten FAP-Inhibitors (ePoster), 62. Jahrestagung der Deutschen Gesellschaft für Nuklearmedizin (DGN), 10. – 13. April 2024, Leipzig. Abstract veröffentlich in: Nuklearmedizin **2024**, *63(02)*: 153-154. DOI: 10.1055/s-0044-1782472.

4. **A. L. Elsner**, D. Bier, D. Schneider, B. Neumaier, B. Zlatopolskiy
   Herstellung und *in vitro* Untersuchung eines radiomarkierten kovalenten FAP-Inhibitors (Wissenschaftlicher Vortrag), 63. Jahrestagung der Deutschen Gesellschaft für Nuklearmedizin (DGN), 02. – 05. April 2025, Bremen. Abstract veröffentlicht in: Nuklearmedizin 2025; 64(01): 75-76. DOI: 10.1055/s-0045-1804367.

5. Zlatopolskiy, B; **Elsner, A.-L.**; Bier, D., Schneider, D., Neumaier, B.
   Synthesis and preliminary in vitro evaluation of an 18F-labeled covalent FAP inhibitor (Poster), 26th International Symposium on Radiopharmaceutical Sciences, iSRS 2025, 11. – 15. Mai 2025, Gold Coast, Australia. Conference Presentation (After Call).

“If you enter this world knowing you are loved and you leave this world knowing the same, then everything that happens in between can be dealt with.”

Michael Jackson